WANL-PR(EEE)-055
NASA-CR-121210

Westinghouse Astronuclear Laboratory

COMPACT THERMOELECTRIC CONVERTER

SYSTEMS TECHNOLOGY

FINAL REPORT

AEC RESEARCH AND DEVELOPMENT REPORT

NOTICE

Westinghouse Astronuclear Laboratory

COMPACT THERMOELECTRIC CONVERTER

SYSTEMS TECHNOLOGY

FINAL REPORT

FORWARD

The work described herein was performed at the Westinghouse Astronuclear Laboratory under subcontract to the Atomics International Division of Rockwell International Corporation. The work was performed for the Space Nuclear Systems Division, a joint AEC-NASA office with project management provided by NASA-Lewis Research Center and the AEC-SNAP Project Office.

DISTRIBUTION

This report has been distributed according to the category "Systems for Nuclear Auxiliary Power (SNAP) Reactor - SNAP Program," as given in the Standard Distribution for Classified Scientific and Technical Reports, M-3679, and according to the NASA Supplementary Report Distribution List at the end of this report.

TABLE OF CONTENTS

Astronuclear
Laboratory

LIST OF ILLUSTRATIONS

LIST OF TABLES

INTRODUCTION

Over the past eight years, the Westinghouse Astronuclear Laboratory has been engaged in the development of the tubular thermoelectric module. During the period from July, 1965, to June, 1969, Westinghouse was under contract to the Atomic Energy Commission (Contract AT(29-2)-2638) on the Compact Thermoelectric Converter Program with the fundamental objectives to develop and demonstrate through test a tubular thermoelectric module of good performance, long life, and high reliability, for application with either reactor or isotope heat sources. During the period from October, 1967, through June, 1973, the further development of the tubular module has been accomplished on the Compact Thermoelectric Converter System Technology Program, under subcontract to Atomics International, Division of Rockwell International, and has been directed specifically at application with the Zirconium-Hydride Reactor developed at Atomics International.

The effort under the earlier Compact Converter Program has been documented[1] and it is the purpose of this final report under the System Technology Program to document only the efforts of the more recent program.

A schematic of the tubular thermoelectric module is shown in the Frontispiece. It consists of alternate washers of n- and p-type lead telluride, separated by thin natural mica washers. Electrical continuity within the circuit is accomplished by cylindrical conductor rings located at the I.D. and O.D. of the lead telluride washers. The conductor rings are also separated by the same mica washers which separate the lead telluride washers. The result is a radially serpentine current path along the length of the module. The circuit is isolated from the structural claddings by thin sleeves of boron nitride. The circuit containment and heat transfer surfaces are provided by the inner and outer cladding, heat being transferred from a heat source at the inner clad, conducted radially outward through the lead telluride to the outer clad where the waste heat is removed by a heat rejection system.

---
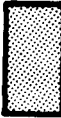
[1] Compact Thermoelectric Converter Final Report, NYOO-3584-15, 20 July 1969

DESIGN FEATURES

- FULLY ENCAPSULATED
- FULLY COMPACTED-VOID FREE
- STRUCTURALLY RUGGED
- NO BONDED JOINTS
- USES PbTe AT HIGH TEMPERATURE
- MECHANICALLY AND ELECTRICALLY ADAPTABLE
- LONGEVITY- SHELF AND OPERATING
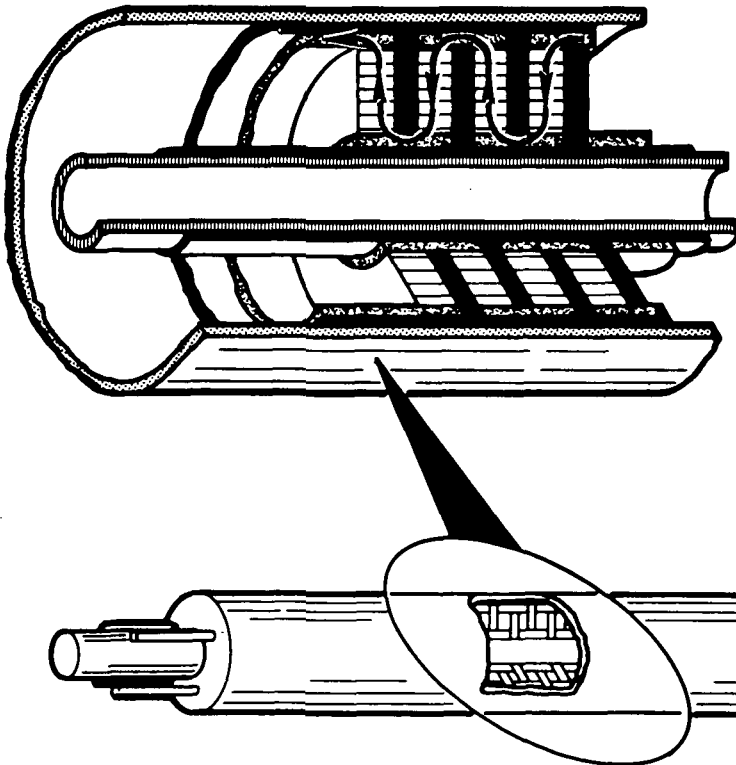
OUTER CLADDING

ELECTRICAL CONDUCTOR

THERMOELECTRIC MATERIAL

ELECTRICAL INSULATION

INNER CLADDING

Frontispiece – Tubular Thermoelectric Module

To identify differences among the tubular modules designed, fabricated, and tested to date, each module has been assigned a sequence and serial number, e.g., TEM-8 S/N-2. The sequence number was changed when a relatively major design change was incorporated. The serial number (S/N) denotes similar modules of a sequence but may incorporate relatively minor changes in design, fabrication or processing. Modules having sequence numbers of TEM-1 through TEM-9U were designed, fabricated, and tested under the earlier Compact Thermoelectric Converter Program while modules having sequence numbers of TEM-13, TEM-14, TEM-15, and TEM-X were designed, fabricated, and tested under the more recent Compact Thermoelectric Converter System Technology Program. However, an exception to the above is that TEM-9U S/N-6, -7, -8, and -9 were designed and fabricated under the earlier program and tested under the recent program, two modules being tested at WANL in static test stands and the other two being tested at Atomics International in liquid metal loops for the purpose of comparing data from identical modules in different test environments. These modules demonstrated the general validity of using static test data to evaluate the performance of converters being developed for use in liquid metal systems.

The TEM-1 through TEM-9U modules had a .5 inch I.D., a 1.66 inch O.D., and a circuit length of 7.2 inches; the TEM-13 and TEM-X reactor power modules had a .75 inch I.D., a 1.64 inch O.D., and a 15 inch circuit length; the TEM-15 sublength technology modules are radially the same as TEM-X modules but had a circuit length of 4 inches; the TEM-14 pump power modules had a .75 inch I.D., a 2.13 inch O.D., and a circuit length of 5.6 inches.

It is important to note the overlap of the two programs because the basic technology effort of the earlier program was continuing during the first year of the later program. In fact, the need for two piece inner conductor rings (discussed later) was identified and demonstrated in TEM-9 modules while the early TEM-13 series modules were in fabrication. For this reason a design change was made after fabrication of the TEM-13C series modules, to incorporate two piece inner conductor rings, prior to having test results on the TEM-13A modules. The fact that design improvements were being identified in the Compact Thermoelectric Converter Program and incorporated into the TEM-13 series modules is the reason

that modules through the TEM-13G series were fabricated prior to recognizing a thermal cycling problem which existed in the longer circuit module but was not a significant problem in the shorter length TEM-9's.

For clarity throughout this report, an attempt is made to discuss all aspects of a particular series of modules in one location. That is, the design, fabrication, test, and destructive examination of a particular series have been collected together to provide complete information on that series. Chronologically, this leads to some confusion. In the case of the TEM-13A modules, for example, all information through destructive examination is presented early in this report, when in fact, the TEM-13G modules were actually on test prior to the destructive examination of the TEM-13A modules.

I. REACTOR POWER MODULES

A. GOALS AND ACHIEVEMENTS

The primary objective of the Compact Thermoelectric Converter System Technology Program, conducted at Westinghouse Astronuclear Laboratory, was to design, develop, fabricate, test, and qualify a thermoelectric power conversion system for space application using a reactor heat source. The state-of-the art tubular thermoelectric generator at the time of the initiation of this program, 1968, had a .5 inch I.D., a 7.2 inch circuit and exhibited a characteristic 20 percent reduction in power output during the first 2,000 hours of operation at a nominal average hot clad temperature, $\overline{T}_H$, of 1000°F. The initial goals of this program were as follows:

1. To provide module parametric calculations covering an extended range of I.D.'s, O.D.'s, circuit lengths and operating temperatures to be used in a system study allowing the selection of an optimum (reference) module design for integration with a ZrH (zirconium hydride) (SNAP 8 type) reactor heat source.

2. To extend the state-of-the art of demonstrated tubular generators to cover the geometry range identified as optimum for the reactor/thermoelectric application.

3. To advance existing technology with respect to reducing module performance degradation to a characteristic rate of 5 percent for a 20,000 hour mission while increasing operating temperature to 1125°F.

4. To design a converter module consisting of an assembly of tubular modules hydraulically interconnected, including manifolds and jackets for hot and cold liquid metals, and provisions for structural support.

During the course of the program from 1968 to the end of 1972, all of these goals were accomplished. In addition, a number of substantial improvements in design and materials were identified and incorporated into the basic generator design. These improvements allowed the consideration of operating temperatures up to 1200°F for five year missions. All of these improvements, have been successfully demonstrated by their incorporation into the current

state-of-the art TEM-X series reactor power modules. A total of twelve TEM-X series reactor power modules were tested prior to January, 1973, with power output degradation rates ranging from 1.4 to 6.1 percent per 10,000 hours, for operating times up to 13,990 hours, average hot clad temperatures as high as 1175°F (1225°F peak), and including up to 63 thermal cycles per module. The individual degradation rates were found to be a strong function of operating temperatures, and this functional relationship was demonstrated to correlate closely with the mathematical model.

Two additional performance improvements have been identified to increase beginning-of-life, B.O.L., efficiency by 30 percent over the demonstrated TEM-X efficiency levels. These improvements, the incorporation of ternary lead telluride thermoelectric materials and electron beam vapor deposited (E.B.V.D.) diffusion barriers, were nearing completion and were scheduled for qualification in full length reactor power modules in calendar year 1973.

B.   TEM-13 REFERENCE REACTOR PROTOTYPE MODULE DESIGN SELECTION

The initial task undertaken by Westinghouse on the Compact Thermoelectric Conver-
ter System Technology Program, was the generation of module performance parametrics to be
used in the selection of a "reference" module design for a 25 KWe reactor/thermoelectric
power conversion system. These parametric calculations were generated using TEMOD, a
FORTRAN computer model for tubular thermoelectric generator performance analysis, developed
under a previous AEC contract.

This initial set of parametric calculations was based on existing 1968 state-of-the-
art (TEM-9 series) design considerations as well as advancements of the technology which
could be realistically projected as attainable in the early 1970's. Table I-1 presents an
itemized list of the range of temperatures and dimensions as well as module component material
selections used in this initial set of parametric calculations. The maximum module average
inner clad temperature was set at 1250°F, corresponding to a reactor outlet of 1300°F and a
100°F axial temperature gradient along the module. The outer clad temperature variations
allow a system trade-off between module performance and radiator weight. All material
selection variations from existing TEM-9 technology were based on preliminary evaluation of
experiments in progress on the TEM-9 technology program. The substitution of refractory con-
ductor rings in place of iron was designed to reduce module degradation by eliminating an
iron/TEGS-2P reaction. A measureable performance improvement was also achieved with
this substitution due to the substantially lower electrical resistivities of the refractory material.
The substitution of inconel 718 for the existing stainless steel outer clad was designed to pro-
vide a modest performance improvement by reducing the radial temperature drop across the
outer clad. Subsequent stress analysis effort, however, indicated that a module designed with
an inconel outer clad could not be successfully autoclaved (compacted) because of the high
strength of the inconel. This modification, although included in the parametric calculations,
was never incorporated into a reactor module.

Results of the module parametric calculations were transmitted to Atomics International
and incorporated into a system parametric study. The end result of this study was the conceptual
design of a 25 KWe, 56 volt reactor/thermoelectric power system. A primary liquid metal loop

TABLE I-1

INITIAL REACTOR POWER MODULE PARAMETRIC INPUT DATA

Item	Calculation Range or Consideration	1968 (TEM-9) State-of-the-Art
1. Average Inner Clad Temperature, $\overline{T}_H$	$1000°F$ to $1250°F$	$1000°F$
2. Average Outer Clad Temperature, $\overline{T}_C$	$400°F$ to $750°F$	$400°F$
3. Inner Diameter	.375 inch to 1.5 inch	.500 inch
4. Outer Diameter	1.20 inch to 3.5 inch	1.66 inches
5. Circuit Length	15.0 inch	7.2 inches
6. End Closures	TEM-9S type	TEM-9S type
7. Thermoelectric Washers	.030 inch axial thickness [1]	.090 inch axial thickness
a. p-type	TEGS-2P material	TEGS-2P material
b. n-type	GE-nl material	GE-nl material
8. Inner Clad	Inconel 718 [2]	Inconel 718
9. Inner Boron Nitride Insulator	.040 inch radial thickness	.040 inch radial thickness
10. Inner Conductor Rings	.015 inch (tungsten)	.015 inch (iron)
11. Outer Conductor Rings	.020 inch (molybdenum)	.020 inch (iron)
12. Outer Boron Nitride Insulator	.037 inch radial thickness	.037 inch radial thickness
13. Outer Clad	Inconel 718 [2]	Stainless Steel 316
14. Mica Insulators	.0015 inch axial thickness	.005 inch axial thickness

Notes: (1) T/E washer radial thickness varied with I.D. and O.D. of module.
(2) Inner and outer clad radial thickness scaled linearly with module I.D. and O.D.

system would be used to transport heat from the reactor through the inner bores of the tubular modules, and a secondary liquid metal loop system would transport the rejected heat from the module outer clads to a space radiator.

As discussed above, one of the program goals was to limit degradation (power reduction as a function of time at fixed operating conditions) to five percent for a 20,000 mission. Thus the 25 KWe system was actually designed for 26.2 KWe at beginning-of-life to compensate for the effects of the anticipated 5 percent power reduction over the duration of the mission.

The system was to be comprised of a total of 96 identical reactor power modules operating in a parallel flow arrangement so that all the modules would have identical operating conditions. The reference module operating temperatures of $\overline{T}_H = 1125^\circ F/\overline{T}_C = 570^\circ F$ were based on a trade off among module performance, module degradation rates, reactor lifetime, radiator size, and overall system weight considerations. Module circuit lengths were increased from the state-of-the-art level of 7.2 inches to 15 inches to reduce the number of individual modules required to produce 26.2 kilowatts. Module radial dimensions were selected to minimize system weight.

Restricting the circuit length to 15 inches necessitated the use of a series/parallel electrical connection of the modules. This arrangement was required because it was not feasible to design a single 15 inch module to deliver 56 volts directly. From a reliability standpoint alone, it was desirable to minimize the number of modules in each series connected string. This, of course, required maximizing the voltage of each module. Preliminary calculations indicated that the maximum voltage attainable in a 15 inch circuit module operating at these temperatures was 14 volts. On this basis, the system was to be comprised of 24 parallel wired "Converter Modules." Each converter module consisted of four series wired reactor power modules.

The "reference" reactor power module (designated TEM-13) circuit dimensions are summarized in Table I-2. These dimensions, it must be pointed out, are post-processing dimensions and not fabrication dimensions. The initial design effort for this, or any other module, was to determine component dimensions which would allow fabrication of the module and would result in the required post-processing dimensions.

TABLE I-2

TEM-13 REFERENCE REACTOR POWER MODULE CIRCUIT DIMENSIONS

A. Radial Dimensions (in Inches)

	Inner Radius	Thickness
Inner Clad (Inconel 718)	.375	.090
Inner Boron Nitride Sleeve	.465	.040
Tungsten Inner Conductor Ring	.505	.015
PbTe Thermoelectric Washers	.520	.143
Molybdenum Outer Conductor Ring	.663	.020
Outer Boron Nitride Sleeve	.683	.037
Outer Clad (Inconel 718)	.720	.020

B. Axial Dimensions (in Inches)

	Thickness
N-type Thermoelectric Washers	.033
P-type Thermoelectric Washers	.036
Mica Intercouple Insulators	.0015
Total Circuit Length	14.98

C. Design Features

No. of Couples = 208

Inner Diameter = .75 Inches

Outer Diameter = 1.48 Inches

C.   TEM-13 END CLOSURE DESIGN AND HEAT LOSS ANALYSIS

1.   End Closure Design Considerations

The basic end closure design concept employed in the reference module, as well as all TEM-13 and TEM-X series reactor power modules, was first utilized on 7.2 inch TEM-9S series modules. The design was established to minimize end closure heat losses while providing the axial support required to maintain adequate module integrity. Figure I-1 shows cutaway schematics of the TEM-9S, TEM-13 reactor power module end closures drawn to scale.

The axial lengths of the various insulating components (Alsimag 222) in the TEM-13 reactor power module end closure were maintained the same as those in the TEM-9S modules except in the stretch neck section of the end closure (see Figure I-1). The purpose of the stretch neck is to allow relative motion between the inner and outer clad resulting from differential thermal expansion during heatup of the module. Since the stretch neck strain is directly proportional to total module length, it was necessary to increase the reactor power module stretch neck length to limit the strain to two percent during operation.

The TEM-13 end closure design also deviated from the TEM-9S end closure in the reduced available volume for the Alsimag insulation in the end section. The volume reduction arises from the fact that although both modules have nearly identical outer diameters, the TEM-13 module has a .75 inch inner diameter whereas the TEM-9 module has a .50 inch I.D. This difference required the use of modified component assembly clearances to achieve proper uniform compaction in the end closure region of the module. The reduction in I.D./O.D. separation also necessitated a reduction in the power pin diameter to .060 inch from .090 inch in the TEM-13 design to facilitate assembly.

2.   End Closure Heat Loss Analysis

Thermal analyses of the TEM-13 reactor power module were conducted using TOSS[1], a digital heat transfer computer code. Boundary conditions were selected to simulate module operation in a reactor application for space $\overline{T}_H = 1125°F/\overline{T}_C = 570°F$ module operation.

[1] D. Bagwell, "Transient and/or Steady State (TOSS) Digital Heat Transfer Code", Union Carbide Nuclear Co., K-1491, 1961.

Conductor Pin

Stretch Neck

.500 I.D.

TEM-9S END CLOSURE

Conductor Pin

Stretch Neck

.750 I.D.
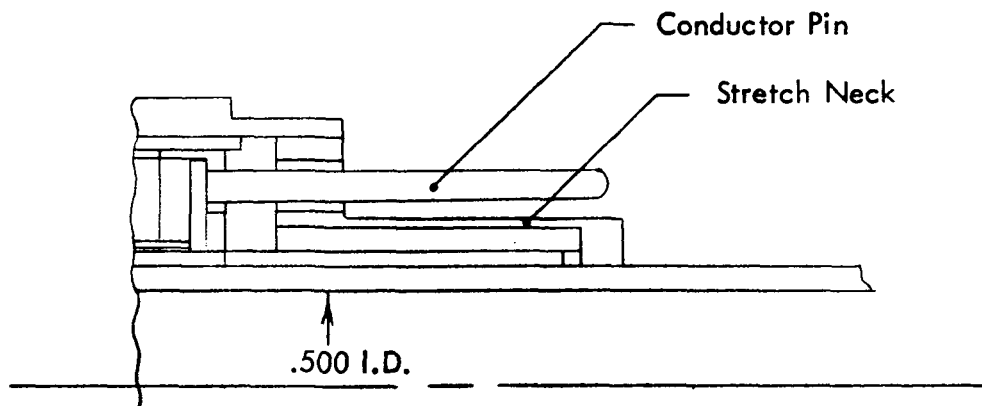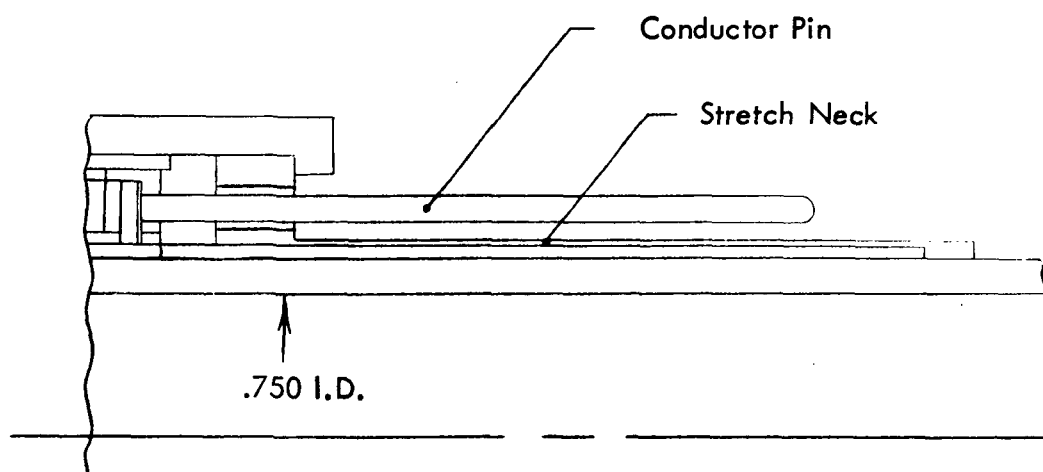
TEM-13 END CLOSURE

Figure I-1. A Comparison of TEM-13 and TEM-9
End Closure Designs

During actual operation, temperatures at the primary inlet end of the module would be higher than those at the other end. To avoid the necessity for analyzing each end of the module separately, "average" temperature conditions were imposed on the model. That is, the inner clad surface temperature was fixed at $1125^\circ F$ along the entire length of the model. The outer clad temperature was fixed at $570^\circ F$ along the region of the module which is in direct contact with the secondary coolant. All other exposed outer surfaces were allowed to radiate to a $570^\circ F$ sink. In addition to the end closure region of the module, the end loss model included 50 percent of the thermoelectric circuit to allow an accurate determination of the thermal interactions between the circuit and end closure. The cutting plane at the center of the thermoelectric circuit was assumed to be an adiabatic surface. Since heat losses through the power pins are minor for a reactor power module, they were neglected.

The TOSS model boundary conditions as well as calculated heat flow patterns are shown in a schematic representation of the TEM-13 end closure in Figure I-2. These results are for a calculation made with a conservative emissivity estimate of 0.25. Arrows show general heat flow paths through each of the end closure components. The rate of heat transfer across each of the end closure boundaries is shown on Figure I-2 in watts. Total end closure heat loss is defined as the sum of the heat loss from each end closure exposed surface as well as the axial heat flow from the end closure into the circuit region of the module radial outboard of the thermoelectric circuit. For this calculation, a total end closure heat loss rate of 166 watts per end was determined.

Similar calculations were performed using several emissivity valves. In the limit ($\in = 0.$, or no radiation) end closure heat losses were reduced to 132 watts per end. Using an emissivity of .6, end losses increase to 229 watts per end. The end losses associated with the operation of a TEM-13 module in a laboratory environment with well insulated end closure surfaces were found to be 150 watts per end (very nearly identical to those of the $\in = .25$ space operation case).

The $\in = .25$ heat loss results were used for all subsequent parametric analyses for reactor power modules, and the laboratory environment boundary condition calculations were used in the evaluation of loop test reactor power module data.
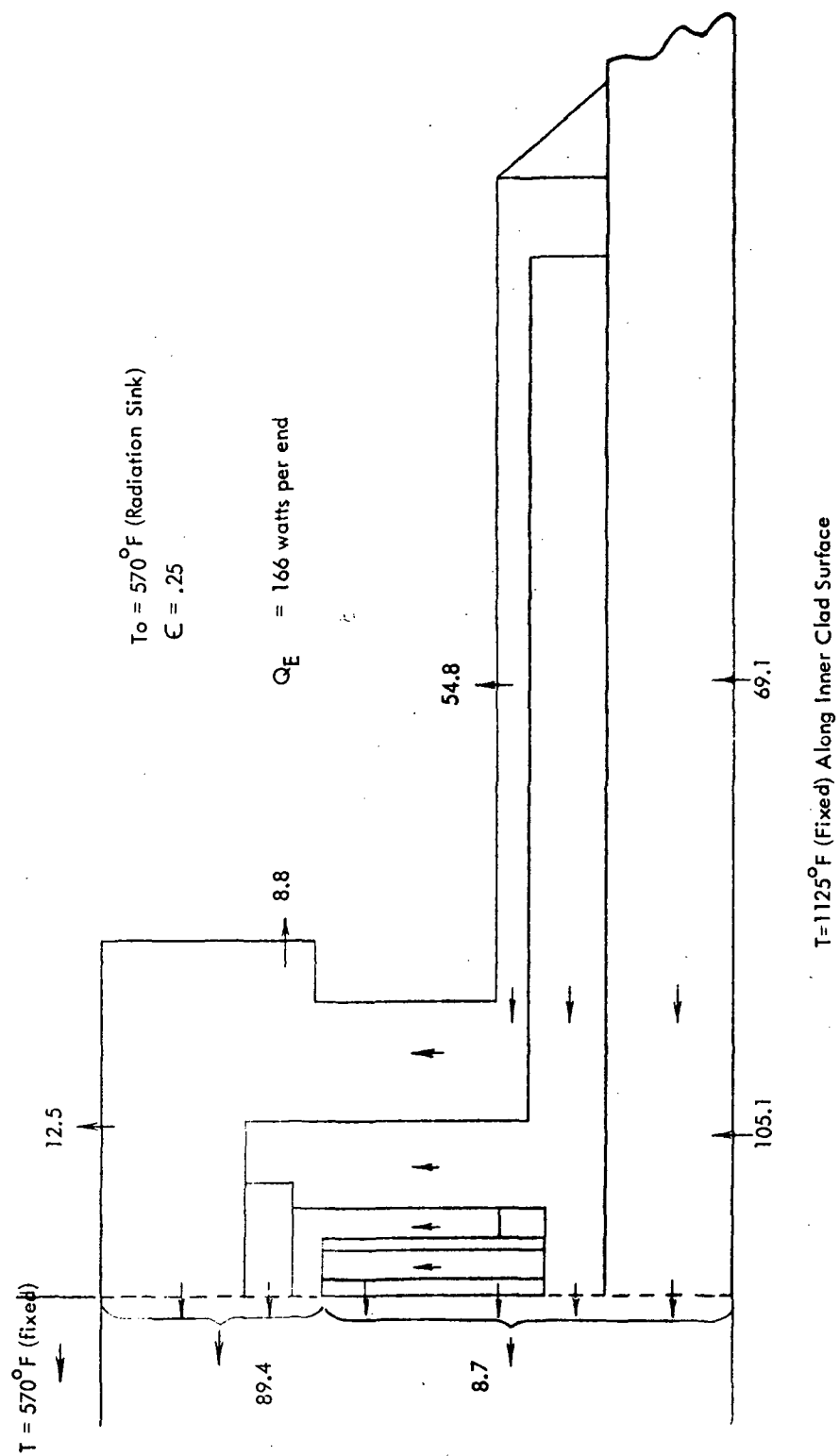
Figure 1-2. TEM-13 End Closure Heat Flow Patterns

$T_0 = 570°F$ (Radiation Sink)

$\epsilon = .25$

$Q_E = 166$ watts per end

T=1125°F (Fixed) Along Inner Clad Surface

T = 570°F (fixed)

54.8

69.1

8.8

12.5

105.1

89.4

8.7

D.   INITIAL TEM-13 SERIES - PROTOTYPE MODULES

1.   Design and Processing

An initial series of TEM-13 prototype reactor power modules were designed and fabricated during the early part of FY 1969. All of the initial prototype designs, designated as TEM-13A, TEM-13B and TEM-13C, as well as all subsequent reactor power modules, differed from the reference reactor power module in that .100 inch stainless steel 316 outer clads were incorporated in place of the .020 inconel clads of the reference design. The radial dimensions of these prototype modules were identical to those of the reference TEM-13 module with the exception that the overall outer diameter was increased to 1.64 inches as a result of the use of the thicker clad.

The individual features and calculated performance parameters for each of the prototype module designs are compared to those of the reference module in Table 1-3. The calculations were made for matched load $\bar{T}_H = 1125^\circ F / \bar{T}_C = 570^\circ F$ operating conditions. Although all of the modules have nominal 15 inch circuits, there are significant component axial dimension differences. The thermoelectric washer and mica insulator thicknesses in the TEM-13A design were the same as those used in TEM-9 series modules designed in a previous program. These dimensions allowed the incorporation of 79 couples within the 15 inch circuit length. The TEM-13C module, on the other hand, incorporated 208 couples with component axial dimensions identical to those of the 14 volt reference module. TEM-13B component dimensions lie between those of TEM-13A and TEM-13C.

Since each module design incorporated essentially identical end closures, end closure heat losses do not vary. However, because of the dimensional variations of the couples, the calculated module voltages and resistances vary considerably, while power output and efficiency can be seen to be much less sensitive to the couple component dimensions. TEM-13B has the lowest power output and efficiency because a smaller portion of the 15 inch circuit is comprised of lead telluride to accomodate the increased total mica thickness.

TABLE I-3

CALCULATED BOL PERFORMANCE PARAMETERS FOR
INITIAL TEM-13 REACTOR POWER MODULES

	TEM-13 Reference	TEM-13A	TEM-13B	TEM-13C
I. DESIGN FEATURE				
1. Module p-leg	.036" TEGS-2P	.093" TEGS-2P	.053" TEGS-2P	.036" TEGS-2P
2. Module n-leg	.033" GE-n	.087" GE-n	.050" GE-n	.033" GE-n
3. Outer Clad	.020" Inconel	.100" Stainless	.100" Stainless	.100" Stainless
4. Mica Washer Thickness	.0015"	.005"	.005"	.0015"
5. No. of T/E Couples	208	79	133	208
6. Total Circuit Length	15.0"	15.0"	15.0"	15.0"
II. CALCULATED OUTPUT				
1. Load Voltage (volts)	14.0	5.18	8.71	13.7
2. Power Output (watts)	273	248	240	252
3. Circuit Heat Input Rate (watts)	5356	5170	5235	5158
4. Circuit Efficiency (pct.)	5.10	4.79	4.59	4.90
5. Total Heat Input Rate (watts)	5688	5502	5567	5490
6. Overall Efficiency (pct.)	4.80	4.51	4.31	4.59

NOTE: All modules assumed to be operating $\bar{T}_H = 1125°F$ and $\bar{T}_C = 570°F$ at matched load conditions.

Two modules of each prototype series were fabricated and processed in the first half of GFY 1969. Processing is a standard two-stage compaction operation to which all tubular modules are subjected to eliminate all assembly clearances and to achieve full theoretical density of the lead telluride washers. The first compaction stage consisted of a 50,000 psi room temperature hydrostatic autoclave cycle and the second stage was a hot gas pressure sintering cycle carried out at 20,000 psi and 700°C (1292°F) for two hours. Both operations were performed in Westinghouse Autoclave Facilities.

2. Static Test Facility Description

After completion of the processing operations, the modules were placed in electrically heated test facilities for "static" testing, conducted at WANL. Figure I-3 is a schematic representation of the static test assembly used in the TEM-13A,B, and C series modules tests. In this test configuration a .625 inch O.D. electrical "main" heater was located within the bore and centered directly under the circuit of the module. Independently controlled "guard heater" windings were located under the end closure regions of the module to simulate end closure temperature profiles anticipated during loop test operation. The volume between the electrical heater O.D. and module I.D. was filled with stagnant liquid metal (NaK-78) to minimize the temperature drop from the heater to the module. An aluminum fin assembly was located over the outer clad of the module to facilitate heat rejection by forced air cooling. The fins were designed to provide an axial temperature profile along the clad of the module simulating liquid metal loop operation.

Thermocouples were located at ten axial positions along both the inner and outer clads of the module as shown in Figure I-3. The inner clad thermocouples were positioned in the space between the heater and module inner clad. The outer clad thermocouples were spot-welded directly to the clad of the module. Thermocouples 1, 2, 9, and 10 were positioned .090 inch on either side of the planes separating the circuit of the module from the end closures. The circuit length was then divided into five segments of equal length by thermocouples 4, 5, 6, and 7. The first and last of the five segments were further instrumented with thermocouples 3 and 8 located at the midpoints.
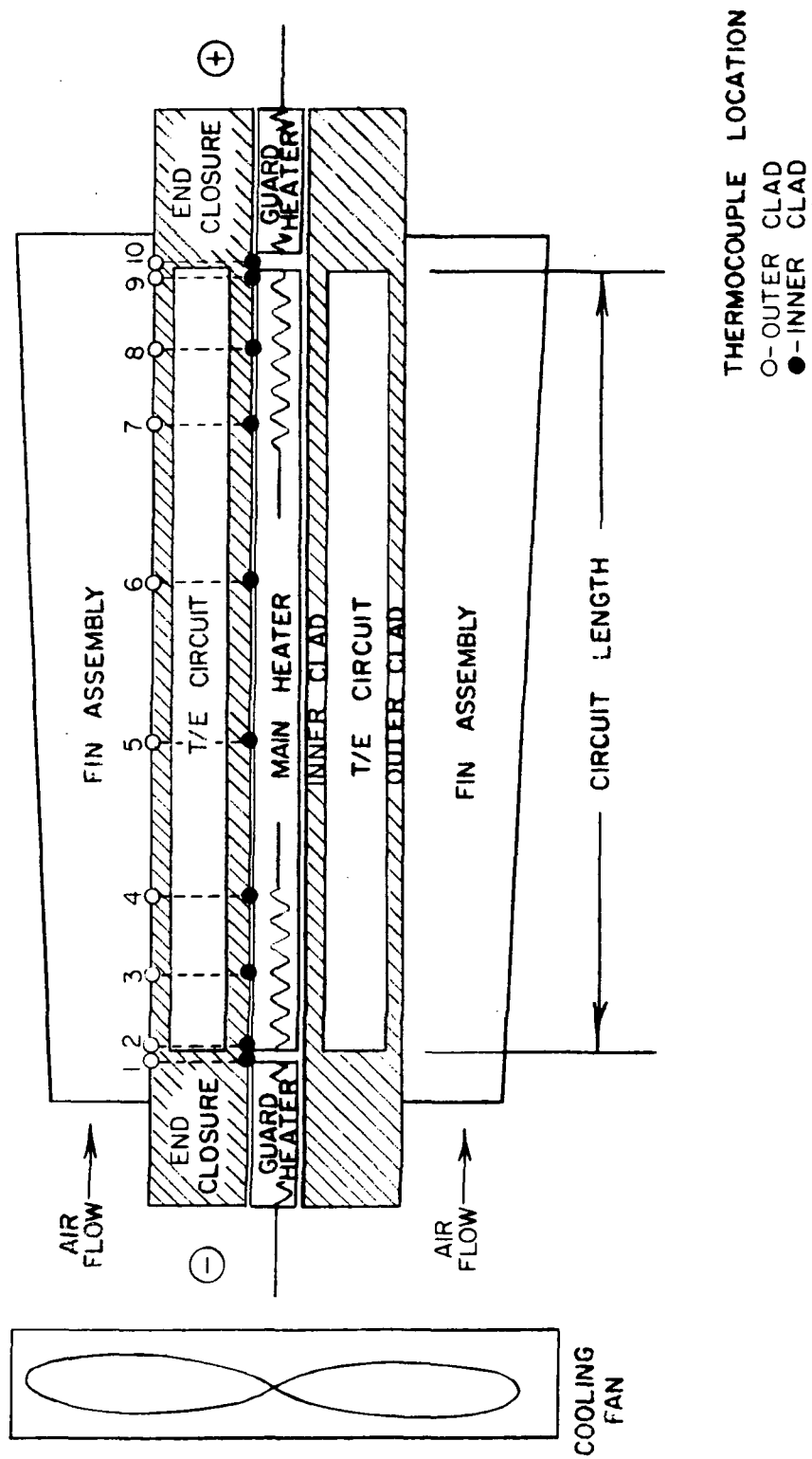
Figure I-3. Instrumentation of Thermoelectric Modules Tested in "Static" Test Stands

To determine the module average hot and cold clad temperatures, $\bar{T}_H$ and $\bar{T}_C$, respectively, a trapezoidal numerical integration technique was applied to the readings from thermocouples 2 through 9 (only the couples located in the circuit region of the module were used). Along with the 20 thermocouple readings, a "standard data set" consisted of instantaneous measurements of heater power, current flow through the module load circuit which was connected across the power pins at each end of the module, and the voltage measured immediately before and after opening a switch in the external load circuit. Measurement of the module open circuit voltage, V_{oc}, in conjunction with the load voltage, V_L, and the load current, I_L, afforded a means to determine the module internal resistance, R_g:

$$R_g = \frac{V_{oc} - V_L}{I_L}$$

3. Heatup Tests

Performance data from these, as well as all other modules on this program, were measured throughout the transient period in which the modules were heated from ambient (room temperature) conditions to their prescribed steady-state operating levels. This allowed a comparison between calculations and experimental data over a wide range of operating temperatures.

During the initial prototype module heatup tests, no attempt was made to control the radial temperature drop across the module. For this reason, there is no correlation between the module average temperature, $\bar{T}$, defined by the expression

$$\bar{T} = 1/2\,(\bar{T}_H + \bar{T}_C),$$

and average module temperature drop, $\Delta\bar{T}$, defined as

$$\Delta\bar{T} = \bar{T}_H - \bar{T}_C.$$

Since the heat throughput and open circuit voltage of a module are proportional to temperature drop, there was no way to predict these parameters as functions of heater power or module average temperature, except near the end of the heatup where the average hot and cold clad

temperatures of each module approach the target steady state levels, 1125°F and 570°F, respectively. However, effective Seebeck coefficient, internal resistance, and thermal impedance are not strong functions of module temperature drop. Therefore, these parameters, which completely specify module performance, can be calculated directly from the experimental data, presented as functions of average module temperature and used to evaluate actual module performance.

The effective Seebeck coefficient, $\bar{a}$, is defined as the ratio of the open circuit voltage to the average radial temperature drop, $\Delta\bar{T}$, across the module. Hence,

$$\bar{a} = \frac{V_{oc}}{\Delta\bar{T}}$$

The thermal impedance, TI, is defined as the ratio of the average radial temperature drop to the circuit heat throughput, Q_C,

$$TI = \frac{\Delta\bar{T}}{\bar{Q}_C} .$$

In this equation circuit heat throughput is that portion of the total electrical heater power which flows into the thermoelectric circuit of the module. Module end closure heat losses, as calculated for the TEM-13 module end closures discussed above, were subtracted from the electrical heater power for each data set to determine Q_C.

Presented in Figures I-4, I-5, and I-6 are the effective Seebeck coefficient, internal resistance, and circuit thermal impedance data, respectively, recorded during the initial heatup of the initial six reactor prototype modules. All the parameters are presented as functions of average module temperature. The calculated parameters for each of the three different designs are also shown on each curve. Although some minor discrepancies exist between experimental data and corresponding calculated curves, the overall correlation was good over the entire temperature range. Figures I-4 and I-5 point out the electrical differences between the three designs quite clearly. The calculated thermal impedance heatup curves for the three prototype module designs were indistinguishable and are shown as shown as a single solid line in Figure I-6. Thermal impedance data from the six modules verified that
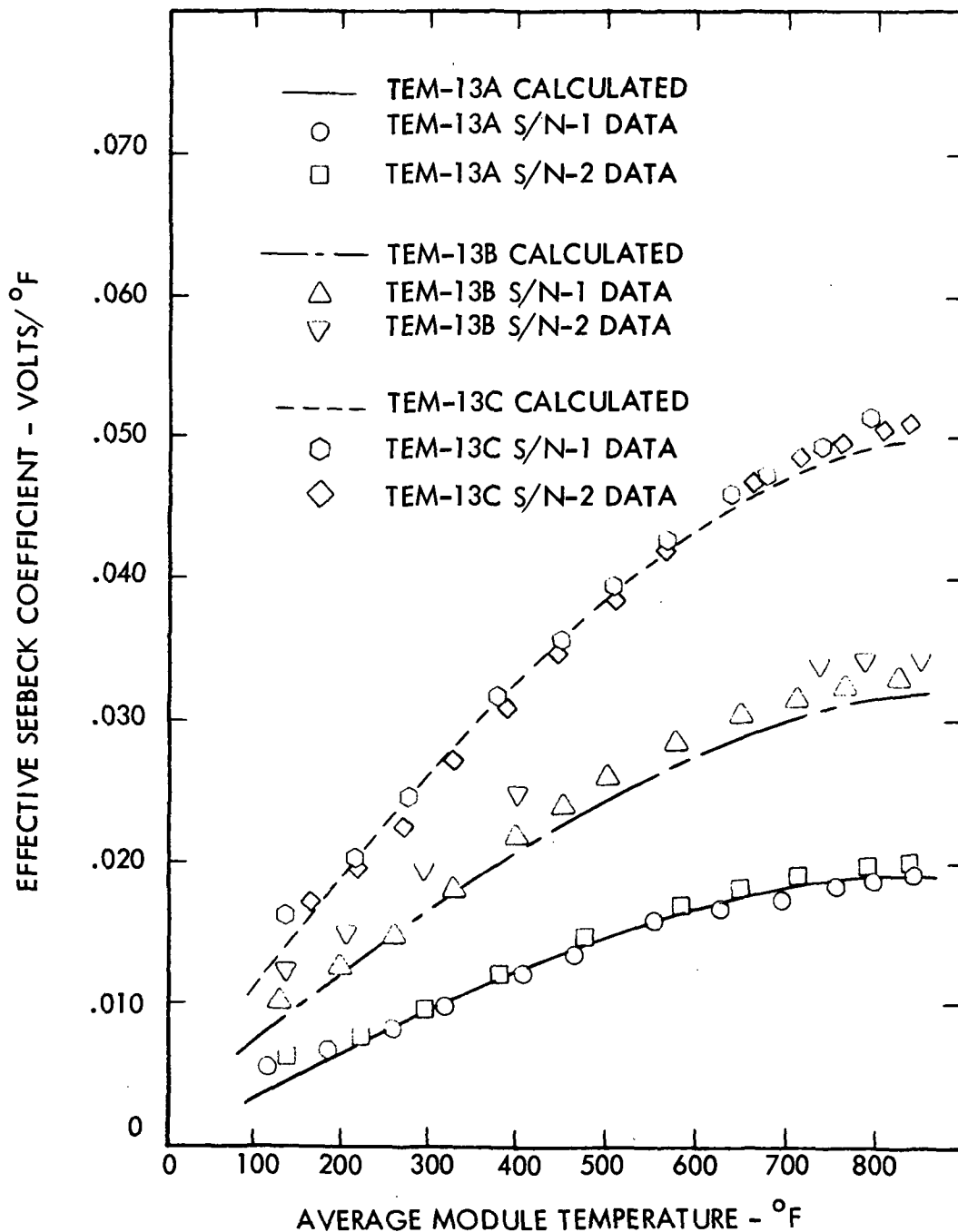
Figure I-4. A Comparison of Calculated and Experimental Effective Seebeck Coefficient
Data Measured during Heatup of Initial Prototype Reactor Modules

Figure 1-5. A Comparison of Calculated and Experimental Internal Resistance Data
Measured during Heatup of Initial Prototype Reactor Modules

Figure 1-6. A Comparison of Calculated and Experimental Module Thermal Impedance
Measured during Heatup of Initial Prototype Reactor Power Modules

the heat throughput is indeed quite insensitive to the design variations incorporated into these modules.

4. Endurance Tests

Of the six initial prototype reactor power modules, four were endurance tested for a period sufficiently long to uncover two design deficiencies affecting module performance stability. The TEM-13B S/N-1 and TEM-13C S/N-1 tests were terminated shortly after their initial heatups due to electrical heater malfunctions. A guard heater failure in the former module caused a shutdown. It was initially intended that the guard heater be replaced and the TEM-13B S/N-1 test resumed. However, subsequent data from its sister module, TEM-13B S/N-2, revealed an unacceptably high degradation rate and attention was focused on identifying the cause and elimination of this degradation rather than the restarting of the TEM-13B S/N-1 test. The TEM-13C S/N-1 test was also terminated due to a heater malfunction. In this case, a breakdown in the electrical heater insulation caused an arc from the heater to the module clad, destroying the heater and severely damaging the module. These incidents promoted heater design modifications for all future static tests.

Figure 1-7 presents power output endurance test data from the remaining four initial prototype reactor power modules, all of which were tested at constant $\bar{T}_H = 1125°F/$ $\bar{T}_C = 570°F$ matched load operating conditions. Almost immediately it was observed that degradation rates were unacceptably high, particularly in the TEM-13B and 13C modules fabricated with thin thermoelectric washers. Figures 1-8 and 1-9 present open circuit voltage and internal resistance data, respectively, from these modules.

The TEM-13B S/N-2 and TEM-13C S/N-2 tests were terminated after relatively short testing times, to allow a destructive examination of the modules. The primary purpose of these destructive examinations was to identify the cause of the high degradation rates.

During the time period in which TEM-13B S/N-2 and 13C S/N-2 were being destructively examined, endurance testing of the two TEM-13A series modules was continued. The TEM-13A S/N-1 test plan called for steady state endurance testing in which the module operating temperatures were to be held constant. TEM-13A S/N-2 was to be thermally cycled to simulate transient operation of the module in the system during a reactor scram.
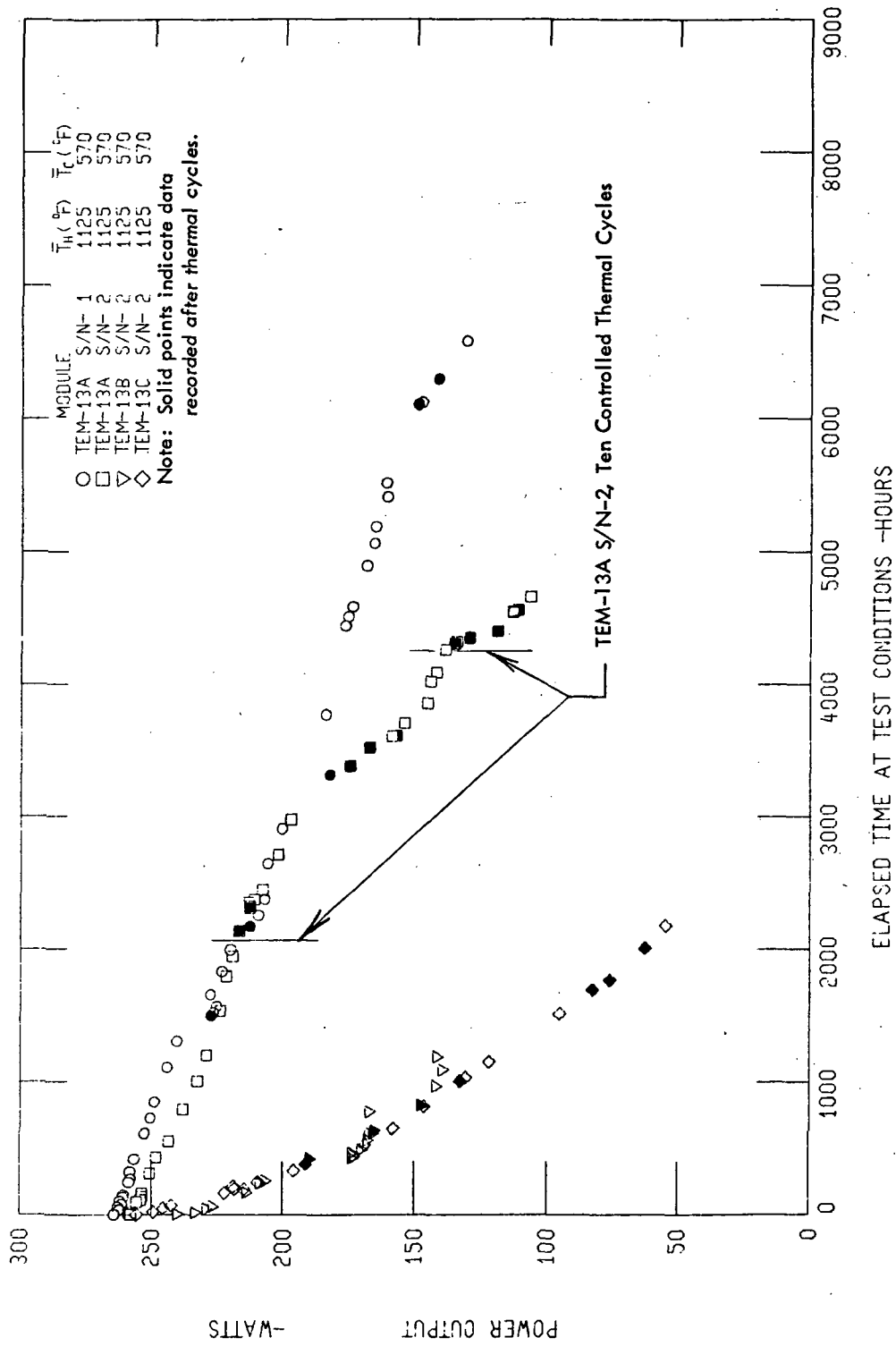
Figure I-7. Power Output Endurance Test Data from Initial Prototype Reactor Power Modules
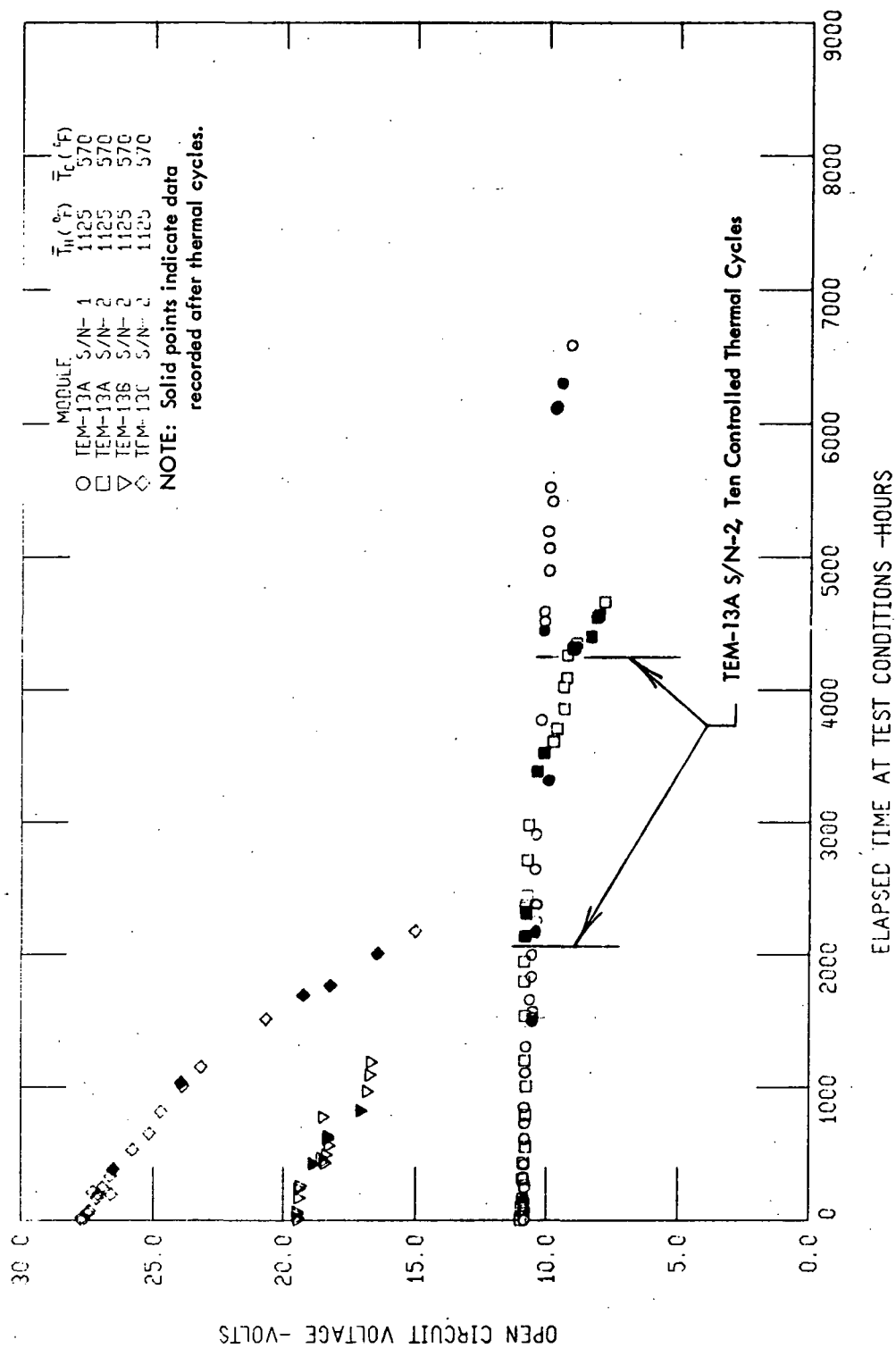
Figure I -8. Open Circuit Voltage Endurance Test Data from Initial Prototype Reactor Power Modules
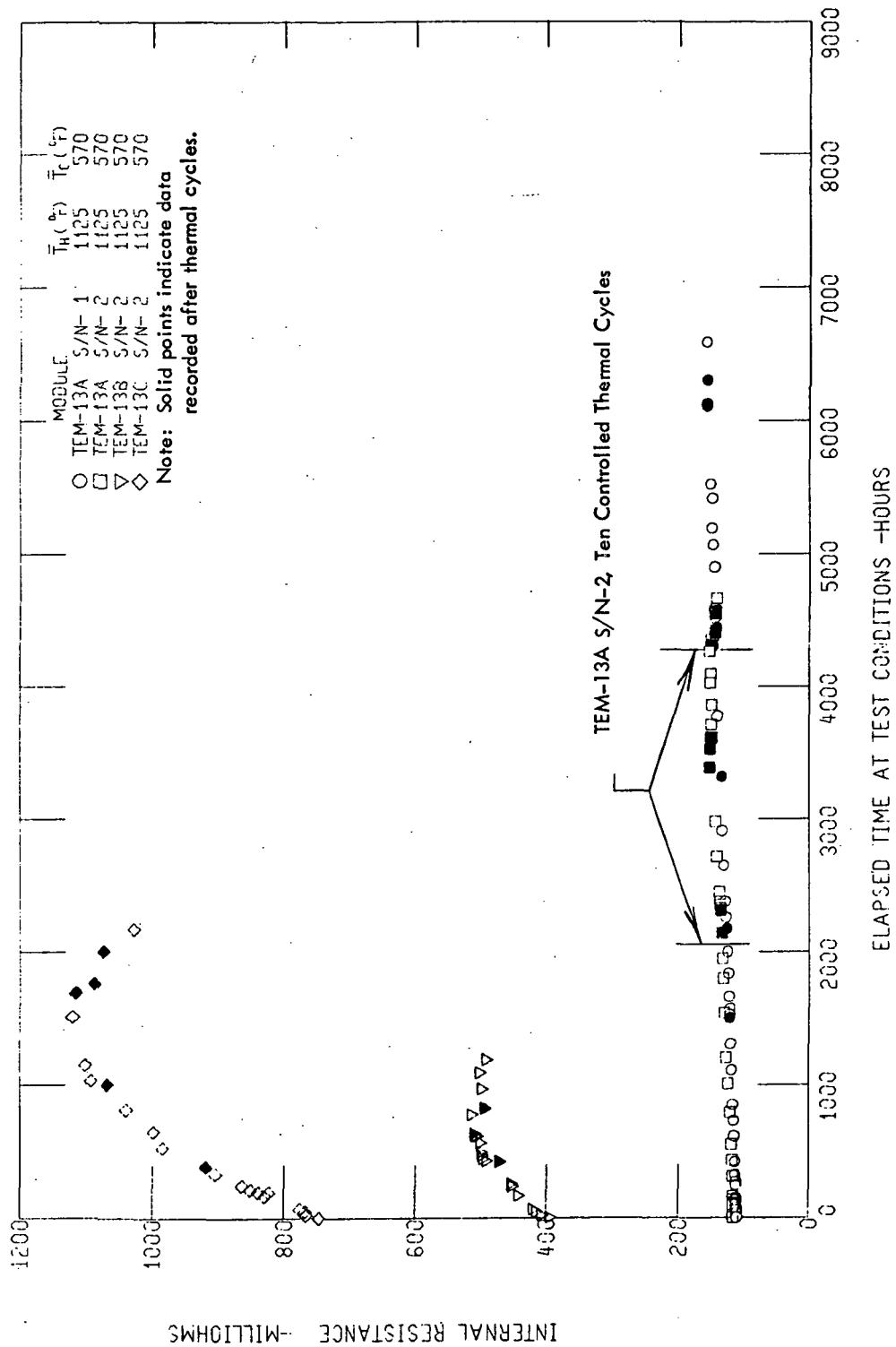
Figure I-9. Internal Resistance Endurance Test Data from Initial Prototype Reactor Power Modules

The module was subjected to a series of ten programmed thermal cycles after each 2000 hours of steady state operation. Each cycle consisted of a reduction of the hot clad temperature from $\overline{T}_H = 1125^\circ F$ to $\overline{T}_H = 500^\circ F$ at a $30^\circ F/minute$ ramp rate and a one hour holding period at the lower operating temperature after which the module was returned to the standard steady state operating conditions again using a $30^\circ F/minute$ ramp rate.

In addition to these controlled TEM-13A S/N-2 thermal cycles, all of the modules were subjected to unscheduled thermal cycles resulting from test interruptions due to power failures and test instrumentation malfunctions. These thermal cycles are much more severe in that temperature ramp rates of approximately $500^\circ F/minute$ are experienced by a module on static test when power is instantaneously interrupted. In addition, similar ramp rates are produced when full power is instantaneously restored after a laboratory power failure. In later module tests, the rapid restart condition was eliminated through the incorporation of test stand control circuits preventing an automatic restart after a power failure.

Data recorded immediately after each unscheduled thermal cycle are shown in solid on Figures 1-7 through 1-9 for each module. The time at which TEM-13A S/N-2 was subjected to controlled thermal cycles is also indicated on the figures. Up until the time that TEM-13A S/N-2 had accrued 3000 hours of operation, during which period the module had been subjected to ten controlled and two uncontrolled thermal cycles, module performance appeared to be unmeasureably affected by transient operation. However, it became apparent, after each successive thermal cycle, that the transient operation was affecting module performance. In particular, step decreases in module voltage, producing subsequent power output decreases, after each thermal cycle indicated the development of inter-couple shorting due to the transient operation of the module.

Shortly after the second set of ten controlled thermal cycles on TEM-13A S/N-2, the two remaining initial prototype modules were removed from test for destructive examination to determine the cause and identify a solution for the thermal cyclic sensitivity problem.

5. Module Destructive Examination Results

TEM-13B S/N-2 was removed from static test after 1187 hours of operation and destructively examined. As mentioned above, the purpose of this examination was to determine the cause or causes of the performance degradation observed during module testing.

A transverse cut was made at the center of the module at a point where the local hot side temperature was approximately 1160°F during testing of the module. The sectioned module was then ground to expose the large mica washer (the mica washer which terminated at the outer diameters of both the inner and outer conductor rings). The mica was then stripped away, exposing the n-type lead telluride washer surface. Seebeck probe traces were taken every 90 degrees around the module circumference, commencing at the inner conductor ring and proceeding in a radial line to the outer conductor ring. Figure I-10 is a typical plot of the Seebeck coefficient versus distance from the inner conductor ring for the n-washer. This plot showed that the washer was converted to p-type over one-half its radial dimension and contaminated over almost its entire surface. Metallurgical examination of the n-type washer indicated that the contamination was caused by excess tellurium. Since the n-type lead telluride is fabricated with a stoichiometric lead-tellurium mixture, it was postulated that the excess tellurium had diffused into the n-type washer from the p-type washer. TEGS-2P material is fabricated with an excess of tellurium to increase the solubility of the sodium dopant. An excess of tellurium has no effect on p-type lead telluride thermoelectric properties but has a gross effect on the n-type material.

Concurrently TEM-13C S/N-2 was being destructively examined. This module was cut transversely into three sections. The center section consisted of the center nine inches of the thermoelectric circuit. This center section was then cut axially, exposing a cross-section of the thermoelectric circuit near the center of the module. Visual examination of this section showed that the large mica washers were separated from the inner conductor rings leaving a gap ranging from .001 to .003 inches. It had been anticipated that this mica washer would form a butt joint with the inner conductor rings during compaction of the module. As a result of this gap, the p- and n-type lead tellurides were in direct contact with one another at each of the mica/conductor ring separations. This condition, of course, allowed free
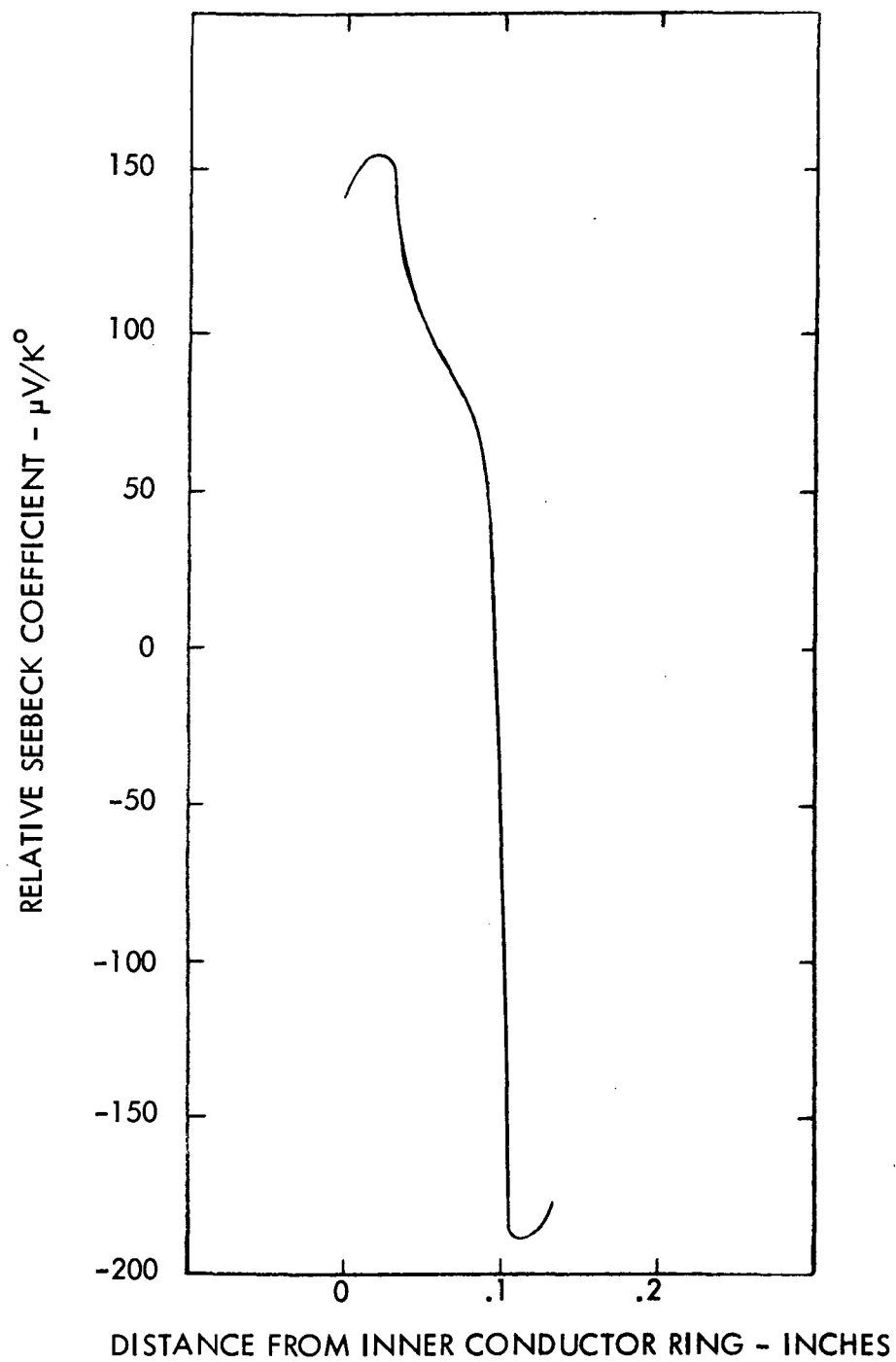
Figure 1-10. Seebeck Coefficient Versus Distance from the Inner Conductor Ring for a
TEM-13B S/N-2 N-Type Washer Operated at 1158°F

diffusion of tellurium from the p- to the n-type washer.

The effects of this direct-contact condition had not been observed in testing of previous TEM-9 series modules for two reasons. First, nearly all of these modules were tested at much lower temperatures, $\bar{T}_H$ = 1000°F, and the diffusion rate of tellurium decreases rapidly with temperature. Second, most of these modules incorporated iron inner conductor rings. Subsequent re-examination of previously destructed TEM-9 series modules showed that the tellurium which had diffused into the n-type material had combined with iron, forming an Fe-Te compound which was found to have small measureable effect on the thermoelectric properties of the n-type material.

TEM-13A S/N-2 was removed from test for destructive examination after 4658 hours of $\bar{T}_H$ = 1125°F/$\bar{T}_C$ = 570°F operation including a total of 20 controlled (30°F/minute ramp rate) and 10 uncontrolled (about approximately 500°F/minute ramp rate) thermal cycles. The destructive examination was performed to study the cause of the modules' observed cyclic sensitivity. The module was cut transversely into three sections: two end sections containing approximately three inches of the thermoelectric circuit and a center section containing approximately nine inches of the circuit. These sections were mounted in epoxy and sectioned axially to expose the circuit for examination. The thermoelectric washers were found to be extensively deformed in a chevron pattern at both ends of the module. Visual examination of the metallographically prepared specimens at high magnification under a microscope revealed that the small mica washers separating the inner conductor rings (see Figure 1-11) were sheared near the point where the mica extends from the inner conductor rings at their inner diameter.

A series of measurements were taken on the metallographically prepared specimens to determine if dimensional changes had occurred in any of the components. The first measurements were taken to determine the axial distance between the inner conductor rings. The measurements showed that, except for a few rings at each end of the module, the distance between most of the conductor rings was greater than 0.005 inch. Since the average measured axial thickness of the mica washers between the lead telluride washers was 0.0042 inch, it was not surprising, therefore, that some lead telluride was found between the inner conductor rings.
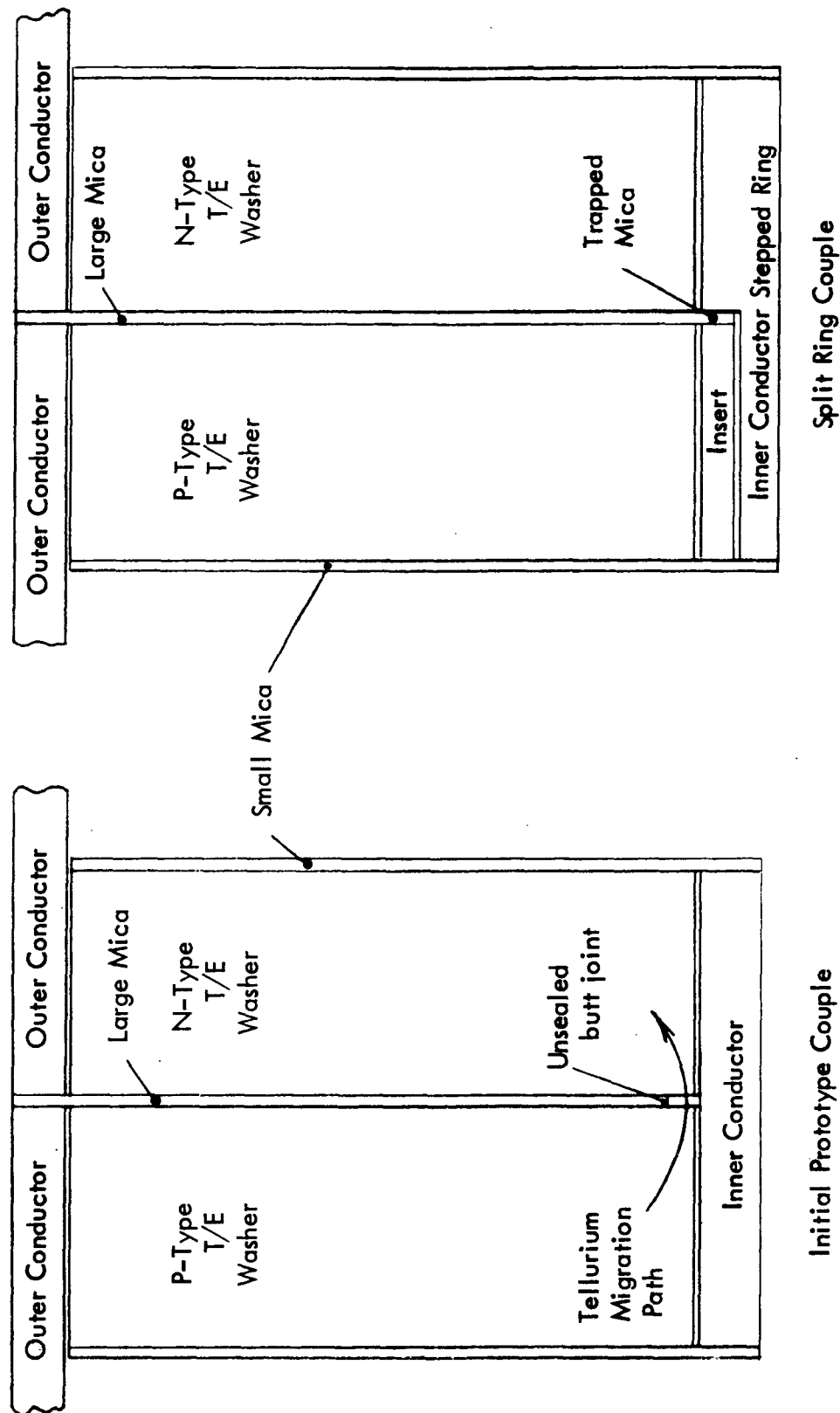
Figure I-11. A Comparison of the Initial Prototype and Subsequent (Split Ring)
Inner Conductor Ring Designs

The axial distance between the molybdenum outer conductor rings was also measured. It was found that the average distance was 0.005 inch with uniform spacing along the module axial length.

Additional measurements were performed on the end sections of the module to determine the axial thickness of the individual lead telluride washers at both the inner and outer conductor ring interfaces. It was found that the axial thickness of the p-type washers was quite uniform along the outer conductor ring, being approximately 0.094 inch. At the negative end of the module the majority of the p-washers were less than 0.094 inch, while at the positive end the axial dimensions were generally greater than 0.094 inch.

The axial thickness measurements performed on the n-type washers showed a somewhat different trend. The n-type washer thicknesses measured at the negative end of the module were more scattered than those of the p-type washers. However, unlike the p-type washers, there was no appreciable thickness difference along the radial thickness of the washers. At the positive end of the module, the axial thicknesses of the n-type washers at the inner conductor ring interface were less than the thicknesses measured at the outer conductor ring interface.

The final dimensional measurement taken was the radial thickness of each washer from the positive and negative ends of the module. The unpolished axial cut sections of the positive and negative ends samples were dismantled and the lead telluride washers removed for measurement. The resulting dimensions showed the average radial thickness of both the n-type and p-type lead telluride washers to be approximately 0.143 inch. This value is the same as the calculated dimension for the radial thickness of the lead telluride circuit in a fully compacted TEM-13 type module.

The testing histories of TEM-13C S/N-1 and TEM-13C S/N-2 made them ideally suited for destructive examination and comparison with each other. During the initial heatup of the TEM-13C S/N-1 module, before it reached test conditions, a heater failure resulted in the module being shutdown and removed from test. Compared to the test history of TEM-13C S/N-2, TEM-13C S/N-1 was essentially in the as-processed condition. TEM-13C S/N-2 experienced ten programmed thermal cycles and five separate heatups, one of which was an

uncontrolled, full power heatup which applied to a full 6000 watts to the main heater. The power output of this module decreased with time during the 2173 hours of test, as shown in Figure I-7.

TEM-13C S/N-1 was cut transversely into several sections, each of which contained approximately 1.5 inches of thermoelectric circuit. The sections were mounted in epoxy and cut axially to expose the circuit configuration. Microscopic inspection of the sections revealed that the circuit was aligned with no noticeable chevroning of the washers, even near the ends of the module. The gaps between the large mica insulators and the inner conductors were observed in this module as in previous modules. The small mica insulators, separating the inner conductor rings, appeared intact except near the very ends of the circuit where an apparent stackup mismatch (total length of outer conductor rings vs. inner conductor rings) was evident. At the ends, the position mismatch between the washers and the inner conductor rings was such that the mica sheared and caused intercouple shorting.

Another phenomenon noted during the microscopic examination of TEM-13C S/N-1 was that the spacing between the inner conductor rings was generally greater than the thickness of the mica between the lead telluride washers. However, the distance between the outer conductor rings appeared very close to the dimensional thickness of the mica between the lead telluride washers.

The two end sections of TEM-13C S/N-2, which had been destructively examined previously to determine the cause of its rapid degradation, were mounted in epoxy and sectioned axially to expose the circuit for examination. An examination of these sections showed that the chevroned washer effect was prevalent throughout each section. Detailed microscopic examination at 100X revealed that many of the mica washers separating the lead telluride washers were either sheared where the mica separated the inner conductor rings or pulled away from the conductor rings or sheared at the lead telluride-conductor ring-mica junction. A similar magnitude of mica movement and/or breakage was noted in the negative end section.

The distance between the inner conductor rings of TEM-13C S/N-2 was measured at 100X using a filar eyepiece. It was evident that the distance between the inner conductor rings was, in most cases, greater than the mica thickness outside the rings. No significant

amount of lead telluride was observed between the rings, and the spacing was filled with expanded mica. The same phenomenon was observed between the inner conductor rings in TEM-13C S/N-1.

6. Summary of Initial TEM-13 Series Results

The initial prototype modules, the first .75 inch I.D. and 15 inch circuit tubular thermoelectric generators fabricated, provided important information to the program. The close correlation between heatup data and calculated parameters indicated that the mathematical model could be used to calculate beginning-of-life (B.O.L.) performance of modules having a wide range of internal geometries.

In addition, test data from these modules identified two serious design deficiencies. Destructive examination data resulted in the confirmation of a need for a design fix, the split inner conductor ring, (see Figure 1-11) which would substantially reduce tellurium migration. In addition, a circuit distortion problem was uncovered and work was started immediately on the identification of a fix to eliminate this problem. Unfortunately, the cyclic distortion problem was not identified until after the next three series of reactor prototype modules, the TEM-13D, 13F, and 13G series, had been designed and fabricated. As a result, the performance of these later modules, too, was found to be extremely cyclic sensitive.

E.   INNER CONDUCTOR RING REDESIGN

Destructive examination results from the on going Compact Converter Program modules (TEM-9's) and the first four modules tested on this program at $\overline{T}_H$ = 1125, TEM-9U S/N - 6, 7, 8, and 9 indicated that the primary mode of performance degradation was due to the transport of tellurium from the p-type material to the n-type material. This transport appeared to be occurring primarily at the butt seal of the large mica and the inner conductor ring.

Figure I-11 shows a schematic representation of the thermoelectric couple design incorporated in the initial prototype reactor modules. Also, shown is the mechanical "fix" incorporated into all subsequent modules to eliminate direct contact of p- and n-type material. The inner conductor was fabricated in two pieces, allowing the large mica insulators to extend into, and subsequently be trapped between the inner conductor components. This inner conductor configuration is referred to as the "split conductor ring" design.

Some radial geometry modifications were required to incorporate the split conductor ring design shown in Figure I-11. It was found necessary to increase the total inner conductor radial thickness to .030 inches to facilitate machining of the inner conductor stepped ring. The TEM-13 reference module design, as well as the initial prototype modules, had inner conductor ring thicknesses of .015 inch as shown in Table I-2. The additional volume required to incorporate the split conductor ring design was obtained without affecting the overall module or lead telluride radial dimensions. This was done by decreasing the inner boron nitride thickness to .025 inch from .040 inch. Calculations showed that these modifications had essentially no effect on module performance.

F.   SECOND GENERATION HIGH VOLTAGE PROTOTYPE MODULES

1.   Degradation Reduction Considerations

Early test data from the initial prototype reactor modules, particularly TEM-13B and TEM-13C which were fabricated with thin thermoelectric washers required for high voltage, exhibited excessively high degradation rates. Destructive examination of these modules indicated the tellurium migration should be decreased through the incorporation of redesigned, split inner conductor rings shown in Figure I-11. In addition, it was determined that improved performance stability could be achieved by increasing the mica insulator axial thickness to .003 inch from .0015 as assumed in the reference TEM-13 design. The latter modification required the reduction to 200 thermoelectric couples from 208 to maintain a total 15 inch circuit length.

Subsequently, two series of second generation high voltage reactor power modules incorporating the split ring inner conductors and thicker mica insulators were designed, fabricated, and placed on test in the early part of CY-1969. These modules were designated TEM-13D and TEM-13F series modules.

2.   TEM-13D Prototype Modules Incorporating TEGS-3P Material

Data from a group of TEM-9 series modules, TEM-9Q design, indicated that high temperature performance stability could be substantially improved by substituting TEGS-3P material, a lead-tin-telluride compound, for the TEGS-2P lead telluride commonly used in tubular modules. The primary reason for this improved stability in these early modules was that the alternate material was found to be chemically compatible with the iron conductor rings used in all modules at that time.

The lead-tin-telluride with its improved stability characteristics, however, has a very serious drawback. The figure-of-merit, a combination of thermal and thermoelectric materials properties that indicate the efficiency of the TEGS-3P material, is about twenty percent lower than that of standard TEGS-2P in the temperature range of interest.

However, because of the extremely high degradation rates observed in early prototype reactor modules, it was decided to incorporate TEGS-3P material into a reactor power module as a backup to the reference design. Reactor modules incorporating TEGS-3P material were designated as TEM-13D series modules.

The TEM-13D design was very similar to the TEM-13C design, with the following exceptions:

a. TEGS-3P lead telluride was incorporated in place of TEGS-2P material.

b. The mica intercouple insulator axial thickness was increased to .003 inch from .0015 inch. This modification required the reduction to 200 from 208 couples to maintain a total 15 inch circuit length.

c. The split inner conductor ring design shown in Figure I-11 was incorporated in this as well as all subsequent module designs on this program.

d. In the TEM-13D modules, all of the inner and outer conductor ring components were fabricated with iron. This modification was made because no information existed concerning the compatibility of lead-tin-telluride with refractory materials such as tungsten or molybdenum.

Table I-4 shows a comparison of calculated matched load, $\overline{T}_H = 1125^\circ F/$ $\overline{T}_C = 570^\circ F$ performance parameters for the TEM-13C and TEM-13D designs. Since the two types of modules had design modifications as well as thermoelectric material modifications, it is difficult to assess the effects of incorporating TEGS-3P material from this comparison alone. Also shown on the table, then, are similar calculations for the TEM-13F design. This type of reactor module, which is discussed more completely in a subsequent section of this report, is essentially identical in design to the TEM-13D module except that TEM-13F employs the standard TEGS-2P material and refractory conductor rings.

A comparison of TEM-13D and TEM-13F calculated parameters shows that the incorporation of TEGS-3P material into a reactor power module results in an efficiency decrease of nearly 8 percent. Perhaps more important is a reduction of over 13 percent in power output. The implications of these performance differences on a reference system module are discussed in the next section of this report.

TABLE I-4

A COMPARISON OF SECOND GENERATION REACTOR MODULE CALCULATED
PERFORMANCE PARAMETERS WITH THOSE OF TEM-13C

Parameter	TEM-13C	TEM-13D	TEM-13F
1. $\bar{T}_H$ ($^\circ$F)	1125	1125	1125
2. $\bar{T}_C$ ($^\circ$F)	570	570	570
3. Matched Load Voltage (volts)	13.7	12.5	13.3
4. Internal Resistance (milliohms)	737	736	716
5. Power Output (watts)	252	214	247
6. Total Heat Input Rate (watts)	5490	5228	5582
7. Overall Efficiency (pct.)	4.59	4.09	4.43

Fabrication of two TEM-13D series modules, S/N-1 and S/N-2, was completed in December, 1968. Measurements taken after completion of the processing cycle but prior to the initiation of testing indicated that both reactor power modules incorporating TEGS-3P material had abnormally high room temperature internal resistance. Whereas the calculated room temperature internal resistance was .124 ohms, that measured for S/N-2 was .155 ohms and S/N-1 actually indicated an open circuit condition. The calculations are based strictly on bulk resistances, with all electrical interface contributions assumed to be negligible. In well-compacted modules, this assumption had been demonstrated to be valid. However, data from these modules indicated that intimate contact between the thermoelectric material and conductor rings had been lost during the cooldown portion of the autoclave cycle. This phenomenon, peculiar to the TEM-13D series modules, was attributed to the use of TEGS-3P thermoelectric washers having different mechanical and thermal expansion characteristics than the standard TEGS-2P material.

Both TEM-13D series modules were instrumented and placed on static test in January, 1969. Internal resistance data recorded during the initial heat-up of these modules is presented in Figure 1-12, plotted as functions of average module temperature. The calculated curve, assuming negligible interface resistances, is also shown. The curve shows that the data from both modules approached the theoretical curve as the temperature was increased. This was anticipated since differential thermal expansion of the module internal components increases all interface pressures as the module temperature is increased. Within $200^\circ F$ of the standard operating conditions, $\overline{T}_H = 1125^\circ F/\overline{T}_C = 570^\circ F$, data from both modules correlated well with the calculated curve.

Endurance test data from these modules, like the initial prototype reactor modules, was extremely sensitive to the cyclic history of the modules. TEM-13D S/N-1 experienced four rapid thermal cycles very early in its test history, resulting in a subsequent drop in voltage and power. The module was removed from test for destructive examination in March, 1969, prior to accruing any substantial endurance test data. Substantial inter-couple shorting was observed upon sectioning the module.
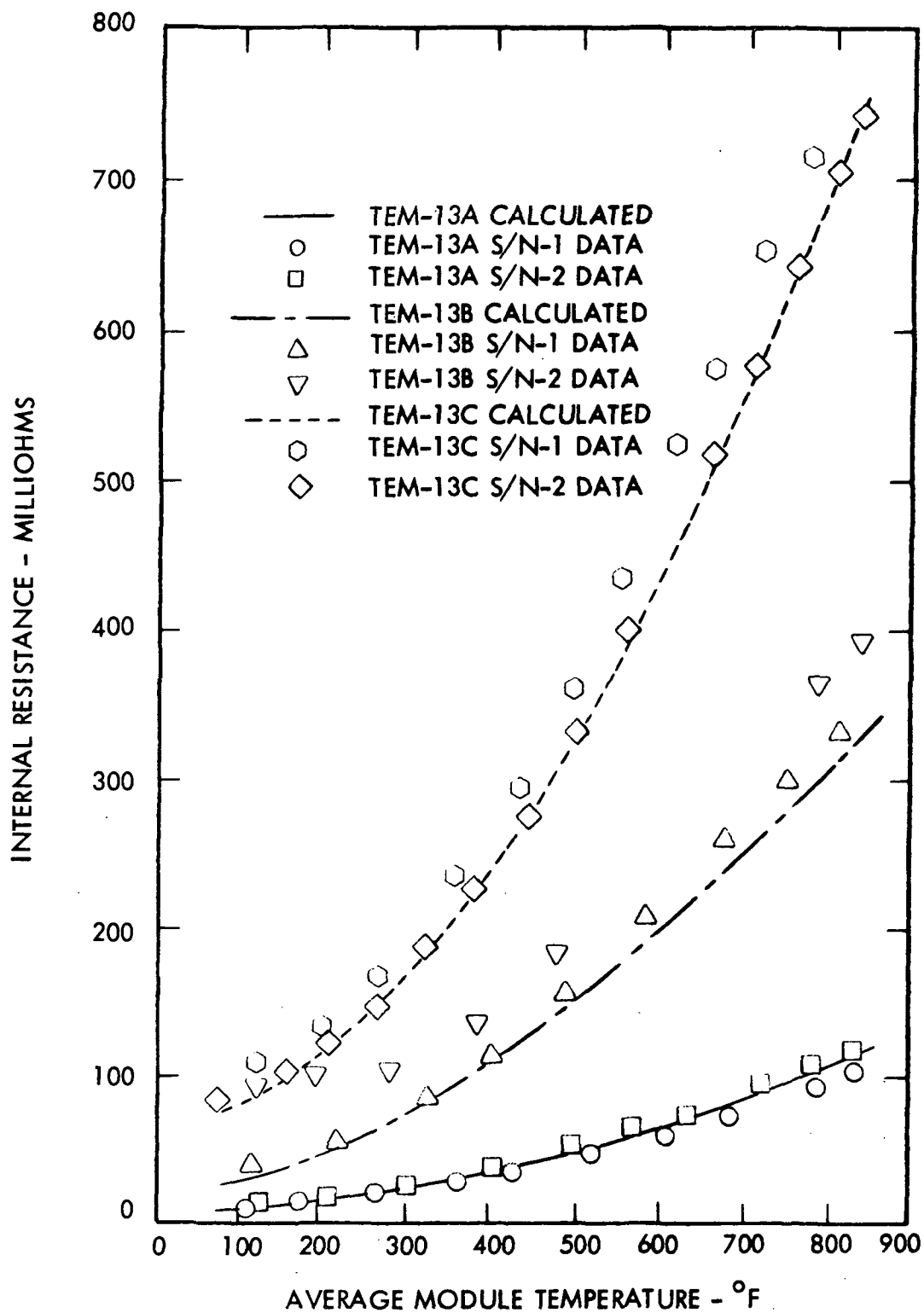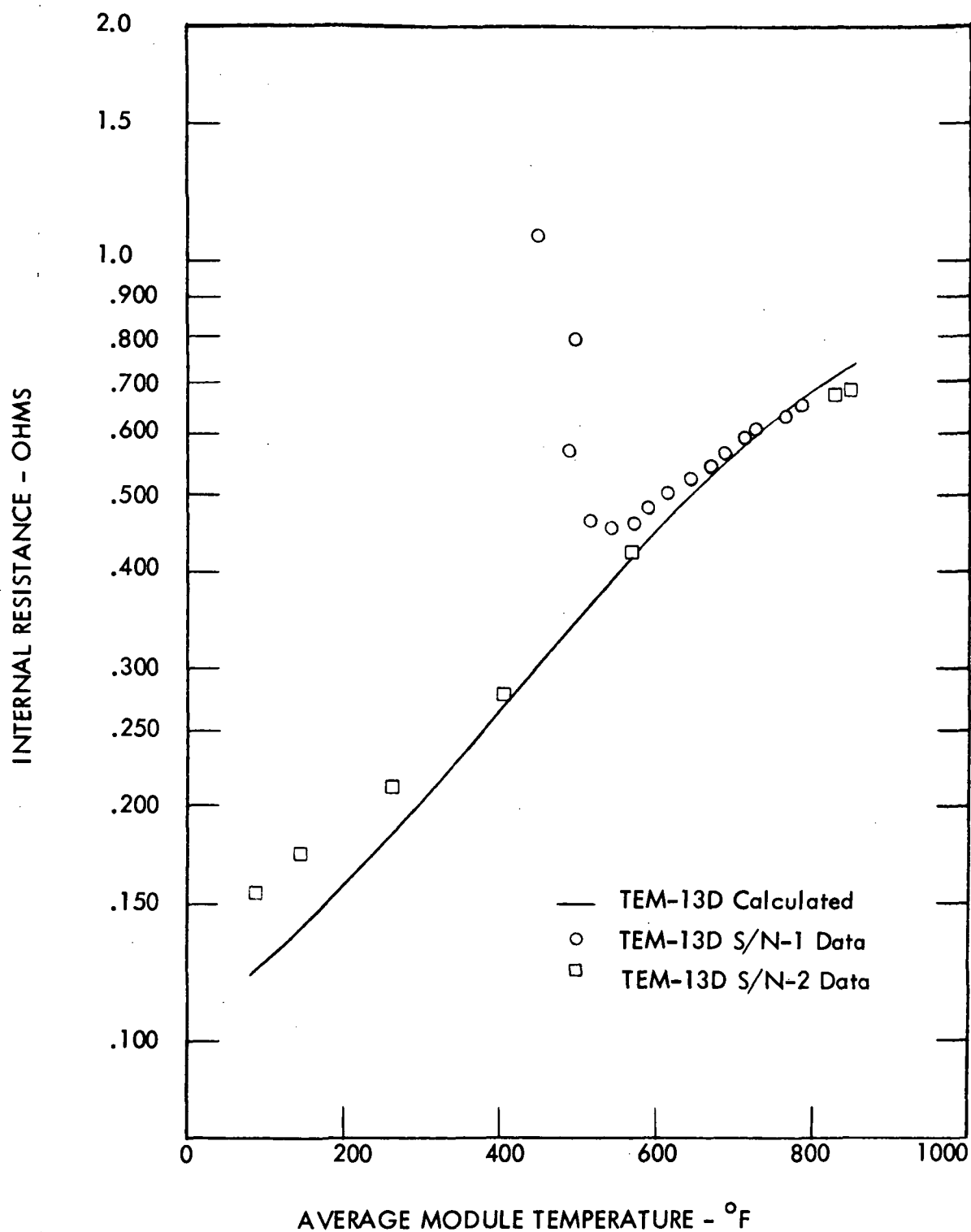
Figure I-12. A Comparison of Calculated and Experimental Internal Resistance
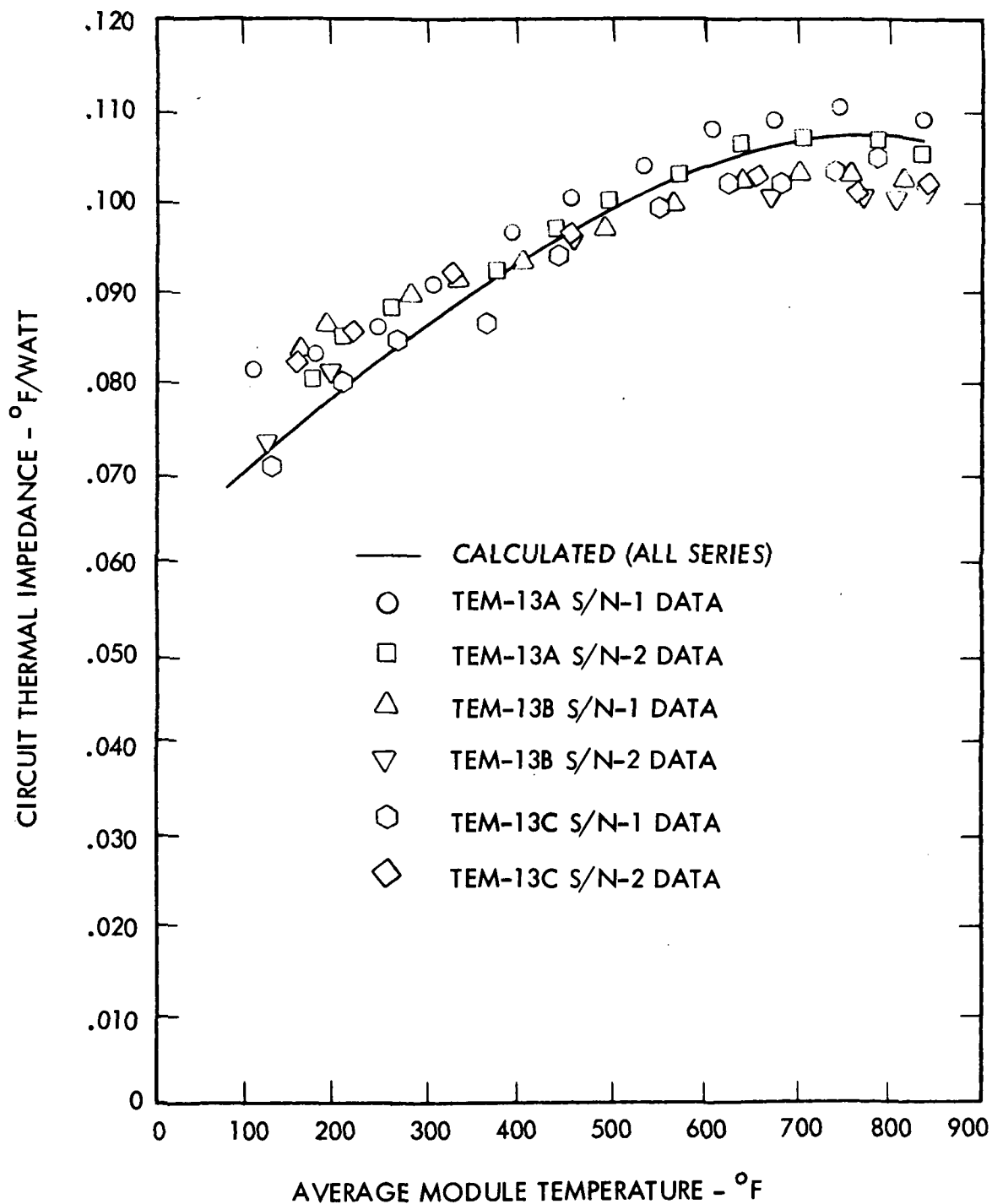Data Measured during Heatup of TEGS-3P Reactor Modules

TEM-13D S/N-2 was endurance tested for a total of 4600 hours. Power output data from this module are presented as a function of testing time in Figure l-13. During the first 2200 hours of operation, TEM-13D S/N-2 experienced only two thermal cycles. The first was caused by a laboratory power failure and the second was conducted to allow an instrumentation modification. TEM-13D S/N-2 performance stability observed during this 2200 hour period was substantially improved over that of the initial high voltage prototype reactor modules (TEM-13B and 13C modules). After this essentially steady-state operating period, the module was subjected to a series of ten thermal cycles identical to those discussed in the TEM-13A test program. Although no discontinuity was observed in the power level at the point where the cycles were performed, data presented in Figure l-13 shows quite clearly that the degradation rate increased. From this, it was later concluded that the primary reason for the improved initial performance stability of TEM-13D S/N-2, was the absence of thermal cycles during this period.

3. TEM-13E Reference Module Incorporating TEGS-3P Material

As discussed above, the substitution of TEGS-3P material for TEGS-2P lead telluride in a specific module results in a substantial reduction in power and efficiency. For this reason, efforts were directed toward establishing the design of a reference reactor module incorporating TEGS-3P lead-tin-telluride. This module design was given the designation, TEM-13E.

The effects of a direct substitution of TEGS-3P lead-tin-telluride for TEGS-2P material in a module can be seen by comparing TEM-13D and TEM-13F calculated parameters shown in Table 1-4. The reduction in power in the TEGS-3P module can be offset either by increasing the number of modules in the system or by extending the lengths of the individual modules. The second alternate was selected to minimize the effects of the material substitution on the system complexity.

Preliminary design calculations indicated that a circuit extension from the TEM-13 reference length of 15 inches to 17.2 was required to compensate for the reduction in power associated with the use of TEGS-3P material. In addition, the number
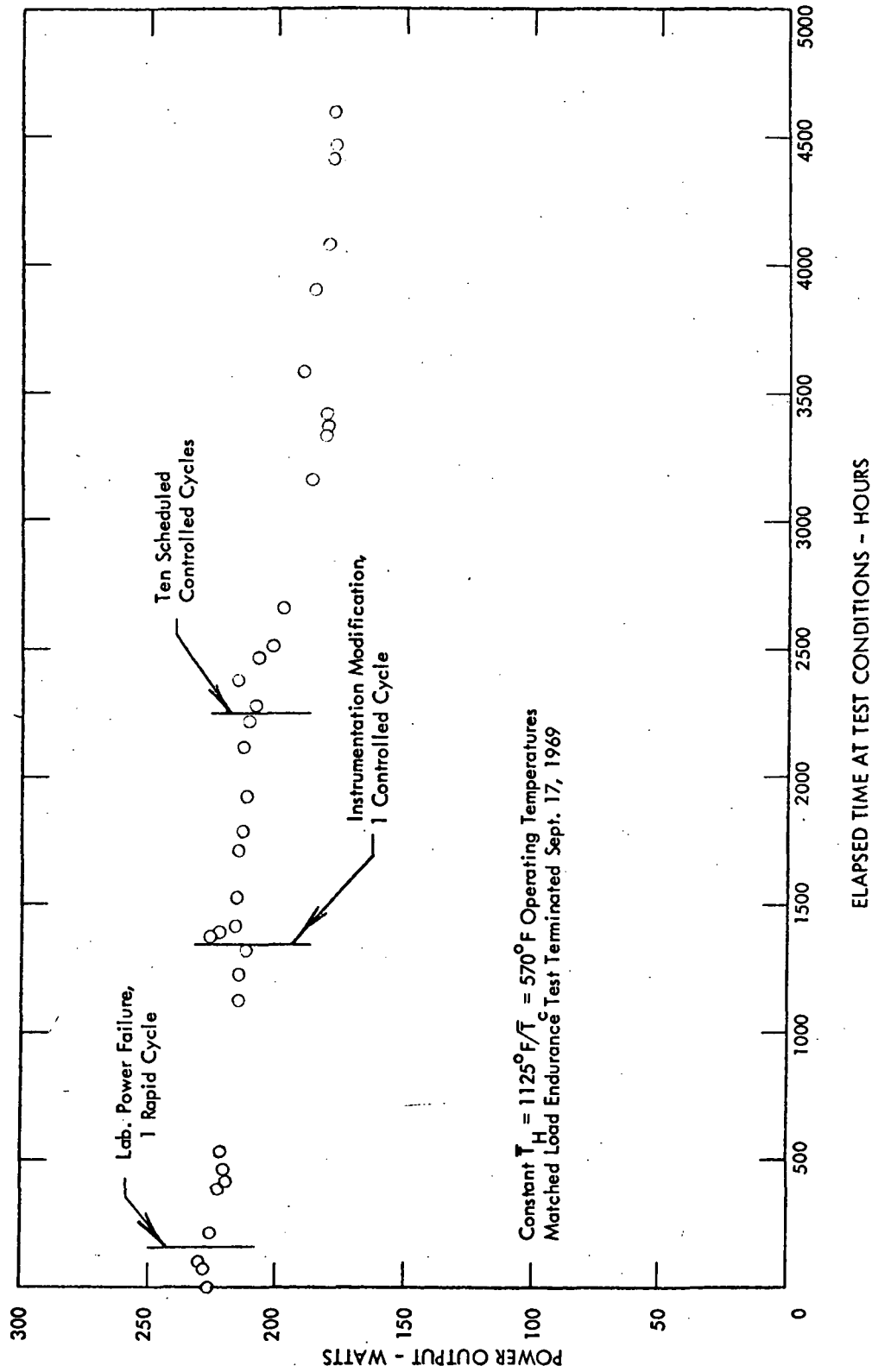
Figure I-13. TEM-13D S/N-2 Power Output Versus Elapsed Testing Time

of thermoelectric couples required to produce 14 volts at matched load $\overline{T}_H = 1125^\circ F/$
$\overline{T}_C = 570^\circ F$ operating conditions was increased to 226 from 208 to compensate for the
lower Seebeck coefficient characterisitic of the TEGS-3P material.

A detailed design of the TEM-13E module was completed. Layout, assembly
and detail drawings of the module were also completed. No modules were scheduled
for fabrication, however, pending results of tests underway on modules incorporating TEGS-2P
material with design improvements incorporated to reduce degradation rates in these modules.
It was quite obvious that a system designed using modules incorporating TEGS-2P lead
telluride could experience a substantial amount of performance degradation and still
out perform a system incorporating TEM-13E series, TEGS-3P material modules.

4. TEM-13F Prototype Modules

The TEM-13F series modules were also designed with split inner conductor
rings to eliminate the direct contact of p- and n-type thermoelectric materials near the
couple hot junctions. The design of the TEM-13F modules was identical to that of the
TEM-13D modules, discussed above, except that TEGS-2P lead telluride was used. In
addition, molybdenum outer conductor rings and tungsten inner conductor ring inserts (see
Figure I-11) were incorporated in the TEM-13F design to provide compatibility with
the p-type lead telluride. In all other respects, the TEM-13D and TEM-13F designs were
identical.

Three TEM-13F series modules were fabricated and placed on static test at
WANL in April, 1969. Heatup data from this group of three modules can be seen in Figures
I-14 and I-15 to correlate very well with the calculated curve for the TEM-13F design
over the entire temperature range. The high degree of performance reproducibility demon-
strated by these three modules is also quite evident.

Table I-5 presents a compilation of beginning-of-life test experimental data
from the three TEM-13F series modules. The experimental data from each module are first
presented as recorded at BOL. The parameters are then listed again with mathematical
adjustments made to compensate for minor deviations from the experimentally measured
clad temperatures and the design operating temperature levels, $\overline{T}_H = 1125^\circ F$ and $\overline{T}_C = 570^\circ F$.
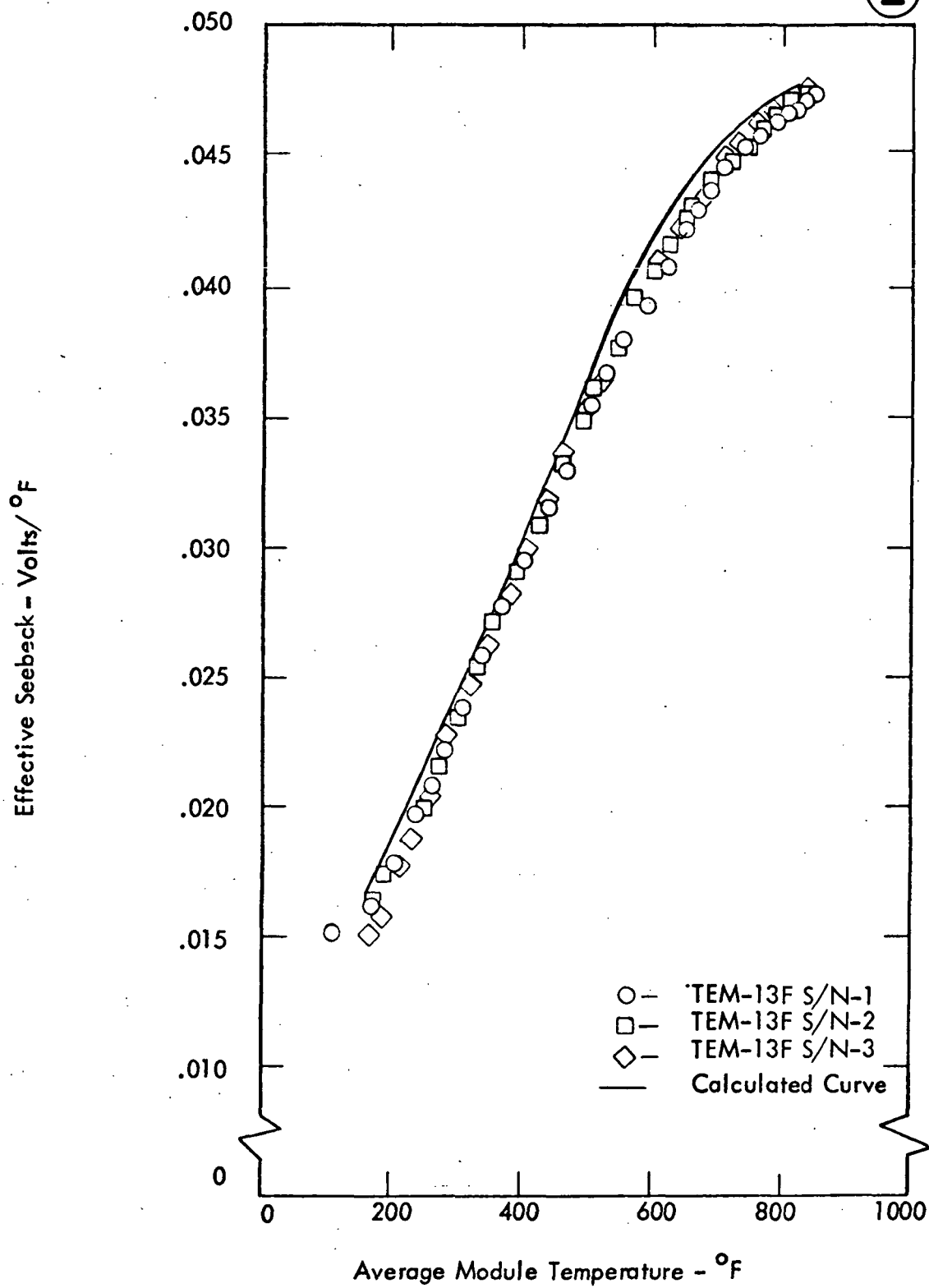
Figure I-14. A Comparison of Calculated and Experimental Effective
Seebeck Coefficient Data Measured during Heatup of TEM-13F Series Modules
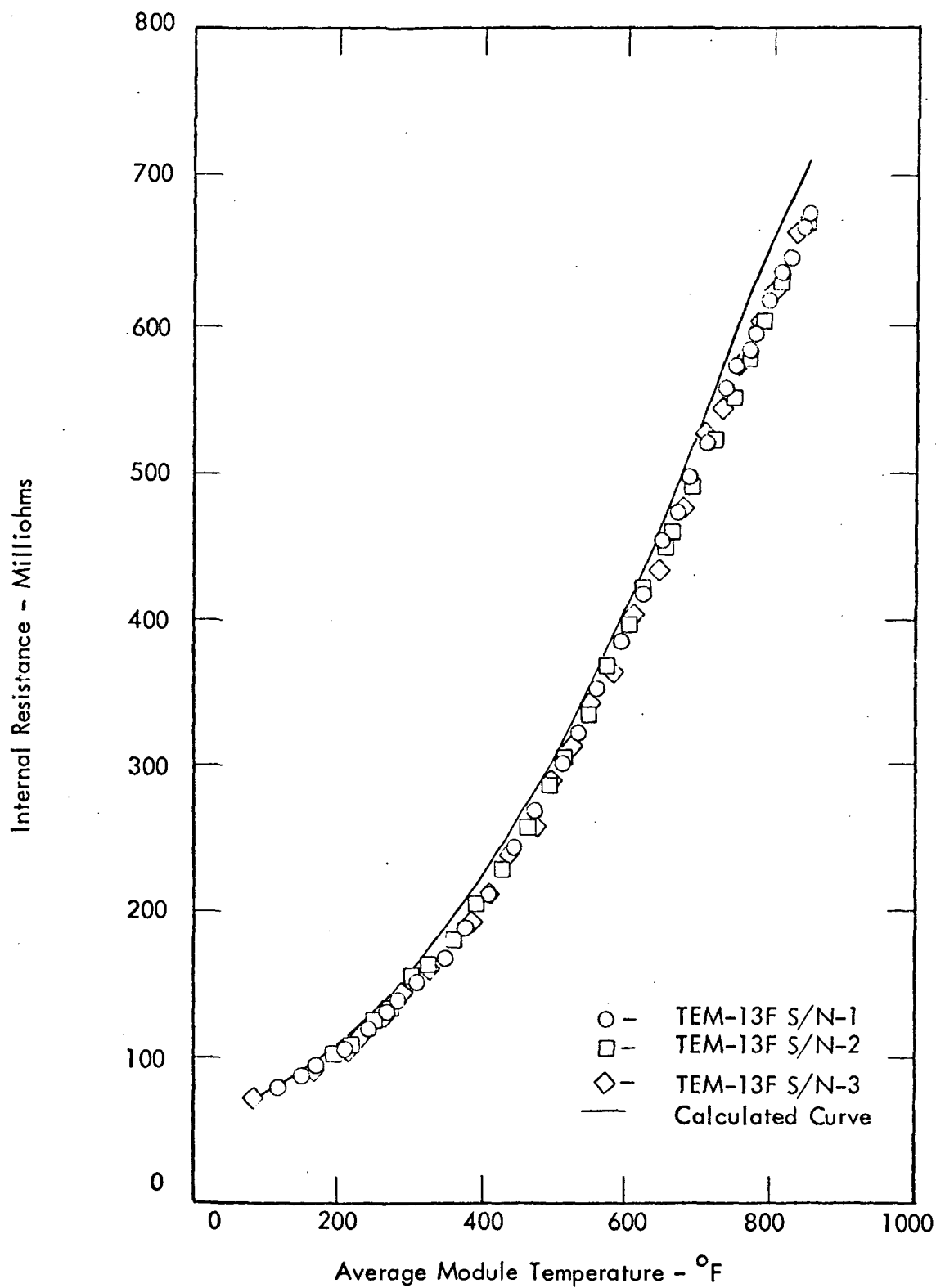
Figure I-15. A Comparison of Calculated and Experimental Internal Resistance Data Measured during Heatup of TEM-13F Series Modules

TABLE I-5

A COMPARISON OF TEM-13F BOL DATA WITH CALCULATED PARAMETERS

I. Actual Recorded Data

Module	$\overline{T}_H$ (°F)	$\overline{T}_C$ (°F)	$\overline{a}$ (Volts/°F)	V_{oc} (Volts)	R_g (ohms)	P_e (Watts)
TEM-13F S/N-1	1128	568	.04721	26.45	.6739	259.5
TEM-13F S/N-2	1125	559	.04721	26.71	.6655	267.9
TEM-13F S/N-3	1123	565	.04744	26.44	.6665	262.2

II. Data Adjusted to $\overline{T}_H = 1125°F$ and $\overline{T}_C = 570°F$

Module	$\overline{a}$ (Volts/°F)	V_{oc} (Volts)	R_g (ohms)	P_e (Watts)
TEM-13F S/N-1	----	26.22	.6732	255.3
TEM-13F S/N-2	----	26.25	.6722	256.4
TEM-13F S/N-3	----	26.32	.6692	258.9
TEMØD Calculations	----	26.28	.7093	243.5

These adjustments are made by applying the partial derivatives of the effective Seebeck coefficient and internal resistance with respect to the average hot and cold clad temperatures over the temperature range between the design and measured operating conditions.

The experimental data and temperature adjusted parameters presented in Table I-5 indicate the very high degree of operational reproducibility of these three modules which were fabricated identically. Also presented in the table are the results of the calculational model, TEMØD, for a TEM-13F module operating at the design conditions. As can be seen the experimental power output data are about 5 percent higher than the predicted level as a result of the internal resistance level of the modules being about 5 percent lower than the calculated level. The primary cause for the resistance descrepancy was found to be related to a .001 inch axial expansion of the lead telluride washers occurring during the module compaction process. This expansion, which was observed during subsequent module destructive examinations, had not been taken into account in the calculational model and produced a 3 percent reduction in module resistance. The discrepancy was not noted in previous modules fabricated with thicker thermoelectric washers, which also expand by .001 inch during compaction, since the resistance reduction associated with this washer expansion is much less as the washer thickness is increased. This effect was taken into account for all subsequent performance calculations.

Although all three TEM-13F series modules were initially tested in static test stands, TEM-13F S/N-3 was removed from static test after 500 hours and shipped to Atomics International for subsequent endurance testing in the liquid metal loop facility. Performance data recorded under loop test conditions correlated well with TEM-13F S/N-3 data recorded on static test. $\overline{T}_H = 1125^\circ F/\overline{T}_C = 570^\circ F$ matched load test conditions were maintained for all TEM-13F series modules.

Power output data recorded from this group of second generation, high voltage, prototype reactor power modules is presented in Figure I-16. A comparison of these data with similar data from the initial high voltage prototype reactor module, TEM-13C S/N-2, shown in Figure I-9, shows that the performance stability was drastically improved through the incorporation of the split inner conductor ring in the second generation modules.
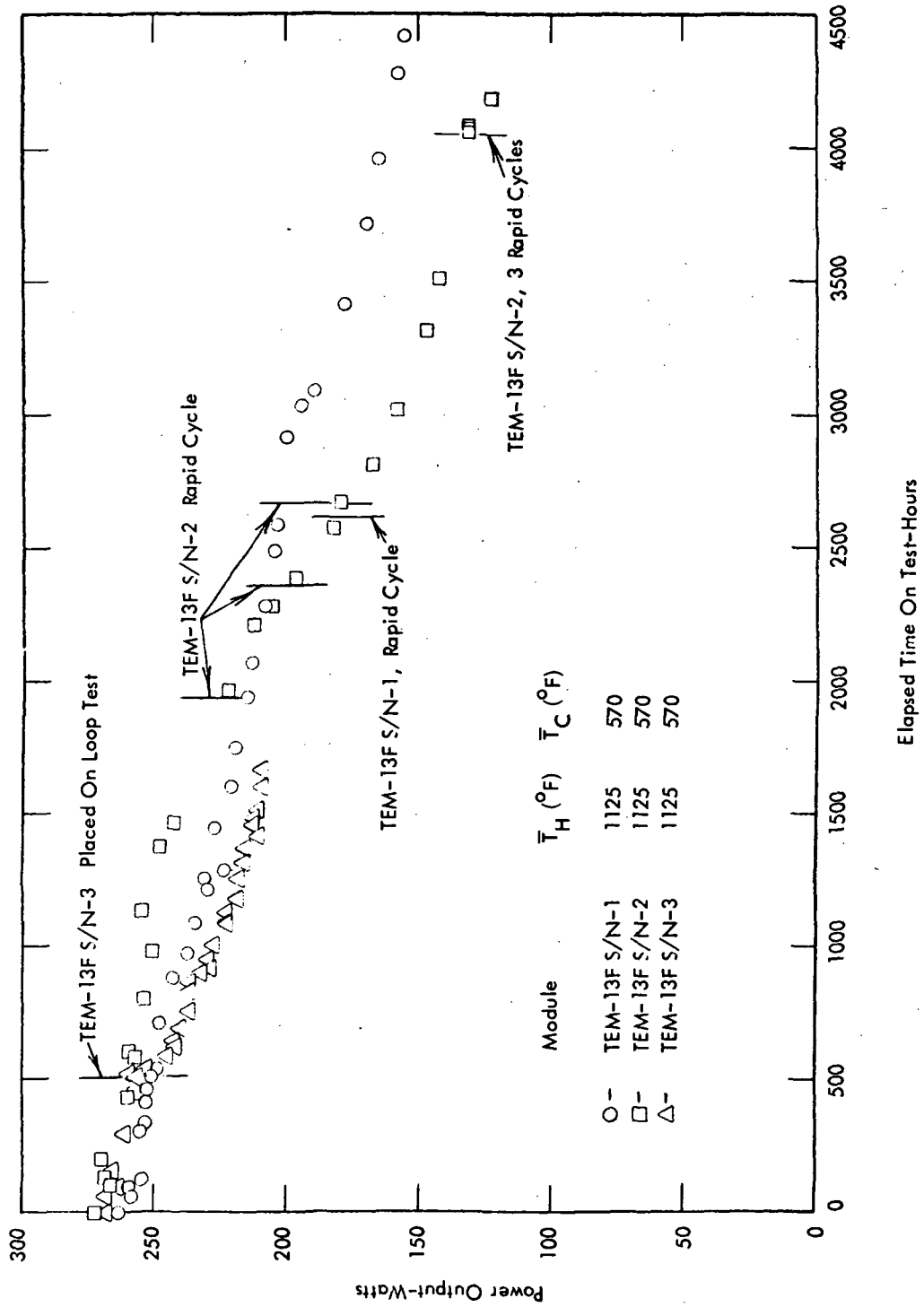
Figure I-16. A Comparison of Electrical Power Output Data from TEM-13F Series Modules

However, like the earlier modules, degradation rates of the TEM-13F modules were seen to be adversely effected by cyclic operation.

Ultimately the three TEM-13F series modules were removed from test for destructive examination. TEM-13F S/N-2, the first module of this series to be examined, was sectioned traversely into three sections. A six inch section from each end of the module was mounted in epoxy and cut axially to expose the circuit configuration. Inspection of the circuit revealed that the washers in the positive end section were so badly misoriented along the inner conductor ring axis that in some cases the p-type washer was in contact with the iron conductor ring at the next couple and the n-type washer was contacting the p-type washer conductor insert ring. The negative end of the module showed that although the washers were chevroned, they still retained contact with their respective inner conductor rings. However, the mica washers which separated the inner rings were fractured.

The inner conductor rings were examined microscopically to determine if any lead telluride had extruded into voids between the rings. No traces of lead telluride extrusion between the rings were observed. In fact, the distance between the rings was extremely uniform as compared to TEM-13 modules that contained inner conductor rings made from material that possessed a lower coefficient of thermal expansion.

Another phenomenon of module distortion was noted during the microscopic examination of the inner conductor rings. The iron rings at both ends of the module appeared to be shorter axially than the remaining rings. Accordingly, the axial dimension of the inner conductor rings was measured to determine the extent of the axial distortion along the inner conductor ring axis. A plot of the change in the nominal axial dimension of the iron inner conductor ring versus position along the module axis shows that the rings near the end of the module had been subjected to enough axial pressure to produce plastic deformation and axial shortening of the ring.

5. Summary of Second Generation TEM-13 Series Module Results

Experimental data from the second generation prototype reactor modules demonstrated that substantial improvements in performance stability could be achieved through the incorporation of the split inner conductor design. Excellent performance

reproducibility was also observed during heatup of these modules. Data from the TEM-13D series modules indicated, as had been anticipated, that a substantial performance penalty resulted from the substitution of TEGS-3P lead-tin-telluride for the standard TEGS-2P material. Performance of modules operated in a two-loop liquid metal loop system was demonstrated to closely duplicate data recorded under static test conditions. Finally, however, this group of modules was found to be sensitive to cyclic operation, indicating the urgent need to identify a means to eliminate this problem.

G. PROTOTYPE 5.25 VOLT REACTOR MODULES

1. Re-establishment of the Reference Module Voltage

In the initial systems analysis performed for the 25 KWe system, an improvement in system reliability was identified as being associated with minimizing the number of individual modules wired in electrical series. This resulted in a reference module design in which the voltage had been set at the maximum fabrication limit of 14 volts. The system voltage requirement of 56 volts was to be achieved by wiring four reactor modules in series.

During FY-1969, the first full year of the Compact Thermoelectric Converter System Technology Program, three factors were identified which indicated the need to re-establish the reference voltage level of the reference module for the 25 KWe system.

The first factor was the reduction in required system voltage to 42 volts from 56 volts. It was this modification that caused initiation of an effort to establish an optimum reference module voltage.

The relationship between system reliability and the number of individual modules wired in electrical series did not change since the initial parametric study. That is, system reliability varies inversely with the number of modules wired in electrical series. This relationship holds because the development of an open circuit in a given module in the system affects that module and all other modules connected in electrical series with it. Maximum reliability then, all other considerations neglected, would result from the design of a 42 volt module design allowing all 96 power modules to be wired in electrical parallel.

However since no tubular module, in the history of this or any previous program, has ever developed an open circuit during operation, the probability of this occurrence was recognized as being minimal. That is, the reliability penalty associated with wiring modules in electrical series was very small.

Two module performance considerations were identified during the initial phase of the program which showed substantial benefits available by reducing the individual module voltage requirement. First, by reducing the required voltage, the number of thermoelectric couples in each module could be decreased. This reduction provides an efficiency increase by

reducing the number of intercouple mica insulators required, hence reducing the mica shunt heat losses. Parametric calculations showed that maximum efficiency in a 15 inch circuit length module is achieved when the module is designed to deliver about five volts.

Another important factor indicating the desirability of decreasing the voltage was the observed relationship between degradation rates and module design voltages. An examination of performance data from the initial prototype reactor modules (see Figure I-7) shows that degradation rates increased rapidly as the voltage was increased. The identification of the primary degradation mechanism present in these modules explains this relationship clearly. Since the high voltage modules had much thinner thermoelectric washers (axially) than the TEM-13A series modules, the percentage of the n-type washers affected by the diffusion of tellurium from the p-type washers was greater at all times. Thus the effects of intercouple tellurium diffusion can be reduced by increasing the axial length of the n-type washers.

Taking these factors into consideration, a 5.25 volt reactor prototype module design was established. It was anticipated, then, that the 25 KWe system would be comprised of 12 groups of reactor power modules wired in electrical parallel. Each group would consist of eight modules wired in electrical series to achieve the 42 volt system voltage requirement.

2. TEM-13G Module Design

The next generation of prototype modules was designed to deliver 5.25 volts when operated into a matched load at $\overline{T}_H = 1125°F/\overline{T}_C = 570°F$ operating temperatures and were designated as TEM-13G series modules. It is important to note that the TEM-13G design was completed and committed to hardware in early 1969, less than one year after the design of the initial prototype reactor modules, and within several months of initiation of TEM-13A series modules tests. At this time, the cyclic sensitivity problem had not yet been identified, hence there were no design improvements related to this problem incorporated into the TEM-13G design.

The TEM-13G design consisted of 79 thermoelectric couples. Figure I-17 is a cross-section drawing of a TEM-13G couple. Nominal component dimensions are listed. The couples, as can be seen, incorporate the split inner conductor ring to reduce intercouple
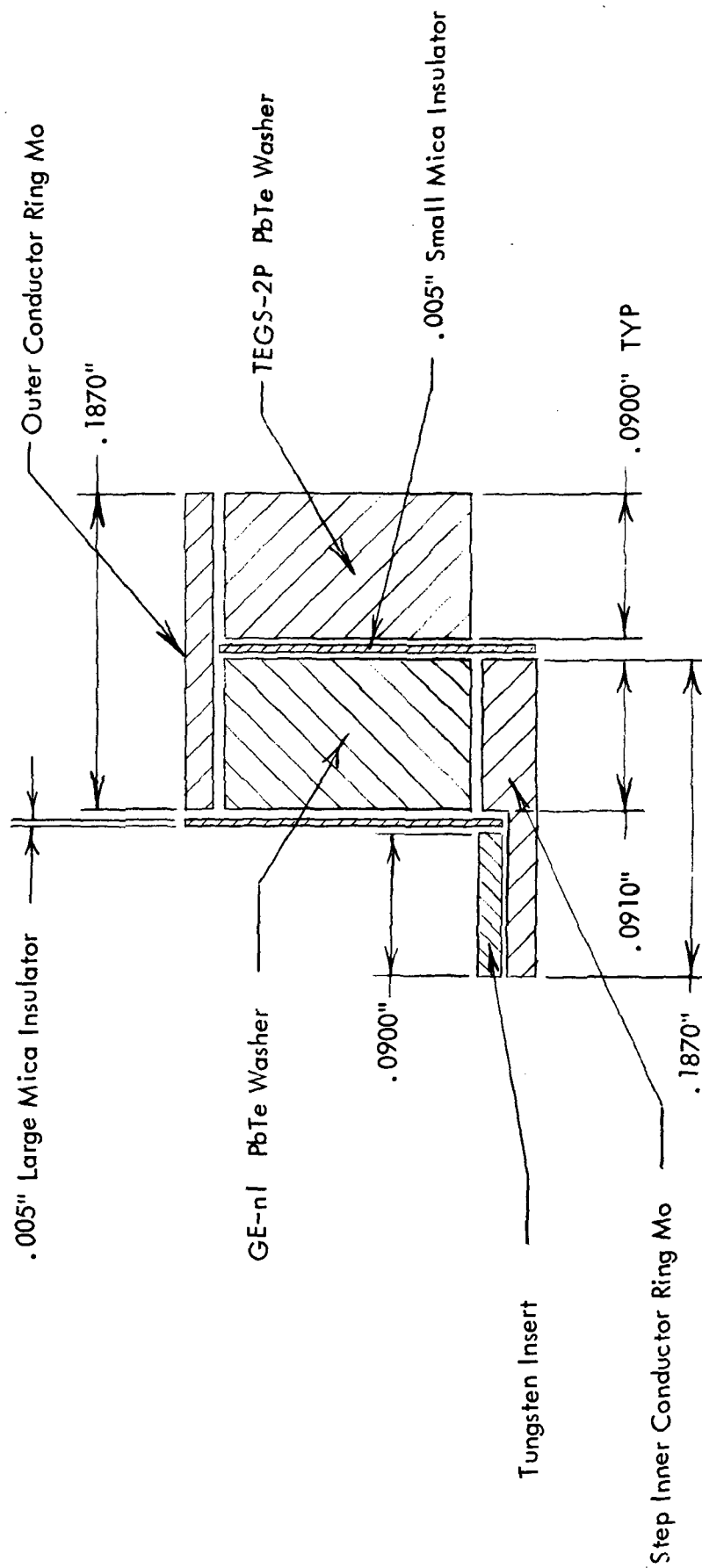
Figure 1-17. TEM-13G Thermoelectric Couple Detail

Outer Conductor Ring Mo

.1870"

TEGS-2P PbTe Washer

.005" Small Mica Insulator

.0900" TYP

.005" Large Mica Insulator

GE-nl PbTe Washer

.0910"

.0900"

.1870"

Tungsten Insert

Step Inner Conductor Ring Mo

tellurium transport. In this design, the stepped inner conductor ring was fabricated with molybdenum rather than iron as in the TEM-13F design. This modification precluded any interactions between iron and TEGS-2P material.

Another change in design was made on the TEM-13G modules to modify the loading of the inner conductor rings during the compaction of the module. Studies indicated that during module processing, the outer conductor rings were loaded (compressed) by a force exerted on them by the internal collector rings. The inner conductor rings, however, relied on loading through Alsimag insulating washers located radially inboard of the collector rings and adjacent to the first and last inner conductor rings in the module. Enlarged photographs of sectioned modules showed that the Alsimag was compressed and sheared, indicating that very little axial load was actually applied to the inner conductor rings. To increase the inner conductor ring loading, a small molybdenum "loading washer" was located axially outboard of the inner conductor rings at each end of the module, as shown in Figure 1-18. These loading rings ensured that the axial compression load was transmitted to the inner conductor rings by distributing this load over a greater Alsimag area to minimize the possibility of shearing.

A relatively minor change which was incorporated into the TEM-13G module design involved increased radial clearance of end closure insulating components. Measurements taken after processing of previous reactor power modules showed a slightly greater diameter at the ends of the module than in the circuit region. This difference resulted from the fact that the Alsimag did not radially compact as much as expected during processing. Since it is desirable to have the most uniform module outer diameter possible, radial assembly clearances in the end closure region of the module were increased. Diametral measurements made on TEM-13G series modules after compaction indicated that as a result of these radial clearance modifications, variations in O.D. along the entire outer clads of the modules were less than .01 inch.

A minor change was made in the Alsimag sleeve (see Figure 1-18) located under the stretch neck of the module. Axial dimensions of the Alsimag sleeve were modified at assembly to ensure contact with the inner boron nitride insulating sleeve. In addition, the sleeve was tapered as shown in Figure 1-18 to allow the retainer ring to move radially inward during compaction.

Outer Clad

Boron Nitride Sleeve

Conductor Ring

Collector Ring

Retainer Ring

Boron Nitride Pin Insulator

Electrical Pin

Stretch Neck

Alsimag Tapered Sleeve

Alsimag Spacer

Alsimag Washer

Molybdenum Loading Washer

Step Conductor Ring

Boron Nitride Sleeve

Inner Clad
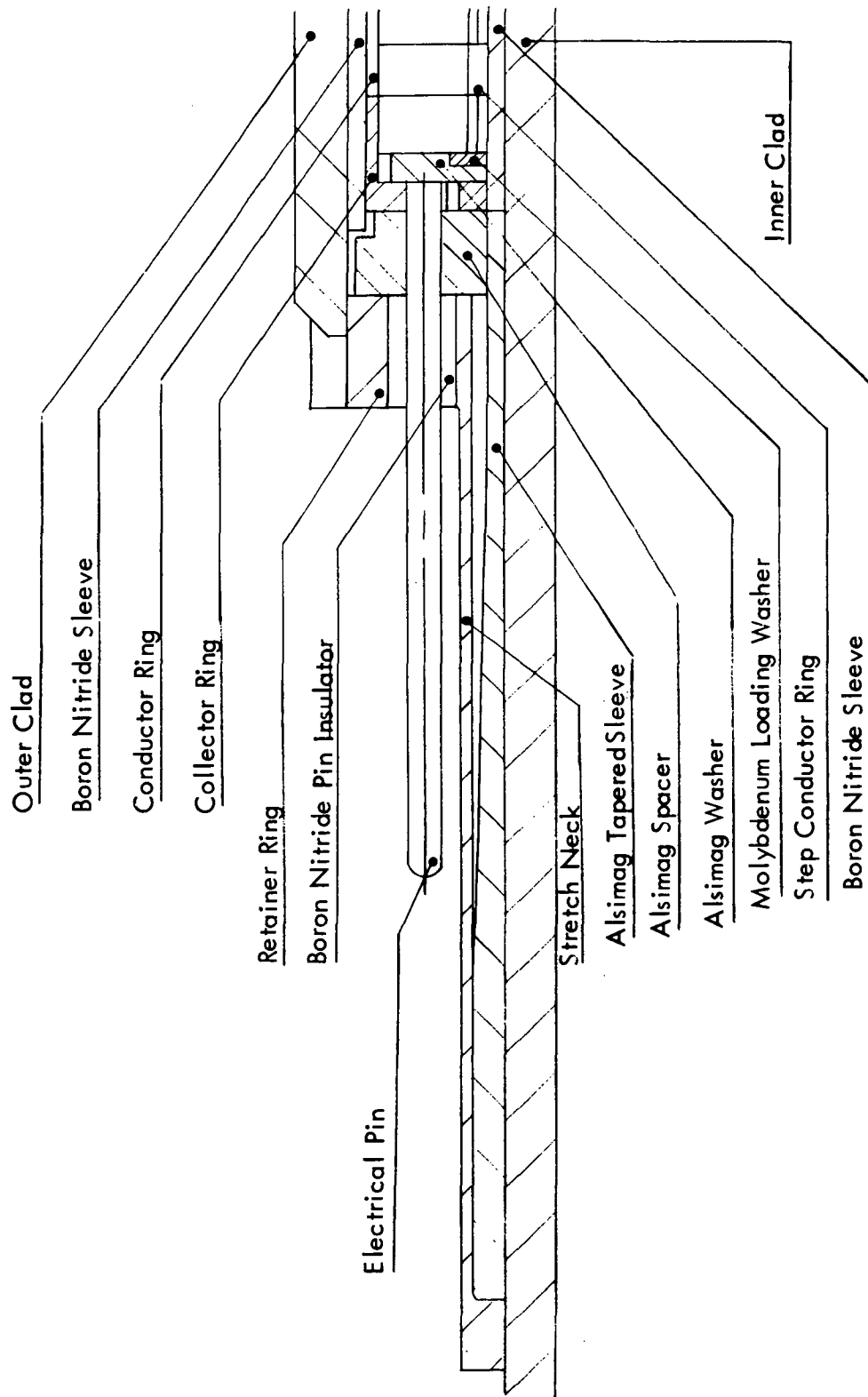
Figure I-18. TEM-13G End Closure Design

The nominal overall circuit length of the TEM-13G module, 15.163 inches, was .034 inch shorter than that of the TEM-13F design. The differences arose from the use of components having nominal dimensions expressed in even .001 inch units. The additional circuit length was accomodated by increasing the Alsimag insulator axial length by .034 inch in the TEM-13G design. This allowed the use of inner and outer clads in the TEM-13G modules having the same overall dimensions of those used in TEM-13F modules.

3. TEM-13G Static Test Assembly Modifications

Prior to testing any of the TEM-13G series modules, an initial modification was made to the static test design. Although this modification had nothing to do with the module design, it did have an affect on performance data, as will be discussed.

All previous modules on test in static test stands, were heated using electrical heaters as shown in Figure I-3. These heaters had main windings which were located directly under the thermoelectric circuits of the modules. In addition, guard heater windings were located on either side of the main heater and used to control end closure heat losses and temperature profiles. However, the required spacing between the main and guard heater windings, 0.5 inch, resulted in the guard heaters being located primarily under the stretch neck region of the module (see Figure I-18). Since very little heat loss occurs in this region of a module, the guard heaters were found to be very ineffective.

Electrical heaters used in the TEM-13G module tests did not have separately controllable guard heaters. Instead, the heater consisted of five series connected elements separated by "dead spaces" of approximately 0.2 inch. The overall heated length of the heater was extended 0.38 inch beyond the thermoelectric circuit at either end of the module to compensate for end closure heat losses. This heater design provided heat generation in the region immediately adjacent to the thermoelectric circuit, the primary heat loss area of the end closures.

The original TEM-13G series modules were instrumented for static test using the same axial thermocouple locations as in all previous reactor module tests. Experimental data from these modules showed that the inner clad temperature profiles were much more sensitive to the individual electrical windings than had been anticipated. Subsequently, it was found

necessary to modify the number and axial positions of the thermocouples. By increasing the number of axial positions to 21, it was possible to use a uniform spacing between thermocouples and provide at least four thermocouples per heater winding element.

Figure I-19 shows the placement of individual thermocouples relative to the electrical heater segments in the ten thermocouple harness and 21 thermocouple harness configurations. It is clear that except for the third and eighth thermocouples in the ten couple harness, all instrumentation was positioned on or very near to the "dead space" between heater elements. This placement resulted in a systematic low indicated average hot clad temperature determination. To eliminate this condition, the 21 couple harness was designed such that the individual thermocouples were evenly distributed along the active and dead spaces of the heater segments (see Figure I-19).

Figure I-20 shows the axial hot and cold clad temperature profiles recorded during static testing of a typical reactor power module instrumented with the 21 thermocouple harness. The sensitivity of the inner (hot) clad temperature profile to the individual heater segments is quite clear. From these data, it was possible to determine that average clad temperatures based on the original ten couple harness thermocouple locations, were approximately $25^{\circ}F$ below the actual average hot clad temperature. As a result of axial heat transfer in the module, the outer clad temperature profile was much more uniform than on the inner clad surface, so that the initial ten cold clad thermocouple locations did provide an accurate determination of $\bar{T}_C$.

A second instrumentation modification resulted from a series of experiments performed to determine the magnitude and uniformity of the radial temperature drop across the Thermon layer used to bond the cooling fins to the outer clad of the module. Data from these experiments indicated that the temperature drop from the outer surface of the module to the base of the cooling fins could vary from $10^{\circ}F$ to $100^{\circ}F$, depending primarily on the thickness and local condition of the Thermon layer. This condition resulted in circumferential temperature variations on the module outer clad which could lead to erroneous cold clad average temperature determinations. To eliminate this condition, a new cooling fin assembly design was implemented during TEM-13G series module tests.
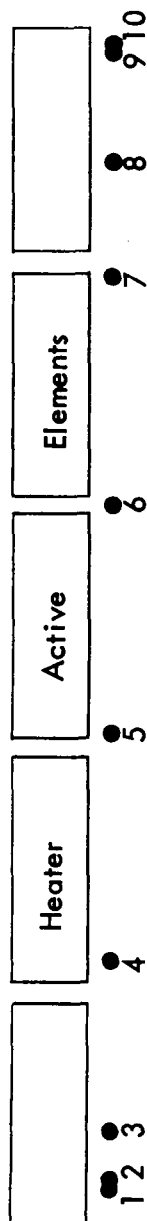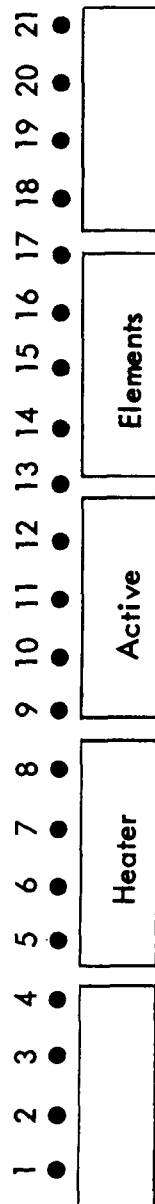
Figure I-19. Thermocouple Placements Relative to Heater Sections for TEM-13G Test Assemblies
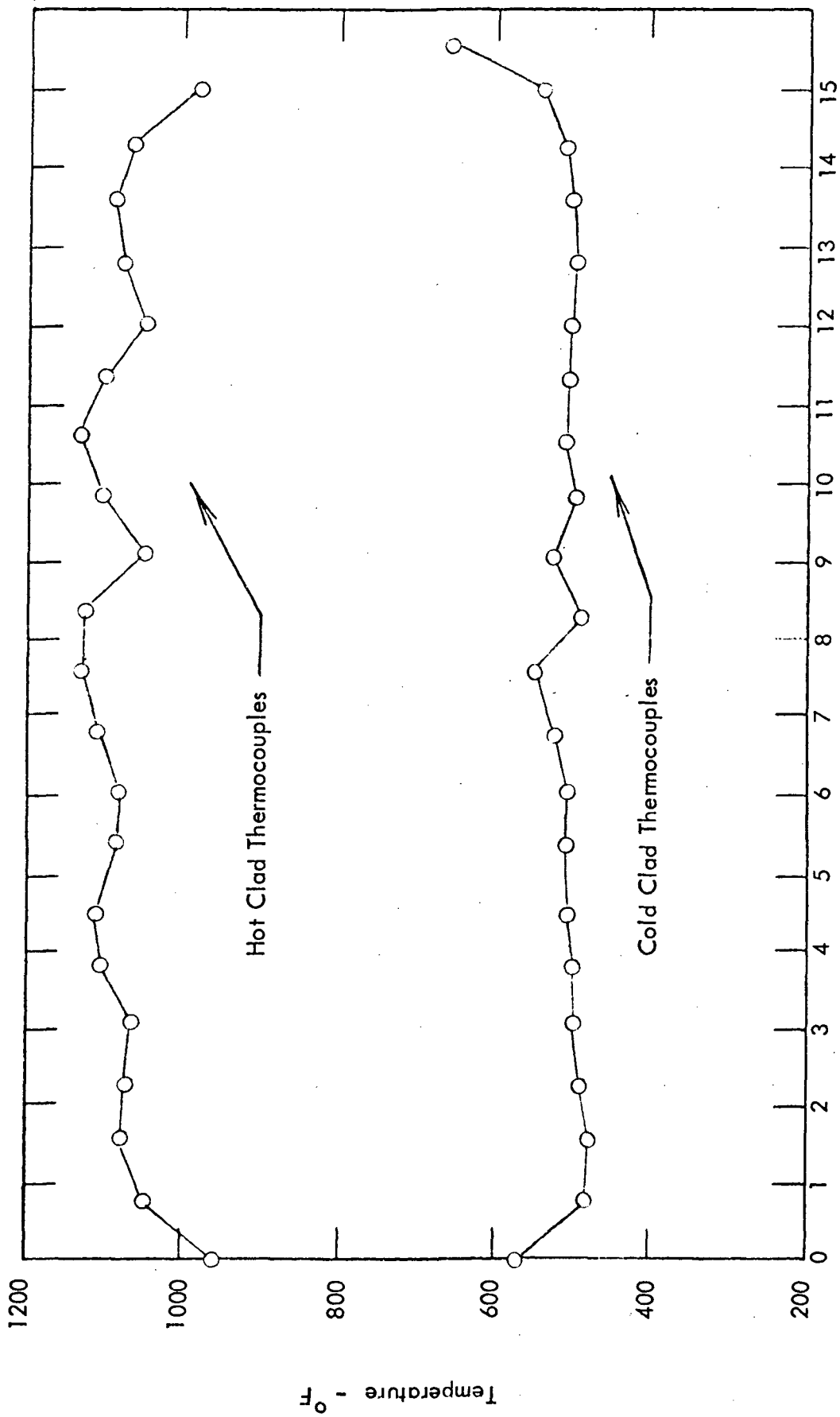
Figure I-20. Axial Temperature Profiles Recorded during Static Testing of a Typical Reactor Power Module

The revised cooling fin assembly was fabricated in four quadrants rather than two halves. Axial grooves were machined in each of the fin quadrants to provide access room for thermocouples which were located in corresponding positions along the outer clad of the module. The I.D. of the fin surfaces was machined .040 inch greater than the O.D. of the module. Metal separator rods having a diameter of .020 inch were placed to run axially on the outer clad of module after Thermon application. The individual fin quadrants were then drawn tightly around the module using stainless steel straps, and bolted into position, thus ensuring uniform thickness of the Thermon layer.

These modifications resulted in a substantial improvement in subsequent module-to -module performance reproducibility as a result of eliminating random and systematic instrumentation error variations.

4. Heatup and Initial Testing of TEM-13G Series Modules

Nine TEM-13G series modules were fabricated during the first half of 1969. Three additional modules, S/N-10, 11, and 12 were fabricated approximately one year later, after the identification of the thermal cyclic sensitivity problem identified during testing of previously fabricated reactor power modules. The purpose for testing each of the TEM-13G series modules is listed in Table I-6, along with a summary of pertinent results.

As is shown in the table, module tests were planned at three different average hot clad temperature levels. These tests were intended to provide experimental degradation rate data at the design operating conditions of $\overline{T}_H = 1125^\circ F$ and at $100^\circ F$ above and below the design levels. Cold clad temperatures were selected for each of the tests to simulate operation of a reactor power module in a space application with a fixed radiator.

Although some of the modules were scheduled for testing in the liquid metal loop at Atomics International, all of these modules were operated in static test stands at WANL before shipment.

The first five TEM-13G series modules were placed on static test at WANL in June, 1969. Evaluation of heatup data from these modules indicated that the degree of performance reproducibility and the correlation between calculated and experimental was not as

TABLE I-6

TEM-13G SERIES MODULES

Module	Purpose	Test Time (Hours) Static	Test Time (Hours) Loop	Summary of Results
S/N-1	Measure degradation rates at design (1125°F/570°F) operating temperatures.	2810	2407	Initial degradation rates extremely low, subsequent data affected by thermal cyclic operation. Need for instrumentation modifications identified.
S/N-2	Compare Loop test performance data with static test data.	415	20208	Same as S/N-1
S/N-3	Measure cyclic sensitivity of TEM-13G Module	1502	0	Same as S/N-1
S/N-4	Measure degradation rates at reduced (1025°F/538°F) operating temperatures	8302	0	Same as S/N-1
S/N-5	Measure degradation rates at increased (1225°F/601°F) operating temperatures	2592	2408	First module to incorporate 21 thermocouple instrumentation. Data correlated very well with calculations.
S/N-6	Installation in Power Converter Module S/N-1	1419	6972	Basic converter module design qualified. Cold side manifold modifications identified.
S/N-7	Same as S/N-6	1388	6972	Same as S/N-6
S/N-8	Same as S/N-6	1394	6972	Same as S/N-6

TABLE I-6

TEM-13G SERIES MODULES

Module	Purpose	Test Time (Hours)		Summary of Results
		Static	Loop	
S/N-9	Same as S/N-6	1588	6972	Same as S/N-6
S/N-10	Cycle 50 times and destructively exam	261	0	Effects of intercouple shorting observed after 28 controlled cycles.
S/N-11	Destructively examine non-cycled module	380	0	Established relationship between amount of circuit distortion and number of thermal cycles.
S/N-12	Initially defined to study cyclic distortion problem. Re-identified to allow correlation of calculations and experimental data over wide temperature range.	0	167	Correlation found to be excellent, maximum 8.1 percent efficiency recorded.

good as had been observed in previous modules. Close examination of the experimental data revealed that the cause of the performance descrepancies was related to test instrumentation deficiencies. In particular, the need to relocate and increase the number of thermocouples was identified, as discussed in the previous section of this report.

The second group of TEM-13G series modules, S/N-6 through S/N-9, were fabricated for incorporation into the first multi-module converter assembly. Prior to installation into this assembly, designated Power Converter Module S/N-1 and commonly referred to as the "Four Pack", each of the individual modules were qualified by a brief static test. All instrumentation improvements discussed in the previous section of this report were incorporated in these static tests.

Figures 1-21, 22, and 23 present comparisons of effective Seebeck coefficient, internal resistance, and thermal impedance data recorded during heatup of these four modules with the corresponding calculated parameters. In each case, excellent module-to-module reproducibility was observed and excellent correlation was achieved between the calculated results and experimental data. These data verified that descrepancies observed in the initial five TEM-13G series modules were caused by instrumentation deficiencies as had been indicated.

Subsequently, one of the initial group of five modules, S/N-5, was removed from test and re-instrumented in a manner identical to that of the second group of modules. A comparison of the beginning-of-life $\overline{T}_H = 1025°F/\overline{T}_C = 538°F$ performance data from the second group of modules along with similar data from TEM-13G S/N-5 after re-instrumentation, is presented in Table 1-7. All of the data can be seen to correlate very well with the calculated parameters for $\overline{T}_H = 1025°F/\overline{T}_C = 538°F$ operation, which are also presented.

After being placed on static test, TEM-13G S/N-6 through S/N-9 were each operated for approximately 500 hours under steady state conditions at $\overline{T}_H = 1025°F/\overline{T}_C = 538°F$ operating temperatures. During this period, all of the modules exhibited extremely stable performance with power output data falling within the band 219 + 6 watts. These modules, thus being qualified, were removed from static test for installation into the Power Converter Module S/N-1. The design and performance of this four pack module assembly is discussed in a later section of this report.
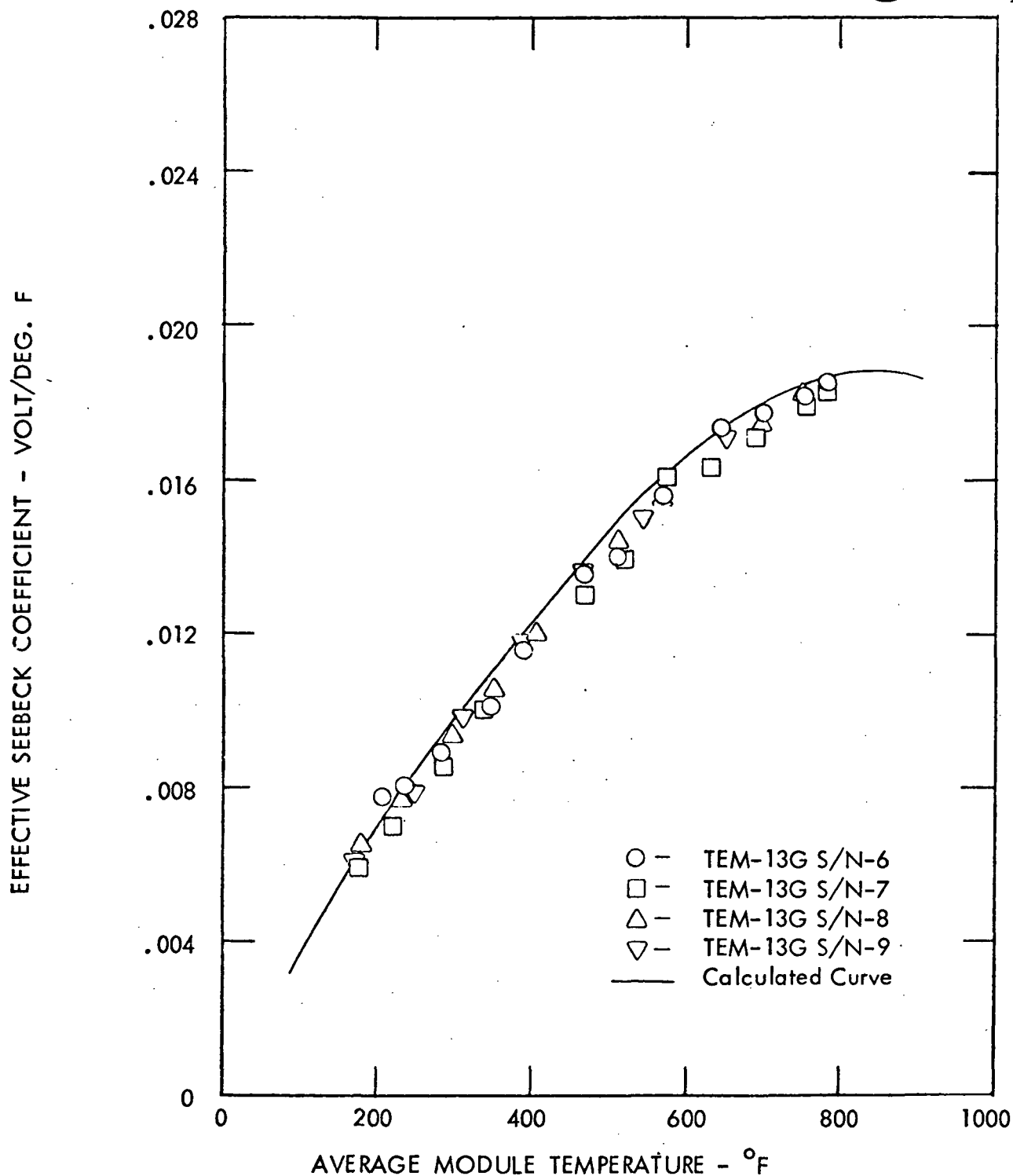
Figure 1-21. A Comparison of Calculated and Experimental Effective Seebeck
Coefficient Data Measured during Heatup of TEM-13G S/N-6 through S/N-9
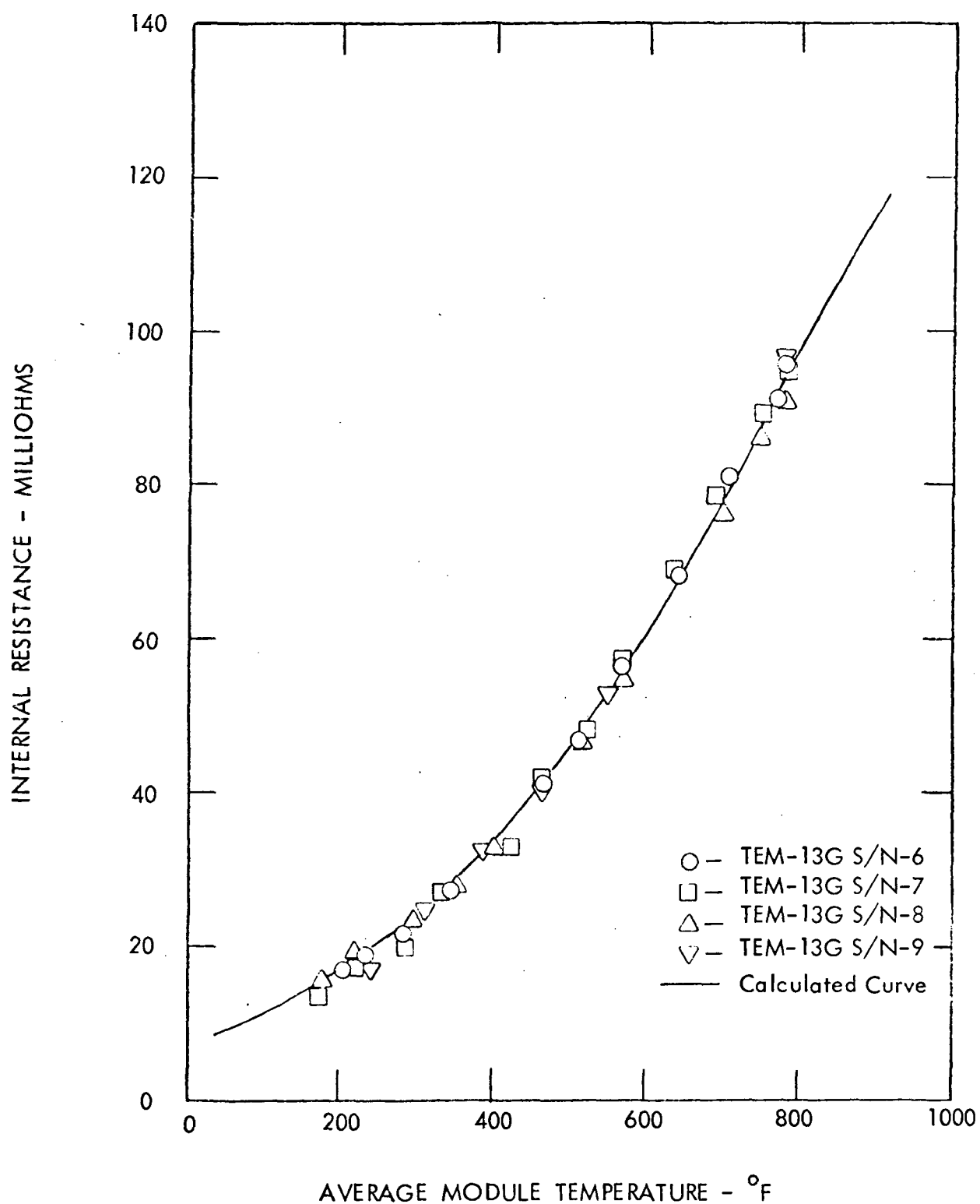
Figure 1-22. A Comparison of Calculated and Experimental Internal Resistance Data
Measured during Heatup of TEM-13G S/N-6 through S/N-9
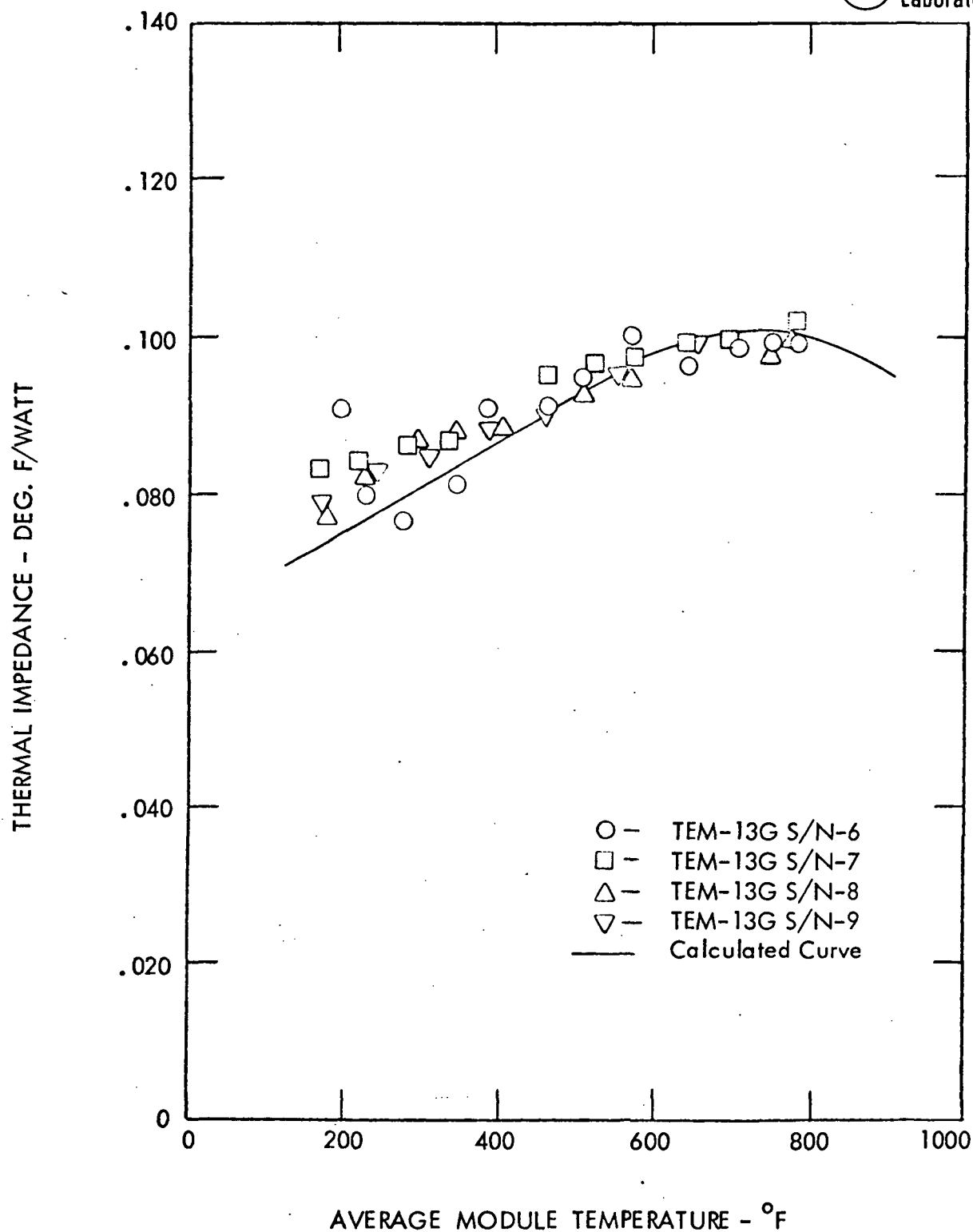
Figure 1-23. A Comparison of Calculated and Experimental Thermal Impedance Data
Measured during Heatup of TEM-13G S/N-6 through S/N-9

TABLE I-7

TEM-13G $\bar{T}_H = 1025°F/\bar{T}_C = 538°F$ BOL DATA

Measured Parameters	Calculated	S/N-5	S/N-6	S/N-7	S/N-8	S/N-9
$\bar{T}_H$ (°F)	1025	1026	1027	1027	1025	1027
$\bar{T}_C$ (°F)	538	538	536	536	539	537
Total Power Input (Watts)	4865	4898	4967	4889	4896	4891
Open Circuit Voltage (Volts)	9.14	9.26	9.21	9.08	9.06	9.09
Circuit Resistance (Milliohms)	93.8	95.9	94.6	94.6	92.1	96.2
Power Output (Watts)	223	224	224	218	223	215
Overall Efficiency (Pct)	4.58	4.57	4.51	4.48	4.57	4.41
Load Voltage (Volts)	4.57	4.62	4.64	4.55	4.51	4.57
Load Current (Amps)	48.7	48.4	48.3	47.9	49.4	47.0

Note: Average clad temperatures determined using 21 hot side and cold side thermocouples.

5. Endurance Tests

Of the initial group of five modules, TEM-13G S/N-2 was the first scheduled for loop testing. This module was removed from static test after accruing 592 hours of $\overline{T}_H = 1025^\circ F/\overline{T}_C = 538^\circ F$ operation, fitted with a heat rejection shroud, and shipped to Atomics International. The module was then restored to $\overline{T}_H = 1025^\circ F/\overline{T}_C = 538^\circ F$ test conditions with liquid metal flow rates adjusted to achieve $200^\circ F$ inlet to outlet temperature drops in the primary and secondary flow channels. Endurance testing of TEM-13G S/N-2 continued until February, 1972, and was terminated after the module had accrued a total of 20,000 hours on test. Overall efficiency, power output, open circuit voltage, and internal resistance data recorded during both static and loop testing of the module are presented as functions of testing time in Figures I-24 through I-27, respectively. Also shown on the curves are similar data from TEM-13G S/N-4 which was endurance tested in a static test stand for 8302 hours at the same nominal average clad temperatures. Performance trends observed for these two identical modules are nearly identical, indicating a very high degree of module-to-module performance reproducibility as well as demonstrating that testing mode (i.e. static and loop testing) has no appreciable effect on module performance, as calculations had indicated.

A statistical analysis of TEM-13G S/N-2 power output data indicated a degradation rate of approximately 10 percent per 10,000 hours during the first 3760 hours of testing. This determination was made by fitting a straight line through the power output data after adjusting the data to compensate for minor fluctuations about the $\overline{T}_H = 1025^\circ F/\overline{T}_C = 538^\circ F$ matched load operating point. These adjustments were necessary to eliminate the effects of performance variations resulting from minor temperature variations (less than $10^\circ F$). Standard linear least-square error techniques were used to determine the straight line fit through the data. During this time, TEM-13G S/N-2 had experienced only three thermal cycles.

At 3760 hours and again at 4580 hours, TEM-13G S/N-2, was subjected to additional thermal cycles resulting from loop system shutdowns at Atomics International. Although no discontinuities in performance resulted from these cycles, degradation rates were observed to have increased. A statistical analysis of data recorded between 3760 hours and 15,336 hours showed that the power output degradation rate had nearly doubled. Yet another increase in degradation rate was observed after a thermal cycle occurring at 15,336 hours.
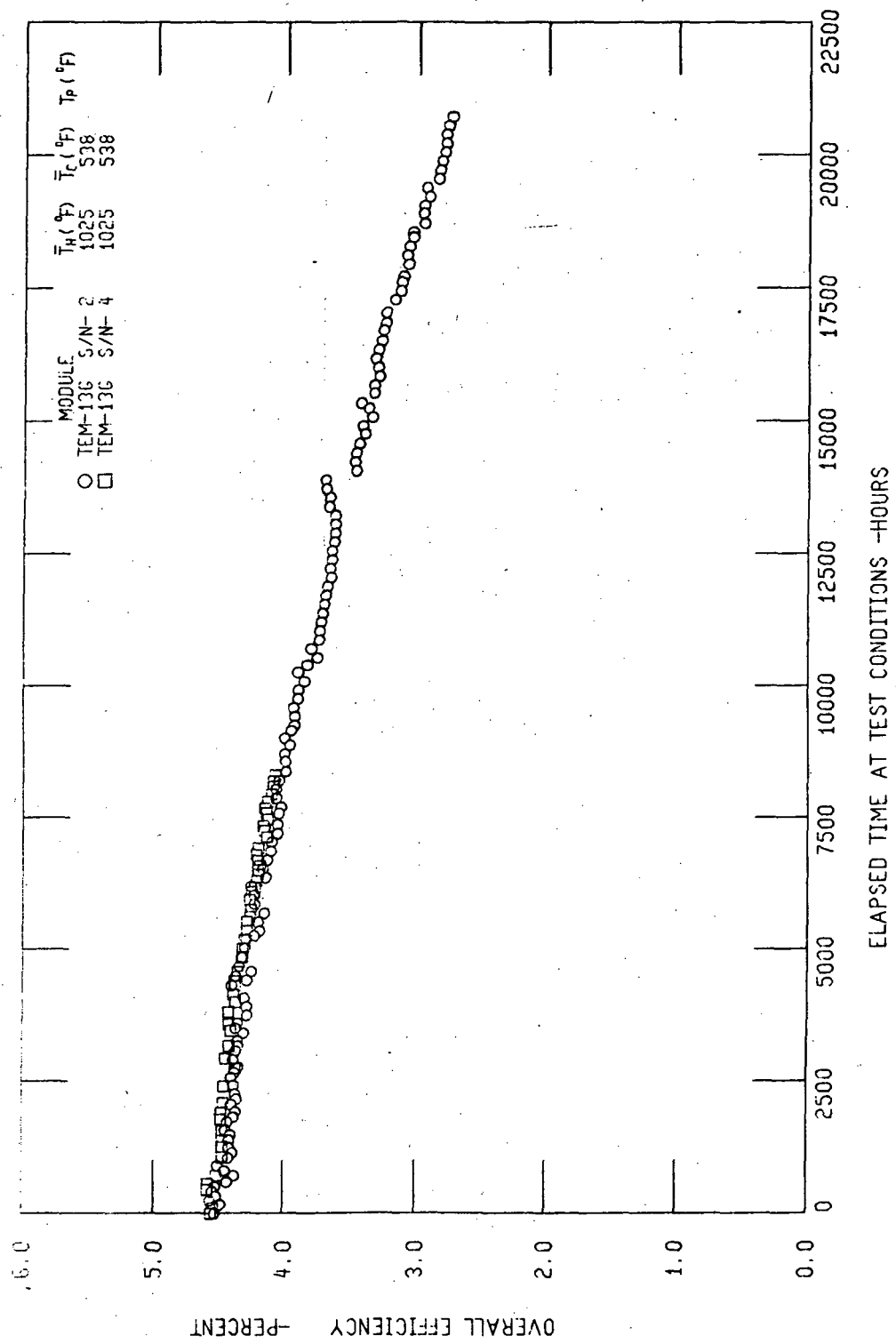
Figure 1-24. A Comparison of Overall Efficiency Data from Two 5.25 Volt Reactor Power Modules Tested at $\overline{T}_H = 1025^{\circ}F/\overline{T}_C = 538^{\circ}F$
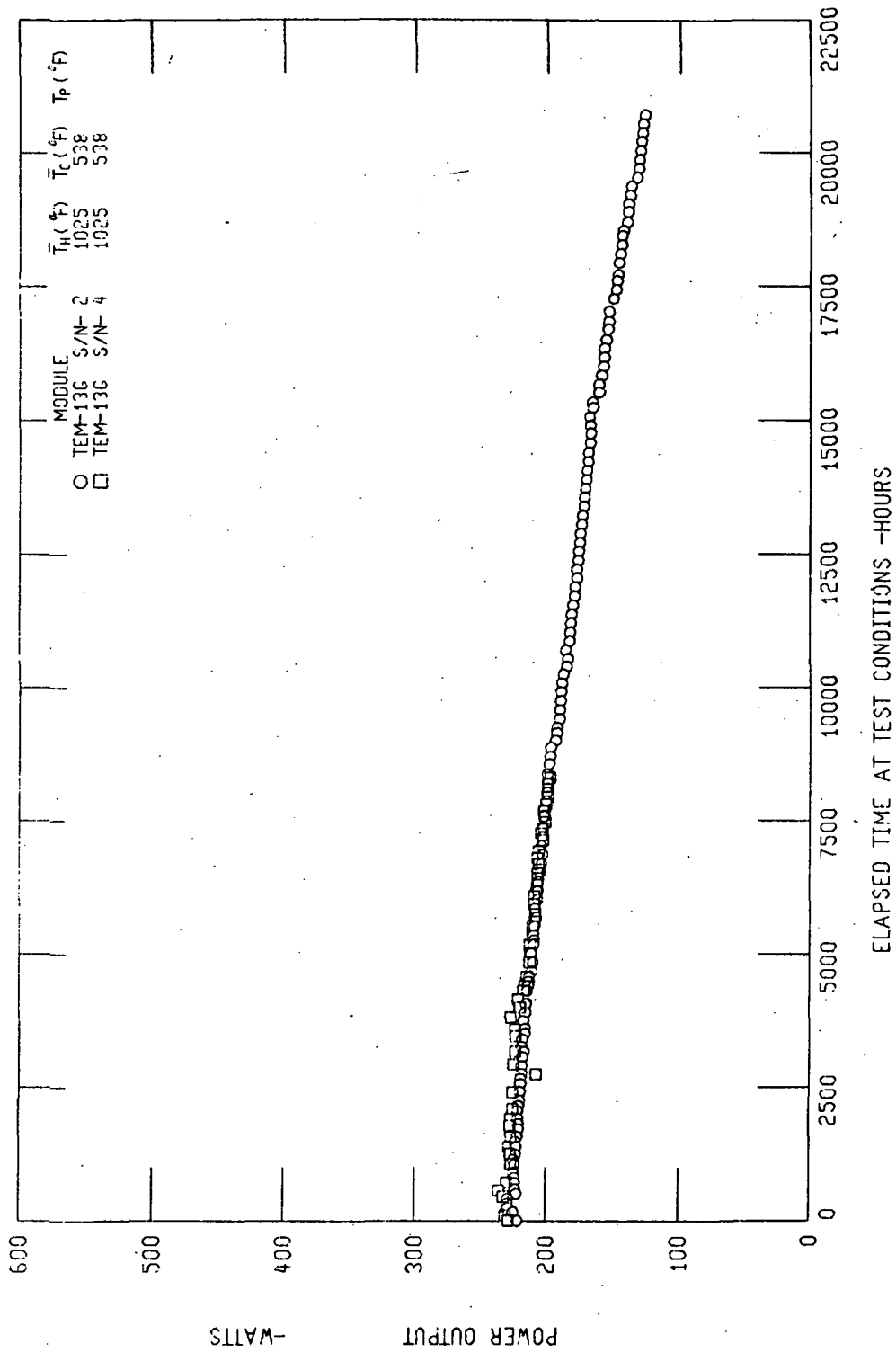
Figure I-25. A Comparison of Power Output Data from Two 5.25 Volt Reactor Power Modules Tested at $\overline{T}_H = 1025°F/\overline{T}_C = 538°F$
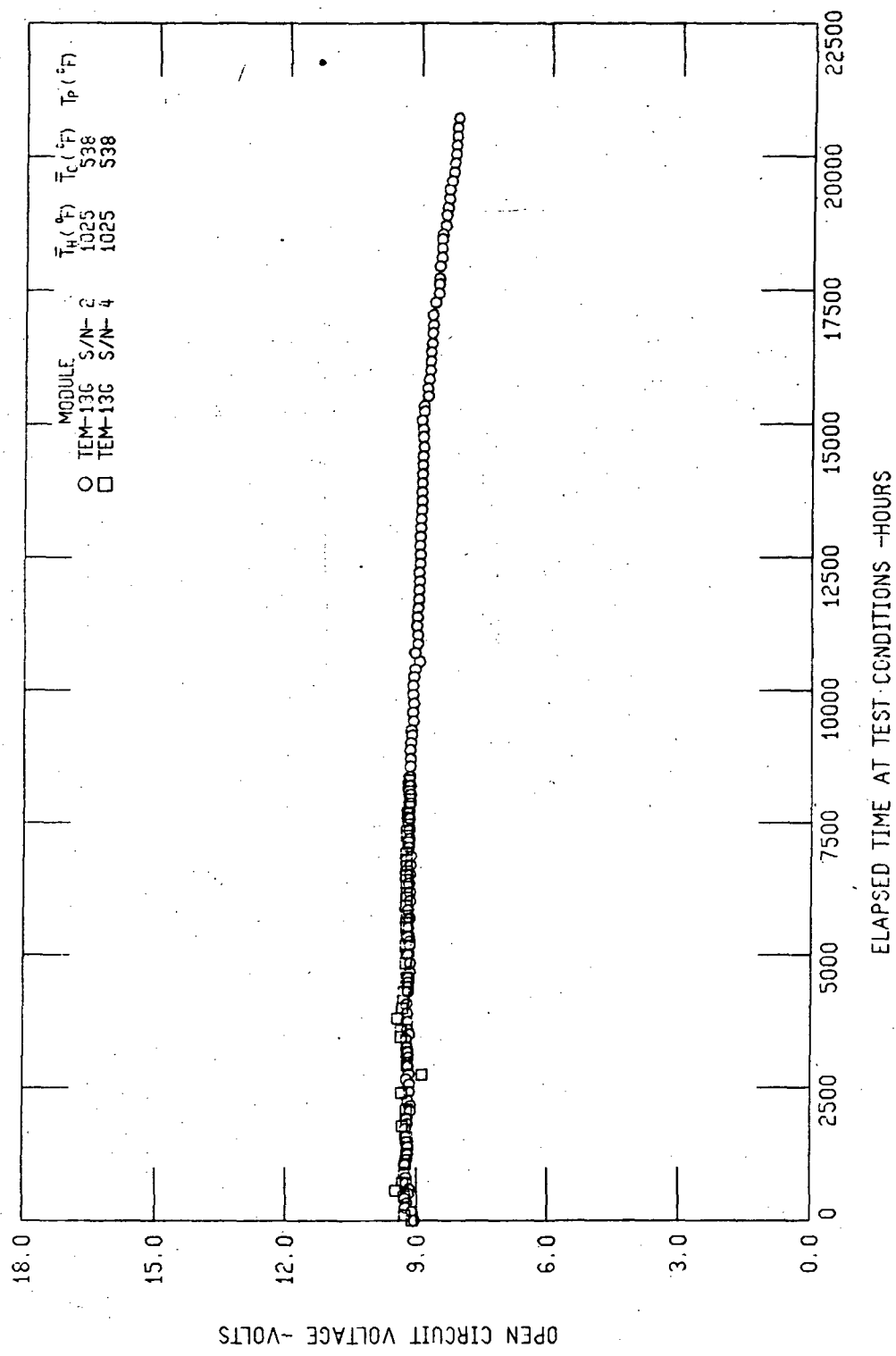
Figure I-26. A Comparison of Open Circuit Voltage Data from Two 5.25 Volt Reactor Power Modules Tested at $\overline{T}_H = 1025°F/\overline{T}_C = 538°F$

Astronuclear
Laboratory
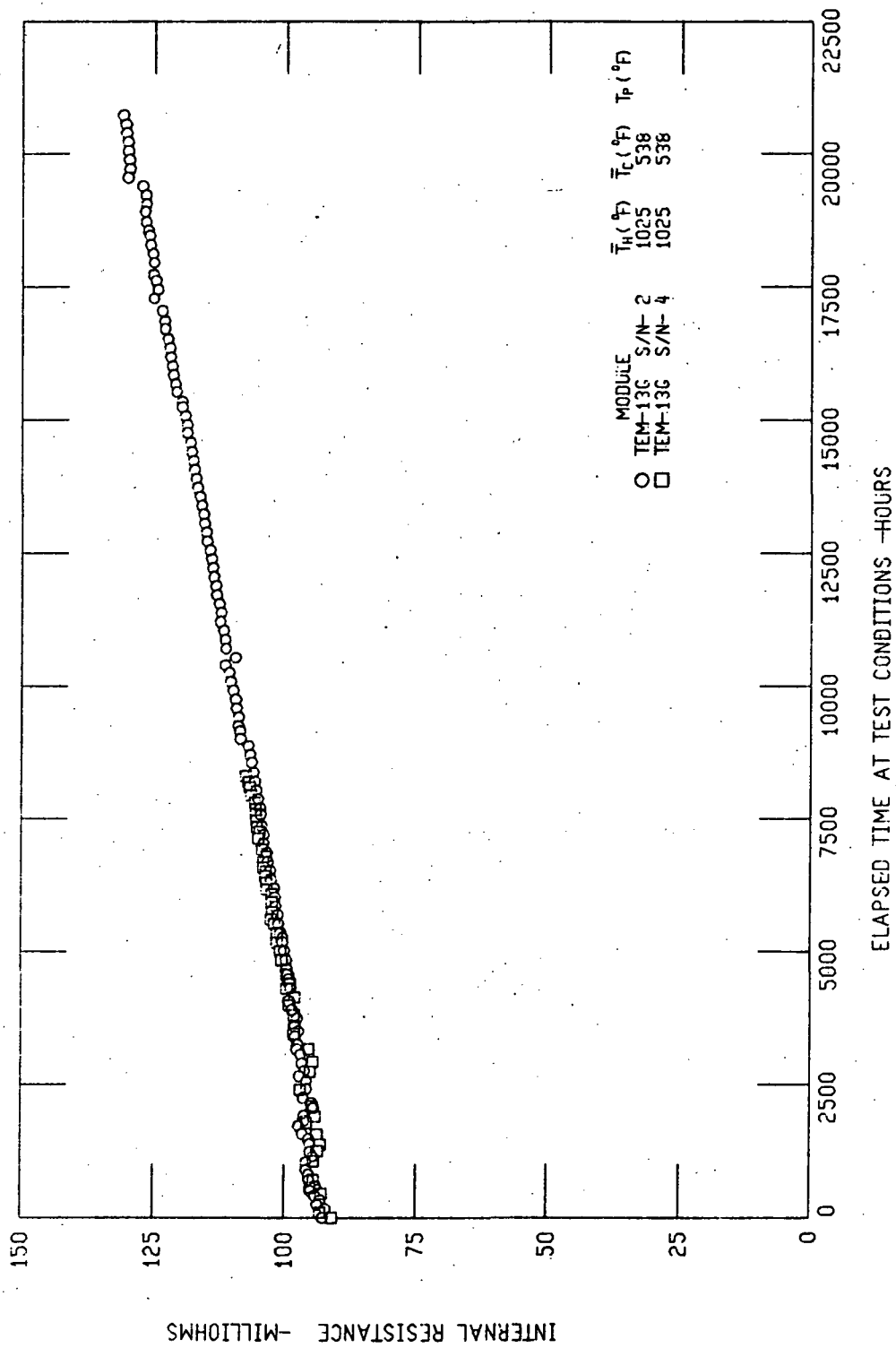
Figure I-27. A Comparison of Internal Resistance Data from Two 5.25 Volt Reactor Power Modules Tested at $\overline{T}_H = 1025^\circ F/\overline{T}_C = 538^\circ F$

From these data it was concluded that degradation rates for the 5.25 volt reactor power modules were functions of module cyclic history. The initial degradation of 10 percent per 10,000 hours recorded for TEM-13G S/N-2 was undoubtedly affected by three thermal cycles occurring during the first 3760 hours of operation of this module.

TEM-13G S/N-4, which was subjected to a total of ten thermal cycles during its 8302 hours of static testing, exhibited degradation rates that were in close agreement to those of S/N-2.

Two other TEM-13G series modules, S/N-1 and S/N-5, were operated initially in static test stands and later shipped to Atomics International for additional loop testing. Cyclic histories of these modules were more severe than those of the previously discussed modules. Some evidence of inter-couple shorting was observed during these tests. Subsequently these modules, along with TEM-13G S/N-3, were removed from test for destructive examination. Basic component distortion patterns observed in these modules were nearly identical to those of modules previously examined.

6. Cyclic Tests

As discussed previously, after the design and fabrication of the initial group of nine TEM-13G series modules, experimental data from previously fabricated modules indicated that the longer reactor power modules were sensitive to cyclic operation. For this reason, three additional TEM-13G series modules were fabricated to determine the extent of sensitivity of this design to thermal cycling.

The first of these modules, TEM-13G S/N-10, was placed on test at $\bar{T}_H = 1125°F/$ $\bar{T}_C = 570°F$ operating conditions, April 23, 1973. The module was subjected to 50 thermal cycles followed closely by a destructive examination of the module. The cycles were identical to those performed on the TEM-13A series modules discussed earlier in this report. A second module, TEM-13G S/N-11 was scheduled to be operated only under steady state conditions at $\bar{T}_H = 1125°F/\bar{T}_C = 570°F$ for the approximate period of time required to complete the S/N-10 cycles. A destructive examination of the latter module, then, would allow a comparison of cyclic tested versus non-cycled modules.

Table I-8 is a compilation of all experimental data recorded for TEM-13G S/N-10. Data sets were recorded in the time period between thermal cycles when the module was being operated at the design $\overline{T}_H = 1125°F/\overline{T}_C = 570°F$ temperatures. Parameters listed on the compilation are elapsed time, E.T.; average hot and cold clad temperatures, THAV and TCAV; internal resistance, RGEN; open circuit voltage, VOC; power output, PE; power input, QMOD; and module overall efficiency, ETA. Also, listed are various parameters adjusted mathematically to compensate for the minor deviations about the $\overline{T}_H = 1125°F/\overline{T}_C = 570°F$ operating conditions. The adjusted parameters are identified by the suffix DES.

The data presented in Table I-8 indicate through the completion of 28 thermal cycles the level of performance of the module was not affected by the transient operation. That is, all adjusted parameters remained essentially unchanged from the B.O.L. level. However, continued thermal cycling resulted in gradual reductions in the adjusted resistance, voltage, power, and efficiency, indicating the development of inter-couple shorting. After completion of 50 thermal cycles, a total power reduction of 8.6 percent was observed.

After completion of thermal cyclic testing, TEM-13G S/N-10 was tested under steady state matched load operating conditions for 100 hours. Data accrued during this time period were very stable and no further reduction in power output was observed. The module was then removed from test for a destructive examination. This module was the first TEM-13 type module ever examined which had experienced controlled thermal cycles and no rapid thermal heatup or cooldown. The destructive examination revealed the circuit was deformed in the familiar chevroned pattern noted in previously examined TEM-13 modules. The total displacement of the inner conductor rings relative to the outer rings was measured to be considerably less than had been encountered in previous reactor power modules which were subjected to fewer, but more rapid thermal cycles.

An identical cyclic test was performed on a TEM-15 series module, S/N-4C, having radial dimensions identical to TEM-13G modules, but designed with a 4.0 inch total circuit length. Destructive examination of the shorter module revealed that the total inner to outer conductor motion was considerably less. In particular, the TEM-15 module circuit looked very similar to the center-most four inch portion of TEM-13G S/N-10. Maximum

TABLE I-8. TEM-13G S/N-10 DATA SUMMARY

TH=1125F, TC=570F TEST CONDITIONS ESTABLISHED AFTER 2.5F/MIN. HEATUP 3/25/70.

NO.	E.I. HOURS	THAV DEG.F	TCAV DEG.F	RGEN M-OHMS	RGDES M-OHMS	VDCML VOLTS	VDCDES VOLTS	PE WATTS	PEDES WATTS	QOD WATTS	ETA PCT.	ETADES PCT.
1	0.0	1125.2	570.5	100.661	100.598	10.315	10.320	264.25	264.68	5454.9	4.842	4.852
2	21.5	1120.6	567.1	100.574	101.207	10.279	10.508	262.63	262.44	5451.5	4.829	4.814
CONTROLLED (30F/MIN.) THERMAL CYCLE NO. 1 COMPLETED 3/24/70.												
3	24.2	1121.8	575.1	101.358	101.191	10.187	10.330	255.93	263.65	5380.1	4.818	4.901
CONTROLLED (30F/MIN.) THERMAL CYCLE NO. 2 COMPLETED 3/24/70.												
4	26.8	1124.6	579.7	101.972	101.160	10.184	10.358	254.21	265.12	5469.4	4.715	4.847
CONTROLLED (30F/MIN.) THERMAL CYCLES NO. 3 THROUGH 8 COMPLETED.												
5	45.4	1118.4	577.6	101.528	101.442	10.101	10.348	251.19	263.89	5477.5	4.696	4.818
CONTROLLED (30F/MIN.) THERMAL CYCLES NO. 9 THROUGH 10 COMPLETED.												
6	52.0	1116.8	574.7	100.999	101.303	10.117	10.344	253.33	264.07	5450.2	4.756	4.845
CONTROLLED (30F/MIN.) THERMAL CYCLES NO. 11 THROUGH 16 COMPLETED.												
7	69.1	1128.1	577.4	102.459	101.545	10.298	10.370	258.70	264.74	5481.6	4.734	4.830
CONTROLLED (30F/MIN.) THERMAL CYCLES NO. 17 THROUGH 28 COMPLETED.												
8	94.2	1127.5	576.7	102.070	101.269	10.317	10.385	260.66	266.26	5492.3	4.762	4.848
CONTROLLED (30F/MIN.) THERMAL CYCLES NO. 29 THROUGH 33 COMPLETED.												
9	121.3	1123.9	574.5	101.374	101.077	10.203	10.298	256.69	262.28	5502.1	4.699	4.767
CONTROLLED (30F/MIN.) THERMAL CYCLES NO. 34 THROUGH 43 COMPLETED.												
10	151.3	1120.9	573.1	99.111	99.190	9.903	10.024	247.37	253.25	5521.5	4.540	4.587
11	151.7	1120.8	573.1	98.663	98.757	9.898	10.020	248.24	254.16	5521.2	4.559	4.603
CONTROLLED (30F/MIN.) THERMAL CYCLES NO. 44 THROUGH 47 COMPLETED.												
12	167.8	1122.5	568.9	98.095	98.405	9.828	9.853	246.16	246.66	5466.9	4.522	4.512
CONTROLLED (30F/MIN.) THERMAL CYCLES NO. 48 THROUGH 50 COMPLETED.												
13	188.6	1120.7	566.4	97.711	98.404	9.789	9.804	245.17	244.21	5466.6	4.502	4.467
14	213.1	1119.6	564.2	97.532	98.510	9.809	9.808	246.62	244.11	5507.6	4.487	4.432
15	237.5	1125.0	575.3	98.981	98.699	9.698	9.816	237.55	244.06	5442.5	4.421	4.484
16	260.7	1121.6	566.0	97.808	98.452	9.829	9.821	246.93	244.93	5500.6	4.494	4.453

SHUTDOWN 4/3/70 (30F/MIN.) FOR DESTRUCTIVE EXAMINATION.

O RAPID CYCLES   50 CONTROLLED CYCLES

distortion was observed near the ends of the TEM-13G series module.

Hence the results from the TEM-13G S/N-10 destructive examination demonstrated that circuit distortion was not only ramp-rate dependent, but was also circuit length dependent.

TEM-13G S/N-11 was tested for 380 hours at steady state $\overline{T}_H = 1125^\circ F/$ $\overline{T}_C = 570^\circ F$ operating conditions. During the test the module was heated to test conditions only twice using extremely low heatup and cooldown ramp rates of $2.5^\circ F/minute$. After testing, this module was also destructively examined. Visual examinations of the TEM-13G S/N-11 circuit revealed that the two heatups produced some washer chevroning, but considerably less than was observed in TEM-13G S/N-10. In addition, there was no evidence of intercouple shorting paths in the latter module.

7. TEM-13G S/N-12 Temperature Mapping Tests

By May, 1970, the degree of sensitivity of reactor power modules to thermal cycling had been experimentally determined. In addition, experimental factors contributing to the development of intercouple distortion had been identified. Various design modifications had been identified to eliminate this condition, and are discussed in detail below. At this time, one untested TEM-13G series module remained. This module was used in "temperature mapping" experiments.

The TEM-13G S/N-12 module was installed into a liquid metal loop system at Westinghouse and a series of short-term "temperature mapping experiments" were conducted. The objectives of this test were: 1) to generate experimental data over a wide range of operating conditions for use in evaluating the accuracy of the primary and secondary boundary layer (film) temperature drops; 2) to correlate calculated module performance with experimental data taken over a wide range of operating temperatures; 3) to compare static and loop test data using common data acquisition system; 4) to generate data for use in debugging computer codes written to reduce loop test data.

The module was operated at three different average hot clad temperature conditions: 950°F, 1085°F, and 1125°F. Secondary loop inlet temperatures and liquid metal flow rates were adjusted to provide data at several cold clad temperatures for each of the selected hot clad temperature operating points.

Open circuit voltage, internal resistance, and power output data recorded during these experiments are presented in Figures I-28 through I-30. Also, shown are corresponding calculated curves plotted parametrically at each of the hot clad temperature conditions. The data exhibit excellent correlation with the calculated curves over the entire temperature range. The strong functional dependency of each of these parameters on both $\overline{T}_H$ and $\overline{T}_C$ is obvious from the slopes of the plotted curves. The high degree of correlation between the calculated and experimental data attests to the accuracy of the module performance calculations and film drop calculations.

Figure I-31 presents module overall efficiency (including end losses) as a function of operating temperatures during the TEM-13G S/N-12 temperature mapping experiments. The data taken at the $\overline{T}_H$ = 950°F level agree quite well with predictions, while at higher temperatures the efficiency data fall above the calculated levels. The discrepancy arises from the fact the performance code overestimates the module power input for high temperature operation. The most probable explanation for this relates to the use of higher than actual high temperature lead telluride thermal conductivities in the performance code.

There is one data point shown on both Figures I-30 and I-31 taken at $\overline{T}_H$ = 1109°F. Although this point was not intended to fall on any of the performance curves, it is included because the 8.01 percent efficiency and 702 watts power output represent the highest level achieved during this series of tests.
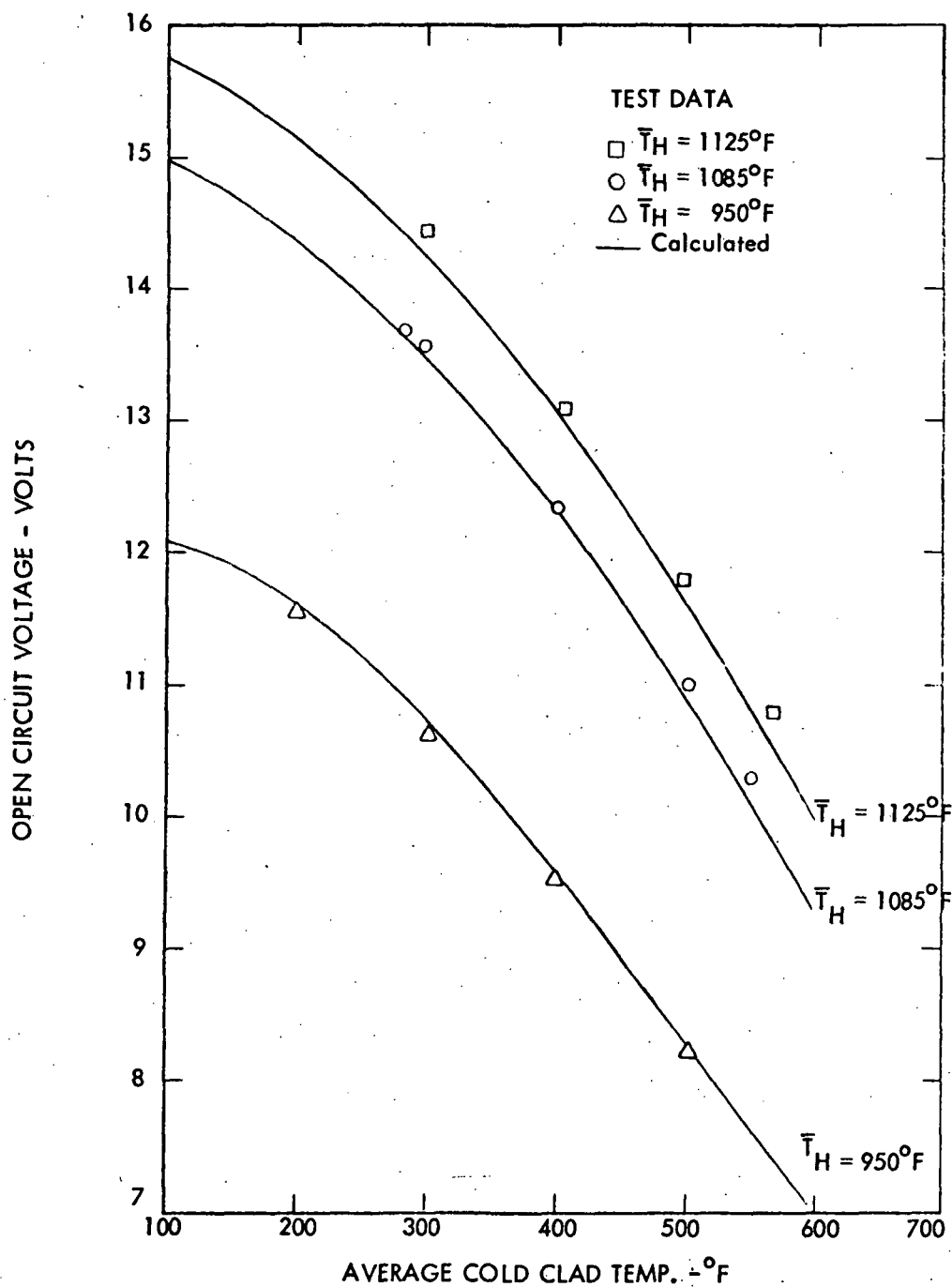
Figure I-28. A Comparison of TEM-13G S/N-12 Open Circuit Voltage
Data with Performance Calculations
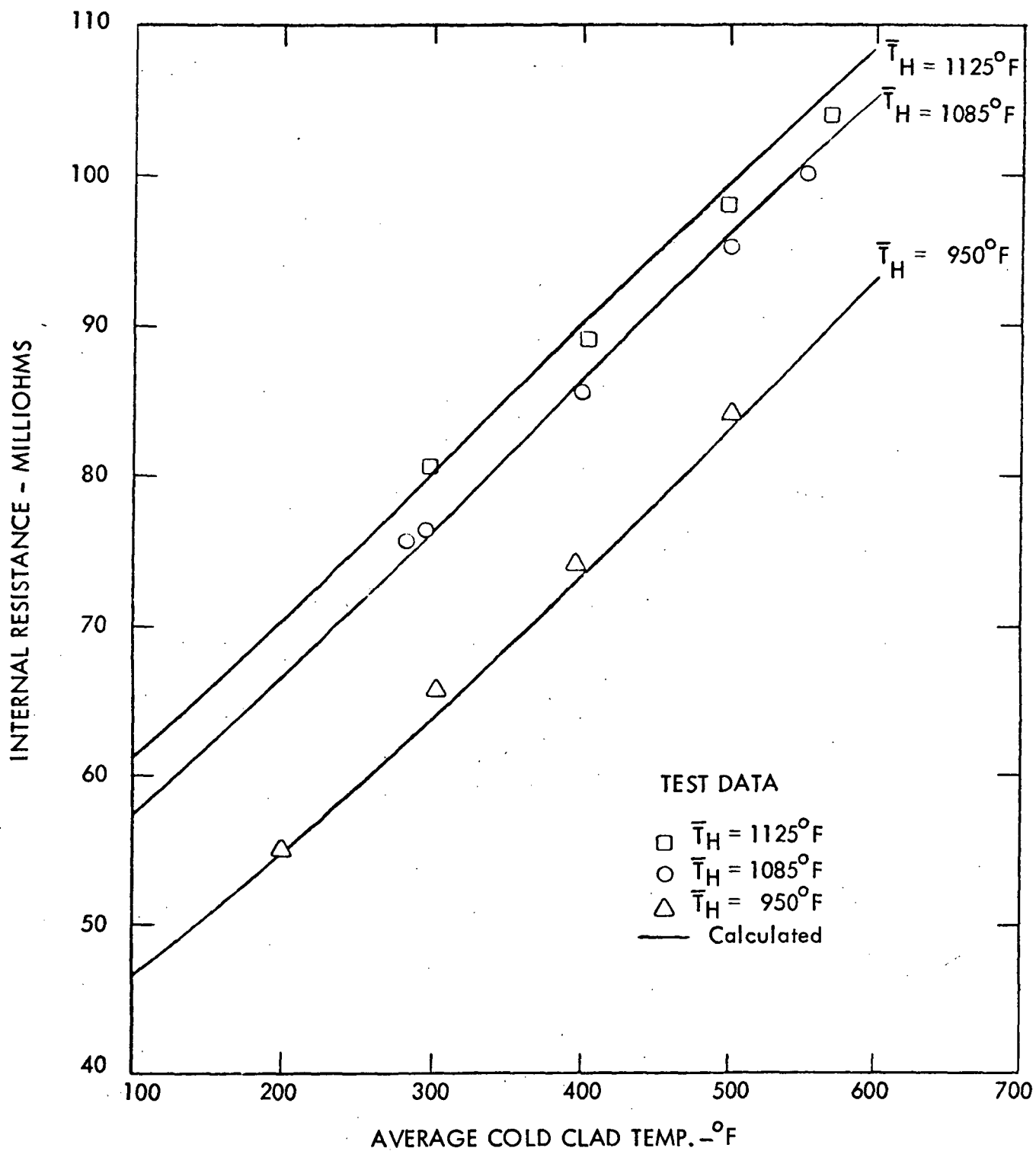
Figure I-29. A Comparison of TEM-13G S/N-12 Internal Resistance
Data with Performance Calculations
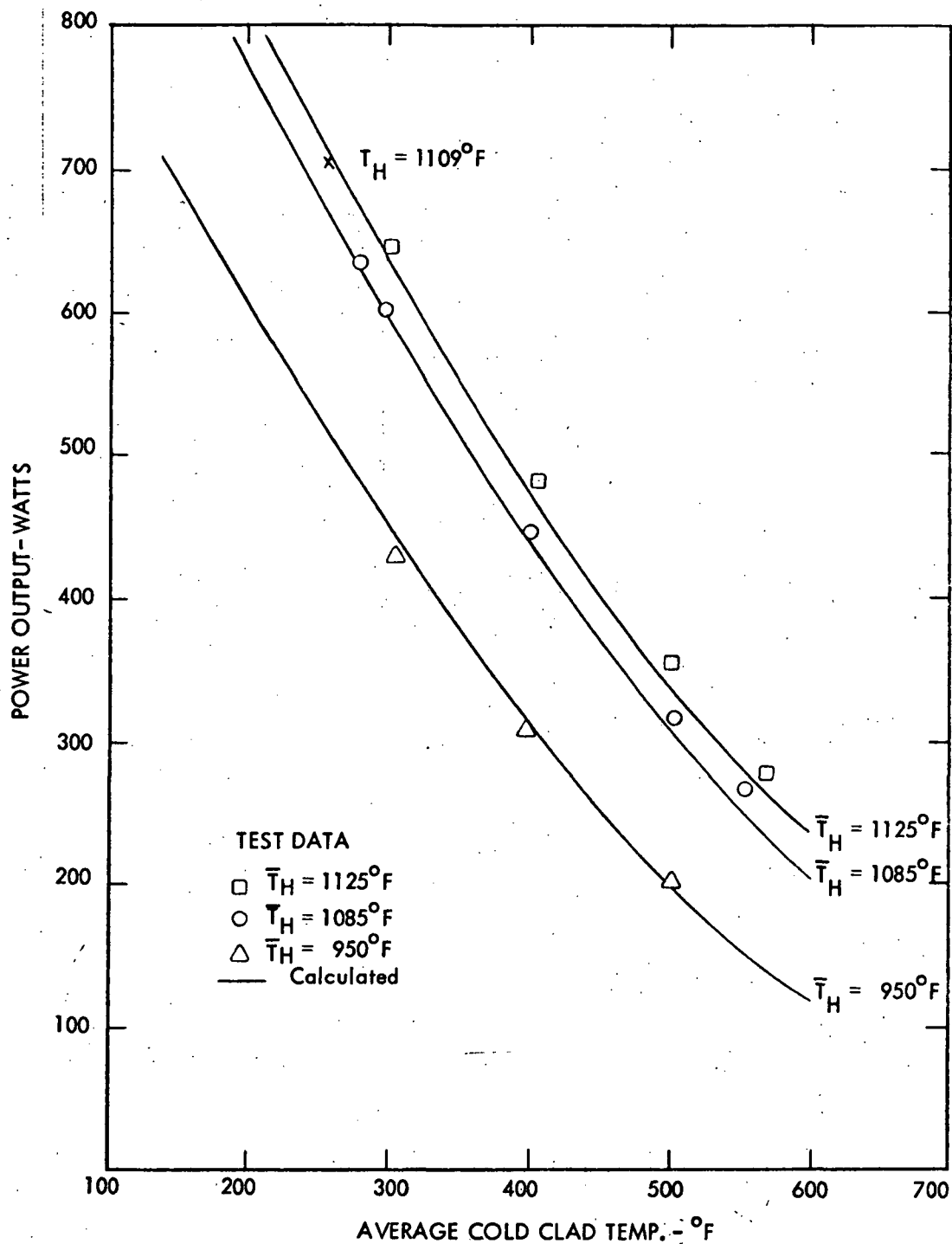
Figure I-30. A Comparison of TEM-13G S/N-12 Power Output
Data with Performance Calculations
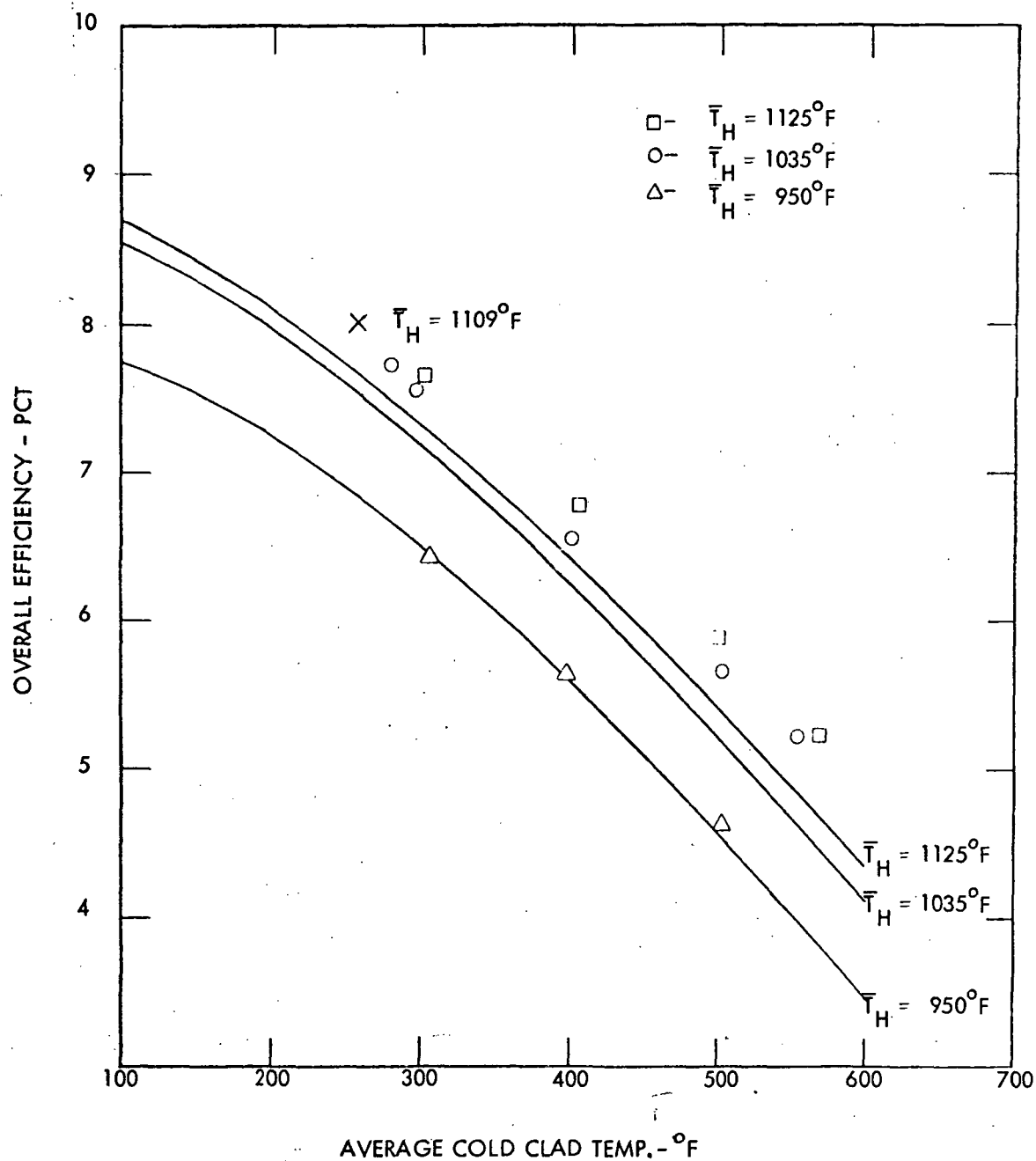
Figure I-31. A Comparison of TEM-13G S/N-12 Overall Efficiency
Data with Performance Calculations

H. CONVERTER MODULE

1. Design and Objectives

One of the initial objectives of the Compact Converter System Technology Programs was to design, fabricate, and test a converter module consisting of an assembly of tubular modules, hydraulically interconnected, including manifolds and jackets for hot and cold liquid metals, and provisions for structural support. Preliminary studies indicated that the 25KWe reactor/thermoelectric power conversion system would be comprised of 96, 15 inch reactor power modules. Conceptual studies indicated that, to minimize the space required by the conversion system, the individual reactor power modules would be packaged together in groups of four. Each group of four modules would be self-contained with one inlet and one outlet for primary liquid metal, along with one inlet and one outlet for secondary flow. The assembly was given the designation "Converter Module" but was commonly referred to as a "Four Pack."

The converter module design was completed in early 1969 and fabrication of parts was initiated by mid 1969. Figure I-32 shows an installation drawing of the final assembly and lists pertinent dimensions. The primary fluid, from the reactor outlet, enters the primary manifold inlet shown near the top of Figure I-32. Flow is directed through the bore of each of the four modules of the assembly and exits through the outlet manifold. Uniform flow distribution was obtained through the use of swirl generators within the bore of each module. The purpose of the swirl generators was to increase the pressure drop through the module and to reduce boundary layer temperature drops during operation. By maintaining relatively high axial pressure drops through the modules relative to those in the manifolds, flow uniformity was assured.

Secondary fluid enters the shroud plenum at the inlet shown in the lower left hand corner of Figure I-32. Here again the secondary fluid is forced to follow a helical flow pattern in the outer shroud of the module to provide uniform flow distribution and to reduce boundary layer temperature drops.

Figure I-32. Converter Module S/N-1 Assembly Drawing

The design provided for counterflow through each of the individual modules. This flow arrangement results in optimum performance in that the radial temperature drop is held nearly constant along the entire circuit length of the module. The secondary manifolds were positioned to minimize cooling from the outer surface of each module in the end closure regions thus minimizing end closure heat losses.

2. **Stress Analysis**

A stress analysis of the converter module design was completed and was based on the use of conventional structural design codes and procedures. The following summarizes the general approach which was used in this analysis.

a.   A three-dimensional flexibility analysis of the complete unit was performed using STASYS, a digital computer program for solving structural analysis problems utilizing a displacement method and finite element direct stiffness techniques.

b.   The stress intensities were determined using three formulae (9, 12 and 13) from the Nuclear Piping Code[1].

c.   The stress indices for branch connections were obtained from Appendix D of the Nuclear Piping Code.

d.   The allowable stresses (Sm values) for formula 9 and formula 12 were obtained, with one exception, directly from Section VIII, Division 1 of the ASME Boiler and Pressure Vessel Code. The 1270°F allowable temperature limit obtained from the code was so restrictive that an investigation was made to determine its basis. This was found to be based on 1 percent creep in 100,000 hours. Since the system had only a 20,000 hour design life, this creep was adjusted to 1 percent in 20,000 hours. The Sm values obtained were 16,300 psi at 410°F, 16,000 psi at 660°F, 13,300 psi at 1045°F, and 7,970 psi at 1270°F.

---

[1]   Draft USA Standard Nuclear Power Piping Code, USAS B31.7, February 1968.

e.   The allowable stresses for formula 13 (alternating stress) were obtained from Code Case 1331-4 for 50 cycles of operation. It was found that this category of stress was never critical for this design. Even when the other stresses (primary or primary plus secondary) were well over the limits, the alternating stress was less than 50 percent of the allowable.

The stress analysis of the original converter module design indicated that certain local stress intensities exceeded code allowables. The worst violations of the code requirements occurred: (1) at the shroud to secondary header joint where the primary plus secondary stress intensity was 70,000 psi and the allowable value is 48,000 psi, and (2) at the primary inlet header joint where the primary plus secondary stress intensity was 67,400 psi, and the limit is 23,900 psi. Subsequently, certain design modifications were identified which would reduce the critical stress intensities. The design changes, which were to be incorporated into subsequent converter module designs are summarized as follows:

a.   The primary header tubes were to be extended such that the spacing between each module and the primary manifold was increased to 6 inches from 2 inches.

b.   The reinforced section at the primary header/primary manifold joint was to be increased to 0.100 inch from 0.065 inch.

c.   The primary manifold wall thickness was to be increased to 0.075 inch from 0.065 inch.

d.   The transition piece joining the module inner clad to the primary header tubes was to be tapered from 0.05 inch at the module end to 0.041 inch at the header tube end. Converter Module S/N-1 employed a 0.035 inch constant section thickness in this transition.

e.   The secondary manifold header stub thickness was to be increased to 0.084 inch from 0.055 inch.

Two sets of external loading conditions were employed in this analysis. First the system was assumed to be a free body so that the effects of thermal stresses and mechanical stresses could be isolated. The free body analysis of the Converter Module including the previously listed modifications indicated a positive design margin for all sections.

The second step in the stress analysis involved postulating a realistic external loading pattern. Since the Power Converter Assembly design, an assembly consisting of six converter modules, as shown in Figure I-33 had not progressed sufficiently to identify the individual converter module piping interactions, there were no clear criteria to use. The approach used, then, was to consider a loading pattern which consisted of all combinations of forces, bending and torque at each piping connection point. The central support member was assumed to be fixed at one end and constrained at the other end in such a manner as to permit motion only in a direction perpendicular to the tubular module and along the axis of the plate.

With loads applied according to the specified pattern it was found that acceptable magnitudes for the piping reactions (at the four connection points) were 50 pounds of force (applied simultaneously along three mutually perpendicular axes) and 100 in.-pounds torsion and bending moments. All forces and moments were assumed to occur simultaneously in the worst direction. Note that these reactions defined an acceptable loading pattern, and were not necessarily optimum. Obviously, if the degrees of freedom in the loading were restricted, higher acceptable magnitudes could be determined.

3. Converter Module Mock-up and Flow Tests

Prior to the fabrication of Converter Module S/N-1, a full size converter mock-up, shown in Figure I-34 was assembled. The objective of this effort was to establish design feasibility, from the fabrication point-of-view, and to gain experience in the welding and inspection operations required. Figures I-35 through I-37 show individual component parts of the metal mock-up in various stages of the assembly procedure.
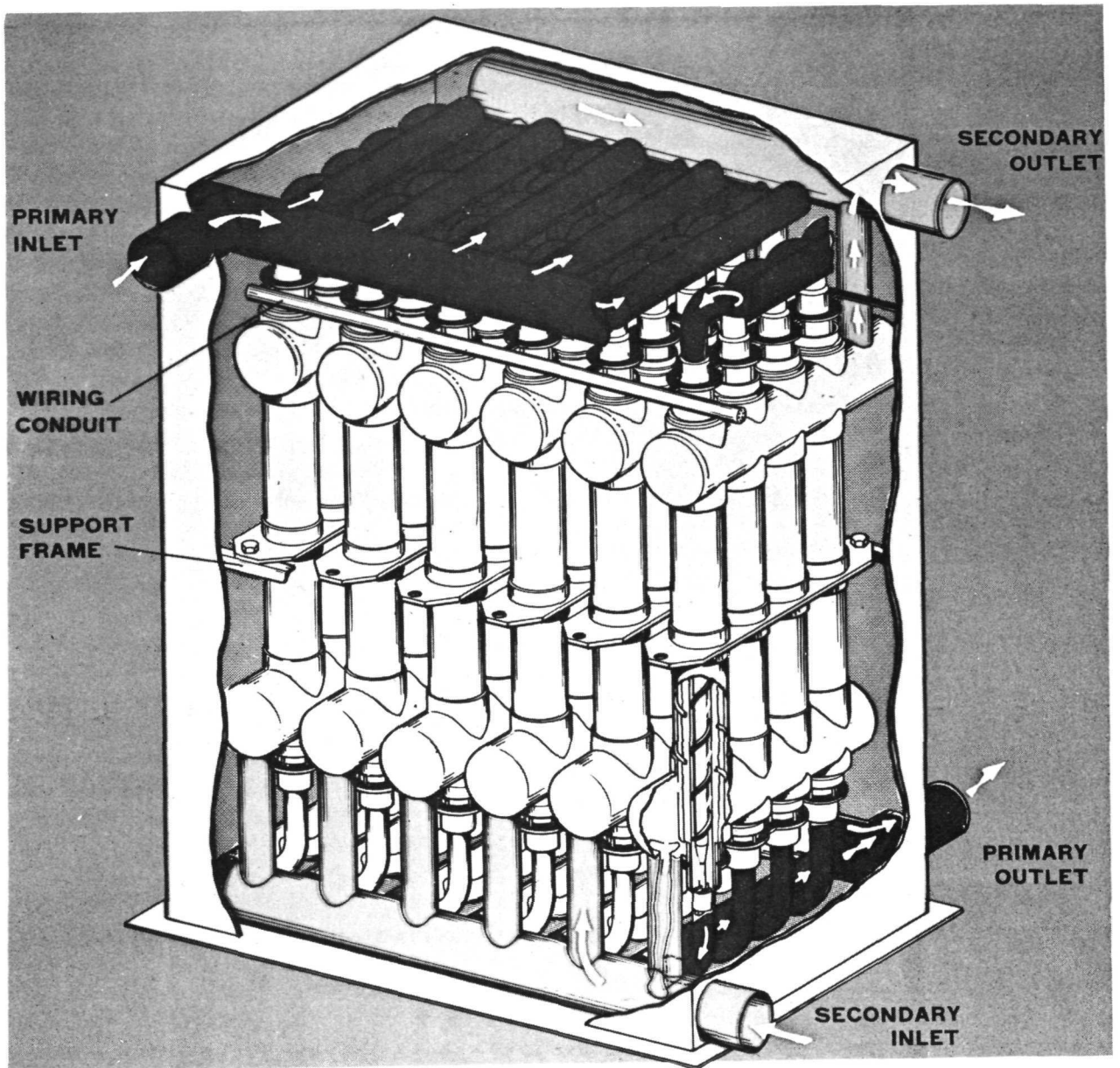
Figure I-33. Power Converter Assembly Conceptual Design

Astronuclear
Laboratory
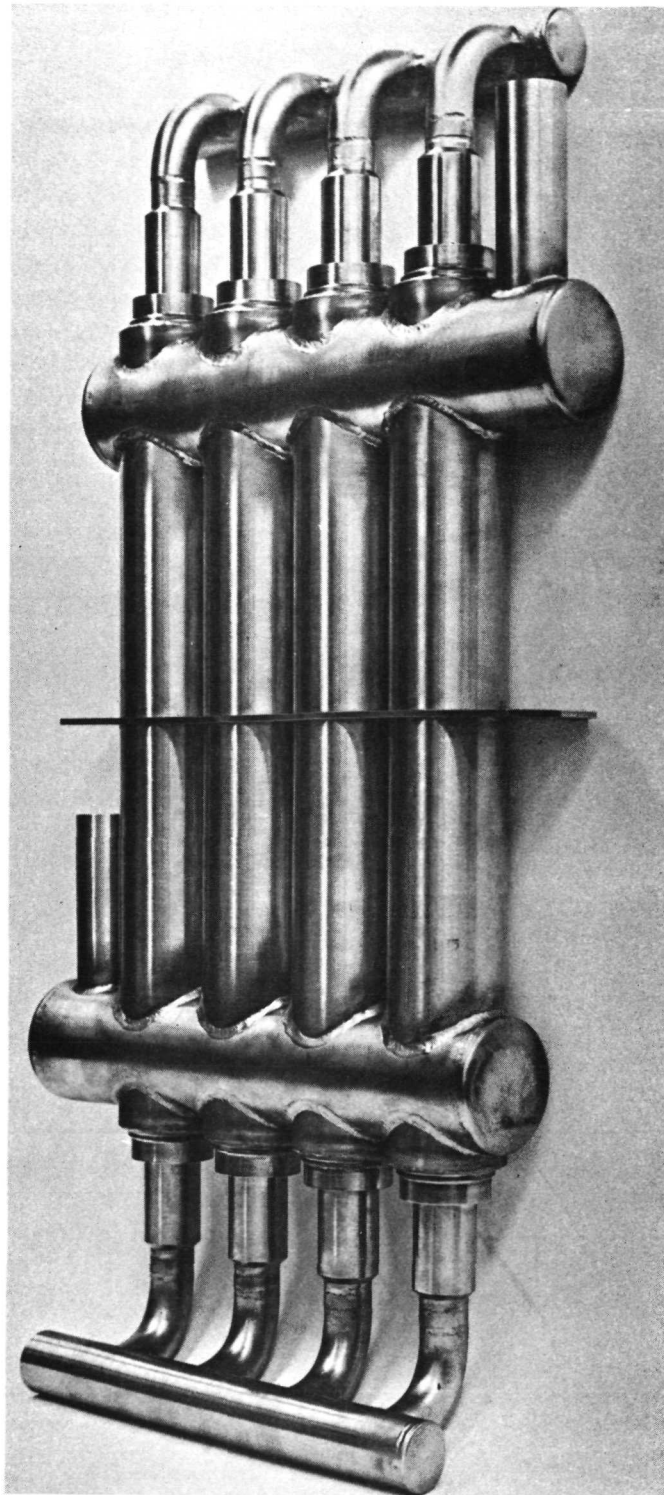
Figure I-34. Converter Module Metal Mockup
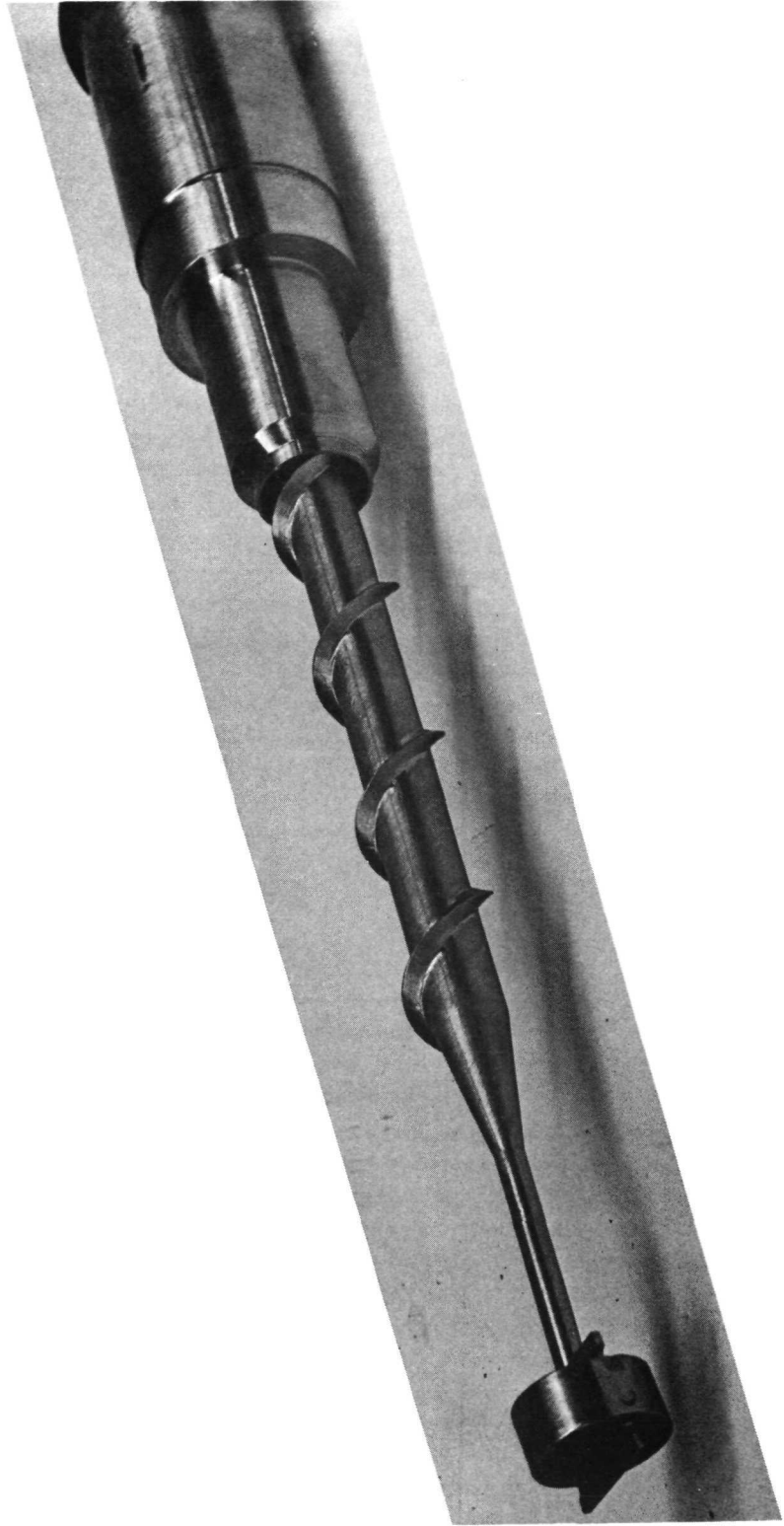
Figure I-35. Simulated Tubular Module with Primary Swirl Generator and Transition
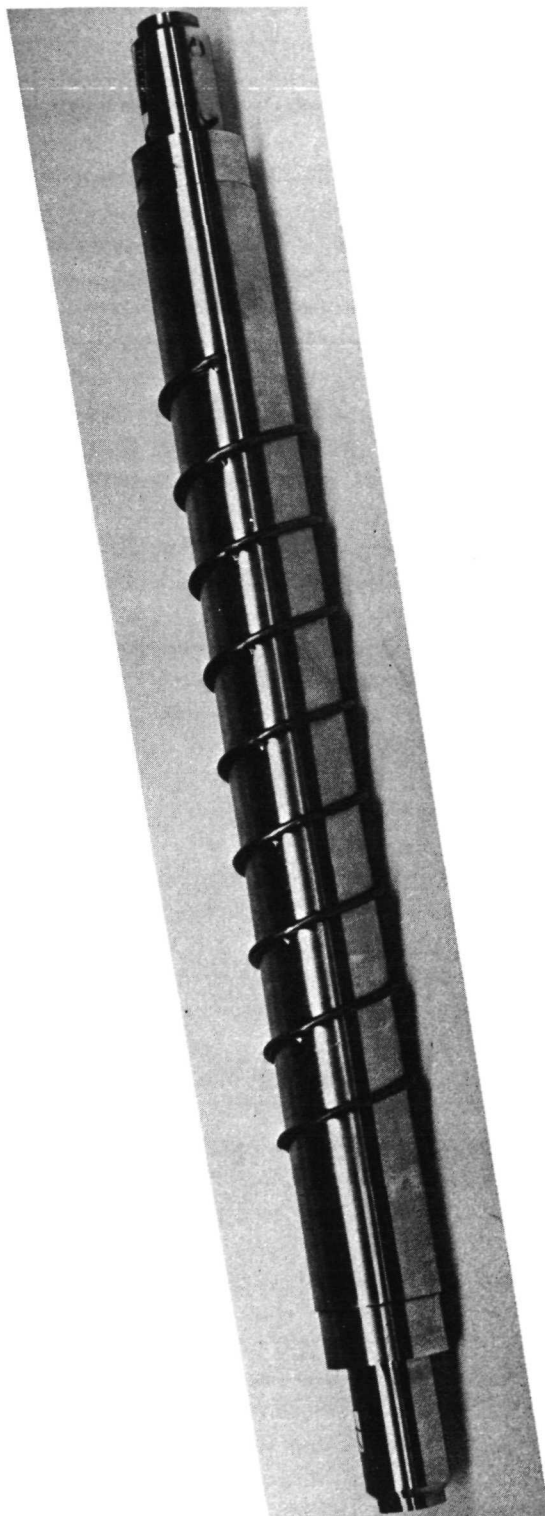
Figure I-36. Simulated Tubular Module with Helix Attached
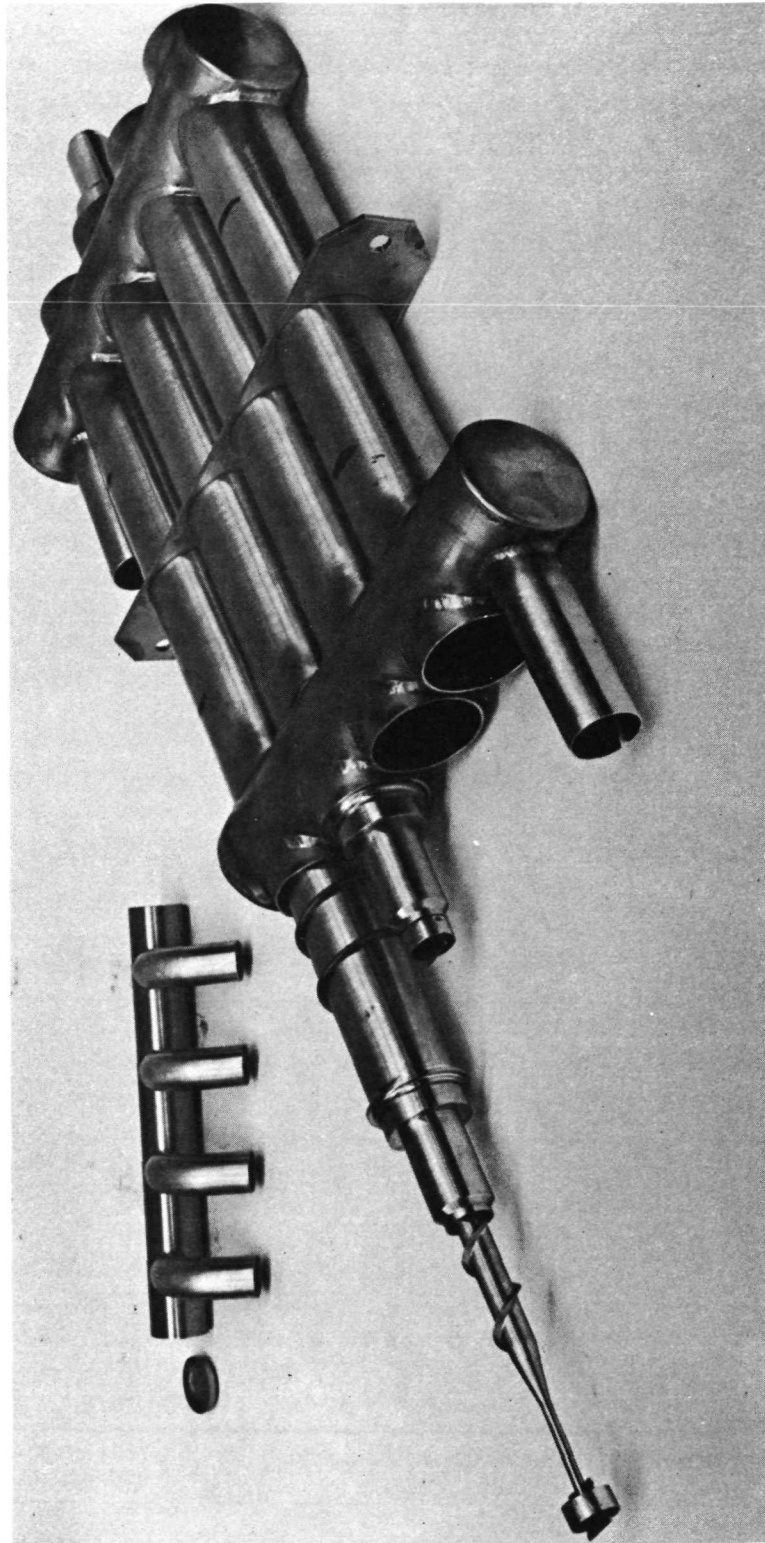
Figure I-37. Heat Rejection Manifold and Converter Module Subassembly

A series of hydraulic flow tests were then conducted to determine the flow distribution within the converter module. Initial flow tests were performed using water flowing through a full-scale plastic mock-up of the primary and secondary flow channels and associated manifolds. The results of these tests were then examined to determine the relationships between pressure drops, flow distribution, and swirl generator pitch. The water tests were conducted using Reynolds numbers consistent with NaK flow.

Based on the results of these initial experiments, a pitch of 1.335 inches was selected for the primary swirl generator. The primary swirl generator, shown during installation into the bore of the simulated tubular module in Figure 1-35, was machined from a solid bar of stainless steel in a form similar to a coarse screw thread.

The secondary (heat rejection) flow channel was established by winding a 0.125 inch diameter wire around the outer surface of the module. Figure 1-36 shows a simulated module with the flow channel helix attached. The 1.25 inches helix pitch was also selected based on the results of the initial water flow tests.

Figure 1-37 shows a simulated module with flow channel hardware, being assembled into the heat rejection manifold of the mockup assembly.

Upon completion of the full size converter module metal mockup assembly, additional hydraulic tests were performed. Results of these tests are shown in Figures 1-38 and 1-39. These plots are the result of the calculation of equivalent NaK primary and secondary flow parameters from the water test data using standard Reynolds analogy techniques. The pressure drop measurements agreed very well with tests conducted on the plastic model.

4. Converter Module S/N-1 Loop Test Performance

The first multiple tubular module conversion device, Converter Module S/N-1, was placed on test in an Atomics International liquid metal loop during the first week of January, 1970. The four modules, TEM-13G S/N-6, S/N-7, S/N-8, and S/N-9, were each static tested for approximately 1500 hours for qualification before assembly into the converter module. A discussion of these initial tests was given earlier in this report.
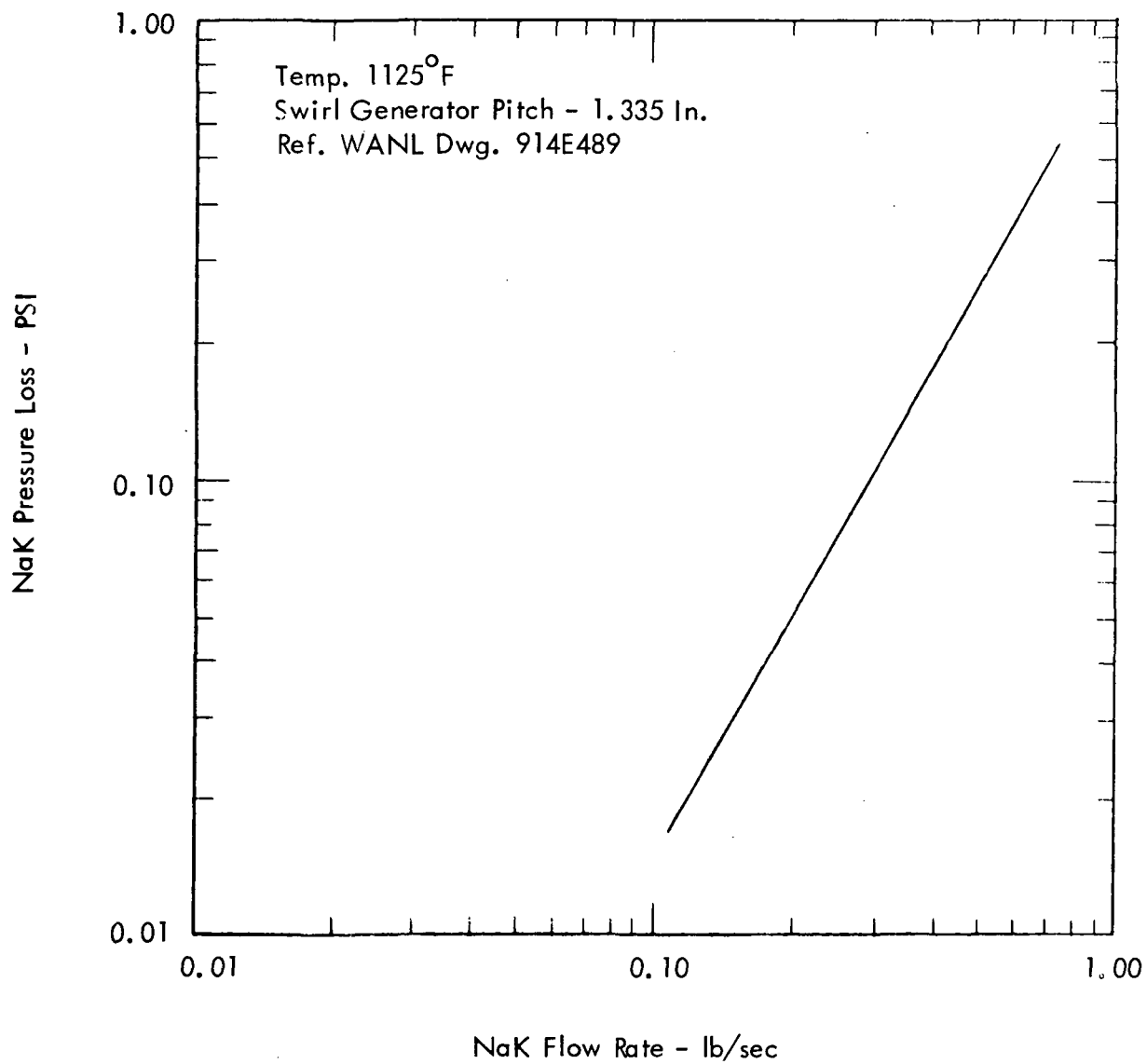
Figure I-38. Predicted Converter Module Primary Side Pressure Drop
Obtained from Mockup Water Flow Tests
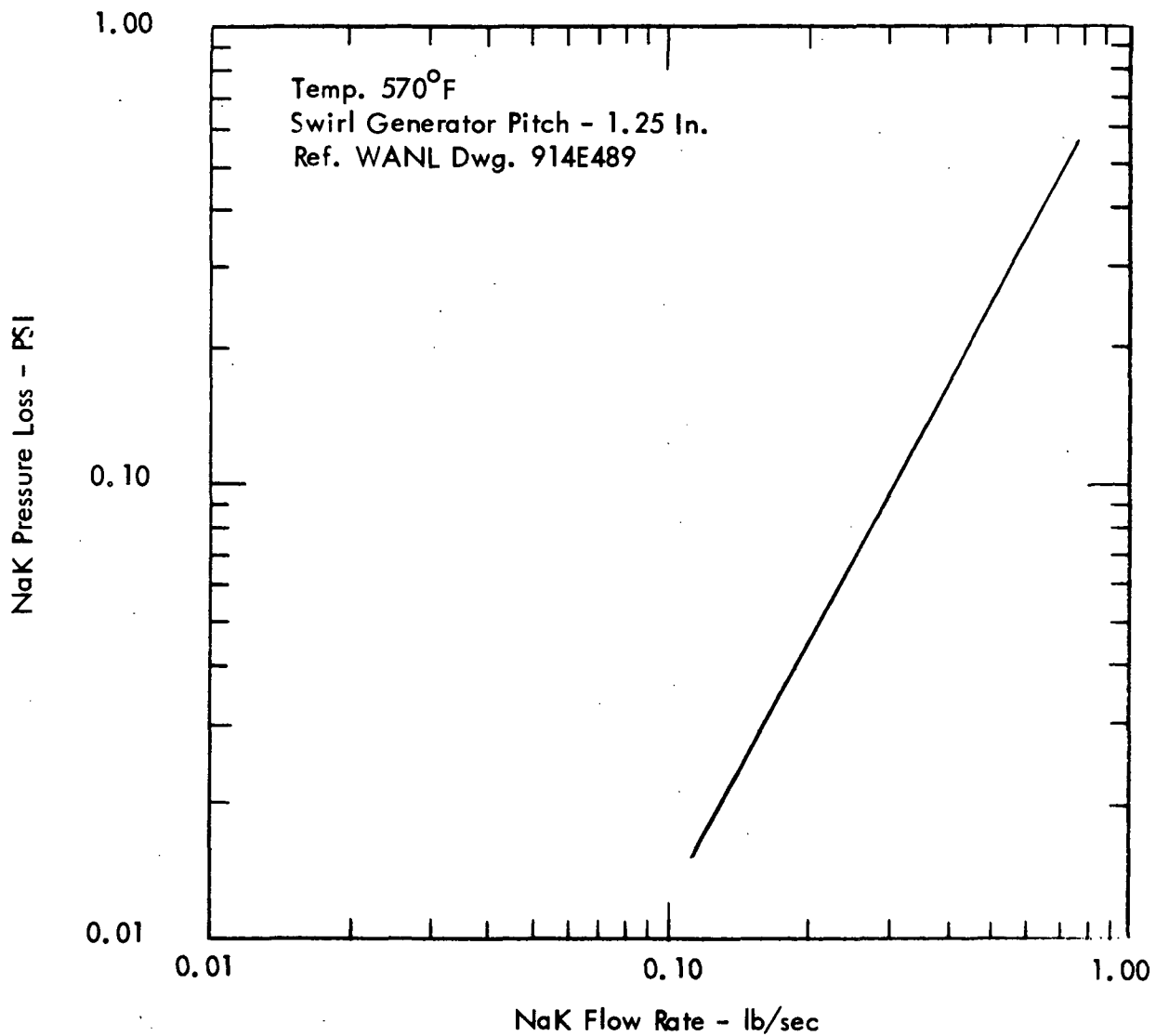
Figure I-39. Predicted Converter Module Secondary Side Pressure Drop
Obtained from Mockup Water Flow Tests

Although the four modules were connected hydraulically within the converter module, they were individually connected to external load resistors so that the performance of each tubular module could be evaluated. The converter module was tested in the Atomics International loop system for a total of 6972 hours.

The basic objective of the test, to demonstrate the mechanical integrity of the multi-module assembly under operational thermal and mechanical stress conditions, was met. The net beginning-of-life power output of the Converter Module, however, was lower than predicted at the target test conditions. Predictions were based on the objective of operating all four of the individual modules with clad temperatures of $\overline{T}_H = 1025°F$ and $\overline{T}_C = 538°F$, with primary and secondary axial temperature drops of 200°F. At these operating conditions, calculations, as well as performance data from a previous module, TEM-13G S/N-2, indicated that each module should produce 222.5 watts resulting in a total expected B.O.L. power for the converter module of 890 watts. The average power measured, however, during the first 140 hours of loop testing (covering the first five data points) was 831 watts.

The experimental data indicated that though the flow conditions for the Converter Module as a whole were close to nominal, none of the tubular modules was actually operating at the prescribed temperature conditions. Analysis of the data indicated that this condition was the result of cross-flow heat transfer in the secondary manifold. The design of Converter Module S/N-1 permitted the upper and lower 2.5 inches of the outer clad of each tubular module to be exposed directly to a cross-flow NaK stream. As a result of this cross-flow heat transfer, the secondary fluid inlet temperature of only the module adjacent to the Converter Module secondary inlet, S/N-9, was at the design level, 431°F. In each successive module the secondary inlet temperature rose substantially above this level as a result of the cross flow manifold heat pickup.

Table 1-9 summarizes the beginning-of-life data from the converter module. The data are first listed on the table as recorded. The primary inlet temperatures were very uniform since the design allowed no cross-flow heat transfer in the primary inlet manifolds.

TABLE I-9

BOL DATA FROM CONVERTER MODULE S/N-1

Parameter	As Recorded					Adjusted to Design Conditions					Calc.
	S/N-9	S/N-8	S/N-7	S/N-6	Total	S/N-9	S/N-8	S/N-7	S/N-6	Total	
1. Primary Inlet Temperature (°F)	1136	1137	1137	1137	1137	1138	1138	1138	1138	1138	-
2. Primary Outlet Temperature (°F)	913	930	939	948	938	1038	1038	1038	1038	1038	-
3. Average Hot Clad Temperature (°F)	1011	1022	1026	1032	-	1025	1025	1025	1025	-	1025
4. Secondary Inlet Temperature (°F)	431	442	447	467	431	431	431	431	431	431	-
5. Secondary Outlet Temperature (°F)	614	643	659	662	632	631	631	631	631	631	-
6. Average Cold Clad Temperature (°F)	528	548	559	570	-	538	538	538	538	-	538
7. Open Circuit Voltage (Volts)	9.21	9.11	8.96	8.68	36.0	9.31	9.35	9.28	9.07	37.0	36.6
8. Internal Resistance (Milliohms)	94.1	95.8	100.2	102.1	392	96.4	95.1	98.1	98.5	388	375
9. Electrical Power Output (Watts)	225	217	200	184	826	225	230	219	209	882	890
10. Thermal Power Input (Watts)	5196	4826	4618	4397	17970	5242	4974	4817	4664	18600	19560
11. Efficiency (%)	4.57	4.75	4.60	4.46	4.60	4.52	4.89	4.83	4.76	4.74	4.58

Primary outlet temperatures varied substantially for each of the modules indicating that there was a variation in heat transferred to each of the modules. The average hot clad temperature of each module, listed in Table I-9, is the arithmetic average of the inlet and outlet temperatures minus the temperature drop across the NaK boundary layer (approximately 13°F for each module).

The effects of the secondary manifold cross flow heat transfer are evident from the individual module secondary inlet temperatures listed in Table I-9. A temperature increase of 37°F was observed in this manifold causing the last module, TEM-13G S/N-6 to operate at a cold side temperature substantially above the $\overline{T}_C = 538^\circ$F level. Average module cold clad temperatures also take into account a 7°F secondary boundary layer temperature drop.

In the second set of data shown in Table I-9, the effects of the temperature deviations were compensated for analytically. In each case the experimental data were adjusted to indicate module performance parameters at the design $\overline{T}_H = 1025^\circ$F/ $\overline{T}_C = 538$ matched load operating conditions. After the adjustments, all parameters were in good agreement with the calculated values, also listed in Table I-9. Power output was within 1 percent of the 890 watt design point and the efficiency was above the calculated level. A similar deviation in the TEM-13G S/N-12 thermal mapping test efficiency data was observed and can be attributed to the use of the higher than actual lead telluride thermal conductivities in the mathematical model.

Figure I-40 presents power output data from the individual tubular modules measured during endurance testing of Converter Module S/N-1. Since performance of TEM-13G series modules had been found to be sensitive to cyclic operation, the times at which the Converter Module was thermal cycled are shown on the figure.

A statistical analysis of the data from the four modules used in the Converter Module Assembly test showed power output degradation rates ranging from 27 to 34 percent per 10,000 hours. Although these rates were higher than those of TEM-13G S/N-2 and TEM-13G S/N-4 tested individually at the same nominal temperatures, the cyclic histories
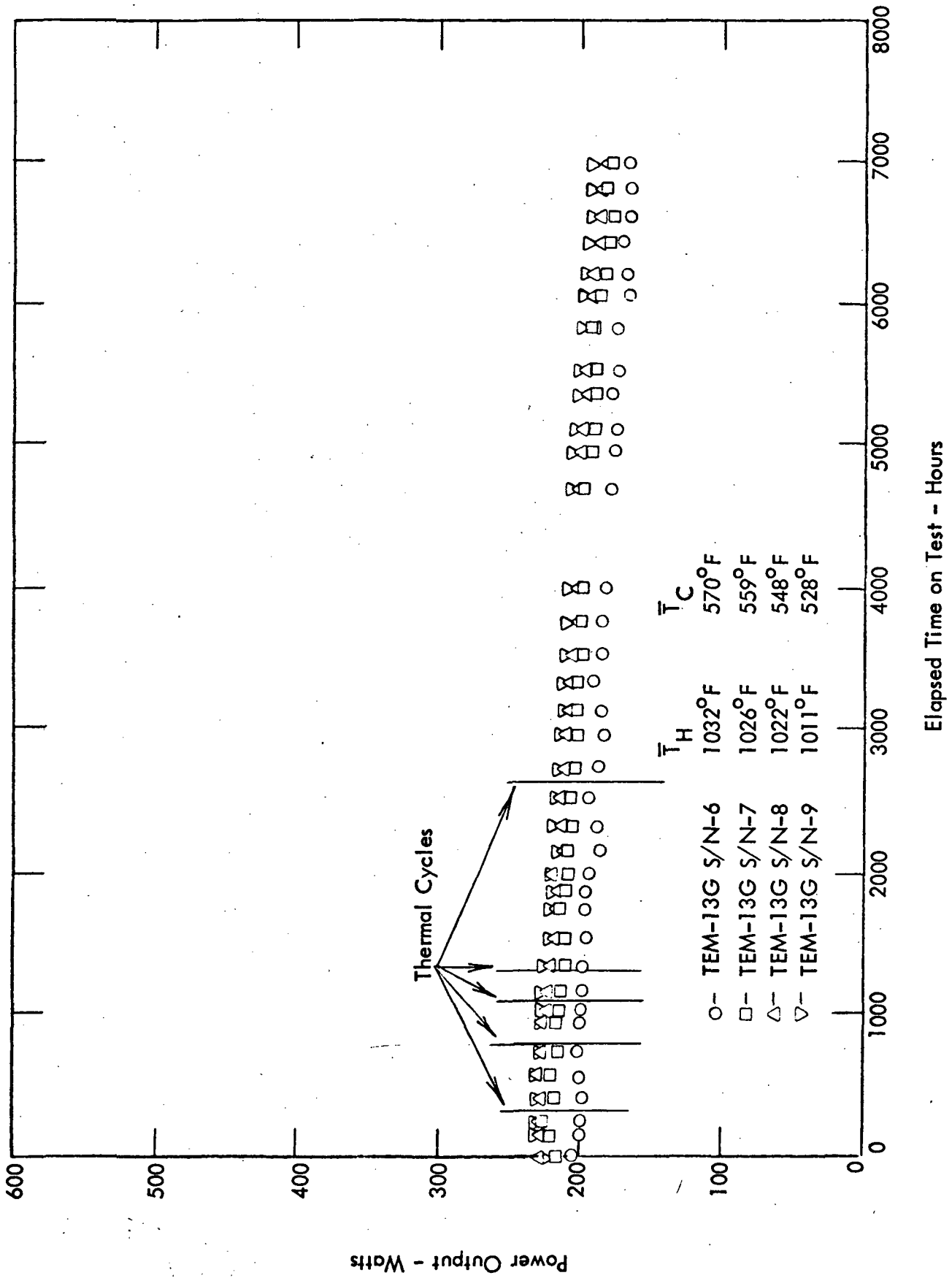
Figure 1-40. Power Output Data from Modules Incorporated into Converter Module S/N-1

of the modules used in the Converter Module Assembly were much different. It was concluded, however, that since stresses imposed on individual modules in the Converter Module Assembly were higher than those of individually tested modules, this could have been a contributing factor to the observed increased degradation rates.

5. Summary of Results of the Converter Module

A substantial effort in the Compact Converter Systems Technology program was directed toward the design of a multi-module converter assembly. The basic objective of demonstrating that such an assembly could be operated under conditions closely simulating those of a reactor/thermoelectric power conversion system was met.

Initial data indicated that the Converter Module design allowed for secondary manifold cross-flow heat transfer, a condition which resulted in a reduction in power output below the design level. A series of flow tests verified that the effects of this cross-flow condition could be reduced by increasing secondary flow rates, as had been predicted. It was anticipated that future multi-module assembly designs would be modified to eliminate this cross flow condition. This modification was never required, however, since later reactor/thermoelectric system designs specified that each module would be shrouded individually.

Endurance test data from Converter Module S/N-1 was affected by thermal cyclic sensitivity of the TEM-13G series modules.

I.   TEM-X SERIES MODULES

1.   Elimination of Cyclic Distortion

Prior to the initiation of the Compact Thermoelectric System Technology Program, design modifications were restricted to modules having one basic overall geometry, namely 0.5 inch I.D. and a 7.2 inch circuit. Modules having these dimensions were found to be very insensitive to thermal cyclic operation. However, data generated on TEM-13 series reactor power modules identified the critical need to identify and eliminate the mechanism producing circuit component distortion during cyclic operation of those modules designed with larger bores and longer circuits.

Performance of reactor power modules was affected by thermal cycling in two ways. First, occasional step decreases in power, resistance and voltage were observed – a sign of internal couple-to-couple electrical short development. Second, increased degrada- tion rates were observed after thermal cycling – a sign of increased inter-couple tellurium transport. Subsequent destructive examination of a large number of TEM-13 series reactor power modules having varying cyclic histories showed extensive component distortion and, in some cases, direct inter-couple shorting as the experimental data had indicated. Results of these destructive examinations are discussed in more detail in earlier sections of this report.

A detailed stress analysis effort was conducted during the latter half of 1969 to examine the mechanical behavior of the tubular module during transient operation. The analysis predicted circuit distortion patterns similar to those observed in a number of reactor power modules which were sectioned after thermal cyclic operation. It was found in the analysis that the circuit distortion was produced by the relative movement of the inner and outer clads of the module. The relative clad motion, in turn, was caused by differential thermal expansion during transient operation.

Differential thermal expansion of the clads had been taken into account in early module designs. Initial stress analysis efforts on the tubular module indicated that the inner clad would slide freely along the inner boron nitride insulating sleeve during heatup of the module. A "stretch neck" was employed in the end closure region of the module to allow for

relative clad motion. However, the stress analysis effort on the TEM-13 series modules showed that due to the high interface pressure levels after module processing and a higher than anticipated coefficient of friction between the inner clad and adjacent boron nitride insulator surface, free expansion of the inner clad during heatup was not achieved. As a result, circuit components were "dragged" back and forth axially during transient operation.

To compound the situation, a racheting effect occurred under conditions produced during laboratory power failures. When a power failure occurred with the module at operating temperatures, both the electrical heater and the electrical fan used to provide the forced air cooling for the module stopped. Cooldown of the module, under these conditions, occurred nearly isothermally. As a result of the isothermal conditions, the radial interface pressures were greatly reduced and the inner clad did not "drag" the inner conductor components back to their initial positions. When power was restored, however, the full heater power was abruptly applied to the electrical heater. Under these transient conditions the inner clad temperature rose by about 500°F before the outer clad temperature had begun to increase. The result was that the lockup between the inner clad and inner conductors occurred very early and the amount of conductor displacement was increased for each cycle.

Additional stress analysis effort indicated that circuit component distortion could be virtually eliminated by matching the inner and outer clad total thermal expansions. Three concepts providing matched thermal growth for both clads were considered. The first concept required the use of a rigid end closure, stiff enough to structurally lock the two clads together. The second concept considered the use of a pre-stressed Inconel 718 inner clad, stretched at room temperature to compensate for axial growth difference between the two clads. The final concept considered the use of a low coefficient expansion material in place of Inconel 718 for the inner clad.

The first and third concepts were committed to hardware for "proof-of-principal" experiments and results are discussed below. The second concept was deferred, pending results of the other experiments. The basic difficulty associated with the pre-stressed clad concept was that the pre-stressing was required prior to fabrication of the module. Initial calculations indicated that the pre-stressed condition would be lost during the hot autoclave process.

2. TEM-X S/N-1: Stiffened End Closure Design

In early 1970, design work was initiated on the first module in which the relative motion of the inner and outer clad, the identified cause of cyclic distortion, was to have been eliminated. This module was designated TEM-X (Experimental) S/N-1. The module design incorporated rigid end closures designed to lock the inner and outer clads together.

The design fix incorporated into TEM-X S/N-1 had two negative aspects associated with it. First, to eliminate relative clad motion, the stretch neck was to be eliminated and replaced with a retainer of increased thickness welded directly to both clads. This resulted in a substantial increase in end closure shunt heat losses. Second, calculations indicated that the stress levels resulting from locking the clads together would cause the stainless steel outer clad to undergo plastic deformation during operation.

The second condition could be eliminated through the use of an inconel outer clad. However, experiments performed in a previous program indicated that proper compaction of the module could not be achieved using an inconel outer clad because of its high strength at processing temperatures. Subsequently, TEM-X S/N-1 was fabricated and processed in a manner identical to that of TEM-13G series modules. After processing the stainless steel outer clad was to be machined to a radial thickness of .050 inch and the TEM-13 G type end closure retaining rings removed. It was planned to shrink fit an inconel outer clad around the module by preheating the clad prior to installation. Reinforced retainers were then to be welded to the inner and outer clads.

Difficulty was encountered during the outer clad machining operation. Because of the high stress levels in the module resulting from the high temperature autoclave cycle, local relaxation occurred during the machining process. A slight axial bowing condition resulted in a non-uniform outer clad thickness near the center of the module after machining. Relaxation of the thinner clad area resulted in additional bowing. As a result of the bowing it was found impossible to machine the module uniformly. Subsequently fabrication of TEM-X S/N-1 was discontinued and the effort to eliminate inner to outer clad motion through the use of stiff end closures was abandoned and emphasis was placed on the development of a low expansion inner clad.

3. TEM-X S/N-2: Low Expansion Inner Clad Design

Of the three concepts generated to eliminate circuit component distortion, the use of low expansion inner clads appeared optimum in that the mechanism was eliminated rather than being designed around. Refractory metals, with coefficients of thermal expansion less than one-half that of stainless steel, appeared ideal for use as inner clad material substitutes. In addition to having low coefficients of thermal expansion, in which total inner and outer clad expansions could be matched, refractory metals have much higher thermal conductivities than inconel, providing a performance improvement.

Several candidate refractory metals were evaluated to determine their suitability. From the available data it appeared that either Ta-10W or T-111 (Ta-8W-2Hf) would provide adequate strength to replace the Inconel 718 inner clad. Although T-111 was attractive because of its proven long-term NaK compatibility, the better availability of Ta-10W combined with concern over possible formation of a Hf-Ni eutectic in T-111 in the coextrusion temperature range made Ta-10W the choice for a short-term proof-of-principle test.

One of the major concerns associated with the use of a low expansion inner clad was the method of joining to the stainless steel end closure components. This problem was eliminated through the use of a bimetal clad design consisting of a 15 inch section of the refractory metal joined to stainless steel segments on either end. The stainless steel clad ends could then be welded to end closure components as in the standard TEM-13 design.

Procurement of a co-extruded Ta-10W/316 SS clad was initiated on a best effort basis. Ta-10W and stainless steel Type 316 were co-extruded successfully. Following the successful fabrication of the Ta-10W/316 SS clad, TEM-X S/N-2 was defined. This module was identical to the TEM-13G series modules in all respects except for the use of the refractory inner clad. Figure I-41 shows cutaway cross section drawings of a TEM-13G series module along with that of TEM-X S/N-2. The Ta-10W section of the TEM-X S/N-2 was under the circuit whereas the stainless steel portion was in the end closure section. The clad was made by hot tandem co-extruding two single Ta-10W/316 SS bimetal joints, electron beam welding the Ta-10W ends of these together, and machining the resultant assembly to the final clad dimension.

TEM-13G S/N-10

INCONEL 718

Ta-10W/316 SS
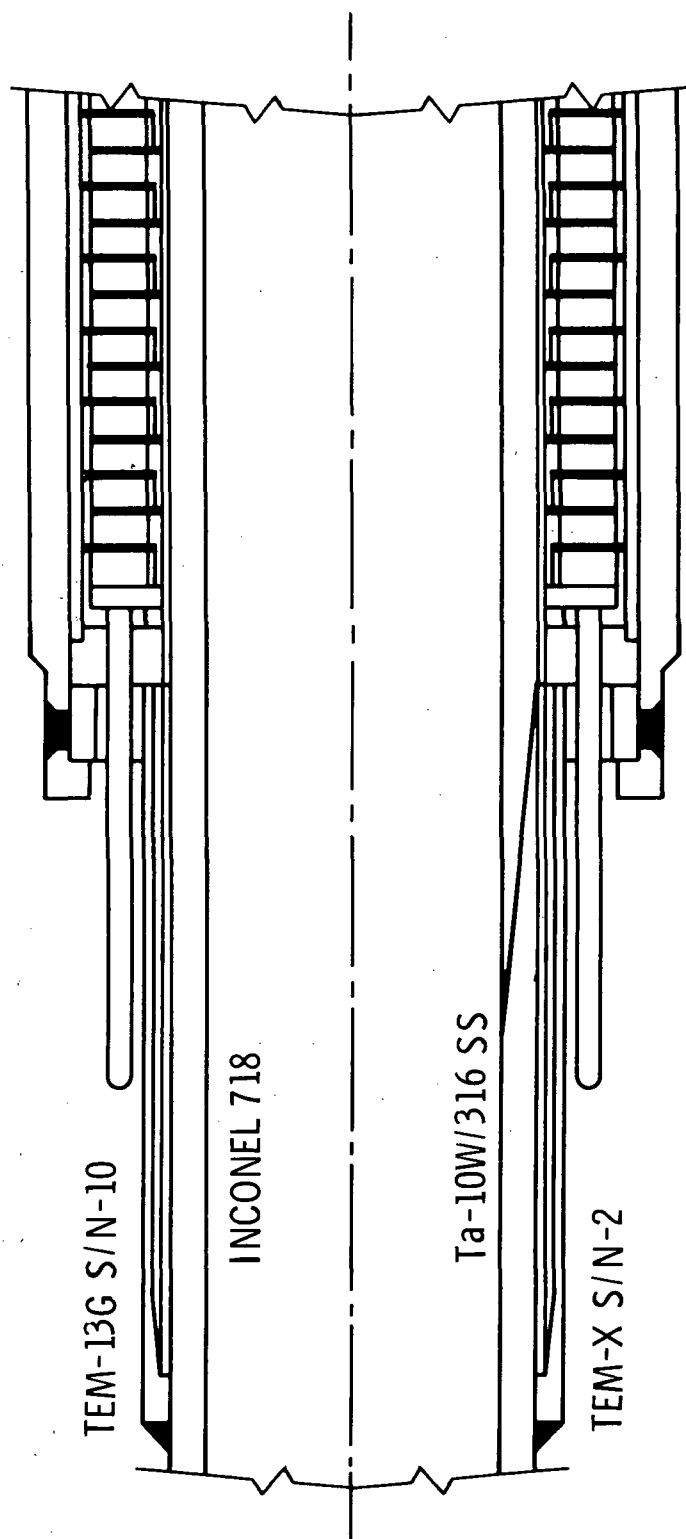
TEM-X S/N-2

Figure 1-41. Reactor Module Redesign for Circuit Stability

4. TEM-X S/N-2: Test Results

Effective Seebeck coefficient, internal resistance, and thermal impedance data recorded during heatup of TEM-X S/N-2, the first module fabricated with a refractory inner clad, are plotted as functions of average module temperature in Figures I-42 through I-44, respectively. Similar data recorded during heatup of TEM-13G S/N-10 are presented for comparison along with calculated curves for the TEM-X S/N-2 and TEM-13G designs. Note that the incorporation of the refractory clad has a noticeable effect on calculated and experimental data from these modules. Because of the higher thermal conductivity of Ta-10W, the voltage (hence effective Seebeck coefficient) of the TEM-X S/N-2 module is higher than that of the TEM-13G module, resulting in improved performance.

Experimental data from both modules can be seen to agree very well with the corresponding calculated curves over the entire temperature range. It is evident from the TEM-X S/N-2 data that proper compaction was achieved during autoclaving of the refractory clad module.

A cyclic test program was specified for TEM-X S/N-2 to determine the success of the clad substitution in reducing or eliminating circuit distortions observed in previous reactor-size (15 inch) modules. After a brief steady state operating period at the design operating conditions, $\overline{T}_H = 1125°F$ and $\overline{T}_C = 570°F$, the module was subjected to a series of 50 controlled thermal cycles. Each cycle consisted of a cooldown from design operating conditions to an intermediate $\overline{T}_H = 500°F$, a one hour steady state soak period, and a return to design operating conditions followed by another one hour soak. All transient operations were conducted at $\overline{T}_H$ ramp rates of 30°F/minute. This was a duplication of the TEM-13G S/N-10 test discussed in a previous section of this report. After a short steady state operating period following completion of thermal cycling tests, the module was removed from test for destructive examination.

Table I-10 presents a summary of performance data recorded during testing of TEM-X S/N-2. During cyclic operation of the module, data were recorded during the steady state soak period at $\overline{T}_H = 1125°F$ and $\overline{T}_C = 570°F$. The data show quite clearly that
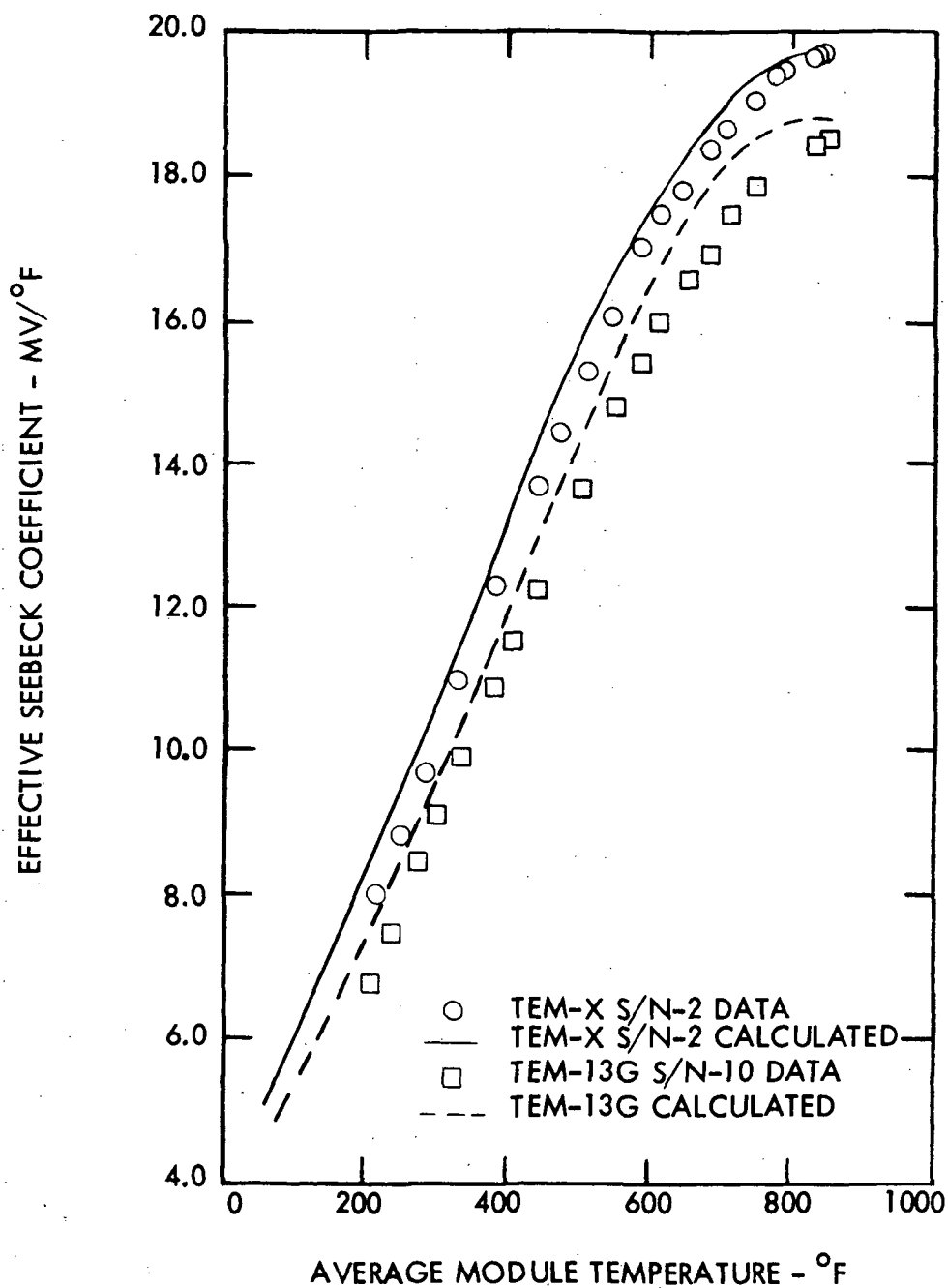
Figure I-42. A Comparison of Calculated and Experimental Effective Seebeck Coefficient
Data Recorded during Heatup of TEM-X S/N-2 and TEM-13G S/N-10
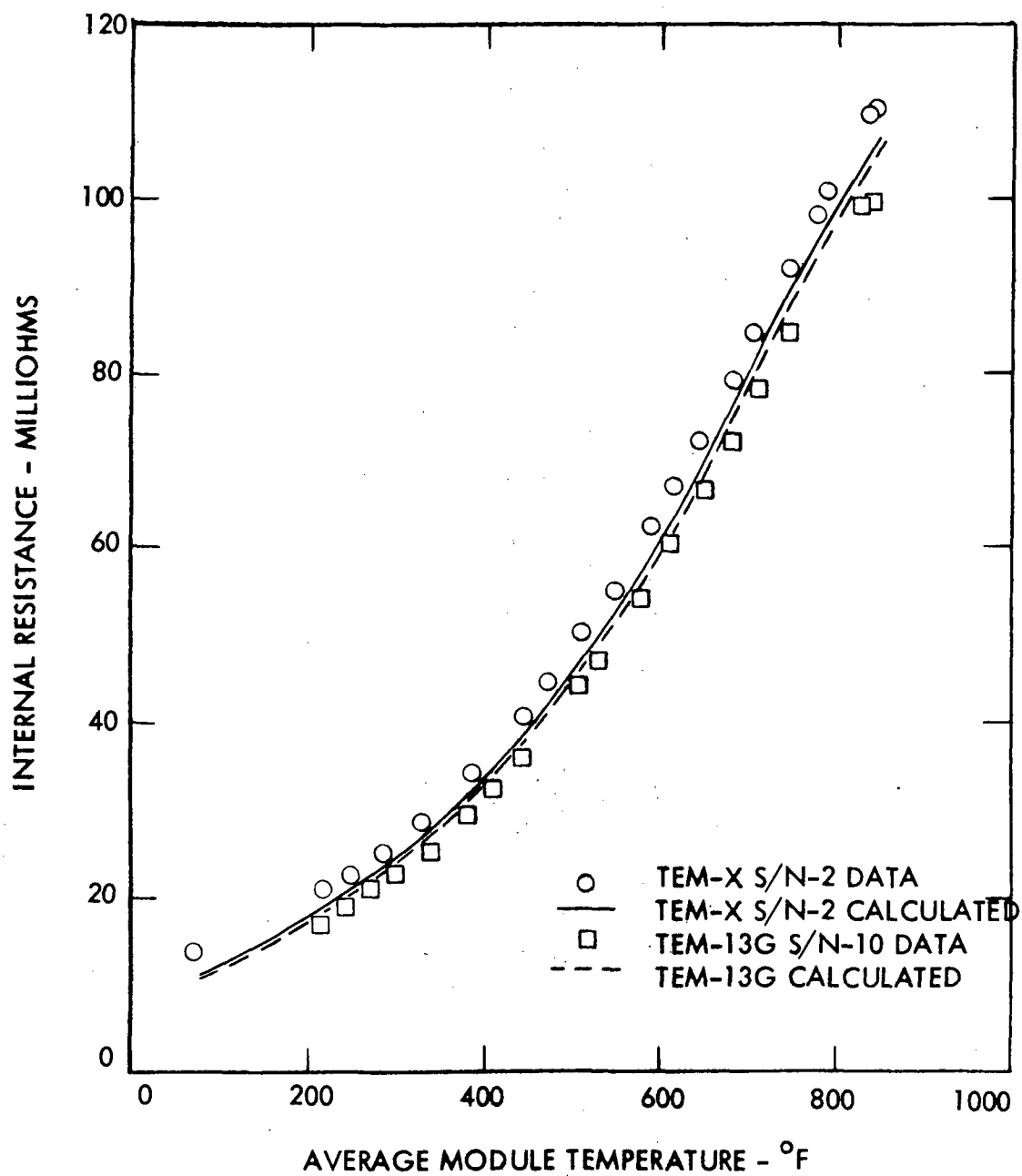
Figure I-43. A Comparison of Calculated and Experimental Internal Resistance
Data Recorded during Heatup of TEM-X S/N-2 and TEM-13G S/N-10
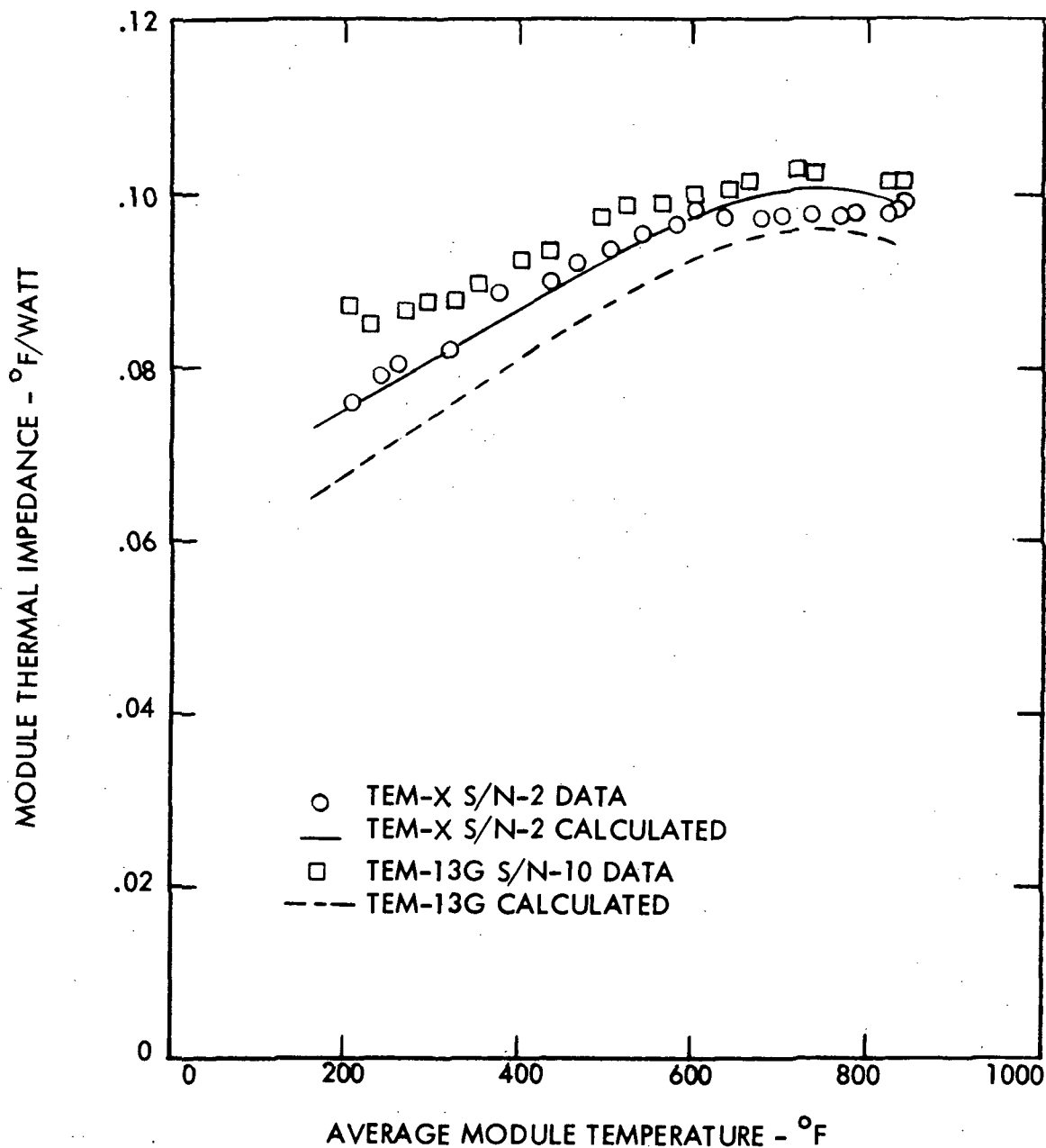
Figure I-44. A Comparison of Calculated and Experimental Thermal Impedance Data Recorded during Heatup of TEM-X S/N-2 and TEM-13G S/N-10

TABLE I-10

TEM-X S/N-2 DATA SUMMARY

Data Point No.	Hours	Total Cycles	P_e (Watts)	R_g (Milliohms)	V_{oc} (Volts)	Q_T (Watts)
1	0	0	272	110.8	10.99	5662
2	1	0	272	110.8	10.98	5665
3	19.2	0	272	110.8	10.98	5683
5	39.8	0	272	110.6	10.97	5676
6	43.3	1	272	110.5	10.97	5571
7	46.0	2	271	110.9	10.96	5572
8	64.0	8	273	110.5	10.99	5553
9	70.3	10	274	110.6	11.00	5608
10	88.0	16	270	110.5	10.93	5581
11	94.6	18	270	110.8	10.95	5576
12	112.3	24	271	110.3	10.94	5612
13	118.8	26	271	110.2	10.93	5568
14	137.1	32	271	110.6	10.94	5560
15	143.4	34	270	110.6	10.94	5549
17	167.8	42	270	110.5	10.92	5593
18	191.8	50	269	110.5	10.91	5594
19	192.7	50	270	110.6	10.92	5611
20	207.3	50	270	110.7	10.93	5610
21	214.5	50	270	110.4	10.92	5617
Calculated			276	107.8	10.92	5910

operation had no measureable effect on module performance. By contrast, TEM-13G S/N-10, subjected to identical cyclic operation, suffered a 21 watt decrease in power output during testing, shown previously in Table I-8. The success of the redesigned refractory inner clad concept is demonstrated by these data. This is more emphatically brought out in Figure I-45 which presents temperature and load adjusted electrical power output for these two modules as a function of the number of thermal cycles completed.

Upon completion of static testing, TEM-X S/N-2 was cooled from the design operating conditions to room temperature at a 30°F/min transient ramp rate. After completion of the cooldown procedure, a final measurement indicated a post testing room temperature module internal resistance of 11.4 milliohms. This level of internal resistance agreed well with both calculations and experimental data from the TEM-13G series modules. This agreement indicated that the substitution of Ta-10W for Inconel 718 resulted in no reduced interface pressures after cyclic operation.

5. TEM-X S/N-2: Destructive Examination Results

After completing the testing discussed above, TEM-X S/N-2 was removed from its static test stand and sectioned to expose the thermoelectric circuit. Figure I-46 is a photograph of TEM-X S/N-2 after sectioning. Also shown for comparison is a similar photograph of TEM-13G S/N-10 after sectioning. The success of the duplex clad is quite clear from a comparison of the two modules shown in the photograph.

The positive and negative ends of TEM-X S/N-2 were also examined to determine the extent of movement of the inner conductor rings with respect to the outer conductor rings. Results of these measurements indicated that a maximum displacement of .005 inch occurred at either end of the module. Maximum displacements exceeding .040 inch were measured during similar measurements made on TEM-13G S/N-10.

TEM-X S/N-2 experimental and destructive examination results gave conclusive proof that the reason for circuit distortion in previously tested reactor power modules was the mismatch between the thermal expansion of the inner and outer clads. Based on these results, the Ta-10W/316 SS bimetal inner clad was committed to use as a standard component in the reactor power modules.
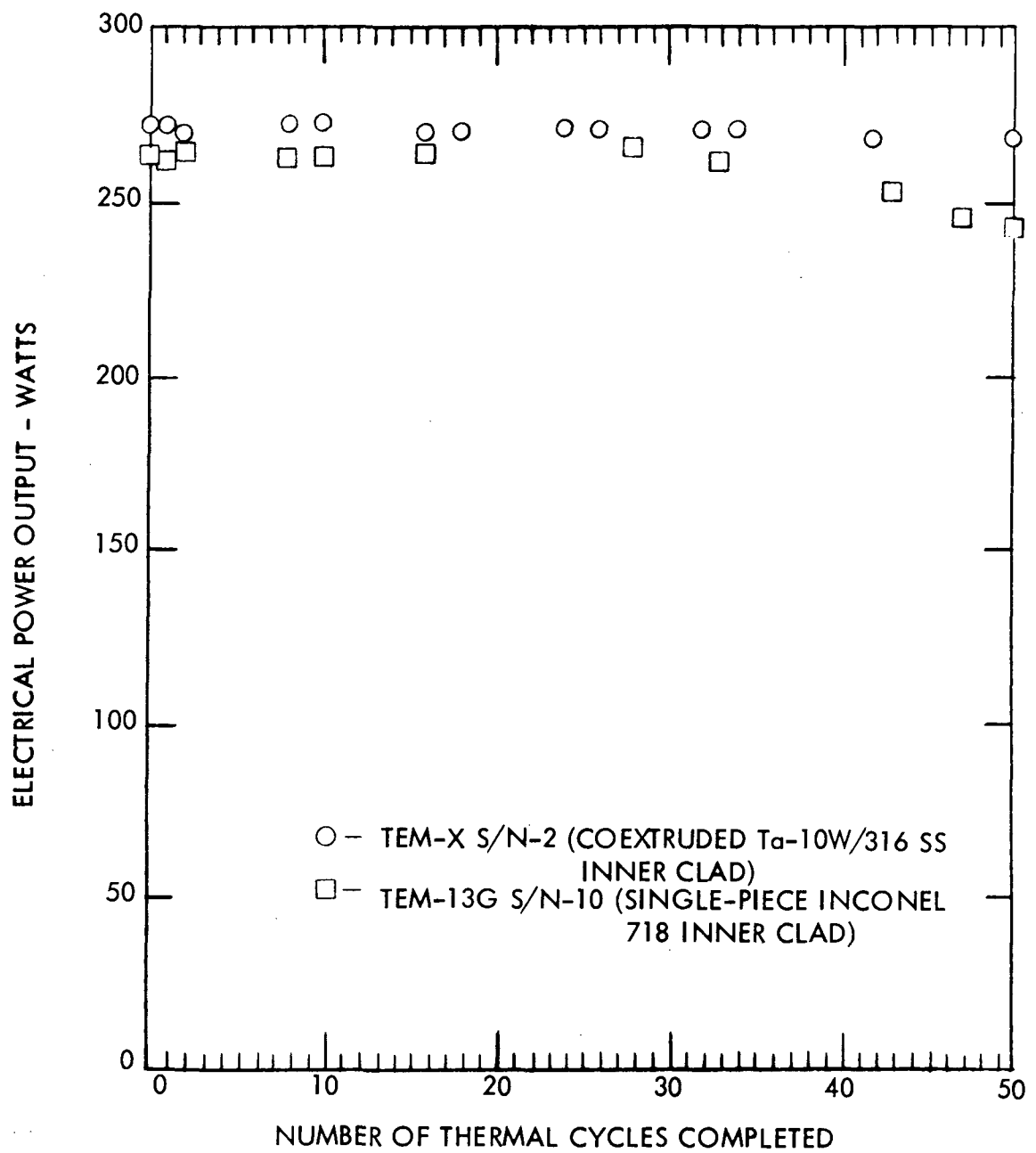
Figure I-45. A Comparison of Electrical Power Output Data as a Function of Thermal Cycles for TEM-X S/N-2 and TEM-13G S/N-2
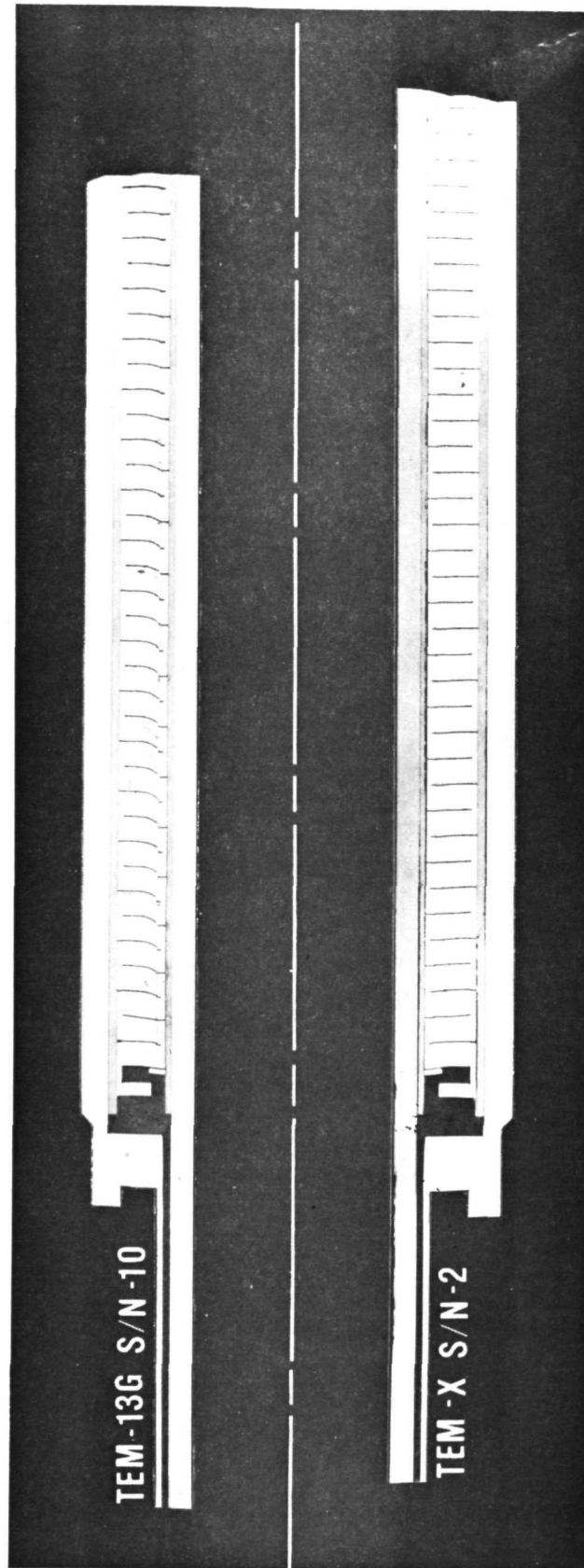
Figure I-46. A Comparison of Destructive Examination Photographs of Two Reactor Power Modules

J. TEM-X S/N-3 SERIES MODULES

1. Design Considerations

Continued system application studies of reactor/thermoelectric systems conducted by Atomics International led, in 1970, to a significant modification to earlier system conceptual designs. In the revised system the reactor power modules were to be removed from their earlier location in the shield gallery area of the spacecraft to an accessible service area beyond the shield. This modification required an intermediate primary heat exchanger but reduced electrical transmission (bus) losses by moving the generators physically closer to the load circuits, thus reducing bus lengths. As a result of this modification in overall system design, a new optimum operating voltage/power ratio was established by the systems contractor.

The TEM-X S/N-3 series modules were to be designed with overall dimensions identical to those of previous reactor modules. The axial dimensions of the circuit components, i.e., the number of couples, were to be selected such that the modules would have a matched load voltage-to-power ratio of ten volts per kilowatt for $\overline{T}_H = 1125^{\circ}F/\overline{T}_C = 570^{\circ}F$. This ratio limited individual electrical bus currents to 100 amps.

The circuit design of the TEM-X S/N-3 module was determined from a parametric study using TEMØD, the thermoelectric module performance prediction code. In this study the number of thermoelectric couples was varied while the total circuit length was held constant at 15 inches. In this manner the voltage to power ratio was varied.

Figure I-47 shows the calculated relationship between the voltage-to-power ratio and number of thermoelectric couples for a reactor module having TEM-13G radial dimensions, a 15 inch total circuit length, a refractory inner clad, and operating at $\overline{T}_H = 1125^{\circ}F$ and $\overline{T}_C = 570^{\circ}F$. In the range of interest (greater than 10 couples) the relationship can be seen to be nearly linear. This follows from the fact that in this range the voltage is directly proportional to the number of couples whereas the power output is very nearly constant. As the number of couples is reduced from ten, however, the power falls off rapidly (due to excessive Joule heating losses in the conductor rings and power take-off pins) whereas the voltage relationship remains linear. This is the cause of the rapid voltage-to-power ratio increase at
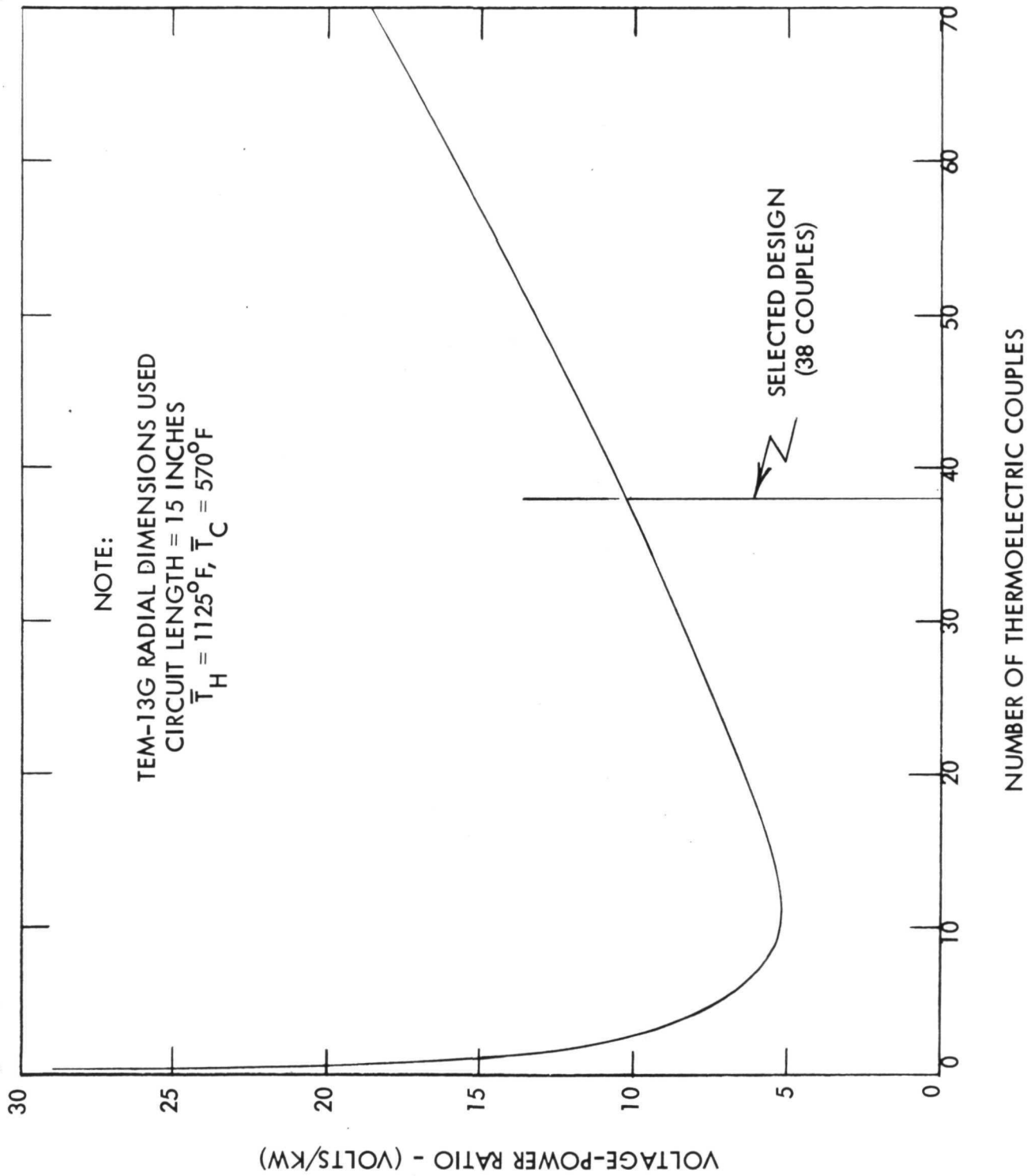
Figure I-47. Relationship between Voltage-To-Power Ratio and Number of Thermoelectric Couples for a TEM-X S/N-3 Module

the low end of the curve. However, this area of the curve was of no practical interest to this program and required no further investigation.

The study revealed that for $\overline{T}_H = 1125^{\circ}F$ and $\overline{T}_C = 570^{\circ}F$ operation, the required voltage-to-power ratio was achieved with a module having 38 rather than 78 couples. Figure I-48 presents a comparison of TEM-13G and TEM-X S/N-3 cross-sections. The following design modifications were incorporated in the TEM-X S/N-3 design:

a. A refractory inner clad, identical to that of TEM-X S/N-2, was in the TEM-X S/N-3 design as shown in Item 1 of Figure I-48 to eliminate component distortion observed during thermal cycling of TEM-3G series modules.

b. Thermoelectric washer axial thicknesses were approximately doubled (.188 inch compared to .091 inch) to meet the voltage-to-power system requirement.

c. The number of conductor pins (Item 2 in Figure I-48) was increased to 8 and their method of attachment to the internal collector ring of the module (Item 3 in Figure I-48) was modified in the TEM-X S/N-3 design. These modifications were required because the reduced number of thermoelectric couples in TEM-X S/N-3 reduced the electrical resistance of the circuit, which increased the significance of the conductor pin resistance. The radial dimensions of the module prohibited the use of larger diameter pins, therefore a larger number of pins was required. The TEM-X S/N-3 pins were threaded into the internal conductor rings to assure positive retention of the pins as shown in Figure I-48.

d. TEM-X S/N-3 incorporated two .005 inch mica insulators between adjacent thermoelectric washers rather than one (Item 4 in Figure I-48). This modification was based on extremely low degradation rates observed in TEM-14 series modules, discussed in Section II of this report, in which thicker inch insulating washers were used. Since thermoelectric washer axial thicknesses were essentially doubled in the TEM-X S/N-3 design, doubling the mica washer thicknesses did not result in a significant performance penalty.

TEM-13G
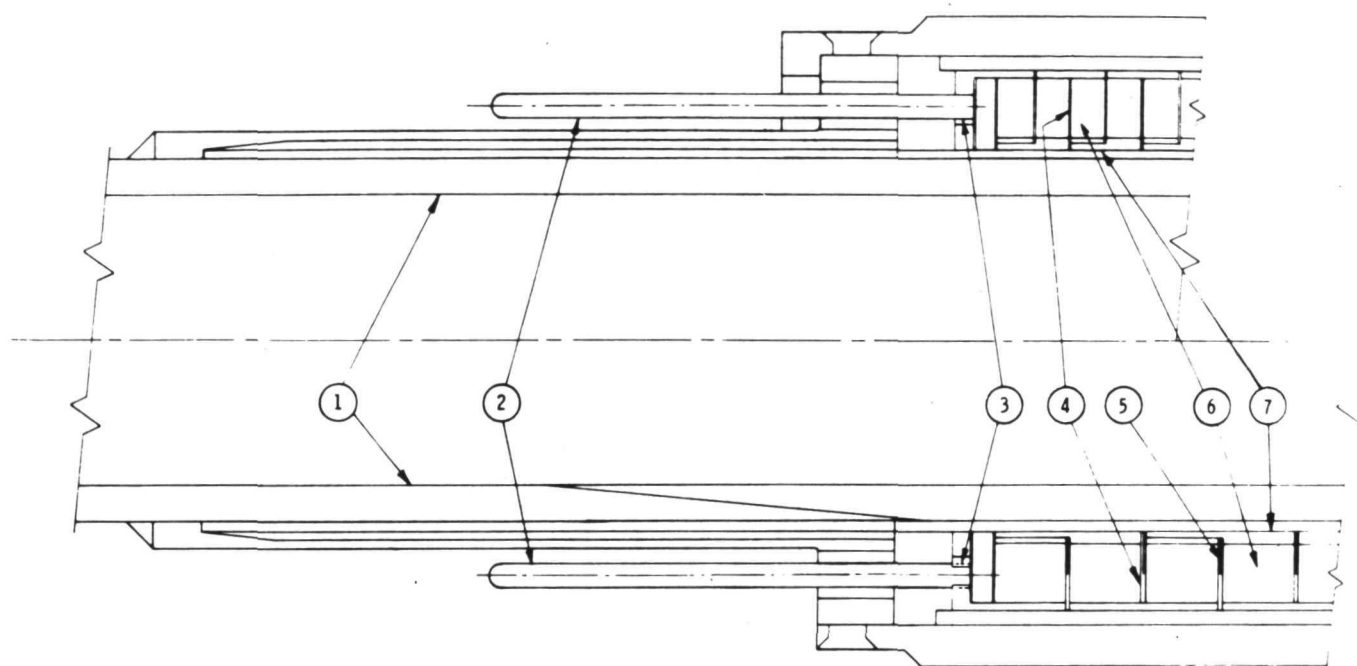
TEM-X S/N-3

		TEM-13G	TEM-X S/N-3
1.	INNER CLAD	INCONEL 718	DUPLEX Ta-10W/316 SS
2.	CONDUCTOR PINS	4 PER END	8 PER END
3.	CONDUCTOR PIN CONNECTION	PRESSED	THREADED
4.	MICA INSULATING WASHER	.005 THK.	.010 THK.
5.	BARRIER	-	.0004W FOIL
6.	LENGTH OF PbTe WASHER	.091	.188
7.	LENGTH OF CONDUCTOR RING	.187	.386
	NUMBER OF COUPLES	79	38

Figure I-48. A Comparison of TEM-13G and TEM-X S/N-3 Module Designs

e.   TEM-X S/N-3 was designed with 0.0004 inch tungsten foil washers extend-
ing radially outward from the couple hot junction (lead telluride/inner conductor
ring interface) to a point midway between the hot junction and cold junction
(lead telluride/outer conductor ring interface). The foil was "sandwiched" be-
tween the two 0.005 inch mica washers as shown in Item 5 of Figure I-48. The
foil provided an absolute diffusion barrier in the region most susceptible to inter-
couple contamination resulting from diffusion of tellurium through the mica in-
sulators. Shunt heat loss through the tungsten foil was reduced by minimizing
the foil axial length (0.0004 inch) and terminating the foil at the radial midpoint
of the thermoelectric washer. The selection of foil diameter was based on a review
of Seebeck probe data from module destructive examinations, which indicated
that diffusion does not occur below the temperature existing at the radial mid-
point of the thermoelectric washers in the TEM-X S/N-3 module.

2.   Initial TEM-X S/N-3 Series Module Results

A total of twelve TEM-X S/N-3 series modules were fabricated between mid-
1970 and January, 1973. A list of the design features of these modules, along with two addi-
tional reactor power modules fabricated with refractory inner clads, is presented in Table I-11.

Fabrication and processing of the first group of three TEM-X S/N-3 series modules
was completed in October, 1970. Post processing internal resistance data from these modules
agreed precisely with theoretical calculations made assuming negligible interface resistances,
indicating proper compaction had been achieved in the autoclave cycle.

The first of these three modules, TEM-X S/N-3, was destructively examined
immediately after processing to determine the effects of the processing cycle on circuit
alignment. The positive end of the module was cut, sectioned, and cast in epoxy. An axial
cut through the end section exposed the circuit for visual examination. Figure I-49 is a photo-
micrograph of the section from TEM-X S/N-3. No deformation of the circuit was noted.
Examination of the negative end showed the same results, i.e., excellent circuit/conductor
ring alignment.

TABLE I-11

DESIGN FEATURES OF TEM-X (REFRACTORY CLAD) MODULES

Serial No.	Length (in.)	No. Couples	Mica Thickness (in.)	Diffusion Barrier	Hermetic Seal	Objectives/Results
2	15	79	0.005	None	None	Demonstrated fix to cyclic distortion problem of TEM-13 Series Modules.
3	15	38	0.010	1/2 W foil	None	Pre-test destructive exam showed well-aligned circuit components.
3A	15	38	0.010	1/2 W foil	None	Development of clad leak demonstrated hermetic seal requirements.
3B	15	38	0.010	1/2 W foil	None	Duplicated TEM-X S/N-3A test.
3C	15	38	0.010	1/2 W foil	End Cap	Long term cyclic test at 1085°F/507°F
3D	15	38	0.010	1/2 W foil	End Cap	Long term cyclic test at 1085°F/507°F in liquid metal loop system.
3E	15	38	0.010	1/2 W foil	End Cap	Inner conductor insert lengths extended.
3F	15	38	0.010	1/2 W foil	End Cap	High temperature loop test module.
3G	15	38	0.010	1/2 W foil	Glass Seal	With 3H and 3J, determine effects of temperature on degradation rates.
3H	15	38	0.010	1/2 W foil	Glass Seal	Identical to 3G.
3J	15	38	0.010	1/2 W foil	Glass Seal	Identical to 3G.
3K	15	38	0.010	1/2 W foil	None	Loop test to simulate loss of hermetic seal during space operation.
3M	15	38	0.010	1/2 W foil	End Cap	Three-piece inner conductor eliminated GEnI/Mo interface. Low temperature/high pressure autoclave cycle incorporated.
4	15	74	0.010	None	Glass Seal	Determine effects of higher voltage design on degradation rates.
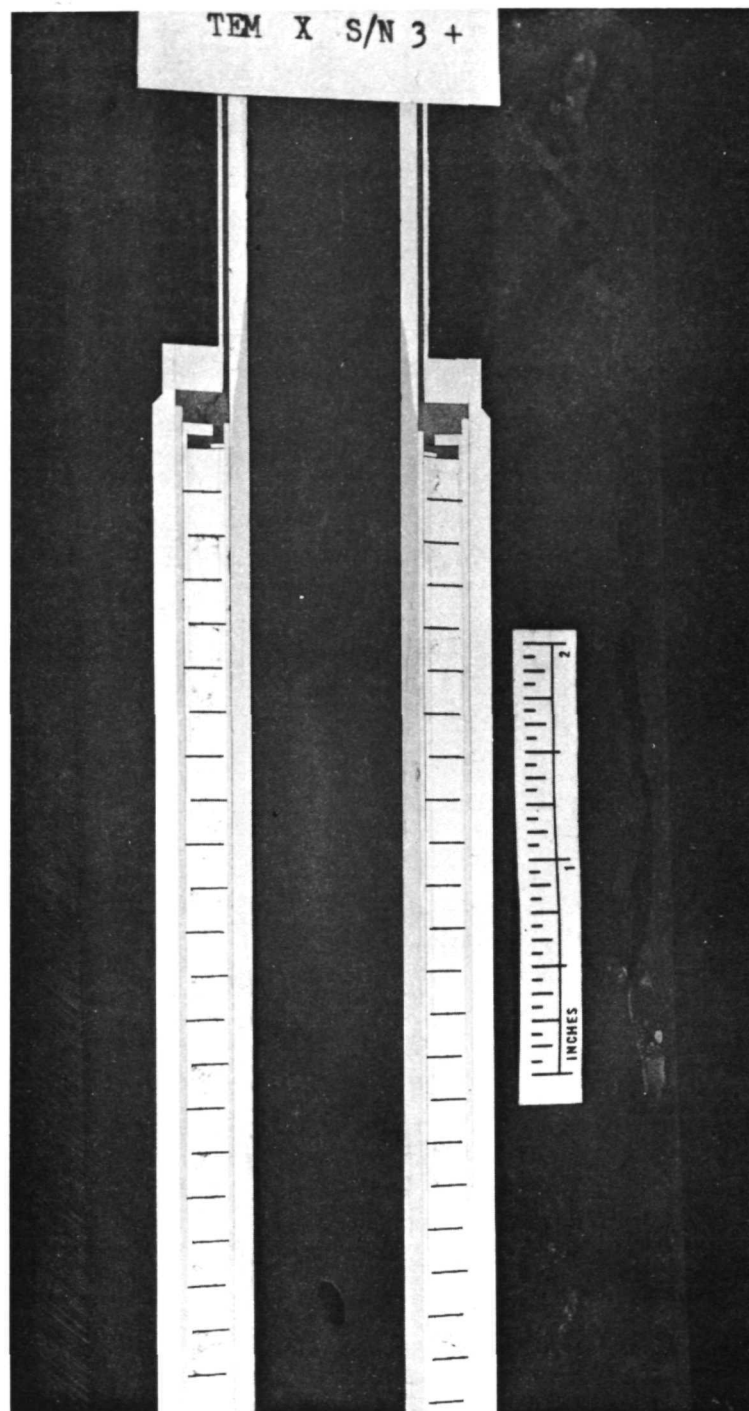
Figure I-49. Photomicrograph of Positive End Section of TEM-X S/N-3

The second and third TEM-X S/N-3 series modules, S/N-3A and S/N-3B, were scheduled for static testing at $\overline{T}_H = 1085°F/\overline{T}_C = 507°F$. The design operating temperatures were modified from the previous levels as a result of more recent system efforts conducted by Atomics International.

Table I-12 presents a comparison of the room temperature internal resistance and beginning-of-life performance data from these and all subsequent TEM-X S/N-3 series modules with the corresponding calculated values for $\overline{T}_H = 1085°F/\overline{T}_C = 507°F$ operation. The module-to-module performance reproducibility was very good for these and all other TEM-X S/N-3 series modules. In addition, the correlation of experimental data with the calculated parameters was considered good. Although the measured B.O.L. open circuit voltages of the first two modules placed on test were approximately 2 to 3 percent below the calculated level, Seebeck coefficient data on the thermoelectric materials used in these modules showed a similar deviation from standard values.

After a brief steady state operating period at the design operating conditions, $\overline{T}_H = 1085°F$ and $\overline{T}_C = 507°F$, TEM-X S/N-3A was subjected to a series of controlled thermal cycles. Each controlled cycle consisted of a cooldown from design operating conditions to an intermediate $\overline{T}_H = 500°F$, a one hour steady state soak period, and a return to design operation condition followed by another one hour soak. All transient operations were conducted at average hot clad temperature ramp rates of 30°F/minute in accordance with the module design specifications. In addition to 49 controlled thermal cycles, the module experienced one rapid shutdown as a result of a laboratory power failure. The power interruption occurred as the module was operating at the design conditions, resulting in a maximum cooldown temperature ramp rate of approximately 460°F/minute. Following the unscheduled shutdown, the module was returned to design operating conditions with a 30°F/minute heatup rate, and the controlled cyclic program continued.

TEM-X S/N-3A completed the thermal cyclic test with no measurable degradation in performance. Table I-13 presents a summary of performance data recorded before and after cyclic testing of TEM-X S/N-3A. Module power output measured at the design operating conditions of $\overline{T}_H = 1085°F$ and $\overline{T}_C = 507°F$ remained constant at 279 ± 3 watts. This

TABLE I-12

A COMPARISON OF CALCULATED AND EXPERIMENTAL BOL PERFORMANCE PARAMETERS FROM TEM-X S/N-3 SERIES MODULES

Module	Room Temperature R_g (Milliohms)		B.O.L $\bar{T}_H = 1085°F$, $\bar{T}_C = 507°F$					
	Circuit	Module	R_g Circuit (Milliohms)	R_g Module (Milliohms)	V_{oc} (Volts)	P_e (Watts)	Q_T (Watts)	η (Pct)
TEM-X S/N-3	2.7	*	**	**	**	**	**	**
TEM-X S/N-3A	2.7	3.0	23.7	24.9	5.24	276	5850	4.73
TEM-X S/N-3B	2.7	*	*	25.0	5.29	280	5930	4.72
TEM-X S/N-3C	2.7	*	*	25.1	5.44	294	6000	4.90
TEM-X S/N-3D (L)	2.7	3.2	*	25.0	5.52	304	5970	5.10
TEM-X S/N-3E	2.6	2.9	*	25.0	5.46	297	5980	4.98
TEM-X S/N-3F (L)	2.6	2.9	*	25.0	5.54	306	5860	5.23
TEM-X S/N-3G	2.8	3.2	*	24.4	5.35	293	6150	4.77
TEM-X S/N-3H	2.7	3.2	*	24.3	5.34	294	6220	4.71
TEM-X S/N-3J	2.7	3.2	*	24.6	5.38	294	6170	4.76
TEM-X S/N-3K (L)	2.6	3.5	*	25.6	5.55	301	5840	5.16
TEM-X S/N-3M	11.4	*	**	**	**	**	**	**
Calculated	2.7	3.0	23.7	24.9	5.40	292	6260	4.67

 * Not Measured
 ** Not Tested
 (L) Indicates Operation in a Liquid Metal Loop System

TABLE I-13

TEM-X S/N-3A DATA SUMMARY

Time (Hours)	P_e (Watts)	R_g (Milliohms)	V_{oc} (Volts)	Q_J (Watts)
0.0	276	24.86	5.24	5847
11.0	276	25.07	5.26	5830
36.7	278	24.63	5.24	5841
107.1	278	24.88	5.26	5814
109.1	279	24.74	5.25	5858
111.1	281	24.79	5.28	5872
FIFTY 30°F/MINUTE THERMAL CYCLES PERFORMED				
541.6	276	24.89	5.24	5834
613.0	276	25.02	5.26	5820
642.9	277	24.88	5.25	5831
685.1	277	24.86	5.25	5836
781.0	278	24.82	5.26	5857
833.2	277	24.91	5.25	5842
1002.6	278	24.82	5.26	5837
1045.9	278	24.87	5.26	5819
1166.4	277	25.10	5.28	5872

test was conducted to demonstrate the cyclic insensitivity of a module fabricated with a refractory inner clad in which total thermal expansion of the inner and outer clad are matched. The data show quite clearly that cyclic operation had no measurable effect on module performance. Similar results were achieved in a similar cyclic experiment performed on a previous reactor power module, TEM-X S/N-2, also designed with a refractory inner clad.

Figures I-50 through I-53 present performance parameters (overall efficiency, electrical power output, internal resistance, and open circuit voltage) recorded during testing of the first two TEM-X S/N-3 series modules. The data are plotted as functions of steady state testing time. TEM-X S/N-3B was a steady state test module which experienced only one thermal cycle as a result of a laboratory power failure. The data presented in these figures indicates both the high degree of reproducibility of performance between identical modules and the complete lack of measureable module degradation. No previous reactor power module, cycled or uncycled, had exhibited this degree of performance stability.

After completion of thermal cyclic testing and an additional 600 hours of steady state $\overline{T}_H = 1085^\circ F$ and $\overline{T}_C = 507^\circ F$ operation, TEM-X S/N-3A was cooled to room temperature to determine the cause of a sudden loss of the two uppermost cold clad thermocouples. Examination of the module revealed that liquid NaK had penetrated through the inner clad into the end closure region of the module. The NaK was used in static test stands to provide a uniform heat conduction path from the electrical heaters to the inner clad of the module as shown previously in Figure I-3. After penetrating the module inner clad, the NaK had attacked the boron nitride electrical pin insulators and escaped to the outside of the module, attacking the cold side thermocouples. At the time of the thermocouple failures, module performance data gave no indication that NaK had attacked the thermoelectric circuit.

Subsequently, TEM-X S/N-3A was removed from the static test stand and destructively examined to determine the cause of the NaK leak. During this examination, the source of the NaK leak was traced to cracked regions in the tantalum portion of the module inner clad, just inboard of the transition region. The cracks had developed in areas where the tantalum extended beyond the boron nitride insulating sleeve. Examination of the clad verified that the bonds had remained intact. Metallographic examination of the cracked
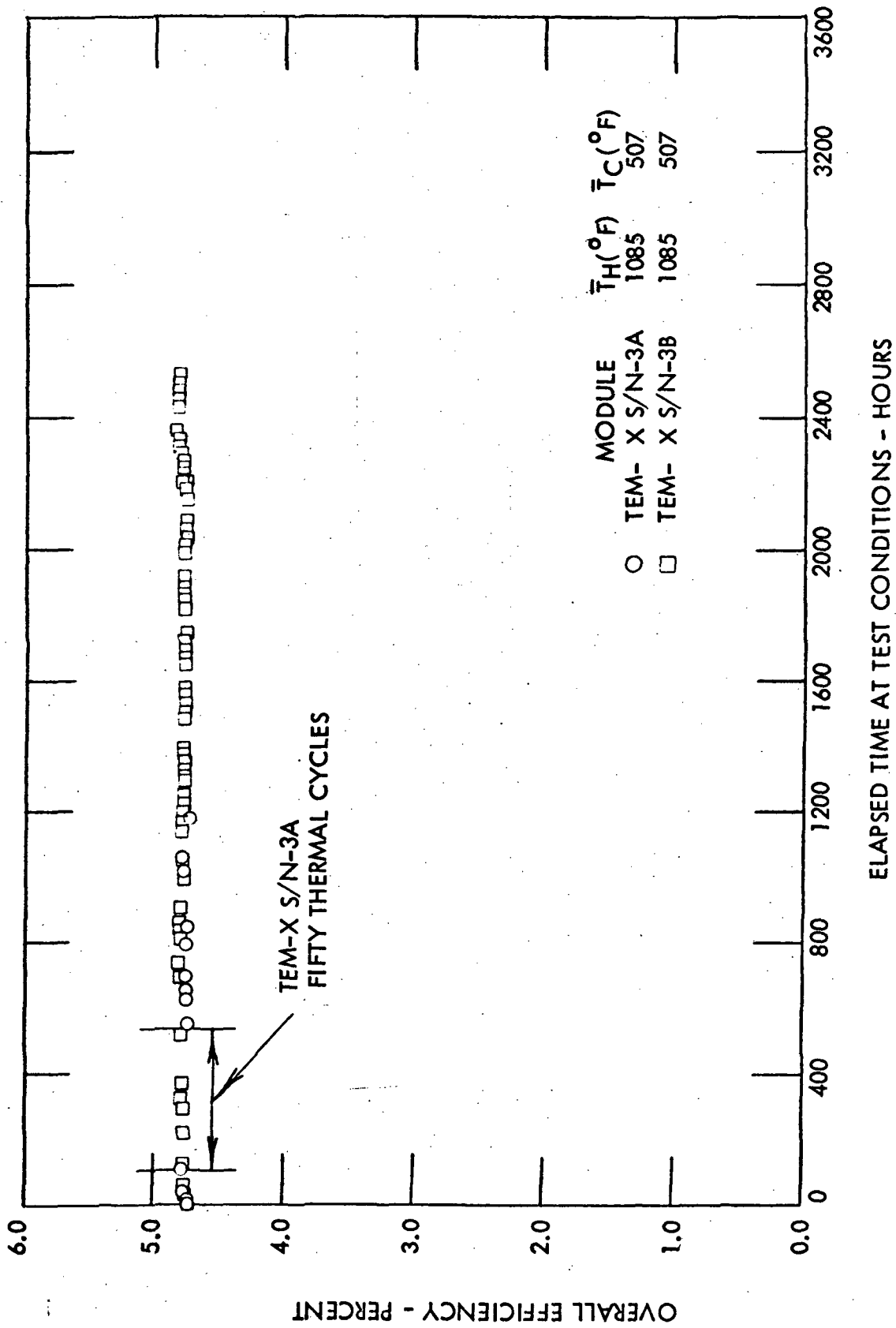
Figure I-50. Overall Efficiency Versus Elapsed Time for the First Two TEM-X S/N-3 Series Modules
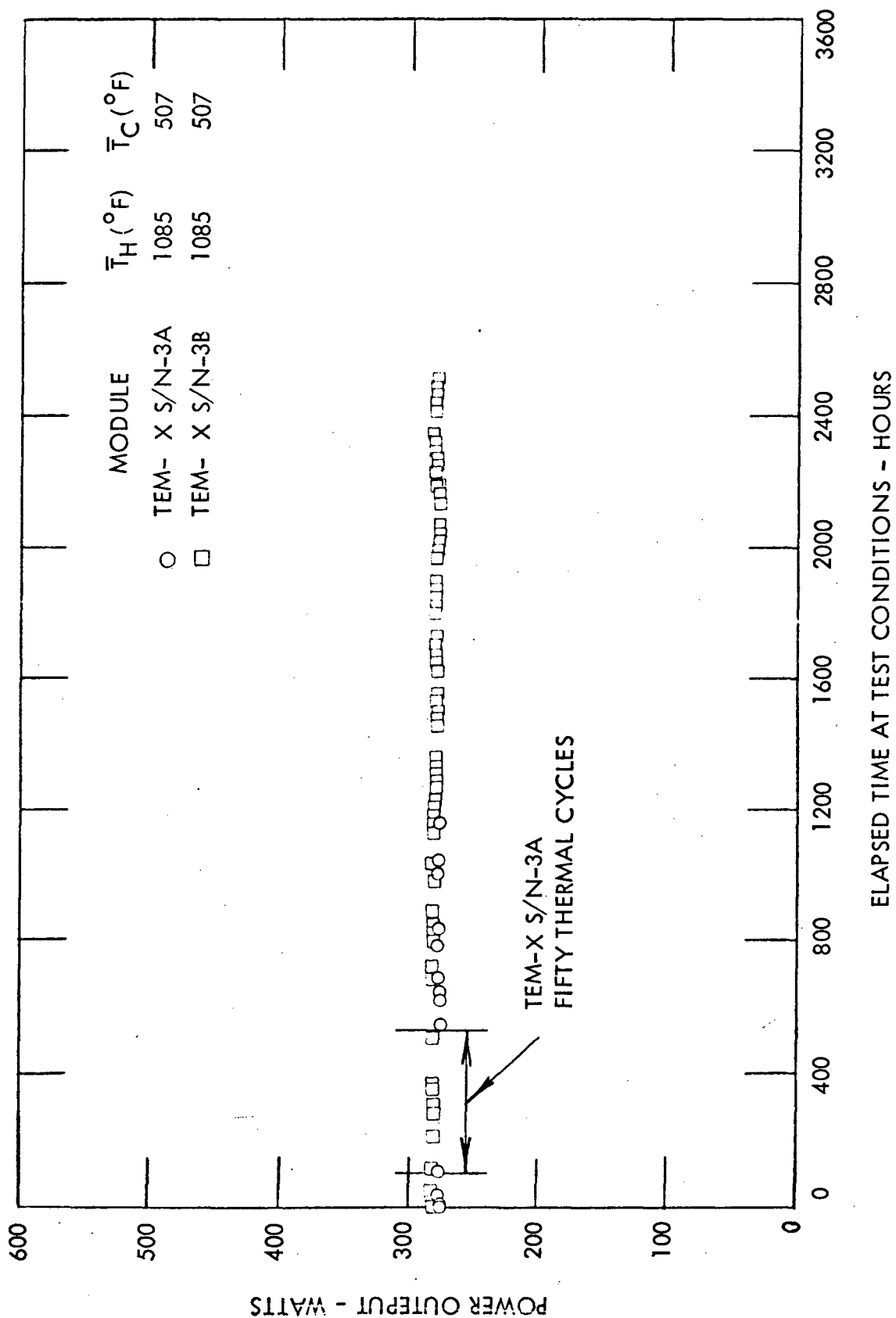
Figure I-51. Electrical Power Output Versus Elapsed Time for the First Two TFM-X S/N-3 Series Modules
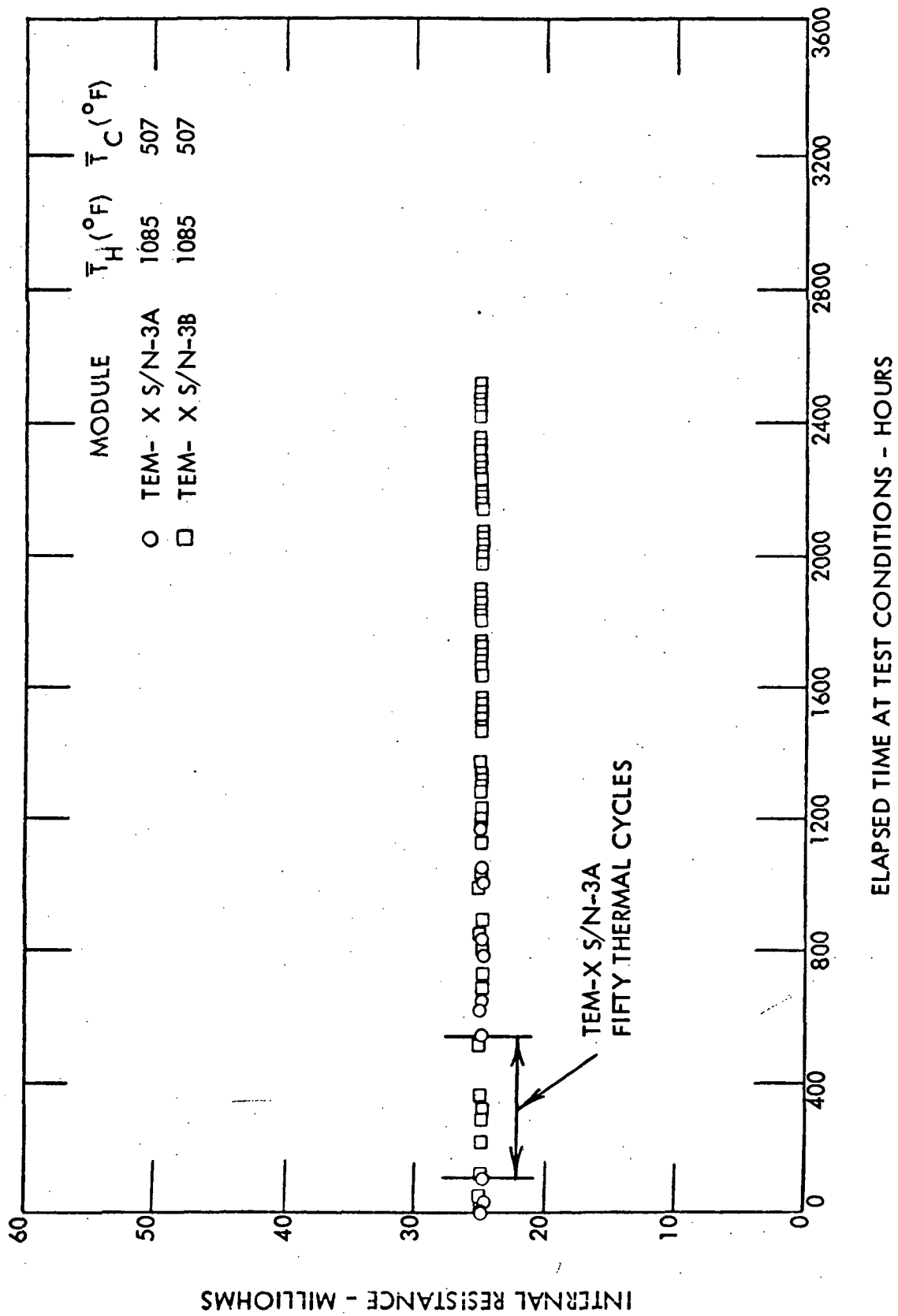
Figure 1-52. Internal Resistance Versus Elapsed Time for the First Two TEM-X S/N-3 Series Modules
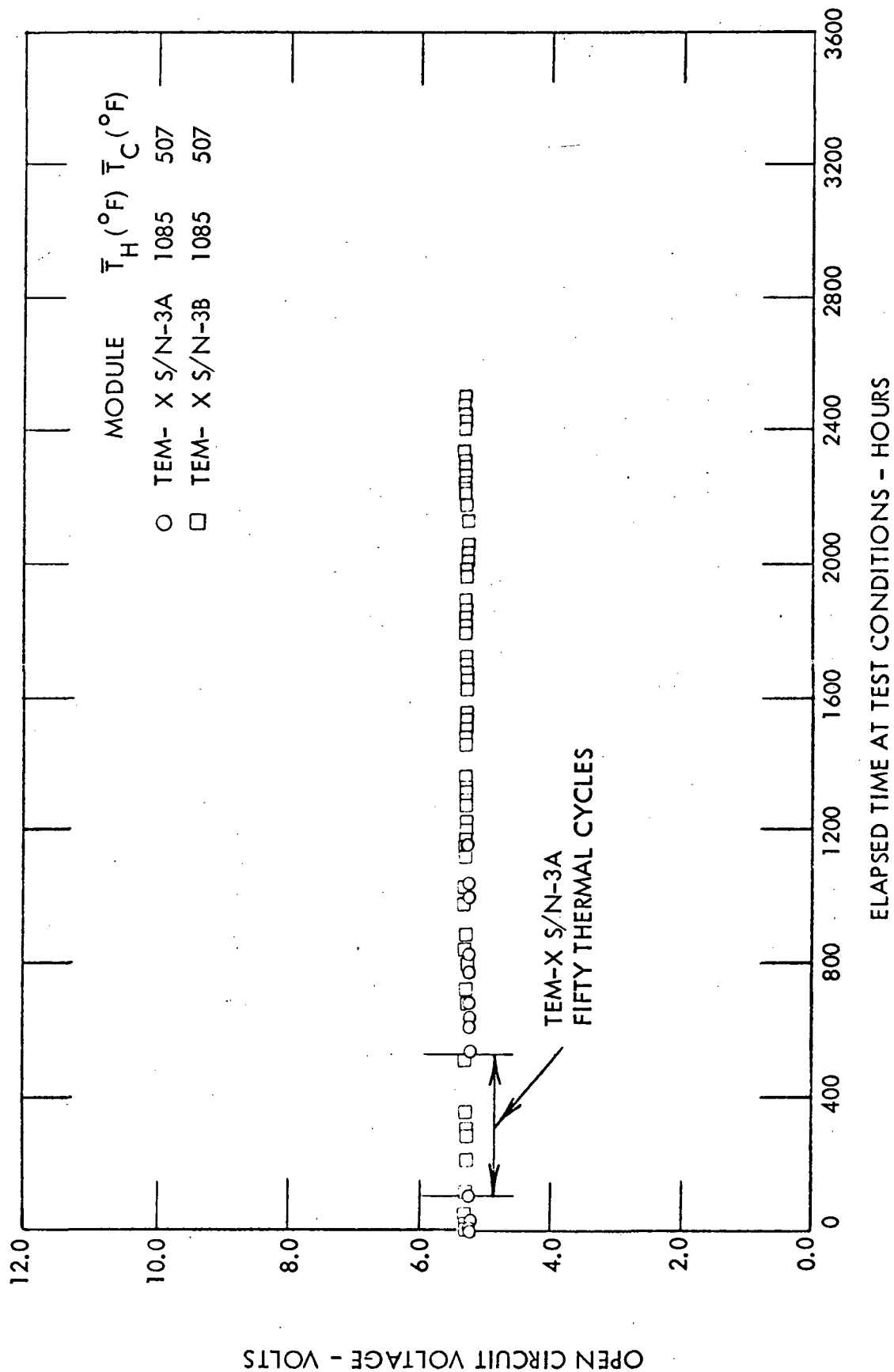
Figure I-53. Open Circuit Voltage Versus Elapsed Time for the First Two TEM-X S/N-3 Series Modules

region disclosed that the cracks were initiated at the outer diameter of the clad, i.e., the failure mode was not a result of NaK attack from the inner diameter. The negative end of the module, which was maintained at 1100°F during testing of the module (100°F higher than the positive end), was still intact. The preliminary analysis indicated that failure was caused by the development of an air leak where the power pins emerge through the BN insulators at the ends of the module. As a result, oxidation attack of the Ta-10W occurred and resulted in cracking of the clad.

A complete investigation was then conducted, using x-ray diffraction, metallography, oxygen analysis of starting stock and processed clads, and chemical analysis of the NaK used in testing. The results confirmed that oxidation of the Ta-10W had occurred and initiated cracks at the outer diameter of the inner clad. These cracks propagated radially inward and resulted in NaK leakage during test. Although in-leakage of air around the end closure power pin seals was strongly believed to be the source of oxygen, the fact that attack of the Ta-10W was confined to a region directly under the Alsimag 222 insulation raised a question concerning Ta-10W/Alsimag compatibility (although free energy considerations do not favor tantalum oxide formation at the expense of Alsimag reduction). However, to establish definitive proof of Alsimag/Ta-10W compatibility, four experimental capsules were designed, fabricated, processed and tested. A capsule consisted of an Alsimag 222 cylinder contained by a Ta-10W cup. This sub-assembly was enclosed in a stainless steel blind-ended sleeve, a plug was welded in the end, the capsule vacuum degassed at 725°F, and then the degassing tube was seal welded. The capsules were all hot isostatically compacted using the same parameters which are used for TEM modules.

After processing, three of the capsules were placed on test at 1200°F and one at 1100°F for times up to 1029 hours. Metallographic examination of these capsules showed no reaction had occurred at the Alsimag/Ta-10W interface. In all cases the Ta-10W was shiny and un-attacked, thus eliminating the possibility that the clad failure was due to an Alsimag/Ta-10W reaction.

While the above failure mechanism investigation was being conducted, the module circuit was sectioned and examined metallographically to check the effectiveness of the bimetal low expansion inner clad in preventing circuit geometry distortion during thermal cycling. As in the TEM-X S/N-2 proof-of-principle experiment, the alignment of circuit components and general geometric appearance of the circuit configuration was excellent; this furnished strong additional proof that the low expansion clad was the answer to obtaining degradation-free operation during thermal cycling.

Testing of TEM-X S/N-3B was terminated after 2584 hours, also as a result of a NaK leak in the inner clad. The loss of NaK resulted in a heater overtemperature and ultimate failure, terminating the test automatically. As in the case of TEM-X S/N-3A, performance data from this module were unaffected by the clad leak up to the time of the heater failure. This module was also destructively examined and results closely duplicated those of TEM-X S/N-3A, discussed above.

3. Hermetic Seal Design Modifications

Results of the initial TEM-X S/N-3 series module tests indicated that the module internals were not completely sealed. During operation in air, trace amounts of oxygen entered the module in the area of the boron nitride electrical pin insulators located at the ends of the module. In previous modules, this air leakage had little or no effect on module operation. However, the use of refractory inner clads in the TEM-X series modules required complete hermetic sealing to protect the clad and ensure successful operation in a laboratory (air) environment.

During the destructive examination of both TEM-X S/N-3A and 3B, it was observed that only those portions of the refractory clad extending beyond the boron nitride electrical insulating sleeve were oxidized. The boron nitride had protected the clad from in-leaking air. As a result of this observation, all newly designed refractory clad modules were fabricated with the boron nitride sleeve extended to ensure complete coverage of the refractory portion of the clad.

Astronuclear
Laboratory

An extensive effort was initiated to develop a direct hermetic seal which could be applied to the module electrical pins, their boron nitride insulators, and the stainless steel retaining ring through which the pins penetrate. Details of the development of the subsequent glass seal are discussed in a later section of this report.

As a temporary expedient to permit testing of additional TEM-X S/N-3 series refractory clad modules, hermetically sealed metal/ceramic end cap assemblies were designed. The static test end cap design, shown in Figure I-54, consisted of an end cap assembly, welded to both the inner and outer clads on each end of the module. Two ceramic/metal seal terminals were brazed to each cap and provided hermetically sealed access ports for two .150 inch diameter nickel power leads. After welding, as shown, the assembly was evacuated and back filled with argon at 7 ± 2 psig. Although the possibility of a leak was remote, further precautions were taken by providing a gas tube connected to a inert gas supply during testing of the module.

A similar protective end cap design was developed for loop tested modules. To eliminate interference between the end cap and shroud of the module required for loop test operation, a telescoping end cap was required. This modification allowed the cap to be slid over the module outer clad during welding of the power leads to the external collector ring located inside the end cap. The end cap was then returned to its final position and welded in three rather than two places.

4.   Performance of TEM-X Modules with End Caps

Four TEM-X S/N-3 series modules were tested using end cap assemblies discussed above. The first of these modules, S/N-3C, was placed on static test April 12, 1971. The other three modules, S/N-3D, 3E, and 3F which were essentially identical in design, followed TEM-X S/N-3C on test very closely.

Effective Seebeck coefficient, internal resistance, and thermal impedance data recorded during heatup of the two static tested modules are presented in Figures I-55 through I-57, respectively. These heatup tests were conducted under open circuit conditions and the calculated open circuit parameters are shown on the figures. The data from both modules can be seen to correlate very well with predictions over the entire temperature range.

POWER LEAD

BRAZE

CERAMIC TO
METAL SEAL

INERT GAS TUBE

BRAZE

ELECT. PIN

LEAK PATH

B. N. INSULATING
SLEEVE

RET. RING

DETAIL A

NaK BULB

10 PSIG ARGON GAS
SUPPLY

TUBULAR
MODULE

A
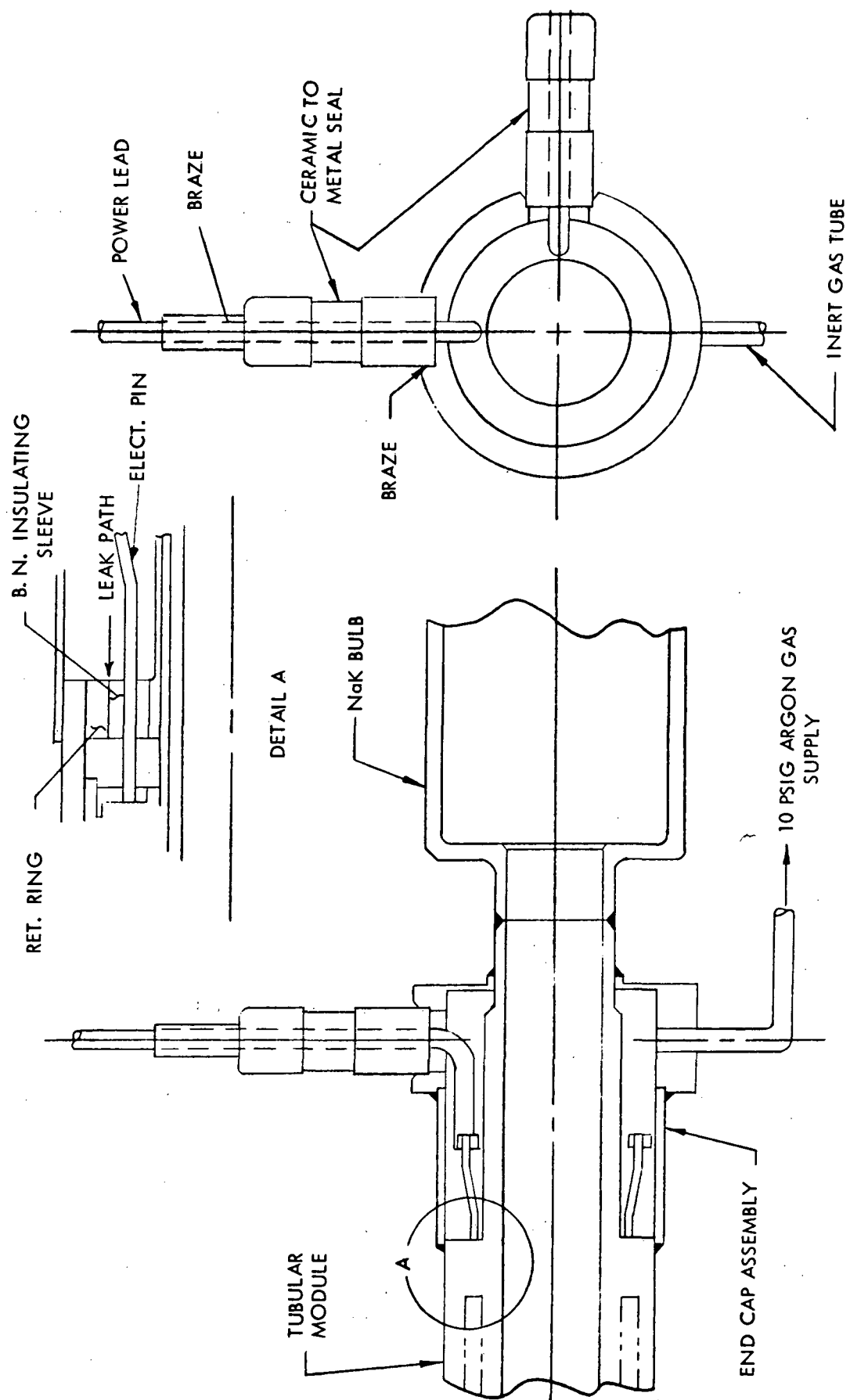
END CAP ASSEMBLY

Figure I-54. Protective End Cap Static Test Assembly
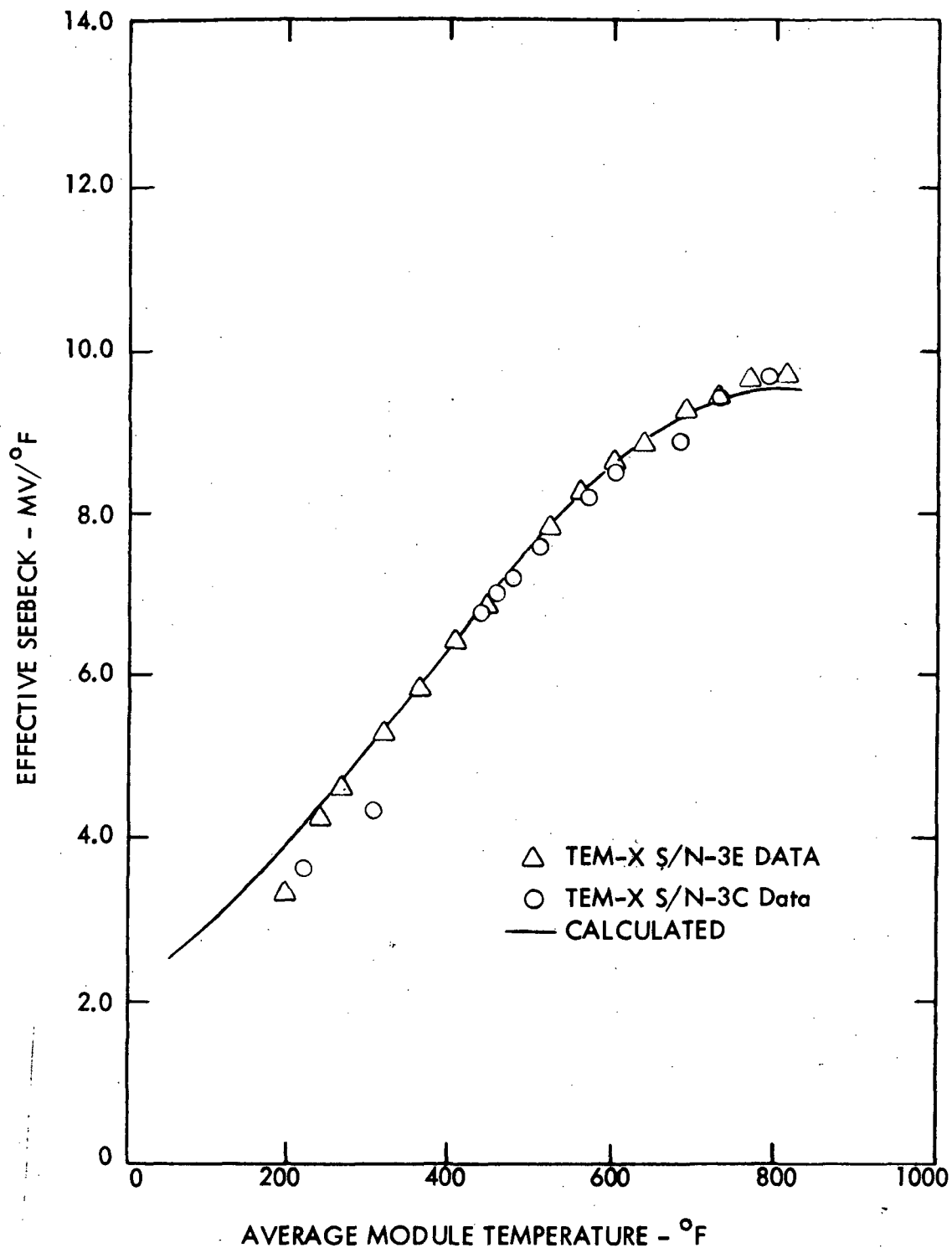
Figure 1-55. A Comparison of Calculated and Experimental Effective Seebeck Coefficient Data Recorded during Open Circuit Heatup of TEM-X Modules with End Caps
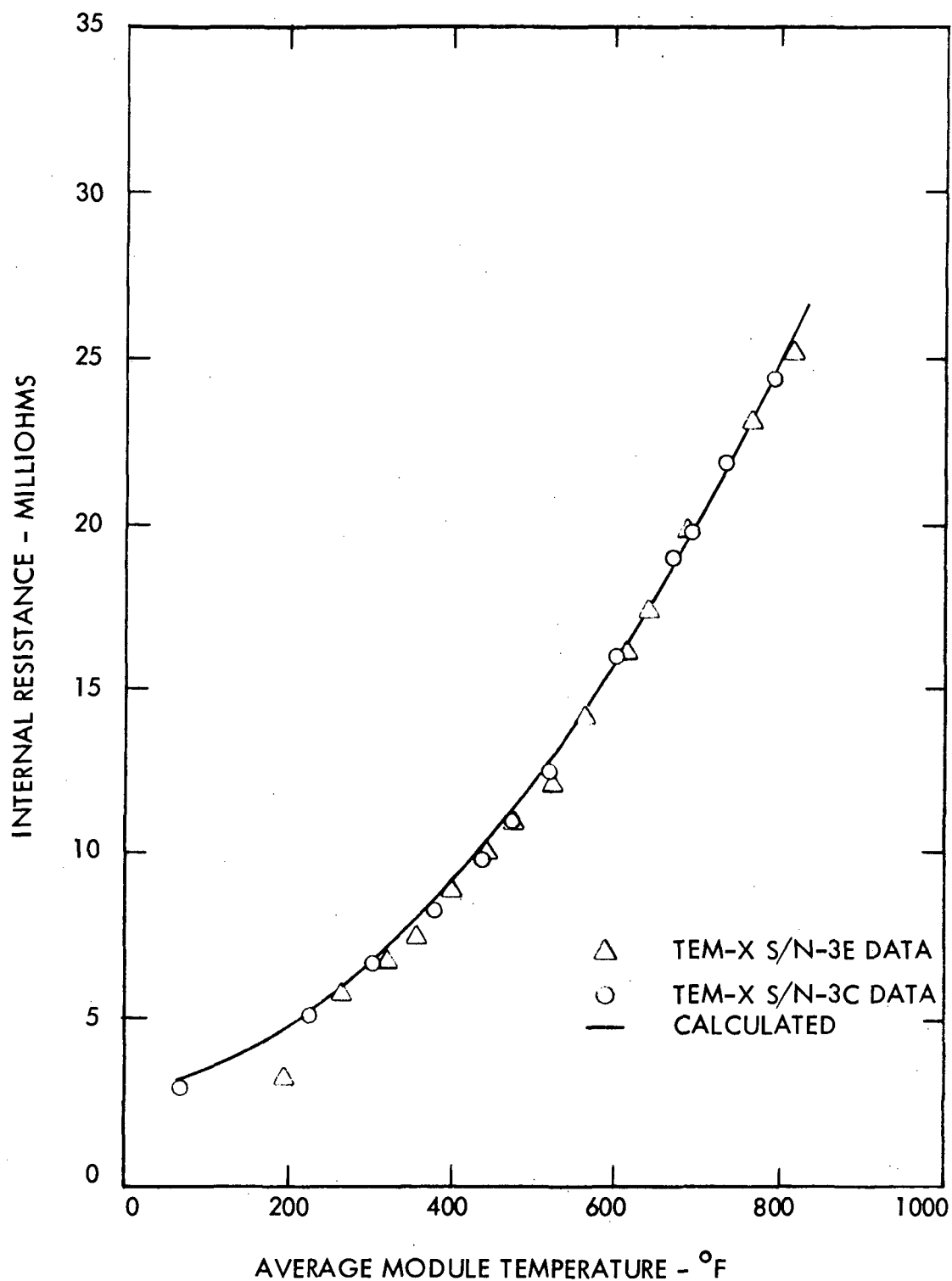
Figure 1-56. A Comparison of Calculated and Experimental Internal Resistance Data Recorded during Open Circuit Heatup of TEM-X Modules with End Caps
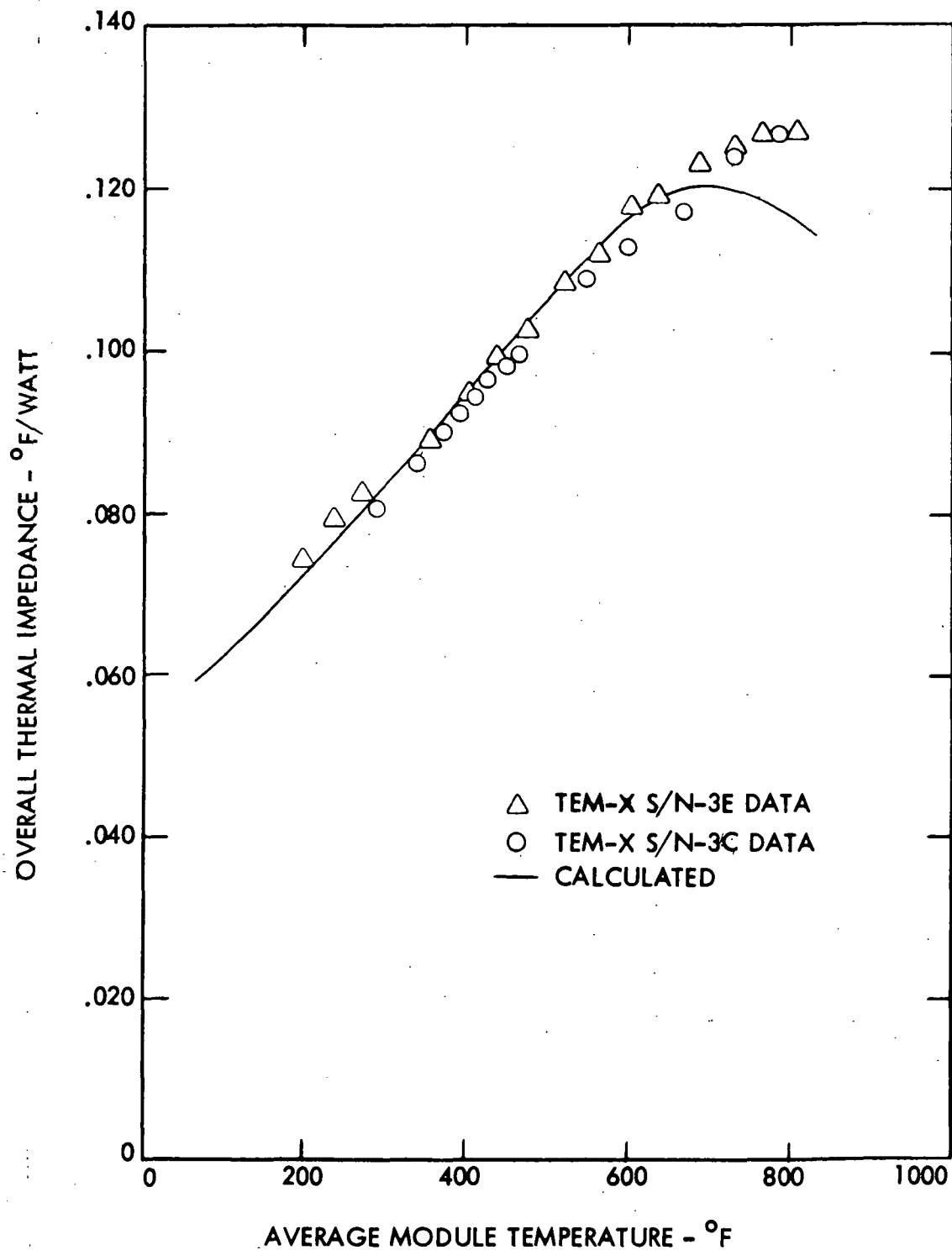
Figure I-57. A Comparison of Calculated and Experimental Thermal Impedance Data Recorded during Open Circuit Heatup of TEM-X Modules with End Caps

The internal resistance data and calculations shown in Figure I-56 do not include the resistance contribution of the end cap power leads shown in Figure I-54. This contribution was eliminated from the data by using one lead on each end of the module as a voltage probe and the other as a power lead. During subsequent matched load testing, however, the two power leads at each end of the module were connected in parallel so that each lead carried only one-half of the load current. During endurance tests the resistance contribution of the end cap power leads, which was substantial, was considered as part of the load resistance. For TEM-X S/N-3C, the pin circuit resistance was measured at 4.63 milliohms at operating conditions, whereas, the module circuit resistance was 25.2 milliohms. The high pin circuit resistance contribution was the primary reason for the effort to develop a directly applied hermetic seal that would eliminate the need for the end cap assemblies.

Some deviation was observed between the calculated and measured thermal impedance data near the design operating conditions (see Figure I-57). The calculated heat input was nearly 300 watts (approximately 5 percent) greater than the measured level. A similar deviation was observed in previous TEM-13 series reactor power modules. Since the deviation existed during open circuit operation, the possibility that the analytical module miscalculated thermoelectric effects such as Peltier heat pumping, was eliminated as a possible explanation for the descrepancy. These thermoelectric heat terms are only present when current flows through the circuit. The deviation was attributed to the use of higher than actual high temperature lead telluride conductivity data in the calculational model. Note that the correlation is quite good at the low temperature range as shown in Figure I-57.

TEM-X S/N-3D and 3F were tested in the liquid metal loop system at Atomics International. All of the modules tested using hermetic seal end caps were operated initially at $\overline{T}_H = 1085^\circ F / \overline{T}_C = 507^\circ F$ matched load conditions. Beginning-of-life performance of these modules is compared to that of all other TEM-X S/N-3 series modules in Table I-12. With the exception of the lower than calculated heat input data, all parameters agreed well with calculations. As discussed above, the resistance of the end cap power leads is included as part of the load resistance for all modules incorporating end caps.

Overall efficiency, electrical power output, open circuit voltage, and internal resistance life test data from this group of modules are presented as functions of testing time in Figures I-58 through I-61, respectively. These four modules had accrued operating times ranging from 9149 to 13,990 hours, and all were operated continuously from the time they were placed on test until the program termination notification was received. Both TEM-X S/N-3C and 3D were subjected to a series of 50 thermal cycles at the times indicated on figures. Subsequent performance data from these modules gave a positive indication that the use of a refractory inner clad provided a module design whose performance was completely insensitive to cyclic operation.

Although modules were normally maintained at matched load conditions and constant average clad temperatures during endurance testing, operating conditions for two modules were modified while the tests were in progress. TEM-X S/N-3E and S/N-3F test temperatures were raised to $\overline{T}_H = 1140°F/\overline{T}_C = 523°F$ after approximately 10,000 hours and 1,000 hours of operation, respectively, at the initial levels of $\overline{T}_H = 1085°F/\overline{T}_C = 507°F$. The time of the modification of test conditions is indicated on Figures I-58 through I-61. These changes in operating conditions simulated the effects of increasing the reactor outlet temperature in a reactor/thermoelectric space power system having a fixed radiator. Data presented in Figures I-58 through I-61 indicate that both modules responded to the test change in a very similar manner. The observed performance level changes were in very good agreement with calculations. In addition, these data indicate the excellent degree of performance stability and reproducibility exhibited by this group of refractory clad reactor power modules.

A statistical analysis (linear curve fit) of all life test data from this group of TEM-X S/N-3 series modules is presented in Table I-14, along with similar data from all other refractory clad modules tested. This analysis was completed by fitting a straight line to the data presented in Figures I-58 through I-61 for each module using the standard least squares technique. The degradation rates were determined by dividing the slope of each line (rate of change) by the y-intercept (beginning-of-life value). Also, shown in the table are similar degradation rate data from all subsequent modules fabricated with refractory inner clads. For modules operated at $\overline{T}_H = 1085°F/\overline{T}_C = 507°F$ operating conditions, power output degradation rates ranged from 1.0 to 4.4 percent per 10,000 of operation. It is significant
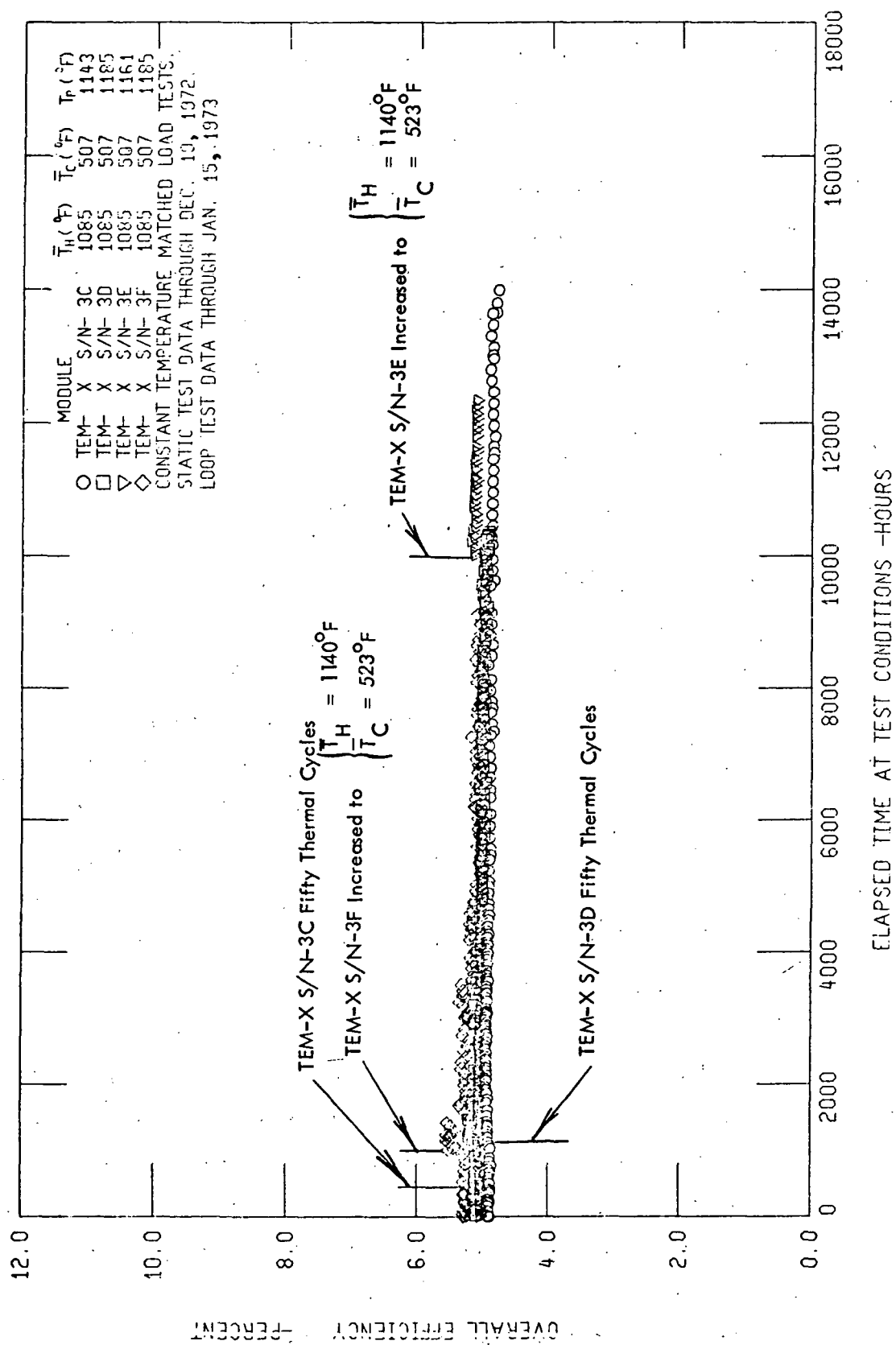
Figure I-58. Overall Efficiency Versus Elapsed Time for Reactor Power Modules Incorporating End Caps
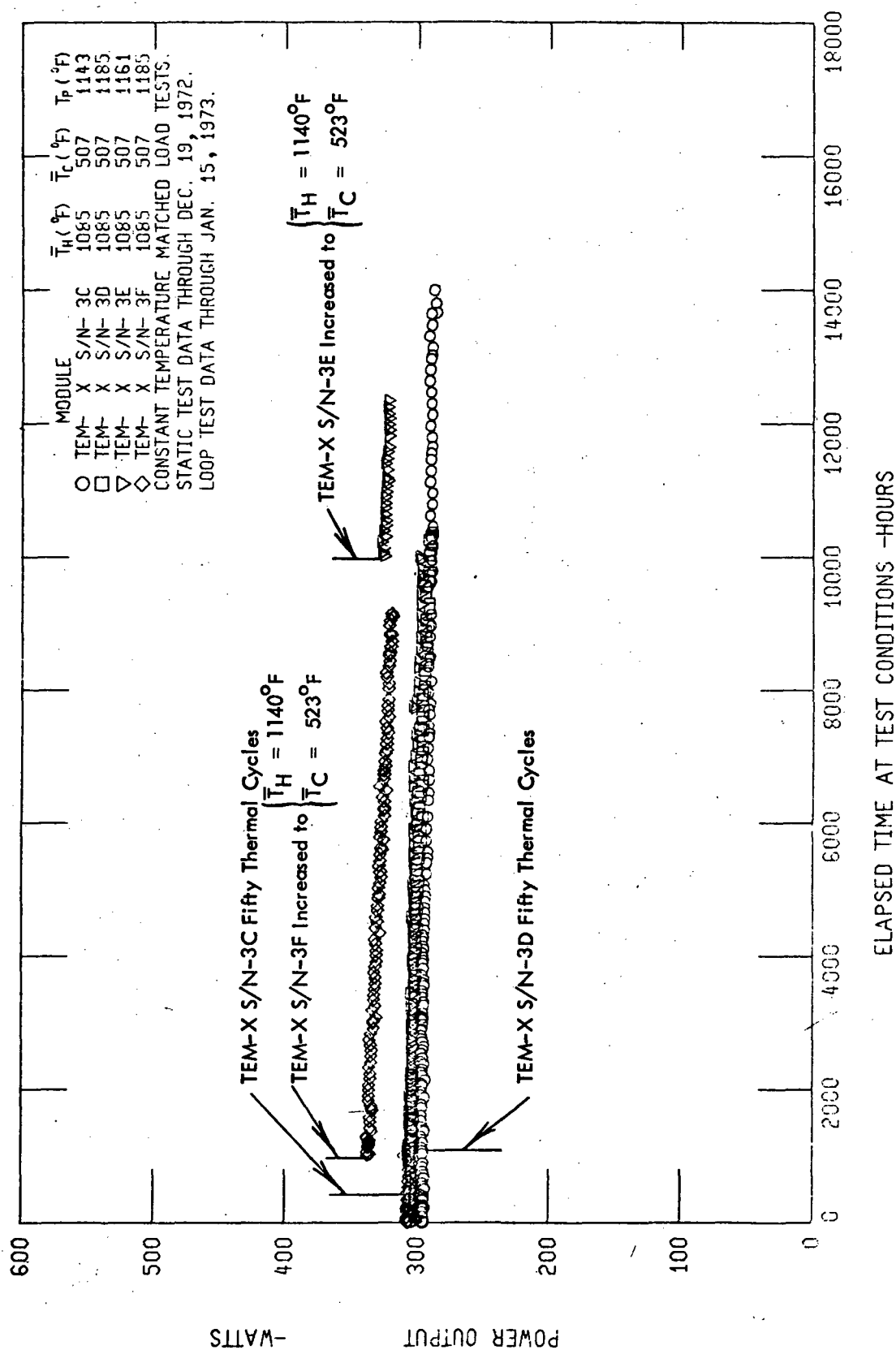
Figure I-59. Power Output Versus Elapsed Time for Reactor Power Modules Incorporating End Caps
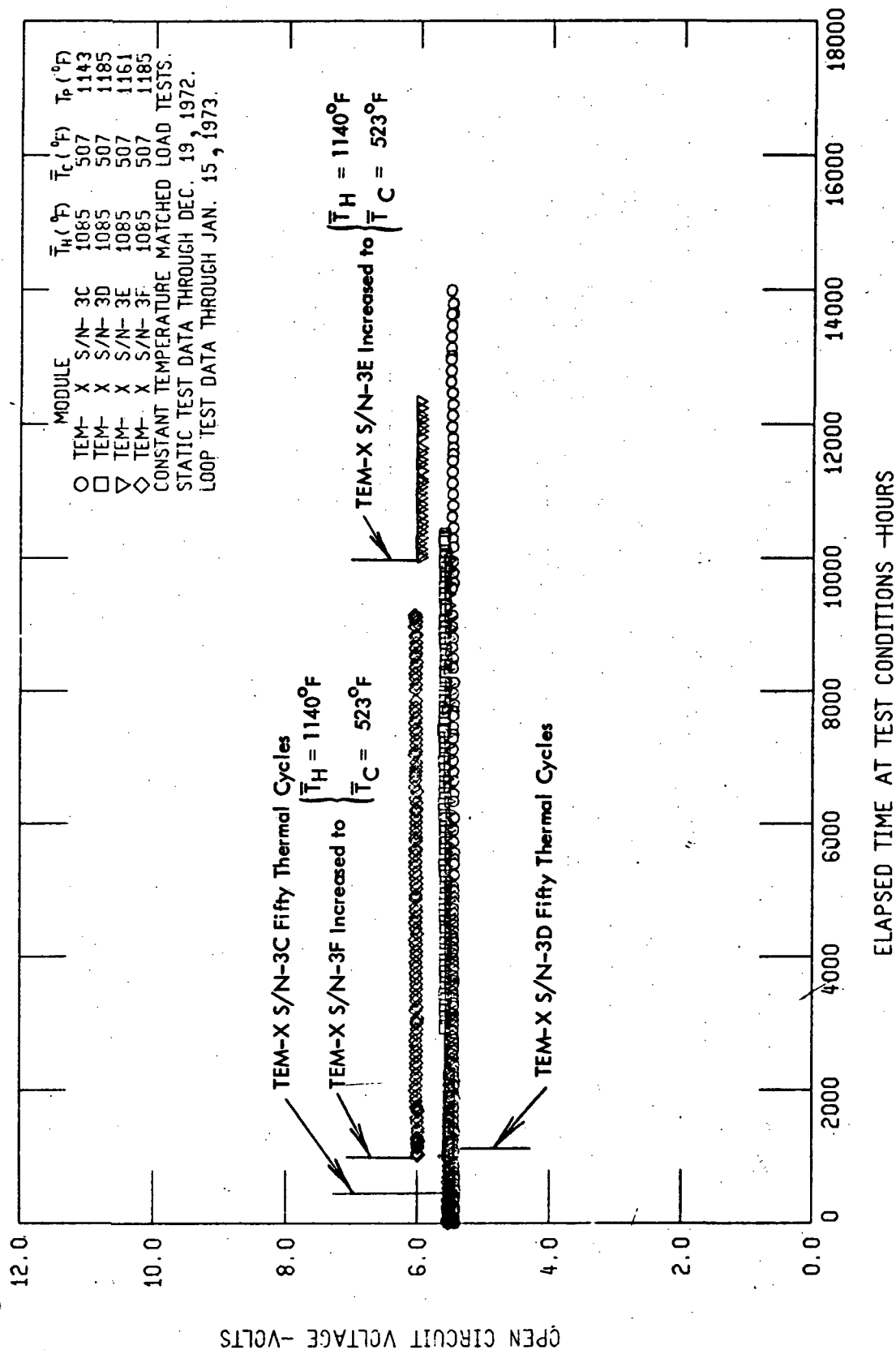
Figure I-60. Open Circuit Voltage Versus Elapsed Time for Reactor Power Modules Incorporating End Caps
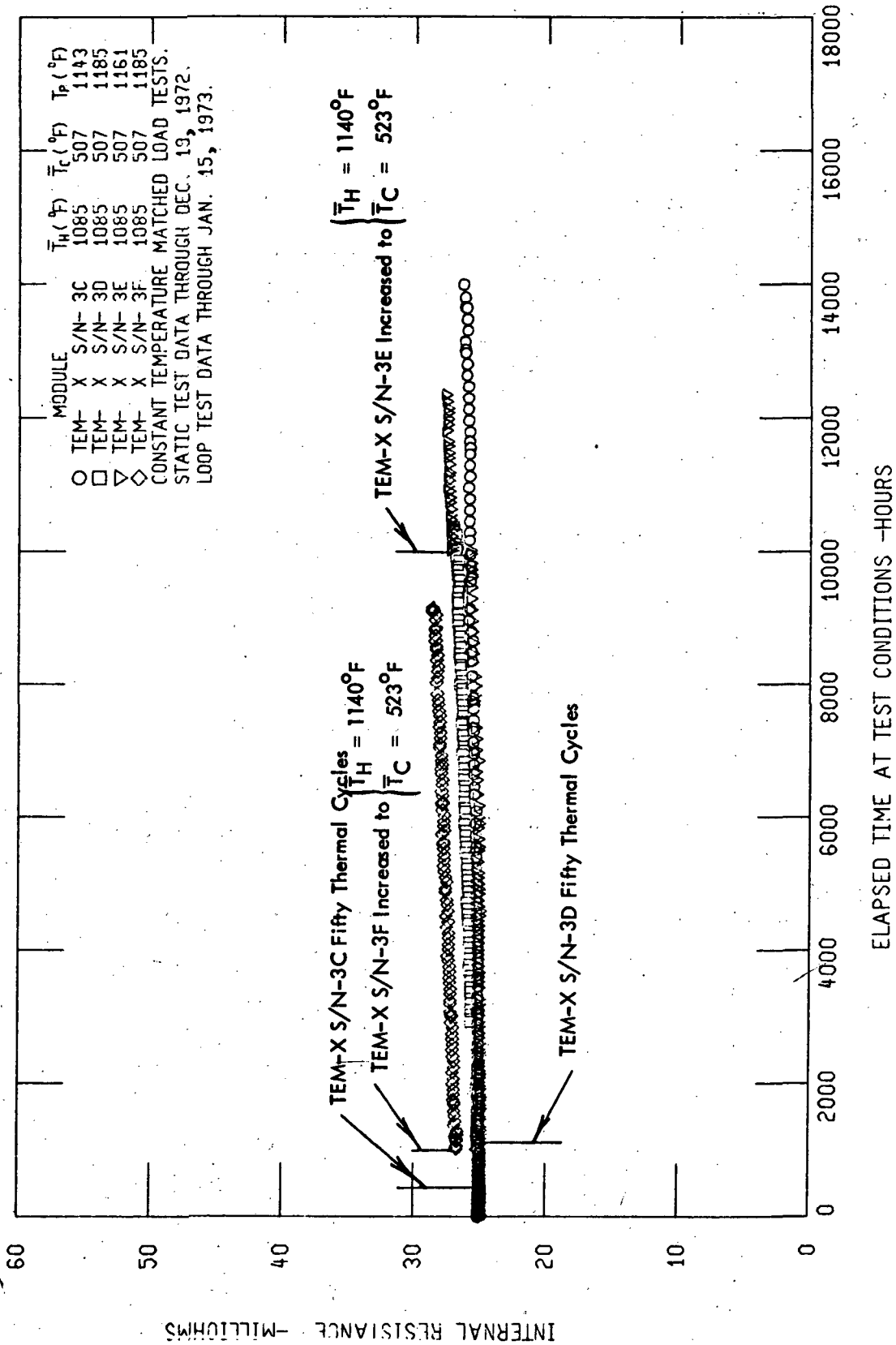
Figure I-61. Internal Resistance Versus Elapsed Time for Reactor Power Modules Incorporating End Caps

TABLE I-14

REFRACTORY CLAD REACTOR MODULE PERFORMANCE STABILITY SUMMARY

Module	$\bar{T}_H/\bar{T}_C(°F)$	Testing Time (Hours)	Rate of Change: % Per 10,000 Hours			Thermal Cycles	
			R_g	P_e	η	Rapid	30°F/min.
TEM-X S/N-2	1125/570-S	216	*	*	*	50	0
TEM-X S/N-3A	1085/507-S	1,166	4.0	-1.9	-2.0	49	1
TEM-X S/N-3B	1085/507-S	2,584	2.8	-2.5	3.0	0	2
TEM-X S/N-3C	1085/507-S	13,990	3.5	-1.7	-0.8	7	53
TEM-X S/N-3D	1085/507-L	10,357	6.4	-4.4	-4.1	10	53
TEM-X S/N-3E	1085/507-S	10,007	3.9	-2.3	-1.3	6	0
	1140/523-S	2,333	6.1	-5.6	-3.1		
TEM-X S/N-3F	1085/507-L	1,011	6.0	-1.0	+4.1	8	2
	1140/523-L	8,138	8.6	-6.1	-6.5		
TEM-X S/N-3G	1085/507-S	4,960	6.4	-1.4	-0.8	3	1
TEM-X S/N-3H	1140/523-S	4,727	7.7	-3.5	-0.8	1	2
TEM-X S/N-3J	1175/535-S	3,504	8.8	-5.1	-4.9	9	1
TEM-X S/N-3K	1085/507L	1,122	*	*	*	1	0
TEM-X S/N-4	1085/507-S	1,433	10.1	-1.6	+1.3	1	0

L   Indicates Loop Test (All test data through January 15, 1973).

S   Indicates Static Test (All test data through December 18, 1972).

*   Insufficient data to allow meaningful performance analysis.

to note that the module with the highest degradation rate, TEM-X S/N-3D, was operated for 25 hours at an average hot clad temperature of 1175°F, 90°F above the prescribed operating conditions as a result of a thermocouple reading error. Since modules tend to exhibit degradation rates consistant with the highest temperatures to which they have been exposed, this is the most likely explanation for the relatively high TEM-X S/N-3D degradation. It is quite obvious, however, that with degradation rates as low as these, it is very difficult to separate real performance variations from random experimental uncertainties.

Also, listed in Table I-14 is a summary of the cyclic test histories of the TEM-X series modules. Thermal cycles are classified in the table as being either "rapid" or 30°F/min. Rapid cycles include all cycles resulting from unscheduled shutdowns due to laboratory power failures or instrumentation malfunctions. All of these conditions resulted in shutdown temperature ramp rates that exceeded the 30°F/min. specification. All of the 30°F/min. cycles were conducted under controlled conditions as specified in the initial test plans or as required in anticipation of scheduled laboratory power outages.

The data from the initial group of TEM-X S/N-3 series modules attest to the success of the program in producing a tubular module with extremely stable performance for both cyclic and steady-state operation. With the exception of the questionable TEM-X S/N-3D data, degradation rates of all TEM-X S/N-3 series modules operated at $\overline{T}_H = 1085°F$ are substantially better than those defined in the initial program objectives of 1968.

5. Performance of TEM-X Modules with Glass Seals

A second group of three TEM-X S/N-3 series modules were fabricated in early 1972. These modules, TEM-X S/N-3G, 3H, and 3J incorporated directly applied glass-to-metal seals at each power pin base, eliminating the need for the end cap assemblies discussed above. Details of the glass-to-metal seal development program are discussed in a separate section of this report.

These modules had thermoelectric circuits identical to the previously discussed TEM-X S/N-3 series modules, but included end closure modifications required to permit the application of the glass-to-metal seals. The modifications consisted of moving the power pin bolt circle outward radially .042 inch to provide additional clearance for seal application.

In addition, the boron nitride pin insulators were recessed .050 inch into the retainer face to capture the glass during application. The glass seals were applied to the modules after completion of the processing (compaction) cycles.

Heatup data from this group of modules reproduced the data presented previously in Figures I-55 through I-57. Beginning-of-life $\overline{T}_H = 1085°F/\overline{T}_C = 507°F$ data from these modules, shown in Table I-12, also correlated very closely with the previous modules as well as the calculated levels.

Endurance testing of TEM-X S/N-3G, 3H, and 3J was conducted in static test stands at three different temperature levels to experimentally determine the relationship between degradation rates and operating temperatures. Figures I-62 through I-65 present overall efficiency, power output, open circuit voltage, and internal resistance data, respectively, from these three modules along with similar data from two additional reactor power modules, discussed below. Operating temperatures for each of the modules are listed in the legends of the figures on which the data are plotted. The first of the three "glass seal" modules had accrued nearly 5000 hours of operation prior to the time the program termination notice was received, with no indicated deterioration of the glass-to-metal seals. A visual inspection of the seals after the modules had been removed from test indicated no signs of deterioration.

A statistical analysis (linear curve fit) of all life test data from these and all other TEM-X series modules is presented in Table I-14. The degradation rate data presented in this table was used to analytically determine the activation energy of the reactor module degradation process (which, physically, is the sensitivity of the degradation rate to operating temperature). This relationship was critical in the design of the Five Kilowatt Demonstration System, discussed in a separate section of this report, since the reference module for the system was designed for optimum end-of-life performance. Since the reactor outlet temperature, hence module operating temperature, was to be varied with operation time in the demonstration system, it was necessary to know the relationship between degradation and operating temperatures in order to accurately design for optimum end-of-life performance.
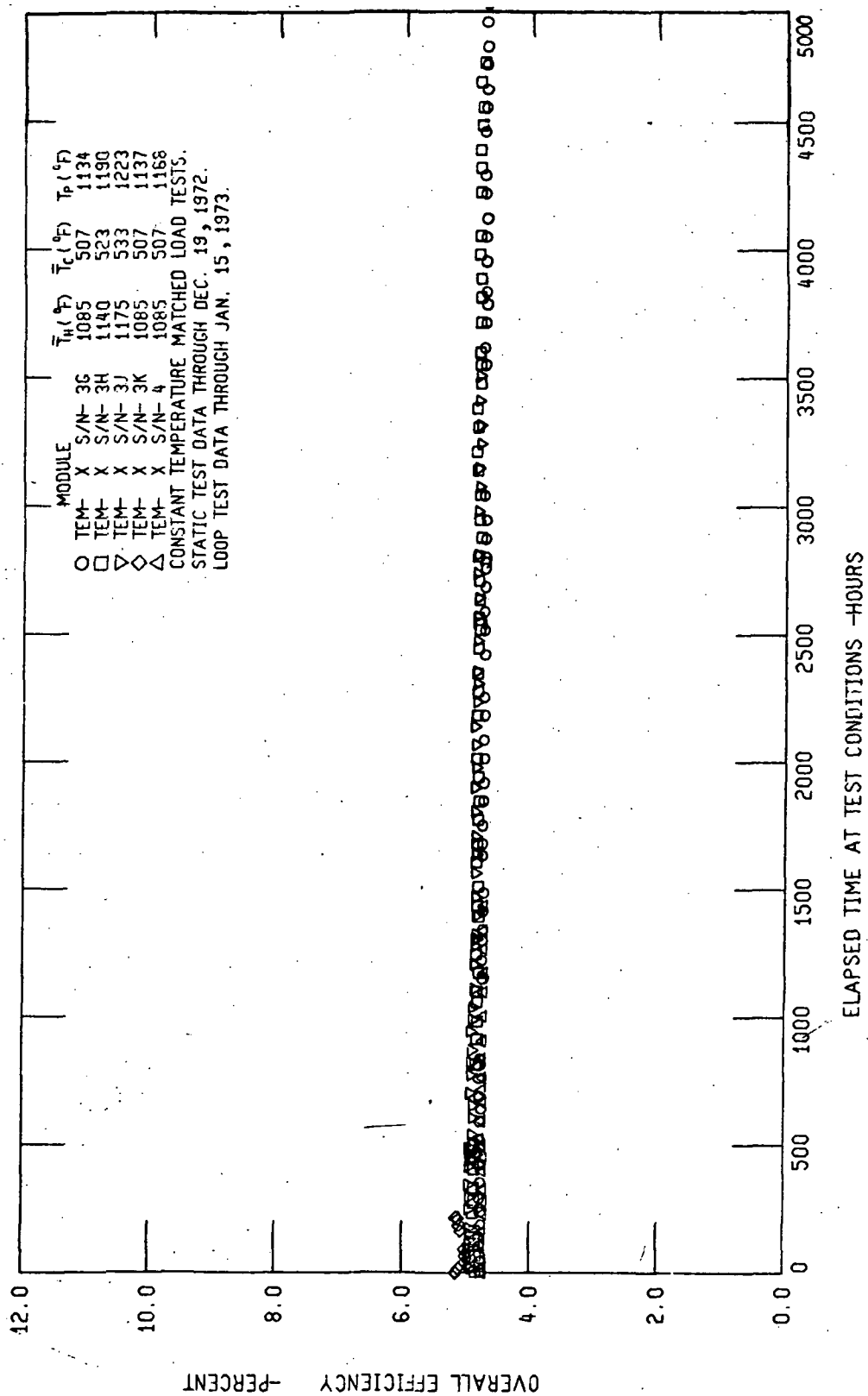
Figure 1-62. Overall Efficiency Versus Elapsed Time for Reactor Power Modules Fabricated without Mechanical End Caps
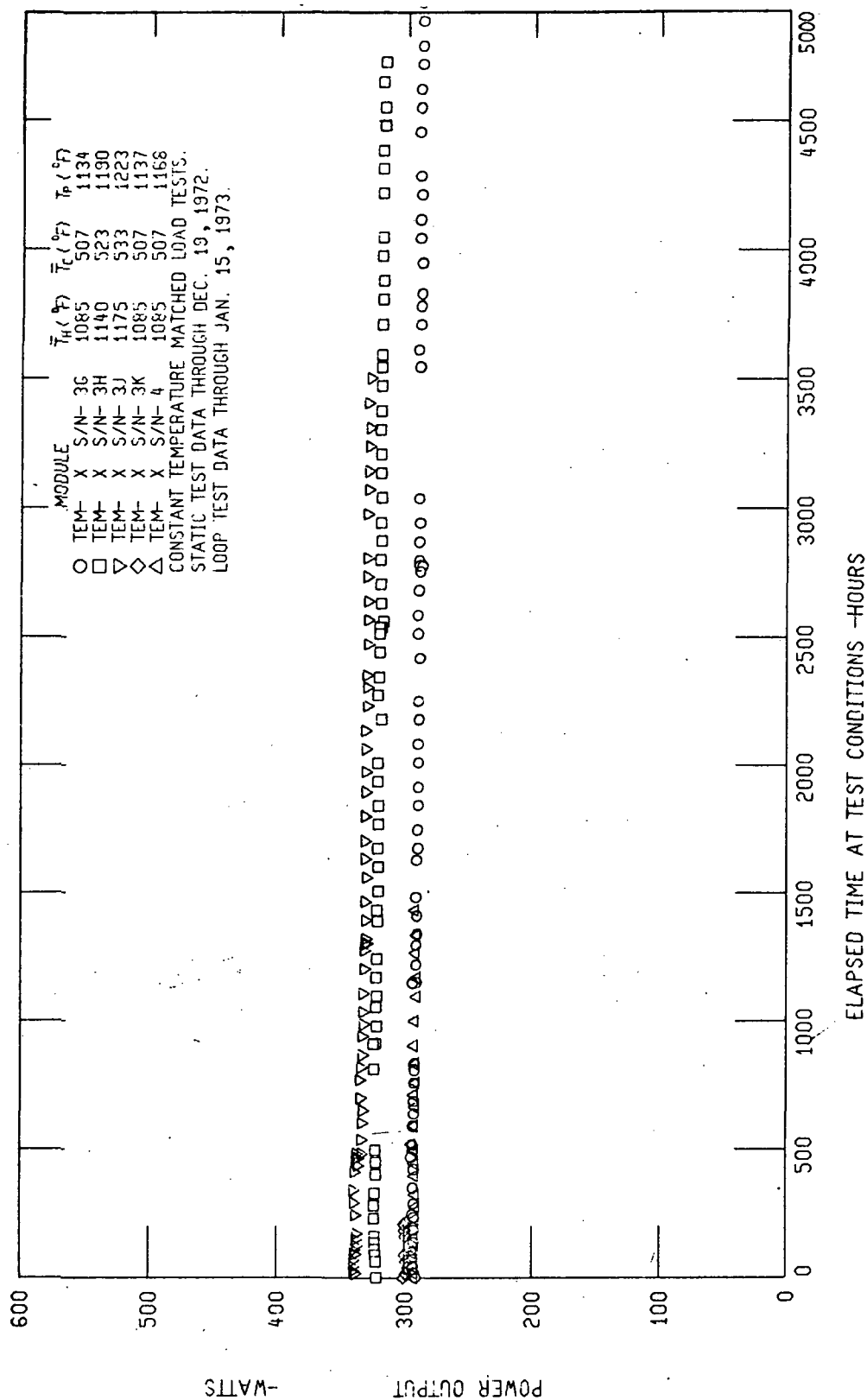
Figure I-63. Power Output Versus Elapsed Time for Reactor Power Modules
Fabricated without Mechanical End Caps
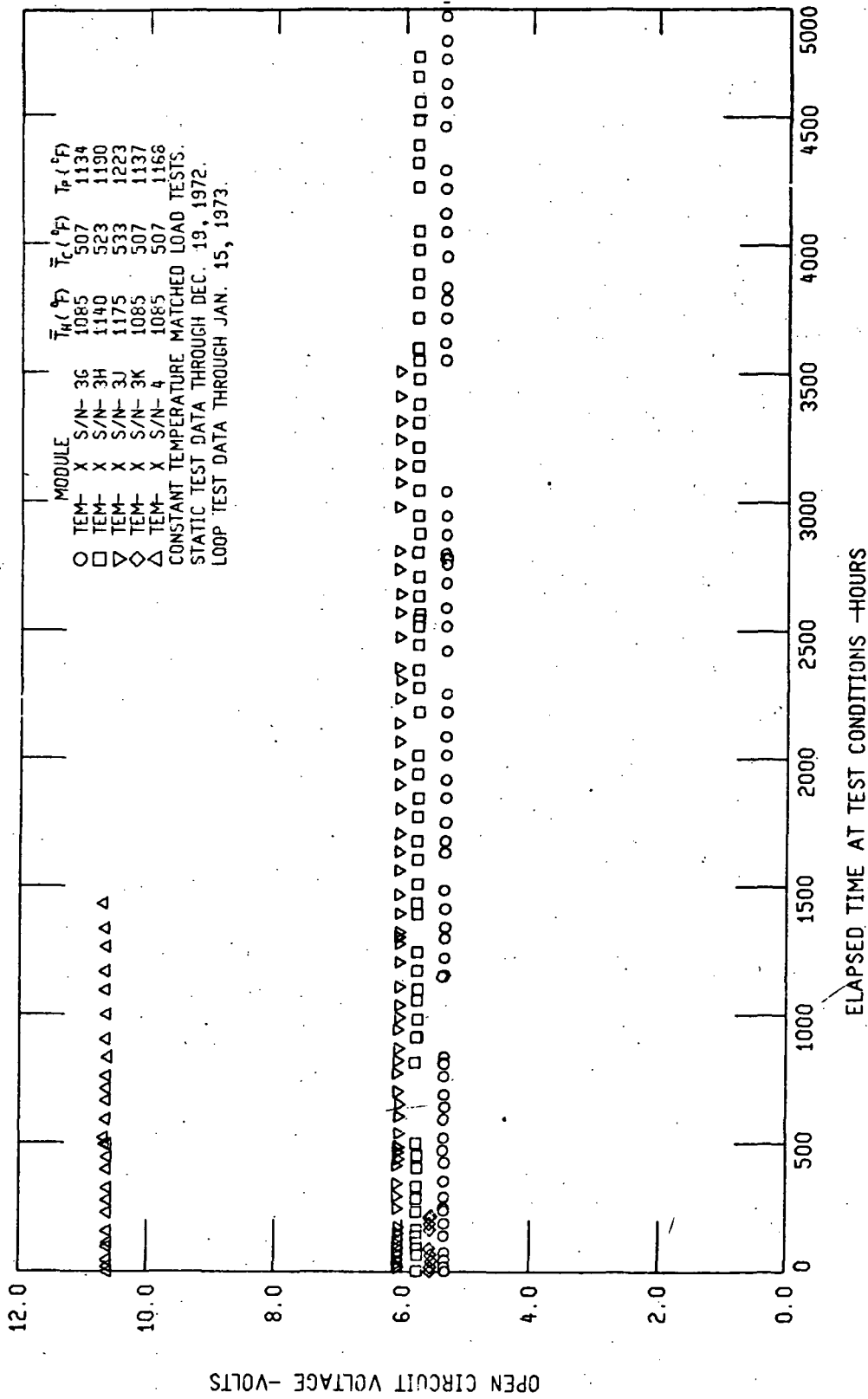
Figure I-64. Open Circuit Voltage Versus Elapsed Time for Reactor Power Modules
Fabricated without Mechanical End Caps

MODULE			$\bar{T}_H$ (°F)	$\bar{T}_C$ (°F)	T_P (°F)
○	TEM- X S/N- 3G		1085	507	1134
□	TEM- X S/N- 3H		1140	523	1190
▽	TEM- X S/N- 3J		1175	533	1223
◇	TEM- X S/N- 3K		1085	507	1137
△	TEM- X S/N- 4		1085	507	1168

CONSTANT TEMPERATURE MATCHED LOAD TESTS.
STATIC TEST DATA THROUGH DEC. 19, 1972.
LOOP TEST DATA THROUGH JAN. 15, 1973.

ELAPSED TIME AT TEST CONDITIONS —HOURS

OPEN CIRCUIT VOLTAGE —VOLTS
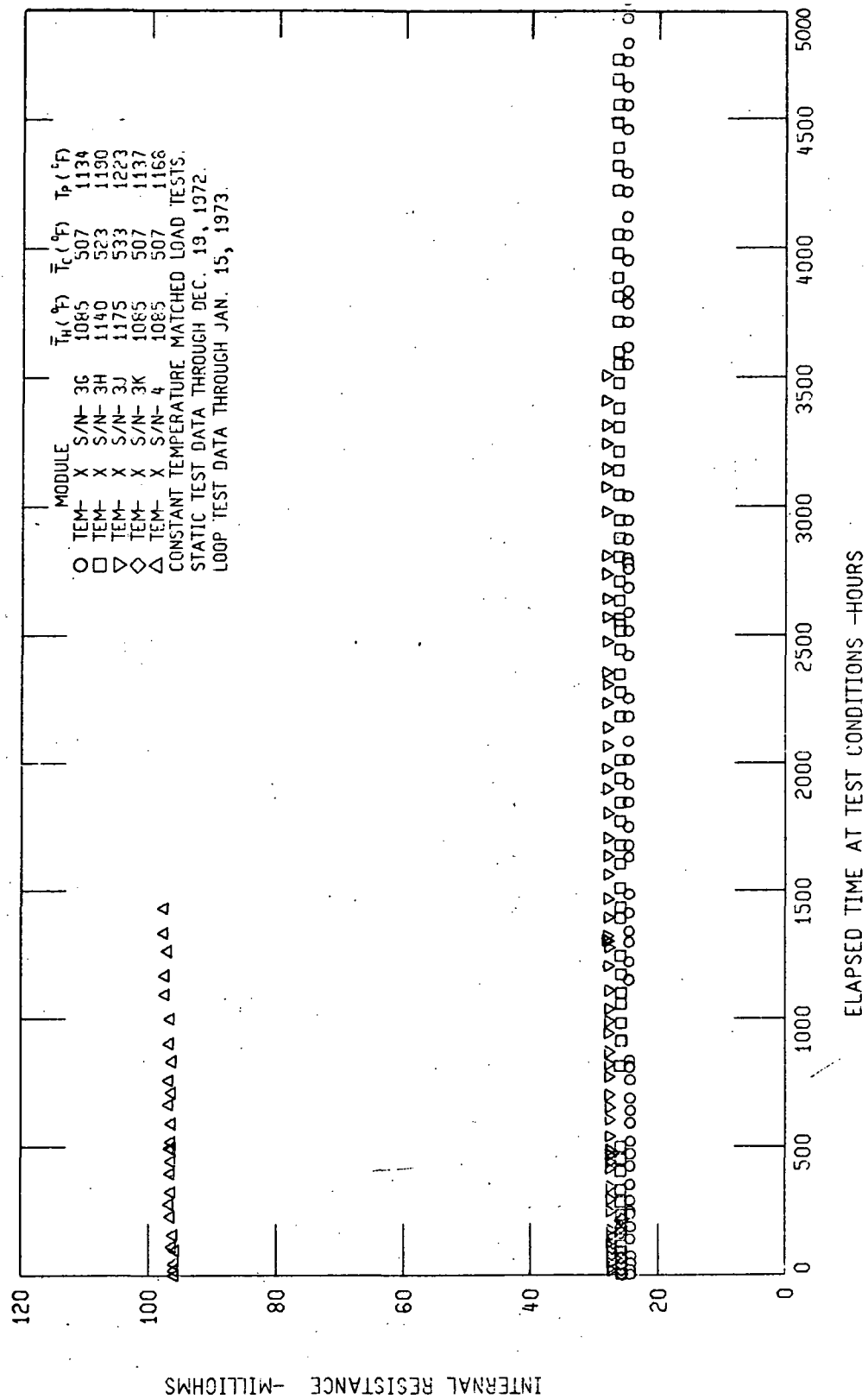
Figure I-65. Internal Resistance Versus Elapsed Time for Reactor Power Modules Fabricated without Mechanical End Caps

Since reactor module activation energy data were not available for use in the initial 5 KWe system design study, the assumption had been made that the activation energy determined from TEM-15 module data would be applicable for reactor modules. Results of the TEM-X degradation analysis indicate that this assumption was valid, at least for reactor modules fabricated with the same thermoelectric materials as used in the TEM-15 series modules.

Based on the hypothesis that the major degradation mechanism is either diffusion or chemical reaction rate controlled, the relationship between degradation rate and operating temperature for a particular module design and testing mode should follow an equation of the form,

$$\text{Rate} = A \exp(-Q/RT).$$

In this equation, known as the Arrhenius relationship, A is a "frequency factor", Q is an "activation energy", R is the ideal gas constant, and T is the rate controlling temperature. The rate of degradation refers to a percent increase per 10,000 hours for internal resistance or a percent decrease per 10,000 hours in the case of power output. For this analysis, the rate controlling temperature was considered to be the average hot clad temperature.

Arrhenius plots of static tested TEM-X and TEM-15A module resistance degradation rate data as a function of inverse absolute temperature are compared in Figure I-66. TEM-15A degradation rate data are presented in a later section of this report. A similar comparison of power degradation rate data is presented in Figure I-67. Using a least squares technique, straight lines were fit for both parameters for both module designs. A linear relationship was obtained by modifying the Arrhenius equation to logarithmic form yielding

$$\log(\text{Rate}) = \log A - (Q/R)(1/T).$$

This is a linear relationship for the log of the rate as a function of inverse temperature having a slope of $(-Q/R)$ and a dependent variable intercept of $(\log A)$.

Based on the least squares analysis of the degradation rates of TEM-X and TEM-15A static tested modules, the activation energies for resistance and power degradation were determined for these two types of modules and are presented in Table I-15. The "best fit" lines are shown in Figure I-66 and I-67, along with the experimental data from which the
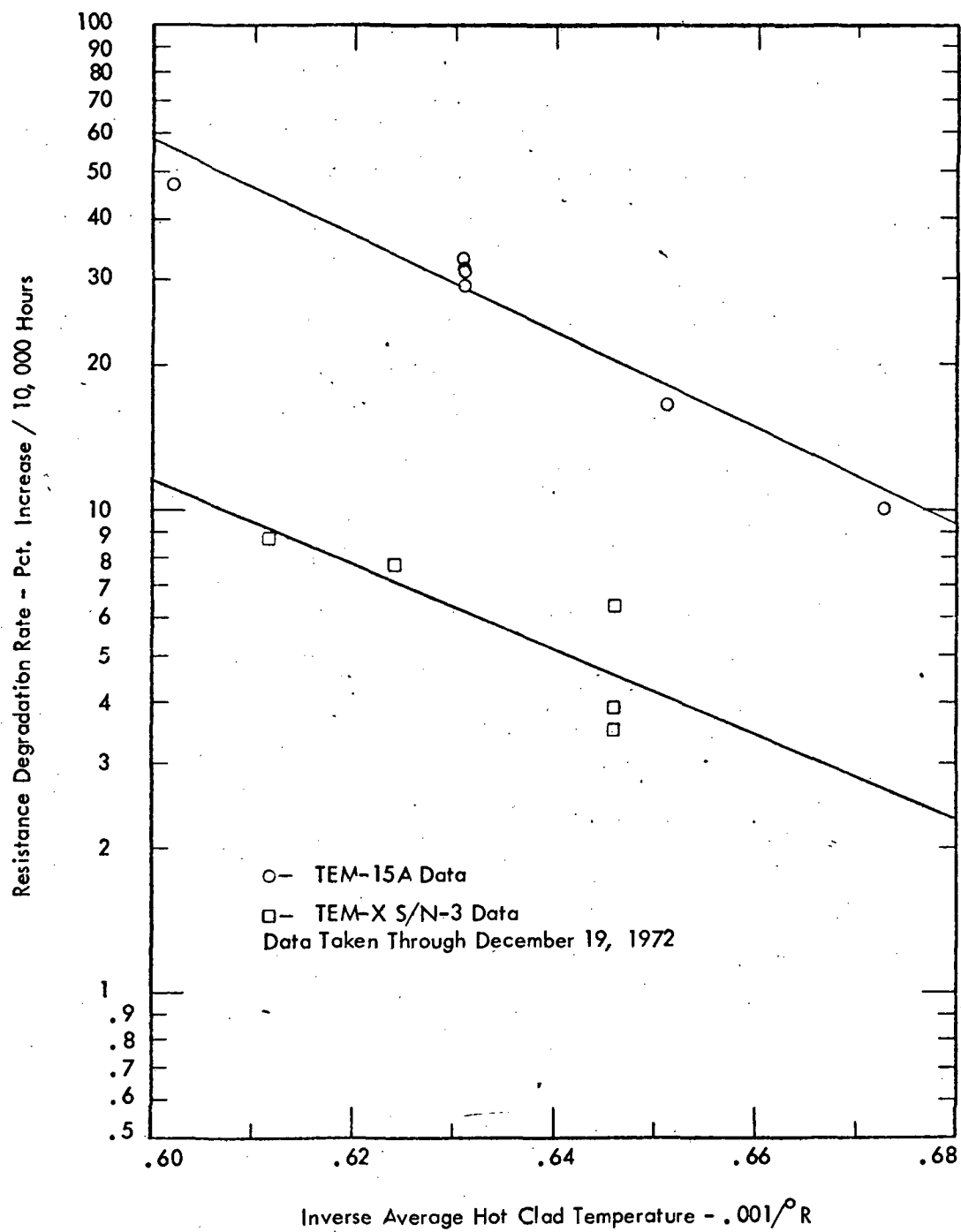
Figure I-66. Static Test Tubular Module Resistance Degradation Rates Versus Inverse Absolute Average Hot Clad Temperature
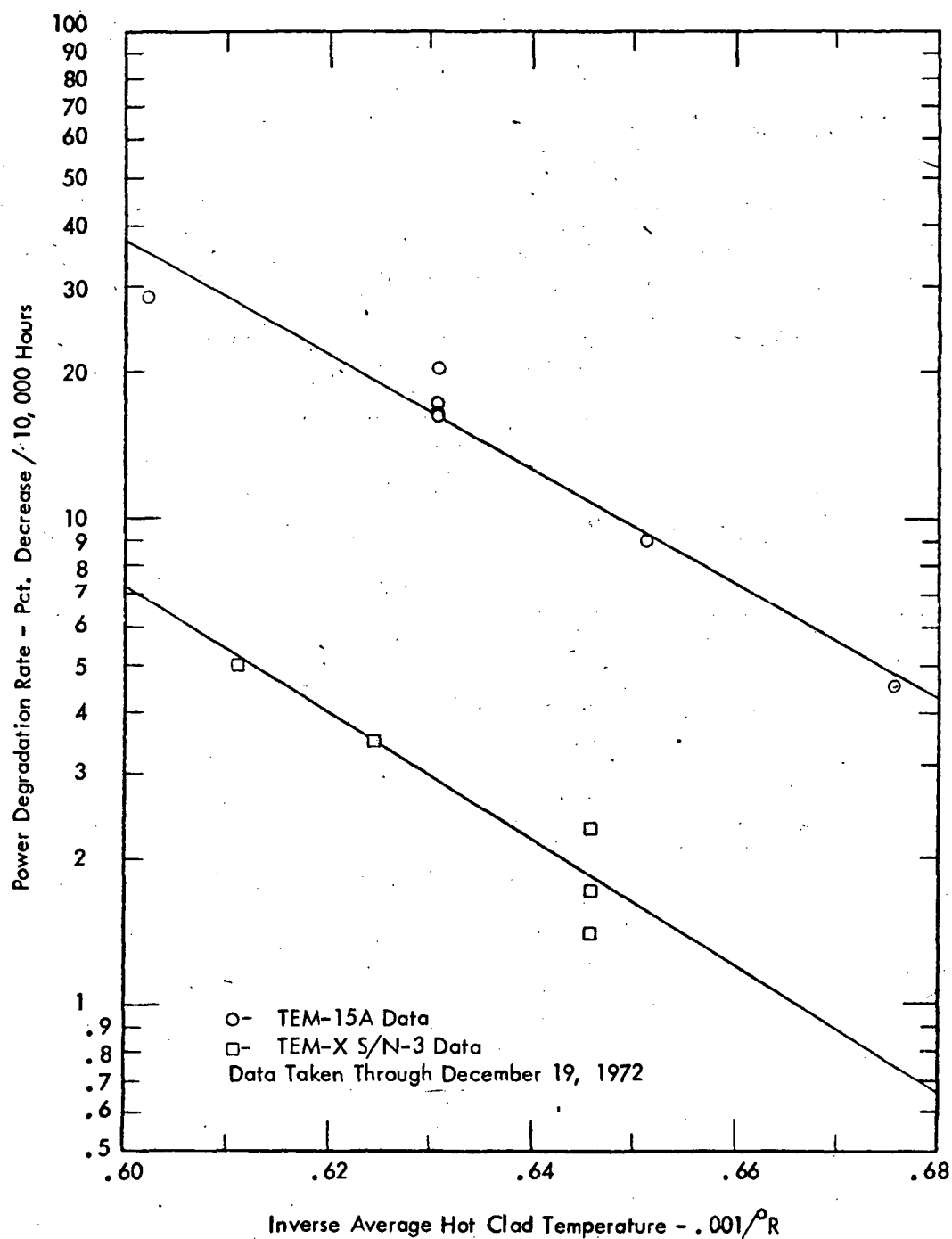
Figure I-67. Static Test Tubular Module Power Degradation Rates
Versus Inverse Absolute Average Hot Clad Temperature

TABLE I-15
TUBULAR MODULE ARRHENIUS RELATIONSHIP CONSTANTS

Module	Frequency Factor (A) (pct/10,000 hrs.)		Activation Energy (Q) (kcal/gm mole)	
Series	R_g	P_e	R_g	P_e
TEM-15A	5.6×10^7	4.2×10^8	25	30
TEM-X	2.5×10^6	5.0×10^9	23	33

lines were derived. The activation energies indicate the sensitivity of the degradation rates to changes in temperatures. The higher the activation energy, the greater the sensitivity. As can be seen, the activation energy of both types of modules are in good agreement. That is, although the TEM-15 module degradation rates are substantially higher than those of the TEM-X series modules, the sensitivity of the rates to the operating temperatures are nearly identical as had been previously assumed.

6. TEM-X S/N-3K Vacuum Test Experiment

An additional TEM-X S/N-3 series module, S/N-3K, was fabricated in early 1972. This module was identical to the previous three modules in all respects, except that the glass-to-metal seals were not applied after processing. The module was tested in the liquid metal loop system in a vacuum environment to determine the effects of glass seal failures during space operation.

Beginning-of-life performance parameters from TEM-X S/N-3K, which was being operated at $\overline{T}_H = 1085°F/\overline{T}_C = 507°F$, are presented along with similar data from all previous TEM-X S/N-3 series modules in Table I-12. Electrical performance data from this module fell within the bands established by previous modules. The TEM-X S/N-3K heat input data were slightly lower than that of previous modules, due to the elimination of convective heat losses from the end closures as a result of vacuum testing. Performance trends for this module can be seen to closely duplicate those of previous modules, insufficient testing time was accrued (1122 hours) to allow a meaningful statistical analysis of the data.

7. TEM-X S/N-3M Autoclave Experiment Module

The next and final TEM-X S/N-3 series module, S/N-3M, was fabricated in the latter half of 1972. (TEM-X S/N-3L was fabricated under a separate contract.) TEM-X S/N-3M incorporated two modifications identified in TEM-15 experiments (discussed in a separate section of this report).

TEM-X S/N-3M incorporated a three piece inner conductor ring design employed in a previous sub-length module, TEM-15H S/N-4. The new design was very similar to the stepped conductor ring design shown previously in Figure I-17, except that tungsten inserts

were used under both the p- and n-type thermoelectric washers. The additional insert, of course, required the elimination of the step on the molybdenum. Performance data from the sub-length module indicated that the elimination of the molybdenum/thermoelectric material interface at the n-leg hot junction produced a measureable reduction in degradation.

Processing conditions used to compact TEM-X S/N-3M were significantly modified from those used in all previous reactor power modules. In a previously conducted sub-length module experiment, TEM-15A S/N-4J, discussed in a separate section of this report, it was determined that full compaction could be achieved at lower autoclave temperatures by utilizing the full 30,000 psi pressure capacity of the autoclave facility at WANL. TEM-15A S/N-4J processing temperatures were restricted to 833°F (445°C) as opposed to 1292°F (700°C) as used in all previous TEM-X series modules. Degradation rates observed during the first 4194 hours of testing of the sub-length module, indicated that degradation rates had been cut nearly in half as a result of this modification.

Subsequently, TEM-X S/N-3M was processed at conditions identical to those of TEM-15A S/N-4J. Post-processing dimensional inspection indicated that TEM-X S/N-3M had compacted to an outer diameter within .001 inch of the average of previous TEM-X series modules. However, the room temperature internal resistance data from TEM-X S/N-3M were substantially higher than observed in previous modules as can be seen in Table I-12. These data indicate that room temperature interface pressure levels are somewhat lower as a result of the modified processing conditions. Proper interface pressure levels should be established during operation of the module, however, as a result of differential thermal expansion.

TEM-X S/N-3M was initially scheduled for loop testing at Atomics International. However, as directed during program termination activities, the module was instrumented for static testing, installed in a static test stand, and prepared for shipment to Jet Propulsion Laboratory for test.

K.   HIGH VOLTAGE REFRACTORY CLAD MODULE, TEM-X S/N-4

The next generation reactor power module design, TEM-X S/N-4, was directed at demonstrating that tubular converters could deliver power levels equivalent to that of the TEM-X S/N-3 series (300 watts) at substantially higher voltage levels while maintaining an acceptable power degradation rate. A reduction in thermoelectric washer axial thickness from .188 inch to .090 inch provides approximately a factor of two increase in voltage.

Because of the relationship between washer thickness, diffusion barrier configuration and degradation rate, a study was performed to determine the final circuit configuration to be incorporated in the high voltage module design. The results of the study are summarized in Table I-16. Respective degradation rates were calculated using TEM-X S/N-3 data as a base, and using empirical factors associated with each barrier configuration as determined from TEM-15 series module data.

Using calculated B.O.L. power levels and associated degradation rates, a power output versus operation time plot was generated for each configuration. The results are shown in Figure I-68. Modules incorporating electron beam vapor deposited tungsten barriers, although they were optimum, were eliminated from consideration for the first high voltage module because of the increased cost and manpower required to perform the vapor depositions. Comparing the curves for the other configurations, it was determined that the .010 inch mica module with no diffusion barrier represented the most reasonable performance trade-off of those modules which could be built at the time (i.e., excluding the EBVD barrier).

Subsequently, TEM-X S/N-4 was fabricated during the first half of 1972, with thermo-electric washers .090 inch thick, axially. This was the washer thickness used in the TEM-13G reactor power modules. In addition, .010 inch mica insulators were incorporated. Glass-to-metal pin base seals, identical to those of TEM-X S/N-3G, 3H and 3J, were applied prior to testing.

Static testing of TEM-X S/N-4 was initiated on June 30, 1972. Experimental data generated during open circuit heatup of the module correlated well with the calculated data over the entire temperature range. Beginning-of-life performance data also agreed well with the calculated levels shown in Table I-16.

TABLE 1-16

BOL PERFORMANCE LEVELS AND PREDICTED DEGRADATION RATES FOR
VARIOUS REACTOR MODULE DESIGNS

Mica Thickness (In.)	Diffusion Barrier	T/E Washer Thickness = .090 in.				T/E Washer Thickness = .188 in.			
		B.O.L. Levels			P_e Deg. Rate (%/10,000)	B.O.L. Levels			P_e Deg. Rate (%/10,000)
		η (%)	P_e (Watts)	V_L (Volts)		η (%)	P_e (Watts)	V_L (Volts)	
.010	W foil (A)	4.28	283	5.55	2.1	4.64	291	2.70	1.0
.010	EBVD (B)	4.90	299	5.61	3.0	5.02	298	2.71	1.4
.010	None	4.90	299	5.61	4.2	5.02	298	2.71	2.0
.005	W foil (A)	4.62	300	5.56	5.0	4.83	297	2.70	2.4
.005	EBVD (B)	5.28	317	5.62	5.5	5.19	306	2.71	2.6
.005	None	5.28	317	5.62	6.7	5.19	306	2.71	3.2

NOTES:

(1) All calculations and predictions based on $\bar{T}_H = 1085°F$, $\bar{T}_C = 507°F$ operation.

(2) All modules incorporate 15.0 inch circuits.

(A) .0004 in. tungsten foil barrier extending radially from hot junction midway through T/E washer.

(B) Electron beam vapor deposited tungsten.
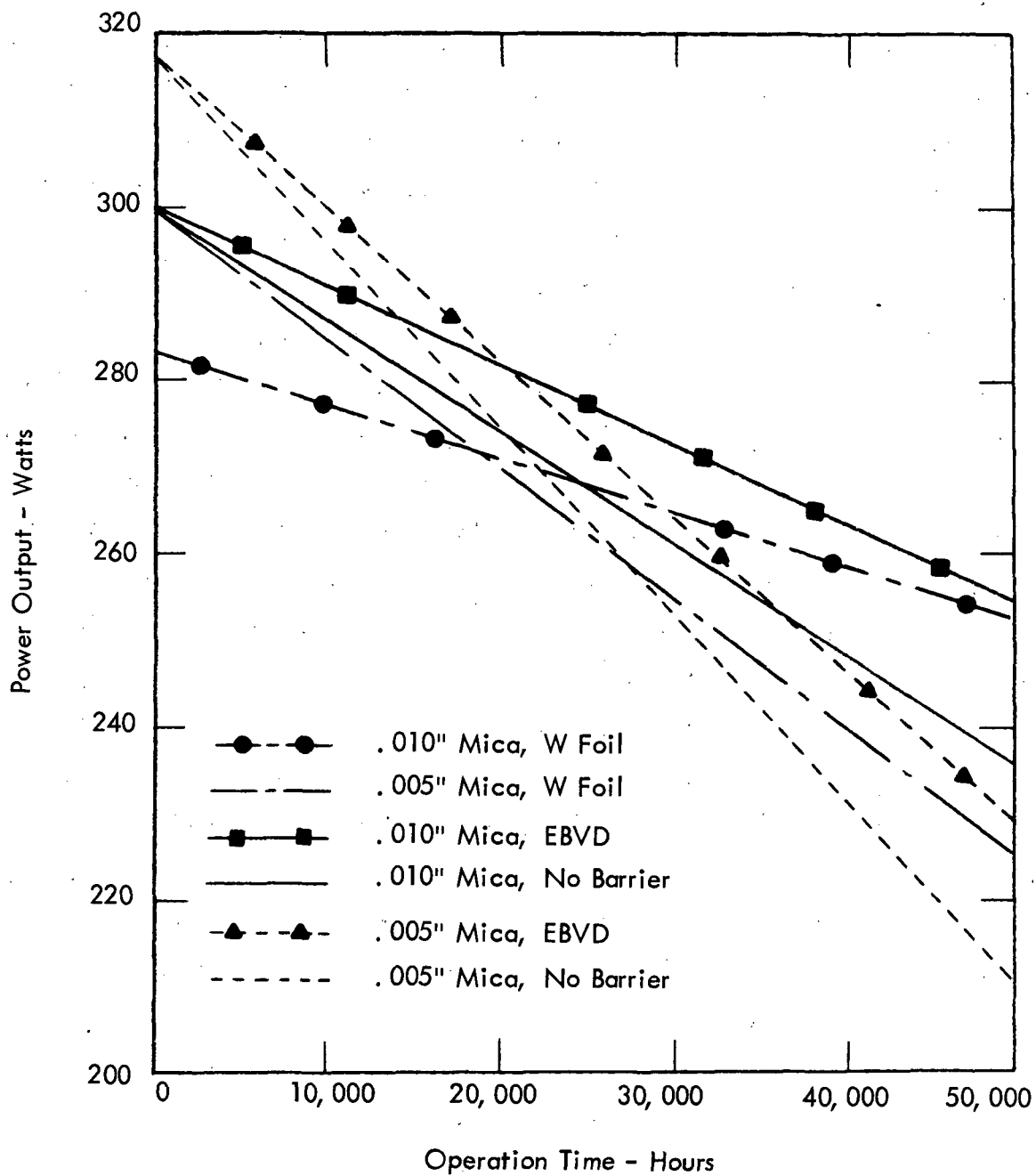
Figure I-68. Predicted Long-Term Performance of .090" Washer TEM-X
Modules with Various Barrier Configurations

TEM-X S/N-4 accrued a total of 1433 hours of operation at $\bar{T}_H = 1085°F/\bar{T}_C = 507°F$ test temperatures. Power output, overall efficiency, open circuit voltage, and internal resistance life test data from this module are presented in Figures I-62 through I-65, respectively, along with similar data from the other glass seal modules. Both the power output and overall efficiency data from this module can be seen to have duplicated similar data from TEM-X S/N-3G which was also operating $\bar{T}_H = 1085°F/\bar{T}_C = 507°F$. These two parameters are relatively insensitive to the modifications incorporated into the TEM-X S/N-4 design. The voltage and resistance data shown in Figures I-64 and I-65, respectively, reflect the sensitivity of these parameters to the number of couples in the module. The voltage of TEM-X S/N-4 is greater than that of S/N-3G by the ratio 74/38 (the ratio of the numbers of couples in the modules). The resistance of the module varies as the square of the number of couples. The basic advantage of the higher voltage module is the reduced matched load current, which reduces bus Joule heating losses. Also, with higher voltage modules, fewer series wired modules are required to achieve a given system voltage requirement. System reliability increases as the number of series wired modules decreases.

In November, 1972, the electrical heater used in the TEM-X S/N-4 test failed causing the module to be shutdown to room temperature. The heater was replaced and the module re-instrumented by mid-December. Testing of TEM-X S/N-4 had been scheduled to be resumed in early January prior to receipt of notification to discontinue work on the program.

Degradation rates observed during the first 1433 hours of TEM-X S/N-4 are listed along with those of all other refractory clad reactor power modules in Table I-14. The indicated 1.6 percent per 10,000 hours power degradation was substantially lower than the predicted rate of 4.2 percent per 10,000 hours. The uncertainty in the experimental data is very large, however, due to the limit testing time of the module. The experimental data shown in Figures I-62 through I-65 indicate clearly that a considerable amount of additional testing time would have been required to separate the effects of the design modification from those of experimental uncertainty with respect to degradation rates.

II. PUMP TUBULAR POWER MODULES

A. GOALS AND ACHIEVEMENTS

Preliminary system studies indicated that the optimum way to thermally link the reactor heat source, thermoelectric generators, and radiator in a reactor/thermoelectric power system was through the use of liquid metal loops. Flow in the individual loop systems was to have been established through the use of electromagnetic pumps. An early effort in theCompact Thermoelectric Converter System Technology Program established the feasibility of using a specially designed tubular module, referred to as a "Pump Tubular Power Module" to provide low voltage-high current (.2 volts at 500 amps) power to operate the electromagnetic (E.M.) liquid metal pumps directly.

Three initial pump power modules, given the designation TEM-14A series were designed, fabricated and placed on static test. All performance objectives were met by these modules, one of which was endurance tested for over 33,000 hours.

A second set of three, essentially identical pump power modules were fabricated in the latter half of 1972. These modules were to be incorporated into an integrated module assembly/electromagnetic pump test to be conducted in the liquid metal test facility at Atomics International.

B.   TEM-14A SERIES MODULES

    1.   Design

        The initial pump power module design was established in 1968, using 0.22 volts
at 500 amps as typical electromagnetic pump requirements. Pump module operating tempera-
tures for this design study were assumed to be $\overline{T}_H = 1125°F/\overline{T}_C = 570°F$, the same as those of
the reactor power modules.

        A parametric analysis of a large number of pump power module designs, all
capable of meeting the specified operating requirements was completed in mid-1968. In this
analysis the module I.D. was fixed at .75 inch to maintain piping commonality with the pre-
viously designed reactor power modules. Variations in inner conductor, outer conductor, and
thermoelectric washer radial thicknesses as well as axial dimensions and number of thermo-
electric couples were considered in the parametric study. From the results of this analysis,
TEM-14A dimensions were selected based on compaction considerations, as well as performance
(efficiency) level.

        Nominal post-processing dimensions of the TEM-14A series modules are listed
in Table II-1. The parametric study indicated that to achieve the 500 amp current requirement,
radially thick conductor rings in conjunction with radially thin thermoelectric washers were
required. The inner conductor ring radial thickness of the selected design was .225 inch com-
pared to the .015 inch thickness used in the initial reference reactor module. Although im-
proved performance was calculated for radially thicker outer conductor rings, .050 inch was
selected to ensure proper compaction of the thermoelectric washers in the autoclave cycle.
The thermoelectric washers of the TEM-14A series modules were approximately 20 times
thicker axially than those of the initial 14 volt reactor power module.

        Figure II-1 shows a schematic of the TEM-14A thermoelectric circuit design.
A comparison of this figure with a similar schematic from a typical reactor power module
shown in Figure I-17, points up the uniqueness of the pump module design. Notice the 7:1
axial to radial thickness ratio of the TEM-14 thermoelectric washer. This ratio was approxi-
mately 1:2 in the TEM-13G design. Notice, also, that the total inner conductor radial
thickness is more than twice that of the thermoelectric washer in the TEM-14 design. The

TABLE II-1

TEM-14A PUMP MODULE POST-PROCESSING DIMENSIONS

A. Radial Dimensions (Nominal)

	Inner Radius (Inch)	Radial Thickness (Inch)
Inner Clad (Inconel 718)	.375	.090
Inner Boron Nitride Sleeve	.465	.040
W/Mo Inner Conductor Rings	.505	.225
Thermoelectric Washers	.730	.100
Mo Outer Conductor Rings	.830	.050
Outer Boron Nitride Sleeve	.880	.037
Outer Clad (316 Stainless Steel)	.917	.150

B. Axial Dimensions (Nominal)

	Axial Thickness (Inch)
GE-nl Thermoelectric Washers	0.696
TEGS-2P Thermoelectric Washers	0.687
Mica Intercouple Insulating Washers	.009
Total Circuit (Active) Length	5.604

C. Design Features

Number of thermoelectric couples = 4

End closures redesigned to accommodate six .200 inch OD pins (in S/N-1)

End closures redesigned to accommodate twelve .200 inch OD pins (in S/N-2 and 3)

Inner Diameter = .75 inches

Outer Diameter = 2.13 inches
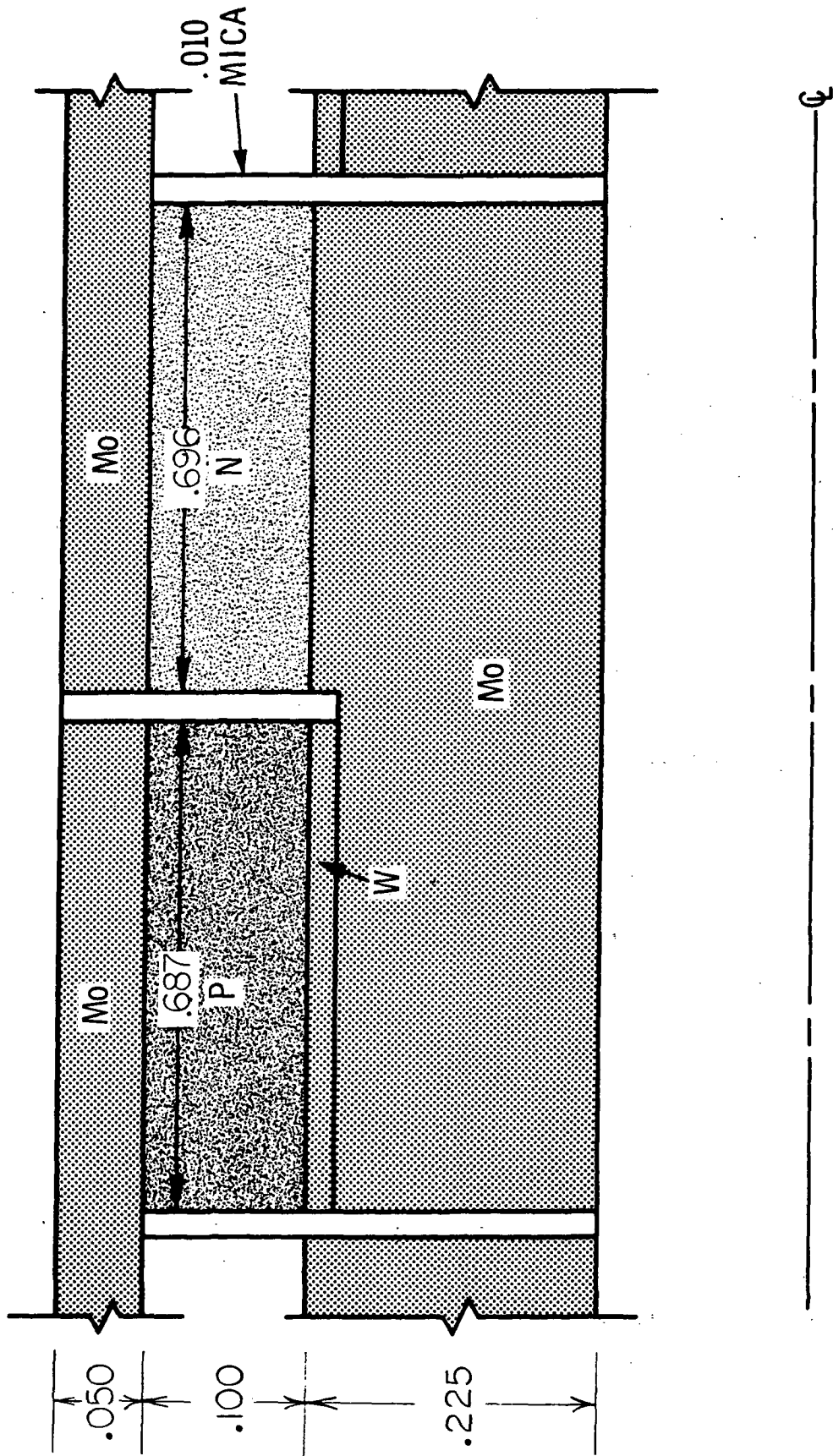
Figure II-1. Couple Design of the TEM-14A S/N-2 and 3 Modules

couple schematic in Figure II-1, shows the use of the two-piece inner conductor ring con-figuration. This design was implemented after the fabrication of TEM-14A S/N-1 which in-corporated single piece molybdenum inner conductors. Hence the couple schematic shown in Figure II-1 is that used in the TEM-14A S/N-2 and S/N-3 designs.

Because of the extremely low circuit resistance of the pump modules, end closure modifications were required to reduce the resistance contribution of the electrical power pins. This reduction was accomplished by increasing the number of pins per end from four (as used in the power module) to six in the pump module and increasing the pin diameters from .060 to .200 inch. In addition, since the pump module would operate in a space vacuum in the system application, molybdenum pins were originally considered as a substi-tute for the conventional nickel pins to further reduce resistance. However, to allow laboratory testing, nickel pins were actually incorporated in the modules, resulting in a substantial increase in module circuit resistance. To compensate for this increase, twelve 0.2 inch electrical pins were incorporated at each end of the second and third pump modules fabricated for ground testing. In addition, the later pump modules incorpor-ated the two piece inner conductor ring design, discussed above, to reduce intercouple tellurium transport. The conductor ring modification had no effect on calculated performance parameters.

2. Test Results

The first pump tubular power module, TEM-14A S/N-1, was fabricated, pro-cessed, and placed on static test at WANL in the latter half of 1968. Two additional modules, S/N-2 and S/N-3, were placed on test in the early part of 1969. The second two modules included the design modifications discussed above.

Testing of the TEM-14 type modules was complicated by the low load circuit resistance required to simulate the 0.44 milliohm E.M. pump electrical resistance. Load circuit resistances were minimized through the use of relatively massive bus leads connected from the module external collector rings to a copper shunting bar. The shunting bar was actually a calibrated resistor and voltage measurements across the bar allowed a determination of load current. In the initial test assembly of the first module, TEM-14A S/N-1, the bus

leads were permanently attached to the shunting bar and no provision was made for open circuit measurements. Since open circuit voltage measurements are required for a determination of module internal resistance, the latter parameter was not determined during initial testing of TEM-14A S/N-1. Subsequent TEM-14A series modules were tested with the bus leads bolted to the shunting bars. Open circuit measurements were made on these modules by removing the bolts and momentarily disconnecting the shunt bar during each data scan.

Beginning-of-life $\overline{T}_H = 1125^{\circ}F/\overline{T}_C = 570^{\circ}F$ performance data from the three TEM-14A series modules are compared to the design calculations in Table II-2. Electrical current, the critical parameter for a pump power module, agreed to within 2 percent of the design level in the S/N-2 and S/N-3 tests. The effect of the high pin circuit resistance in TEM-14A S/N-1 is quite evident in these data.

As can be seen from the data presented in Table II-2, the efficiency level of the TEM-14A pump modules is substantially lower than that of typical reactor power modules. There are three major factors inherent in the pump module design which lead to efficiency reductions:

a. The high current requirement results in substantial conductor ring and electrical power pin Joule heating losses. Over 15 percent of the electrical power generated is converted to Joule heat in the electrical power pins of TEM-14A S/N-2 and 3.

b. Low voltage, high current pump module electrical requirements necessitate designs with radially thin thermoelectric washers. Efficiency, unfortunately, is proportional to thermoelectric washer radial thickness.

c. End closure heat losses of pump modules are increased by losses through the electrical leads. In addition, the pump modules have shorter thermoelectric circuits than power modules making their end losses a greater percentage of the total module heat requirements.

TABLE II-2

A COMPARISON OF EXPERIMENTAL AND CALCULATED BOL PUMP MODULE PARAMETERS

Parameter	Module			Design*
	S/N-1	S/N-2	S/N-3	
1. Average Hot Clad Temperature (°F)	1125	1125	1125	1125
2. Average Cold Clad Temperature (°F)	570	570	570	570
3. Electrical Load Resistance (milliohms)	.44	.44	.44	.44
4. Open Circuit Voltage (volts)	**	.443	.451	.466
5. Load Voltage (volts)	.201	.198	.228	.220
6. Module Internal Resistance (milliohms)	**	.452	.448	.491
7. Load Current (amps)	438	497	508	500
8. Total Power Input (watts)	3200	3480	3600	3365
9. Power Output (watts)	89	109	113	110
10. Overall Efficiency (percent)	2.78	3.13	3.14	3.27

Notes:

   * Design calculations based on initial parametric studies.

   ** No open circuit voltage or internal resistance measurements made on TEM-14A S/N-1.

Electrical current and power output data recorded during endurance testing of the TEM-14A series modules are presented in Figures II-2 and II-3, respectively. The first module, TEM-14A S/N-1, was tested essentially continuously since October, 1968, except for a short period required to replace a failed electrical heater in the test stand after 17,847 hours of operation. During the heater replacement, the load circuit was modified to allow open circuit measurements during subsequent testing of the module. TEM-14A S/N-2 was tested continuously since April, 1969.

The TEM-14A S/N-3 test plan specified cyclic operation followed by a destructive examination to determine the sensitivity of the pump module design to cyclic operation. The module was subjected to five sets of ten thermal cycles, each performed with 30°F/min. hot clad temperature ramp rates. Each of the sets were followed by a steady state $\overline{T}_H = 1125^\circ$F/ $\overline{T}_C = 570^\circ$F operating periods of approximately 1000 hours. None of the cycles produced any measureable deleterious effects on module performance. TEM-14A S/N-3, as a matter of fact, had the lowest degradation rate of the three TEM-14A series power modules. After completion of the last cycle and a total of 7727 hours of steady state testing, TEM-14A S/N-3 was removed from test for destructive examination.

Table II-3 presents a summary of performance stability data from the three TEM-14A series modules. Degradation rates were determined using the statistical analysis discussed in Section I of this report. Cyclic histories of each of the modules are also summarized on the table. Internal resistance data from TEM-14A S/N-1 were monitored only after modifying the load circuit at 17,847 hours and resistance degradation rates were determined using only subsequent data.

Extremely stable performance was demonstrated by the TEM-14A series pump power modules. The two long-term tested modules exhibited power degradation rates ranging from 3.9 to 4.7 percent per 10,000 hours. A slightly increasing power was observed during the 7727 hours of TEM-14 S/N-3 testing. The primary reason for the high degree of performance stability demonstrated by these modules during relatively high temperature testing ($\overline{T}_H = 1125^\circ$F), was related to the circuit design of the modules. Tellurium contamination was restricted to a relatively small axial portion of the n-type washers, thus reducing the effects of the degrading process.
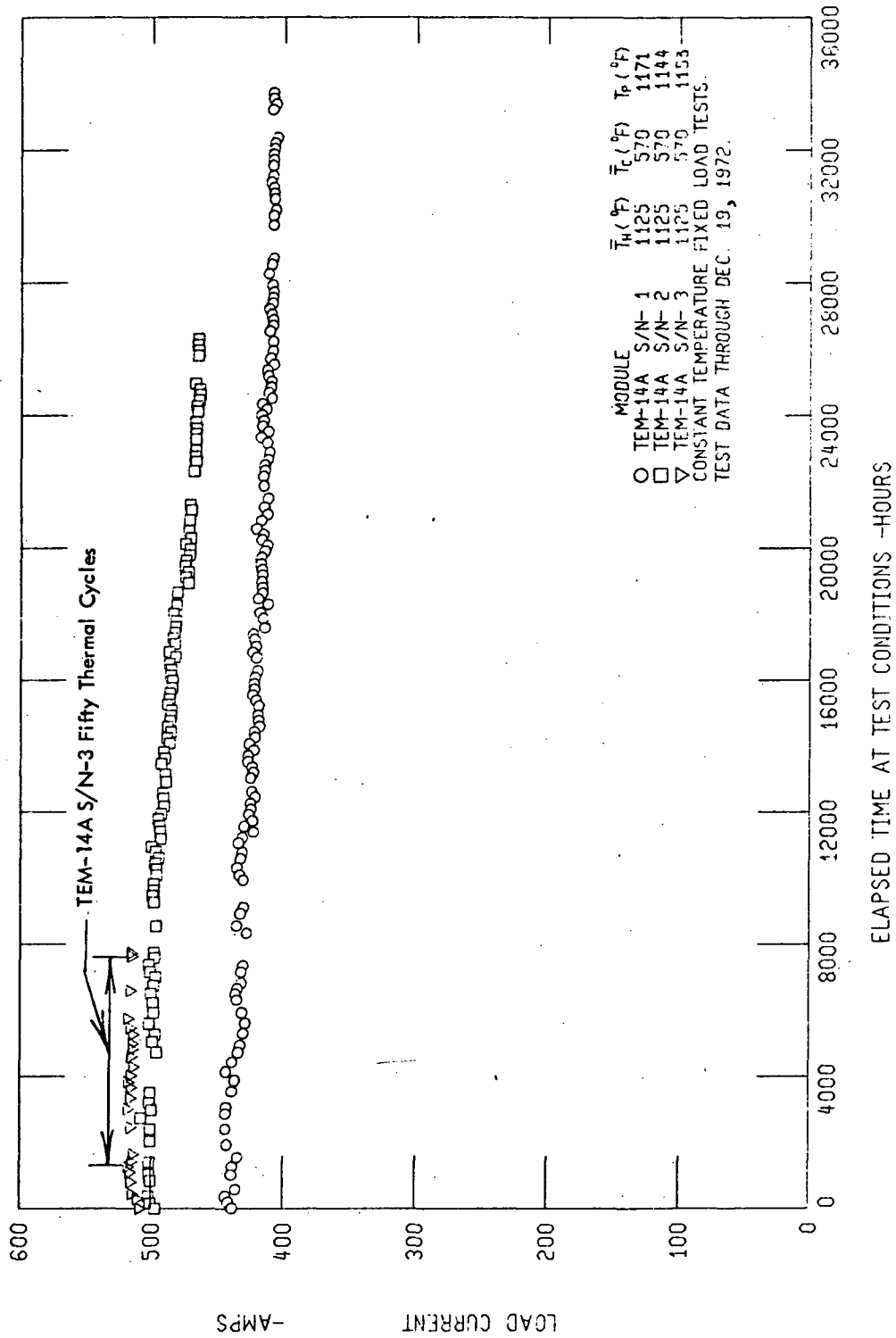
Figure II-2. Electrical Current Data from Prototype Pump Power Modules
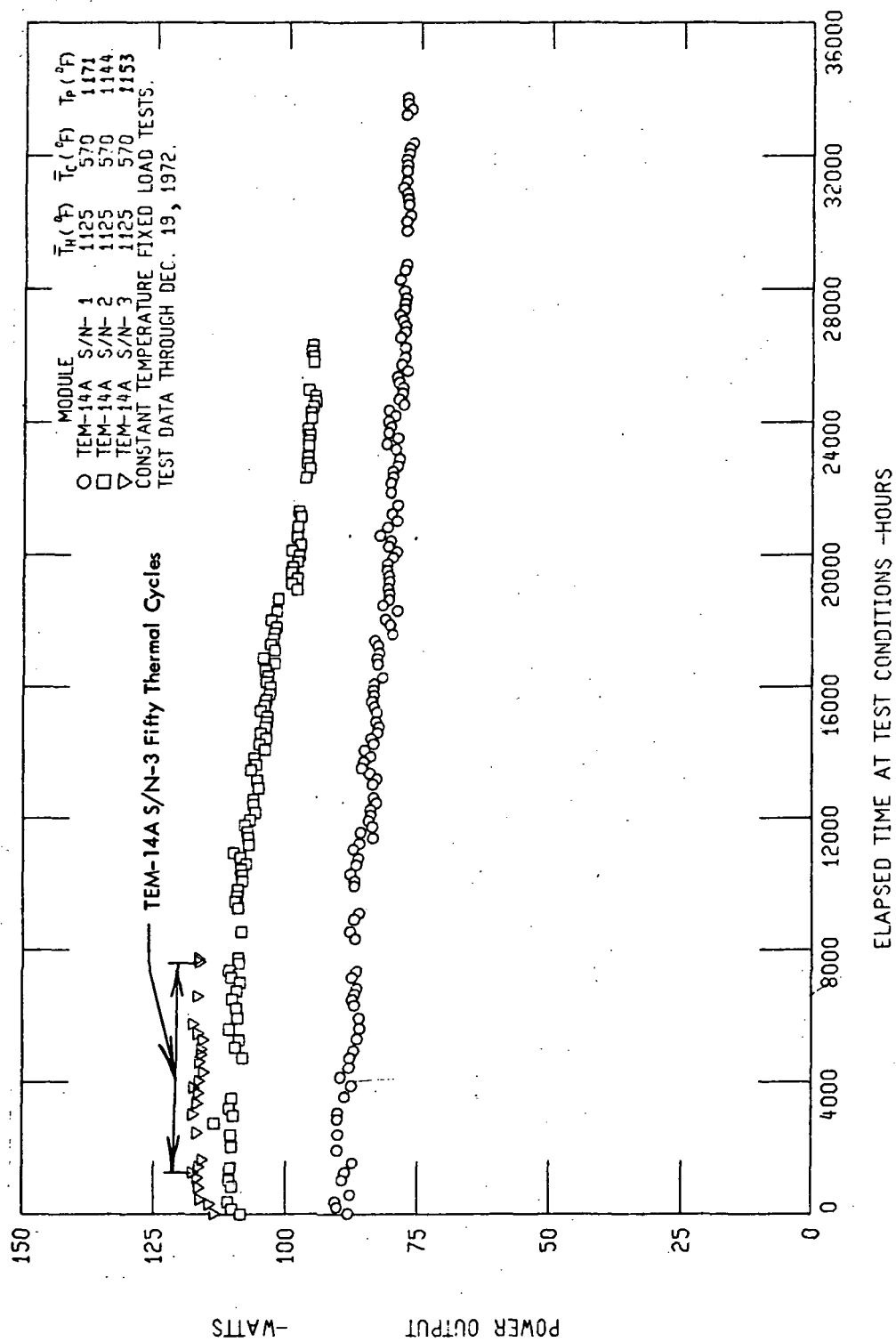
Figure II-3. Power Output Data from Prototype Pump Power Modules

TABLE II-3

PUMP MODULE PERFORMANCE STABILITY SUMMARY

Module	Testing Time (Hours)	Rate of Change: % Per 10,000 Hours			Thermal Cycles	
		R_g	P_e	η_o	Rapid	30°F/Min.
TEM-14A S/N-1	33713	1.1*	-3.9	-4.6	14	1
TEM-14A S/N-2	26294	5.1	-4.7	-4.3	13	0
TEM-14A S/N-3	7727	4.5	+1.3	-0.4	2	50

* Included S/N-1 resistance data taken after reinstrumentation only.
All modules tested at $\bar{T}_H = 1125^{\circ}$F/$\bar{T}_C = 570^{\circ}$F.
All data included through January 9, 1973.

Astronuclear Laboratory

3. Destructive Examination Results from TEM-14A S/N-3

TEM-14A S/N-3 was removed from static test after 7727 hours of $\overline{T}_H = 1125^\circ F/$ $\overline{T}_C = 570^\circ F$ and completion of 50 thermal cycles as discussed above. Sections were cut from the module end and center and disassembled to examine the interface formed by the inner conductor ring and the lead telluride washers. Samples were removed by scraping the outer diameters of the inner conductor rings and the inner diameters of the lead telluride washers. The results of the examination are summarized as follows:

a. No evidence of compound formation or reaction products was found in samples scraped from the tungsten inner conductor rings nor from the inside diameter of the p-type washer.

b. Scrapings from the first inner conductor ring at the negative end of the module showed a strong $PbMoO_4$ pattern via x-ray diffraction. No such pattern was seen on films of the scrapings taken from the inside diameter of the matching lead telluride washer.

c. Scrapings from the module center n-type washer and inner conductor rings showed very weak patterns of $PbMoO_4$, with the weaker pattern being from the sample scraped from the lead telluride washer. Previous samples scraped from another portion of the center ring and washer revealed no diffraction lines for $PbMoO_4$.

These results indicated that there is a slight reaction between molybdenum and n-type lead telluride in the presence of a limited amount of oxygen. Tungsten, however, does not seem to exhibit the same phenomenon. The effect of the above reaction on module performance is not known, but the replacement of molybdenum by tungsten appears necessary to eliminate any possible deleterious reactions that could increase module degradation. It should be noted that despite this minimal surface contamination, no changes were noted in the Seebeck coefficient values of the n- and p-type washers, even near the conductor ring/ thermoelectric junction region. In fact, there was no measured power degradation of this module after testing for 7727 hours at the $\overline{T}_H = 1125^\circ F$ level (see Table II-3).

C.   TEM-14B SERIES MODULES

A second generation of tubular modules designed to deliver low-voltage, high-current power to electromagnetic liquid metal pumps were defined in FY 1973 and identified as TEM-14B series modules. Three TEM-14B series modules, S/N-1, -2, and -3, were to be incorporated into an integrated module assembly/electromagnetic pump test to be conducted in the liquid metal test facility at Atomics International during calendar year 1973.

The TEM-14B series modules were similar in design to the TEM-14A series modules discussed above except that 50 percent radial thickness tungsten foil diffusion barriers were incorporated between each adjacent pair of thermoelectric washers. Because of the small number of couples (four), the thermal penalty associated with the incorporation of foil barriers is immeasureably small. However, the performance stability improvement resulting from the incorporation of foil barriers should be measureable.

All Westinghouse hardware for the integrated module assembly/electromagnetic pump test was completed by December, 1972. In addition the three modules were fabricated and processing was completed in early December. Three sets of shrouds and primary flow channel swirl generators required for loop operation were fabricated. Three sets of nickel external collector rings (a total of nine rings) were fabricated and shipped to Atomics International where they were brazed to the electrical bus assemblies. In addition, a welding fixture to support the three modules during welding of the electrical bus/collector ring assemblies was designed and fabricated.

Two sets of flexible electrical bus assemblies, each brazed to three external collector rings, were received from Atomics International in late December. Installation of the bus/collector ring assemblies was initiated in accordance with assembly procedures.

Figure II-4 is a photograph of all hardware required for mating of the bus/collector assembly to the three modules. The ends of the modules can be seen extending from the module welding fixture. The external collector rings, each brazed to a flexible bus assembly, are mounted on a temporary holding fixture and can be seen in the figure laying in front of, and below the modules. The collector rings fit simultaneously over the ends of the modules
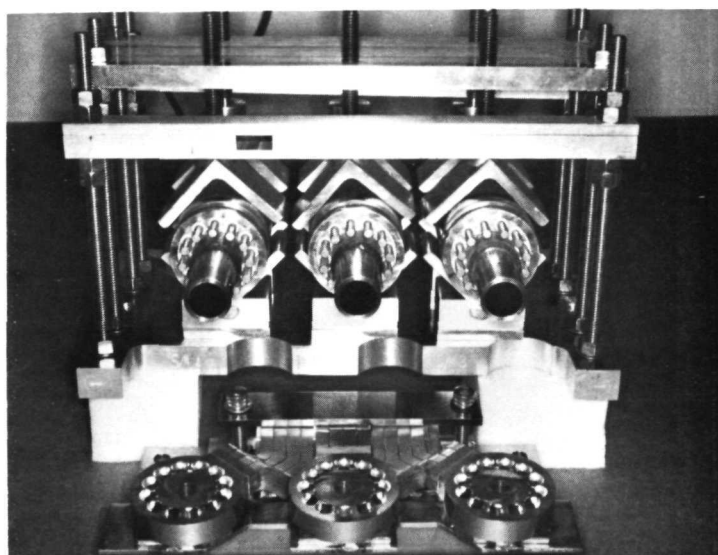
Figure II-4. Photograph of the TEM-14B/Electrical Bus Bar Assembly Hardware

so that the twelve electrical pins, seen extending from ends of each module, fit into the holes in the collector rings. Each of the pins would then be welded to the collector ring. Effort on the module/bus bar assembly was terminated upon notification to close out the program.

In addition to the design work, an end closure/electrical bus heat loss analysis was completed. The object of this effort was to determine thermal losses expected in the integrated TEM-14B module assembly/electromagnetic pump test and to determine electrical pin temperatures. The effects of various module/pump throat electrical connection options was also studied. The results indicated that the end closure heat loss rates are very insensitive to the module/pump throat electrical connection options, primarily because heat flow out of the module into the bus at one end is nearly balanced by heat flow into the module at the other end. The total end heat loss rate per module operating at $\overline{T}_H = 1140^\circ F/\overline{T}_C = 523^\circ F$ is 570 watts. The maximum electrical pin temperature for any configuration is $911^\circ F$, at these operating temperatures.

The thermal analysis indicated two minor end closure design modifications which could be made to substantially reduce heat losses in future modules. The primary end heat loss results from axial flow of heat from the inner conductor ring across a .050 inch Alsimag (aluminum oxide/silicon/magnesium ceramic) insulator into the internal collector ring located in the module end closure. This alsimag axial thickness could be tripled by moving the collector ring closer to the ends of the module with very minor modification to the end closure design. In addition, the inner boron nitride electrical insulator could be terminated directly under the circuit, thus reducing radial heat transfer from the inner clad of the module to the internal collector ring. The boron nitride would be replaced by Alsimag which is a much better thermal insulator. These modifications were to have been recommended for the TEM-14C modules which were to be incorporated into the 5KWe demonstration test.

D. SUMMARY OF PUMP POWER MODULE RESULTS

The successful development of the pump power module, which represented a radical departure from previous tubular modules design, fabrication, and test experience, not only verified that such a module could be produced but also established that the mathematical models used in the design of tubular modules are applicable over a wide range of conditions.

All requirements were met by the first series of pump power modules fabricated. The 500 amp current requirement, for instance, was met to within 1.5 percent at the design operating conditions. Performance stability demonstrated by this group of TEM-14A series modules exceeded all expectations, and thermal cyclic testing of one module demonstrated the insensitivity of the pump module design to transient operation. The long-term perform-ance capabilities of the tubular module incorporating lead telluride thermoelectric materials were, once again, clearly demonstrated by the performance data from the TEM-14A series modules, the first of which had accrued over 33,700 hours of high temperature operation prior to program closeout.

III. SUBLENGTH TECHNOLOGY MODULES

A. GOALS AND ACHIEVEMENTS

One of the most important goals of the Compact Thermoelectric Converter System Technology Program, conducted at Westinghouse Astronuclear Laboratory, was to identify and eliminate or control all factors contributing to performance degradation. Extensive progress was made toward this end, primarily through implementation of experiments and evaluation of data generated on "sublength technology" modules. These modules were given the numerical designation TEM-15. This phase of the program was initiated in July, 1969.

The TEM-15 series modules were designed with radial dimensions identical to those of the TEM-13G reactor power modules, discussed in Section I of this report, but with total circuit lengths reduced to 4.0 inches from 15.0 inches. This length reduction reduced the cost of the modules and the instrumentation complexity required to permit performance evaluation. All TEM-15 series modules were fabricated with Inconel inner clads identical except in length to those used in the TEM-13G series reactor power modules.

Prior to the initiation of the TEM-15 design effort, the primary degradation mode had been identified as being caused by the diffusion of tellurium around mica/inner conductor ring interfaces into the n-type lead telluride washers. This degradation mode was uncovered by results of destructive examination of TEM-9 series modules fabricated in a previous technology program. Based on this information, all TEM-15 series modules incorporated the stepped inner conductor ring design discussed in Section I of this report and depicted in Figure I-17. Initial TEM-15 experiments, then, were directed at studying means to further reduce tellurium contamination.

Nominal thermoelectric washer thicknesses of all TEM-15 series modules was .050 inch which was considerably thinner than those of reactor power modules contemplated in 1969. These TEM-15 dimensions were established to accentuate the effects of the primary mode of degradation, i.e., intercouple contamination. This was done to accelerate TEM-15 degradation rates, thus allowing a more rapid evaluation of the effects of each modification.

Initial TEM-15 experiments were defined to evaluate the effects of various design assembly clearances, fabrication processes, and intercouple diffusion barriers on module performance. Figure III-1 depicts the initial matrix of modules investigated and identifies the modules fabricated initially.

A letter suffix was assigned to each of the initial modules to identify the type of insulating barriers used to separate the n- and p-type thermoelectric washers. TEM-15A series modules utilized the conventional single piece .005 inch mica insulators with no diffusion barriers. TEM-15B modules utilized a layer of nominal 0.0005 inch tungsten foil "sandwiched" between two layers of mica. TEM-15C series modules incorporated two mica insulators with a thin film diffusion barrier coating applied to each of the 0.0025 inch thick mica mating surfaces. A serial number applied to each module identified the assembly clearance and fabrication process incorporated. Figure III-2 depicts variations in the couple assemblies incorporated in the initial TEM-15 module experiments.

During the course of the program, a substantial number of additional experiments were performed using TEM-15 series modules. Table III-1 is a list of the processing and design features of every TEM-15 series module fabricated on the program from 1969 to the termination. All of these modules, with the exception of TEM-15A S/N-4A and TEM-15P S/N-1, were tested in static test stands at WANL. TEM-15A S/N-4A was in the first group of sublength modules fabricated and was destructively examined immediately after processing to study compaction completeness and circuit alignment. TEM-15P S/N-1 was the last sublength module fabricated on the program. The program termination notice was received prior to initiation of TEM-15P S/N-1 testing.

INSULATING RING INVESTIGATION

TEM-15A

0.005 MICA

TEM-15B

0.0045 MICA (2 PIECES)
+0.0005 W (FOIL) BARRIER

TEM-15C

0.005 MICA (2 PIECES) WITH
THIN FILM BARRIER - W, Mo
OR W + Mo

INSULATING RING

MICA RADIAL CLEARANCE

WELD SHRINKAGE CONTROL

ASSY AXIAL PRELOAD

MODULE DESIGNATOR

LEGEND:

EB - ELECTRON BEAM WELDING

TIG - TUNGSTEN/INERT GAS WELDING

LO & HI - ARE PRELOADS TO BE DETERMINED WITH HI
PROBABLY EQUAL TO 1100 LBS. PRESENTLY IN USE

① - CIRCLED NUMBERS INDICATE INITIAL MODULES,
EXAMPLE: TEM-15A-1

Figure III-1. Initial TEM-15 Design Matrix
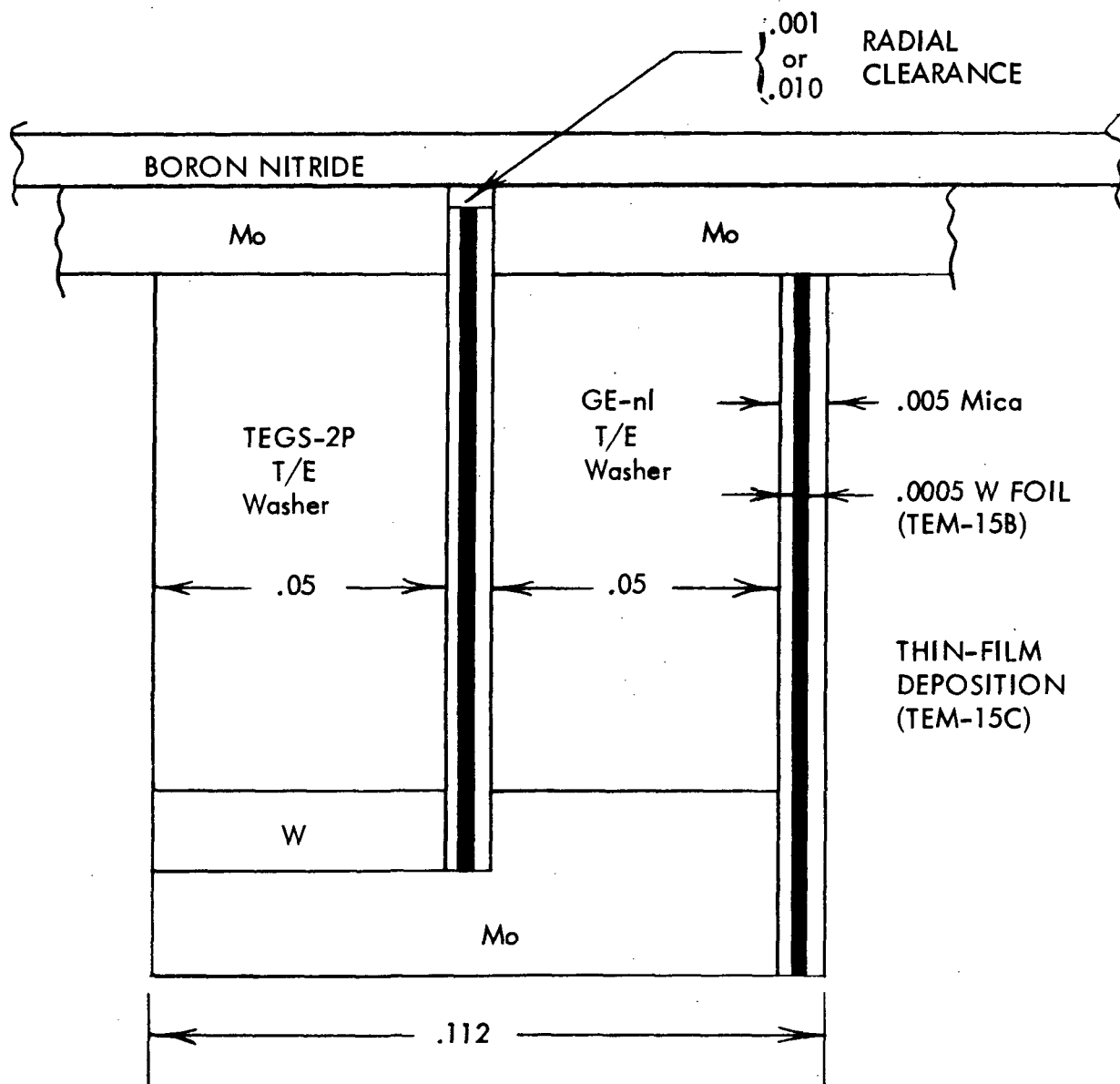
Figure III-2. TEM-15 Couple Assembly

TABLE III-1

PROCESS AND DESIGN FEATURES OF TEM-15 SERIES MODULES

Module	Process and Design Innovation
15A S/N-1	Same as 15A-4 except 300 lb axial preload and EB welded.
15A S/N-4	Baseline design: 36 couples, .050 inch T/E washers, .005 inch mica, .001 inch mica radial clearance, 1100 lb axial preload, TIG welded, hydrogen purged, tungsten insert under p-type washer with axial clearance at assembly.
15A S/N-4A	Same as 15A-4. (Destructively examined after processing.)
15A S/N-4B	Same as 15A-4. (Thermal cycled at 2.5°F/min ramp rate.)
15A S/N-4C	Same as 15A-4. (Thermal cycled at 30°Fmin ramp rate.)
15A S/N-4D	Same as 15A-4. (Steady state endurance tested.)
15A S/N-4E	Same as 15A-4 except not hydrogen purged.
15A S/N-4F	Same as 15A-4 except not hydrogen purged and tungsten insert clearance eliminated.
15A S/N-4G	Same as 15A-4F. (Tested at $\overline{T}_H = 1025^\circ$F, $\overline{T}_C = 480^\circ$F)
15A S/N-4H	Same as 15A-4F except leak-tight glass seals incorporated.
15A S/N-4J	Same as 15A-4F except processing conditions modified.
15A S/N-5	Same as 15A-4 except 300 lb axial preload, EB welded, and .010 inch mica radial clearance incorporated.
15A S/N-8	Same as 15A-4 except .010 inch mica radial clearance incorporated.
15B S/N-4	Same as 15A-4 except each intercouple insulator consists of .0004 inch W foil (full radius) sandwiched between two .0025 inch mica washers.
15B S/N-4A	Same as 15B-4 except each intercouple insulator consists of .0004 inch W foil (1/2 radius) sandwiched between two .005 inch mica washers (33 couples).
15B S/N-4B	Same as 15B-4 except W foil prevented from extending beyond mica at O.D. and tungsten insert clearance eliminated.
15B S/N-4C	Same as 15B-4B except W foil reduced from full to 1/2 radius.
15B S/N-4D	Same as 15B-4B except W foil extended through inner conductor ring.

TABLE III-1 (Continued)

Module	Process and Design Innovation
15C S/N-4	Same as 15A-4 except each intercouple insulator consisted of 2000 - 4000 Å Mo barriers deposited between two 0.0025-inch mica washers.
15C S/N-4A	Same as 15A-4F except each intercouple insulator consisted of 500 - 1500 Å tungsten barriers EB deposited between two 0.0025-inch mica washers.
15C S/N-8	Same as 15C-4 except .010-inch mica radial clearance incorporated.
15D S/N-4	Same as 15A-4 except .010-inch mica insulators incorporated. (33 couples)
15E S/N-4	Same as 15A-4 except APX-4 type PbTeSe substituted for TEGS-2P material.
15F S/N-4	Same as 15A-4F except ANX-6 type PbTe-GeTe substituted for Ge n-type material.
15H S/N-4	Same as 15A-4F except W inserts used under n-type washers at the inner conductor rings.
15P S/N-1	Same as 15H-4 except p-type ternary material substituted for both TEGS-2P and GE-nl washers.

B.   TEM-15A SERIES BASELINE TECHNOLOGY MODULES

TEM-15A series modules were designed for a series of experiments to investigate the influence of variations in component dimensions, assembly procedures, processing conditions and operating temperatures on module performance stability. All of these modules were fabricated with standard .005 inch thick mica insulators. No attempt was made in any TEM-15A series module, to control thermoelectric washer interactions through the use of diffusion barriers. (Diffusion barrier experiments were incorporated into a later series of modules and are discussed below.)

A total of thirteen TEM-15A series modules were fabricated and twelve tested on the program. None of the design variations incorporated in these modules had any effect on calculated beginning-of-life performance. The modifications were made to determine their effects on performance stability (degradation rates). In general, heatup data from these modules indicated that beginning-of-life performance reproducibility was excellent.

Table III-2 lists the results of a statistical analysis to determine degradation rates of the individual TEM-15A series modules. Degradation rates were determined using techniques discussed in Section I of this report.

TEM-15A S/N-4 was the "baseline" design. That is, this module incorporated all of the assembly clearance, fabrication techniques and processing conditions used in the TEM-13G reactor power module designs. Four identical TEM-15A S/N-4 series modules; S/N-4, S/N-4A, S/N-4B, and S/N-4C were fabricated to study the effects of thermal cycling on module performance. TEM-15A S/N-4A was destructively examined immediately after processing and was not placed on test. Destructive examination measurements showed nearly perfect alignment of internal components in this module.

Two other modules of this initial group, S/N-4B and 4C, were tested for relatively short time periods during which they were thermally cycled at $2.5^{\circ}F/$minute and $30^{\circ}F/$minute ramp rates, respectively, 50 times. Cyclic operation produced no measurable performance variations or degradation rate increases in these modules. TEM-15A S/N-4 was tested for a time period comparable to that of the thermally cycled modules, was thermal cycled one

TABLE III-2

PERFORMANCE ANALYSIS SUMMARY OF BASELINE TECHNOLOGY MODULES

Module	Test Conditions $\overline{T}_H/\overline{T}_C$ (°F)	Testing Time (Hours)	Rate of Change: % Per 10,000 Hours			Thermal Cycles	
			R_g	P_e	η	Rapid	30°F/min.
TEM-15A S/N-1	1125/570	25,276	31.0	-16.5	-14.3	11	1
TEM-15A S/N-4	1125/570	2,349	30.3	-21.6	- 7.5	0	1
TEM-15A S/N-4A	1125/570	Not Tested					
TEM-15A S/N-4B	1125/570	2,175	30.3	-19.0	-21.4	0	50
TEM-15A S/N-4C	1125/570	875	*	*	*	1	50
TEM-15A S/N-4D	1125/570	25,471	33.3	-17.2	-14.9	9	2
TEM-15A S/N-4E	{1125/570, 1125/570}	3,090 / 9,406	29.3 / 49.4	-13.8 / -25.9	- 9.6 / -23.3	1 / 3	0 / 1
TEM-15A S/N-4F	{1125/570, 1200/637}	10,146 / 4,369	29.2 / 47.0	-20.2 / -28.5	-15.8 / -27.1	5	2
TEM-15A S/N-4G	{1025/480, 1075/525}	5,051 / 4,225	10.1 / 16.6	- 4.5 / - 9.0	- 2.5 / - 7.9	5	0
TEM-15A S/N-4H	1125/570	5,129	21.9	-12.6	-10.6	1	1
TEM-15A S/N-4J	1125/570	4,194	21.7	- 9.5	- 5.0	0	50
TEM-15A S/N-5	1125/570	24,214	31.3	-16.3	-14.2	13	51
TEM-15A S/N-8	1125/570	2,442	27.7	-21.6	-12.6	1	51

* Data recorded after 190 hours of $\overline{T}_H$ = 1200°F operation.
All data included through January 9, 1973.

time and removed from test. Subsequent destructive examination data from these modules showed that although the amount of inner-to-outer conductor ring displacement was a function of number of cycles and cyclic ramp rates, in no case was the distortion significant enough to conceivably affect performance. The primary reason that the TEM-15 series modules were much less cyclic sensitive than the TEM-13 series modules is that the circuit lengths were much shorter. Very little distortion had been observed in the center four inch portion of the TEM-13 series modules.

Three of the initial group of TEM-15A series modules were specified as long-term steady state endurance tests. These modules were tested at $\overline{T}_H = 1125^\circ F/\overline{T}_H = 570^\circ F$ matched load conditions continuously, except for laboratory power failure caused shutdowns, for testing times exceeding 25,000 hours. Electrical power output and overall efficiency data from this group of long-term TEM-15A series modules are presented as functions of testing time in Figures III-3 and III-4, respectively. As can be readily seen from the data presented in these figures, excellent long-term performance reproducibility was achieved in these modules, indicating that none of the minor design, processing, or fabrication modifications investigated in this series of experiments has had a gross effect on module performance.

A comparison of the data shown in Figures III-3 and III-4 with similar data presented in Section I of this report shows that the power and efficiency levels of the sub-length modules are lower than those of typical reactor power modules. The power output reduction, of course, results from the use of shorter thermoelectric circuits in the sub-length modules. Module power output is directly proportional to circuit length, all other parameters held fixed. The lower efficiency levels of sublength modules result from two factors. First, the TEM-15A series modules utilize relatively large mica insulator/thermoelectric washer axial thickness ratios. This results in increased mica shunt heat losses in the sublength modules. Second, although both types of modules use identical end closures and thus have identical end closure heat loss rates (about 300 watts), these losses represent a significantly larger portion of the total sublength module power requirement (about 1800 watts). Typical reactor power modules have a total power requirement of about 5000 watts, hence the effects of end closure heat
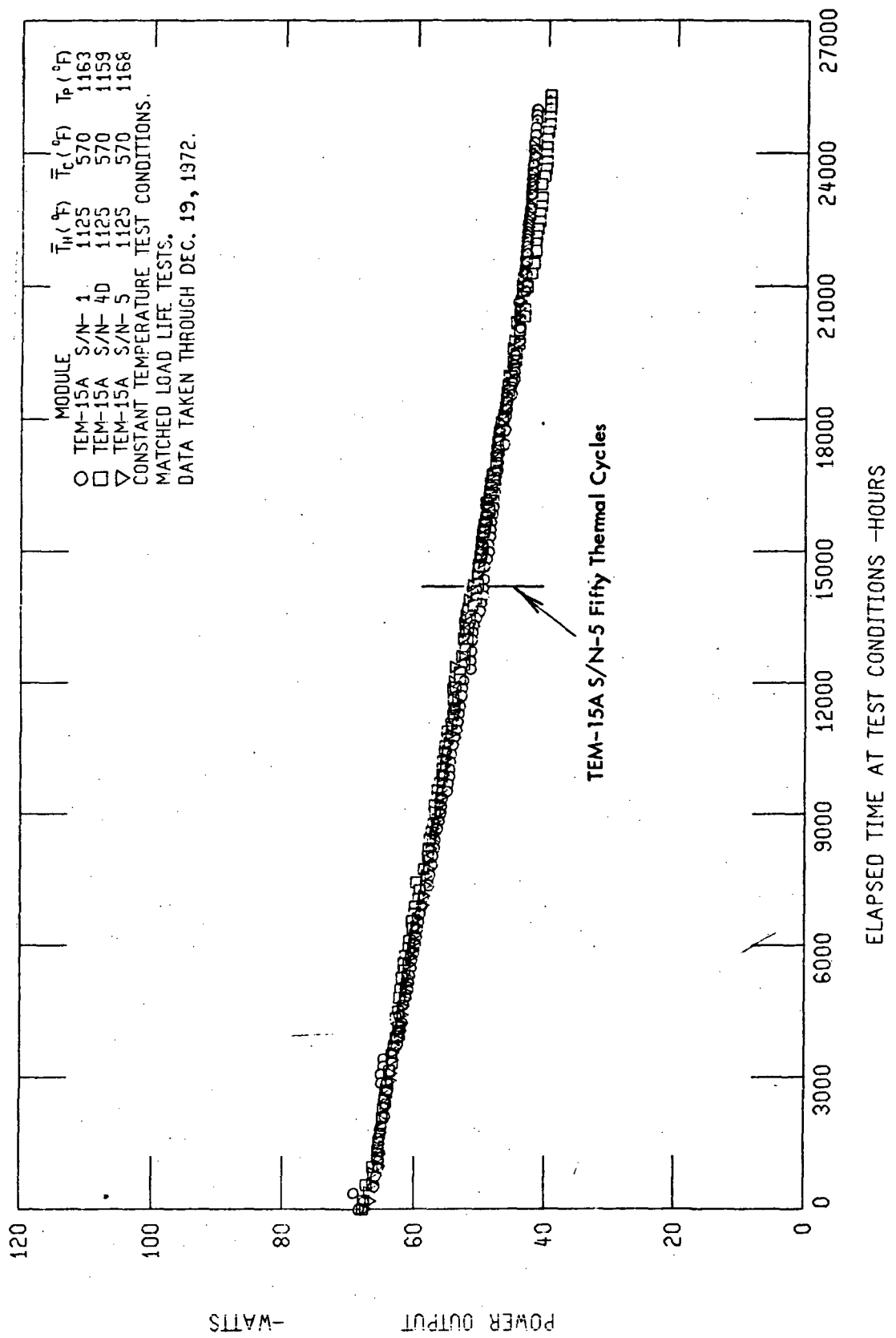
Figure III-3. A Comparison of Power Output Data from Long-Term TEM-15A Series Modules
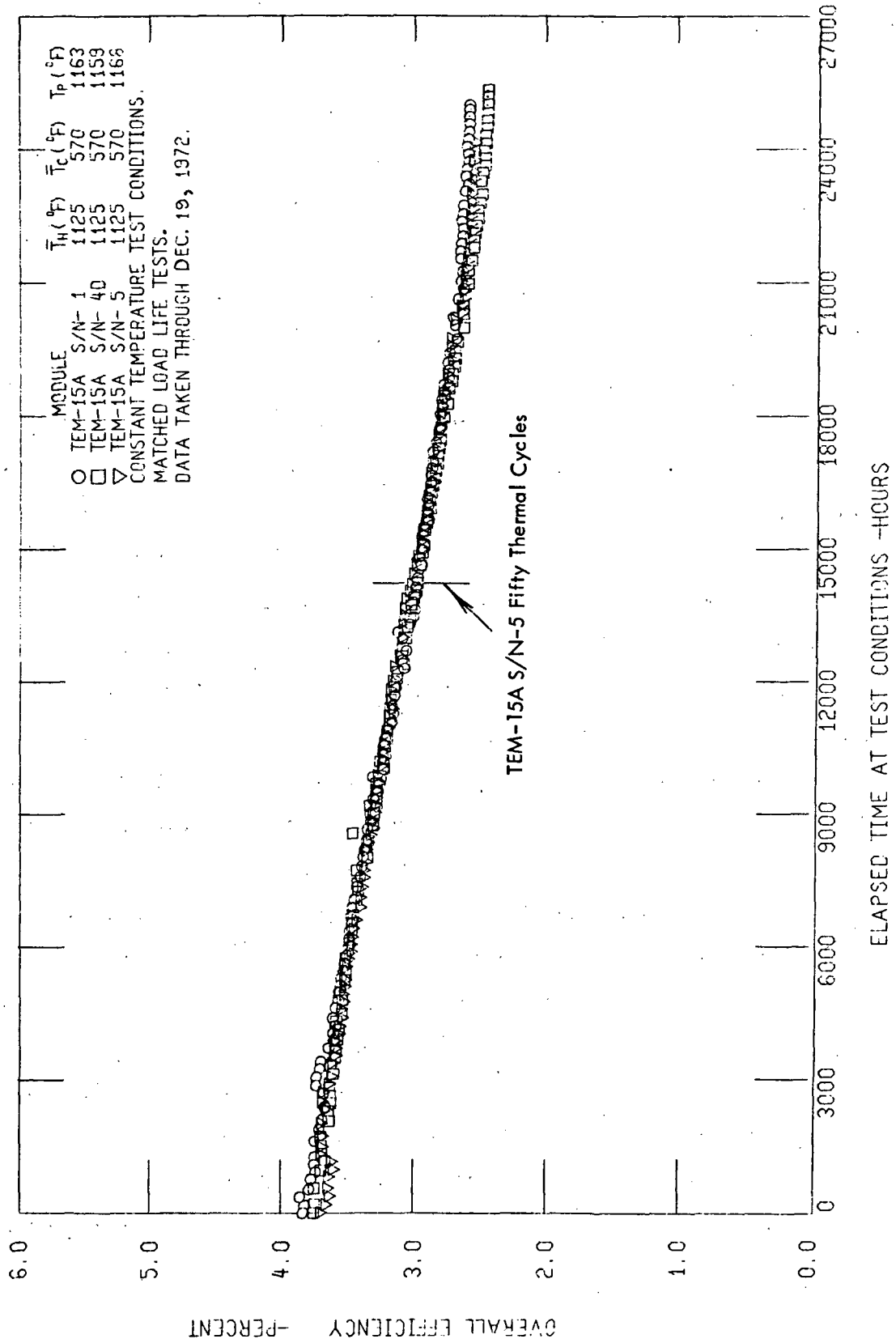
Figure III-4.   A Comparison of Overall Efficiency Data from Long-Term TEM-15A Series Modules

losses on overall efficiency are substantially less for reactor power modules.

More recent data from the long term TEM-15A series modules (data taken after 20,000 hours of operation) indicated that the degradation had begun to deviate from the initial linear trend. Data presented in Figures III-3 and III-4 showed that degradation rates had begun to reduce. This phenomenon would be expected to occur either as the concentration gradient of the migrating specie (tellurium) tends to become equalized or as the reaction which produces the degradation tends toward completion. During the first 20,000 hours of operation, these modules had degraded by approximately 35 percent of their initial power levels. Hence, this deviation from linear degradation would not be expected to occur in thermoelectric power system in which the total degradation of the modules would be restricted to less than 10 percent of the initial level, such as the 5 KWe demonstration system.

It is quite obvious from the data presented in Figures III-3 and III-4 that the 50 thermal cycles performed on TEM-15A S/N-5 after about 14,000 hours of steady state testing had no effect on subsequent performance of the module. The degradation rate analysis of data from this module, presented in Table III-2, also shows the lack of sensitivity to thermal cycling.

TEM-15A S/N-4E was the first sublength technology module fabricated after the identification of the refractory inner clad as a solution to the cyclic distortion problems encountered in TEM-13 series reactor power modules. This module was identical to the baseline TEM-15A S/N-4 module except that the module was not hydrogen purged after fabrication. Hydrogen purging had been performed on all previous modules to reduce trace amounts of oxygen in the thermoelectric circuits. The hydrogen purge step was eliminated to evaluate its effect on module performance stability. It was recognized that the hydrogen purge would have to be eliminated in refractory clad TEM-X series modules because of the formation of hydrides during this operation.

Elimination of this purge operation produced no measurable effect on TEM-15A S/N-4E beginning-of-life performance levels or on degradation rates determined during

the first 3000 hours of $\overline{T}_H = 1125°F/\overline{T}_C = 570°F$ operation. Subsequently the hydrogen

purge step was eliminated from all TEM-15 and TEM-X series modules.

After 3000 hours of operation, the average hot clad temperature of TEM-15A

S/N-4E was increased to $\overline{T}_H = 1200°F$. After 190 hours, the module was returned to the

initial $\overline{T}_H = 1125°F/\overline{T}_C = 570°F$ operating temperatures. Degradation rates recorded during

the 9000 hours of operation after the temporary temperature increase were substantially

higher than those before, as shown in Table III-2. The post $1200°F$ degradation rates

of TEM-15A S/N-4E are in excellent agreement, however, with rates determined for a

later module, TEM-15A S/N-4F, which was held at $\overline{T}_H = 1200°F$ operating conditions.

This indicates that modules assume degradation characteristics related to the peak temper-

atures to which the modules are operated. Hence, no reductions in degradation in a thermo-

electric system can be achieved by reducing operating temperatures during low power

requirement periods. This also explains the higher $\overline{T}_H = 1085°F$ degradation rates of TEM-X

S/N-3D, discussed in Section I of this report, after the initial $\overline{T}_H = 1175°F$ operation.

Testing of three additional TEM-15A S/N-4 series modules; S/N-4F, S/N-4G

and S/N-4H was conducted at various temperature levels to determine the relationship

between operating temperatures and degradation rates. Power output and overall efficiency

data from these modules are presented as functions of testing time in Figures III-5 and

III-6, respectively. Testing temperatures of two of these modules, S/N-4F and S/N-4G

were modified at the times indicated on the curves. Degradation rates for these modules

have been calculated and listed for all sets of operating conditions in Table III-2. A

discussion of the temperature – degradation rate relationship of these and reactor power

modules is given in Section I of this report.

Performance data from the final TEM-15A series module fabricated, S/N-4J,

are also presented in Figures III-5 and III-6. Processing (gas-pressure-sintering) conditions

were modified in this module to achieve full compaction at lower temperature and higher

pressure than the standard autoclave cycle used for all previous TEM-15 series modules.

Data presented in Table III-2 indicate that after 4194 hours of operation, TEM-15A S/N-4J
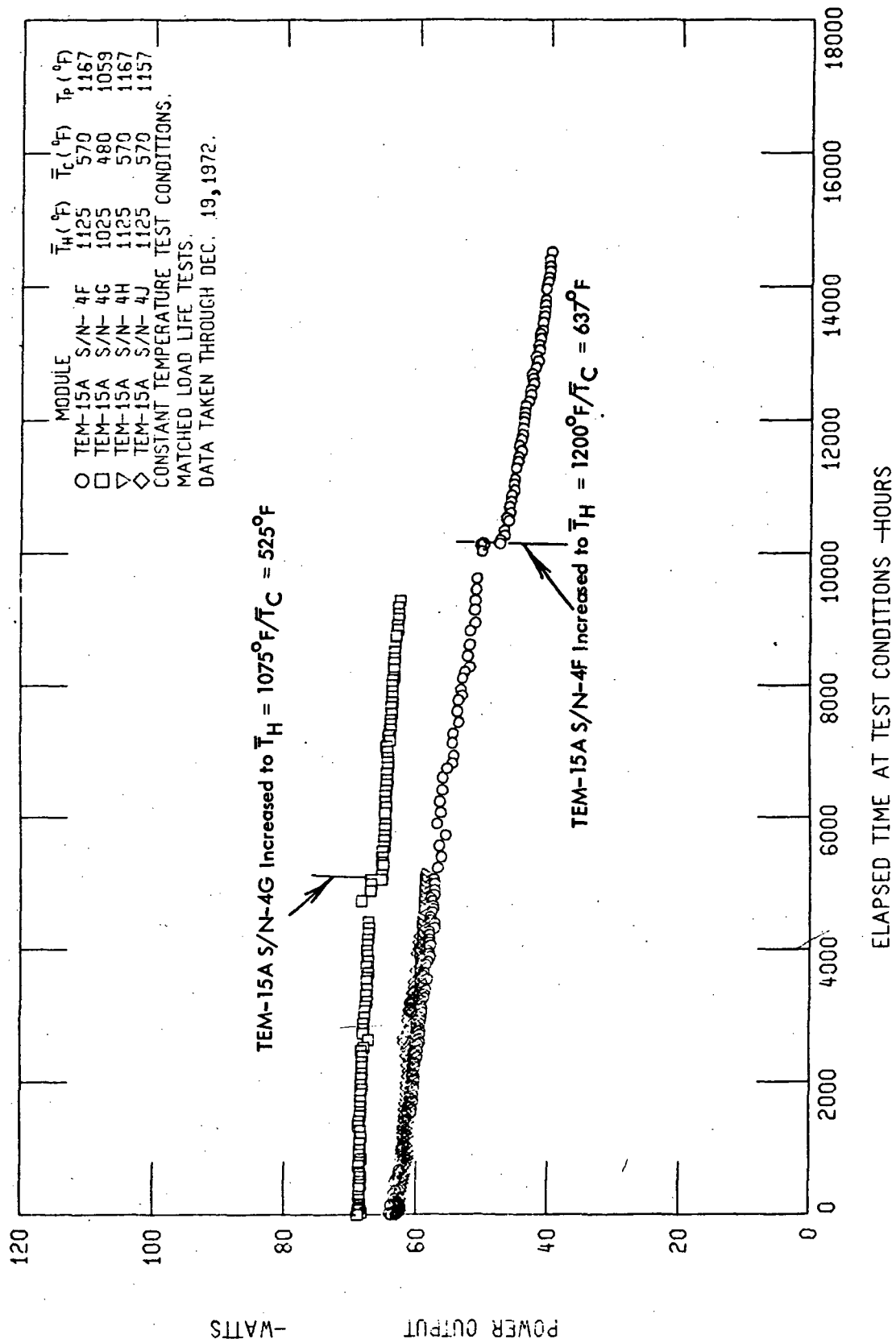
Figure III-5. A Comparison of Power Output Data from Recent TEM-15A Series Modules
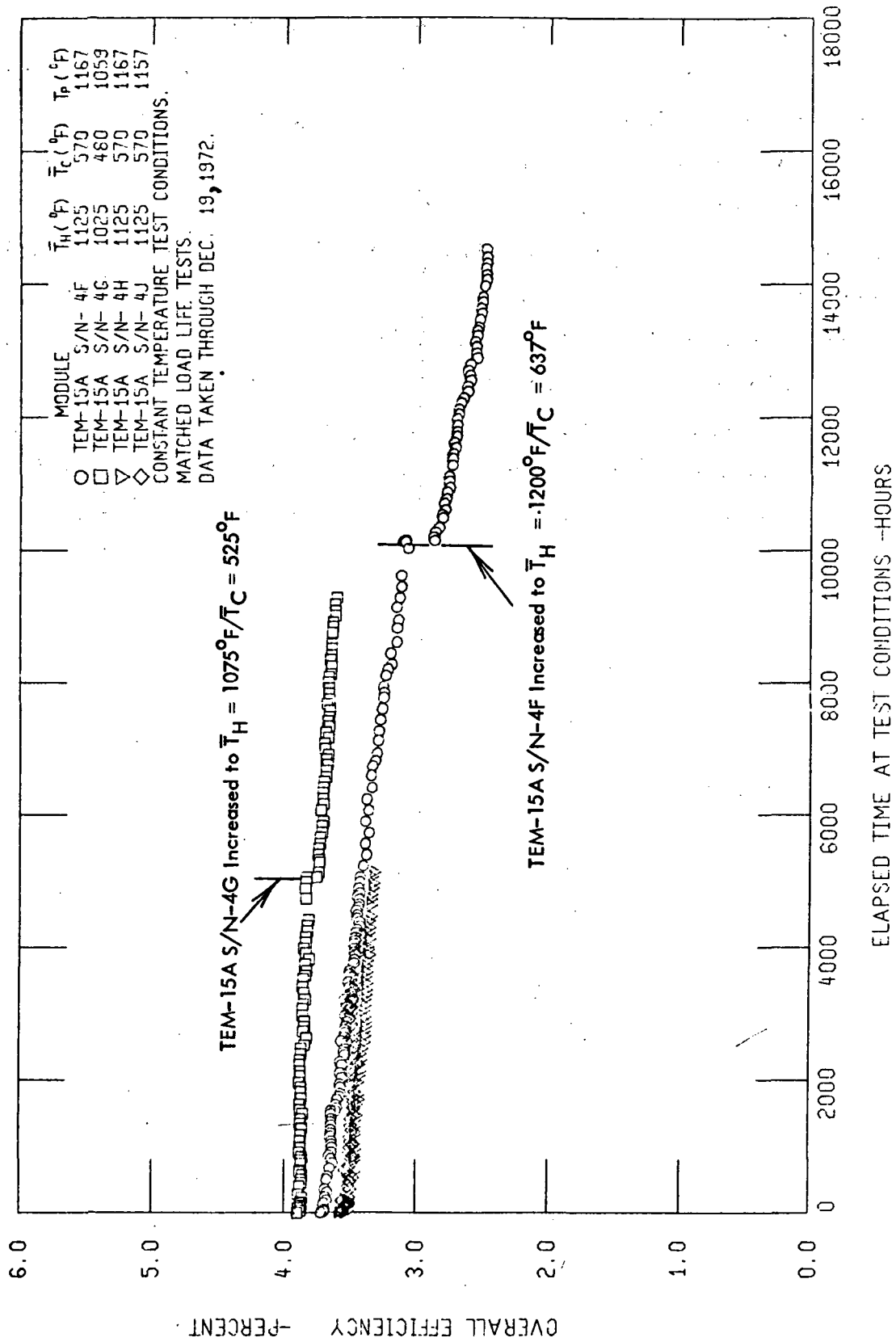
Figure III-6. A Comparison of Overall Efficiency Data from Recent TEM-15A Series Modules

had a power degradation rate nearly one-half as large as the rate displayed by identical modules tested at the same temperatures: $\overline{T}_H = 1125°F/\overline{T}_C = 570°F$. Based on these data from this module, it was decided to use the revised processing conditions on the final full-length reactor power module, TEM-X S/N-3M.

The rationale for this change in process conditions was that some modules, destructively examined prior to test, showed indications of free tellurium around the p-type washer and it was thought that the existance of this free tellurium after processing may have been contributing significantly to the degradation observed. The premise was therefore made that the free tellurium within this p-type material was being melted and subsequently squeezed out of the washer during the high temperature processing. The processing temperature for TEM-15 S/N-4J was therefore established at 440°C, which is below the melting temperature of tellurium, with a pressure increase to 30,000 psi to achieve compaction.

C.   TEM-15B SERIES TUNGSTEN FOIL BARRIER MODULES

The TEM-15B designation applies to all sub-length reactor technology modules incorporating tungsten foil diffusion barriers positioned between two mica electrical insulators.   Five TEM-15B series modules were fabricated and tested on the program and the individual design features of each of the modules are listed in Table III-1.

The first four of the five TEM-15B series modules were experiments to determine the effects of the foil/mica insulator variations on module performance. Electrical power output and overall efficiency data from these four modules, all tested at $\overline{T}_H = 1125^\circ F/$ $\overline{T}_C = 570^\circ F$ operating temperatures are presented in Figures III-7 and III-8. A comparison of these data with similar performance data from TEM-15A series modules discussed above, shows that the use of diffusion barriers resulted in substantial reductions in both power and efficiency at beginning-of-life. Calculations had indicated that substantial heat flux increases result from the use of the tungsten foil. The increased heat flux, in turn, produced increased radial temperature drops across the clads, boron nitride insulating sleeves and conductor rings of the module, thus reducing the temperature drop across the lead telluride material. This reduced thermoelectric temperature drop produced an attendant drop in power output. The different barrier configurations incorporated into the individual TEM-15B series modules produced beginning-of-life performance variations which were in excellent agreement with calculations.

Although the power output and efficiency levels of the TEM-15B series modules were somewhat lower than those of the non-barrier TEM-15A series modules, substantially improved performance stability was demonstrated. Degradation rates exhibited by each of the TEM-15B series modules are summarized in Table III-3. Characteristic power output degradation rates for modules incorporating tungsten foil barriers and .005 inch mica insulators were 13 percent per 10,000 hours for $\overline{T}_H = 1125^\circ F/\overline{T}_C = 570^\circ F$ operation compared to 17 percent per 10,000 hour degradation rates of non-barrier TEM-15A series modules operated at identical temperatures. In addition, a comparison of data from TEM-15B S/N-4B and 4C verified that substantial performance improvements are achieved with

TABLE III-3

PERFORMANCE ANALYSIS SUMMARY OF ADDITIONAL TEM-15 SERIES MODULES

Module	Test Conditions $\overline{T}_H/\overline{T}_C$ (°F)	Testing Time (Hours)	Rate of Change: % Per 10,000 Hours			Thermal Cycles	
			R_g	P_e	η	Rapid	30°F/min
TEM-15B S/N-4	1125/570	3,637	17.9	- 6.9	- 5.7	2	0
TEM-15B S/N-4A	1125/570	19,723	14.8	- 7.8	- 6.4	6	1
TEM-15B S/N-4B	1125/570	14,656	18.3	-12.7	-10.6	5	1
TEM-15B S/N-4C	1125/570	10,918	22.1	-14.5	-10.9	5	0
TEM-15B S/N-4D	1125/570	5,269	*	*	*	0	50
TEM-15C S/N-4	1125/570	2,753	29.0	-13.8	-13.9	2	0
TEM-15C S/N-4A	{1125/570 {1125/570**	4,433 6,830	20.2 23.4	-10.6 -16.0	- 7.5 -13.4	5	1
TEM-15C S/N-8	1125/570	22,727	26.0	-14.2	-11.9	10	1
TEM-15D S/N-4	1125/570	20,961	20.9	-11.5	- 9.1	9	1
TEM-15H S/N-4	1125/570	15,067	23.6	-14.4	-11.7	5	1

All data included through January 9, 1973.

* Module design prohibited meaningful performance stability analysis
** Data recorded after momentary overtemprature to 1360°F
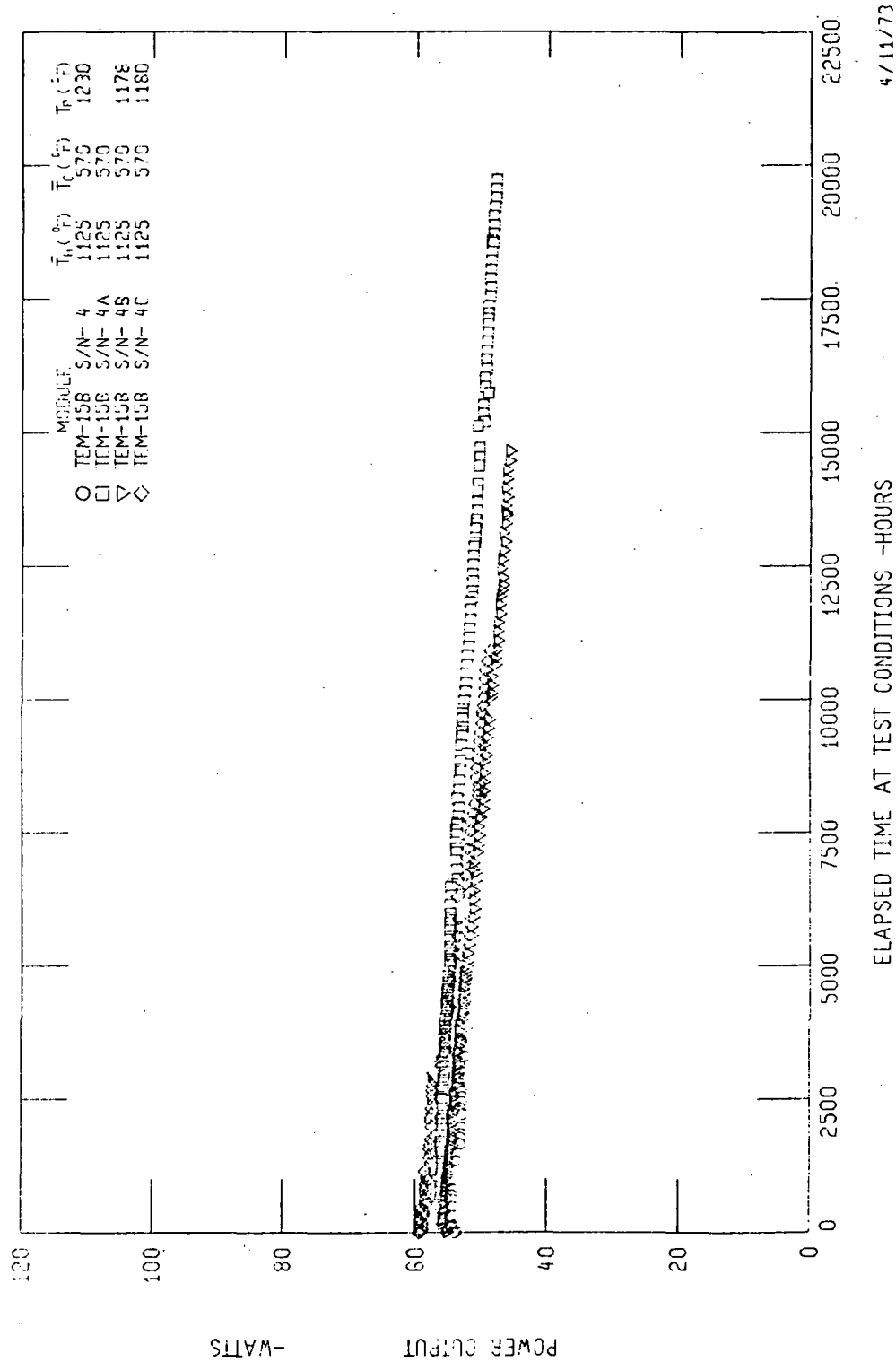
Figure III-7. A Comparison of Power Output Data from TEM-15B, Tungsten Foil Barrier Modules
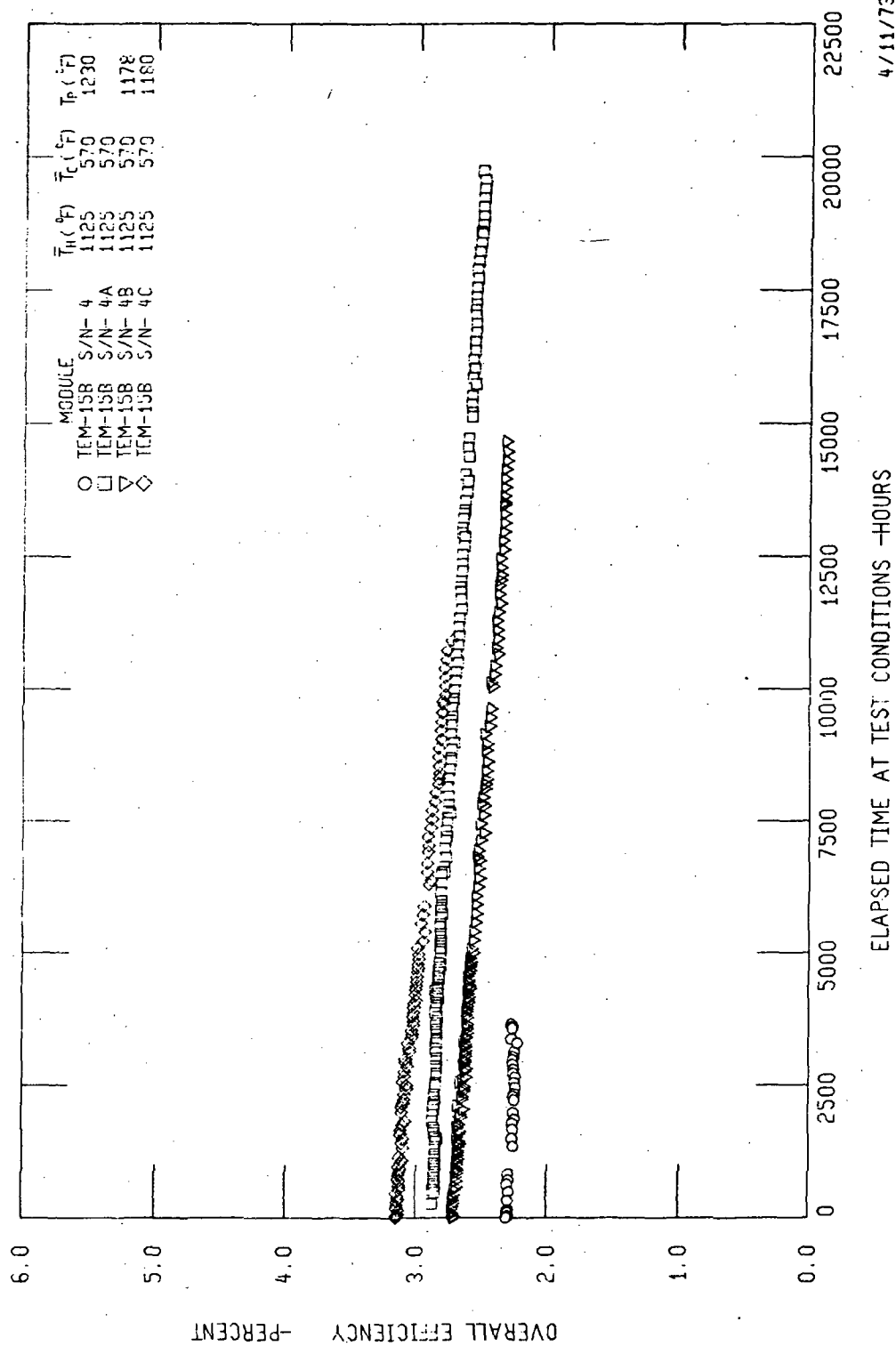
Figure III-8. A Comparison of Efficiency Data from TEM-15B, Tungsten Foil Barrier Modules

little or no power degradation penalty by terminating the foil barriers midway radially in the thermoelectric washers. Temperatures beyond the midpoint are too low to sustain tellurium diffusion.

Both the data plots and the degradation analysis show that the performance stability of the 0.010 inch mica module (TEM-15B S/N-4A) was substantially better than that of either module incorporating 0.005 inch mica. The power output degradation exhibited by this module was less than 8 percent per 10,000 hours, a factor of two reduction compared to TEM-15A series modules. This is the barrier configuration used in the TEM-X series reactor modules. The B.O.L. performance penalty associated with the use of tungsten foil barriers was greatly reduced in reactor power modules because of axially thicker thermoelectric washers and fewer intercouple insulators per unit length at the thermoelectric circuit.

Destructive examination of TEM-15B S/N-4, the only module of this group to be destructively examined, indicated that residual degradation observed in modules incorporating tungsten foil intercouple diffusion barriers was caused by tellurium transport around the ends of the tungsten foils. An additional module, TEM-15B S/N-4D was designed to prove this. Tellurium transport around the ends of the tungsten foils was combatted by extending the foil radially inward through the entire inner conductor ring to the boron nitride insulating sleeve. This required fabricating the inner conductors as two separate rings. Because of the uncertainties involved in the introduction of axial electrical interfaces, this experiment was defined to determine the effects of increasing the tellurium diffusion path length, but was not intended to identify a couple design to be incorporated into a reactor module.

Beginning-of-life performance data from TEM-15B S/N-4D indicated that the axial conductor ring interface resistance component was more than twice the value of the bulk resistance of the module. In standard modules which incorporate no axial electrical interfaces, there is no measurable interface resistance component. Because of the high TEM-15B S/N-4D interface resistance which actually decreased with time, it was impossible to evaluate the effects of reduced intercouple tellurium transport based on experimental data.

It was intended that these effects would be determined based on results of a destructive examination. The program was terminated prior to initiating this destructive examination.

D.   TEM-15C SERIES ELECTRON BEAM VAPOR DEPOSITED MODULES

TEM-15C series modules were experiments in which thin films of molybdenum or tungsten formed by electron beam vapor deposition (E. B. V. D.), were used to retard the transport of tellurium between adjacent thermoelectric washers. In this design two .0025 inch thick mica insulators were used between each adjacent pair of thermoelectric washers as shown in Figure III-2. A deposition film of 1000 to 2000 angstroms was placed on one side of each mica piece, and the mica oriented so that the coated faces were together. Since the total electron beam deposited film was approximately 3 percent as thick as the tungsten foil barriers incorporated in the TEM-15B series modules, shunt heat losses were negligible.

Three TEM-15C series modules were designed, fabricated and tested in this program. Design features of each of these modules are listed in Table III-1. The first two modules, S/N-4 and S/N-8, incorporated molybdenum barriers. Degradation rate reductions were observed in these modules, as is shown in Table III-3. However, the thin film molybdenum barriers did not exhibit the same degree of performance stability observed in foil barrier TEM-15B series modules.

Subsequently, TEM-15C S/N-4 was removed from static test and destructively examined after 2753 hours of $\overline{T}_H = 1125^\circ F/\overline{T}_C = 570^\circ F$ operation. Data from this examination showed that the molybdenum had reacted with the diffusing tellurium to form a molybdenum-telluride compound, thus, substantially reducing the effectiveness of molybdenum as a diffusion barrier.

The second module of this series, TEM-15C S/N-8 remained on static test. Power output and efficiency data from this module, which had accrued over 22,500 hours of testing, are shown in Figures III-9 and III-10, respectively.

The final TEM-15C series module, S/N-4A, was essentially identical to S/N-4 except that thin film tungsten barriers were utilized. Performance data from this module are also shown in Figures III-9 and III-10. Degradation rate data are presented in Table III-3. During the first 4433 hours of operation, TEM-15C S/N-4A exhibited degradation
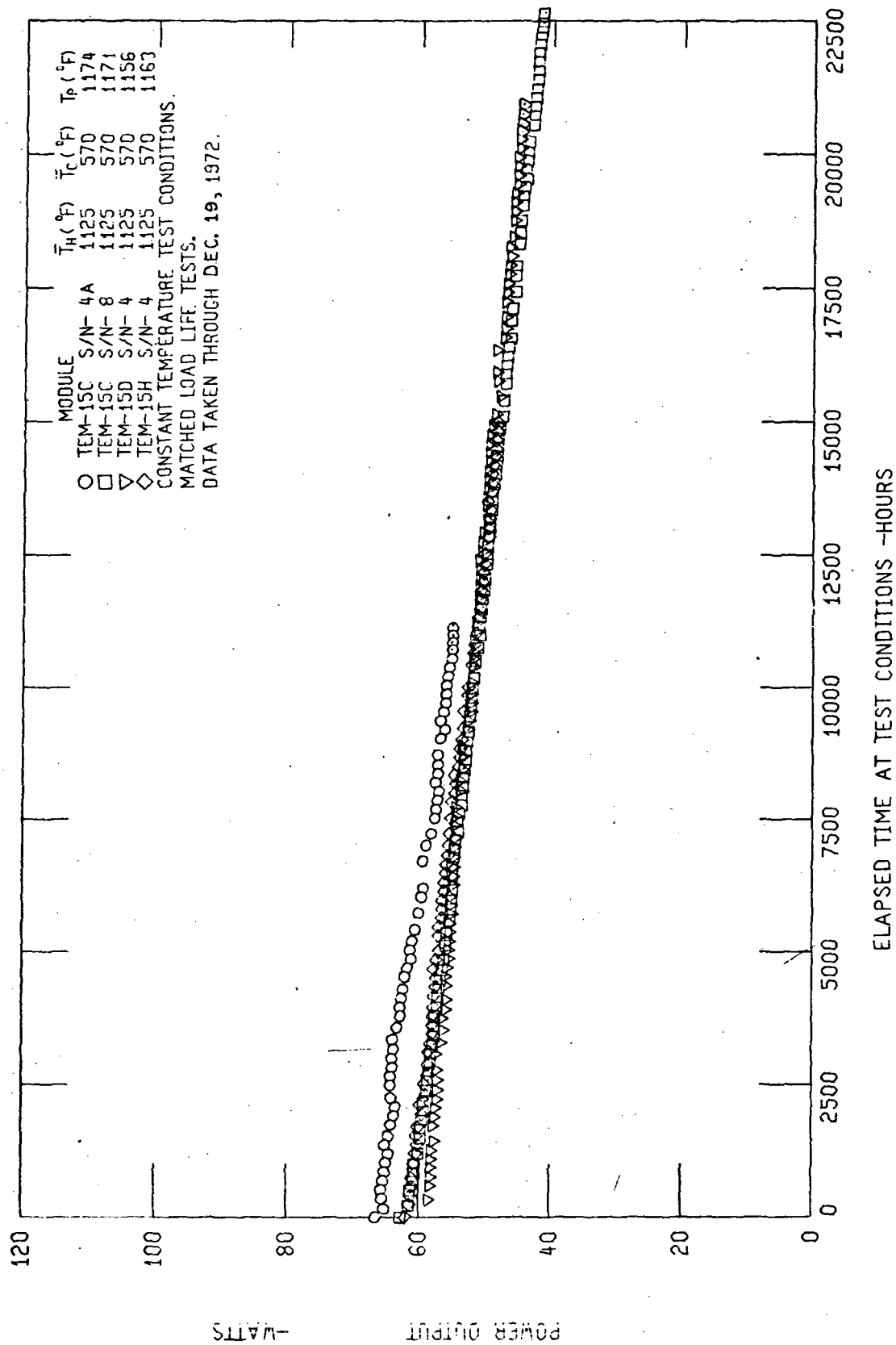
Figure III-9. A Comparison of Power Output Data from Improved Performance Stability TEM-15 Series Modules
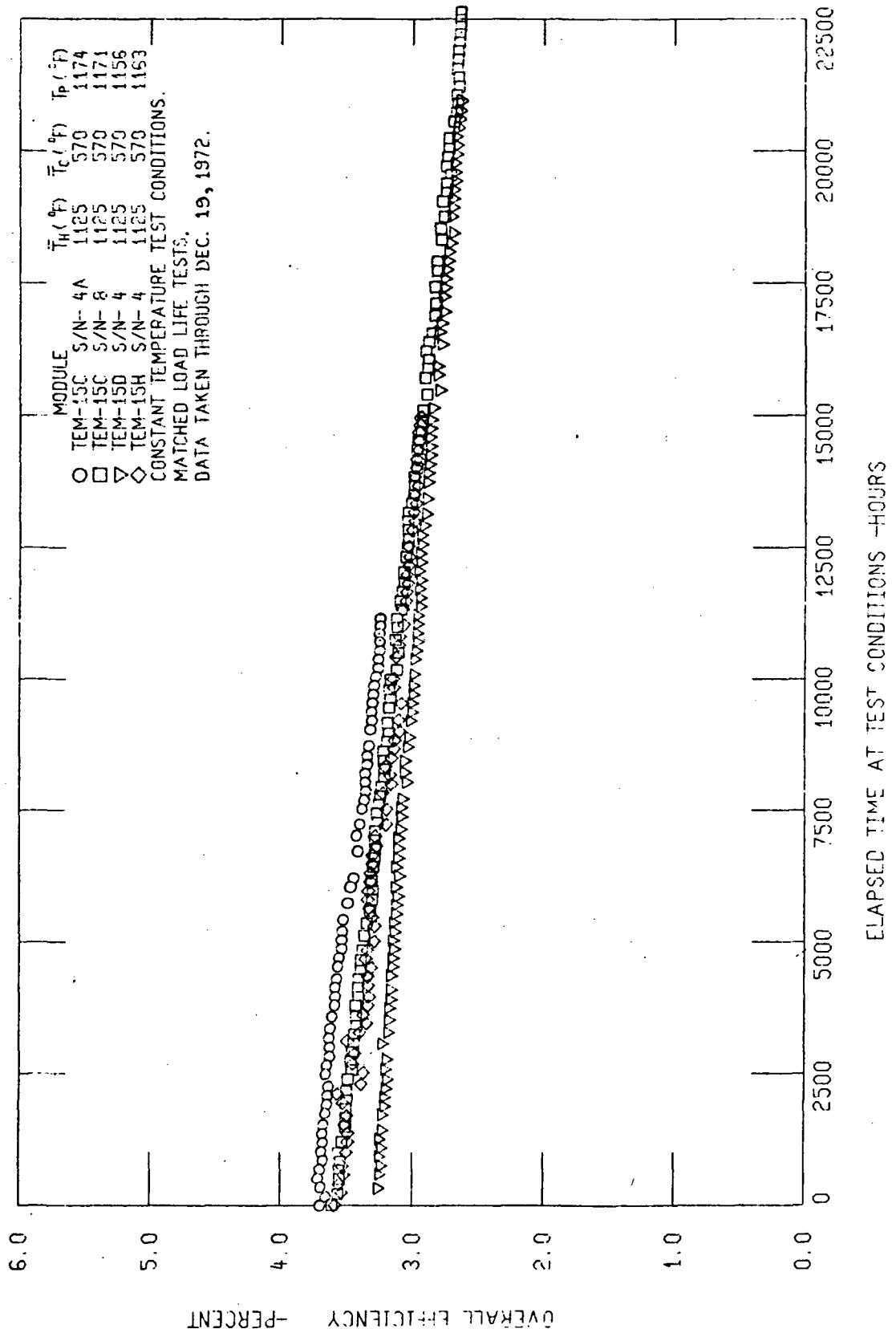
Figure III-10. A Comparison of Overall Efficiency Data from Improved Performance Stability
TEM-15 Series Modules

rates as low as had been observed for tungsten foil barrier modules. These results were of particular significance because the thin film barriers provide substantially improved B.O.L. performance relative to the standard foil barrier through the elimination of shunt heat losses. Based on these results, a substantial effort in the first half of GFY 1973 was directed toward the improvement of tungsten foil deposition techniques to allow their incorporation in reactor power modules.

After 4433 hours of operation, TEM-15C S/N-4A experienced a rather severe momentary overtemperature as a result of controller malfunction. During the incident, the module inner clad temperature rose to 1360°F before the heater power was shutoff. After standard $\overline{T}_H = 1125^{\circ}F/\overline{T}_C = 570^{\circ}$F test conditions were restored, somewhat acceleration rates were observed. Table III-3 lists the TEM-15C S/N-4A degradation rates before and after the overtemperature.

E.   ADDITIONAL TECHNOLOGY MODULE EXPERIMENTS

In addition to baseline TEM-15A and barrier TEM-15B and C series modules, five one-of-a-kind sublength technology modules were fabricated during the course of Compact Thermoelectric Converter System Technology Program. The individual design features of each of those modules are listed in Table III-1.

1. Material Experiment Modules

Three of the modules; TEM-15E S/N-4, TEM-15F S/N-4 and TEM-15P S/N-1 were material experiment modules related to the ternary thermoelectric material program. The first two of these modules were tested in static test stands. Results of these tests are discussed in a later section of this report as an integral part of the ternary material development program discussion. The final material experiment module, designated TEM-15P S/N-1, was fabricated and processed during the latter half of 1972. This module incorporated ternary p-type thermoelectric material in both legs of each couple. The purpose of this experiment was to generate electrical resistivity and thermal conductivity data for the new material and to allow a determination of degradation rates associated with the ternary p-type material. Plans to test the module, however, were suspended as a result of the program close out notice.

2. TEM-15D S/N-4: .005 Inch Mica Module

TEM-15D S/N-4 was sublength technology module designed with .010 inch mica insulators containing no additional diffusion barrier mechanisms. This module was designed with 33 thermoelectric couples as opposed to 36 used in all previously fabricated TEM-15 series modules except TEM-15B S/N-4A which also incorporated .010 inch mica. The reduction in the number of couples was required to accommodate the increased mica thickness within the 4.0 inch (nominal) circuit length. The purpose of this experiment was to determine the effects of mica thickness alone on module degradation.

TEM-15D S/N-4 was placed on static test May 26, 1970 at $\overline{T}_H = 1125^{\circ}F/\overline{T}_C = 570^{\circ}F$ operating temperatures and was tested essentially continuously until the end of the program.

Power output and efficiency data from the module are presented in Figures III-9 and III-10, respectively. A reduction in the B.O.L. levels of both parameters was the result of replacing a portion of the thermoelectric material with mica in this design.

Substantial performance stability improvements were observed in TEM-15D S/N-4 as a result of the increased mica thickness. These data are shown in Table III-3. The power output degradation of TEM-15D S/N-4 was approximately one-third lower than that of the baseline TEM-15A series modules operated at the same temperatures. Based on these data, a reactor power module, TEM-X S/N-4, was fabricated and tested with the same intercouple insulating configuration used in TEM-15D S/N-4.

3. TEM-15H S/N-4: Three Piece Inner Conductor Ring Module

The final sublength technology module, TEM-15H S/N-4 was identical in design to the TEM-15A baseline technology modules except that a tungsten insert was incorporated under both the p- and n-type lead telluride washers. The result was a three-piece inner conductor ring. This modification was made to eliminate a surface reaction between molybdenum and n-type lead telluride observed at the hot junctions of destructively examined modules.

Static testing of TEM-15H S/N-4 was initiated March 2, 1971. Performance data recorded during steady state $\overline{T}_H = 1125°F/\overline{T}_C = 570°F$ operation of the module are shown in Figures III-9 and III-10. A statistical analysis of these data indicated that modifications incorporated into the TEM-15H design resulted in a measurable reduction in degradation rates. The results of this analysis are shown in Table III-3. As a result of the success of this experiment, the final reactor power module fabricated in this program incorporated the three-piece inner conductor ring design to further improve performance stability.

IV. TERNARY THERMOELECTRIC MATERIALS

A. INTRODUCTION

From its inception in 1958 to date, the development of tubular thermoelectric module technology has incorporated p-type PbTe (3M Company TEGS-2P) and PbTe-SnTe (3M Company TEGS-3P), and n-type PbTe (3M Company TEGS-2N and -3N, General Electric Company GE-NL), as the p- and n-type leg materials in the thermoelectric couple. Until fairly recently, no materials work had been reported that indicated the existence of different p- and/or n-type materials which had superior Figure of Merit (Z) over the tubular module operating temperature range and which were likely to be chemically and mechanically compatible with the general tubular module materials/structure/fabrication combination.

In 1968 and 1969, however, reports[1] of work performed by Radio Corporation of America for the U. S. Atomic Energy Commission indicated that certain dilute p- and n-type PbTe-base alloys might be advantageously considered as improved tubular module materials. Accordingly, a work task was instituted at WANL under this program to investigate the application of these materials on both analytical and experimental bases.

It is well established that in materials such as PbTe, large substitutional alloy additions of either anion or cation species (or both) will substantially lower the lattice contribution to the thermal conductivity. However most investigations, conducted with alloy addition concentrations of order 25 to 50 atomic percent, showed that a reduction of carrier mobility was effected along with the lowering of lattice thermal conductivity, and that the overall effect on thermoelectric performance was little or no improvement.

RCA, working initially with n-type PbTe - GeTe alloys, reported that if the concentration of alloy addition was restricted to the dilute region (less than 10 atomic percent), substantial lowering of the lattice thermal conductivity could still be achieved, but degradation of electrical properties was much less severe and a substantial overall

[1] "Improved Compatible Materials for Thermoelectric Power Generation", RCA Laboratories, Princeton, N.J., Report Nos. NYO-3886-1 (February, 1968), - 2 (November, 1968), - 3 (April, 1969) and - 4 (August, 1969).

improvement in thermoelectric performance was obtained. They then found a similar situation in the case of p-type PbTe - PbSe alloys. The WANL program included investigations of both types of alloys, and these are discussed separately in the remaining main sections of this task report.

The first phase of the WANL work, conducted from mid-1970 through mid-1971 resulted in the preliminary identification of optimized p- and n-type compositions and the fabrication and testing of TEM-15 type experimental modules in which those compositions were evaluated. This work is discussed in the following sections as "Previous Development." Although the results at that time indicated a need for continuing the experimental work to complete the characterization and optimization of these materials and more thoroughly develop their application to the tubular module, further work on the task was canceled. In mid-1972, with the availability of additional funding, the work was resumed, and the bulk of this report is concerned with activity since that time.

B. N-TYPE PbTe - GeTe TERNARY ALLOYS

1. Previous Development

Working initially with crystal ingots grown from the melt by the vertical Bridgeman method, and later with specimens fabricated by an elaborate hot pressing procedure from powder obtained from quenched, homogeneous polycrystalline ingots, RCA concluded that their n-type composition $Pb_{.951}Ge_{.05}Te\ (PbI_2)_{.001}$ was the best of the compositions they investigated for use in the temperature range which coincides with the tubular module operating region.

It was decided at the outset to conduct the WANL investigation of PbTe-GeTe alloys in such a way that the technology developed in the investigation would be as directly applicable as possible to use of the material in the tubular module. For example, materials were prepared by forming polycrystalline ingots, and test specimens were fabricated from these using powder metallurgical techniques. While this approach undoubtedly yields specimens of somewhat lesser quality than, say, a grown and sliced Bridgeman crystal, it is more important to consider that the specimen fabrication techniques are directly applicable to the fabrication of tubular module washers; furthermore, properties measured on powder metallurgy specimens are more representative of material behavior in an operating tubular module than are properties measured on single crystal specimens.

In accordance with this rationale, specimens of $Pb_{.951}Ge_{.05}Te(PbI_2).001$ were prepared and tested by WANL, but the Seebeck coefficients, α, and electrical resistivities, ρ, measured over the temperature range 300 to 850°K, were not the same as the values reported by RCA for these materials. Also, in the course of investigating various materials processing conditions, including hydrogen heat treating temperatures from 550°C to 750°C, it was found that the material was unstable with respect to processing temperature. As processing temperature increased, both α and ρ decreased, indicating an increase in the electrical carrier concentration. Evidence was obtained which indicated that a Ge-rich, nearly-submicroscopic precipitate phase, was developing in the material as process temperatures were increased, and this was presumed at the time to be the source of the changing material properties.

To investigate the lack of correspondence between the properties of RCA and WANL prepared $Pb_{.951}Ge_{.05}Te(PbI_2)_{.001}$, a series of additional specimens having small modifications in their lead and iodine content were prepared and tested. The compositions of these specimens are given in the left-hand column of Table IV-1; the electrical properties of specimens of each composition were measured on material which had been processed at both $650^{\circ}C$ and $750^{\circ}C$. Also, to determine whether a reduction in Ge content would increase the thermal stability of the material structure, a corresponding series of reduced Ge specimens were similarly prepared and tested; the compositions of these latter specimens are given in the right-hand column of Table IV-1.

Briefly, the test results on the above specimens indicated the following:

a. None of the specimens tested exhibited both α and ρ values which closely corresponded to the RCA reported values.

b. Reducing the Ge content of a material of given iodine content decreased (but did not eliminate) the previously discussed thermal instability.

c. Despite (a) and (b) above, several of the compositions tested exhibited α and ρ values which promised overall energy conversion characteristics superior to the GE-NL n-type PbTe.

It was found, in the course of further investigation, that the electrical resistivity values measured on standard cold pressed specimens were a much stronger function of specimen density than was the case with unalloyed n-type PbTe. Because of this density effect, specimens were prepared to near theoretical density by hot pressing. However, the resulting samples had many surface and bulk cracks. Nonetheless, Figure IV-1 gives the estimated figure of merit data for five compositions based on measurements made on the hot pressed specimens. Superimposed on Figure IV-1 are solid curves representing figure of merit data from the RCA work on the $Pb_{.951}Ge_{.05}Te(PbI_2)_{.001}$ material and also for GE-NL n-type PbTe. Based on the information presented in Figure IV-1, the WANL ANX 6 composition $Pb_{.95}Ge_{.05}Te(PbI_2)_{.0007}$ was selected as the optimum PbTe-GeTe alloy for experimental module TEM-15F S/N-4.

TABLE IV-1

COMPOSITIONS OF EXPERIMENTAL N-TYPE PbTe-GeTe ALLOYS

Compositions Based on $Pb_{.95}Ge_{.05}Te$		Compositions Based on $Pb_{.97}Ge_{.03}Te$	
Molecular Formula	WANL Designation	Molecular Formula	WANL Designation
$Pb_{.95000}Ge_{.05}Te(PbI_2)_{.00035}$	ANX 8	$Pb_{.97000}Ge_{.03}Te(PbI_2)_{.00035}$	ANX 12
$Pb_{.95035}Ge_{.05}Te(PbI_2)_{.00035}$	ANX 9	$Pb_{.97035}Ge_{.03}Te(PbI_2)_{.00035}$	ANX 13
$Pb_{.9500}Ge_{.05}Te(PbI_2)_{.0007}$	ANX 6	$Pb_{.9700}Ge_{.03}Te(PbI_2)_{.0007}$	ANX 10
$Pb_{.9507}Ge_{.05}Te(PbI_2)_{.0007}$	ANX 7	$Pb_{.9707}Ge_{.03}Te(PbI_2)_{.0007}$	ANX 11
$Pb_{.950}Ge_{.05}Te(PbI_2)_{.001}$	ANX 5	$Pb_{.970}Ge_{.03}Te(PbI_2)_{.001}$	ANX 4
$Pb_{.951}Ge_{.05}Te(PbI_2)_{.001}$	ANX 1 (RCA Comp.)	$Pb_{.971}Ge_{.03}Te(PbI_2)_{.001}$	ANX 3

Symbol	Composition	Specimen No.	Final Density (% Theor.)
▽	Pb$_{.9707}$ Ge$_{.03}$ Te(PbI$_2$)$_{.0007}$	2122 (ANX11)	99.15
O	Pb$_{.951}$ Ge$_{.05}$ Te(PbI$_2$)$_{.001}$	2113 (ANX1)	99.47
+	Pb$_{.95}$ Ge$_{.05}$ Te(PbI$_2$)$_{.001}$	2119 (ANX5)	99.48
△	Pb$_{.9700}$ Ge$_{.03}$ Te(PbI$_2$)$_{.0007}$	2121 (ANX10)	99.55
X	Pb$_{.95}$ .Ge$_{.05}$ Te(PbI$_2$)$_{.0007}$	2120 (ANX6)	99.84
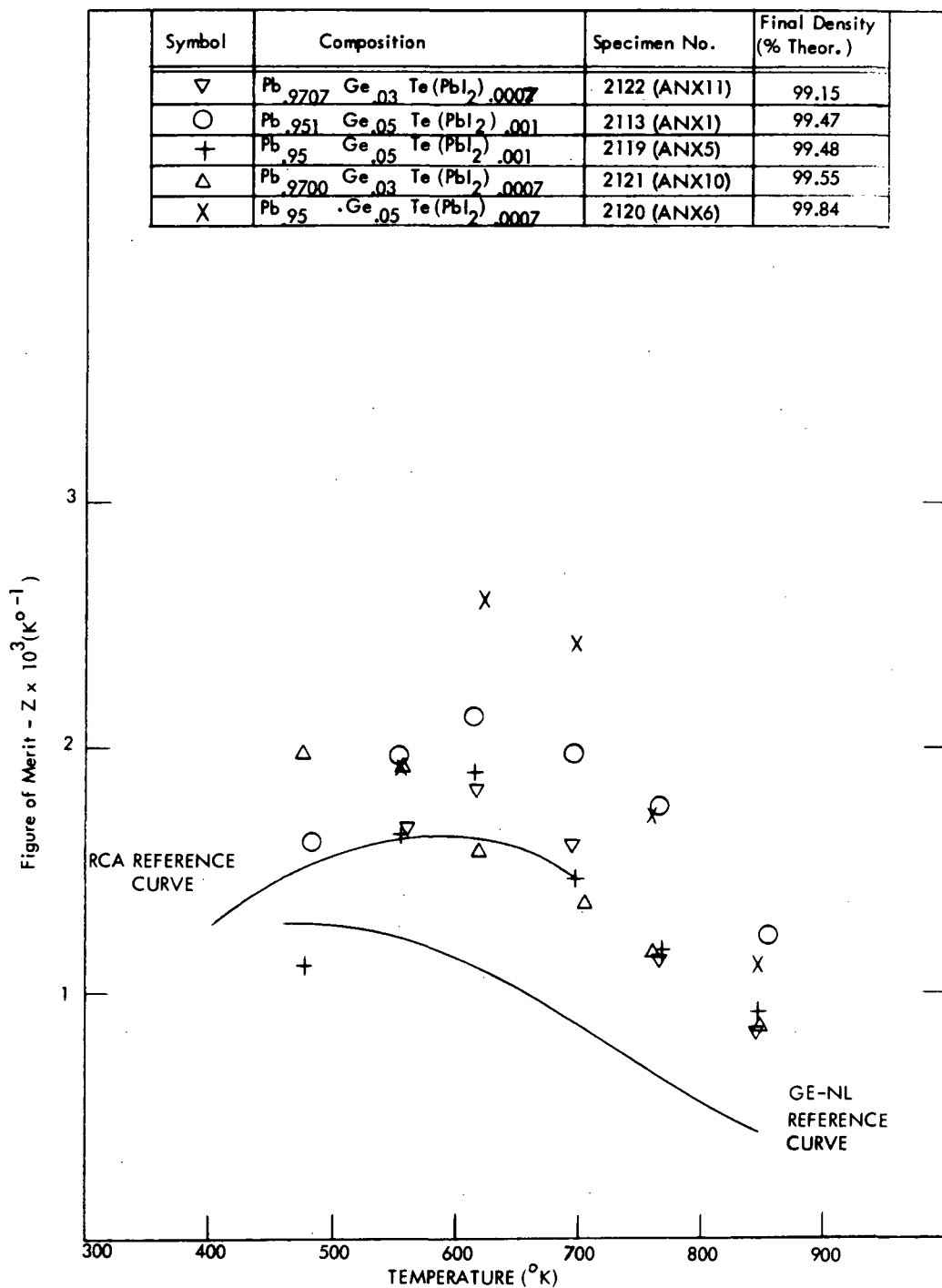
Figure IV-1. Figure of Merit of Hot Pressed Specimens of PbTe-GeTe Alloys

2. Sublength Technology Module TEM-15F S/N-4

TEM-15F S/N-4, a sublength technology module of the type discussed

previously in Section III, was fabricated in the first half of 1971. It contained thermoelec-

tric washers made of TEGS-2P p-type PbTe and ANX 6 n-type $Pb_{.95}Ge_{.05}Te(PbI_2)_{.0007}$.

A large batch of the ANX 6 material was prepared (for making the module washers) by

crushing three polycrystalline ingots to powder and heat treating the powder at $750^{\circ}C$

for one hour in flowing hydrogen. Electrical test specimens were then cold pressed

from this powder, and they in turn were heat treated at $750^{\circ}C$ for two hours in flowing

hydrogen. (It was upon the properties of ANX 6 specimens processed in both powder

and pressed form at $750^{\circ}C$ that the selection of the ANX 6 composition had been based.)

On the basis of test results obtained on these specimens, the material was accepted for

module use.

Before washers could be fabricated, however, additional information became

available which indicated that GeTe was being lost from the ANX 6 material during

$750^{\circ}C$ heat treating due to preferential vaporization of that molecular species. This

information included the results of relative weight loss versus temperature experiments,

shown in Figure IV-2, and a fairly complete set of vapor pressure data for various alloy

compositions in the PbTe-GeTe system[1].

Although the available data was incomplete and not thoroughly analyzed,

it was decided in view of the impending cancellation of further work to use this material

batch for module washers but to limit the heat treating temperature for the pressed washers

to a value where loss of GeTe would be minimized. Accordingly, the washers for TEM-15F

S/N-4 were heat treated at $587^{\circ}C$ for two hours in flowing hydrogen.

The module was then fabricated and processed in the same manner as the

"baseline" TEM-15A S/N-4 modules except that the inner conductor tungsten insert clear-

ance was eliminated and a simple vacuum degassing process was substituted for the earlier

hydrogen purge/vacuum degassing cycle. Following fabrication, the module was placed

---

[1] S. G. Karbanov et al, "Physico-Chemical Study of the System PbTe-GeTe", Izv. AN SSR
Neorgan. Materialy 5, No. 2, pp. 270-274 (1969).
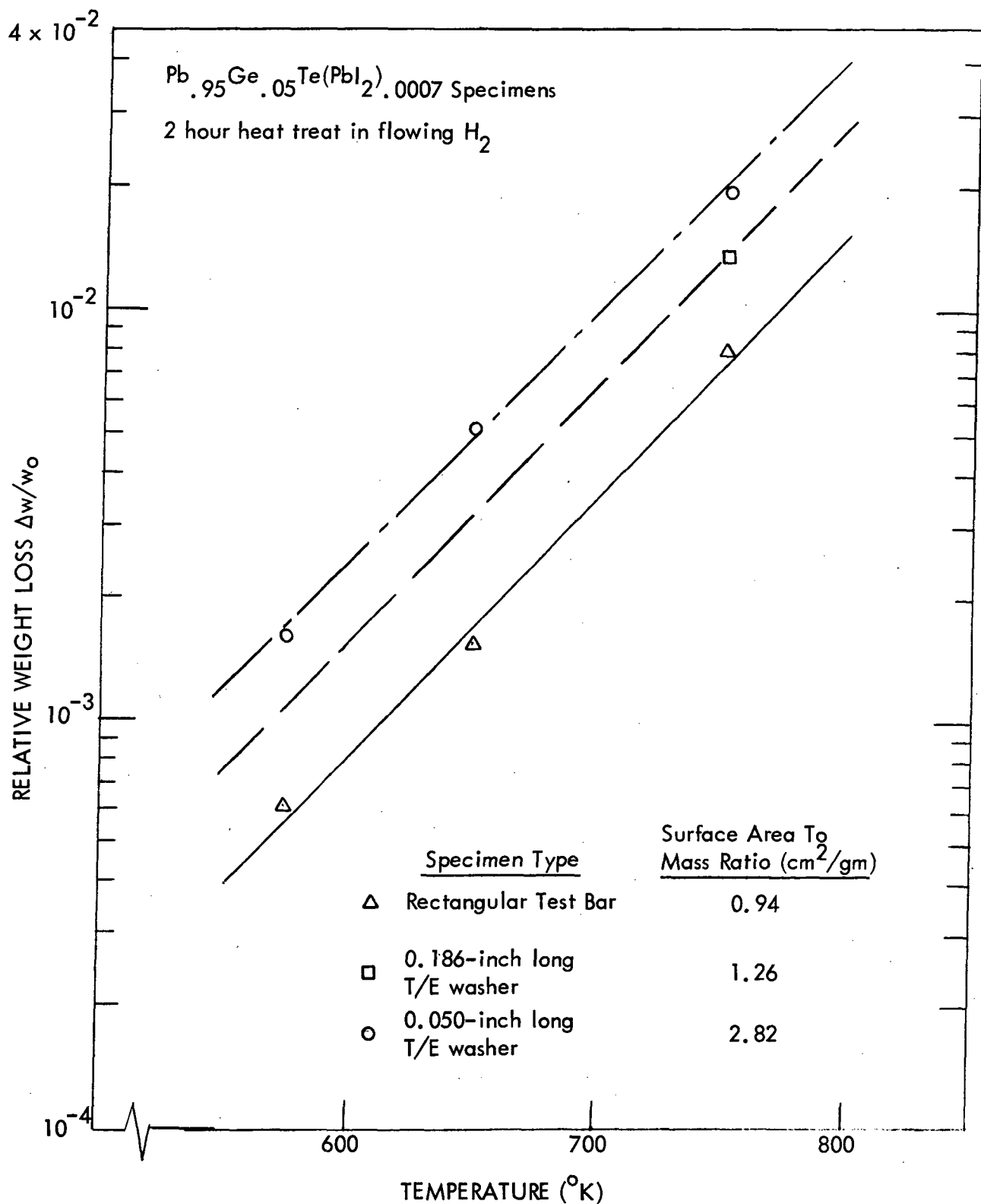
Figure IV-2. Relative Weight Loss of ANX 6 N-Type
Ternary Material Versus Temperature

on static test at $\bar{T}_H$ = 606°C (1125°F) and $\bar{T}_C$ = 296°C (570°F), where it was found that BOL power output was lower than anticipated and the degradation rate higher than that of comparable modules. The BOL experimental data and calculated values are shown in Table IV-2.

TABLE IV-2

CALCULATED AND EXPERIMENTAL TEM-15F S/N-4 BOL DATA

Fixed Load = 88.9 milliohms $\bar{T}_H$ = 606°C, $\bar{T}_C$ = 296°C

Parameter		Data	Calculated	Percent Deviation of Actual from Calculated
V_{oc}	- volts	4.79	4.95	- 3.3
R_g	- milliohms	91.7	87.0	+ 5.1
P_e	- watts	62.5	70.4	- 12.6
Q_{in}	- watts	1734	1632	+ 6

A year after this module was built, funding was again allocated for ternary material development. Accordingly, the first step in the investigation was the destructive examination of the TEM-15F S/N-4.

Chemical analysis of the ANX 6 formulation was carried out on specimens taken from various stages of material processing and from washers taken from the tested module. The results of the analyses and the composition of the material as formulated are shown in Table IV-3. The analyses of germanium confirm suppositions that germanium had been lost from the alloy during processing. The chemical results indicate a 20 - 22 percent loss in germanium for the heat treated powder and a 28 percent (total) loss for the washers that were made from the powder, heat treated again and used in the module. There appeared to be no change in germanium content during operation in the module internal environment. Thus, it is apparent that part of the anticipated decrease in lattice thermal conductivity was not achieved because of the GeTe loss.

TABLE IV-3

CHEMICAL ANALYSIS OF ANX 6

		Relative Atomic Abundance			
		Pb	Te	Ge	I
1.	ANX 6 Make-up Composition	0.9507	1.000	0.050	0.0014
2.	ANX 6 Powder	0.9602	1.001	0.039	0.0012
	Heat treated 2 hours at 750°C	0.9595	1.000	0.040	0.0012
3.	Unused ANX 6 Washers	0.9625	1.001	0.036	0.0012
	(2) + washers heat treated two hours at 585°C	0.9644	1.003	0.033	0.0011
4.	ANX 6 Washers from TEM-15F S/N-4	0.9630	1.001	0.036	0.0011
	(2) + (3) + 4865 hours test	0.9630	1.002	0.035	0.0012

It was thus decided that, in the resumption of work on this task, heat treating would be performed at temperatures compatible with minimum vaporization loss of GeTe, and the composition being worked with would be changed to the higher-doped ANX 1 compound $Pb_{.951}Ge_{.05}Te(PbI_2)_{.001}$. The latter change was considered necessary to increase the electrical carrier concentration and hence reduce the electrical resistivity in the direction of the RCA reference properties.

Electron microprobe examination disclosed reaction products of $Ge_x Te_y Mo_z$ and $Ge_x Mo_y$ at the ANX 6/molybdenum conductor ring interfaces. This reaction was observed to have occurred at both the hot and cold side surfaces. Seebeck probes on the n-type washer showed a significant portion of the ANX 6 material had been altered with respect to its initial electrical properties. The changes were attributed to tellurium migration from the p-type material, although it is possible that the molybdenum/ANX 6 reaction could have contributed to the high internal resistance measured at BOL. It was also postulated that the high resistance arose because the hot isostatic compaction process did not produce sufficient densification and decreased resistance in the ANX 6 material.

Without quantitative calculations as to the amount of n-type material affected, it appeared that the higher degradation rate of TEM-15F S/N-4 (compared to other standard TEM-15 modules) resulted from a higher mobility for tellurium migration in this particular module, possibly a greater susceptibility of the ANX 6 material to tellurium transport degradation, and compatibility problems with the molybdenum conductor rings.

3. Current Materials Processing

The current procedure for the manufacture of PbTe-GeTe alloys consists of accurately weighing lead, tellurium, germanium, and PbI_2 doping ingredients and placing into a carbon coated quartz tube. The tube is evacuated to less than $< 10^{-5}$ torr and sealed. The sealed tube is then heated in incremental steps to $1000^{\circ}C$ and rocked for two hours. The reacted products are quenched from above $975^{\circ}C$ into water. The cooled ingot is removed from the quartz tube, ground into powder, and screened. The material that is retained between -50 +270 mesh is used to produce cold pressed washers and test bars. The washers and bars are then heat treated for 2 hours at $575^{\circ}C$ in flowing hydrogen prior to electrical testing or assembly into a module.

4. Material Property Evaluation

Evaluation of the thermoelectric properties of PbTe-GeTe alloys consisted of measuring Seebeck coefficient (α) and electrical resistivity (ρ) as point functions of temperature, and also measuring Seebeck voltages across specimens having large temperature differences imposed upon them. Preliminary thermal conductivity measurements were initiated, but these were not completed and no data was obtained due to termination of the program. In addition to the above, x-ray diffraction measurements were performed on various specimens to determine crystal lattice parameters.

a. Seebeck and Resistivity Measurements

Ternary material qualification specimens were installed in a resistance-probe harness, shown in Figure IV-3, which was then installed in a special test fixture and placed within a large quartz tube. The tube was then positioned in the bore of a resistance-heated tube furnace as shown in Figure IV-4. The furnace was used to heat the specimen/fixture assembly to the approximate steady state reference temperatures 475, 550, 620, 700, 770 and 850°K, at which data points were obtained. At each such reference temperature, a small heater in the test fixture provided an additional heat input at one end of the specimen bar to create a 20 - 25C° axial temperature drop along the bar and permit making Seebeck voltage measurements. Seebeck coefficient and electrical resistivity values were calculated from the voltage, resistance and temperature data. To minimize surface oxidation and retard sublimation, an argon atmosphere at a slight positive pressure was maintained in the tube throughout the eight hour test run.

Eleven ingots of ANX 1 composition ($Pb_{.951}Ge_{.05}Te(PbI_2)_{.001}$) were prepared in various charge sizes (three-quarter, half, and full) to yield approximately 454 grams (full charge) of material. All ingots were successfully quenched with the carbon coating intact on the quartz tube. The
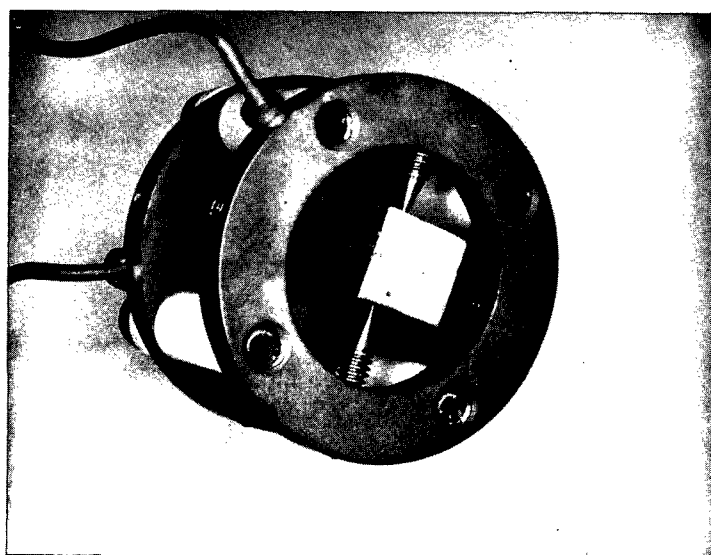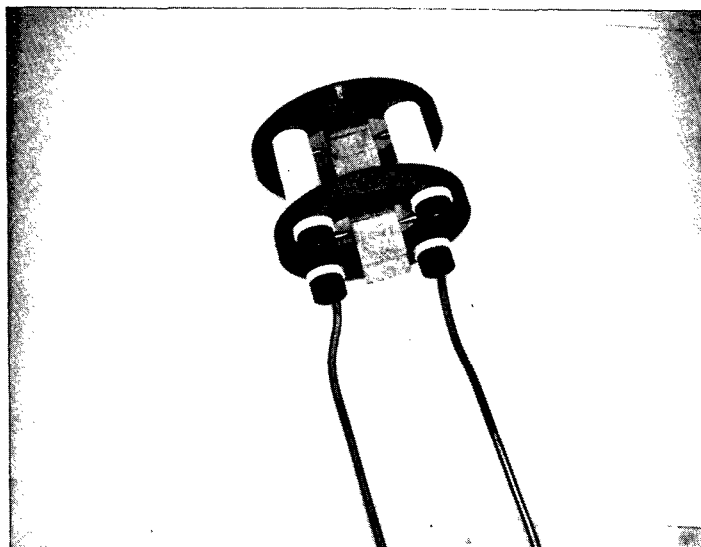
Figure IV-3. Special Test Harness to Hold Qualification Bars and Obtain
Resistance Data at Operating Temperatures
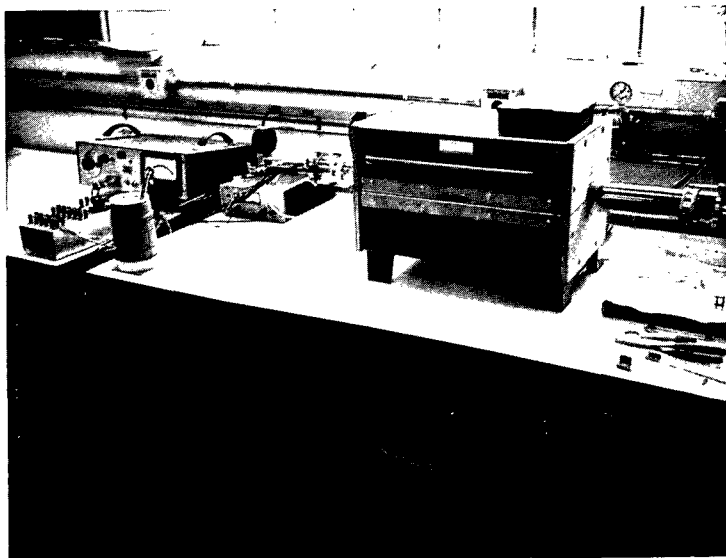
Figure IV-4. Seebeck and Resistivity Test Apparatus Used to Obtain
Thermoelectric Property Data from Qualification Bars

ingots were reduced to powder and fabricated into test bars for electrical
property measurements by cold pressing un-heat treated powder (-50 +270
mesh) and then heat treating the bars in flowing hydrogen for two hours
at 575°C. This treatment duplicated the process procedure for standard
n-type PbTe and minimized the loss of germanium through sublimation.
Electrical test bars from ingots ANX 1-9, 10, 11, 12, 13, 14, 15, 17, 18,
19 and 21 were tested over the temperature range 295 to 850°K. Results
of these tests are shown in Figure IV-5, Figure IV-6 and Figure IV-7
along with the RCA n-type ternary reference curves (solid lines) for Seebeck
and resistivity. No variations in electrical properties were noted between
different batch sizes. In general, except for ANX 1 - 11 which produced
very anomalous data, the Seebeck data indicates all specimens had compar-
able properties; however, there was considerable scatter in the electrical
resistivity. The scatter was thought to be caused by variations in specimen
density, a phenomenon noted in previous experiments with this material.
Hot pressing to 99 percent theoretical density did not alter the Seebeck
coefficient of the material, but reduced the electrical resistivity to the
desired values, as is discussed below.

b. Measurement of Seebeck Voltage over Large Temperature Differences

Seebeck voltage characteristics of PbTe-GeTe qualification bars were
measured for all n-type ternary materials with serial numbers between
ANX 1-9 and ANX 1-21. One end of the ANX test specimen was heated
by conduction through a tungsten disc, while the other end was cooled
by a water cooled base plate. Seebeck voltage (millivolts) was plotted
on the vertical axis of an X-Y recorder with hot junction temperature
(°C) as the horizontal component. At any point in the test cycle, a change
in voltage (ΔV) versus a change in temperature (ΔT) would describe the
Seebeck coefficient ($\Delta V/\Delta T$).
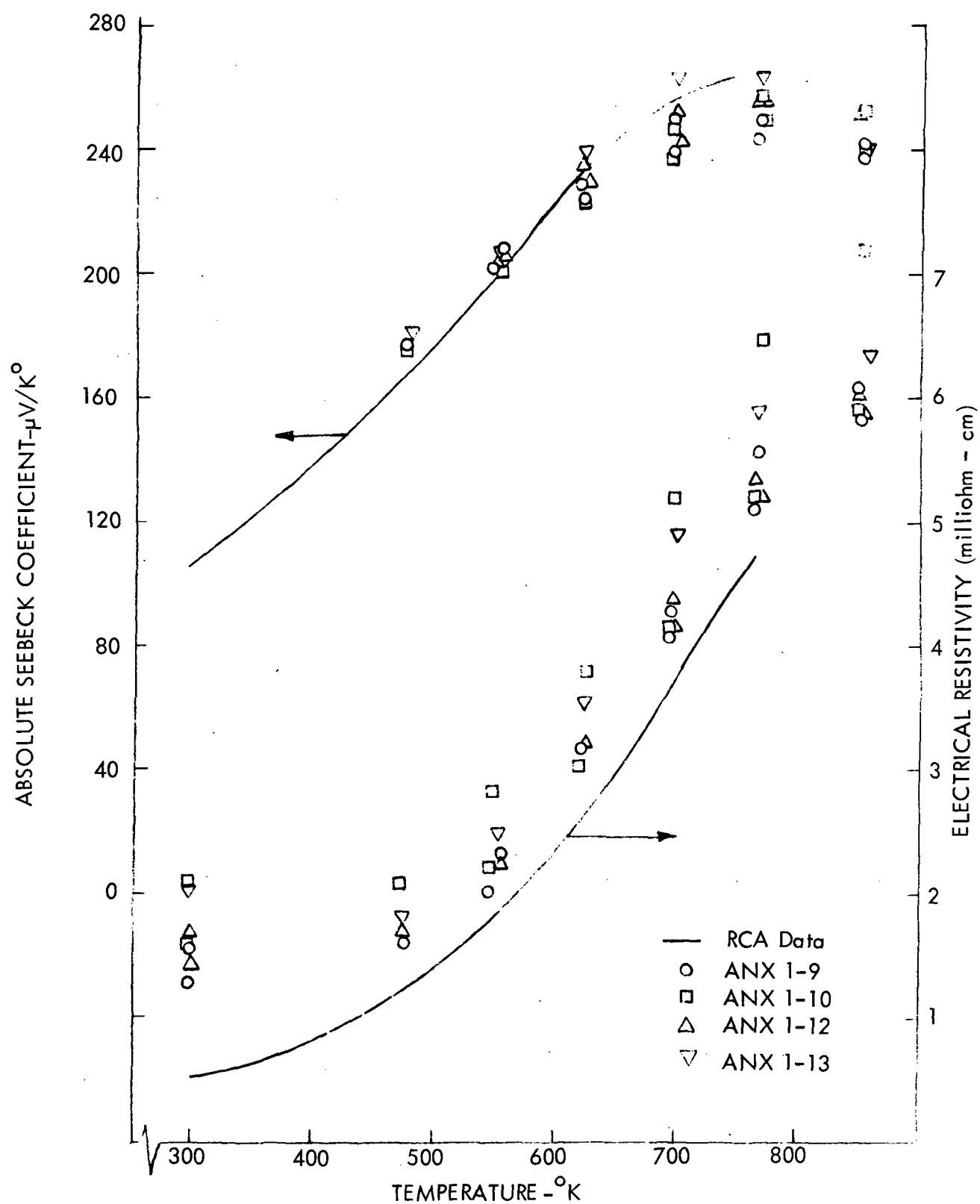
Figure IV-5. Electrical Properties Versus Temperature for Cold Pressed ANX 1 Alloys
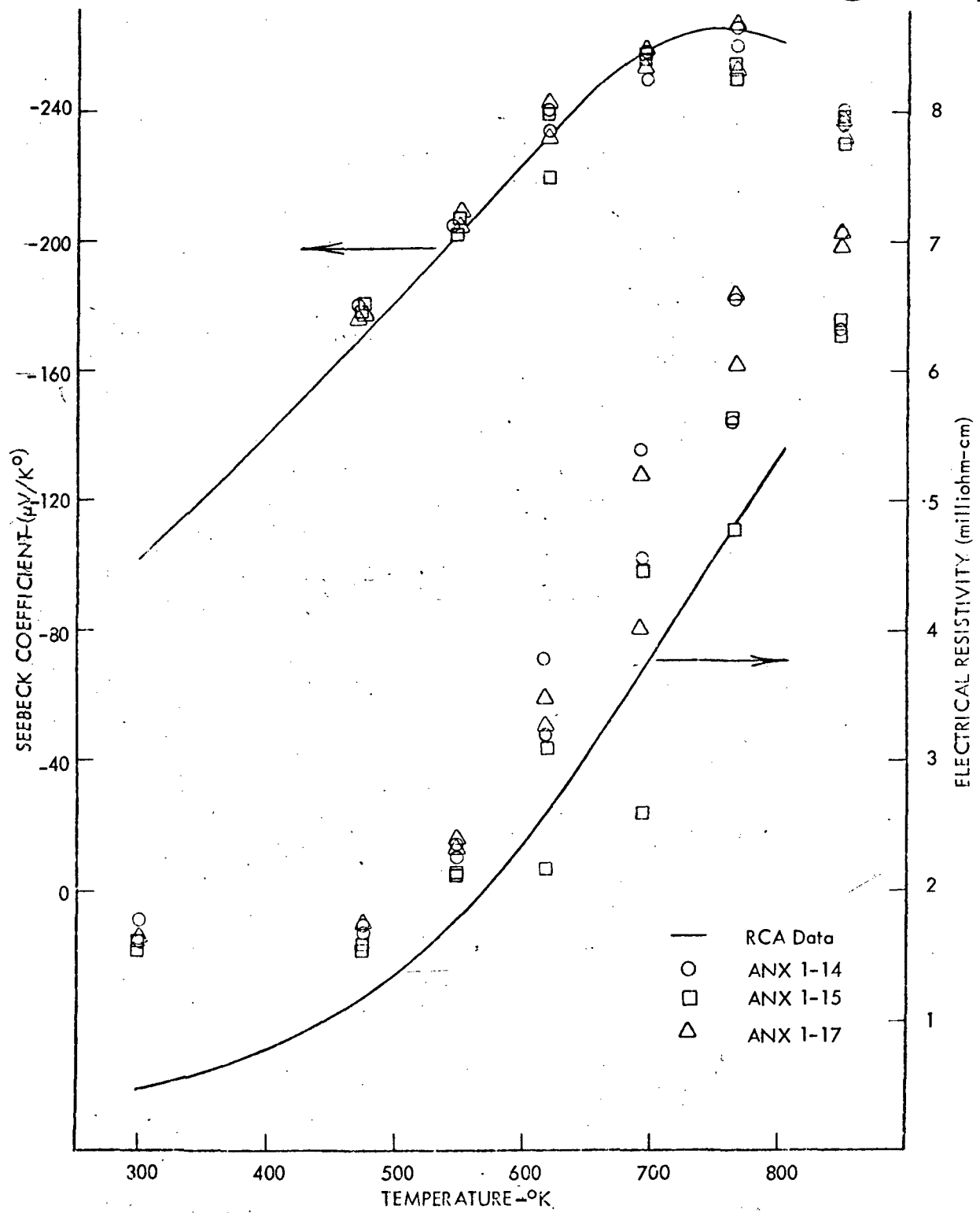
Figure IV-6. Electrical Properties Versus Temperature for Cold Pressed ANX 1 Alloys
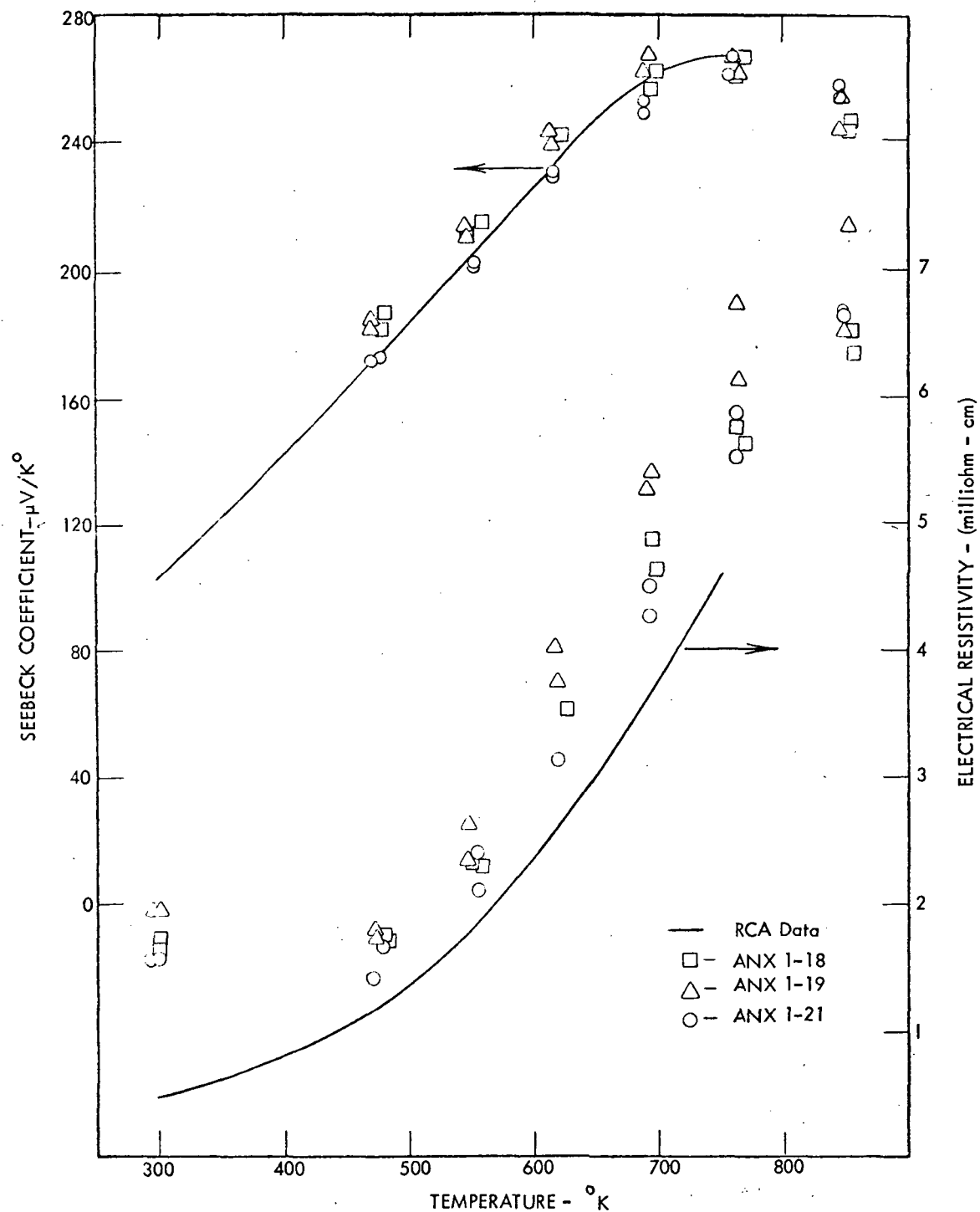
Figure IV-7. Electrical Properties Versus Temperature for Cold Pressed ANX 1 Alloys

All high ΔT experiments were performed in an inert atmosphere under a water cooled metallic bell jar. Figure IV-8 is a photograph of the test apparatus for the high ΔT experiments. Shown in the photograph are the X-Y recorder, digital voltmeter, water cooled bell jar, and power control system (under desk). Figure IV-9 is a photograph of the inside of the bell jar, with a closer view of a qualification test bar, tungsten disc and heater housing. Thermocouple readings were measured at the tungsten disc and directly under the qualification bar.

The main purpose of these experiments was to determine material performance over a temperature range consistent with the operating temperatures of a reactor power module in which the material would be used. Consequently the high ΔT experiments were performed with hot-junction temperatures of 319.00°C (606°F), 592.75°C (1099°F) and 650.00°C (1202°F) and with cold junction temperatures maintained at 8.75°C (47.8°F).

Table IV-4 lists the qualification bars and n-type ternary materials tested in the high ΔT apparatus. By comparing the performance of each qualification bar from one ingot to another, the small, medium, and large melts of n-type ternary material were assessed for potential voltage output.

Typical results of one of the high ΔT experiments are listed in Table IV-5. A comparison of the voltage data with calculations made by integrating the Seebeck coefficient data from the experiments discussed in the previous section showed good agreement for all specimens tested.

c. Thermal Conductivity Experiments

Preliminary experiments were performed with known test specimens in the thermal conductivity test apparatus. Both 0.500 inch diameter and 1.00 inch diameter samples of known standards were tested in a modified thermal conductivity instrument, (Model TCC GM-R22 manufactured by Dynatech
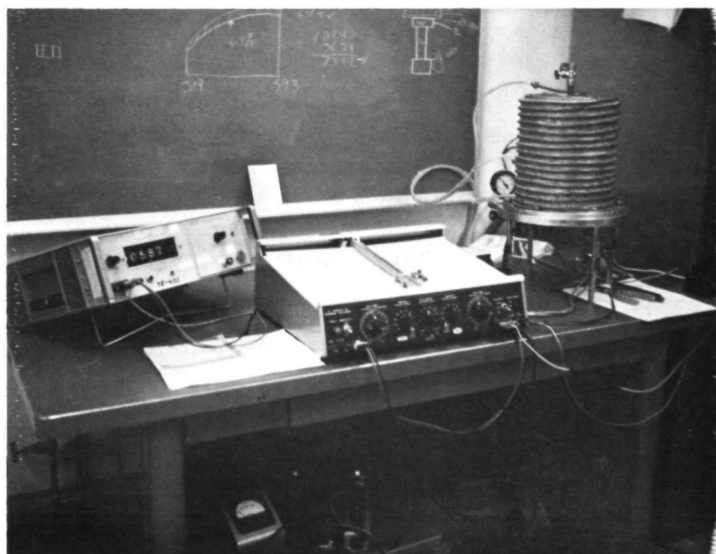
Figure IV-8. Test Apparatus for High ΔT Facility
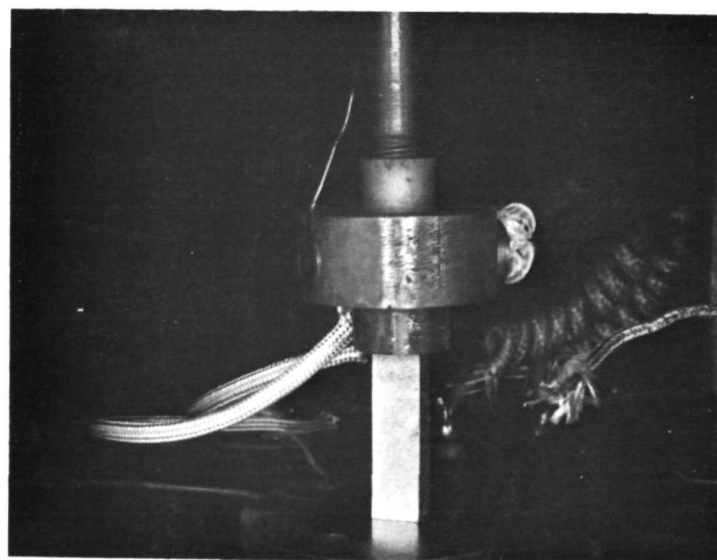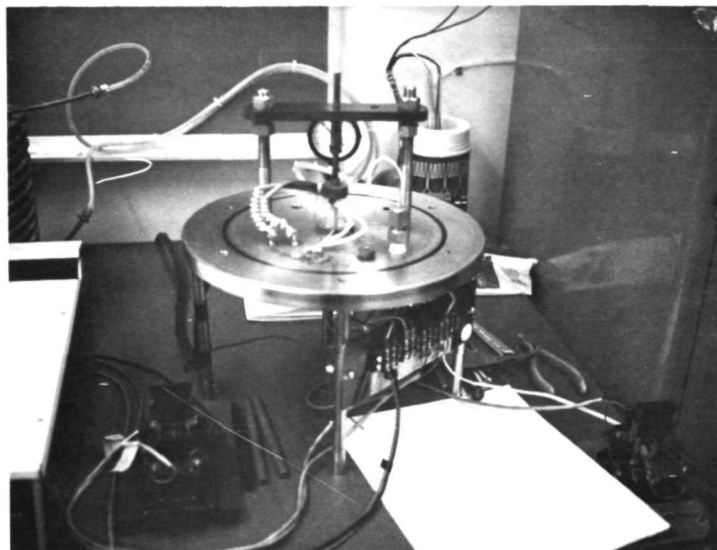
Figure IV-9. Ternary Material Qualification Bar Installed on Water Cooled Base Plate

TABLE IV-4

HIGH ΔT TEST SPECIMENS FOR PbTe-GeTe MATERIAL

N-Type Ingot Designation	Specimen Number
ANX 1-9	Q1044R, Q1045, Q1046
ANX 1-9*	Q1142R, Q1143, Q1144
ANX 1-10	Q1048R, Q1049, Q1050
ANX 1-12	Q1055R, Q1056, Q1057R
ANX 1-13	Q1110R, Q1111, Q1112
ANX 1-14	Q1114R, Q1115, Q1116
ANX 1-15	Q1118R, Q1119, Q1120
ANX 1-17	Q1122R, Q1123, Q1124
ANX 1-18	Q1126R, Q1127, Q1128
ANX 1-19	Q1130R, Q1131, Q1132
ANX 1-20*	Q1138R, Q1139, Q1140
ANX 1-21*	Q1174R, Q1175, Q1176
ANX 1-21**	Q1178R, Q1179, Q1180

*   Heat treated at 700°C for 100 hours

**   Non-heat treated specimens

TABLE IV-5

HIGH ΔT TEST RESULTS WITH N-TYPE TERNARY MATERIALS

ANX 1-15 (PbTe-GeTe) Ternary Material

Specimen No. Identification Description	Q 1119	Q 1120
Th_1	319.00	319.00
Tc_1	8.75	8.75
ΔT ($^\circ$C)	310.25	310.25
Normalized Voltage (mv)	54.84	54.15
Th_2	592.75	592.75
Tc_2	8.75	8.75
ΔT ($^\circ$C)	584.00	584.00
Normalized Voltage (mv)	124.67	123.65
Th_3	650.00	650.00
Tc_3	8.75	8.75
ΔT ($^\circ$C)	631.25	631.25
Normalized Voltage (mv)	138.00	137.14
ΔV (592.75 - 319.00)	69.83	69.50
ΔV (650.00 - 319.00)	83.16	82.99

Corporation, Cambridge, Massachusetts). Qualification tests were relatively easily performed with the 1.00 inch diameter specimen, but the use of a 0.500 inch Pyroceram standard resulted in extreme difficulties in arriving at a balanced equilibrium where the heat through the two heat meters was in good agreement.

Large size (1.00 inch diameter) thermal conductivity specimens of lead germanium telluride materials were unavailable. Therefore, considerable time and effort was expended in perfecting the test procedure with 0.500 inch diameter specimens.

Some difficulty was encountered in specimen preparation when two small thermocouple holes had to be drilled radially 0.250 inch to the centerline of the 0.500 inch diameter cylinder. One ANX 1 hot pressed cylinder was successfully instrumented and partially tested prior to the cancellation of all thermal conductivity experiments.

Initial thermal conductivity experiments were attempted at 400°C with ANX 1-type material, but due to extensive loading stresses during thermal expansion, the specimen cracked, split, and invalidated the results.

Other hot pressed samples of ANX 1-type ternary material and n-type lead telluride were available for test prior to all work stoppage, but all tests were terminated as directed.

d. X-Ray Diffraction Measurements of Lattice Parameters

X-ray diffraction (XRD) patterns obtained on powder from quenched ingots or powder heat treated in hydrogen produced broad diffuse lines which made measurement of lattice parameters impossible. Sharp XRD lines could be produced by annealing a quenched ingot in situ at 700°C for 168 hours, or by annealing powder from a quenched ingot in a sealed

ampoule at the same temperature for 100 hours. A series of annealing
experiments were conducted to evaluate the use of x-ray diffraction
as a tool which could measure alloy composition; i.e., germanium content,
after various processing steps.

The XRD studies, along with a recent paper by Hohnke et al.[1], allowed
an understanding of the phenomena and results previously observed. Speci-
fically, the new phase diagram determined by Hohnke (in contrast to
Shelimova's work[2]) shows complete solubility of germanium telluride in
lead telluride down to about 570°C. Below this temperature, spinodal
decomposition occurs for compositions whose mole fraction is given by
0.05 < GeTe < 0.96. In addition, Hohnke found the lattice parameter
to be a linear function of germanium telluride content to 60 mole percent
germanium telluride. Table IV-6 summarizes the results obtained from
various specimens used in this (WANL) study. The results shown in Table
IV-6 can be superimposed on an expanded plot of Hohnke's values for
lattice parameter versus germanium telluride content, Figure IV-10. It
is evident that the broad lines obtained previously resulted from microscopic
coring of the alloy, despite the rapid quench. Further, it is apparent that
for a nominal 5 percent germanium telluride composition, certain parts
of the individual grains will be composed of compositions in excess of
5 percent germanium telluride, and these compositions will decompose
into two distinct phases at elevated temperatures where diffusion is faster.
Appearance and growth of an almost pure germanium phase had been
observed when using the electron microprobe to examine samples prepared
at WANL in 1970.

[1] D. K. Hohnke, H. Holloway and S. Kaiser, J. Phys. Chem. Solids, 33, P. 2053 (1972).

[2] L. E. Shelimova, N. K. Abrikosov and V. V. Zhdanova, Russian J. of Inovg. Chem. 10, p. 650 (1965).

It is now clear that heat treating, which was done at a temperature where complete solid solution exists, and at which diffusion must be extremely rapid, produces a homogenous 5 percent germanium telluride alloy. This alloy (5 percent germanium telluride in lead telluride) is at the limit of germanium telluride solubility and will remain single phase regardless of subsequent cooling rates and further times at temperatures below the solidus (approximately 800°C). It is further evident, from Figure IV-10, that heat treating the homogenized powder in a flowing hydrogen stream systematically reduces the germanium telluride content, as evidenced by the increase in lattice parameter with increasing time and temperature. In fact, the lattice parameter measurements indicate that processing at 750 $\pm$ 20°C under flowing hydrogen effectively removes all of the germanium telluride from the alloy. XRD lattice parameters results obtained on crushed hot pressed specimens which were annealed at 700°C in sealed ampoules for 100 hours indicated that no germanium telluride was lost during the hot pressing procedure.

The above results, coupled with the electrical property measurements made, show that while the homogenization anneal did not significantly alter the electrical characteristics, judicious processing of the powder was extremely important. It is rather apparent that powder should not be heat treated prior to use for fabrication. The X-ray diffraction method, because of its extreme sensitivity and rapidity, is a more desirable technique than wet chemistry for germanium determination.

5. Compatibility Experiments

Ternary materials compatibility tests were divided into two types of experiments which exposed ANX 1 materials to different insulating and electrical contact materials. The first series of experiments, die tests, were short term accelerated exposures at a test

TABLE IV-6

LATTICE PARAMETER OF ANX 1 MATERIAL - Å

Sample	No powder Treatment	Powder annealed in sealed ampoule for 100 hrs at 700°C	Powder Annealed in Flowing H_2					
			575°C		650°C		750°C	
			2	4	2	4	2	4
Ingot quenched from 1000°C	Broad lines	ANX 1-9 – 6.4401 ANX 1-14 – 6.4409 ANX 1-15 – 6.4400 ANX 1-17 – 6.4402	Broad lines	–	–	–	–	–
Ingot quenched from 1000°C. Annealed in-situ at 700°C for 168 hours	6.4391		6.4442	6.4458	6.4523	6.4553	6.4600	6.4611
Ingot quenched from 1000°C. Annealed in-situ at 700°C for 168 hours. Powder (−20 +35) hot pressed		6.4404						
Ingot quenched from 1000°C. Powder (−20 +35) Hot Pressed		ANX 1-14/HP025 – 6.4405 ANX 1-15/HP026 – 6.4404 ANX 1-17/HP027 – 6.4404						
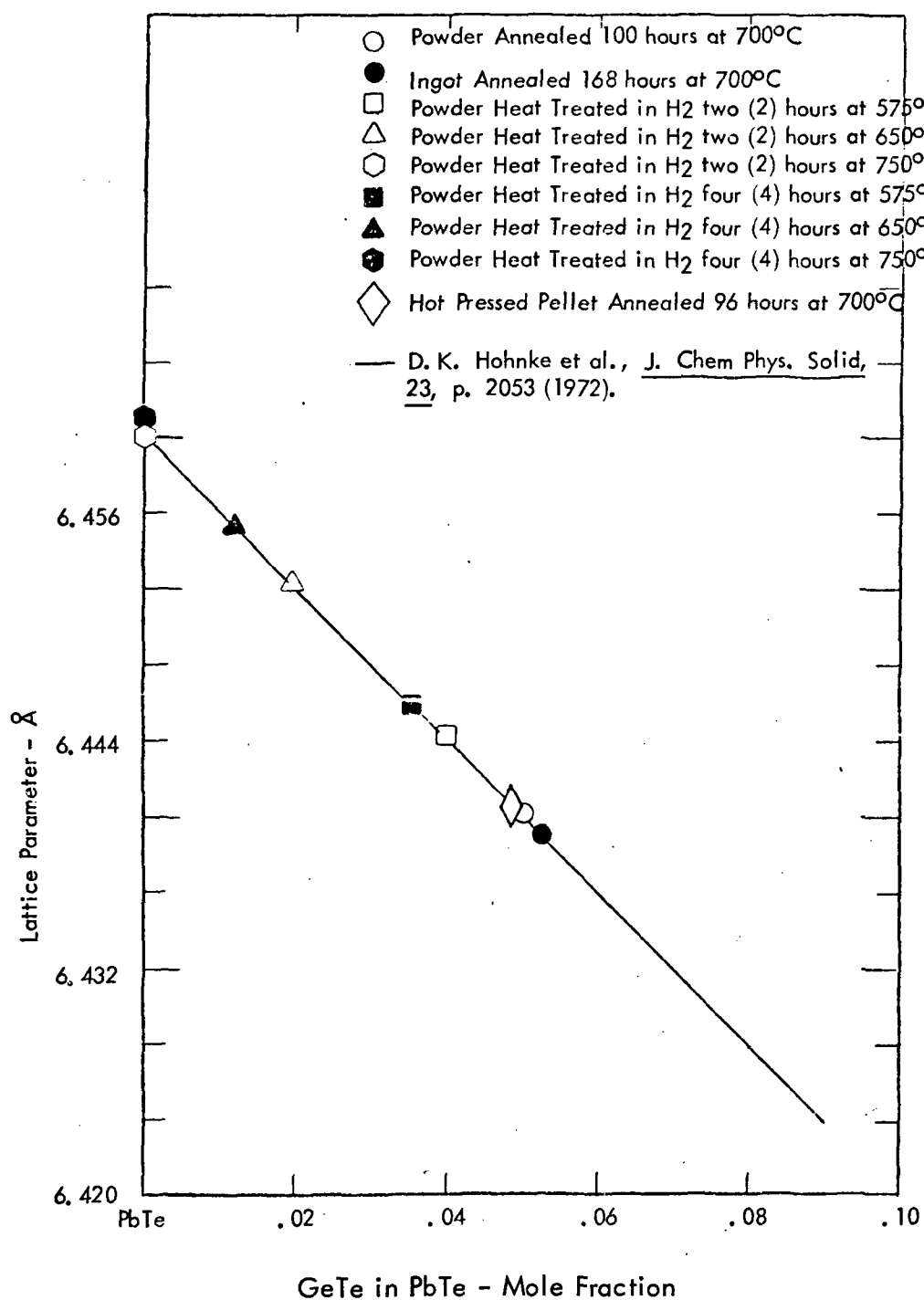
Figure IV-10. Lattice Parameter Versus Mole Fraction
GeTe in PbTe

temperature of 700°C in a hydrogen atmosphere. The second series of experiments, capsule tests, consisted of 1000 hour tests in a void-free, hermetically sealed capsule at a temperature of 636°C. Both types of tests were performed with ANX 1 ternary material to determine material interactions and long term stability of the thermoelectric material.

a. Short-Term Tests

Compatibility tests of short term duration (2, 4, and 6 hours) were performed with lead germanium telluride in hydrogen at temperature of 700°C. ANX 1 material in the cold pressed and sintered pellet form (0.50 diameter x 0.30 inch length) was placed in contact with molybdenum, tungsten, phlogopite mica, and standard p-type lead telluride during the short term testing in hydrogen. Twelve tests were completed with lead germanium telluride ternary material in contact with each of the four materials for 2, 4, and 6 hours.

(1) Testing Procedure

Short-term compatibility experiments were performed in a vacuum furnace with pure hydrogen as a cover gas. A sample of each test material was loaded into a graphite die (Figure IV-11) in direct contact with the flat side of an ANX ternary pellet. Graphite punches were used to maintain contact between the ternary n-type pellet and the respective compatibility sample. The sequence of operations started by evacuating the air from the furnace at room temperature and back filling with pure helium. After a second evacuation and backfill with helium, the pure hydrogen was introduced and continuously flowed through the furnace throughout the compatibility test run. Electric heaters within the furnace controlled the graphite temperature 'during warmup and at the test temperature. An Instron compression test apparatus was used to apply 3000 psi pressure to the graphite punches while both the ternary n-type pellet and compatibility sample were at 700°C.
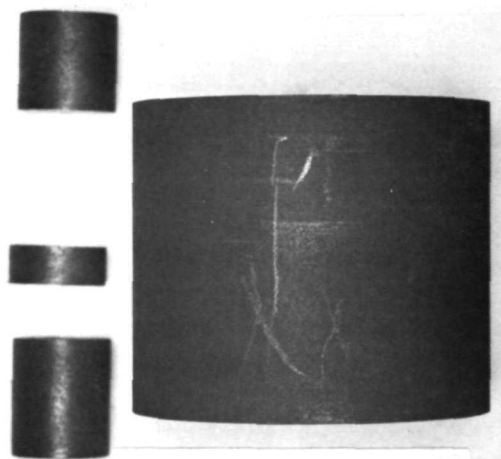
Figure IV-11. P-03* Graphite Die and Punches Used in Short-Term Compatibility Tests
* Product of Pure Carbon Company, Inc., St. Marys, Pennsylvania

(2) Evaluation Methods

(a) Specimen Preparation

After furnace cooldown, the graphite compatibility die was removed from the test chamber and potted in an epoxy compound. The assembly was later sectioned into two halves along the longitudinal axis and polished. One section was used for electron beam microprobe examination, and the other half was tested for Seebeck voltage output. All twelve compatibility samples were prepared by similar processing procedures.

(b) Electron Beam Microprobe Analysis

Each of the compatibility tests were examined with the electron beam microprobe for possible diffusion of the specific elements involved. No reactions were detected at the tungsten or mica interfaces with the n-type ternary material, but there was a detectable reaction at the molybdenum/ANX interface. This reaction was only apparent for the longest time (6 die test hours). It appeared that this was the same reaction seen in the examination of the TEM-15F S/N-4 experimental module.

(c) Seebeck Voltage Probe Analysis

Each compatibility test specimen was probed with the Seebeck apparatus to check the change in Seebeck coefficient with distance from the interface of the simulated diffusion couple. The n-type ternary material's electrical properties were not affected by either the tungsten or the mica, but were affected by the molybdenum, as can be seen from the data in Figure IV-12. Although the molybdenum/ANX reaction could only be detected by the electron beam microprobe for the longest time (6 hours), the electrical property changes were evident after two hours.
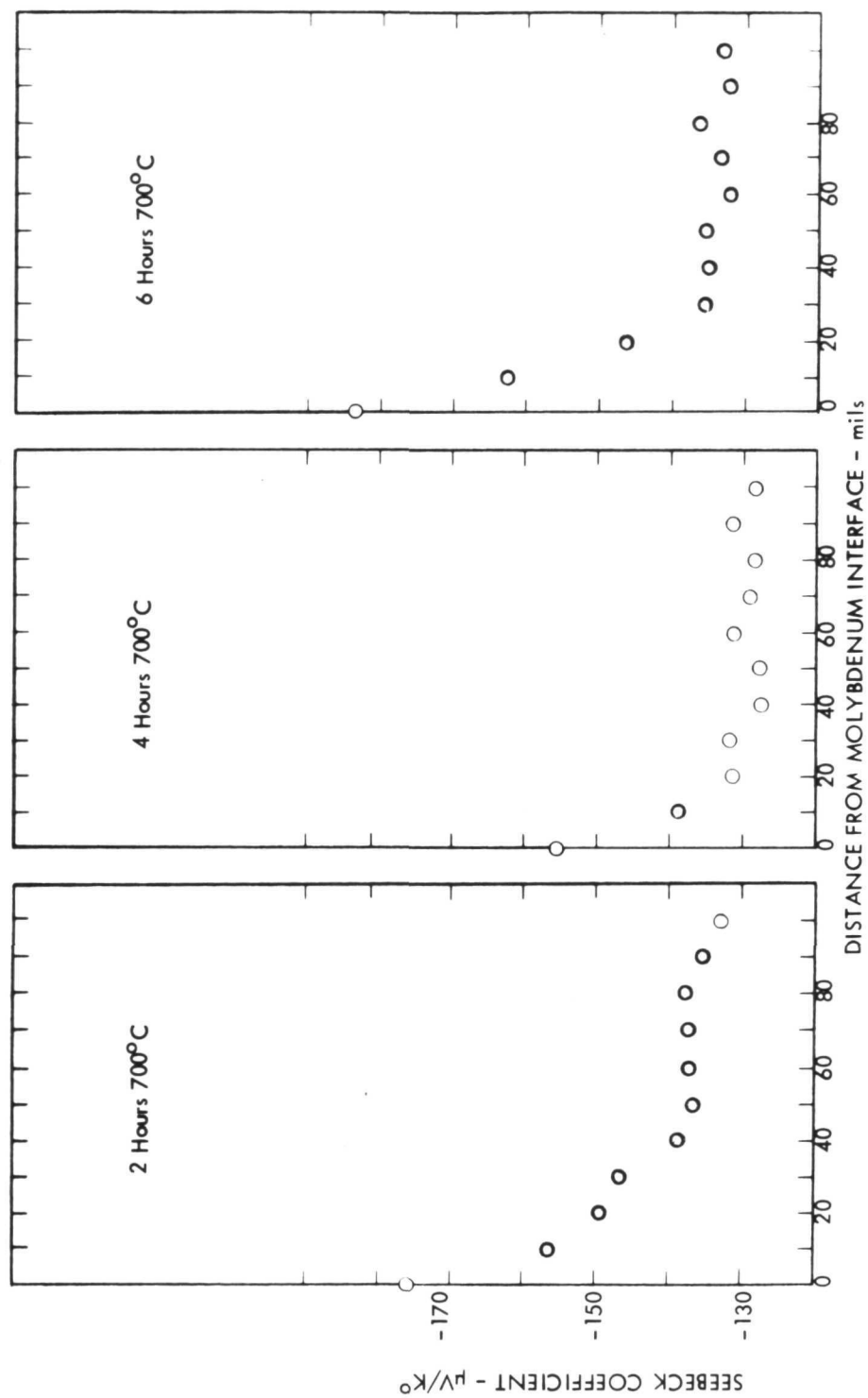
Figure IV-12. Seebeck Coefficient of ANX 1 PbTe-GeTe Versus Distance from Molybdenum Interface

The contamination of the ANX (lead germanium telluride) by tellurium diffusion from p-type telluride is quite apparent, as can be seen from data presented in Figure IV-13. The data tend to indicate, quantitatively, at least, that the ANX is as susceptible to contamination by tellurium as standard n-type lead telluride.

b. 1000-Hour Capsule Tests

After short term compatibility tests were completed with PbTe-GeTe materials, a new experimental capsule design was prepared to allow stability measurements during long-term testing at 636°C (1175°F). ANX 1 pellets were scheduled for steady state testing for at least 1000 hours at a minimum temperature of 607°C. Several variations of capsules were planned for testing, but only one type of capsule was actually fabricated and tested. Premature phasing-out of the program resulted in only three ANX 1 capsules being assembled and tested for 1000 hours.

(1) Design, Fabrication and Capsule Designation

Design revisions were made to the experimental capsule to isolate each ANX 1 pellet with the materials of interest for the full duration of life testing. Each capsule contained five isolated pellets in contact with boron nitride on their circumferential surface and tungsten at both flat ends. Figures IV-14 and IV-15 illustrate the EXC-capsule as assembled and also the final product after processing and machining. Metallic spacers were installed between pellets to permit a definite break in Seebeck voltage from one pellet to the next. In the post testing examination, the Seebeck voltage probing was conducted along the longitudinal axis for all five pellets with definite separation of data for each ternary pellet tested for 1000 hours. Every effort was made to utilize exiting materials and components from previous capsule fabrication. Two layers of boron nitride were assembled between the ternary pellet and the stainless steel outer case. Stainless steel electrical contact were
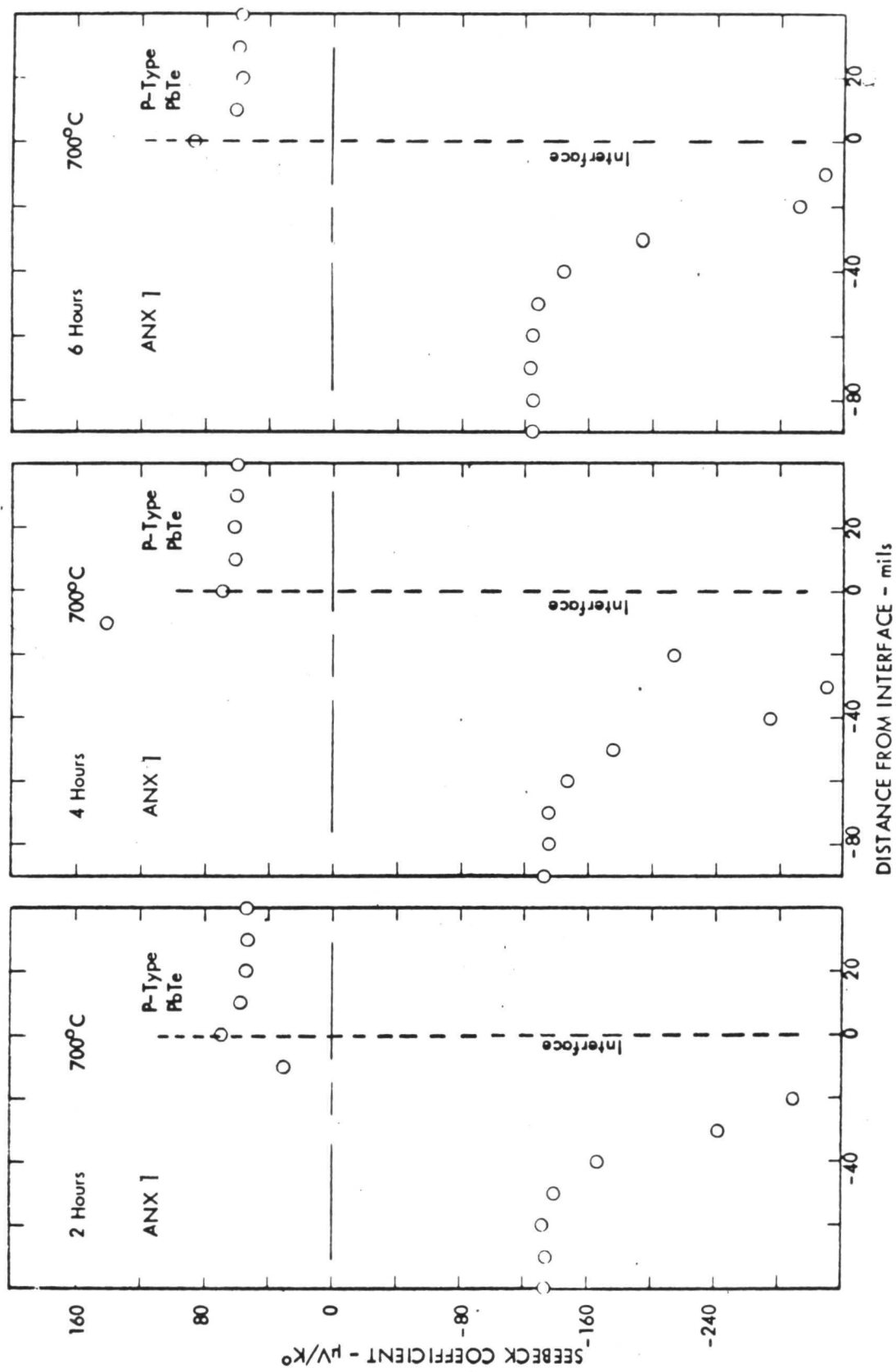
Figure IV-13. Seebeck Coefficient Versus Distance from Interface – ANX 1/P-Type PbTe
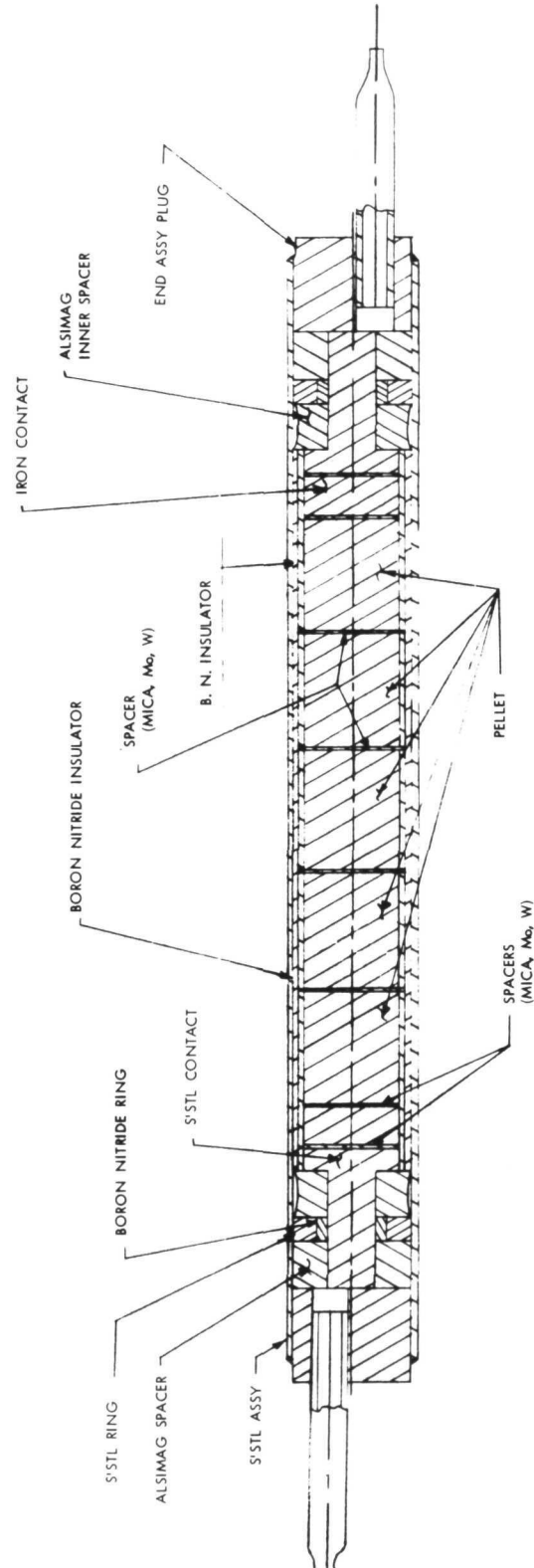
Figure IV-14. EXC-Capsule as Assembled

Labels on figure: END ASSY PLUG, ALSIMAG INNER SPACER, IRON CONTACT, SPACER (MICA, Mo, W), B. N. INSULATOR, BORON NITRIDE INSULATOR, PELLET, S'STL CONTACT, BORON NITRIDE RING, SPACERS (MICA, Mo, W), S'STL RING, ALSIMAG SPACER, S'STL ASSY
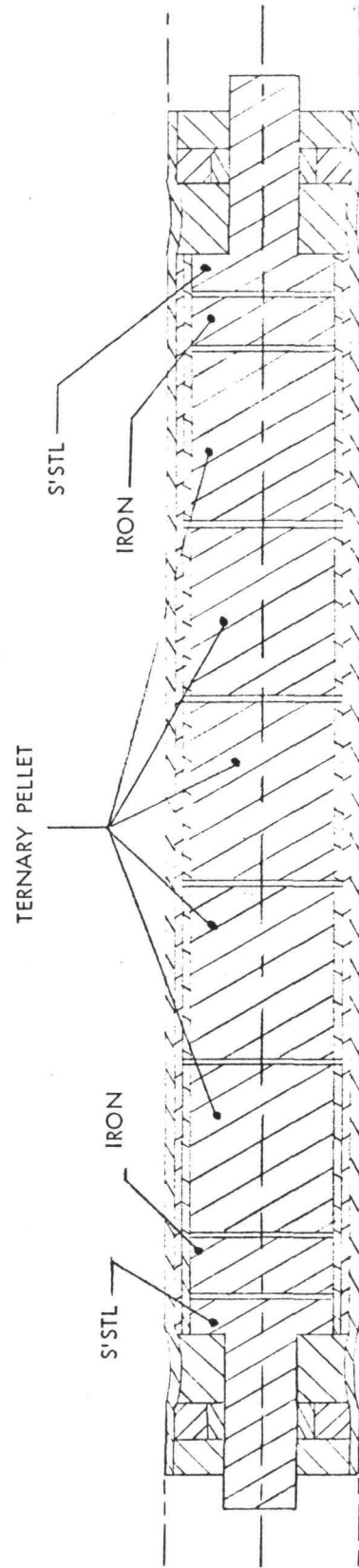
Figure IV-15. EXC Capsule after Processing and Machining

utilized because of the external air environment during the 1000 hours at 636°C. Boron nitride and Alsimag spacers insulated the electrical contacts from the outer case and permitted resistance measurements to be taken at operating temperature.

Every component in the EXC-capsule, except the boron nitride, was heat treated to a higher temperature than the static test temperature of 636°C, to remove the possibility of contamination and to simulate the assembly of TEM-X modules. Stainless steel, tungsten, and iron were heat treated in hydrogen at 825°C for one hour and then placed in vacuum storage to await final assembly. Boron nitride was machined dry and stored in high vacuum chambers without cleaning or heat treating. ANX 1 pellets were cold pressed from screened powder (-50 + 270) and sintered in hydrogen prior to assembly.

Final assembly operations were performed in an argon dry box by adding components from left to right as shown in Figure IV-14. Final closure at the end plug was provided by a welded seal. Heat treatment and evacuation steps were analogous to tubular module fabrication procedures. Evacuation tubes were first pressed and then sealed with an electron beam weld. Each capsule was later subjected to cold isostatic pressing and hot isostatic pressing similar to the processing of a standard tubular module.

Final machining was performed to expose the stainless steel contacts and remove part of the Alsimag spacer. After clean up, the capsules were made available for instrumentation.

Table IV-7 is a complete list of EXC-capsules fabricated for 1000 hour compatibility tests. The list includes three ANX capsules as well as eight APX capsules discussed in the next section of this report.

The individual pellets in each capsule are listed by position and serial number. Each pellet is also identified with a specific lot of ANX or APX ternary material. In addition, the spacer components between individual pellets are identified as to thickness and material. The PbTe-GeTe powder used in the ANX 1 capsules originated from ingots ANX 1-9 and ANX 1-10, which were blended to form ANX 1 - 20A.

(2) Instrumentation and Test Apparatus

Each EXC-capsule was instrumented with three chromel alumel thermo-couples that were beaded and spot welded to the stainless steel case. One thermocouple was located at the center line of the No. 3 pellet and the other two couples were located at the outside extreme locations of No. 1 and No. 5 pellets. By measuring the temperature at three locations, the average pellet temperature was determined throughout the 1000 hour test period.

Two 304 stainless steel wires were spot welded to each stainless steel contact to provide current and voltage leads to measure internal resistance at operating temperature. By passing alternating current through the capsule and measuring the voltage drop from contact to to contact, the resistance values for EXC-capsules were determined by Keithley milliohmeter readings. Capsule resistance measurements ranged from 33.0 milliohms initially to 36.0 milliohms after 1000 hours of testing at 636°C.

The bulk resistance contribution of the stainless steel, iron and tungsten was calculated to be approximately 1.0 milliohm at operating temper-atures. Thus the total resistance of the ANX 1-20A pellets rose from 32 to 35 milliohms during the 1000 hours of 636°C operation. These resistance data relate to average resistivity increases from 4.9 to 5.4 milliohm centimeters, an increase of 9.4 percent.

TABLE IV-7

PELLET IDENTIFICATION CHART FOR TERNARY EXC-CAPSULES

Capsule Serial Number	Spacer Material	Pellet 1	Spacer Material	Pellet 2	Spacer Material	Pellet 3	Spacer Material	Pellet 4	Spacer Material	Pellet 5	Spacer Material
EXC-001	.014"W	2394 APX10-33A	.014"W	2408 APX10-33B	.014"W	2401 APX10-33A	.014"W	2405 APX10-33B	.014"W	2400 APX10-33A	.014"W
EXC-002	.014"W	2388 APX10-33A	.014"W	2404 APX10-33B	.014"W	2393 APX10-33A	.014"W	2410 APX10-33B	.014"W	2359 APX10-33A	.014"W
EXC-003	.014"W	2351 ANX1-20A	.014"W	2353 ANX1-20A	.014"W	2359 ANX1-20A	.014"W	2361 ANX1-20A	.014"W	2365 ANX1-20A	.014"W
EXC-004	.014"W	2345 ANX1-20A	.014"W	2346 ANX1-20A	.014"W	2364 ANX1-20A	.014"W	2349 ANX1-20A	.014"W	2369 ANX1-20A	.014"W
EXC-005	.014"W	2347 ANX1-20A	.014"W	2354 ANX1-20A	.014"W	2356 ANX1-20A	.014"W	2357 ANX1-20A	.014"W	2358 ANX1-20A	.014"W
EXC-006	.014"W	2402 APX10-33B	.014"W	2385 GE-N	.014"W	2409 APX10-33B	.014"W	2387 GE-N	.014"W	2413 APX10-33B	.014"W
EXC-007	.014"W	2389 APX10-33B	.014"W	2379 GE-N	.014"W	2390 APX10-33A	.014"W	2384 GE-N	.014"W	2391 APX10-33A	.014"W
EXC-008	.027"W .005" Mica	2395 APX10-33A	.005" Mica	2403 APX10-33B	.005" Mica	2397 APX10-33A	.005" Mica	2407 APX10-33B	.005" Mica	2398 APX10-33A	.005" Mica .027"W
EXC-009	.027"W .005" Mica	2406 APX10-33B	.005" Mica	2392 APX10-33	.005" Mica	2411 APX10-33B	.005" Mica	2396 APX10-33A	.005" Mica	2412 APX10-33B	.005" Mica .027"W
EXC-010	.014"Mo	2415 APX10-33C	.002"Mo .010"W .002"Mo	2416 APX10-33C	.002"Mo .010"W .002"Mo	2414 APX10-33B	.002"Mo .010"W .002"Mo	2417 APX10-33C	.002"Mo .010"W .002"Mo	2418 APX10-33C	.014"Mo
EXC-011	.014"Mo	2419 APX10-33C	.002"Mo .010"W .002"Mo	2420 APX10-33C	.002"Mo .010"W .002"Mo	2421 APX10-33C	.002"Mo .010"W .002"Mo	2422 APX10-33C	.002"Mo .010"W .002"Mo	2423 APX10-33C	.014"Mo

Astronuclear Laboratory

The calculated resistivity values obtained from the capsules were lower than values previously obtained from qualification bars or even hot pressed specimens. In addition, the test temperature was steady state at 909°K (636°C) in contrast to 850°K which was an established point in Seebeck and resistivity testing. At the lower temperature the resistivity values for ANX 1-20A material would be even lower.

Test apparatus for EXC-capsule work consisted of laboratory bench furnaces which could maintain 636°C test temperature for more than 1000 hours. Figure IV-16 illustrates two such furnaces under steady state operations. Four EXC-capsules could be instrumented and loaded into one furnace for long term testing. Three furnaces were operated simultaneously during the 1000 hour tests with EXC-capsules.

(3) Post-Test Specimen Preparation
After the 1000 hr. test time had elapsed, the electric furnace was slowly reduced to room temperature and the EXC-capsules were withdrawn from the furnace. All stainless steel lead wire and chromel alumel thermocouples were removed and each capsule was potted in an epoxy compound and sectioned longitudinally. Both capsule halves were ground and polished for Seebeck voltage probing and electron beam microprobe scanning. Figure IV-17 shows photographs of polished halves of EXC-005.

(4) Electron Beam Microprobe Analysis
One half section of each capsule was further sectioned in order to obtain samples of proper size for the microprobe. Sections from those ANX 1 EXC capsules tested for 1000 hours were examined with the microprobe for materials compatibility. Each section examined contained one full pellet and half of each adjacent pellet with compatibility material of interest in between each pellet yielding four contact surfaces for examination.

Figure IV-16. Two Bench Furnaces Operating at 636°C and Life Testing EXC-Capsules
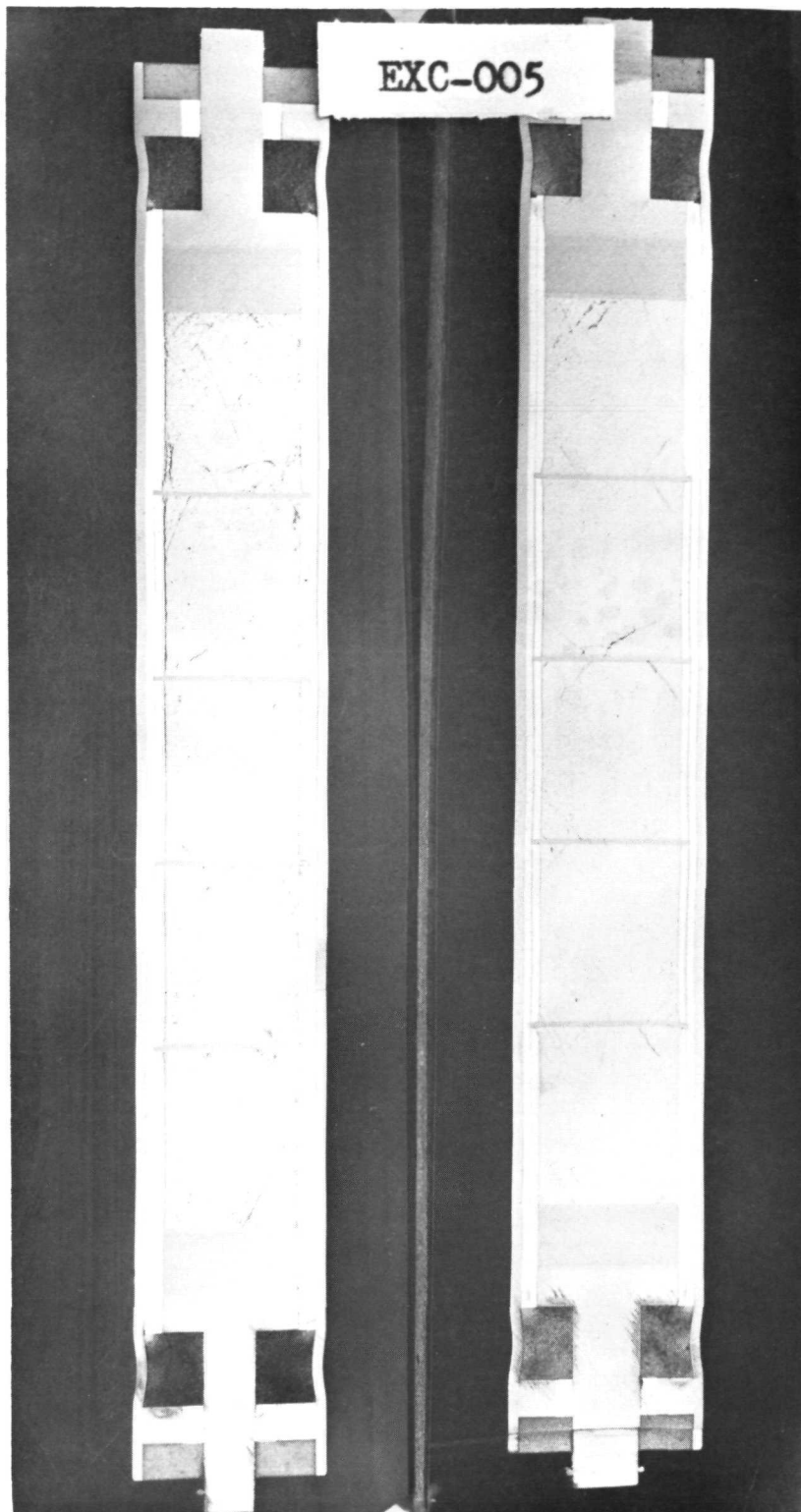
Figure IV-17. Polished Halves of EXC-005 Capsule

The three EXC-capsules that were examined each contained tungsten as the spacer material. No reactions were evident in any of the samples examined with the microprobe where the tungsten was in contact with the ANX 1 pellet.

(5) Seebeck Voltage Probe Analysis

The half of the polished EXC-capsules not sectioned for microprobe analysis was used for Seebeck voltage probe analysis. Voltage probes, spaced by .010 inch apart were made down the centerline of each ternary n-type pellet. Each pellet was probed individually with the initial probe commencing in the adjacent pellet or iron contact and continuing over the spacer material in contact with the pellet at each face. It should be noted that from this type of probing the first data point (interface between pellet and spacer material) actually represents a reading between 0 and 10 mils from the interface. In any case there were no significant changes in Seebeck voltages at the contact surfaces compared to the rest of the pellet.

(6) Hot Pressing n-Type Thermoelectric Materials

(a) Hot Pressing Procedure

In order to perform hot pressing operations in a hydrogen atmosphere, modifications were required to a vacuum furnace to meet fire and safety regulations. Vacuum tight fittings, valves, and plumbing were required to manifold a three gas system (helium, hydrogen, and argon) into the hot zone of the test furnace. In addition, emergency and standard operational procedures were required to safely handle the hydrogen environment at elevated temperatures (700°C). To provide the hot pressing capability, two graphite rams were used to exert pressure within the hot pressing die. An INSTRON recording system indicated the relative position and total load being exerted by the rams. By changing scales, the load could be controlled from 10 to 10,000 lbs., depending

on the test requirements. Graphite electric heaters provided the hot zone and maintained temperature conditions for hot pressing operations.

Special controllers were used to start up the sequence of events and program the furnace for several hours prior to the hot pressing run. In a similar controlling mode, the furnace temperature was decreased in small increments (no faster than 100°C/hour) until all power was shut-off. Total time for one hot pressing run was 20 to 21 hours, depending on the speed and punctuality of the operator at each step of the operation. A brief outline of the steps required to hot press n-type materials are listed in Table IV-8.

In general, it was necessary to reduce the diameter and/or length of the resulting cylinder after hot pressing. The reduction was accomplished by mounting the specimen in a lathe and turning down the outside diameter in .010 inch steps. All machining was performed dry, using a vacuum system for dust collection. The machined cylinder was then placed in a die and the top and bottom surfaces were rubbed over 600 grit polishing paper. By reversing the cylinder, both top and bottom surfaces were ground smooth and parallel to each other. A two inch diameter steel die maintained perpendicularly between the cylinder walls and the flat ends. Final polishing was obtained with 00 paper which permitted sizing the length dimension to an accuracy of .0005 inch.

After final sizing, the cylinder was boiled in methanol and acetone (50/50 mixture) for ten minutes to remove any foreign matter. The specimen was removed from the hot liquid, air dried, and placed in vacuum storage overnight. Prior to testing, the samples were heat treated for two hours in hydrogen at 575°C.

TABLE IV-8

STEPS REQUIRED TO HOT-PRESS N-TYPE T/E MATERIAL

1. Situate undensified powdered PbTe-alloy within die.

2. Vacuum out-gas (at .01 mm pressure and room temperature) PbTe-alloy powder for at least three hours.

3. Vacuum out-gas PbTe-alloy powder at 200°C for 8 hours.

4. Increase powder temperature to 400°C under full vacuum and hold for 2 hours.

5. Introduce high purity helium, purge, and evacuate.

6. Repeat step 5.

7. Fill chamber with high purity helium.

8. Admit high purity hydrogen to chamber and increase temperature to 700°C and hold one hour.

9. Introduce high purity helium into chamber displacing hydrogen.

10. Evacuate chamber and compress powder to 90 percent theoretical.

11. Introduce high purity hydrogen and adjust temperature to 700°C.

12. Apply 7500 psi hydrogen for 30 minutes.

13. Evacuate chamber.

14. Cool furnace from 700°C to 500°C in two hours at a linear rate.

15. Cool furnace to room temperature at a linear rate not to exceed 100°C per hour.

16. Evacuate chamber and die and introduce argon.

(b) N-Type Lead Telluride Preparation and Results

Initial procedural checkout tests of the hot pressing facility were performed with standard n-type PbTe. Quenched n-type material was reduced to powder in an argon dry box to produce powder lots of -20 +35, and -50 +270 mesh (U. S. Standard Sieve Size). Qualification bars were cold pressed, heat treated, and tested for Seebeck voltage and resistivity measurements to establish a reference base line for cold pressed and sintered n-type PbTe.

Three successful hot pressing runs were made with n-type PbTe to qualify the hot pressing facility. In each experimental run, n-type hot pressing powder was loaded into a 5/8 inch diameter die and compacted under 6500 psi pressure for one half hour at a temperature of 700°C. Temperature profiles were controlled and monitored on both the heatup and cooling cycles. Crack-free solid n-type cylinders (0.625 inch diameter x 0.7 inch length) were obtained from all three experimental runs. To verify the integrity and density of the hot pressed cylinder, the diameter was turned down on a lathe from 0.625 to 0.273 inch before and after machining. The relative non-smooth surface of the larger cylinder is caused by the graphite surfaces of the punches and die. Weight and volume measurements indicated a theoretical density of 99.1% for the machined cylinder compared to 98.95% for the total 5/8 inch diameter pellet. After hot pressing and machining, HP001 and HP003 were subjected to a heat treatment in hydrogen at 575°C for two hours. Seebeck and resistivity measurements were made on the hot pressed samples and the results compared to similar type data obtained on cold pressed and sintered qualification bars. The data obtained on hot and cold pressed samples showed good agreement.

Only the resistivity value of the large (.625 inch diameter) sample showed some deviation because of the large area-to-length ratio. However, all Seebeck coefficients were in agreement with each other. Consequently, all hot pressed specimens for Seebeck and resistivity testing were machined to 0.273 diameter to obtain the best and most accurate thermoelectric property data for both n- and p-type material.

During the thermal conductivity experiments, difficulties were encountered in obtaining equilibrium conditions with 0.500 inch diameter test specimens. An alternate standard was available in the 1.00 inch diameter size which proved to be highly successful in obtaining stable temperature conditions. Because of the better results with the larger standard, an attempt was made to hot press a very large sample of PbTe material (1.060 diameter x 1.000 length). Graphite punches were fabricated for the redesigned die body and the molybdenum reinforcement ring was remachined to accept the larger die size. N-type powder was used with the new hot pressing tools on the initial trial run. The procedure was the same for previous hot pressing runs except that the total load on the graphite punches was increased to 7000 lbs. to maintain high pressure on a 1.060 inch diameter cross-section. During STEP 12 (Table IV-8) at 700°C, the graphite die shattered and opened one of the graphite heaters in the furnace. The hot pressing run was aborted and the hydrogen was removed from the furnace as quickly as possible. After cool down, the graphite pieces were removed from the furnace and the hot pressed specimen was salvaged. Figure IV-18 illustrates the hot pressed sample on n-type PbTe machined to 1.000 diameter x 0.896 length. Further effort on the large size specimen was deferred until all smaller sizes (0.625 diameter) of each material were prepared for thermal conductivity tests.
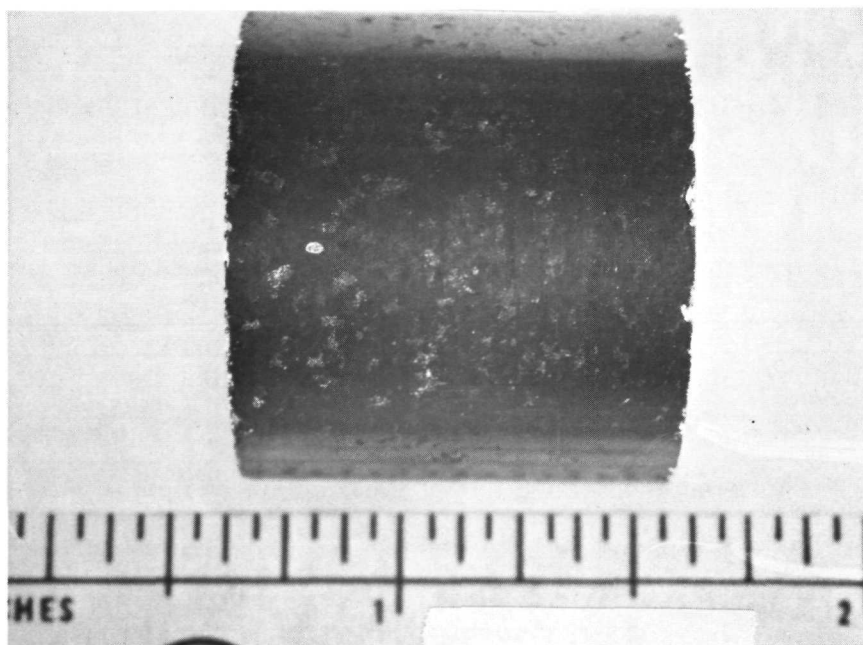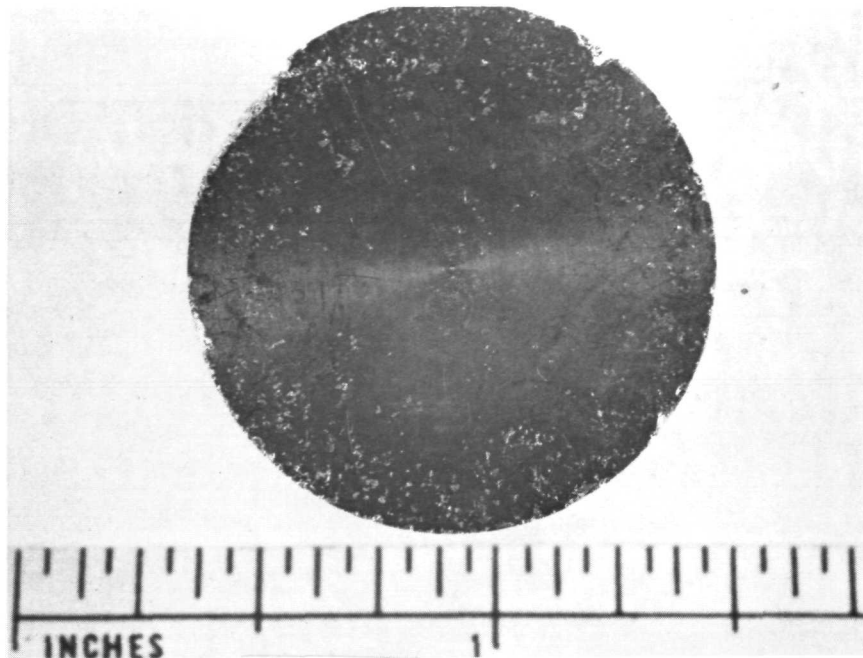
Figure IV-18. HP030 - Hot Pressed Cylinder of N-Type Material
(Hot Pressing Conditions - 7500 psi at 700°C)

After the hot pressing facility was refurbished, one additional run was made with n-type PbTe to prepare a smaller sample (0.625 diameter x 0.7 length) for thermal conductivity testing.

(c) N-Type PbTe-GeTe - Preparation and Results

Hot pressing of PbTe-GeTe was initiated after sufficient p-type hot pressed samples were available for thermal conductivity tests. Quenched ANX 1-type ingots were reduced to powder in an argon dry box to produce powder lots of -20 +35, and -50 +270 (U. S. Standard Sieve Size). These two lots of powder had individual grain sizes from 500 to 841 microns, (-20 +35), and 53 to 297 microns, (-50 +270). Coarse powder was used exclusively for hot pressing; while fine powder, (-50 +270), was used for (1) cold pressing quali-fication bars, pellets, and washers, (2) chemical analyses, and (3) x-ray diffraction experiments.

Because of difficulties in reaching equilibrium in the thermal conductivity experiments, the 5/8 inch diameter hot pressed ANX 1 samples were deferred until December, 1972. Instead, the size of the hot pressing die was reduced from 5/8 inch diameter to 1/2 inch diameter to reduce the quantity of hot pressing powder for each run and reduce the required machining by 125 mils. The hot pressing procedures followed the steps described in Table IV-8, except that the initial hot pressing pressure was 6,500 psi rather than 7,500 psi. The second and third hot pressing runs used pressures of 7,000 and 7,500 psi respectively. By increasing the pressure from 6,500 psi to 8,000 psi, the density changed from 98.6% to 99.0%. ANX 1-type thermoelectric material PbTe-GeTe was found to require a higher pressure during hot pressing than n-type PbTe.

Table IV-9 lists the fourteen hot pressed cylinders of PbTe-GeTe material that were prepared during this program. Eight hot pressed samples were machined to 0.273 diameter and heated for two hours in hydrogen at 575°C. Seven cylinders were used for Seebeck and resistivity measurements, while the eighth specimen was recrushed for x-ray diffraction measurements.

Results of electrical testing HP-018 (ANX 1-15) are illustrated in Figure IV-19. The solid curves represent RCA data. It is evident that hot pressing has materially reduced the electrical resistivity without changing the value of the Seebeck coefficient. Comparison should be made with the data obtained on cold pressed samples, as shown in Figure IV-5. It was anticipated that the standard hot isostatic process required to achieve module compaction would sufficiently densify the PbTe-GeTe to a state where the electrical resistivity would correspond to the data shown in Figure IV-19.

The thermal conductivity specimens were further processed by drilling two radial holes to a depth of 0.250 inch and spaced 0.500 inch apart along the axis of the sample. Two matched thermocouples were installed in the holes to monitor pellet temperature during thermal conductivity testing and the PbTe-GeTe specimen was mounted in the thermal conductivity test apparatus. Hot pressed specimen (HP-024) containing ANX 1-13 ternary material was successfully instrumented and measurements of thermal conductivity had begun when all thermal conductivity measurement effort was terminated.

TABLE IV-9

HOT PRESSED CYLINDERS OF PbTe-GeTe MATERIAL

Specimen Number	Hot Pressing Pressure (psi)	Thermoelectric Material
HP-016*	6, 500	ANX 1-13
HP-017*	7, 000	ANX 1-14
HP-018*	7, 500	ANX 1-15
HP-019*	7, 500	ANX 1-17
HP-020*	7, 500	ANX 1-18
HP-021*	7, 500	ANX 1-21
HP-022*	7, 500	ANX 1-19
HP-023**	8, 000	ANX 1-21
HP-024***	8, 000	ANX 1-13
HP-025	8, 000	ANX 1-14
HP-026	8, 000	ANX 1-15
HP-027	8, 000	ANX 1-17
HP-031	8, 000	ANX 1-19
HP-032	8, 000	ANX 1-15

*   Samples machined from 0. 500 diameter to 0. 273 diameter for Seebeck and resistivity measurement.

** Sample recrushed for x-ray diffraction work.

***Sample (0. 500 Dia. x 0. 611 length) used in thermal conductivity tests.
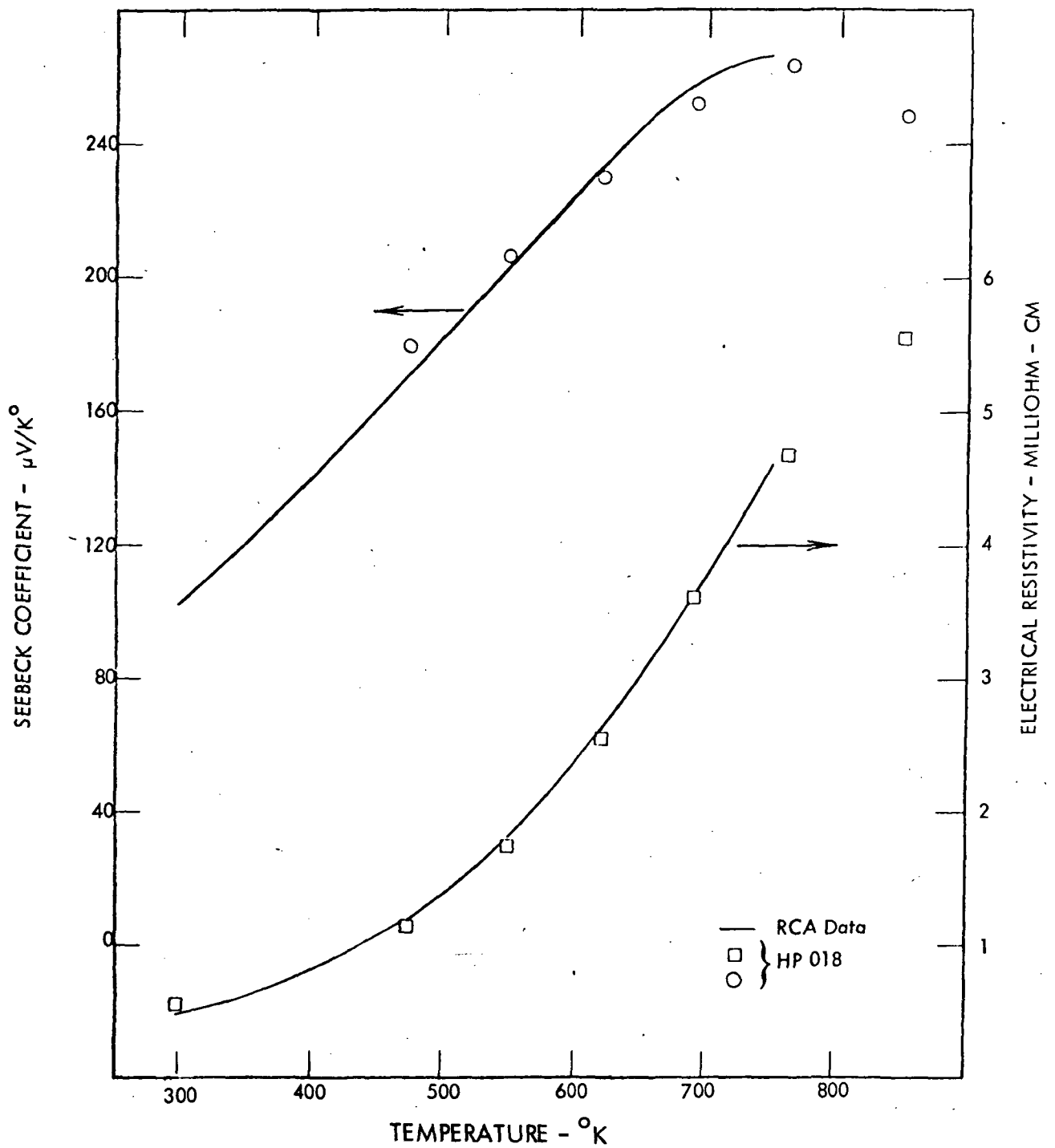
Figure IV-19. Electrical Properties of Hot Pressed PbTe-GeTe Versus Temperature

C.   P-TYPE PbTe-PbSe TERNARY ALLOYS

1.   Previous Development

Electrical property measurements on specimens from the p-type ingots made by WANL to the RCA-reported optimum composition $PbTe_{.95}Se_{.05}Na_{.007}$ indicated that the WANL material had much too low an electrical carrier concentration.

It was postulated that this was due to a severely limited solubility of sodium in the strictly stoichiometric $PbTe_{.95}Se_{.05}$ alloy. It was further postulated, based on a knowledge of standard p-type lead telluride, that the sodium solubility could be increased by adding excess tellurium to the composition. Accordingly, additional compositions were prepared incorporating both excess tellurium and higher sodium content. The six compositions investigated are listed in Table IV-10.

Analyses of Seebeck coefficient and electrical resistivity measurements made on cold pressed and heat treated specimens, Figures IV-20 and IV-21, together with analytical figure of merit estimates, indicated that the highest sodium content formulations $PbTe_{.96}Se_{.05}Na_{.01}$ and $PbTe_{.9643}Se_{.05}Na_{.01}$ possessed the highest figures of merit of the listed compositions over the temperature range of interest. However, due to the hard, brittle nature of these p-type materials, specimens having acceptably high densities could not be fabricated by cold pressing techniques. To permit measurement of true electrical resistivity values, a hot pressing technique was developed for fabricating specimens to near-theoretical density.

Figures of merit calculated from Seebeck and resistivity measurements on hot pressed, high density specimens were found to be higher than values obtained from cold pressed specimens of the same composition. This was very encouraging because the physical state of a hot pressed pellet is more representative of a thermoelectric washer in a fabricated module than is the state of a cold pressed test specimen. The figure of merit vs. temperature curve calculated for hot pressed $PbTe_{.96}Se_{.05}Na_{.01}$ was quite comparable to the reference curve for the RCA-reported optimum composition.

At this point in the previous work, $PbTe_{.96}Se_{.05}Na_{.01}$ (APX 4) was designated the optimum ternary p-type composition for application to the tubular module. Thermal con-

TABLE IV-10

COMPOSITIONS OF EXPERIMENTAL P-TYPE PbTe – PbSe ALLOYS

WANL Designation	Molecular Formula	Excess Te:Na* Atom Ratio
APX 1 (RCA Comp.)	$PbTe_{.95}\ Se_{.05}Na_{.007}$	0
APX 2	$PbTe_{.957}\ Se_{.05}Na_{.007}$	1:1
APX 3	$PbTe_{.960}\ Se_{.05}Na_{.007}$	10:7
APX 6	$PbTe_{.9585}Se_{.05}Na_{.0085}$	1:1
APX 4	$PbTe_{.96}\ Se_{.05}Na_{.01}$	1:1
APX 5	$PbTe_{.9643}Se_{.05}Na_{.01}$	10:7

* Excess Te = (Te atoms + Se atoms) – Pb atoms
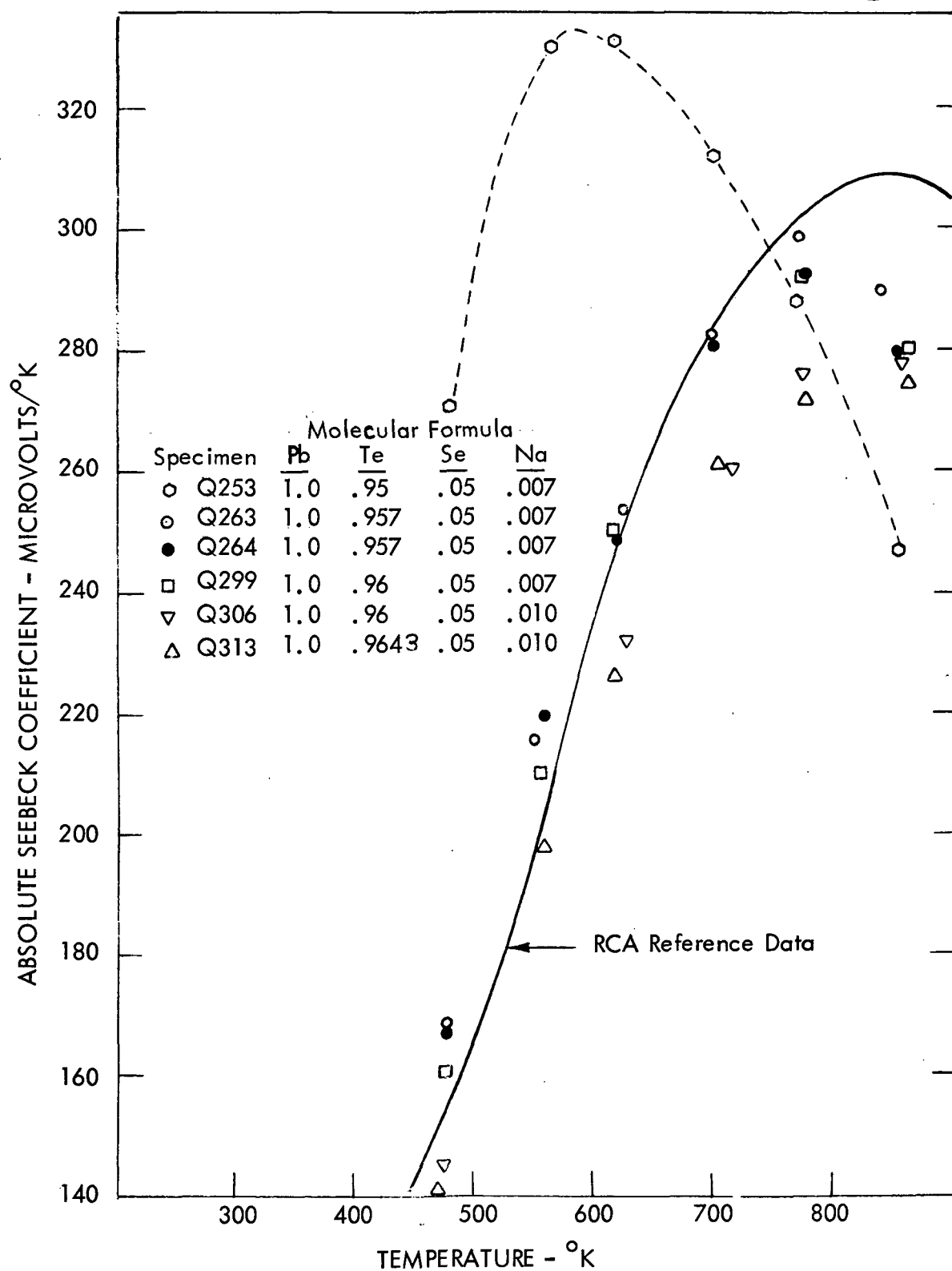
Figure IV-20. Seebeck Coefficient of P-Type PbTe – PbSe Alloys – Powder
and Cold Pressed Specimens Heat Treated at 650°C in H_2
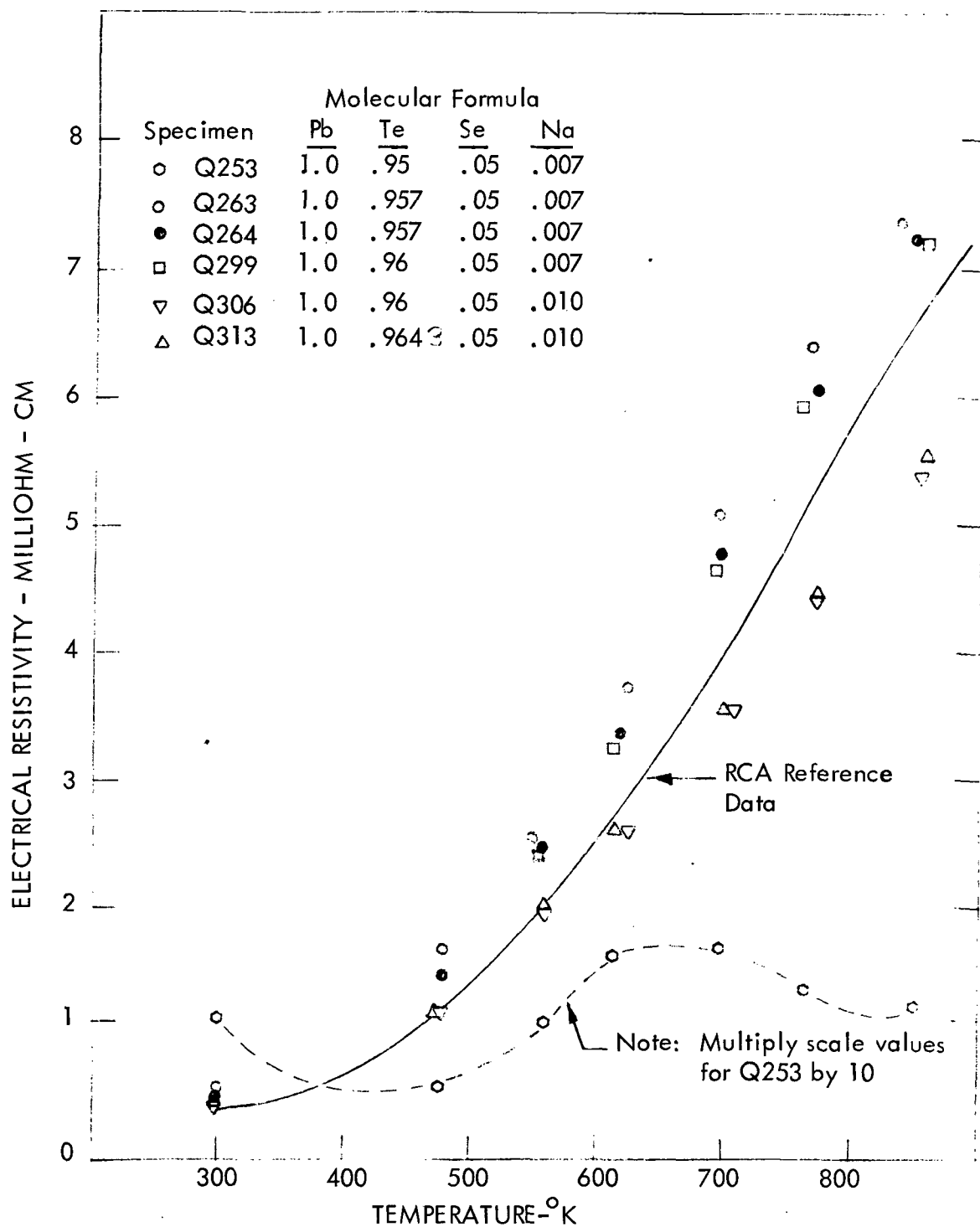
Figure IV-21. Electrical Resistivity of P-Type PbTe - PbSe Alloys - Powder and Cold Pressed Specimens Heat Treated at 650°C in H₂

conductivity measurements were then made on an APX 4 specimen over the temperature range
300 to 8°K by Resalab, Inc. The results, together with the RCA reference data for their
reported optimum composition, are plotted in Figures IV-22. The correspondence between the
two data sets is very good, and this reinforced the belief that use of the ternary p-type mater-
ial would substantially improve tubular module operating performance.

2. Sublength Technology Module, TEM-15E S/N-4

TEM-15E S/N-4, a sublength technology module of the type previously discussed
in Section III, was fabricated late in 1970. The module design was identical to that of the
"baseline" TEM-15A S/N-4 module except that the APX 4 composition $PbTe_{.96}Se_{.05}Na_{.01}$
was used for the p-type thermoelectric washers (standard GE-NL n-type PbTe was used for
the n-type washers). Two polycrystalline APX 4 ingots were prepared and crushed to -50 +270
mesh powder, and the resultant powder lots heat treated at 650°C for two hours in flowing
hydrogen. Electrical test specimens were then cold pressed and they in turn were heat treated
at 650°C for two hours in flowing hydrogen. The results of electrical property tests on these
specimens indicated that the powder lots were identical and acceptable for module use.

The powder lots were then blended together and module washers fabricated from
the resultant batch, with the cold pressed washers being heat treated at 650°C for two hours
in flowing hydrogen. Assembly and fabrication of TEM-15E S/N-4 then proceeded in a manner
identical to TEM-15A S/N-4. The module was placed on static test in November 1970 and the
test data demonstrated that the thermal conductivity of the APX 4 alloy was about twenty per-
cent lower than conventional p-type lead telluride. However, the electrical resistivity of the
module was higher than was calculated, and the change in electrical properties proceeded at
a rate which was faster than that established by the TEM-15A S/N-4 series. Accordingly, the
module was removed from test after 1000 hours and destructively examined.

Based on the test data and the destructive examination results, it was concluded
that no incompatibility problem existed between the APX 4 alloy and the tungsten inner con-
ductor ring. It was also concluded that the initial high resistance of the module was a result
of tellurium loss during the relatively high 650°C heat treatment of the washers, particularly
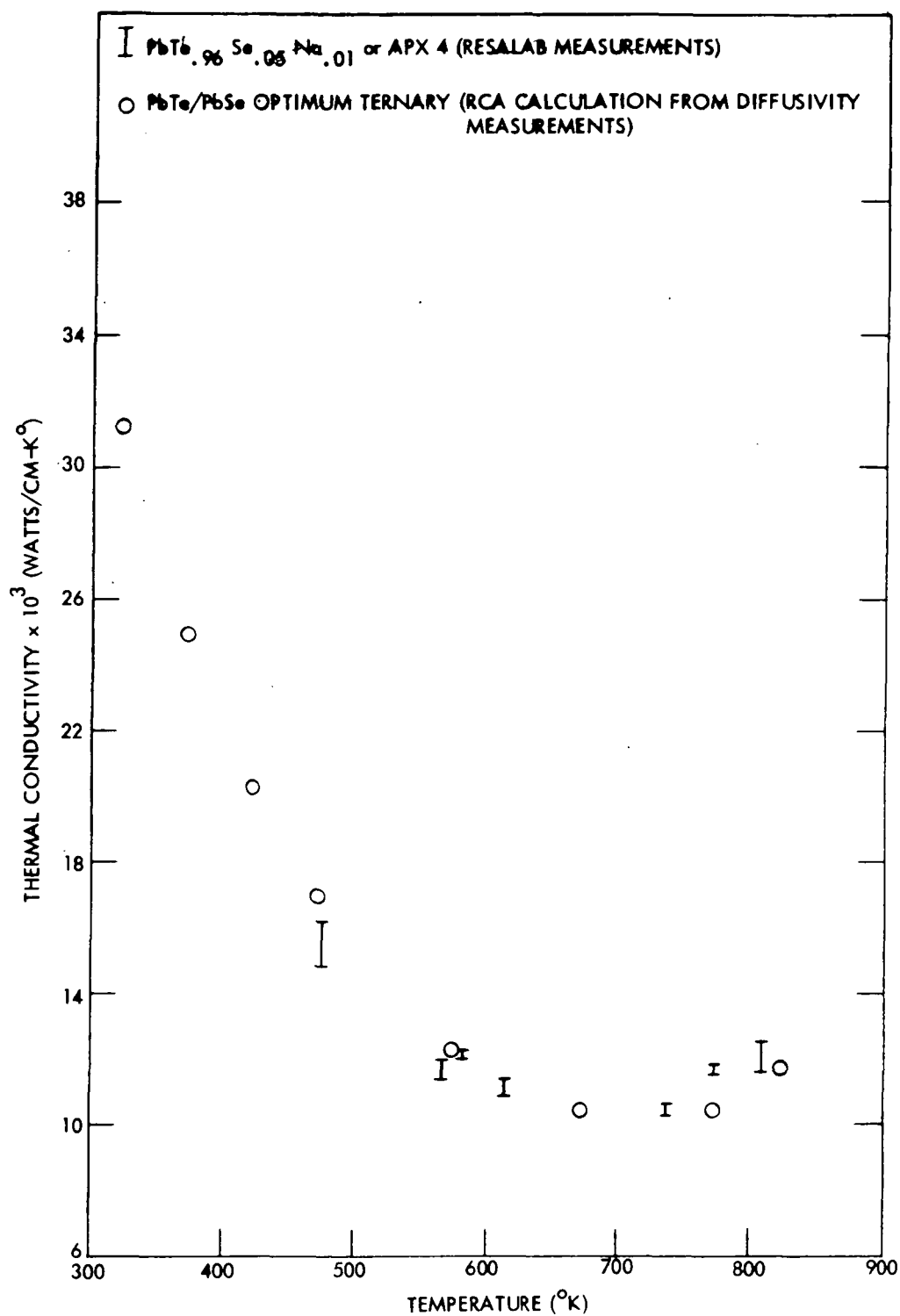
Figure IV-22. Thermal Conductivity of P-Type Thermoelectric Materials

in view of their high surface to volume ratio. Because of this tellurium loss, the p-type washer experienced changes in its electrical properties. The net result was that both the n-and p-type material contributed to the module degradation rather than only the n-type changes that were being observed in modules incorporating standard p- and n-type lead telluride materials.

From the problems just discussed, the TEM-15E S/N-4 data demonstrated that the ternary APX alloys possessed thermal conductivities substantially lower than that of standard p-type lead telluride, and thus held promise for increased module efficiency once the optimum combination of composition and processing temperature were determined.

From the results obtained in the first phase of ternary p-type alloy work, it appeared that it would be necessary to utilize an excess Te:Na ratio greater than 1:1 in order to achieve complete solubility of the sodium addition and maintain this solubility throughout elevated temperature processing and operation. Also, it appeared that the compositions with highest sodium content possessed the highest figures of merit over the module operating temperature range. In accordance with these facts, it was decided that when work on this task was resumed the composition to be investigated would be $PbTe_{.965}Se_{.05}Na_{.01}$, WANL designation APX 10, having an excess Te:Na ratio of 1.5:1. It was also decided that heat treating temperatures would be minimized in order to limit the loss of tellurium during processing.

3. Current Materials Processing

The current procedures for manufacturing p-type PbTe-PbSe alloys are essentially identical to those discussed previously for n-type PbTe-GeTe alloys. In the p-type case, however, sized powder is heat treated at $550^\circ C$ for one hour in flowing hydrogen, and cold pressed washers or test specimens are heat treated at $575^\circ C$ for two hours in flowing hydrogen prior to use in module assembly or electrical property measurement.

Difficulty was experienced early in the program when several quartz tubes containing one-pound melts of $PbTe_{.965}Se_{.05}Na_{.01}$ exploded during the quenching step. Because of this, the existing preparation procedure was reviewed step-by-step, and several changes instituted to eliminate the explosion problem and improve the ingot-to-ingot reproducibility

of electrical properties. The principal changes made were reducing the ingot size by one-half, applying multiple carbon coatings to the quartz tube inner surfaces, and substituting elemental metallic sodium for the sodium-lead alloy previously used to introduce sodium to the formulation. It was found that reducing the melt size was the most important factor in eliminating the explosion problem.

4. Material Property Evaluation

To fully characterize the APX 10 alloy, a number of different measurements and analyses were performed to develop an understanding of the material formulation and performance. A total of 36 ingots were prepared in the course of the investigation, although several early ones were destroyed during quenching and others were judged to be contaminated and were not used.

To verify that the APX 10 compositional formulation $PbTe_{.965}Se_{.05}Na_{.01}$ was being maintained within acceptable limits and without contamination by impurity elements, each useable ingot was checked by wet chemistry, emission spectrography, atomic absorption spectrophotometry and x-ray diffraction measurements. In addition to qualifying the composition, extensive measurements of Seebeck coefficient and electrical resistivity as a function of temperature, and Seebeck voltage over large temperature differences, were performed. Thermal conductivity measurements were planned but were not performed due to termination of the program. The various aspects of the APX 10 characterization techniques are described in the following subsections:

a. Seebeck and Resistivity Measurements

Ingots of APX 10 material were reduced to powder using a mortar and pestle in an argon-filled glove box. Powder was sized to -50 + 270 mesh using stainless steel sieves, and heat treated as described previously. Rectangular electrical test bars (0.250 x 0.235 x 0.875 inches) were then cold pressed and heat treated as previously noted. The bars were maintained in vacuum storage until tested. Seebeck coefficient and electrical resistivity measurements were made using apparatus and procedures identical to those previously described for n-type PbTe - GeTe alloys.

Table IV-11 lists the APX 10 material lot numbers and test bar serial numbers tested during this program, and Figure IV-23 shows typical test results obtained on these specimens. It is obvious that the properties of the APX 10 material do not duplicate the RCA reference data, as both the Seebeck and resistivity of the APX 10 material are significantly lower. This is largely due to the higher sodium content and resultant higher carrier concentration in the WANL alloy. However, the APX 10 properties are superior to the RCA data for application over the specific tubular module operating temperature range. The power number (α^2/ρ) of the APX 10 material is comparable to that of standard p-type lead telluride, so that the lower thermal conductivity of APX 10 should result in a higher figure of merit and improved module performance.

b. Measurement of Seebeck Voltage Over Large Temperature Differences

Seebeck voltage characteristics of APX 10 test bars were measured for all material lots between APX 10-21 and APX 10-34. These tests were conducted identically to the manner previously described for n-type PbTe - GeTe specimens.

Table IV-12 is a list of the APX 10 specimens tested in the high ΔT apparatus, and typical test data are given in Table IV-13. In general, as in the n-type case, excellent agreement was obtained between measured Seebeck voltages and voltages calculated by integrating Seebeck coefficient data over the given temperature range.

c. X-Ray Diffraction Measurement of Lattice Parameter

Powder samples from individual APX 10 ingots were submitted for accurate lattice parameter determinations. The precision with which the lattice parameters could be measured was determined by measuring values for four different powder samples from the same melt. The data yielded a result of ± 0.0005 Å for the technique used.

TABLE IV-11

SEEBECK AND RESISTIVITY TEST SPECIMENS FOR PbTe$_{.965}$Se$_{.05}$Na$_{.01}$

P-Type Ingot Designation	Specimen Number
APX 10-8	Q-1026
APX 10-13B	Q-1029
APX 10-17	Q-1031, Q-1032
APX 10-18	Q-1035, Q-1036
APX 10-19	Q-1038, Q-1039
APX 10-21	Q-1059, Q-1060
APX 10-22	Q-1065, Q-1066, HP-007
APX 10-23	Q-1069, Q-1070, HP-008
APX 10-24	Q-1073, Q-1074
APX 10-25	Q-1079, Q-1080
APX 10-26	Q-1081, Q-1082
APX 10-27	Q-1085, Q-1086
APX 10-28	Q-1089, Q-1090
APX 10-29	Q-1093, Q-1094, Q-1094R
APX 10-30	Q-1099, Q-1100, Q-1100R
APX 10-31	Q-1103, Q-1104
APX 10-32	Q-1105, Q-1106
APX 10-33A (Capsule Material)	Q-1145, Q-1146
APX 10-33B (Capsule Material)	Q-1148
APX 10-33C (Capsule Material)	Q-1150, Q-1151
APX 10-34C (TEM-15P S/N-1 Material)	W-422, W-423
APX 10-34C (Washer Material Recycled)	Q-1181, Q-1183, Q-1184
APX 10-40 (TEM-15G* Material)	Q-1185, Q-1186, Q-1187

*Sublength technology module scheduled for fabrication after program termination.
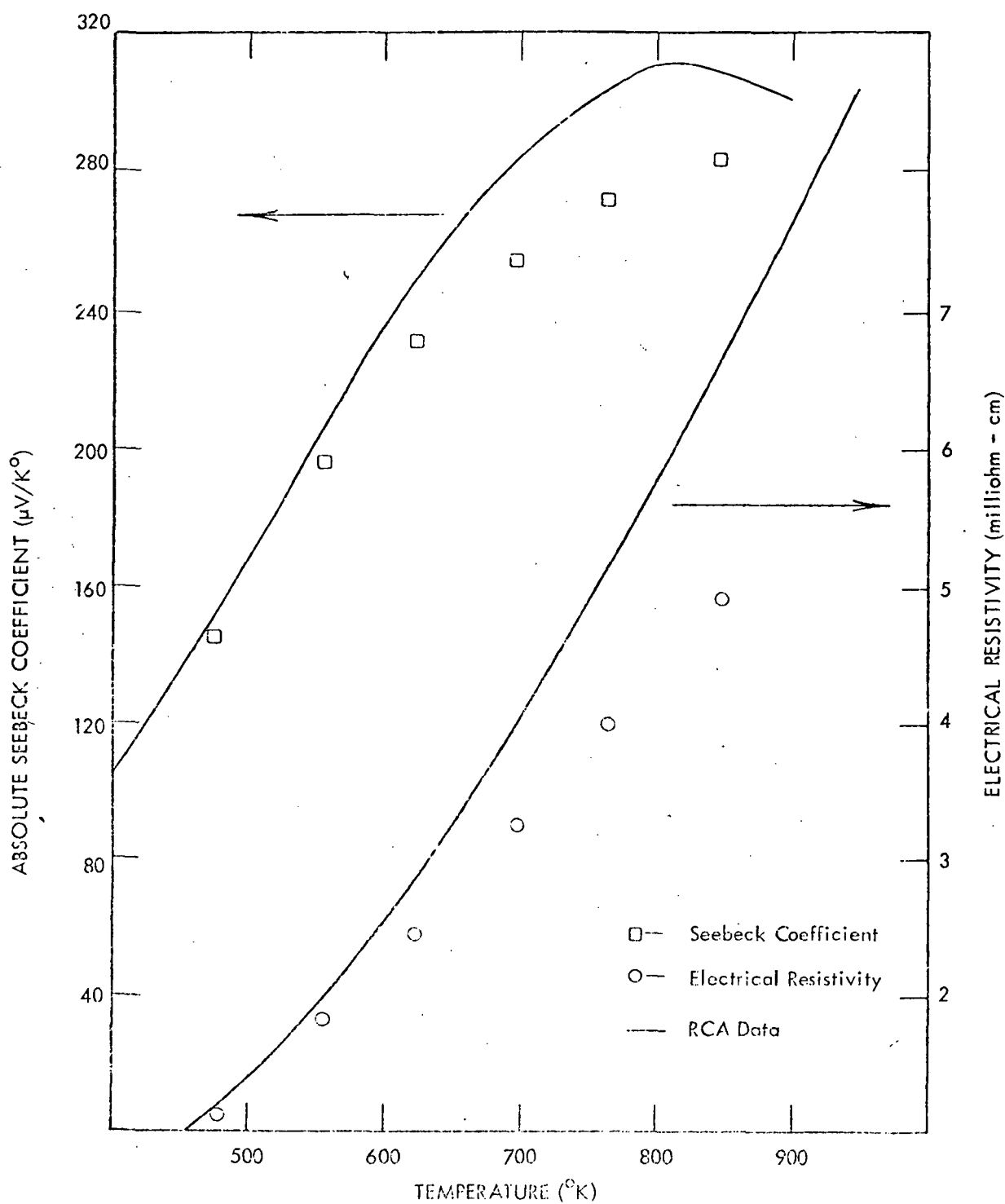
Figure IV-23. Electrical Properties Versus Temperature for APX 10-23

TABLE IV-12

HIGH ΔT TEST SPECIMENS FOR PbTe$_{.965}$Se$_{.05}$Na$_{.01}$

P-Type Ingot Designation	Specimen Number
APX 10-21	Q-1059R, Q-1060R
APX 10-22	Q-1065R, Q-1067, Q-1068
APX 10-23	Q-1069R, Q-1071, Q-1072
APX 10-24	Q-1074R, Q-1075, Q-1076R
APX 10-25	Q-1077, Q-1078, Q-1079R
APX 10-26	Q-1081R, Q-1083, Q-1084
APX 10-27	Q-1085R, Q-1087R, Q-1088
APX 10-28	Q-1089R, Q-1091, Q-1092
APX 10-29	Q-1093R, Q-1095R, Q-1096R
APX 10-30	Q-1097, Q-1098, Q-1099R
APX 10-31	Q-1101, Q-1102, Q-1103R
APX 10-32	Q-1105R, Q-1107R, Q-1108
APX 10-34C	W-424, W-425

TABLE IV-13

HIGH ΔT TEST RESULTS WITH P-TYPE TERNARY MATERIAL

APX 10-23 Ternary Material $(PbTe_{.965}Se_{.05}Na_{.01})$

Specimen No. Identification Description	Q 1071	Q 1072
Th_1	319.00	319.00
Tc_1	13.75	13.75
ΔT (^{o}C)	305.25	305.25
Normalized Voltage (mv)	37.75	37.77
Th_2	592.75	592.75
Tc_2	13.75	13.75
ΔT (^{o}C)	579.00	579.00
Normalized Voltage (mv)	113.32	113.16
Th_3	650.00	650.00
Tc_3	13.75	13.75
ΔT (^{o}C)	636.25	636.25
Normalized Voltage (mv)	129.68	129.94
ΔV (592.75 - 319.00)	75.57	75.39
ΔV (650.00 - 319.00)	91.93	92.17

From each ingot, a portion of non-heat treated powder and a second portion of powder that was heat treated in flowing hydrogen for one hour at 550°C, were used in determining the lattice parameters. The determinations were then averaged and plotted on an expanded plot (Figure IV-24) of lattice parameter vs. mole fraction PbSe in PbTe as determined by Steininger[5]. The lattice parameter of 6.4429 $\overset{\circ}{A}$ obtained from the non-heat treated APX 10 samples agrees very well with the Steininger value of 6.4435 $\overset{\circ}{A}$ for 5.0 mole percent PbSe in PbTe. The data indicates that the ingots are reproducible and contain the as-formulated composition value of 5 mole percent PbSe.

The heat treated APX 10 samples yielded diffraction lines that were broader than those obtained on the non-heat treated powder. The average of lattice parameter values determined from the middle of the broad lines was 6.4478 $\overset{\circ}{A}$, which represents approximately 3.7 mole percent PbSe. However, if the lattice parameters were calculated using the leading and trailing edges of the broad lines, a maximum value of 6.4545 $\overset{\circ}{A}$ and a minimum value of 6.4444 $\overset{\circ}{A}$ were obtained which represented 1.7 and 4.7 mole percent PbSe, respectively.

In order to understand more fully the effect heat treating has on the lattice parameter of the APX 10 composition, two sets of experiments were conducted. One study conducted consisted of heat treating powder from ingot APX 10-21 for various times and temperatures in flowing hydrogen. The other involved the annealing of powders (after various processing steps) in sealed argon-filled ampoules for 100 hours at 700°C. The results of these studies are shown in Table IV-14. From the data, the following observations were made:

(5)
J. Steininger, Met. Trans., Vol. 1, p. 2939 (1970).
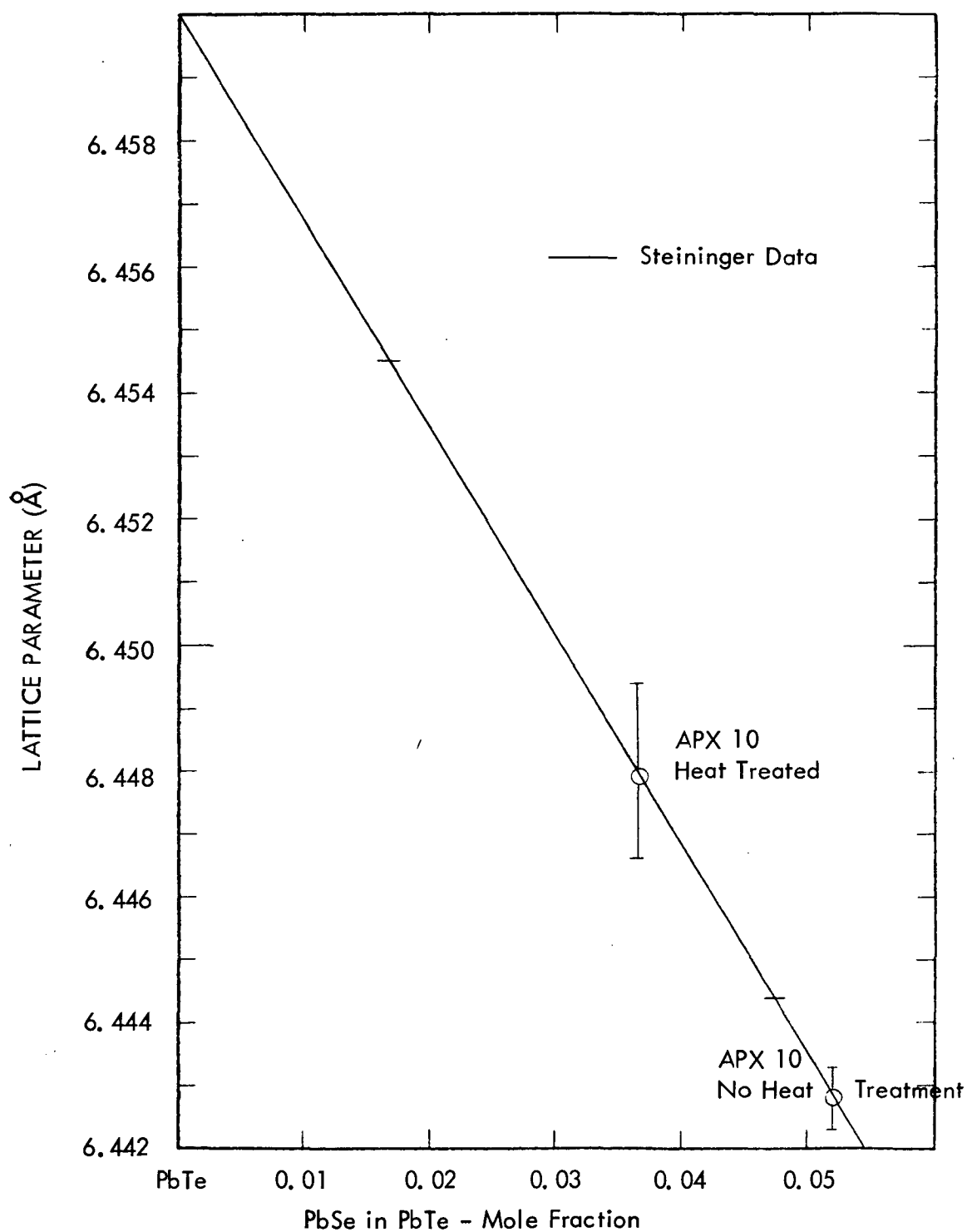
Figure IV-24. Lattice Parameter Versus Mole Fraction PbSe in PbTe

TABLE IV-14

X-RAY DIFFRACTION LATTICE PARAMETER RESULTS ON APX 10-21 POWDER

Lattice Parameter (Å)	Type Treatment	
6.4427 ± 0.0005	No heat treatment	Average of 4 separate measurements, no line broadening
6.4486	Heat treated 1 hr at 550°C in H_2	Line broadening edges 6.4517/6.4452
6.4473	Heat treated 2 hrs at 550°C in H_2	Line broadening edges 6.4507/6.4440
6.4472	Heat treated 4 hrs at 550°C in H_2	Line broadening edges 6.4507/6.4441
6.4466	Heat treated 2 hrs at 750°C in H_2	Slight line broadening--not enough to measure
6.4474	Heat treated 4 hrs at 750°C in H_2	Slight line broadening--not enough to measure
6.4420	Powder H.T. 1 hr at 550°C in H_2, pressed into test bar, bar H.T. 2 hrs at 575°C in H_2, bar crushed to powder, powder sealed in argon-filled quartz tube and annealed 100 hr at 700°C.	Slight line broadening
6.4430	Nonheat treated powder annealed for 100 hrs in sealed argon-filled tube at 700°C	Slight line broadening
6.4446	Powder heat treated for 1 hr at 550°C in H_2 then annealed for 100 hrs at 700°C in sealed argon-filled tube	Slight line broadening
6.4434	Nonheat treated powder[1] annealed for 1 hr at 550°C in sealed argon-filled tube	No line broadening

[1] APX 10-13B powder instead of APX 10-21

(1) Samples heat treated at 550°C in H_2 for from one to four hours have expanded lattices.

(2) If samples from (1) are annealed in a sealed argon-filled tube for 100 hours at 700°C, the lattice parameter returns to its original non-heat treated value.

(3) If non-heat treated powder is heated in a closed argon atmosphere (annealed in a sealed tube) to a temperature which causes lattice expansion when heated in flowing hydrogen, the lattice does not expand.

(4) Heat treatment of non-heated powder at higher temperatures than 550°C in flowing hydrogen does not result in line broadening.

The following conclusions are drawn from the above observations:

(1) Interstitial hydrogen may be introduced in the 550°C heat treatment in flowing hydrogen causing an expansion of the lattice.

(2) There is a critical temperature between 550°C and 750°C at which the interstitial hydrogen is released and sublimation of PbSe and/or Se occurs.

(3) The hydrogen heat treatment at 550°C does not affect the material composition; i.e., cause a loss of PbSe and/or Se.

d. Analysis of Sodium Content by Atomic Absorption

Determination of the sodium content of APX 4 alloy $PbTe_{.96}Se_{.05}Na_{.01}$ (during the destructive examination of the TEM-15E S/N-4 module) by emission spectrography indicated a level of order 0.03 weight percent in most specimens. If this was truly the case it represented a serious problem, since the as-formulated level was 0.069 weight percent and this would mean that over half the dopant addition was being lost during processing. However, investigation disclosed that the accuracy of the spectrographic

technique could not be guaranteed to be better than 1/3 to 3 times the amount reported.

This tolerance was judged to be completely unacceptable for examination and characterization purposes, so other potential analysis techniques were investigated. The method settled upon was atomic absorption spectrophotometry, which had an accuracy of $\pm$ 5 to 10 percent of the amount present. This technique was used to analyze both APX 4 and APX 10 ternary alloys and also some standard p-type PbTe specimens. The results of these analyses are given in Table IV-15. In all cases, the weight percentages obtained by atomic absorption are substantially higher than spectrographic values obtained on the same materials and are in good agreement with the material makeup compositions.

5. Compatibility Experiments

Ternary alloy compatibility tests were divided into two general environment/time/temperature categories. The first of these was a series of die tests where accelerated short-term exposures were performed at 700°C in a hydrogen atmosphere. The second category was a series of 1000 hour EXC capsule tests at a temperature of 636°C.

The tests were intended to determine interactions between the APX 10 alloy and the other module circuit materials, and also to evaluate the long term stability of the APX 10 material in terms of its electrical properties. All test procedures and evaluation methods used were identical to those discussed previously for n-type PbTe – GeTe alloys. The results obtained were as follows:

a. Short-Term Die Tests

A total of twelve die tests were performed with APX 10 pellets in contact with tungsten, molybdenum, phlogopite mica or standard n-type PbTe for 2, 4 and 6 hours at 700°C in a hydrogen atmosphere.

TABLE IV-15

ATOMIC ABSORPTION ANALYSIS FOR SODIUM

		Weight Percent No.
Qualification Specimens from	W308*	0.061
Original APX 4 Powder Lot	Q757*	0.066
Specimens Reclaimed from	Q617*	0.058
15E-4 Module Washers	Q618*	0.055
Control Specimen Reclaimed from Unassembled Washers	Q621*	0.061
Standard p-type lead telluride powder	No. 1	0.061
	No. 2	0.061
	No. 2R	0.061
APX 10 - 8 Powder	---	0.058
-13B	---	0.060
-17	---	0.069
-19	---	0.053
-22	---	0.062
-23	---	0.061
-25	---	0.057
-27	---	0.058
-28	---	0.062
-30	---	0.052
-31	---	0.062
-32	---	0.062

* Samples previously reported by spectrographic analysis to contain 0.03 weight percent sodium.

Electron beam microprobe examination of the sectioned and polished dies revealed no interface reactions between the APX 10 alloy and tungsten, molybdenum or mica.

Seebeck probe traverses across the compatibility interfaces indicated that the APX 10 electrical properties remained unaffected in all cases. However, as shown in Figure IV-25, the standard n-type PbTe exhibited the classic degradation due to migration of excess tellurium from the p-type alloy.

b.   Long-Term Capsule Tests

After completion of the short-term die tests, a series of capsule tests were performed to evaluate the compatibility and stability of the APX 10 alloy during 1000-hour operation at 636°C (1175°F). Eight capsules, identical in design to those previously discussed for n-type PbTe - GeTe alloys, were assembled and tested with APX 10 pellets in contact with tungsten, moly-bdenum and phlogopite mica (both air and vacuum heat-treated). In two of these, APX 10 pellets were spaced alternately with standard n-type PbTe pellets, with tungsten foil spacers separating the two thermoelectric materials. The detailed assembly configurations of the eight capsules were given previously in Table IV-7.

Figure IV-26 is a photograph of some APX 10 capsule pellets positioned on a heat treating fixture just after removal from the hydrogen furnace. Figure IV-27 is an x-ray radiograph of all eleven EXC capsules (three ANX 1 capsules and eight APX 10 capsules) fabricated under this program. A care-ful examination will disclose interpellet spacers in most capsules extending beyond the outer diameters of the thermoelectric pellets and having much higher densities than the boron nitride which surrounds the pellet circumfer-ential surfaces. The dark lines appearing in EXC-008 and 009 are the low density phlogopite mica spacers used in those capsules; the mica spacers toward the right ends of these capsules are not visible because of parallax
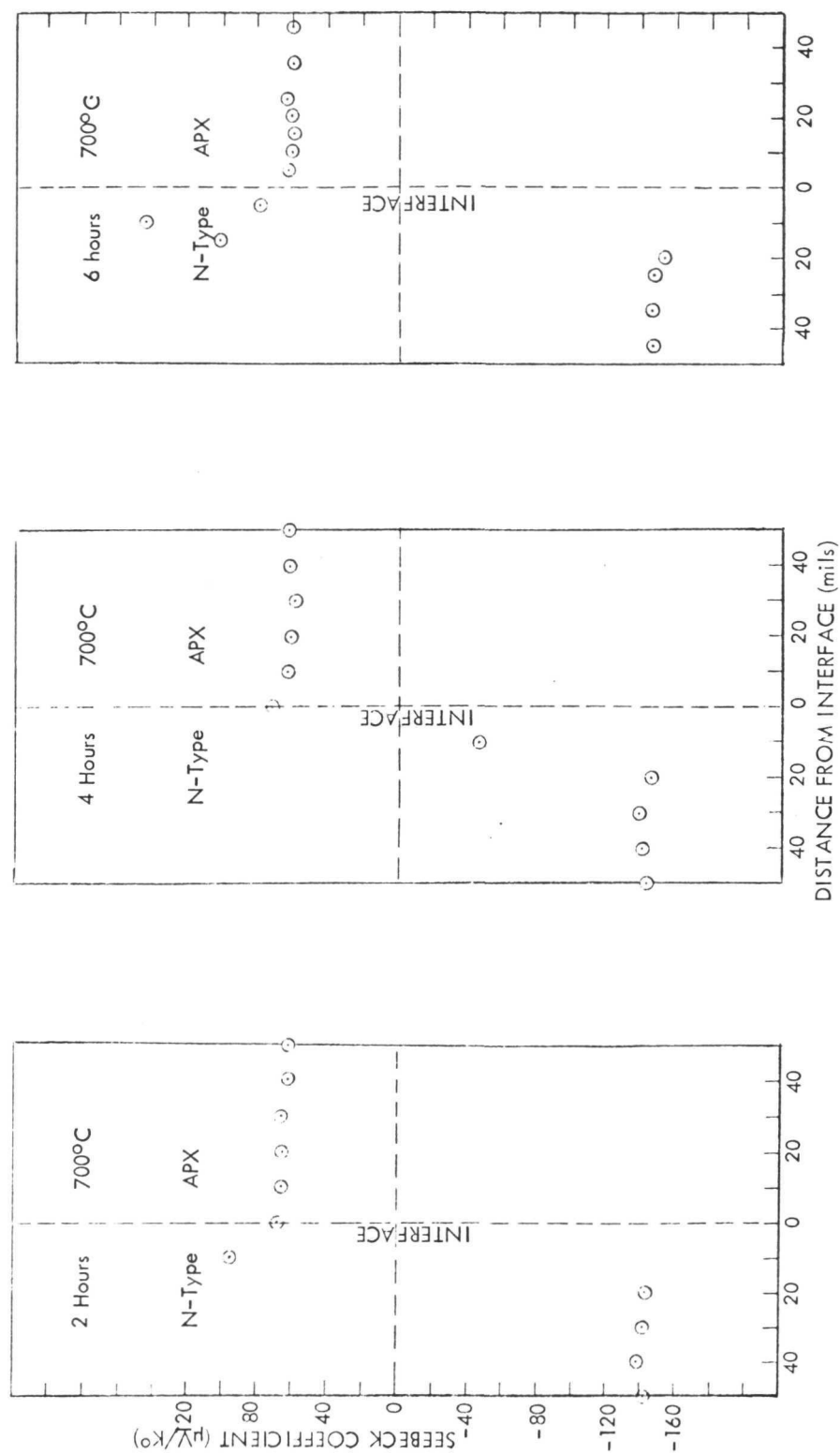
Figure IV-25. Seebeck Coefficient Versus Distance from Interface
for P-Type $PbTe_{.965}Se_{.05}Na_{.01}$/Standard N-Type PbTe
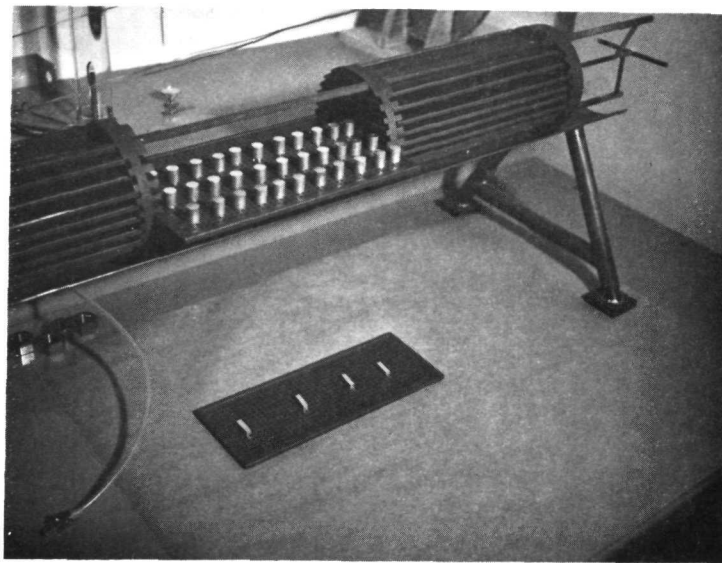
Figure IV-26. APX 10 Pellets (0.50 Diameter x 0.625 Length)
Positioned on Furnace Fixture after Heat Treatment in Hydrogen
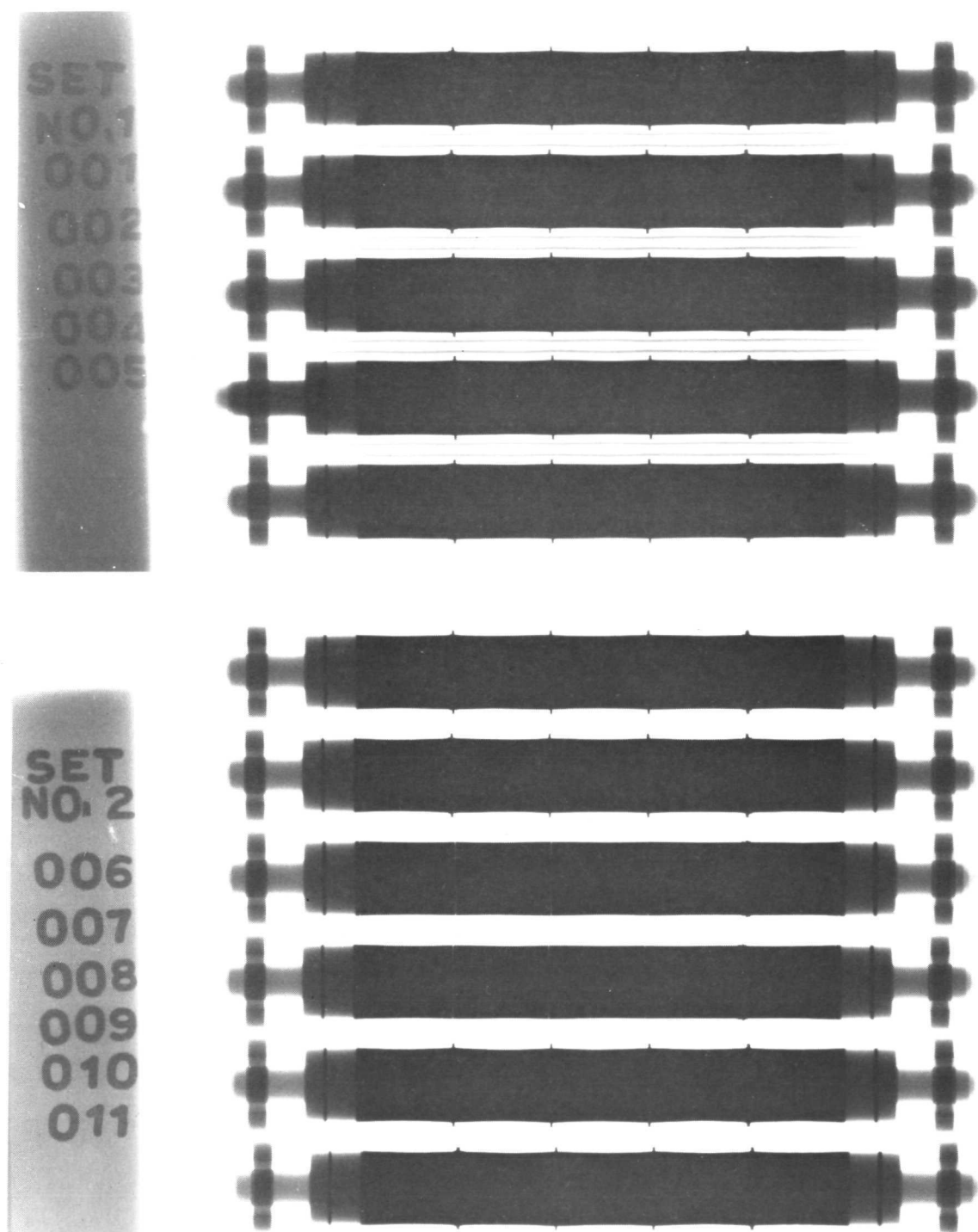
Figure IV-27. Radiographic Exposures of Eleven EXC-Capsules after Hot Isostatic
Pressing and Final Machining

effects in the x-ray beam/film positioning arrangement. In general, the as-fabricated capsules appeared to be very uniform in size, shape and internal geometry.

The eight APX 10 capsules were instrumented and tested in the same manner as the ANX 1 capsules previously discussed. Measured resistance values during the $636°C$ tests ranged from 32.0 milliohms initially to 37.0 milliohms after 1000 hours. After accounting for the resistance contributions of the stainless steel, iron and tungsten or molybdenum components, it was calculated that the APX 10 electrical resistivity increased from 4.7 to 5.5 milliohm-centimeters (17 percent) during 1000 hours of $636°C$ testing.

Capsules EXC-008 and -009 were assembled with 0. 560 diameter x 0.005 inch thick mica spacers between all adjacent pellets and at the outboard faces of the first and last pellets. The purpose of these capsules was to establish a standard to which later assemblies containing identical mica spacers plus various tungsten diffusion barriers could be directly compared.

During the testing of the three ANX 1 capsules and six APX 10 capsules containing electrically conductive tungsten and/or molybdenum spacers between all thermoelectric pellets, the end-to-end capsule circuit resistance measured at temperature (635-640°C) did not exceed 0.04 ohm in any case throughout the test duration. Thus, in testing APX 10 capsules EXC-008 and -009, all resistance in excess of 0.04 ohms could be attributed to the mica interpellet spacers. Figures IV-28 and IV-29 illustrate the resistances of these capsules as a function of test time. In both cases, the initial megohm-range resistance had deteriorated to hundreds of ohms by the end of 1000 test hours. Also, the resistance between the capsule internal circuit and the originally electrically isolated outer clad had decreased by two orders of magnitude. It thus appeared that the 0.005 inch mica spacers were being gradually penetrated and/or circumvented by electrically conductive
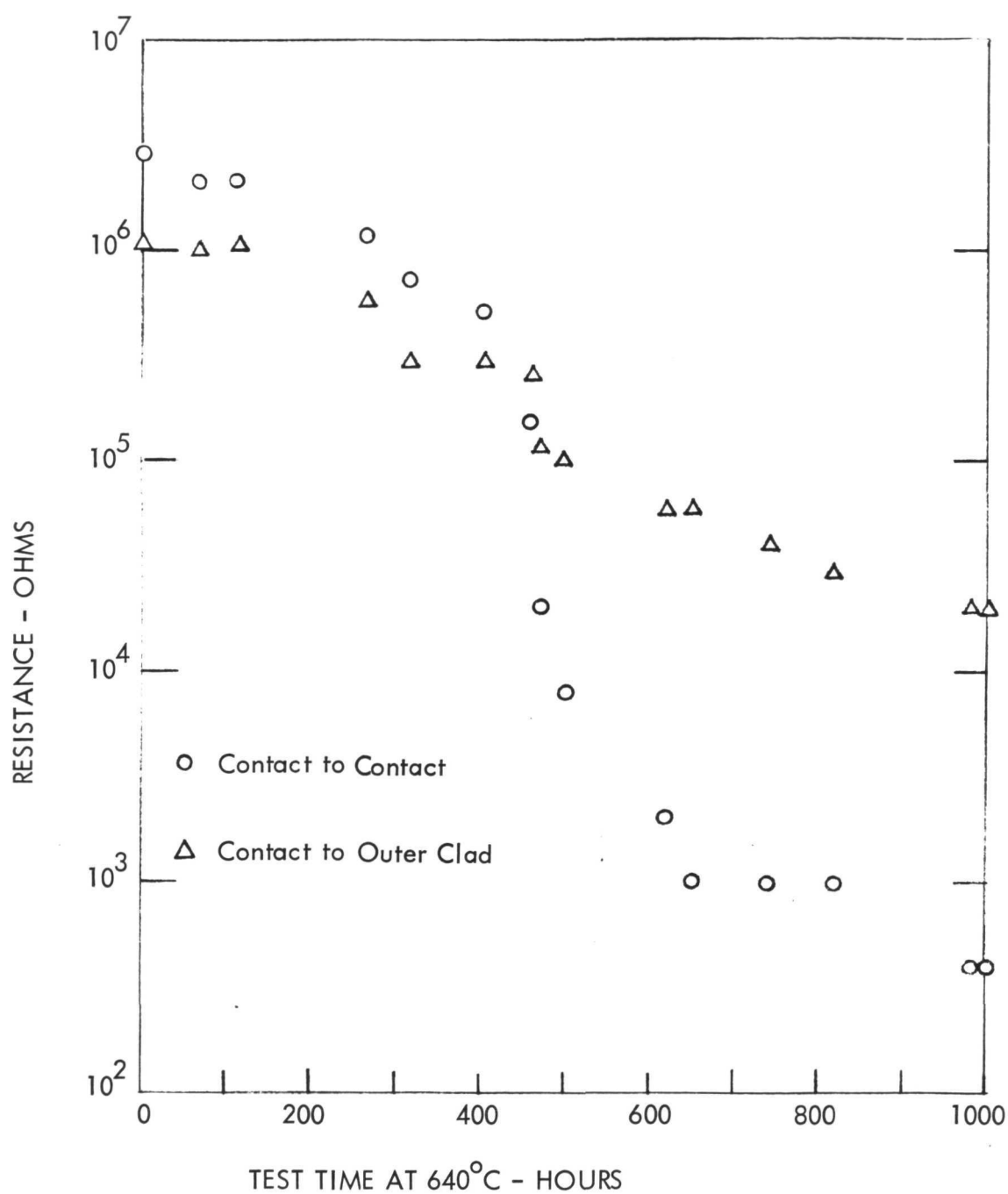
Figure IV-28. Electrical Resistance Data from EXC-008
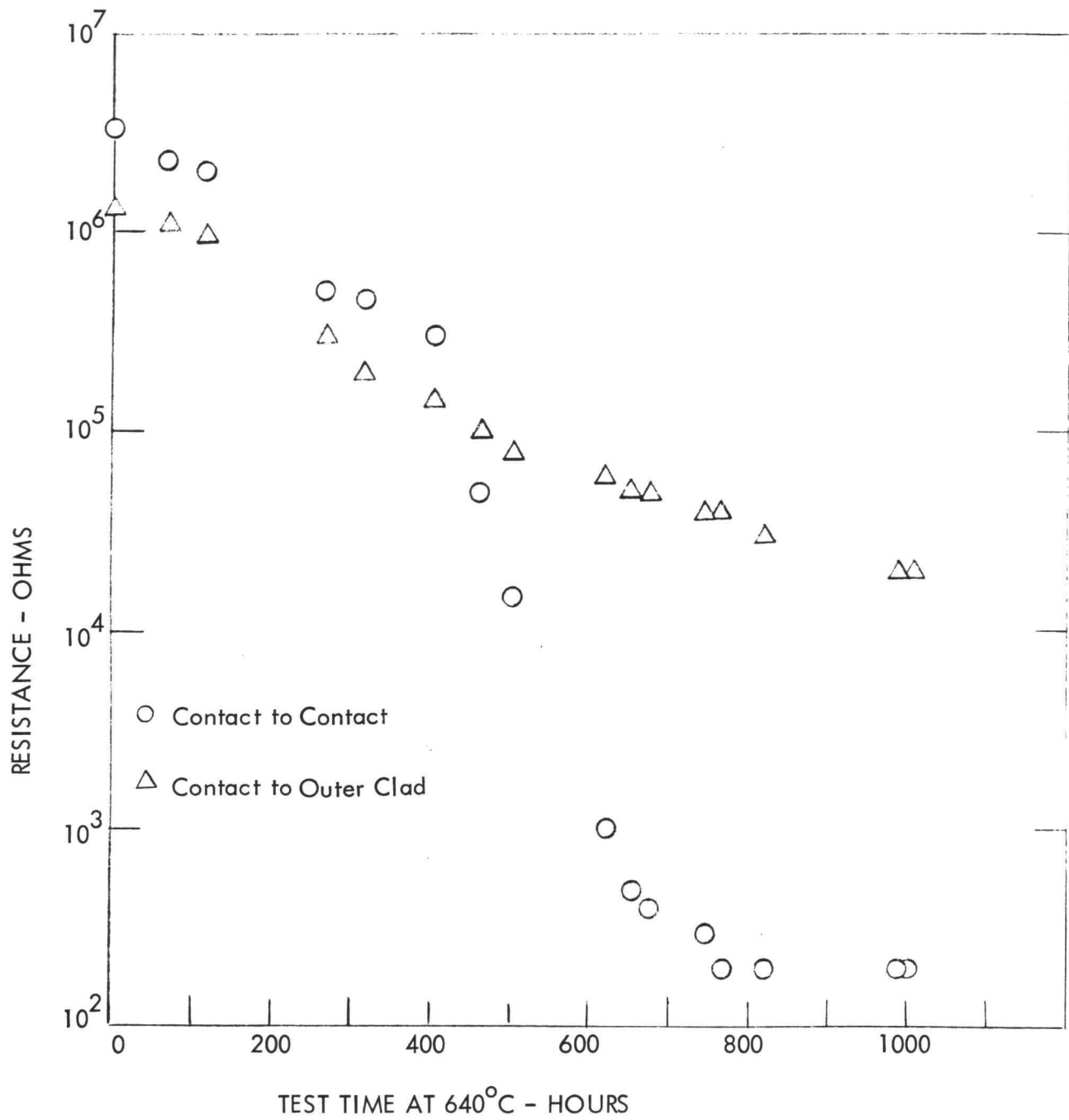
Figure IV-29. Electrical Resistance Data from EXC-009

material (presumed, by analogy with the known behavior of standard p-type PbTe, to be elemental tellurium.) This situation was investigated further in the course of electron beam microprobe and Seebeck probe analyses as discussed below:

(1)   Post-Test Specimen Preparation

After the 1000 hour test time had elapsed, the electric furnaces were slowly cooled to room temperature and the EXC capsules withdrawn. All instrumentation was removed, and each capsule was potted in an epoxy compound and sectioned longitudinally. Both halves of each capsule were ground and polished, as shown for EXC-008 in Figure IV-30.

(2)   Electron Beam Microprobe Analysis

One half-section of each capsule was further sectioned to provide samples of suitable size for microprobe scanning. Each such sample contained one full pellet plus half of each adjacent pellet and the interposed spacers, giving a total of four compatibility/contact surfaces for examination. Sections from all eight APX 10 capsules were studied.

In all capsules containing APX 10 pellets in contact with tungsten spacers (see Table IV-15), a slight selenium/tungsten interaction was observed. Figures IV-31, show an APX 10/tungsten interface in EXC-001, as exhibited by photographs of both a backscattered electron scan and elemental x-ray traces. The backscattered electron intensity is directly proportional to the density of the material being examined, so that the tungsten spacer appears white (high intensity) and the APX 10 material light gray in the electron display. The x-ray traces for Te, Pb and W indicate that no Te/W or Pb/W interactions
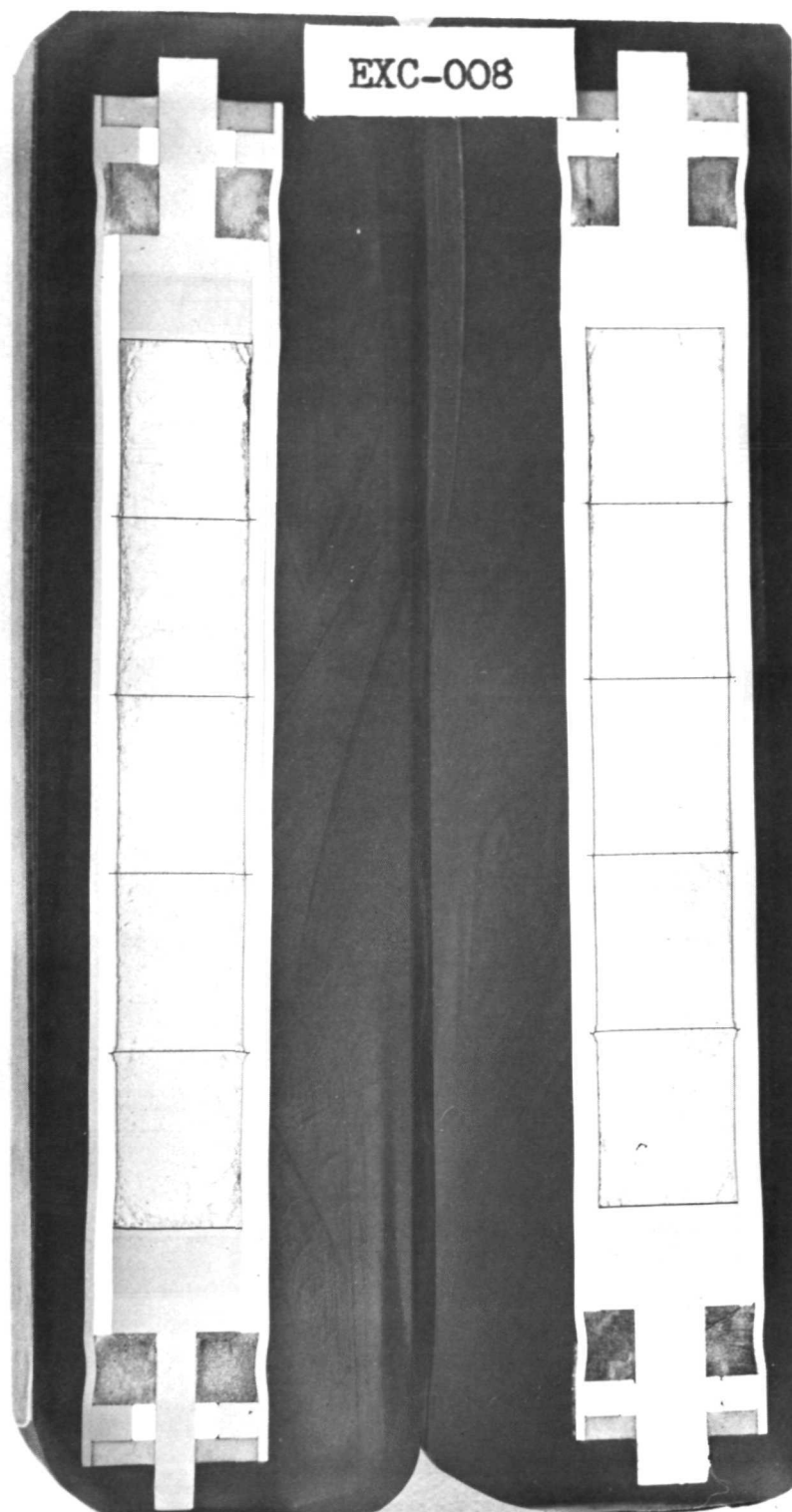
Figure IV-30. Photograph of EXC-008 Polished Capsule Halves

have occurred, but the Se trace shows a band of Se concentrated at
the interface and diffusing slightly into the tungsten. The interaction
zone is about 4 μ m thick after 1000 hours at 636°C. Similar zones
were seen at all other APX 10/tungsten interfaces examined.

In all capsules containing APX 10/molybdenum contact interfaces, a
more severe compatibility problem was observed with both selenium
and tellurium interacting with the molybdenum spacers. The corres-
ponding backscattered electron scan and elemental x-ray traces are
shown in Figures IV-34, -35 and -36. The interaction zone width is
about 10-12 μ m and was present at all APX 10/molybdenum inter-
faces examined.

No incompatibility interactions were seen in the capsules containing
APX 10/mica contact interfaces, and in general no evidence of tel-
lurium transport from the APX 10 material (except for the direct,
highly localized reactions with tungsten and molybdenum just dis-
cussed) was seen in any of the eight capsules examined. In view of
this, the deteriorating resistance of capsules EXC-008 and -009 can-
not be explained. Further investigation was precluded by termination
of the program.

(3)   Seebeck Voltage Probe Analysis

The second half-section of each APX 10 capsule was used for Seebeck
voltage probe analysis. Voltage probe traces were made along the
axis of each pellet in each capsule section, with a 0.010 inch spacing
between individual probe readings. Since the first point of a given
trace is located in the adjacent spacer material (or pellet), the first
data point in a given pellet lies anywhere from 0 to 0.010 inch
from the contact interface. No significant Seebeck voltage changes
near the contact interfaces were seen in any pellet in any of the
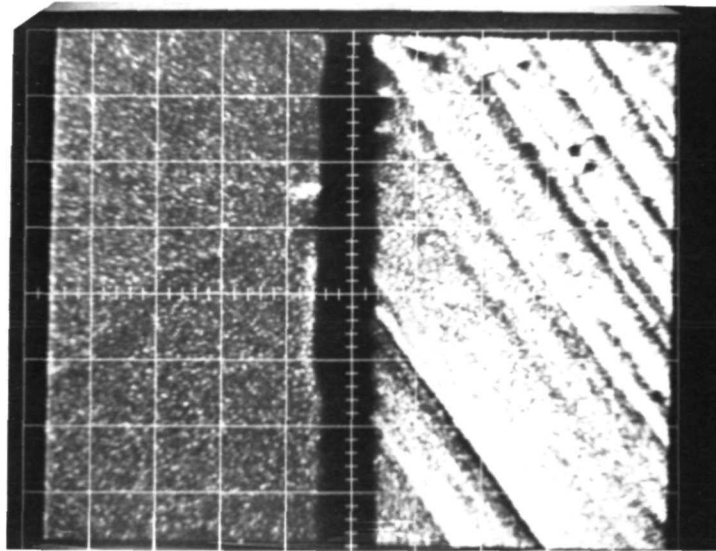
APX 10   W

Backscattered Electron Scan
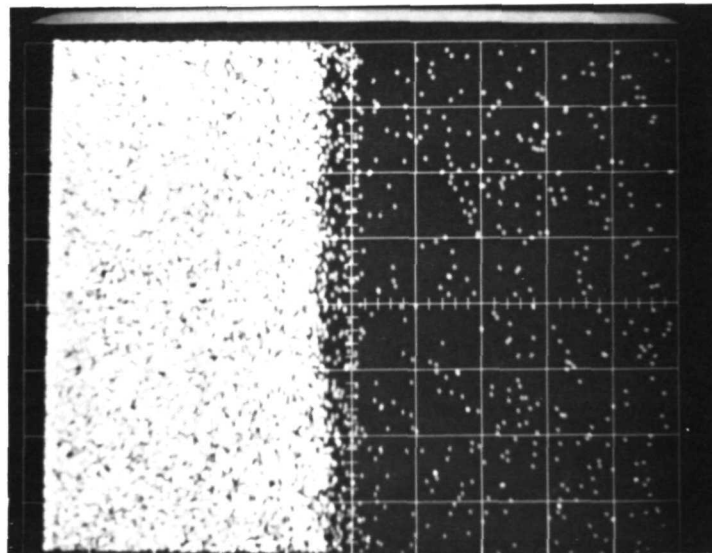
1000X

Te X-Ray Scan

Figure IV-31. EXC-001 Electron Microprobe Analysis
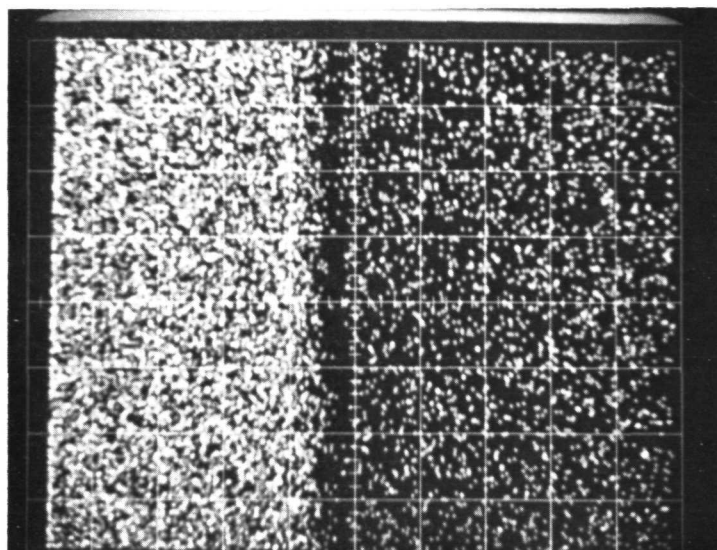
Pb X-Ray Scan

1000X
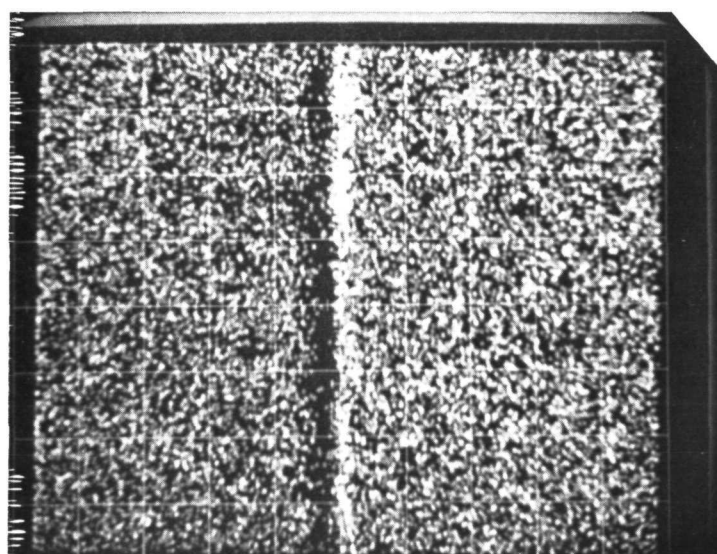
Se X-Ray Scan

Figure IV-32. EXC-001 Electron Microprobe Analysis
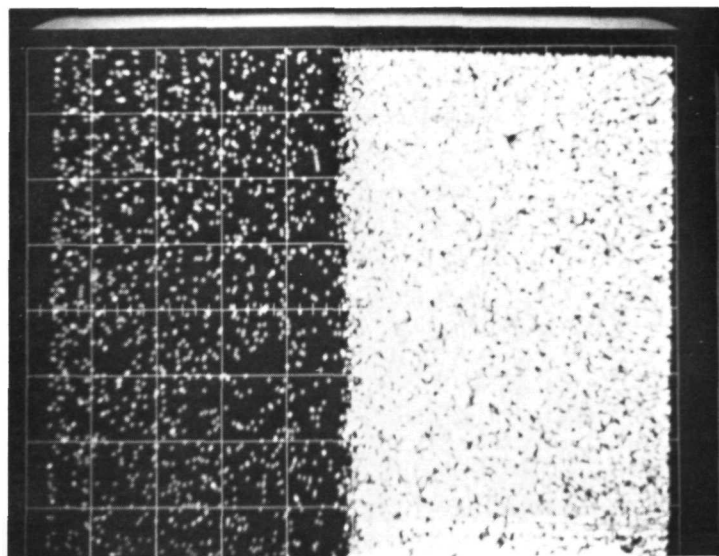
W X-Ray Scan

1000X

Figure IV-33. EXC-001 Electron Microprobe Analysis
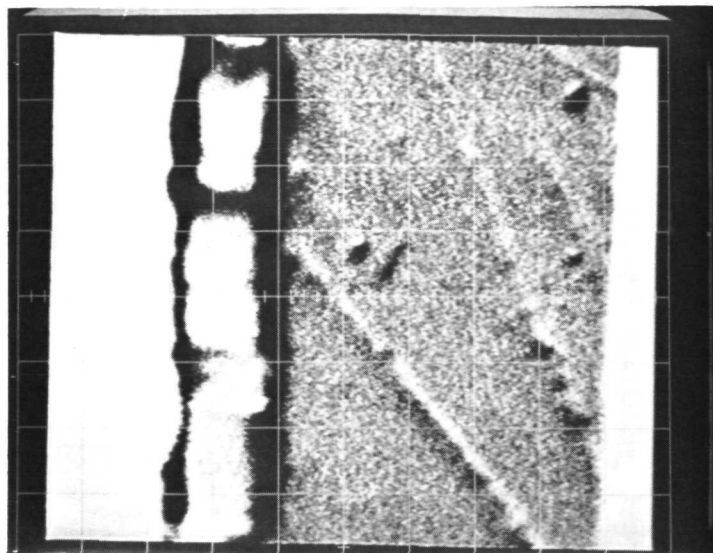
APX 10   Reaction Zone   Mo   W

Backscattered Electron Scan
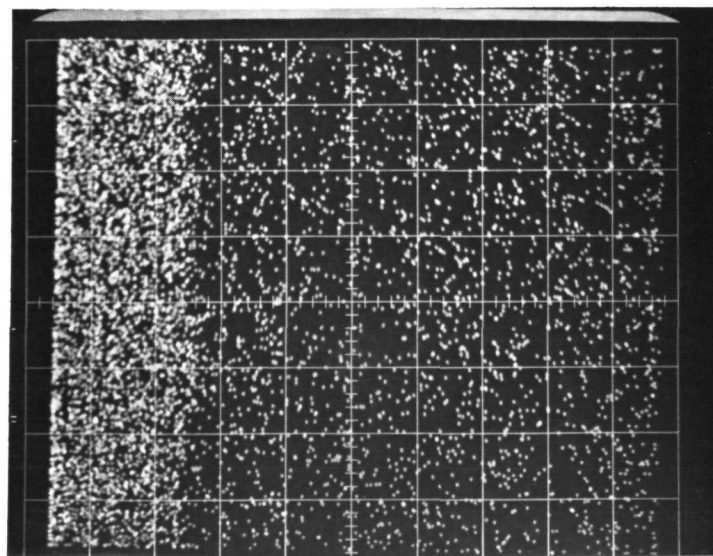
1000 X

Pb X-Ray Scan

Figure IV-34. EXC-010 Electron Microprobe Analysis
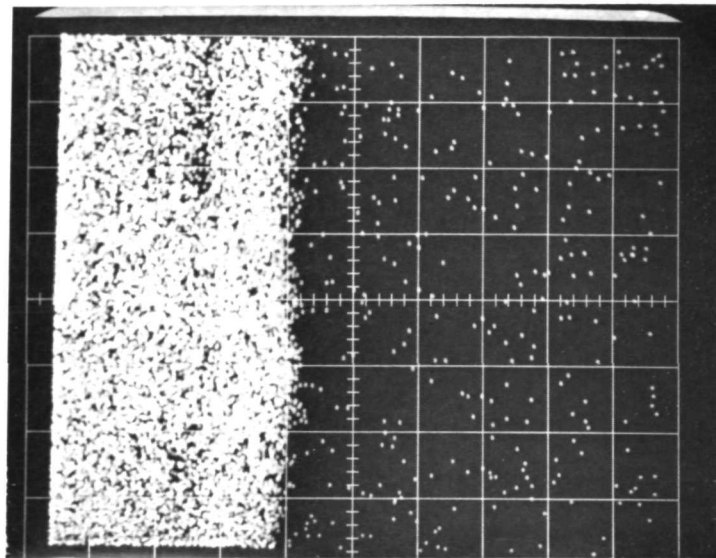
Te X-Ray Scan

1000X
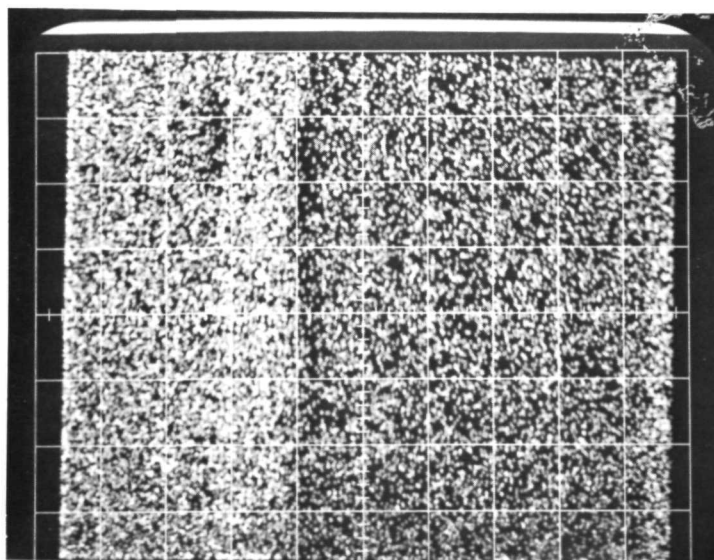
Se X-Ray Scan

Figure IV-35. EXC-010 Electron Microprobe Analysis
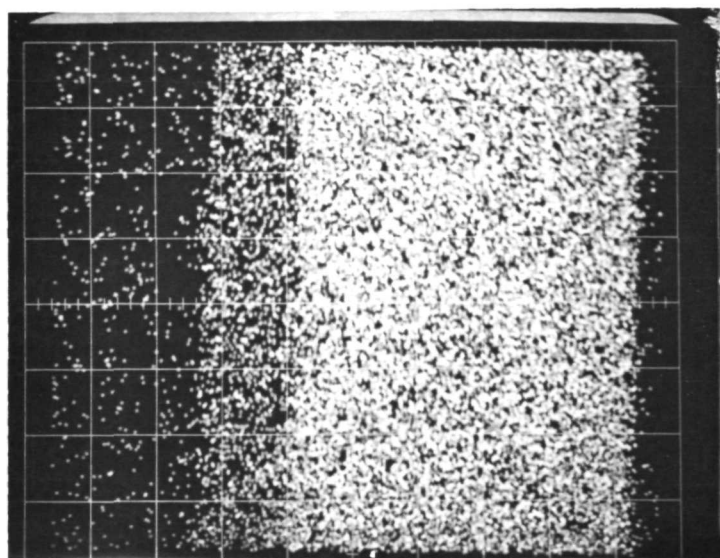
Mo X-Ray Scan

1000 X
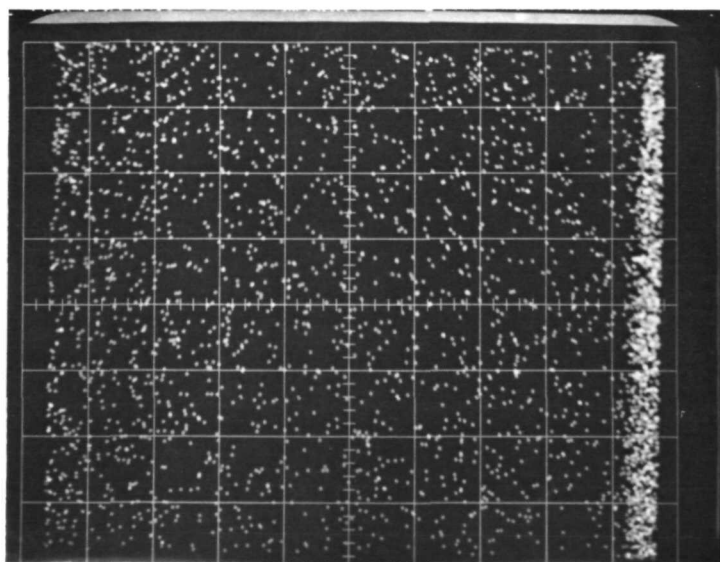
W X-Ray Scan

Figure IV-36. EXC-010 Electron Microprobe Analysis

APX 10 capsules. This indicates that the reactions disclosed by electron beam microprobe analysis were highly localized and did not affect the bulk electrical properties of the APX 10 material over a significant distance from the contact interfaces.

6. Hot Pressing of P-Type Thermoelectric Materials

    a. Hot Pressing Procedure

    Since only one hot pressing equipment facility was equipped for hydrogen atmosphere operation, both n- and p-type materials were processed in the same unit. The features and operation of this system were described previously in the section on n-type PbTe - GeTe alloys. In addition to hot pressing runs, all short-term compatibility die tests were also performed in this system. To minimize the potential for cross-contamination between consecutive experiments, the furnace was baked out at 950°C in hydrogen prior to each die test or hot pressing run.

    The steps required to hot press the p-type PbTe - PbSe alloys are outlined below:

    STEP 1. Vacuum outgas at room temperature for several hours the undensified powdered PbTe - PbSe alloy which is situated within the die. (10^2 mm pressure)

    STEP 2. Outgas in vacuum at 200°C for 8 hours (overnight).

    STEP 3. Increase temperature to 300°C with full vacuum maintained and hold for two hours.

    STEP 4. Introduce high purity helium, purge, and evacuate.

    STEP 5. Repeat Step 4.

    STEP 6. Fill with high purity helium.

STEP 7.   High purity hydrogen is admitted to the chamber and the
temperature increased to 650°C over a 2-hour period.
(<u>Minimum</u> 1 hour dwell at 650°C)

STEP 8.   Introduce high purity helium and displace the hydrogen
from the furnace.

STEP 9.   The helium is pumped out and the powder is compressed
for 15 seconds to a density of 90% of theoretical. <u>High
purity helium</u> is then admitted to the chamber. (Total time
under vacuum is to be limited to 2 minutes.)

STEP 10.   Hydrogen is introduced into the chamber to displace the
helium.

STEP 11.   The temperature of the die is adjusted to the desired value
of 700°C.

STEP 12.   7500 psi pressure is applied for a period of 60 minutes;
then remove all pressure.

STEP 13.   Cool the furnace in two hours at a linear rate from 700°C to
500°C in a hydrogen atmosphere.

STEP 14.   Introduce <u>high purity helium</u> and displace the hydrogen.

STEP 15.   Set the automatic equipment to control the cooling of the
furnace at a linear rate not to exceed 100°C/hr.

STEP 16.   Evacuate chamber and die; then introduce argon. Open.

(1)   APX 10 Material

After qualifying the hot pressing facility and procedures with n-type
(PbTe) lead telluride powder, two changes were made for the APX 10
hot pressing runs. First, the size of the hot pressing die was reduced

from 5/8 inch diameter to 1/2 inch diameter to reduce the quantity of hot pressing powder for each run. Second, the time at temperature was increased to 60 minutes rather than 30 minutes to increase the density of the hot pressed APX 10 pellet.

Some difficulty was encountered in hot pressing APX 10 material under 6,500 psi at 700°C. The pellet was partially hot pressed and non-homogeneous with one end containing numerous voids. Consequently, the pressure was increased in small increments for successive pressings until the APX 10 powder was successfully densified. Figure IV-37 illustrates the surface condition of the bottom end of a 1/2 inch diameter APX 10 pellet after hot pressing for one hour under varying pressure from 6,500 psi to 7,500 psi. Once the pressing conditions were established, the size of the die was increased to 5/8 inch diameter so that hot pressed pellets would be large enough to be machined to a size compatible with the thermal conductivity apparatus (0.500 inch diameter by 0.611 inch length). Two samples of APX 10-26 and APX 10-27 are shown in Figure IV-38 after hot pressing and machining to 0.500 diameter.

Table IV-17 lists the nine specimens of APX 10 material that were hot pressed during this program. The first six pressings were varied to establish the correct pressing pressure. HP-004 specimen was subjected to metallographic examination and HP-006 was tested in the high ΔT apparatus. A comparison of Seebeck voltage was made between qualification bar Q-1076 (cold pressed and sintered) and HP-006 specimen (hot pressed) to determine if the Seebeck properties were affected by hot pressing procedures. The data is tabulated in Table IV-18 where the voltage output is given for both specimens when subjected to temperature differences of 293, 561 and 617°C. These results indicated that the hot pressing procedure was not altering the Seebeck coefficient
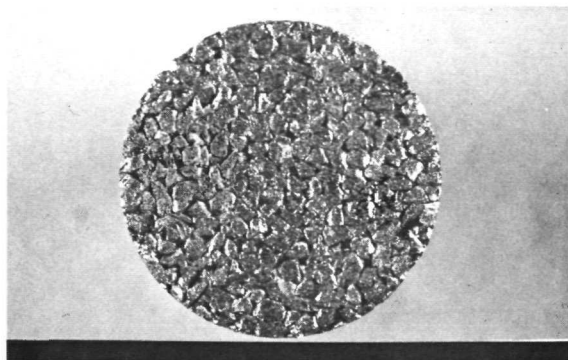
a. Pressed for
1 hour at
700°C, 6500 psi

b. Pressed for
1 hour at
700°C, 7000 psi
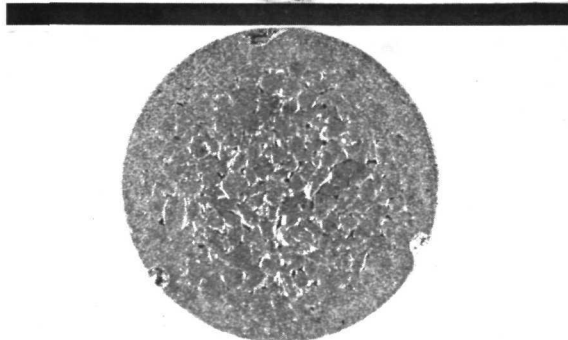
c. Pressed for
1 hour at
700°C, 7250 psi
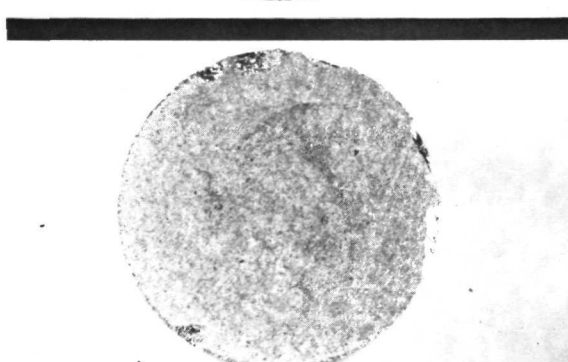
d. Pressed for
1 hour at
700°C, 7500 psi

Figure IV-37. Bottom View of 1/2-Inch Diameter APX Pellet
after Hot Pressing under Varying Load Conditions
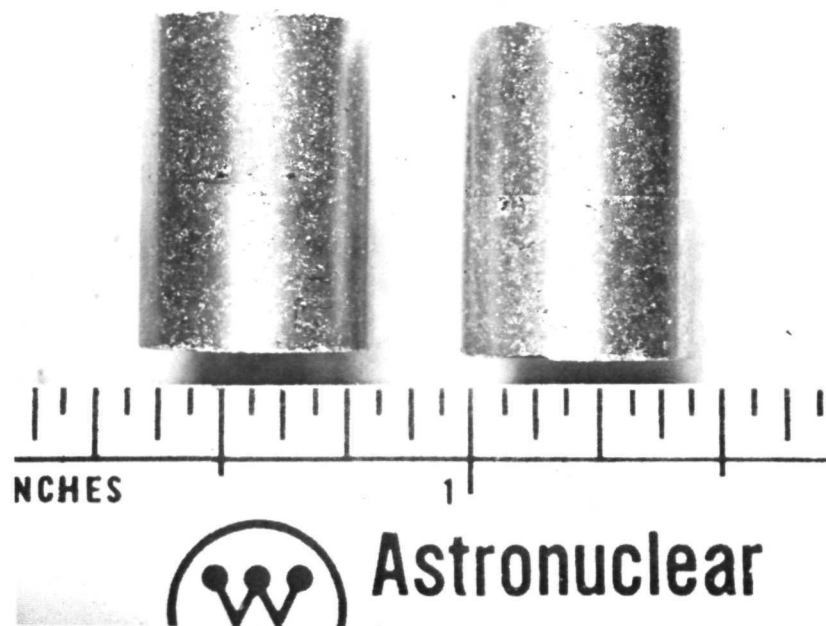
Figure IV-38. Hot Pressed Cylinders of APX 10-26 and APX 10-27
P-Type Ternary Material Machined to 0.500 Inch Diameter

TABLE IV-16

HOT PRESSED CYLINDERS OF APX 10 MATERIAL

Specimen Number	Hot Pressing Pressure (psi)	Thermoelectric Material
HP 004	6, 500	APX 10-22
HP 005*	6, 500	APX 10-23
HP 006*	7, 000	APX 10-24
HP 007*	7, 250	APX 10-22
HP 008**	7, 375	APX 10-23
HP 009**	7, 500	APX 10-24
HP 010***	7, 500	APX 10-25
HP 011***	7, 500	APX 10-26
HP 012***	7, 500	APX 10-27

*   Partially pressed cylinders illustrated in Figure IV-37

**   0. 50 inch diameter cylinders machined to 0. 273 inch diameter

***   0. 62 inch diameter cylinders machined to 0. 500 inch diameter for thermal conductivity tests.

TABLE IV-17

COMPARATIVE TEST OF HOT PRESSED APX 10-24 WITH COLD PRESSED QUALIFICATION BAR

	APX 10-24 Qualification Bar Q-1076	APX 10-24 Hot Pressed Cylinder 006
$T_{H1}(^{\circ}C)$	319	319
$T_{C1}(^{\circ}C)$	26	26
ΔT (C°)	293	293
Voltage (mV)	39.2	38.6
$T_{H2}(^{\circ}C)$	593	593
$T_{C2}(^{\circ}C)$	32	32
$\Delta T_{2}(C^{\circ})$	561	561
Voltage (mV)	110.7	110.7
$T_{H3}(^{\circ}C)$	651	651
$T_{C3}(^{\circ}C)$	34	34
$\Delta T_{3}(C^{\circ})$	617	617
Voltage (mV)	126.8	127.5

of the APX 10-24 material over the temperature range of interest.

Additional electrical property data were obtained from HP-007,
HP-008, and HP-009 hot pressed specimens. Of the three cylinders,
two specimens (HP-008 and HP-009) were machined to 0.273 diameter
prior to testing, while HP-007 was tested at a diameter of 0.498 and
a length of 0.80. Comparison of results with cold-pressed qualifica-
tion bars from the same materials are illustrated in Figure IV-39. As
expected, the increased density of the hot pressed material is reflected
in a significantly lower electrical resistivity, while the Seebeck
coefficient is unaffected.

(2)   Standard P-Type Lead Telluride

It was decided that, if the thermal conductivities of hot pressed
specimens of both APX 10 and p-type PbTe could be measured in the
same apparatus, the superiority of the ternary alloy could be assessed
on the basis of the most direct possible comparison. Thus, hot pressing
work was initiated on standard p-type PbTe to provide 0.500 inch
diameter x 0.611 inch long thermal conductivity specimens.

The hot pressed APX 10 specimens discussed in the previous subsection
had been made from powder particles in the 841 to 500 micron size
range (-20 +35 U. S. Standard Seive Size). However, p-type PbTe
powder was available only in the 500 to 53 micron (-35 + 270) range.
To provide a relatively coarse powder for hot pressing, so that the
differences in particle boundary contributions to the measured thermal
conductivities would not obscure the comparison to be made, the
p-type PbTe was screened into two powder lots. The coarse lot, con-
sisting of 500 to 297 micron (-35 +50) particles, was used for hot
pressing, while the 297 to 50 micron (-50 + 270) lot was used for cold
pressing washers and test specimens.
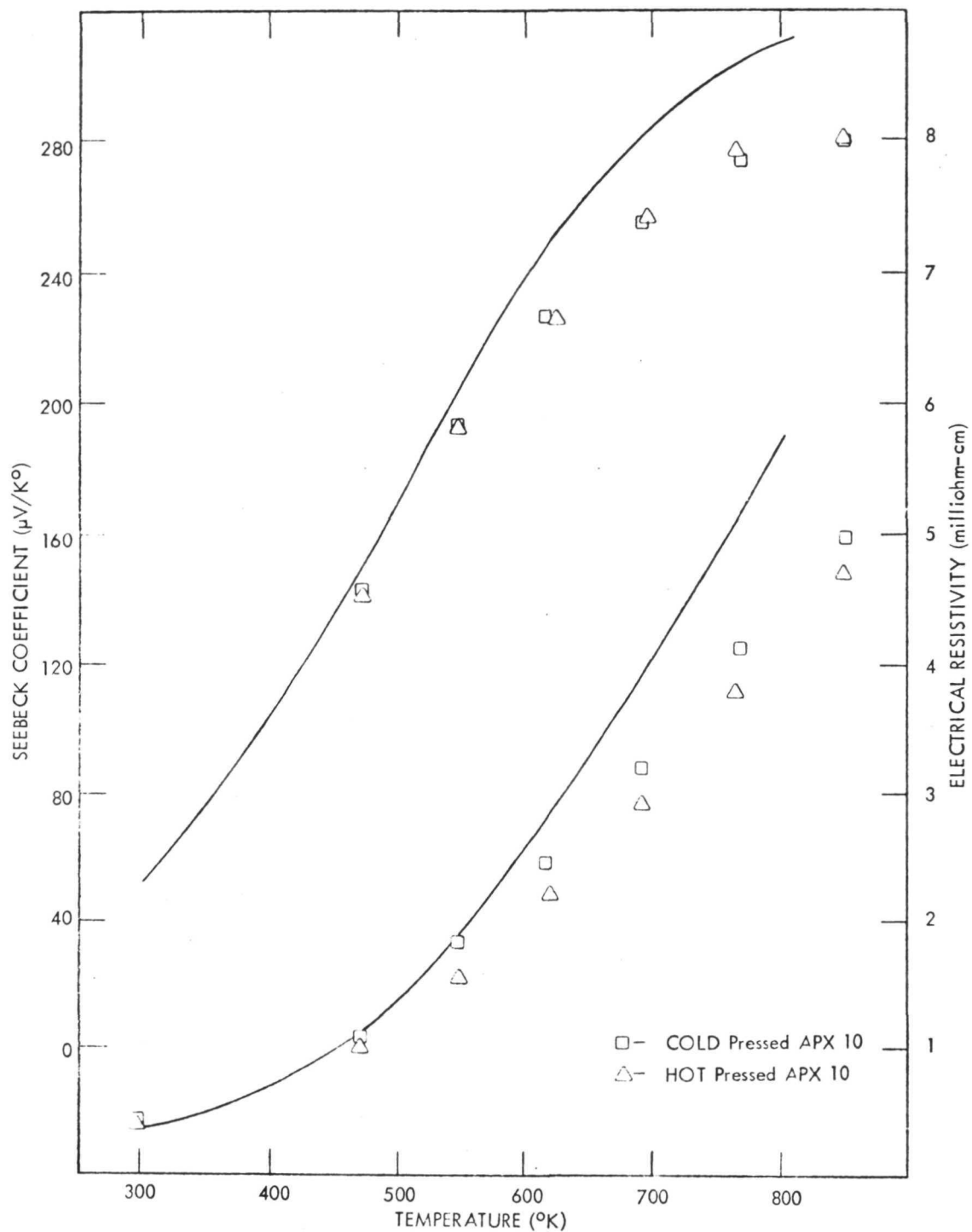
Figure IV-39. Electrical Properties Versus Temperature for APX 10 Specimens

Hot pressing of p-type PbTe specimen HP-013 was then attempted using a procedure identical to that described previously for the APX 10 material. However, the response of the p-type PbTe to this procedure was less than satisfactory; first, the pellet was strongly bonded to the graphite punches after the one hour - 700°C - 7500 psi pressing cycle, and second, it broke into irregular pieces during subsequent machining. To correct this problem, 0.625 inch diameter pyrolytic graphite discs were prepared and interposed between the hot pressing punches and the PbTe powder; also, the 700°C - 7500 psi dwell time was reduced from one hour to 30 minutes. Under these conditions, two 0.625 inch diameter p-type PbTe pellets (HP-014 and -015) were successfully hot pressed and released for thermal conductivity measurement.

b.   Sample Preparation for Thermal Conductivity Measurement

Hot pressed cylinders of APX 10 and p-type PbTe were reduced to 0.500 inch diameter x 0.611 inch long cylinders using machining techniques similar to those previously described for n-type materials. They were then given a "cleanup" heat treatment for two hours at 575°C in hydrogen, and stored under vacuum until used.

To permit installation of the thermocouples required in the thermal conductivity measurement procedure, it was necssary to drill two 0.04 inch diameter x 0.25 inch deep holes in each specimen. In attempting to drill these holes in three APX 10 specimens, the cylinders were destroyed due to cracking and/or chipping initiated by the drilling operations. Additional p-type cylinders were being processed when the thermal conductivity measurement effort was terminated (ANX 1 specimens had already been drilled and instrumented successfully at this point).

D.   CONCLUSIONS

1. N-Type PbTe - GeTe Alloys

a. Of the compositions investigated, the ANX 1 formulation $Pb_{.951}$ $Ge_{.05}$ Te $(PbI_2)_{.001}$ exhibits the best energy conversion characteristics over the con-templated tubular module operating temperature range. (This assumes that proper processing temperatures are used, as indicated below. Note that this formulation is the same as the RCA reference composition.)

b. ANX 1 material should be prepared by rapidly quenching a homogeneous melt from a temperature of $975^\circ C$ or greater. Powder obtained from crushed ingots should not be heat treated. Cold pressed module washers or test specimens should be heat treated for two hours in hydrogen at $575^\circ C$. This temperature is high enough to avoid spinodal decomposition and maintain a single-phase microstructure, and also eliminate any as-quenched composi-tional inhomogeneities via diffusion, yet low enough to avoid depletion of the GeTe content through selective sublimation of that molecular species.

c. The Seebeck coefficient and electrical resistivity as a function of tempera-ture were determined for hot pressed ANX 1 material and presented in Figure IV-19. The hot pressed condition is considered to be most represen-tative of the physical condition of an ANX 1 washer in a fabricated module.

d. The measurement of thermal conductivity as a function of temperature re-mains to be performed in completing the characterization of the ANX 1 formulation. This could be done either by direct measurement on hot pressed specimens, as was being attempted under this task when the program was terminated, or by comparing the thermal impedance of an all-ANX 1 experimental module to that of an all-Ge- NL n-type PbTe module operating over a range of average temperatures and using a small radial temperature gradient.

e. The accuracy of the Seebeck coefficient measurements made on ANX 1 specimens was proven to be extremely good by virtue of the precision with which Seebeck voltages calculated by intergration of the experimental Seebeck coefficient vs. temperature curve could be correlated with Seebeck voltages measured directly from specimens subjected to high temperature gradients.

f. The ANX 1 alloy is chemically/electrically compatible with pure tungsten and with phlogopite mica at temperatures up to 700°C. It is not compatible with molybdenum at 636 or 700°C, and thus molybdenum hot side conductor rings should not be used in an ANX 1 module. (Molybdenum can probably be safely used for cold side conductor rings; although an interaction will occur during hot isostatic compaction, its extent and effects should be tolerable or negligible because of the short exposure time involved.)

g. The ANX 1 formulation is just as susceptible to tellurium transport degradation as is standard n-type PbTe, and thus the same transport/diffusion barrier requirements exist for an ANX 1 module as for the currently standard devices.

2. <u>P-Type PbTe - PbSe Alloys</u>

a. Of the compositions investigated, the APX 10 formulation $PbTe_{.965}Se_{.05}Na_{.01}$ exhibits the best energy conversion characteristics over the contemplated tubular module operating temperature range. (This assumes that proper processing temperatures are used, as discussed below.)

b. APX 10 material should be prepared by rapidly quenching a homogeneous melt from a temperature of 975°C or greater. If powder obtained from crushed ingots is heat treated for one hour in hydrogen at 550°C, and cold pressed module washers or test specimens heat treated for two hours in hydrogen at 575°C, then depletion of the PbSe content through selective sublimation of that molecular species is avoided, and reproducible electrical

properties are developed which are satisfactorily representative of the final fabricated (i.e. fully densified) state. However, it appears that hydrogen is dissolved interstitially into the APX 10 lattice during the 550°C heat treatment, as manifested by a significant increase in the lattice parameter of material so processed. Further, this hydrogen is rejected from the lattice at some undetermined higher temperature between 550 and 700°C, so that its presence in module washers would probably produce some undesirable effects during elevated temperature module fabrication processing and/or operation. Further work is thus required to seek a heat treating temperature between 550 and 700°C at which neither lattice expansion due to solution of interstitial hydrogen nor PbSe depletion due to selective sublimation occur to a deleterious extent.

c.   The Seebeck coefficient and electrical resistivity as a function of temperature were determined for hot pressed APX 10 material and presented in Figure IV-39. As in the n-type case, the hot pressed condition is considered to be most representative of the physical condition of an APX 10 washer in a fabricated module.

d.   The measurement of thermal conductivity as a function of temperature remains to be performed to complete the explicit characterization of the APX 10 formulation. As in the n-type case (1-d above), this could be done either by direct measurement or by an in-module comparative measurement (with the comparison in this case being made against standard TEGS-2P p-type PbTe). Before this is done, however, it would be possible to make a reasonably good estimate of $k(T)$ for APX 10 by using the $k(T)$ values measured by Resalab, Inc. for the APX 4 formulation (Figure IV-22). From those measurements and the measured electrical resistivity, a lattice contribution $k_l(T)$ would be calculated for the APX 4 alloy. This $k_l(T)$ would then be assumed valid for APX 10 also, since the two compositions are

virtually indistinguishable from the phonon propogation viewpoint. Finally, using the measured electrical resistivity in Figure IV-39, an electronic contribution $k_e(T)$ would be calculated for APX 10, and the total $k(T)$ for the APX 10 alloy determined from $k(T) = k_l(T) + k_e(T)$.

e. As in the n-type case, the good accuracy of Seebeck coefficient measurements made on APX 10 specimens was confirmed by the excellent correlation between Seebeck voltages measured directly from specimens subjected to high temperature gradients and values obtained by integrating the experimental Seebeck coefficient vs. temperature curves. The high ΔT Seebeck voltage measurements were also used to confirm that cold pressed and heat treated APX 10 specimens had Seebeck coefficients identical to hot pressed specimens, which helped prove that the hot pressing procedure did not affect the APX 10 material composition.

f. Atomic absorption spectrophotometric analyses of APX 10 (and APX 4) specimens proved that the sodium content of processed and fabricated material was essentially the same as in the material make-up composition. This alleviated the uncertainties which had arisen when previous emission spectrographic analyses indicated that over half the make-up sodium was lost. Emission spectrography is not a satisfactory technique for accurate dopant concentration analysis in these materials.

g. The APX 10 alloy is chemically/electrically compatible with phlogopite mica at temperatures up to 700°C. It is not compatible with molybdenum at 636°C, although the degree of interaction is somewhat less than in the ANX 1/molybdenum case. Thus molybdenum hot side conductor rings should not be used in an APX 10 module. On the same basis as discussed for the n-type case (1-f above), molybdenum is probably a satisfactory material for cold side conductor rings.

Unlike the n-type case, the APX 10 alloy exhibits a slight interaction with pure tungsten at 636°C. Although the extent of the Se/W reaction zone is only 4 μm after 1000 hours at 636°C, further work is required to quantitatively establish the time and temperature dependence of the reaction, and its effect on the APX 10 transport properties and on the effective APX 10/tungsten contact resistivity must be assessed to determine whether the interaction can be ignored and tungsten safely used as a hot side conductor ring material in an APX 10 module.

h.   The APX 10 material exhibits behavior similar to that of standard p-type PbTe in acting as a source of elemental tellurium which can transport to the adjacent n-type washers and cause electrical property degradation of the n-type material. Thus the same transport/diffusion barrier requirements exist for an APX 10 module as for the currently standard devices.

V. DIFFUSION BARRIERS

A. ELECTRICAL CONTACTS (RADIAL BARRIERS)

In the early embodiment of the tubular module, Armco iron was the material used for the electrical conductor rings which directly contact the p- and n-type PbTe washers at their inner (hotter) and outer (colder) circumferences. However, electron microprobe and Seebeck probe studies together with EXC capsule experiments conducted during the early years of the Compact Converter Program revealed that a diffusion-enhanced interaction between the iron and p-type PbTe was deleteriously affecting the electrical properties of the latter and thus causing a major fraction of the module performance degradation being observed at that time. Thus, a study was initiated to find a method for suppressing this interaction through use of a substitute contact material or diffusion barrier.

An extensive series of compatibility experiments was performed in which niobium, zirconium, molybdenum and tungsten were tested in EXC capsules and compatibility dies in contact with both p- and n-type PbTe at temperatures up to 750°C. The results were evaluated principally via electron beam microprobe examinations, with some Seebeck probe testing as well. This work has been extensively reported previously[1], and the details will not be repeated here; briefly, tungsten was the only material which was totally compatible with both n- and p-type PbTe, while molybdenum was compatible with n-type but exhibited a slight interaction with p-type (much less severe, however, than the inter-action between iron and p-type PbTe). Niobium and zirconium were both found to exhibit severe interactions with the PbTe materials.

Molybdenum and tungsten contacts were then introduced to the module design in various ways, as listed and discussed below:

a. A thin tungsten foil strip was introduced as a diffusion barrier between the inner (hotter) iron conductor ring and the PbTe washers. This produced a signifi-cant reduction in short-term performance degradation rate, but the problem of

---

[1] Compact Thermoelectric Converter Phase II-C Final Report, NYOO-3584-15, July 20, 1969, Section II.

completely covering the iron surface with foil while not shearing through the
mica separator washers with the sharp foil edges was never completely solved;
also, the assembly process was complicated to a formidable degree.

b.   In addition to (a), a tungsten foil strip was incorporated between the outer
(colder) iron conductor rings and the PbTe washers after it was discovered that
in the 2 hour − 650/750°C module isostatic compaction process, enough inter-
action occurred between the outer iron conductor and p-type PbTe washer to sig-
nificantly reduce the initial module performance level. This innovation also
produced a significant improvement in performance but suffered from the same
problem and complications as in (a).

c.   Solid molybdenum inner, and later outer, conductor rings were substituted
for the iron/tungsten foil combinations. This was very satisfactory from the
assembly and "coverage" viewpoints, and was quite successful in terms of low
degradation, high-initial-level module performance. Only the slight interaction
between the inner molybdenum ring and the p-type PbTe washer remained a
source of degradation; the cold junction operating temperature was too low
and the hot isostatic compaction time too short for this interaction to develop
at the outer conductor interface.

d.   To eliminate the last known source of contact-interaction degradation, the
molybdenum inner ring was modified by cutting a step into the p-type washer
contact area and filling this step with a solid tungsten ring diffusion barrier. The
resulting two-piece or "split" inner conductor ring design was discussed previously
and is shown in Figure I-11. This design modification essentially eliminated contact
interaction degradation from the tubular module.

e.   Very recently, a slight interaction between molybdenum inner rings and
n-type PbTe washers was detected by electron beam microprobe examination
of modules which had been operated for very long periods of time. To elimin-

ate this last tiny increment of degradation, and also to prepare for the introduction
of ternary (Pb, Ge) Te and Pb(Se, Te) alloys to the module (which do not appear
to be as compatible with molybdenum as are p- and n-type PbTe), a tungsten
ring diffusion barrier was also incorporated between the n-type washer and the
main (molybdenum) inner conductor ring.

B.   FOILS (AXIAL BARRIERS)

Results of electron beam microprobe examinations and Seebeck probe measurements
on metallographically prepared specimens from tubular modules, test capsules and compati-
bility dies have shown that phlogopite mica, used in thicknesses up to 0.010 inch to electri-
cally insulate adjacent p- and n-type PbTe washers in the module circuit assembly, is
not an effective barrier to the axial transport of elemental tellurium from the p-type (tellurium
rich) to the n-type (neutral or tellurium deficient) washer. Since no substitute insulating
material possessing an adequate combination of mechanical and physical properties, fabri-
cability, and chemical compatibility has been identified to date, it has been necessary
to investigate various transport barrier concepts to permit continuing the use of phlogopite
mica while eliminating the electrical property degradation which results from accumulation
of transported tellurium in the n-type material.

The first concept investigated involved the incorporation of a .0004 inch thick
tungsten foil washer sandwiched between two half-axial-thickness mica washers at each
insulator position in the circuit, with the intent that the foil act as a physical diffusion
barrier to transporting tellurium. Tungsten was selected because it is the only metal which
has been shown to be chemically inert to both p- and n-type PbTe, and the .0004 inch
thickness corresponds to the thinnest foil that was commercially available. The concept
was evaluated in several EXC capsules and in sub-length technology modules TEM-15B
S/N-4 and 15B S/N-4B (See Section III of this report). Testing of these devices revealed
that the barrier was very successful in reducing degradation due to axial transport of
tellurium through the mica (although there remained an increment of degradation due
to transport around the mica). However, the significant performance loss due to radial
heat flow through the .0004 inch tungsten foil was a serious drawback to this concept.

The situation was somewhat improved when it was determined from the results
of extensive Seebeck probe studies on metallographically prepared module sections that
the transport-degraded region of n-type PbTe washers in non-barrier modules was confined
to the inner (hotter) half of the washer radial thickness, as shown schematically in Figure
V-1. It was then reasoned that a tungsten foil washer dimensioned to cover only the inner
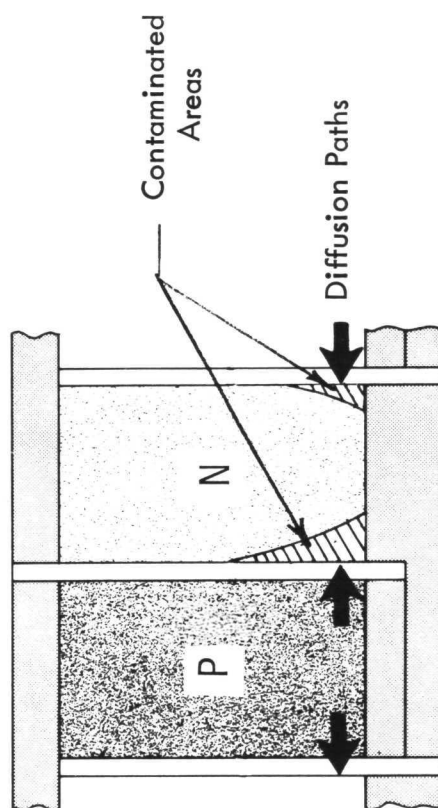
Figure V-1. Schematic Representation of Degradation of N-Type PbTe Washer Due to Transport of Excess Tellurium from P-Type PbTe Washer

radial half of the mica washer would be perfectly adequate as an axial transport barrier, and would perform much better from the shunt heat loss viewpoint (since the outer radial half of the heat flow path would then be mica with its much lower thermal conductivity). This modified concept was evaluated in experimental modules TEM-15B S/N-4A and 15B S/N-4C, where it was found that the reduction in degradation rate due to elimination of axial tellurium transport was indeed maintained, and that shunt heat losses were reduced 50 percent as compared to the full-radial-thickness foil case.

In view of the above results, the half-radial-thickness tungsten foil barrier concept was incorporated as a standard design feature in full-size tubular modules. A total of 12 reactor power modules (TEM-X S/N-3 series) and 3 electromagnetic pump power modules (TEM-14B S/N-1, -2 and -3) were fabricated using this barrier scheme.

C.   THIN FILMS (AXIAL BARRIERS)

1.   Introduction

Despite the adoption of the foil barrier as a standard design feature, the shunt heat losses through the foil/mica layers created an obstacle to the development of a highest-attainable-efficiency module. A barrier concept which circumvents this problem is the use of a thin metal film deposited on either the mica or PbTe washer surfaces to form a physical diffusion barrier. At film thicknesses less than about 5,000 $\overset{o}{A}$ (2×10^{-5} inches), the radial heat loss through such a metal layer would be negligible. For reasons already noted, tungsten is a highly attractive candidate for a barrier film material. If high quality tungsten films can be successfully applied to the components, and if the tungsten is effective as a tellurium diffusion barrier, then the use of such a film should eliminate degradation due to axial tellurium transport without introducing any deleterious side effects[1] during the device operating life.

Experimental deposition of both molybdenum and tungsten films on mica substrates, and iron and tungsten films on PbTe substrates, was investigated using electron beam vapor deposition (EBVD), RF and DC sputtering and chemical vapor deposition techniques, with the bulk of the actual work involving the first of these. Facilities at WANL, (W) Research and Development Center, (W) Lima Aerospace Electrical Division, (W) Baltimore Systems Development Division and outside suppliers were utilized. Process variables investigated included source material purity, substrate temperature, source-to-substrate distance, deposition atmosphere, deposition time and rate, substrate cleaning by glow discharge bombardment, film thickness and post-deposition annealing.

Some success was achieved in depositing fairly good quality 1000 - 1500 $\overset{o}{A}$ molybdenum films and 500 - 1000 $\overset{o}{A}$ tungsten films on mica, and experimental modules were built to evaluate both of these. In later work tungsten films up to 1500 $\overset{o}{A}$ thick were successfully deposited, but equipment problems and program termination precluded further advancement toward the 5000 $\overset{o}{A}$ film thickness goal.

---

[1] Such as potential long-term chemical contamination.

2. Description of Relevant Material Characteristics [1], [2], [3], [4]

Phlogopite (natural amber) mica is a complex mineral silicate found in natural deposits in many parts of the earth. The chemical composition varies somewhat from one deposit to another, but is typified by the formula $K H_2 Mg_3 Al (SiO_4)_3$ which may also (more informatively) be writted as $K_2O \cdot Al_2O_3 \cdot (MgO)_6 \cdot (SiO_2)_6 \cdot (H_2O)_2$. In certain varieties, fluorine atoms are substituted for some of the oxygen atoms. Two crystal structures have been reported for natural phlogopite micas. Some varieties exhibit a hexagonal structure with the (approximate) lattice parameters $a_o = 5.3$ Å and $c_o = 29.98$ Å. In other cases are found monoclinic structures which resemble distorted hexagonal arrays; these have lattice parameters of order $a_o = 5.3$ Å, $b_o = 9.2$ Å, $c_o = 10$ to 20 Å and $\beta = 95$ to 100 degrees. In both types of structures there is very strong bonding in one plane of the unit cell (the basal plane in the hexagonal case) and very weak bonding in the principal lattice direction intersecting the strong bonding plane. This results in a macroscopic structure which tends to be split into thin laminae parallel to the strong bonding plane. It is fairly easy to accurately split the mica into thin sheets (down to about 0.0002 - 0.0003 inch thick) but, concurrently, it is almost impossible to obtain sheets 0.001 inch or more thick which are completely free of laminar faults.

(1) F. M. Clark, Insulating Materials for Design and Engineering Practice, Part III: Mica and Mica Products, Wiley, New York, 1962.

(2) WANL-TME-1306, Literature Summary of Thermoelectric and Thermoelectric Module Material Properties, R. L. Novak and R. Skalka, September 21, 1965.

(3) Electrical and Physical Data on Mica Insulating Film and Sheet for the Design Engineer, W. F. Griffith, Perfection Mica Company, Nov. 1965.

(4) R. F. Bunshah (ed.), Techniques of Metals Research, Volume 1, Techniques of Materials Preparation and Handling, Part 3, Interscience, New York, 1968.

Because of the laminar macrostructure, the mica is noticeably hygroscopic; sheets absorb moisture onto the internal laminar surfaces as well as the outer surfaces. In applications such as the thermoelectric module this moisture is objectionable and must be removed by drying at elevated temperatures. An 800°C - 30 minute vacuum drying cycle is used for module components. In sheets containing more than a few laminar faults, the moisture evolution during this cycle causes surface cracking, blistering and physical separation of the laminae over large areas, and 50 percent or more of the dried components are often scrapped for this reason. Although difficult to photograph, some appreciation of this problem can be gained from Figure V-2, where two originally indistinguishable 2 x 2 x 0.0025-inch mica squares are shown after processing in the same drying cycle. (The absorbed moisture discussed above should not be confused with the water of constitution which is given off as the material decomposes chemically in the $850-1000^\circ$C temperature range.)

The physical property of phlogopite mica which is of great significance in this discussion is the coefficient of linear thermal expansion. Most reference sources indicate that in directions parallel to the plane of lamination this has a value of 12 to 15 x $10^{-6}/C^\circ$ in the 0 - 200°C temperature range. (Perpendicular to the plane of lamination, values as high as 10^{-3} to $10^{-2}/C^\circ$ are given.)

Tungsten is a body centered cubic refractory metal having a lattice parameter of 3.158 $\overset{\circ}{A}$. It has the highest melting point, 3410°C, of all the pure metals. In the 0 - 200°C temperature range its expansion coefficient is about 4.6 x $10^{-6}/C^\circ$. Chemically, tungsten is relatively inert near room temperature, but becomes highly reactive (especially with atmospheric gasses and carbon) at temperatures above 400 - 500°C or so.

Molybdenum is another body centered cubic refractory metal, very similar to tungsten in many respects; it has a lattice parameter of 3.147 $\overset{\circ}{A}$, melting point of 2610°C and a 4.9 x $10^{-6}/C^\circ$ expansion coefficient in the 0 - 200°C range. It is somewhat more chemically reactive than tungsten in most instances; in particular, an interaction between molybdenum and n-type PbTe has been identified which is deleterious to the electrical properties of the latter.
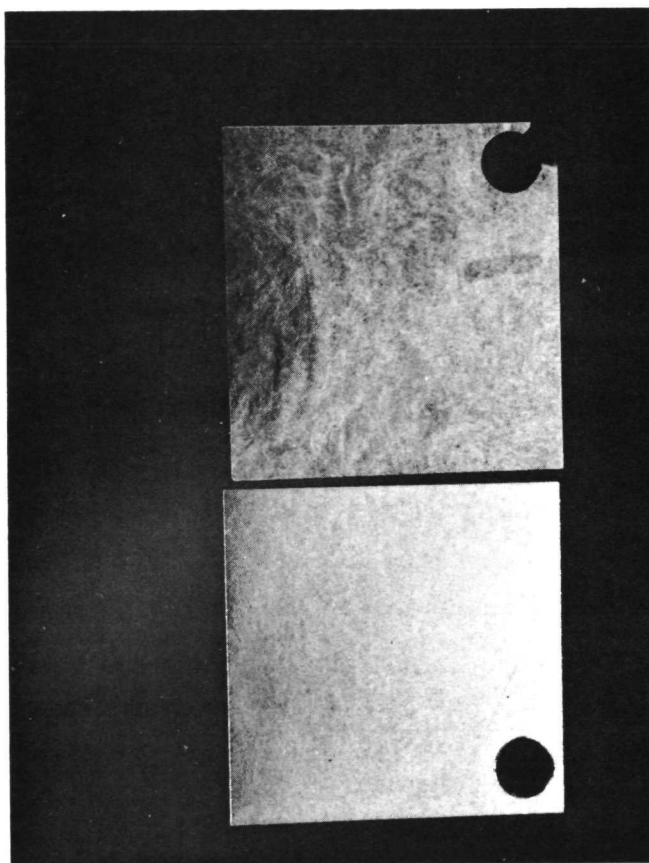
Figure V-2. Nominally Identical Phlogopite Mica Specimens Exhibiting Widely Different Delamination States after Processing in an 1800°C – 30 Minute Drying Cycle

Iron is a body centered cubic metal (at the temperatures of interest here) having a 2.866 $\overset{o}{A}$ lattice parameter, $1536^{o}C$ melting point and $11.8 \times 10^{-6}/C^{o}$ expansion coefficient in the $0 - 200^{o}C$. It reacts readily with many other materials (including p-type PbTe) at moderate temperatures, but is virtually inert to n-type PbTe.

PbTe is a compound semiconductor which exhibits the NaCl (B1) crystal structure with a parameter of about 6.45 $\overset{o}{A}$ (with small variations over the range of off-stoichiometric existence.) Its melting point is about $923^{o}C$, but the vapor pressure of the solid is extremely high and the material sublimes at a significant rate in open systems above $150^{o}C$ or so. PbTe has an expansion coefficient of about $19 \times 10^{-6}/C^{o}$ in the $0\text{-}200^{o}C$ range. It is an extremely reactive material even at moderate temperatures.

Before describing in detail the experimental work that was performed, we note a priori some of the major problems to be dealt with in implementing the thin film deposition on mica substrates, these include:

a.   The substrate surface will be crystallographically parallel to the strong bonding plane as previously discussed. It is unlikely that any low index planes in the tungsten or molybdenum lattices would match up closely with the substrate surface (although this cannot be proved due to lack of a precise atom-position model of the mica crystal structure), so it is expected that a distorted, highly defected transition region would be developed in the deposited film adjacent to the mica. This would probably result in poor (mechanically weak) bonding between film and substrate.

b.   In the plane of the film, there will be a factor of 4 mismatch in thermal expansion coefficient. Thus very high thermal stresses will be developed in the film/substrate interface region when the temperature changes significantly from the deposition temperature. Such a temperature change is quite unavoidable; if a relatively high deposition temperature is used, the components must be cooled to room temperature for removal from the deposition chamber and assembly into the module, and if a low deposition temperature

is used, the components will be heated during processing and operation of the assembled module. Since the film/substrate bond will be weak at best, it is almost inevitable that the film will be mechanically separated from the substrate due to the thermal stress. If the separation occurred uniformly, such that the film became an ultrathin foil adjacent but not bonded to the mica, then its utility as a transport barrier would not be impaired. More probable, however, is the occurrence of separation over small regions bounded by cracks in the film. The resultant film segments might then fall away, or at least peel back from, the mica substrate.

c.   Since the mica is hygroscopic, even if the substrates are processed in the drying cycle prior to deposition, some moisture will be reabsorbed during transport to any installation in the deposition chamber. This absorbed layer will probably adversely affect film quality, and thus should be removed in situ just prior to film deposition.

d.   It is fairly well established in thin film technology that metal films of 1000 $\overset{o}{A}$ or less thickness deposited below a temperature θ_3 characteristic of the particular metal tend to have an amorphous, non-crystalline structure. The value of θ_3 tends to be highest for body centered cubic metals and tends to increase with increasing melting point. Thus with tungsten and molybdenum we probably encounter the highest possible values of θ_3; that is, to obtain a crystalline as-deposited film, a higher substrate temperature would be required for tungsten than for any other metal. The little quantitative information available indicate that θ_3 for tungsten is probably 400 to 500°C. In terms of the capabilities of most deposition equipment systems (except chemical vapor deposition systems), this is a very extreme requirement and could only be met with a special and expensive apparatus. During most of the program, equipment of this type was not available, and it was necessary to take the approach of depositing an amorphous film on the mica and then annealing

the coated component to effect an amorphous-to-crystalline structural
transformation in the film. This transformation must be achieved if there is
to be any reasonable chance for the film to function as a diffusion barrier.

In the case of film deposition on PbTe substrates, in addition to thermal
expansion mismatch, the following must be considered:

a.   The PbTe washers used in tubular modules are produced by powder
metallurgy techniques and are about 91 percent of theoretical density when
assembled into the module circuit. The surfaces upon which films would be
deposited are thus not continuous flat planes as in the mica case, but rather
a series of relatively flat islands surrounded by deeply grooved boundaries.
When the washers are compacted to 100 percent of theoretical density during
subsequent module processing, the final film structure will have a network of
discontinuities corresponding to the original surface particle boundaries, and
the film material deposited in the original boundary grooves will be "folded"
into the interior of the washer as final compaction progresses.

b.   The high vapor pressure of PbTe will create problems if elevated substrate
temperatures are either (1) used to promote crystallinity in the as-deposited
film or (2) unavoidably obtained due to electron bombardment (sputtering) or
radiant heating (EBVD).

3.   Electron Beam Vapor Deposition

As previously noted, most of the actual experimental deposition work has utilized
the EBVD process. Nearly all of the EBVD work was performed in three equipment
systems at WANL. The first system used was a 36 inch diameter by 48 inch long welding
chamber fitted with a 10 inch oil diffusion pump vacuum system and a vertical beam EB
welding gun and power supply. A small molybdenum or tungsten cylinder (typically 0.5
inch diameter by 0.25 inch long) was placed on a copper block and positioned directly
under the electron gun. Mica sheet specimens (2 x 2 or 2 x 3 inches) were placed in
various holding fixtures to position them as desired with respect to the vapor source.

The chamber could then be evacuated and the source partially or completely melted with the electron beam; material evaporating from the molten surface would then expand into the chamber and deposit on the mica surface. In some cases, radiant heating lamps were positioned inside the chamber to heat the mica substrates prior to and/or during deposition. A large number of runs were made in this system using various combinations of substrate location and substrate temperature (in the range 25 to about 200°C) and a chamber pressure just prior to each run of about $2-4 \times 10^{-6}$ torr.

A process was eventually developed for applying good quality molybdenum films in this system. $2 \times 2 \times .0025$ inch sheets were coated with 200 - 800 Å films using ambient substrate temperatures. The coated sheets were then hydrogen annealed at 800°C for 1 hour, after which the coating/annealing sequence was repeated two more times. The final Mo film thickness was in the range 1000 to 2000 Å. One module insulating ring was then punched from each coated sheet. These barrier components were evaluated in sublength technology modules TEM-15C S/N-4 and 15C S/N-8, discussed in Section III of this report. In the TEM-15 circuit design, two rings were used at each mica position (Mo-coated faces together), so that the total barrier thickness was 2000 to 4000 Å at each position. Testing of these modules indicated that their rate of electrical output degradation was less than in otherwise identical non-barrier modules, but the improvement was disappointingly small. Accordingly, it was decided to abandon further work on molybdenum coatings and concentrate on the development of a tungsten deposition process.

Working with tungsten in the same equipment system, films obtained were generally extremely poor and their characteristics extremely non-reproducible. No films of remotely promising quality could be obtained having thickness greater than 100-200 Å. The problems involved with the poor results were compounded by frequent breakdown of the electron gun and power supply and by frequent unavailability of the system for use on this project.

Near the end of the period during which the above system was in use, a series of EBVD experiments were conducted at the Westinghouse Baltimore Systems Development

Division using a vastly superior equipment system. This apparatus featured a 270° deflected electron gun, permitting placement of substrates in the optimum positions over the molten source; quartz lamp substrate heaters permitting heating of the substrate to about 400-450°C; provision for in situ cleaning of the substrate surface by glow discharge ion bombardment; and rapid pumpdown to the 10^{-6} - 10^{-7} pressure range, permitting many experiments to be run per working day (vs. two days per experiment with the other system). Despite these features and advantages however, the results of tungsten-on-mica depositions remained poor. Only extremely thin films exhibited promising quality. Deposition of intermediate layers of chromium or aluminum oxide did not improve the characteristics of thicker films. The only positive result of this work was the observation that noticeable improvements in film appearance and adhesion to the substrate were obtained by argon glow discharge cleaning the substrate just prior to deposition or by splitting the mica sheets to expose a "freshly cleaved" surface just prior to evacuating the chamber.

Attempts were also made to deposit iron films on n-type PbTe, but the results were poor; the films were dull and "powdery" and appeared to be completely non-adherent.

To permit further investigation of the above and eliminate some of the problems previously discussed, a second EBVD system was set up at WANL. A surplus arc welding chamber, 30 inches in diameter by 48 inches long and equipped with a 6 inch oil diffusion pump vacuum system, was obtained and fitted with the vertical beam electron beam welding gun system that had been used in the first chamber. This new chamber was reserved for use on the vapor deposition project, and was thus fitted with more elaborate and useful fixturing and accessories including a water-cooled heat sink for holding the vapor source, universal adjustable substrate holders, a shutter for blocking the source-to-substrate vapor path when desired, and a high voltage power supply, feedthrough and instrumentation to permit glow discharge cleaning of the substrates. Substrate heaters were not included as results previously obtained with hot substrates were even worse than in the cold substrate cases. A large number of experiments were run in this system, principally concerned with investigating the effects of substrate position, glow discharge cleaning and duration

of the deposition run. Eventually it was determined that by using the following procedure, fairly good tungsten films 300-800 Å thick could be deposited on 2 x 2 x 0.0025 inch phlogopite mica substrates which had been processed in the 800°C - 30 minute vacuum drying cycle prior to deposition:

a. Evacuate the chamber to about 2×10^{-5} torr (the lowest attainable pressure for this system).

b. Clean the substrates by argon glow discharge bombardment for 10 minutes at a pressure of 20-25 microns and a discharge current of about 25 millamperes DC.

c. Re-evacuate the chamber to 2×10^{-5} torr.

d. Melt the upper end of a .25 inch diameter by .50 inch long tungsten cylinder to form a molten hemisphere vapor source.

e. Deposit tungsten on the mica for 1 minute using a source-to-substrate distance of 8 inches.

f. Cool for 30 minutes (or more), then perform a second 1 minute deposition run.

This procedure was used with the apparatus setup shown in Figure V-3 with a typical yield of 50-60 percent acceptable specimens (details of acceptable and unacceptable specimens are presented in a later section). All attempts to lengthen the deposition run duration or to increase the number of depositions per specimen produced unacceptable results.

A sufficient number of acceptable specimens having film thicknesses of order 500 Å was made to fabricate experimental module TEM-15C-4A. Testing of this module revealed a reduction in the rate of electrical output degradation sufficient to justify the procurement of a sophisticated ultrahigh vacuum EBVD system with which to continue the development of a tungsten-on-mica deposition process which would yield 5000 Å tungsten films.

Working in the same equipment system, a preliminary attempt was made to deposit tungsten onto the flat faces of P-Type PbTe pellets. However, the resultant films were completely non-adherent, both in the as-deposited condition and following a one hour,
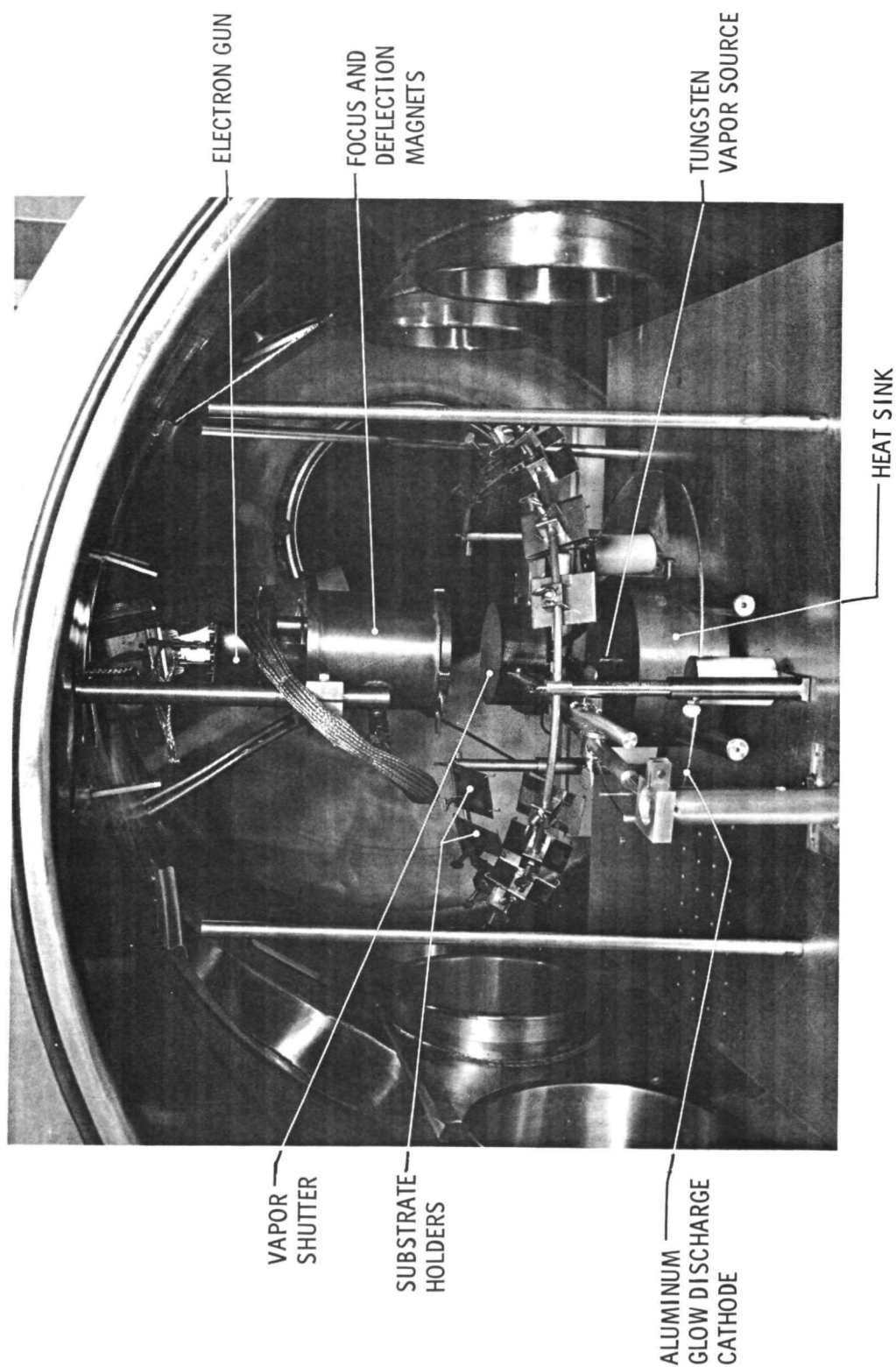
Figure V-3. EBVD Apparatus Used for Making TEM-15C S/N-4A Module Components

ELECTRON GUN

FOCUS AND DEFLECTION MAGNETS

TUNGSTEN VAPOR SOURCE

HEAT SINK

VAPOR SHUTTER

SUBSTRATE HOLDERS

ALUMINUM GLOW DISCHARGE CATHODE

Astronuclear Laboratory

Figure V-4. Ultrahigh Vacuum Ultek/Airco-Temescal EBVD System

Figure V-5. Work Chamber Interior of Ultrahigh Vacuum EBVD System —
Note Substrate Dome, Quartz Lamp Substrate Heaters and Electron Beam Source
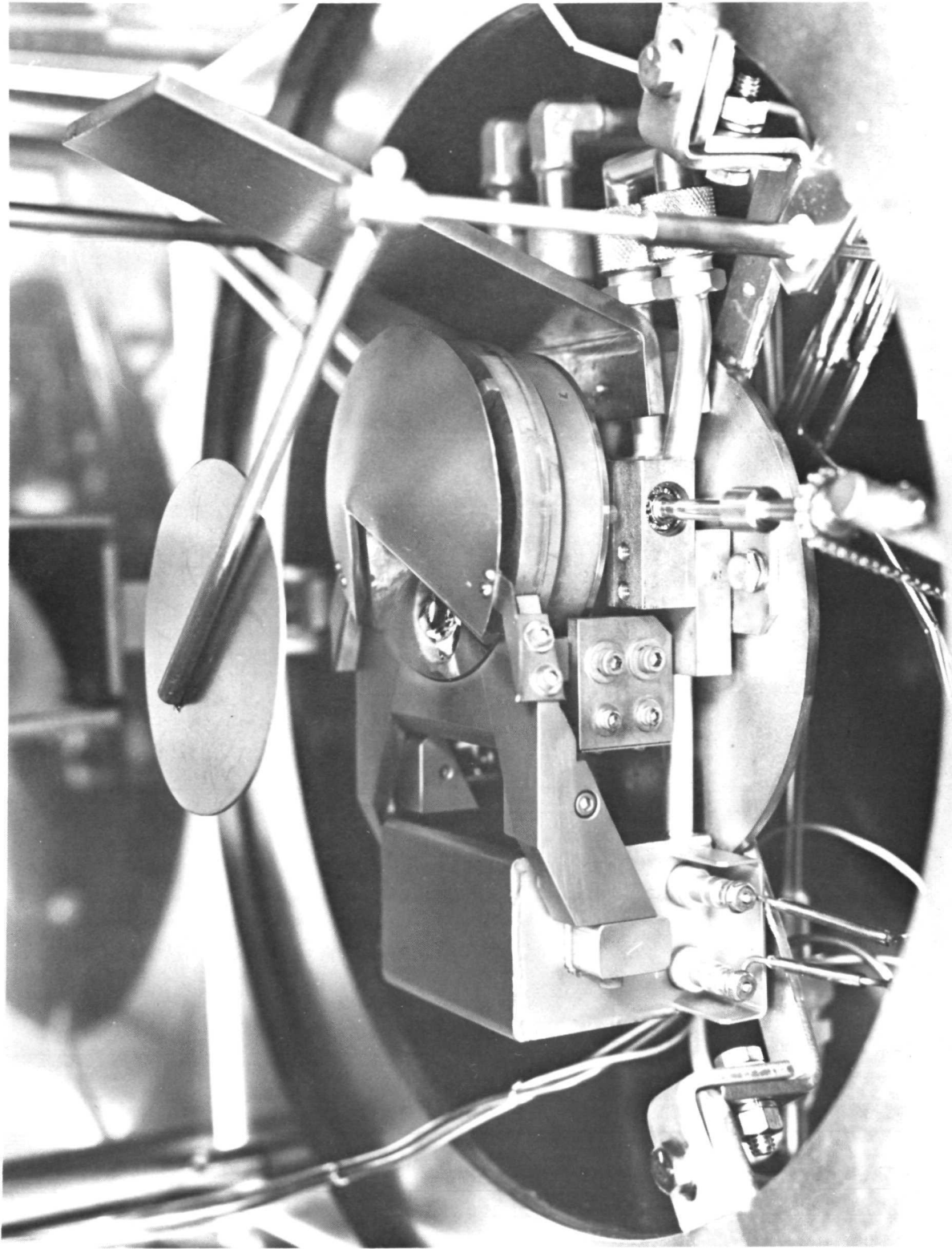
Figure V-6. Airco-Temescal 270° – Deflected Four-Crucible Electron Beam Source Mounted in Ultrahigh Vacuum EBVD System

725°C hydrogen anneal.

Finally, as alluded to above, a third WANL EBVD system was procured and set up. This was an Ultek RCS ultrahigh vacuum system (ion pump + titanium sublimation pump + cryopump) fitted with a 24 inch diameter stainless steel water-cooled bell jar and a contaminant-free rough pumping system (carbon vane blower + sorption pumps). It was equipped with an Airco-Temescal 270° - deflected 4-crucible electron beam source, 8 kw power supply and x-y beam sweep control; fixed-dome substrate holder having a capacity of 137   1.5 inch diameter mica discs; 2.5 kv AC glow discharge substrate cleaning system; and an 8 kw quartz lamp substrate heater system rated for heating the substrates to 500°C. Most of the features of this system can be seen in Figures V-4, V-5 and V-6.

The installation and set up of this system was plagued with a series of problems, most of which involved inadequacies in the integration of the EBVD components, substrate fixturing, substrate heater components and glow discharge components with the basic vacuum system. Although most of these problems were eventually resolved, the time spent in this work precluded the accomplishment of much experimental deposition work prior to termination of the program. Nevertheless, good quality, adherent tungsten films of about 1500 Å thickness were being deposited on mica at substrate temperatures in the 350-450°C range just before work was stopped.

4. Sputtering

The first series of sputtering experiments was performed in a DC system located at the (W) Lima Aerospace Electrical Division. Tungsten-on-mica and chromium-on mica films of 1000 - 3000 Å thickness were deposited at a substrate temperature of about 200°C. The tungsten films were "powdery" and completely non-adherent, but the chromium films were of good quality and quite adherent. Attempts were then made to deposit tungsten on a chromium subcoating, but the double film invariably flaked away from the mica in tightly curled flakes, presumably due to a very high residual stress condition.

At about the same time that the previously discussed EBVD experiments were being conducted at (W) Baltimore, a second series of sputtering experiments was being

performed at the (W) Research and Development Center using an RF system. This work was performed in a high performance Varian RF/DC sputtering system, where depositions were attempted using substrate temperatures as high as 550°C. Among the other process variables investigated were the effect of glow discharge substrate cleaning ("off-sputtering") for as long as one hour prior to deposition, and the effect of a thin sputtered layer of aluminum oxide interposed between tungsten and mica.

The results of the sputtering experiments were substantially the same as those of the EBVD work at that time: that is, good quality films could only be obtained at thicknesses up to a few hundred Angstroms, no good films could be obtained using high substrate temperatures, and significant improvements in film quality were obtained by glow discharge cleaning the substrate surface and by splitting the mica to expose a "freshly cleaved" surface just prior to evacuating the chamber. The sputtering work was terminated because there did not appear to be any inherent advantage to using sputtering as opposed to the EBVD process, and it was thus considered preferable to continue working with the (EBVD) facilities physically located at WANL.

Finally, a set of evaluation specimens were prepared by an outside vendor, Varian Vacuum Division. These tungsten films, of unknown thickness, were of high quality and exhibited excellent adhesion to the mica substrates. Had these been obtained early in the program, they probably would have influenced the direction of work toward the sputtering process in preference to EBVD, but they were not made available for evaluation until after procurement of the Ultek ultrahigh vacuum EBVD system was committed.

5. Chemical Vapor Deposition

Early in the tungsten film barrier concept program an outside vendor, San Fernando Laboratories, was retained to deposit tungsten coatings on a set of mica specimens using their version of the chemical vapor deposition (CVD) process. A set of evaluation specimens was delivered having coatings in the 10,000 - 13,000 $\overset{o}{A}$ thickness range. In all cases the coatings were badly blistered and virtually non-adherent to the mica. Also, the uncoated back surface of the mica was severely discolored. In view of these "best

effort" results, it was decided that the CVD approach was not promising and the work was terminated.

6. Characteristics of As-Deposited Tungsten Films

Evaluation of experimentally deposited films was made principally on the bases of visual and microscopic appearance and adhesion to the mica substrate as determined by certain qualitative tests. Visually, film appearance varied from a bright, smooth, mirrorlike metallic surface through various degress of milkiness or cloudiness to a completely dull, dark "powdery" deposit. The microscopic aspects of these variations will be discussed below in some detail. Attempts to make a meaningful film adhesion measurement by various tape-pull techniques were not successful because a thin surface layer of mica easily fractures and pulls away from the bulk mica sheet, making it nearly impossible to differentiate between mica fracture and poor film adhesion. Eventually a simple rub test was resorted to, and it was actually possible to make distinct judgements on the adhesion of a given film using this approach.

The first discussion of specific film characterisitics concerns films deposited in the second WANL EBVD system, where the bulk of the actual EB experimental work was performed; this is the system in which the components for experimental module TEM-15C S/N-4A were made.

Figure V-7 is a 75X photograph of a film which would be judged perfect on the basis of visual examination. This film is about 500 $\overset{o}{A}$ thick, and only a few fine cracks and small pits or inclusions are seen in the 0.060 x 0.047-inch area of the photograph. A film of this character usually (but not always) exhibits good to excellent adhesion. Figure V-8 was prepared specifically to illustrate one of the principal problems associated with the mica substrate (rather than the deposited film), namely the array of elongated blisters which have developed in the surface (blisters are also faintly visible in Figure V-7). It appears that these develop during glow discharge cleaning, but only speculation exists at present concerning the mechanism of their development.

Figure V-9 shows a film which is relatively free of cracks but has a high density of pits and inclusions. Films having this type of appearance were obtained periodi-

Figure V-7. Good Quality 500 Å Tungsten Film –
As-Deposited, 75X

Figure V-8. Elongated Blisters in Mica Surface Layers,
75X

cally throughout the work, but their occurrence could not be correlated with any particular aspect of the deposition process.

Figures V-10 and V-11 correspond to the visual observation of an increasing degree of cloudiness or milkiness in the films. The photographs show this to be associated with the development of an increasingly fine network of cracks, reducing the film to an array of fragments having the appearance of a "two-dimensional" grain structure. A fragment network of this type was inevitably observed to develop in films whose thickness approached 1000 $\overset{o}{A}$, irrespective of the details of the deposition run or process. However, networks very frequently were observed in much thinner films as well, and it is believed in these cases that their appearance is due to the development of temperature gradients (and hence thermal stress gradients) in the specimen during deposition. Although it is not evident in Figure V-11 because of the two-dimensionality of the photograph, edge lifting and peelback begins to occur in the film fragments as their size approaches that shown. Adhesion tests on network specimens indicate that adhesion deteriorates rapidly with decreasing fragment size.

Figure V-12 illustrates a somewhat different, but also frequently encountered, film defect structure. Several sets of long, parallel cracks or tears are found to intersect at fairly discreet angles, and extensive peelback has occurred at the edges of the tears. Films of this type are virtually completely non-adherent. The occurrence of these arrays may be more related to the mica substrate than to the tungsten film or the deposition process. Similar arrays of lines which do not appear to be cracks or tears are at least faintly visible in Figures V-7 through V-10. Also, the array is very similar to the array of deformation faults and cracks invariably observed in the mica insulators during destructive examination of modules which have been isostatically compacted. In some cases an array of tears is observed in a second or third "layer" of a film, with peelback occurring from an earlier tungsten layer rather than from the mica as shown in Figure V-12.

For the purpose of making module washers for experimental evaluation, 2 x 2 x 0.0025 inch mica squares were coated with 300 - 800 $\overset{o}{A}$ films as previously described. A given square was accepted for module use if it contained a washer-size film area of
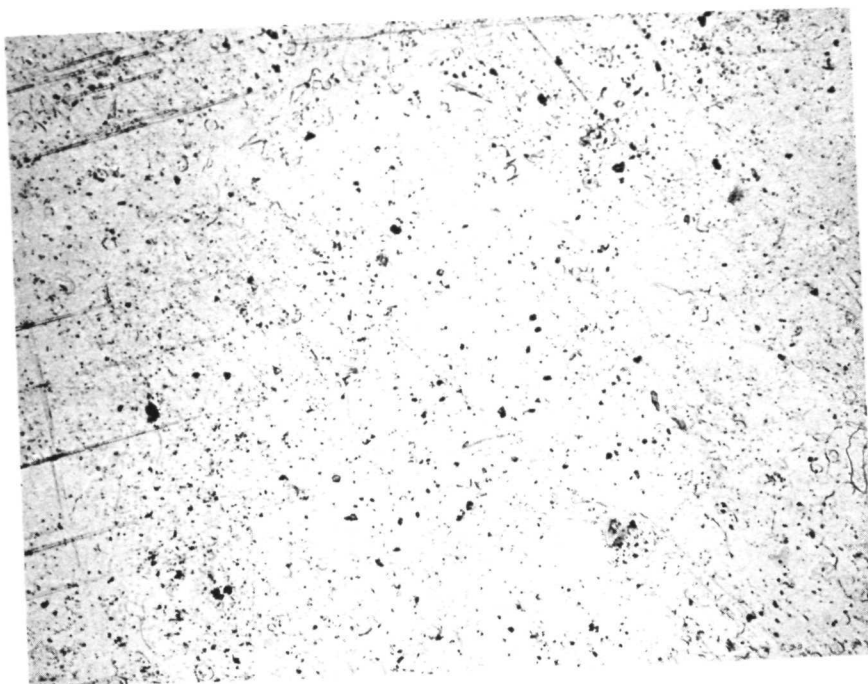
Figure V-9. Crack-Free 500 Å Tungsten Film with High Density of Pits or Inclusions - As-Deposited, 75X

Figure V-10. Coarsely Fragmented 500Å Tungsten Film - As-Deposited, 75X

Figure V-11. Finely Fragmented 500 Å Tungsten Film with Slight
Peeling - As-Deposited, 75X

Figure V-12. Arrays of Parallel Tears with Severe Peeling in 500 Å
Tungsten Film - As-Deposited, 75X

quality equivalent to that shown in Figure V-7. Typically, 50 - 60 percent of the specimens in a given run were accepted. Some feeling for the difficulty of selecting acceptable specimens can perhaps be imparted by noting that all of the film characteristics shown in Figures V-7 through V-12 were photographed at different locations of a single 2 x 2 inch specimen.

Next, we briefly discuss films deposited in the Ultek RCS ultrahigh vacuum system just before termination of the program. Figure V-13 shows various characteristics of a 1500 Å film, deposited at a substrate temperature of 450°C, which appeared visually to be perfect and exhibited excellent adhesion. Most of the area of this film had a very low defect density, as in Photograph A. The most prevalent defects present were highly localized fragmented regions, as in B; sets of parallel linear tears or cracks, as in C; and (rarely) areas of high pit or inclusion density, as in D.

The achievement of depositing good quality films at high substrate temperatures in the ultrahigh vacuum environment belies the results previously obtained in the oil-pumped EBVD and sputtering systems. It must be concluded that the problems experienced in the latter cases were due to outgassing, hydrocarbon contamination or some other factor indigenous to the lower quality vacuum environment.

Finally, Figure V-14 shows some characteristics of the sputtered films deposited by Varian Vacuum Division. Photograph A is an area depicting the lowest density of defects obtained in flat films (see below); this does not approach the freedom from defects obtained in the better EBVD films. In B is seen a finely fragmented film very similar to the EBVD film of Figure V-11, and C shows a film containing numerous large tears with severe edge peelback. Unlike the EBVD case, the above films all exhibit excellent adhesion despite their high defect density. Photograph D shows a sputtered film with low defect density, but the film itself is severely corrugated or ridged in a randomly oriented manner. Only films of this type had defect-free areas approaching those obtained by EBVD. No explanation is available for the development of the corrugation network.
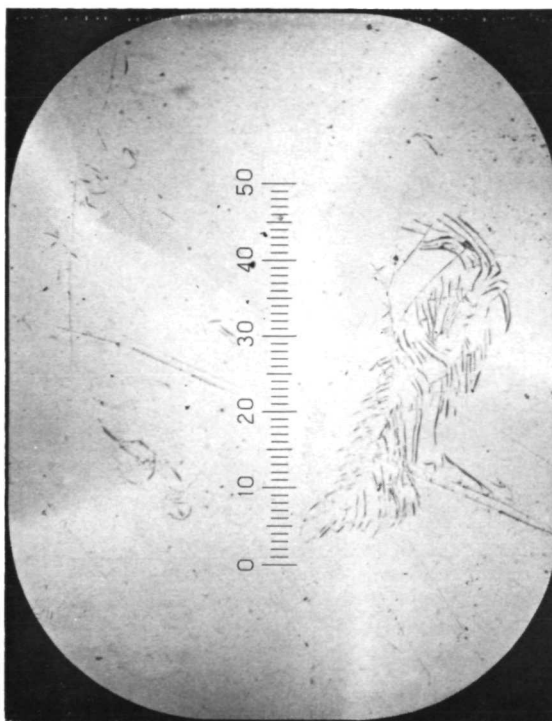
A. Typical Nearly-Defect-Free Area, 100X
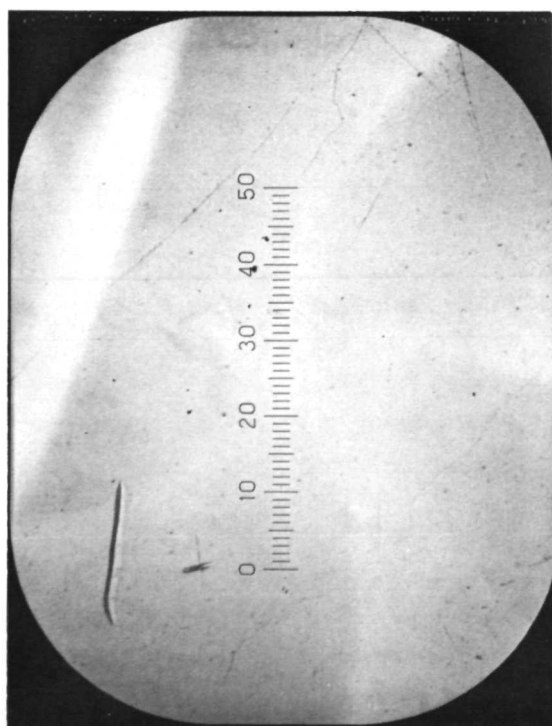
B. Localized Fragmented Region, 100X
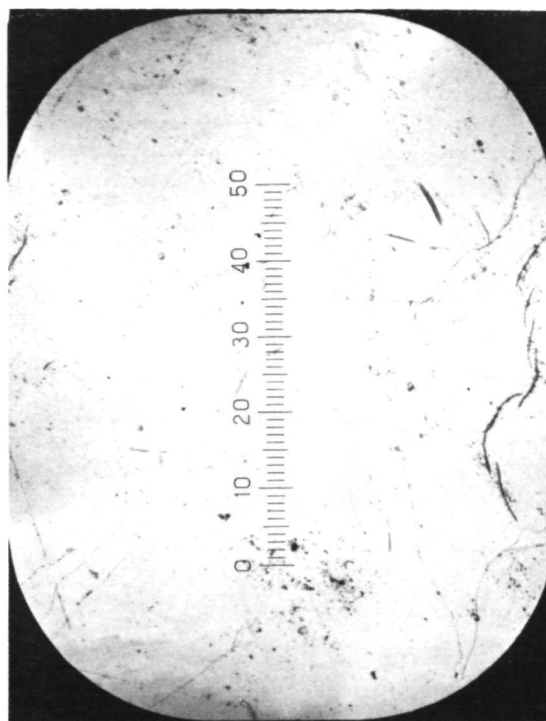
C. Sets of Linear Tears or Cracks, 100X
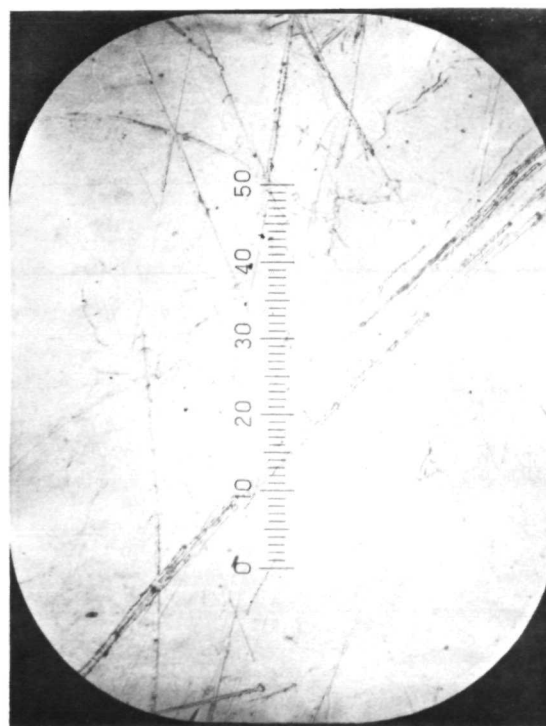
D. Region of High Pit or Inclusion Density, 100X

Figure V-13. Characteristics of 1500 Å Tungsten Film Deposited by
EBVD in Ultrahigh Vacuum at 450°C Substrate Temperature

B. Finely Fragmented Film, 100X

D. Corrugated Film with Low Defect Density, 100X
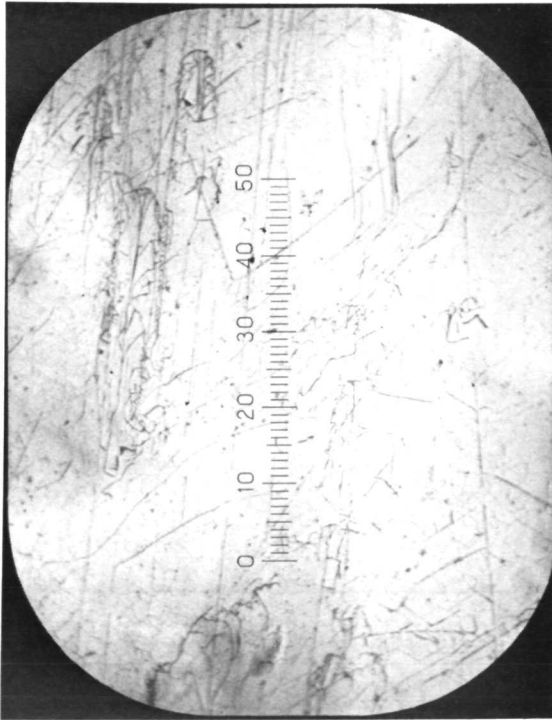
A. Minimum Defect Density in Flat Films, 100X
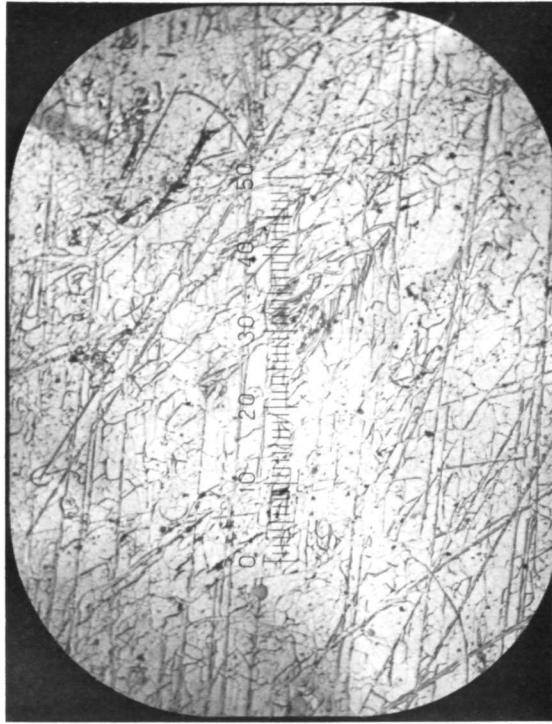
C. Large Tears with Severe Edge Peelback, 100X

Figure V-14. Characteristics of Tungsten Films Deposited by Sputtering at Varian Vacuum Division

7. Processing of Tungsten Coated Mica

As noted previously, the thin tungsten films deposited at relatively low substrate temperatures are amorphous in the as-deposited state, but must be structurally crystalline if they are to function as a physical diffusion barrier. Several experiments were performed on annealing as-deposited films at various temperatures and in various heat treating atmospheres, after which the films were scraped off and x-ray powder diffraction patterns taken to see whether a given anneal had promoted the amorphous-to-crystalline structural transformation. It was found that a tungsten diffraction pattern was obtained after annealing at temperatures as low as $600^\circ C$, although $650 - 700^\circ C$ produced a stronger pattern. Varying the annealing atmosphere from argon to hydrogen to vacuum had no apparent effect on the diffraction pattern.

Two complicating observations were also made during the annealing experiments. First, a tungsten carbide ($a - WC_2$) diffraction pattern was inevitably superimposed on the pure tungsten patterns obtained. It is believed that some tungsten carbide is formed as the vaporized tungsten, transporting from the vapor source toward the mica substrate, reacts with hydrocarbon contaminants in the residual chamber atmosphere to form WC_2 molecules which then deposit on the mica. It is felt, however, that tungsten carbide is a completely innocuous contaminant phase, and no effort was directed toward its elimination. (Carbide formation probably would not occur in the Ultek ultrahigh vacuum system, as the hydrocarbon concentration in the system is presumably very low.)

Second, it was found that annealing usually reduced the adherence of films which had good appearance and adherence in the as-deposited condition; this is presumably due to the thermal expansion mismatch previously discussed. (Not surprisingly, it was also found that annealing did not improve the characteristics of films which exhibited poor as-deposited appearance and/or adherence.) In view of this latter situation, it was decided that components would not be annealed prior to assembly into the module; the isostatic compaction temperature currently used in processing assembled modules is sufficient to produce the required structural transformation in the tungsten films.

Module washers for TEM-15C S/N-4A were punched from tungsten coated mica blanks using the same hardened tool steel punching dies that are used for uncoated mica; a test punching and an unpunched coated blank are shown in Figure V-15. Microscopic examination of a few punched module washers revealed no film defects that could be attributed to the punching operation.
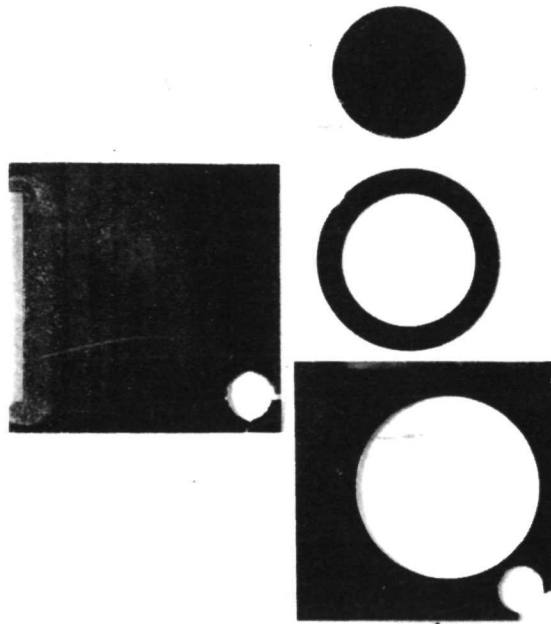
Figure V-15. Unpunched Coated Blank and Test Washer Punching from 2 x 2 x 0.0025-Inch Mica with 500 Å Tungsten Film

VI. LOW EXPANSION BIMETAL INNER CLAD

A.   INTRODUCTION

Experimental data from early reactor power module tests along with data generated during destructive examination of these modules indicated that severe module circuit component distortion resulted from differential thermal expansions of the module clads during transient operation. Subsequent stress analyses efforts showed that the distortion could be eliminated through the substitution of a low expansion inner clad material for the previously used Inconel 718 inner clads.

The design of a refractory metal inner clad to be used in a proof-of-principal test (TEM-X S/N-2) is discussed in detail in Section I of this report. The clad for this, and all subsequent reactor power modules on this program, was made by (hot) tandem co-extruding two single Ta-10W/316 stainless steel bimetal joints, electron beam welding the Ta-10W ends of these together, and machining the resultant assembly to the final clad configuration. As discussed in Section I, performance data generated during subsequent refractory metal clad reactor power module performance data along with post-test destructive examination results showed that the circuit distortion problem had been successfully eliminated.

Additional materials evaluation work was required, however, to ensure that the integrity of the bimetal joint was not imparied during cyclic or long term operation of the module and to develop a seal to eliminate in-leakage of air into the module during operation in a laboratory (air) environment. The latter effort was very critical in that trace amounts of air were found to produce oxygen attack of the refractory metal clad during operation, thus initiating cracks which allowed liquid metal to leak into the module.

B.   EVALUATION OF THE TEM-X S/N-2 INNER CLAD

As discussed in Section I of this report, TEM-X S/N-2 was a proof-of-principal experimental module designed to demonstrate that circuit component distortion could be eliminated through the use of a low expansion refractory metal inner clad. Test data and destructive examination data from this experiment, as discussed in Section I, gave conclusive proof that the reason for previously observed circuit distortion was the total thermal expansion mismatch between the inner and outer clads.

During the post-test destructive examination of TEM-X S/N-2, the entire length of the inner and outer diameter of the bimetal clad was examined visually and metallographically. No evidence of NaK corrosion or oxidation was observed at any point along the clad axis. The center section, where the two extruded bimetal joints were electron beam welded together, was removed and metallographically prepared for examination via light microscopy. Figure VI-1 is a photomicrograph of the weld zone from TEM-X S/N-2. The microscopic examination revealed no indications of impurities, porosity or inclusions.

The electron beam welding was done at a pressure in the 10^{-5} torr range. Experimental work[1] has shown that EB welding of refractory materials at pressures less than 10^{-3} torr results in weld zone oxygen levels which are equal to or less than the oxygen content in the base material. Consequently, essentially oxygen-free welds are assured at the center of the Ta-10W clad by proper control requirements during EB welding.

The tandem transition joint between the 316 ends and the Ta-10W center portion was removed, mounted separately, and examined via light microscopy and the electron beam microprobe. Figure VI-2 is a photomicrograph of a portion of the joint area. The photo is representative of the entire bond area examined. No separation of the two materials was evident. The diffusion bond reaction is characterized by a thin layer of intermetallic formation (.0001 to .0002 inch) at the Ta-10W/316 SS interface. EB microprobe traces across the joint bond area showed the intermetallic layer was composed of nickel, chromium and tantalum.

---

[1] NASA Contract Report No. 54088, Quarterly Report, March, 1964, "Determination of the Weldability and Elevated Temperature Stability of Refractory Metal Alloys."

O.D

I.D.
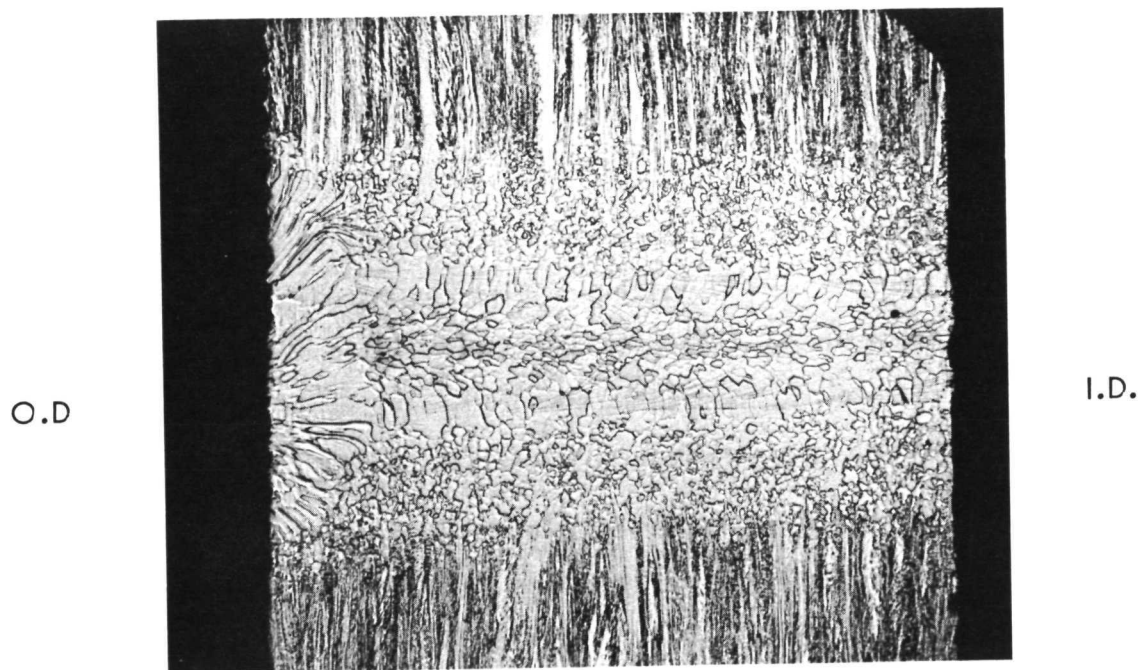
Figure VI-1. Electron Beam Weld Zone from TEM-X-2 Inner Clad (40X)

Ta-10W

316 SS
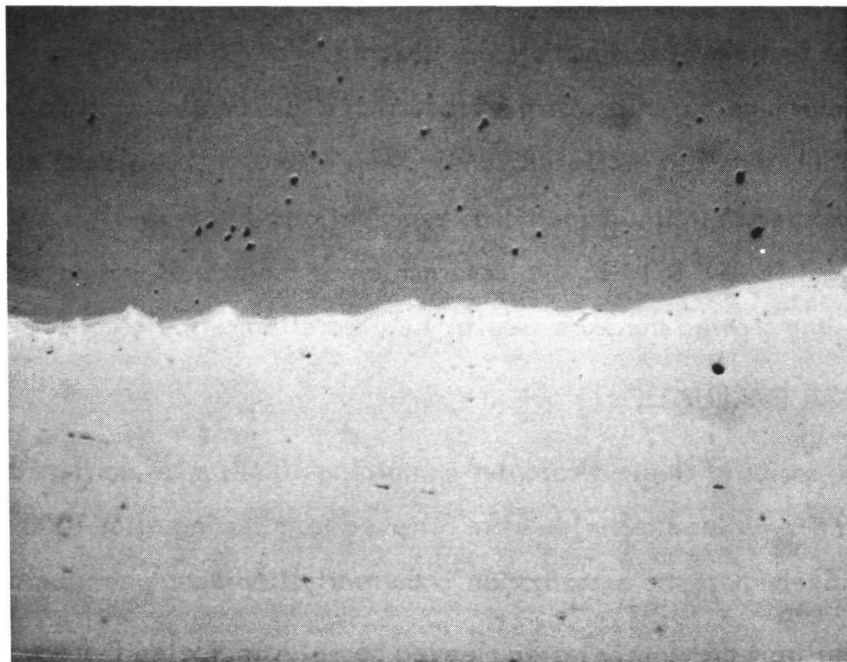
Figure VI-2. Photomicrograph of Bond from TEM-X-2 Inner Clad Showing
Intermetallic Diffusion Zone (500X)

The width of the intermetallic layer is controllable during the fabrication process by varying the extrusion temperature. It was decided that a lower extrusion temperature would produce a two-fold benefit; not only would the intermetallic layer be reduced in thickness, but the bond would be strengthened because the strength ratio of the stainless steel to the Ta-10W would increase. There was also evidence that a stronger joint results as the length of the tapered transition region is increased. The joint from TEM-X S/N-2 had a bond length which varied from 0.5 to 1 inch. In later implementations of the bimetal clad, the extrusion temperature was limited to the range 982 to 1038°C, and slight changes were made to the billet preforms to yield a final transition region length of about 1.5 inches.

C.   QUALIFICATION OF THE TA-10W/316 SS CLAD FOR LONG TERM USE

1. Introduction and Background

In view of the demonstrated success of the Ta-10W/316 SS low expansion inner clad in eliminating module circuit distortion during thermal cycling, a program was initiated to perform detailed qualification of this clad for long-term operational system use. The specific objectives of this program were as follows:

a.   Ensure that the NDT and inspection techniques used to evaluate the TEM-X bimetal clads are adequate for detecting defect conditions which might lead to problems during long-term system operation.

b.   Determine the detailed effects (if any) of thermal cycling on the physical, mechanical and metallurgical characteristics of the bimetal clad in general and the intermetallic bond region in particular.

c.   Using available literature data from prior and continuing outside programs, estimate the diffusional growth rate of the intermetallic bond region at temperatures in the vicinity of 650°C. Using this estimate, select three suitable test temperatures and experimentally measure the intermetallic growth rates at these temperatures.

d.   Based on the growth rates measured in (c), calculate the operating time at peak inner clad operating temperatures required for the thickness of the intermetallic bond region to reach the critical 5×10^{-4} inch value that previous work[1] has shown to cause mechanical embrittlement of similar bimetal diffusion bonded assemblies. This period of time would then represent a probable limit to the useful operating life of a bimetal clad module.

---

[1] R. W. Buckman, Jr. and R. C. Goodspeed, "Evaluation of Refractory/Austenitic Bimetal Combinations," WANL-PRE-(EE)-004, August, 1969, Final Report, Contract NAS-37634.

e. Also based on the growth rates measured in (c), analytically determine a temperature T* which in 100 hours of exposure will produce the same amount of intermetallic growth as would 44,000 hours of exposure to the 650°C peak inner clad operating temperature. Then actually anneal an experimental specimen for 100 hours at T*, and verify the analytical results.

To provide specimens for the experimental work, six Ta-10W/316 tandem extruded single joints were procured from Nuclear Metals. These joints were extruded at a nominal temperature of 1010°C. The machined specimen dimension (inches) were .932 O.D. x .750 I.D. x 10.8 long (later shortened to 8.0 inches by cutting off the Ta-10W ends), with a nominal transition joint length of 1.62 inches; a typical joint is shown in Figure VI-3.

2. Nondestructive Testing and Inspection

Various nondestructive testing and inspection techniques were used to evaluate the bimetal joint specimens in the as-received state and after exposure to various experimental conditions. To detect surface and surface-connected defects, liquid penetrant testing incorporating a solvent-removable visible dye penetrant was used in accordance with WANL PS-294564-1, Class O. A borescope was used to look for defect indications in the specimen bores. Helium leak testing for gas-permeable defects penetrating the entire specimen wall was performed using the most sensitive scale of a Veeco MS-9 mass-spectrometer-type leak detector. Dimensional measurements were made using conventional inspection instruments, with all values measured being indexed and recorded to permit comparison of pre- and post- test conditions. Radiographic inspection was performed in accordance with MIL-STD-271.

It had been anticipated that the most sensitive and useful technique for nondestructively evaluating the condition of the intermetallic bond region itself would be immersion ultrasonic testing using a water couplant; both pulse-echo and through-transmission ultrasonic examination had been used to inspect module clads and to evaluate
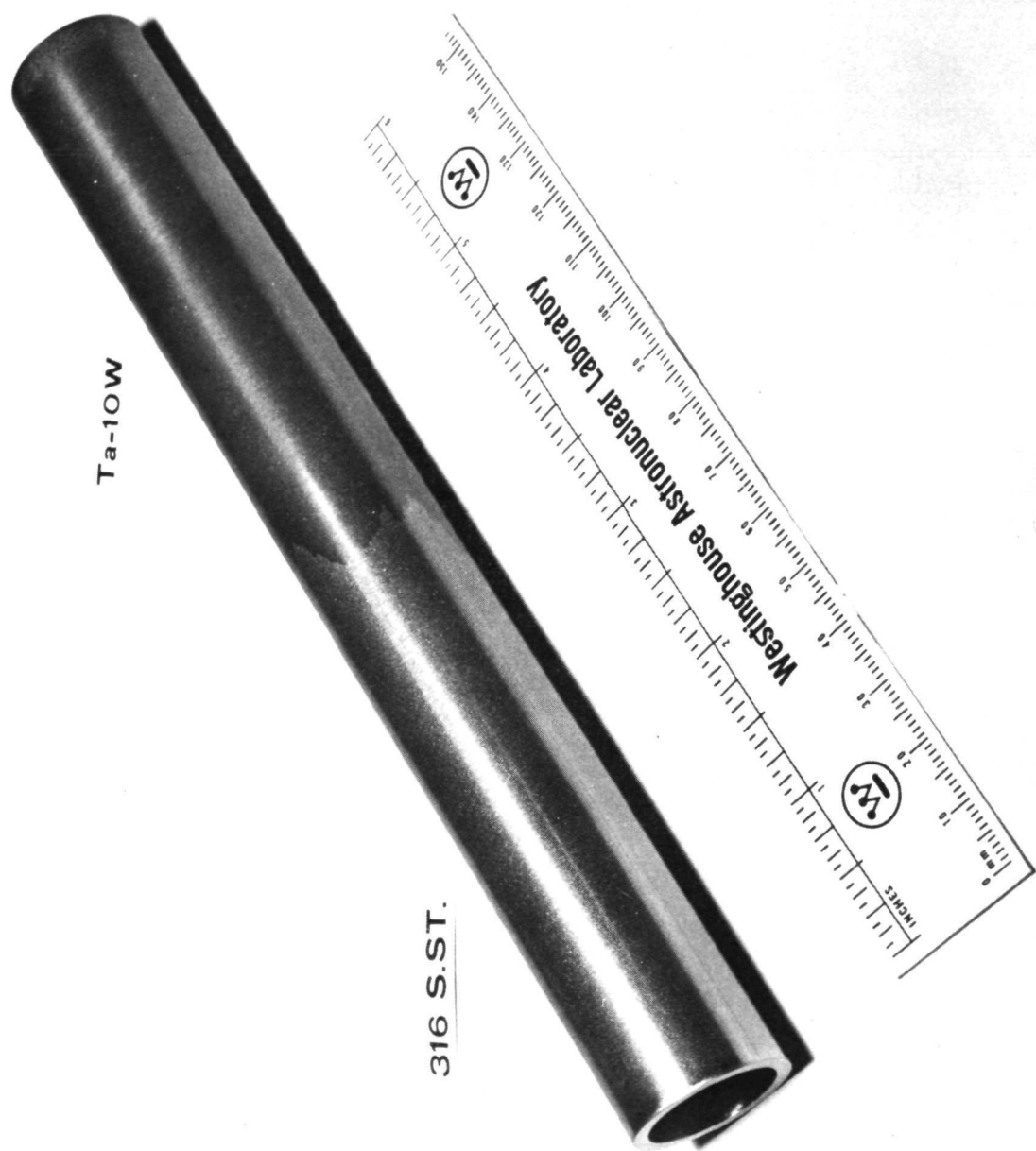
Figure VI-3. Ta-10W/316 SS Bimetal Joint Qualification Specimen

similar bonds in another program[1]. At the time that the six specimen joints were ordered, the ultrasonic equipment which was used to inspect module clads had been dismantled and put up for disposition (fabrication of new reactor power modules was not a funded task of the Compact Converter Program at that time), and the experienced operator was no longer available. To permit on-site performance of ultrasonic testing during this qualification program, the equipment was redesignated for such use, a new operator identified, and the test equipment/fixturing setup reassembled with incorporation of some fixturing improvements over the previous arrangement.

A precision standard for evaluation of the bond region, which simulated both localized defects and large-area unbonding, was then designed and procured. Using this standard and also an early bimetal joint which was known to be defective, a series of setup and checkout tests were made to ensure proper functioning of both equipment and personnel. The results of these tests were somewhat disappointing; good reproducible indications could easily be obtained for the localized defects, but indications of large area unbonding were extremely difficult to interpret, and the reliability of the latter interpretation appeared to be overly dependent upon operator skill and experience. It was finally necessary to abandon the use of an unbonding standard, and each test run on each tubular specimen was set up on the basis of detecting the presence of small-diameter dots of thin paper tape affixed to the inner surface.

At first it appeared that this latter approach was satisfactory; when an unbonding indication was obtained on one of the as-received specimens, it was exactly reproduced several times even when other specimen tests were interposed between repetitions. It was later found, however, that specimens which had originally been judged defect-free exhibited unbonding indications when re-tested in the same condition some months later. Thus, although the results of ultrasonic tests will be noted below as though they were completely reliable, they must in fact be regarded with some suspicion. If the program

---

[1] D.R. Stoner, "Evaluation of Tantalum/316 Stainless Steel Transition Joints", NASA CR-121111, December, 1972.

were to be continued, either more work would be done to qualify a totally reliable ultra-sonic technique, or a different technique (probably eddy current testing) would be developed to detect unbonding.

The six single joint specimens were inspected and tested in the as-received state using all of the above methods, with results given in Table VI-1. The results of inspection and testing after exposure to the various experimental conditions will be given in the appropriate subsections below.

3. Thermal Cycling and Mechanical Property Tests

A paramount objective of the qualification program was to demonstrate that the bimetal joint could withstand the specified reactor module thermal cycling conditions without experiencing physical or mechanical damage or deterioration which would affect module performance or integrity. The specified cycle configuration consists of heating and cooling at the approximate rate of 16.7 C^o/min between the limits 260 and 593°C.

Before any experimental work was performed, a study was conducted of available information from other programs which have considered the effects of thermal cycling on refractory metal/stainless steel transition joints[1], [2]. In one case[1], a 3.0 inch I. D. x 0.095 inch wall Nb-1Zr/316 SS joint was subjected to 20 thermal cycles between 149 and 843°C at rates of 11.6 (heating) and 5.8C^o/min. (cooling), 500 more cycles between 788 and 871°C at 16.7C^o/min., and finally 58 cycles identical to the first 20. No structural defects were found in this specimen after cycling, but a 0.052 to 0.055-inch radial reduction had occurred in the joint region.

In a second more extensive program[2], 1.75 inch I.D. x 0.123 inch wall Ta/316 SS joints were subjected to 100 thermal cycles between 121 and 732°C at a rate of 5.1C^o/min.

[1] H. M. Cameron, "Thermal Cycling Test on a 3-inch Diameter Nb-1 Zr to 316 Stainless Steel Transition Joint," NASA TMX-2118, November, 1970.

[2] D. R. Stoner, "Evaluation of Tantalum/316 Stainless Steel Transition Joints," NASA CR-121111, December, 1972.

TABLE VI-1

RESULTS OF INSPECTION AND NONDESTRUCTIVE TESTING OF AS-RECEIVED
SINGLE BIMETAL JOINT SPECIMENS P/N 982D323G03A

Type of Test	Specimen Serial Number					
	C23838	C23839	C23840	C23841	C23842	C23843
Dimensional Inspection	OK	OK	OK	OK	OK	OK
Helium Leak Test (Tube internally evacuated, helium sprayed over O.D.)	NAD*	NAD	NAD	NAD	NAD	NAD
X-Ray Radiography	NAD	NAD	NAD	NAD	NAD	NAD
Liquid Penetrant (all surfaces)	NAD	NAD	NAD	NAD	NAD	NAD
Borescope Examination (of tube I.D.'s)	NAD	Boring Tool Chattermarks	NAD	Boring Tool Chattermarks	NAD	NAD
Ultrasonic Tests: 10/24/72 Test	NAD	NAD	Unbonding indications	NAD	NAD	NAD
2/5/73 Test	Unbonding indications	-	-	-	-	Unbonding indications

*NAD = no apparent defects

All four specimens remained helium leak tight after cycling, but all four had developed fissures (cracks) in the 316 I.D. adjacent to the intermetallic bond region, and one had also developed fissures in the Ta O.D. adjacent to the bond region. No unbonding of the intermetallic region itself was observed. All four specimens exhibited diametral reductions in the joint region, ranging from 0.005 inch (specimens internally helium pressurized to 250 psig at 732°C) to 0.017 - 0.065 inch (specimens tested with open bores).

In considering the applicability of these results to the reactor module inner clad, we had in the TEM-X case a much smaller I.D. (0.750 inch) while maintaining a comparable wall thickness (0.091 inch). These, combined with the considerably reduced upper temperature limit for cycling (593°C), meant that the radial displacements due to thermal expansion would be very much smaller, and hence the extent of the yielded zone and amount of plastic flow in the TEM-X joint region would be far less than in the reference cases. Furthermore, the strength of the Ta-10W refractory metal component in TEM-X was substantially higher than that of the Nb-1 Zr or Ta reference specimens (67/37/35 kpsi, 0.2% YS at R. T.; 80/50/45 kpsi, UTS at R.T.; typical values for comparable specimens[1]), which would further reduce the extent of the yielded zone, the amount of plastic flow and the probability of fissuring in the refractory metal side of the joint. In defense of the above argument is the fact that 11 TEM-X modules with Ta-10W/316 SS inner clads were operated on test, with up to 13,990 hours of operating temperature exposure and up to 53 thermal cycles, without any indications of transition joint failure.

The possibility of developing diametral shrinkage in the TEM-X transition zone was not quite so easily dismissed; although such shrinkage would be far less than in the reference cases, it clearly could be non-zero. An immediate look into this situation was taken by making I.D. profile measurements on a TEM-X clad which was subjected to 50 thermal cycles between 260 and 593°C at 16.7C^o/min. in a liquid metal loop system at Atomics International. The results indicated that no significant diametral changes

---

[1] D. R. Mash, D. W. Bauer and M. Schussler, "Fabricating the Refractory Metals," Metal Progress, February, 1971.

(localized to the transition zone) had occurred. However, a more precise evaluation of this situation was made during measurement of specimens from experiments conducted under this task, as discussed below.

A tensile specimen design for evaluating the transition joint was evolved in conjunction with mechanical testing consultants at the Westinghouse Research and Development Center, and friction-type tensile grips for this specimen configuration were designed and procured. A sketch of the tensile specimen is shown in Figure VI-4; five of these could be machined from a given bimetal joint specimen.

One specimen (C23842) was selected at random from the defect-free group and machined into five tensile specimens to be used for establishing the mechanical deformation and strength characteristics of the intermetallic joint (relative to the Ta-10W and 316 SS base alloys) for the as-received condition, and room temperature tensile tests were made on three of these. In testing the first specimen, C23842-E shown in Figure VI-5, some slippage was experienced in the friction-type tensile grips; this resulted in a less-than-smoothly varying distribution of plastic tensile strain along the specimen gage length, as shown in Figure VI-6. However, the important result of the test is that fracture eventually occurred in the 316 stainless steel portion, well removed from the intermetallic bond region. After correcting the grip slippage problem, a second specimen (C23842-A) was tested at a higher strain rate; as shown in Figures VI-7 and VI-8 the fracture again occurred in the 316 stainless steel portion, but this time a very smooth plastic strain distribution was obtained.

Finally, to investigate the fracture mode when the specimen was constrained to fail in the intermetallic bond portion, a third specimen (C23842-B) was cut down to a small cross section in the bond portion as shown in Figure VI-9. This was then tested at a crosshead speed selected to give about the same strain rate in the cut down section as that used in testing the second specimen above. Failure of this specimen occurred in the following sequence:

    a. An initial fracture occurred in the Ta-10W near the thin end of that material, as shown in Figure VI-10.
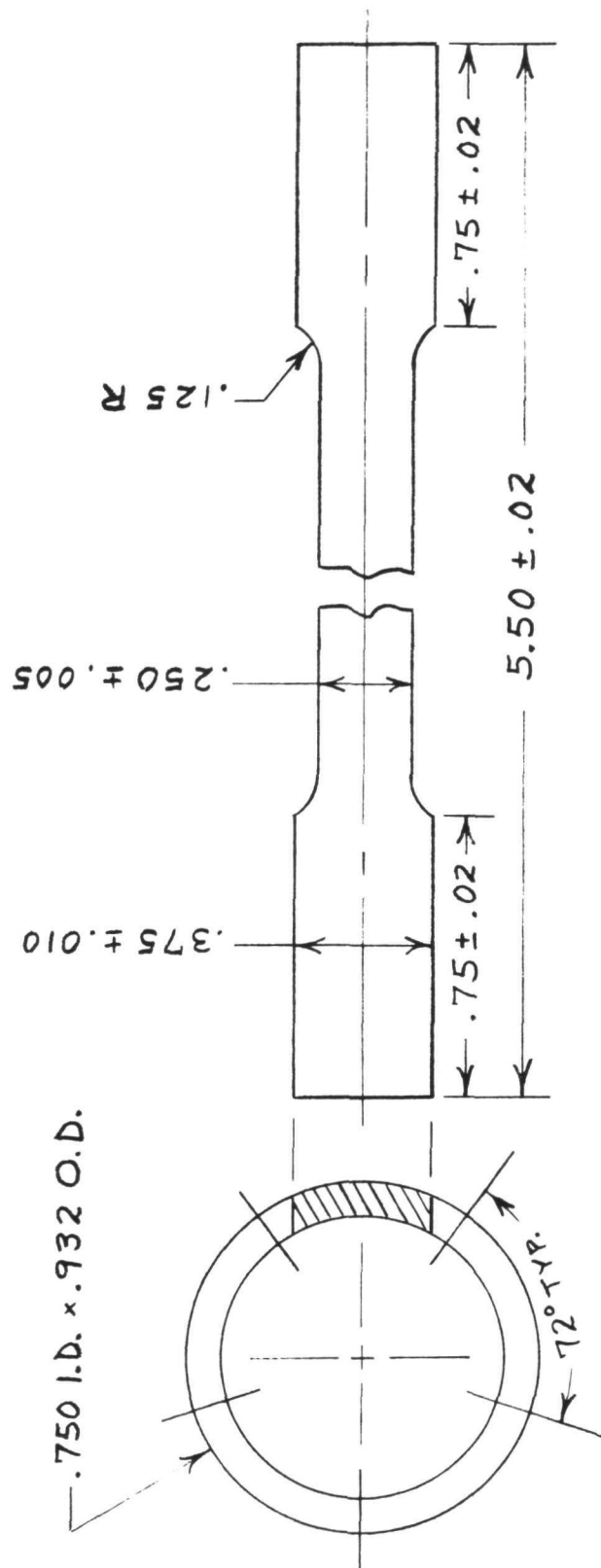
Figure VI-4. Tensile Specimen Design for Mechanical Property
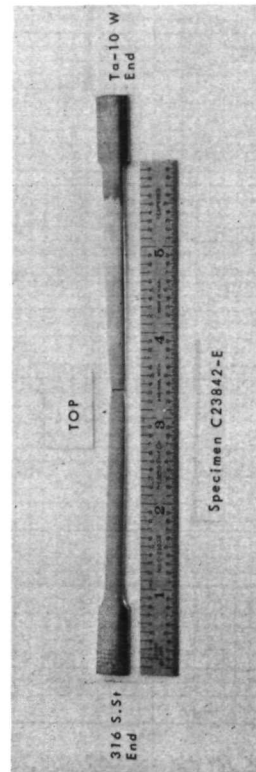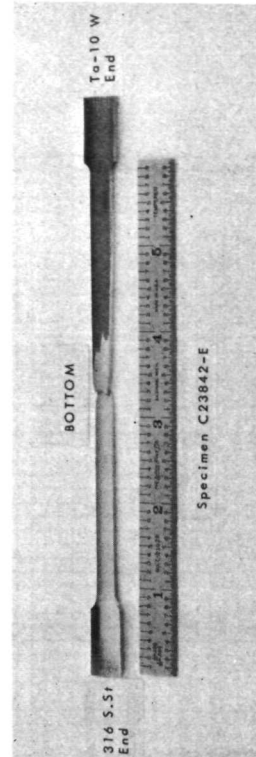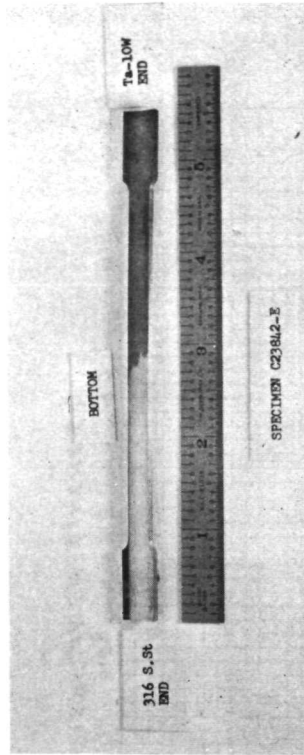Testing of Ta-10W/316 SS Bimetal Joints

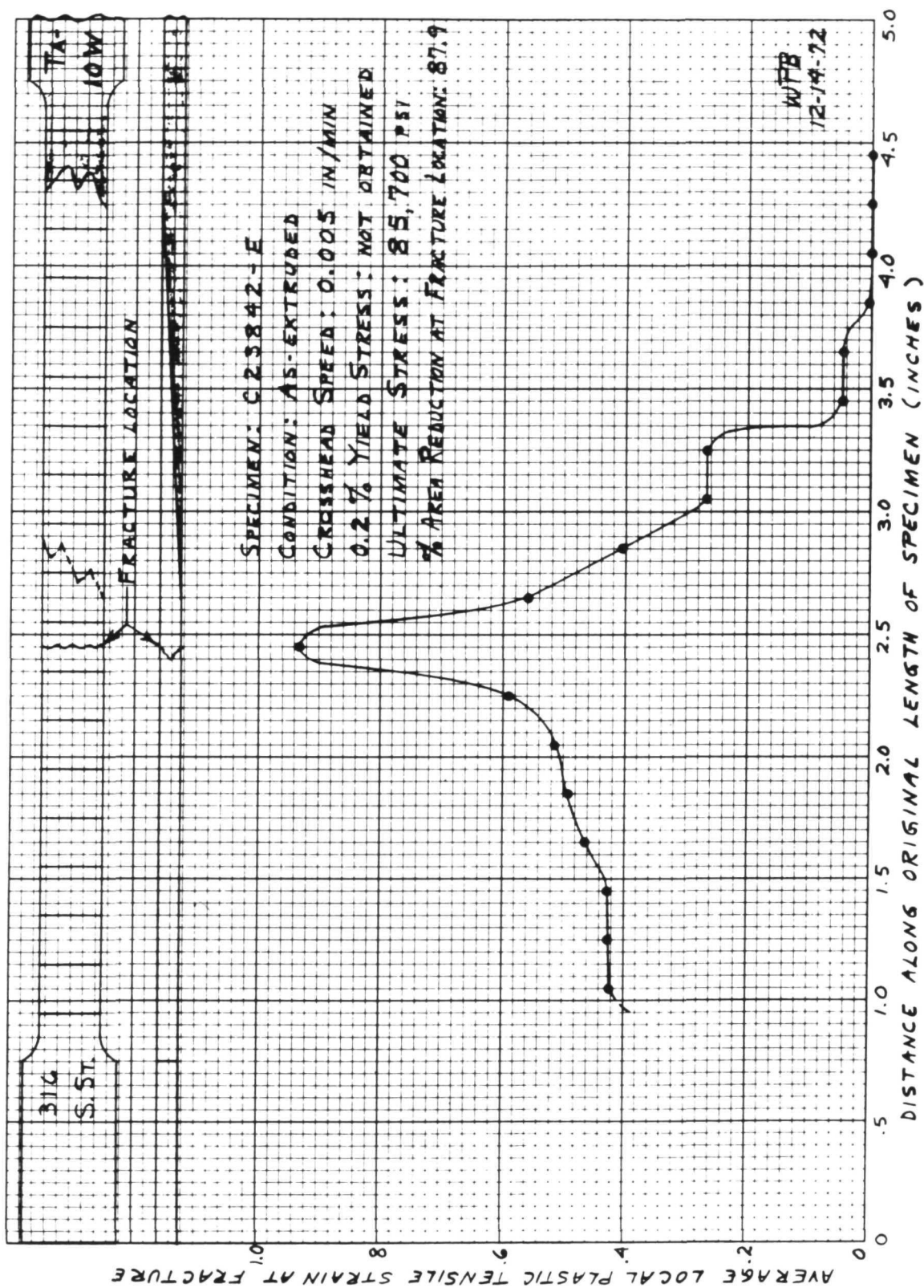Figure VI-5. Bimetal Joint Tensile Specimen No. C23842-E

Figure VI-6. Results of Tensile Test on As-Received Specimen No. C23842-E
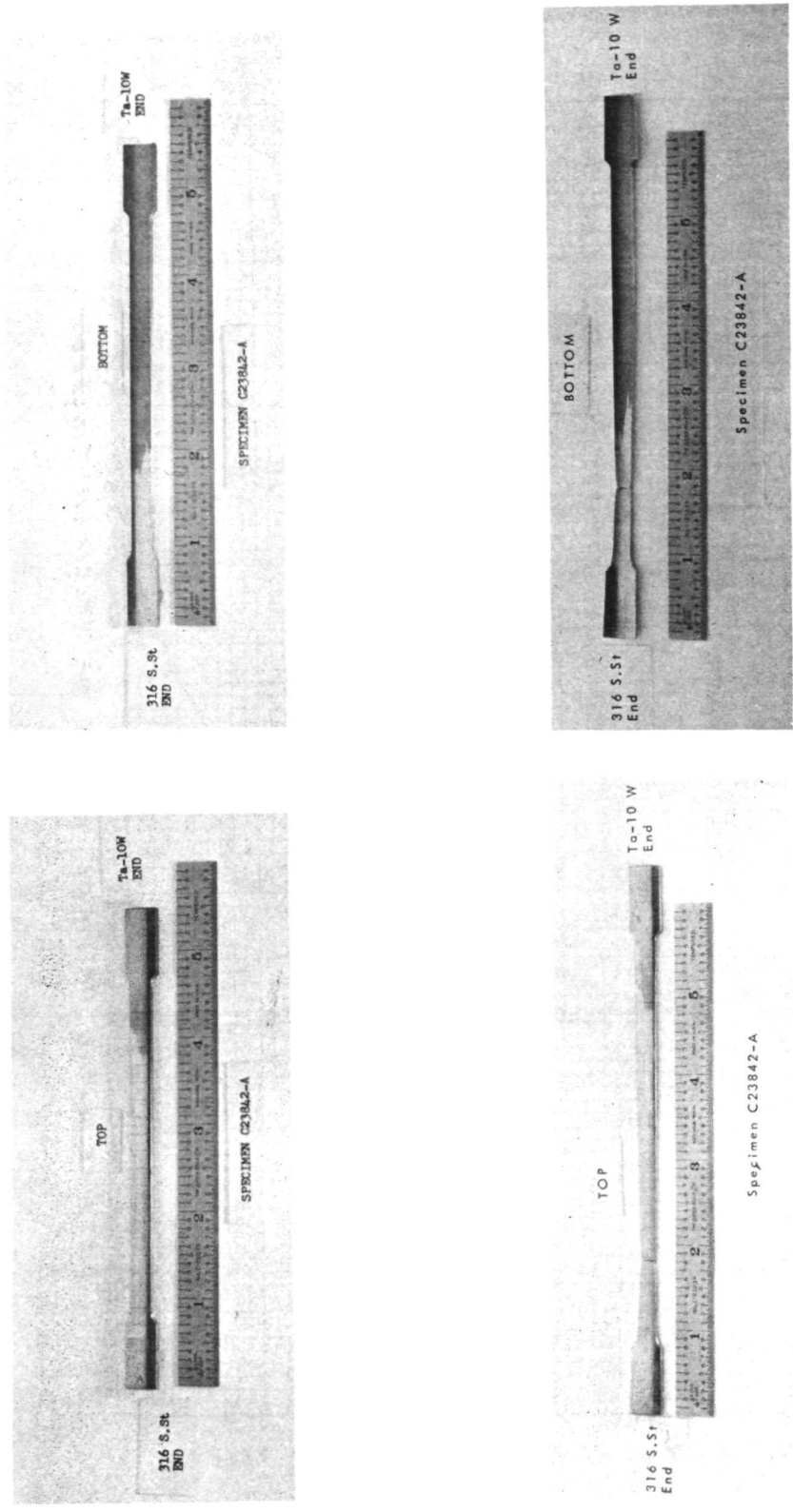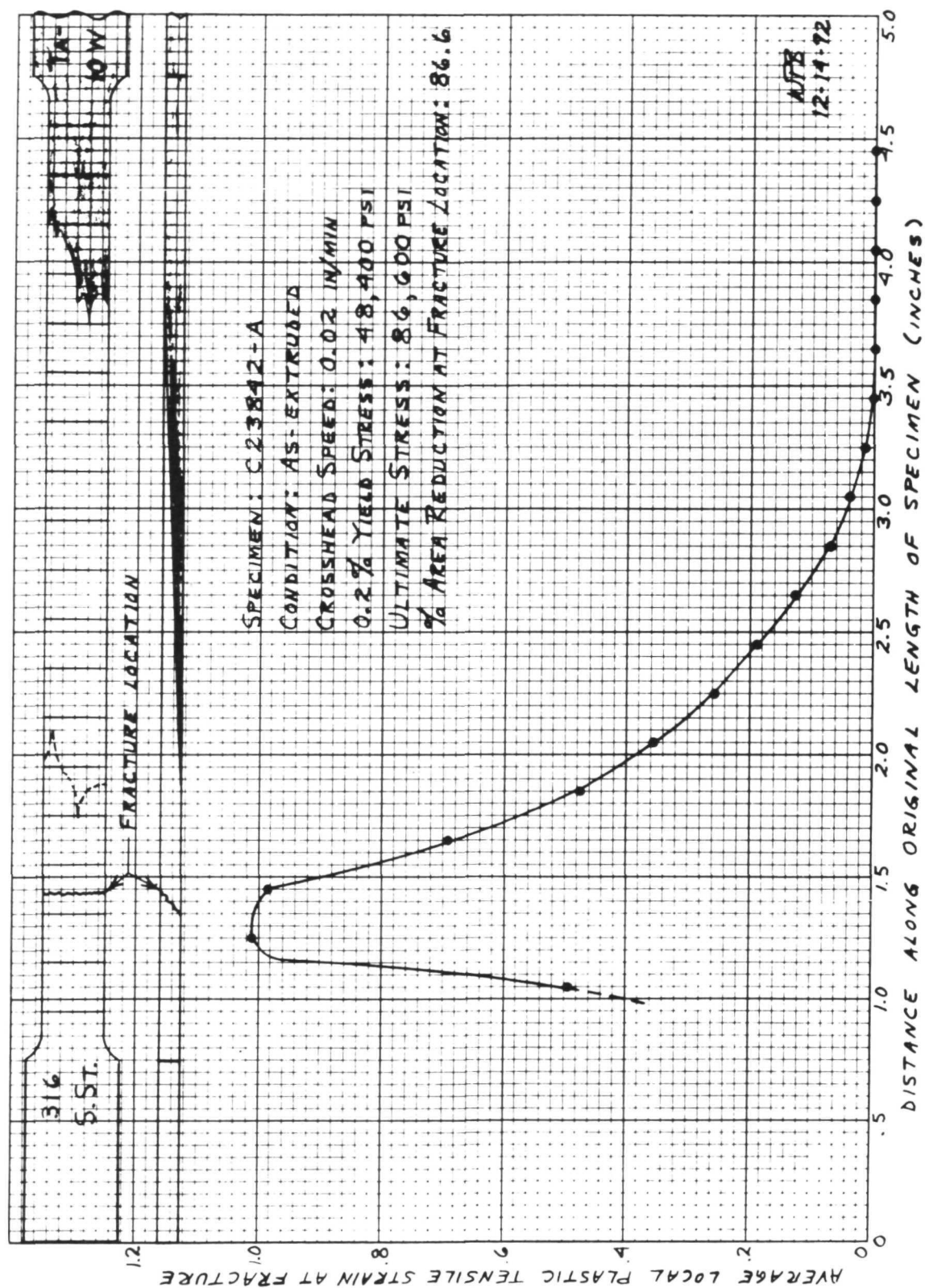
Figure VI-7. Bimetal Joint Tensile Specimen No. C23842-A

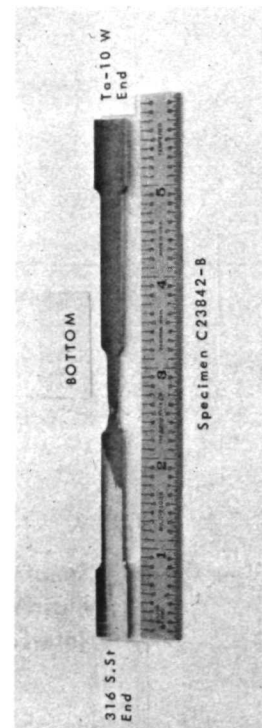Figure VI-8. Results of Tensile Test on As-Received Specimen No. C23842-A

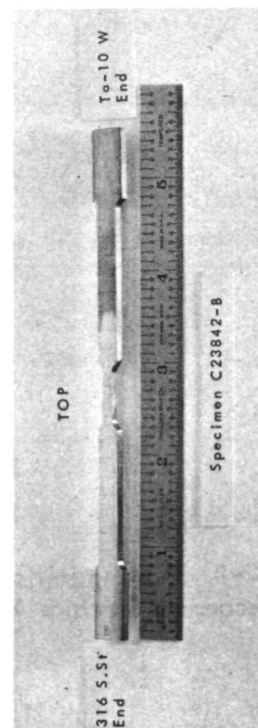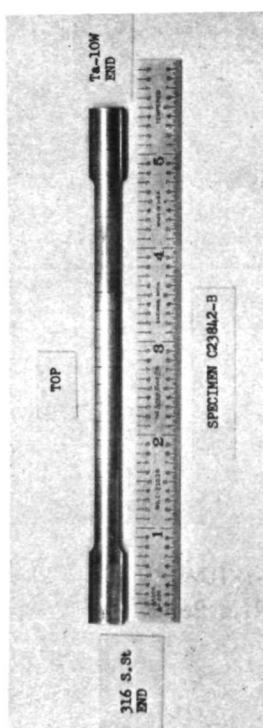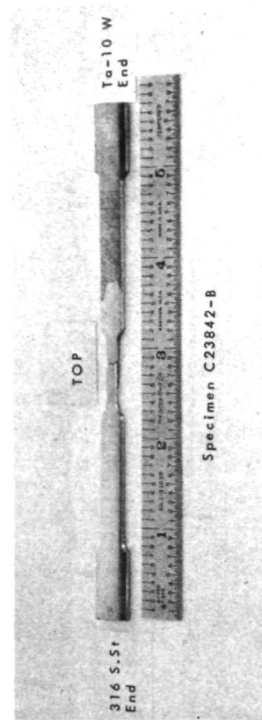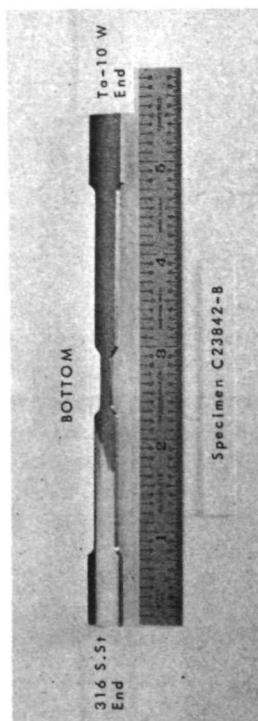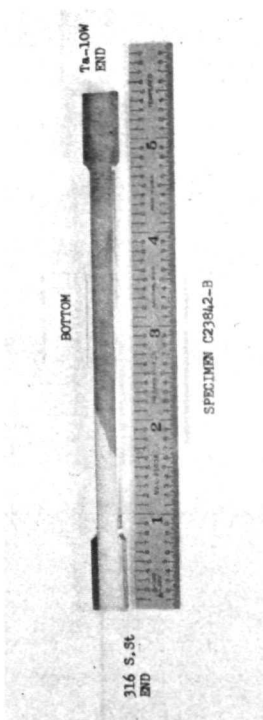Figure VI-9. Bimetal Joint Tensile Specimen No. C23842-B,
Constrained to Fail in Intermetallic Bond Region

b. As deformation continued, yielding of the 316 stainless steel was able to accommodate the displacement in that material, but the intermetallic bond itself (which is less ductile than the stainless) could only accommodate the displacement by a slow propogation of the initial fracture along the bond interface. This condition can also be seen in Figure VI-10.

c. When fracture along the bond interface reached approximately the midpoint of the joint, propogation ceased. The remaining test displacement was accommodated by yielding of the 316 stainless steel in the region of bond fracture, finally terminating in fracture of that material. The plastic strain distribution and other data for this test are shown in Figure VI-11.

Two important conclusions were drawn from the results of the above tests. First, when the base metal and intermetallic bond regions are equally stressed, fracture occurs in the stainless steel rather than in the bond region along the bond interface. Second, even if the joint is stressed in such a way that failure must occur in the bond region, the principal failure mode is a tensile-type fracture in the Ta-10W side of the bond interface rather than a delaminating-type fracture along the interface. It thus appears that, in the as-received (extruded) condition, preferential mechanical failure along the inter-metallic bond interface does not occur, and the as-received Ta-10W/316 SS joint must be considered satisfactory from the mechanical property viewpoint.

A Varian ion-pumped ultrahigh vacuum furnace with split-can tantalum heaters was fitted with a cam-type temperature controller and set up for thermally cycling the bimetal joint specimens. The ultrahigh vacuum environment was judged necessary to avoid contamination of the Ta-10W specimen portion with the interstitial impurity elements (C, N, O) which are commonly found in lower-quality vacuum atmospheres and which are known to severly affect the mechanical properties of refractory metals at concentrations as low as a few hundred ppm.
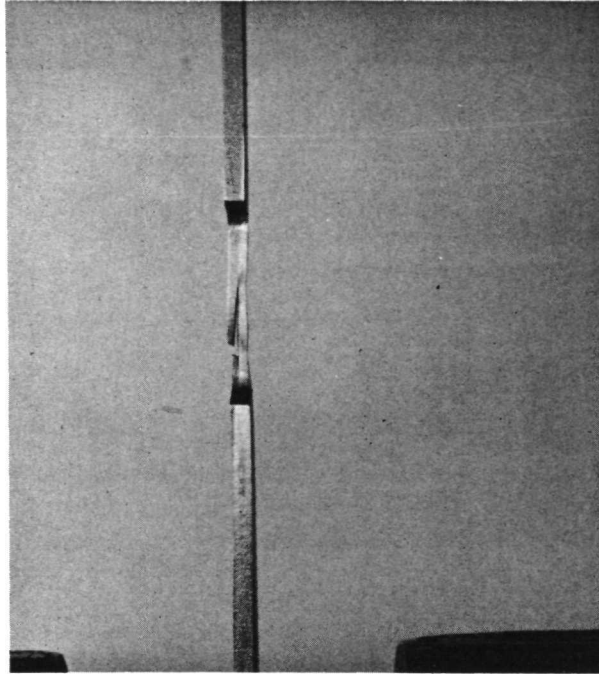
Figure VI-10. As-Received Tensile Specimen No. C23842-B, Showing Initial Fracture in Ta-10W
Plus Propogation of Secondary Fracture along Intermetallic Bond Interface
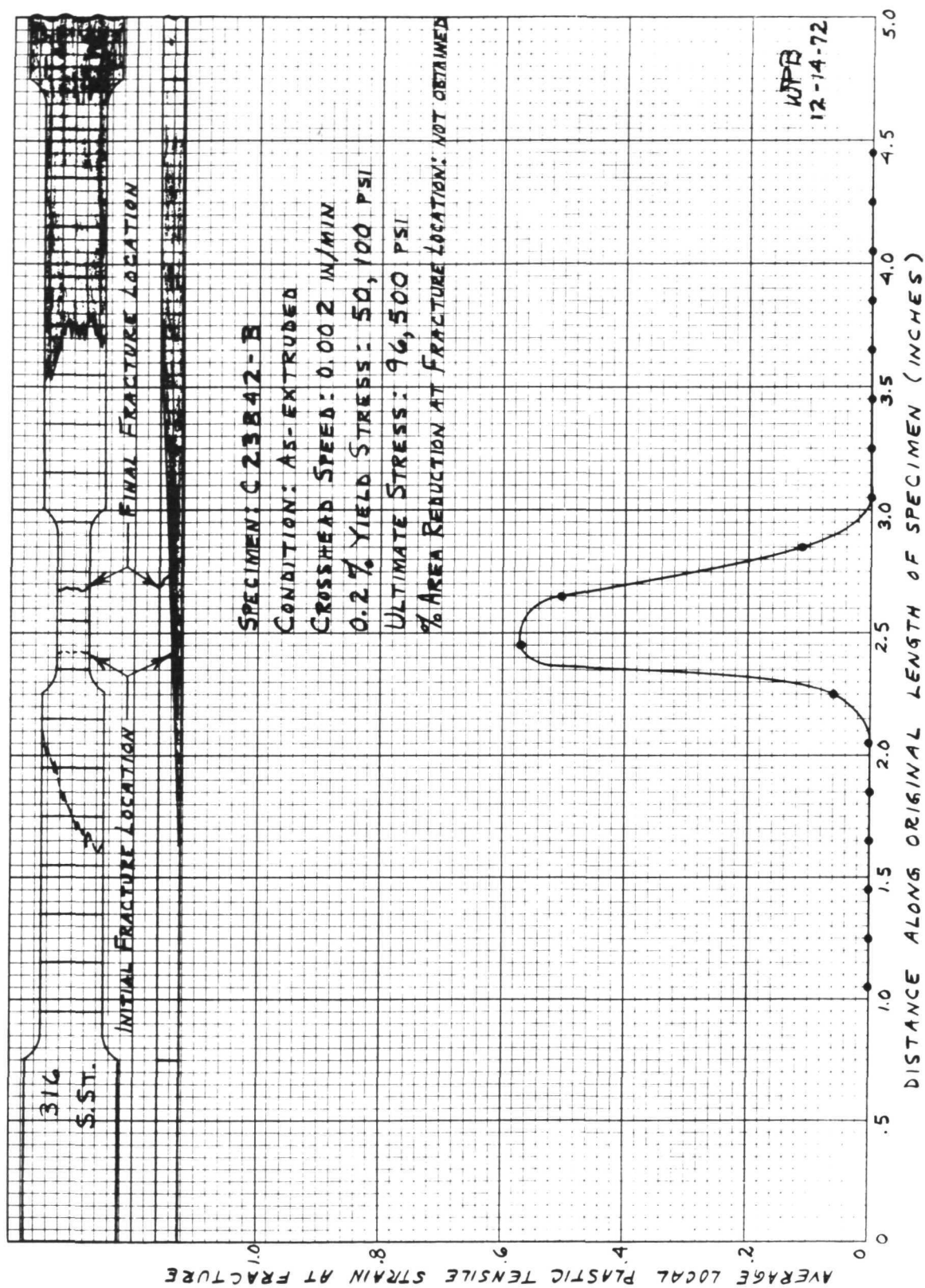
Figure VI-11. Results of Tensile Test on As-Received Specimen No. C23842-B

SPECIMEN: C23842-B
CONDITION: AS-EXTRUDED
CROSSHEAD SPEED: 0.002 IN/MIN
0.2% YIELD STRESS: 50,100 PSI
ULTIMATE STRESS: 96,500 PSI
% AREA REDUCTION AT FRACTURE LOCATION: NOT OBTAINED

DISTANCE ALONG ORIGINAL LENGTH OF SPECIMEN (INCHES)

AVERAGE LOCAL PLASTIC TENSILE STRAIN AT FRACTURE

INITIAL FRACTURE LOCATION
FINAL FRACTURE LOCATION
316 S.ST.

WPB
12-14-72

To permit precision profiling of the controller cam to give the desired time-temperature cycle configuration, setup tests were made using a stainless steel dummy specimen and later the bimetal joint specimen which had exhibited unbonding indications during ultrasonic testing in the as-received condition. Grit blasting of the outer specimen surfaces was found necessary to increase the specimen emissivity to a value which permitted achievement of the desired $16.7C^{\circ}/min$ cooling rate. Instrumentation consisted of one control thermocouple, located at the axial center of the intermetallic bond region, and three monitoring thermocouples distributed along the specimen length. Pressure was measured with an ionization gage. The specimen was held in the furnace hot zone by a tungsten wire hanger threaded through two small holes drilled through the tube wall at the Ta-10W end.

Specimen C23840, which had exhibited unbonding indications during ultrasonic testing in the as-received condition, was installed in the furnace and subjected to 50 thermal cycles. It was then removed from the furnace and ultrasonically tested; unbonding indications of greater severity than in the as-received case were obtained. Helium leak testing indicated no apparent defects, but some liquid penetrant indications were obtained on the inner surface. Inner and outer diameter profile measurements were then made, and the averaged results are plotted in Figure VI-12 together with similar data representing the as-received condition. It is doubtful that the dimensional changes shown, which are at most .0004 inch diametral variations, are of any significance with respect to the physical/mechanical condition of the bimetal joint; most of the indicated changes are within the limits of error of the measuring and averaging technique (+ .00015 inches).

Specimen C23841 was then randomly selected from the remaining group of defect free joints, installed in the furnace and subjected to 50 thermal cycles during which the pressure typically varied from 2×10^{-8} torr at $260^{\circ}C$ to 5×10^{-7} torr at $593^{\circ}C$. The actual time - temperature cycle configuration for this test is shown in Figure VI-13. The specimen was then removed from the furnace and ultrasonically tested, with some unbonding indications being obtained. Helium leak testing and liquid penetrant inspection indicated
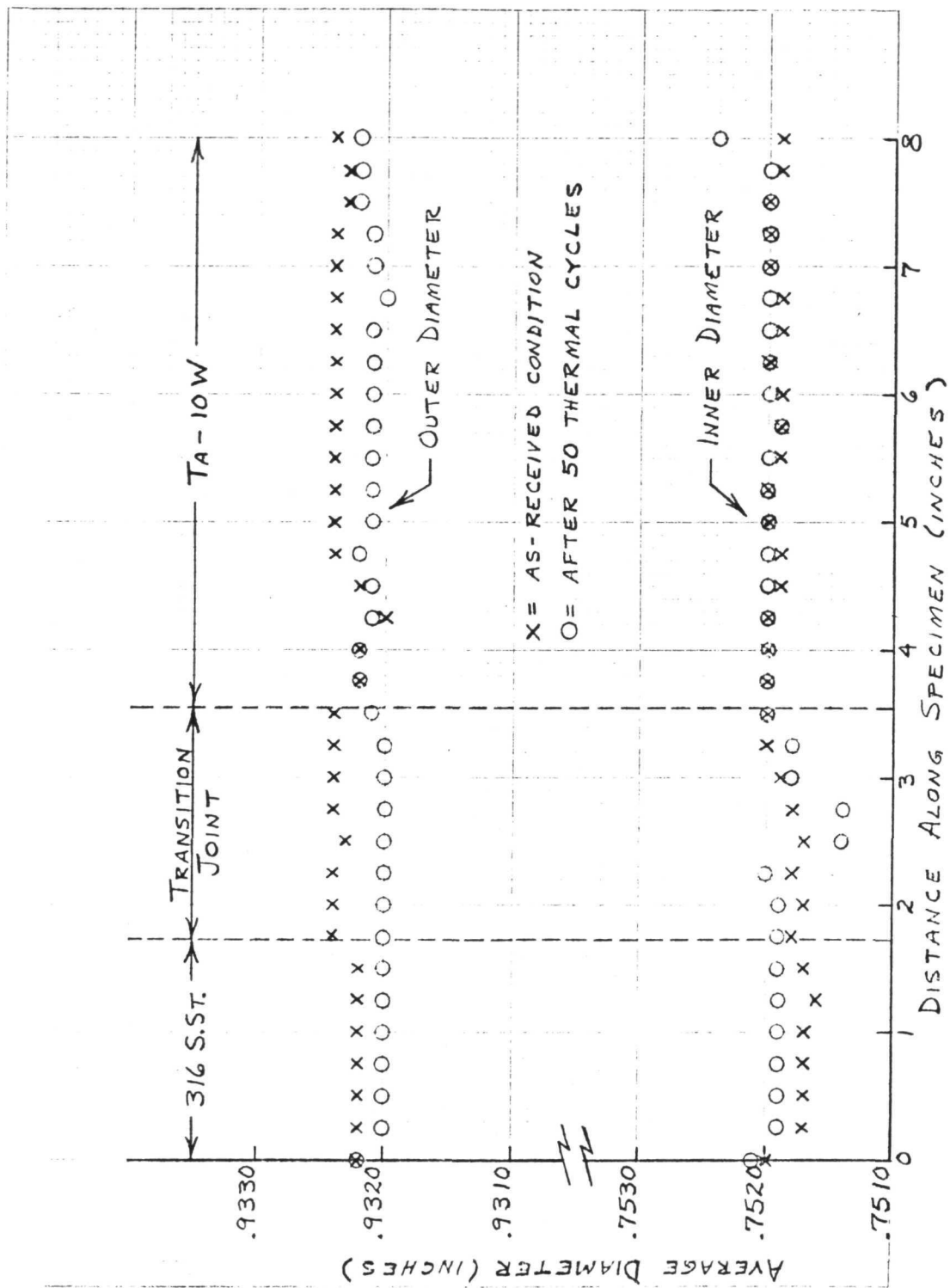
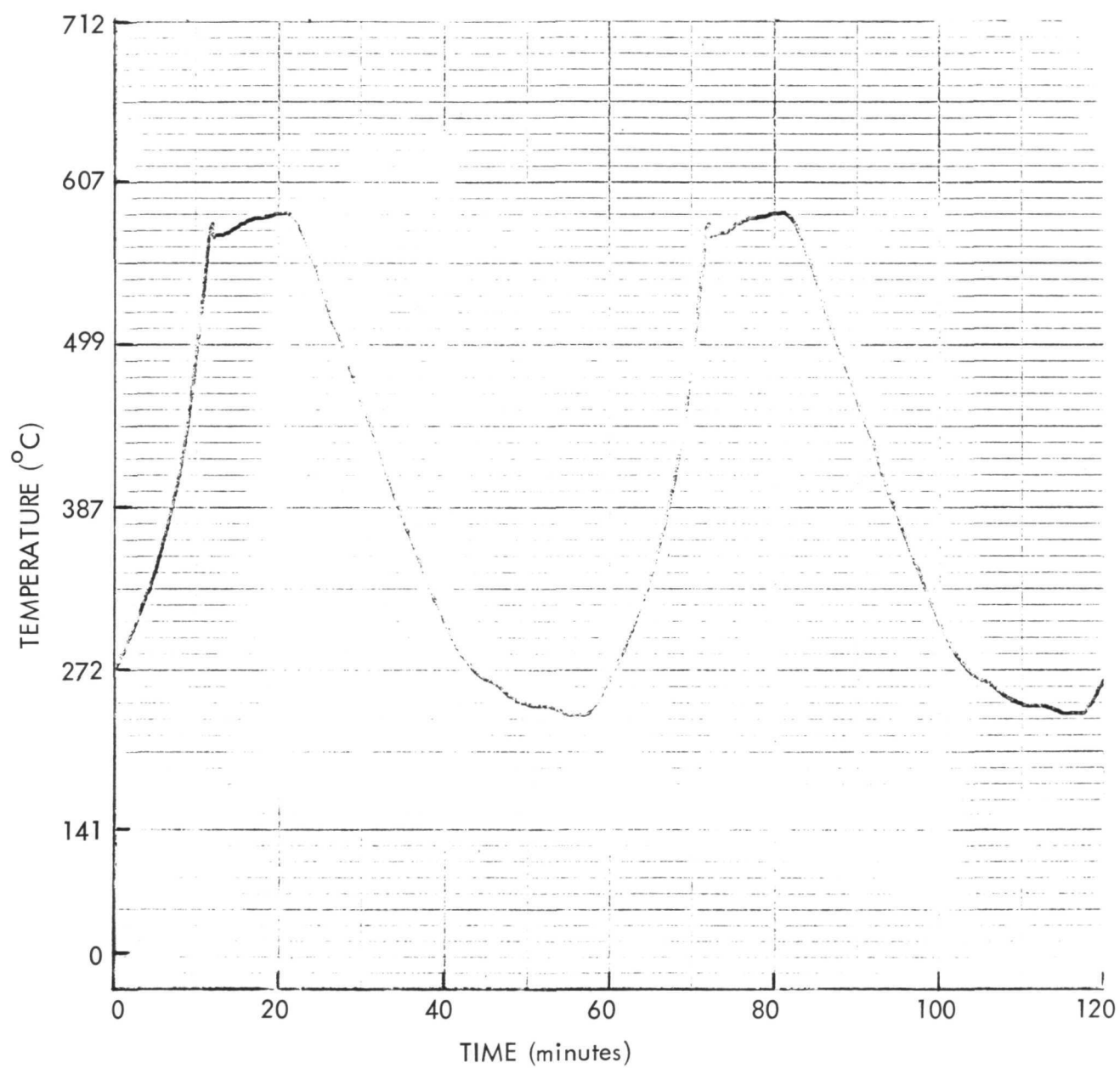Figure VI-12. Average Diameter Profiles for Bimetal Joint Specimen No. C-23840

Figure VI-13. Temperature-Time Configuration of
Bimetal Joint Thermal Cycle Tests

no apparent defects. After measuring inner and outer diameter profiles the specimen was cleaned, reinstalled in the furnace and subjected to a second set of 50 thermal cycles which was identical to the first set. It was again nondestructively tested, with results similar to those obtained after the first 50 cycles, and diameter profile measurements were repeated. The averaged diameter data is plotted in Figure VI-14, which again indicates that no significant dimensional changes occur in the bimetal clad due to thermal cycling.

C23841 was then machined into five tensile specimens, two of which were cut down to force failure to occur in the intermetallic bond portion as previously described. Two regular and two cut-down specimens were then tensile tested at room temperature. Figures VI-15 and VI-16 show the plastic strain distributions and other test results for the two regular specimens (C23841-C and -E), whose tests differed only in the strain rates used. Both specimens fractured in their stainless steel portions, well removed from the intermetallic bond region and quite similarly to the fracturing of as-received specimens as previously described (see Figures VI-5 through VI-8). This indicates that no significant embrittlement of the intermetallic bond (or of the Ta-10W) occurred during thermal cycling, and also that no fissures (cracks) were produced near the intermetallic bond as seen in somewhat similar joints in another study[1]; such fissures, if present, would propogate into total fractures under the tensile test loading. The yield stress values obtained for the regular specimens are sufficiently close to the previously obtained as-received values to indicate that thermal cycling does not strain harden the stainless steel.

The microstructure of the regular specimens along the intermetallic bond is shown in Figure VI-17, together with comparative photomicrographs of Specimen C23841-B which was not tensile tested. These pictures show that only at the extreme tip of the bond region, at the 316 end, does the stainless steel grain structure begin to exhibit the elongated, strained appearance characteristic of the deformation produced by uniaxial loading; the grains are equiaxed and deformation-free along the entire remainder of the bond region. It thus appears that, under axial loading, the intermetallic bond is "screeened" from any

[1] D. R. Stoner, "Evaluation of Tantalum/316 Stainless Steel Transition Joints", NASA CR-121111, December, 1972.
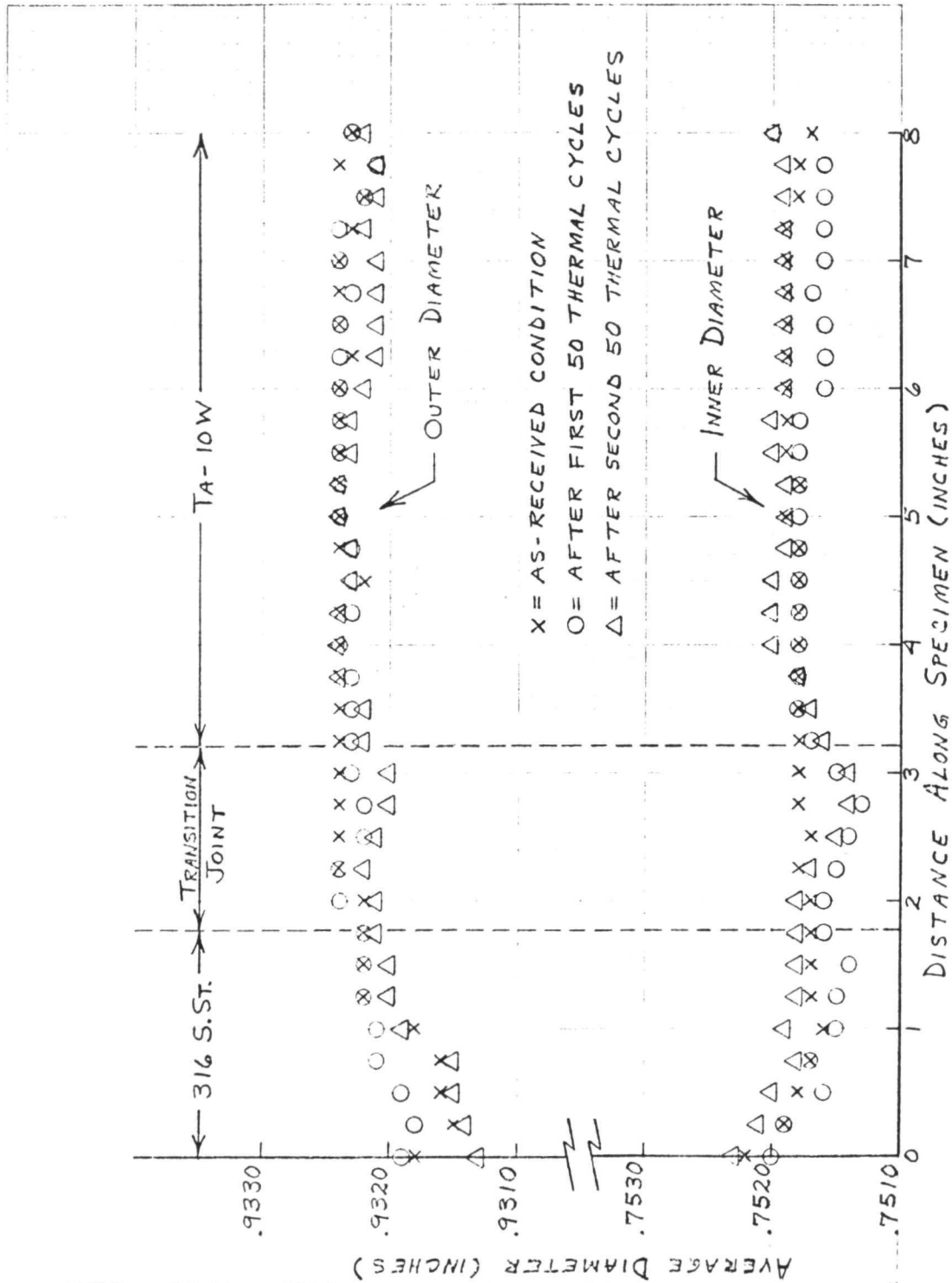
Figure VI-14. Average Diameter Profiles for Bimetal Joint Specimen No. C23841
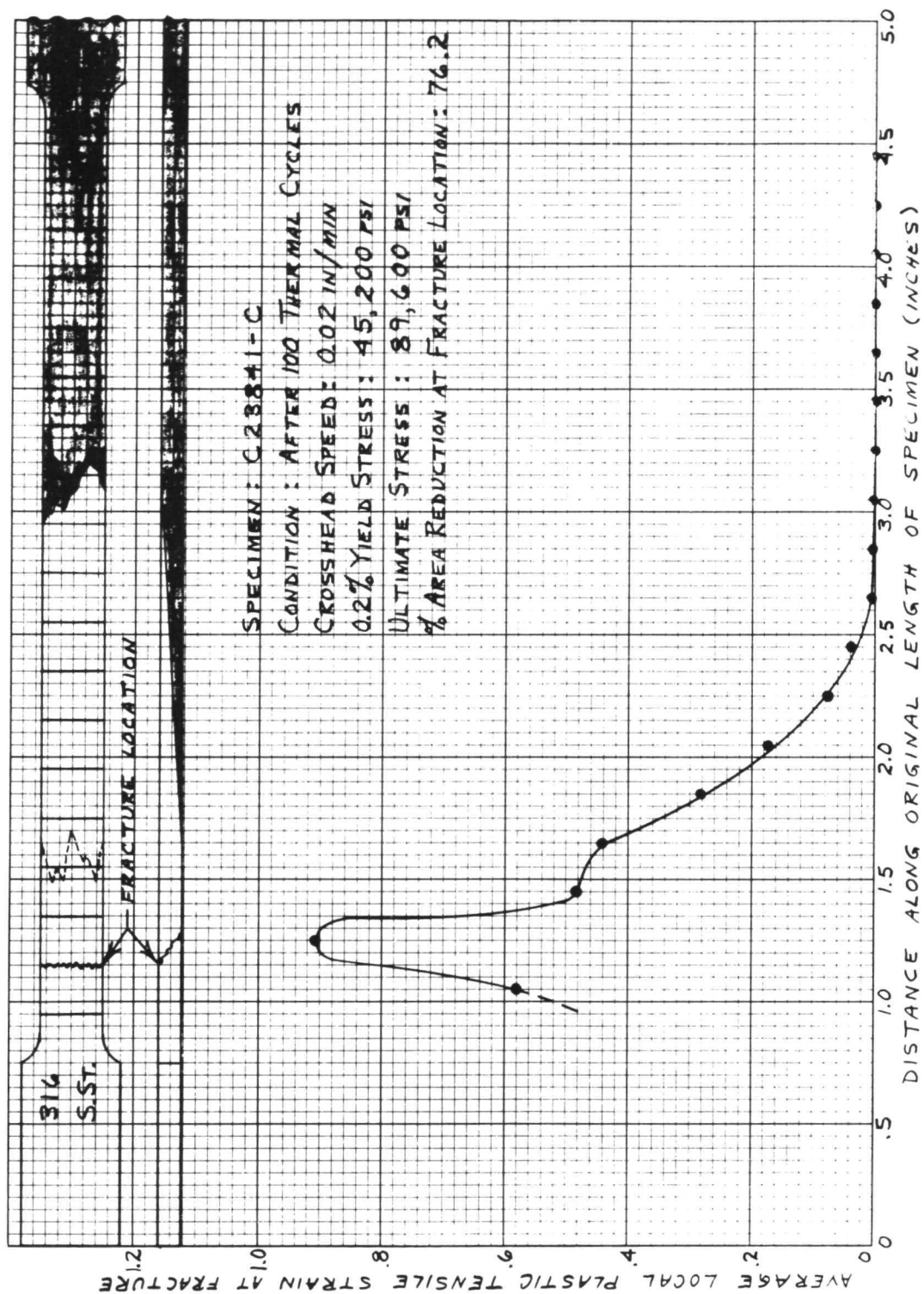
Figure VI-15. Results of Tensile Test on Thermally Cycled Specimen No. C23841-C

Specimen: C23841-E

Condition: After 100 Thermal Cycles

Crosshead Speed: 0.1 in/min

0.2% Yield Stress: 40,200 psi

Ultimate Stress : 87,900 psi

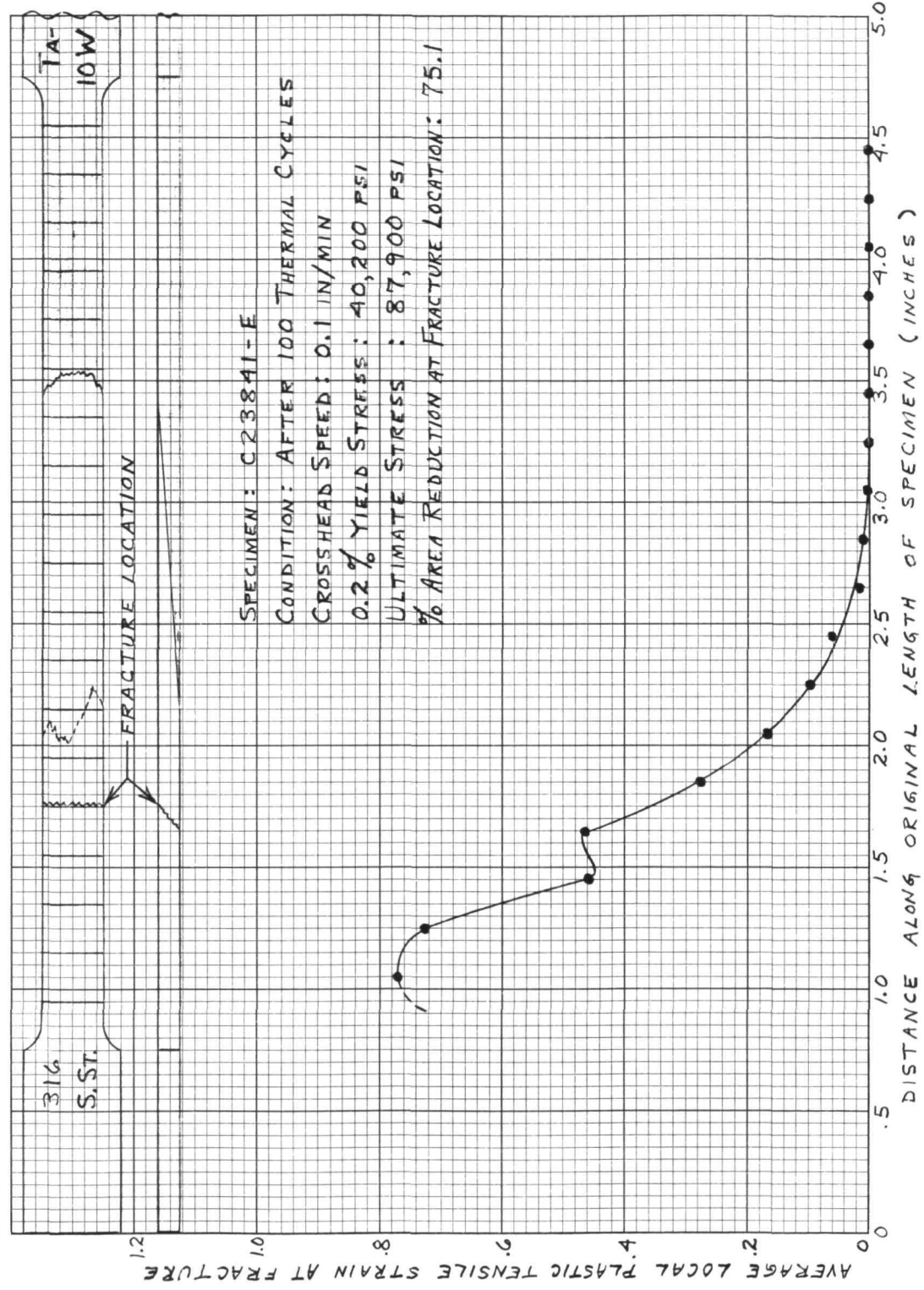% Area Reduction at Fracture Location: 75.1

Figure VI-16. Results of Tensile Test on Thermally Cycled Specimen No. C23841-E
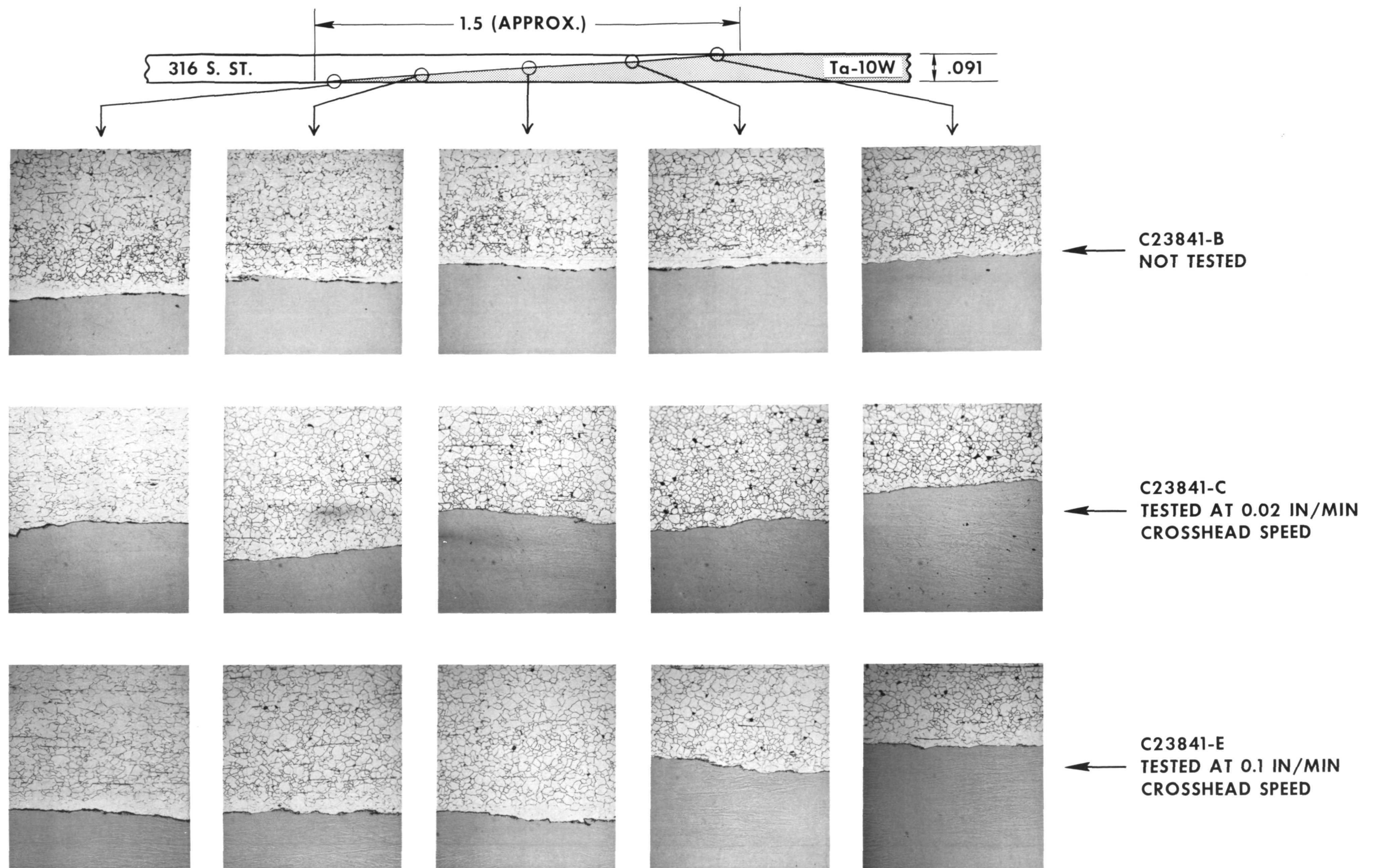
Figure VI-17 Microstructure at Intermetallic Bond Interface of Thermally Cycled
Tensile Specimens not Fractured in Bond Portion – Etched to Exhibit 316 Grain Structure .200 x
(Reduced 60 Percent for Reproduction)

significant deformation by yielding and eventual fracture in the bulk 316 stainless steel portion, and that this situation is not altered by the effects of 100 thermal cycles.

The plastic strain distribution and other test results for cut-down specimen C23841-D are shown in Figure VI-18, and photographs of the specimen before, during and after testing are displayed in Figure VI-19. C23841-D was tested at a crosshead speed selected to give about the same strain rate in the cut-down section as that used in testing regular specimen C23841-C. The failure sequence for this specimen was as follows:

a. Tensile-type fracture in the 316 stainless steel along a plane of maximum shear stress (see center photograph of Figure VI-19).

b. Yielding of the 316 to accommodate continuing deformation, together with slow propogation of the initial fracture in both directions along the bond interface.

c. Final tensile-type fracture in the Ta-10W (see right-hand photograph of Figure VI-19).

This differs from the failure sequence of as-received cut-down specimen C23842-B, described previously, in two respects. First, the initial fracture in this case was in the 316 rather than the Ta-10W; and second, the extent of yielding and secondary fracture propogation along the intermetallic bond interface is much less here than in the as-received specimen.

The microstructural appearance of the fracture area is shown in the upper half of Figure VI-20. The extent of heavy deformation in the 316 is seen to approximately correspond to the extent of secondary fracture propogation along the intermetallic bond interface. Beyond this point, the 316 structure is relatively equiaxed and deformation-free, as confirmed by comparison with the end photomicrographs of the grain structure far from the fracture location.

The corresponding data, photographs and photomicrographs of cut-down specimen C23841-A are shown in Figures VI-21, VI-22 and the lower half of VI-20. This specimen was tested at a crosshead speed five times higher than that used on C23841-D.
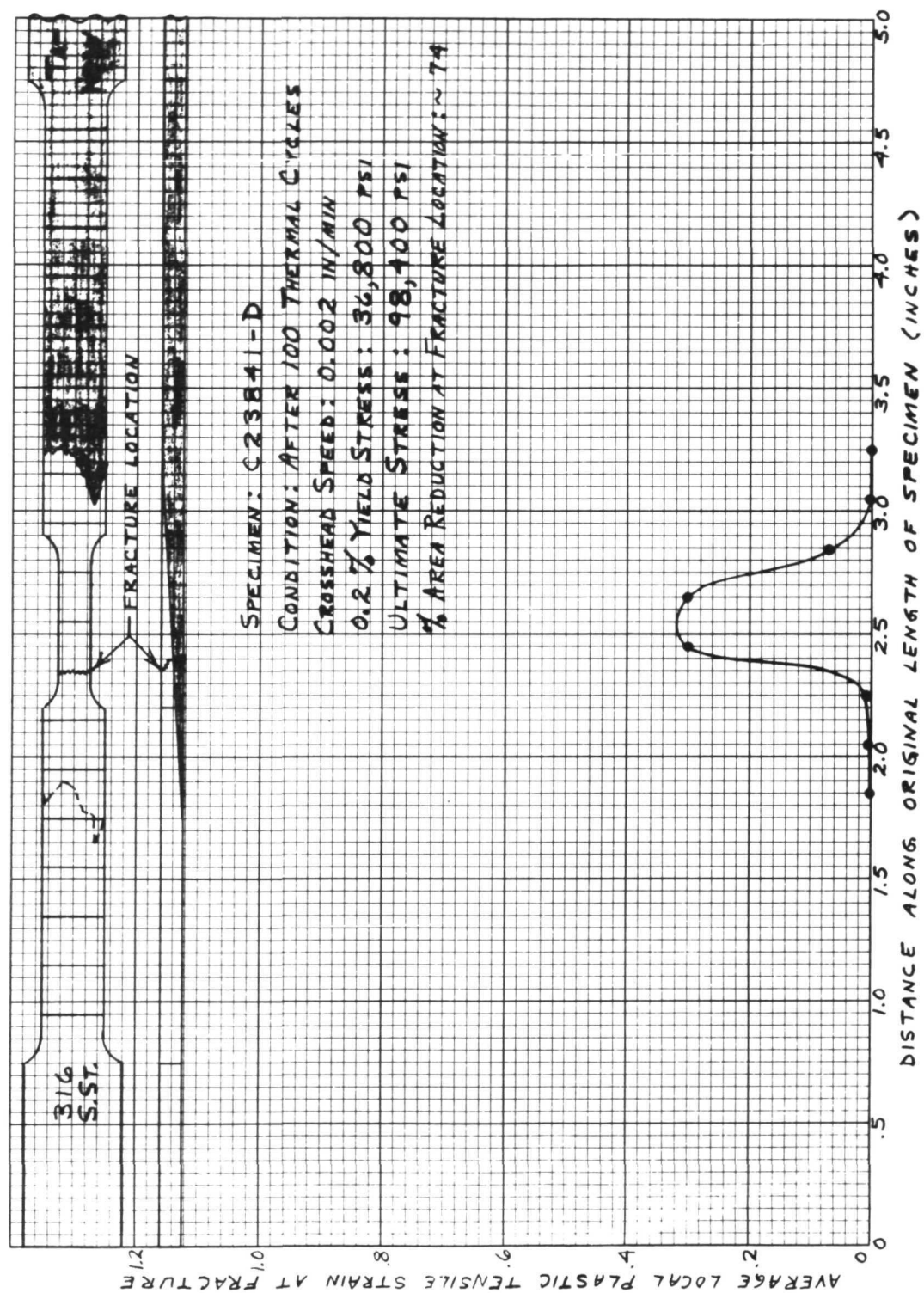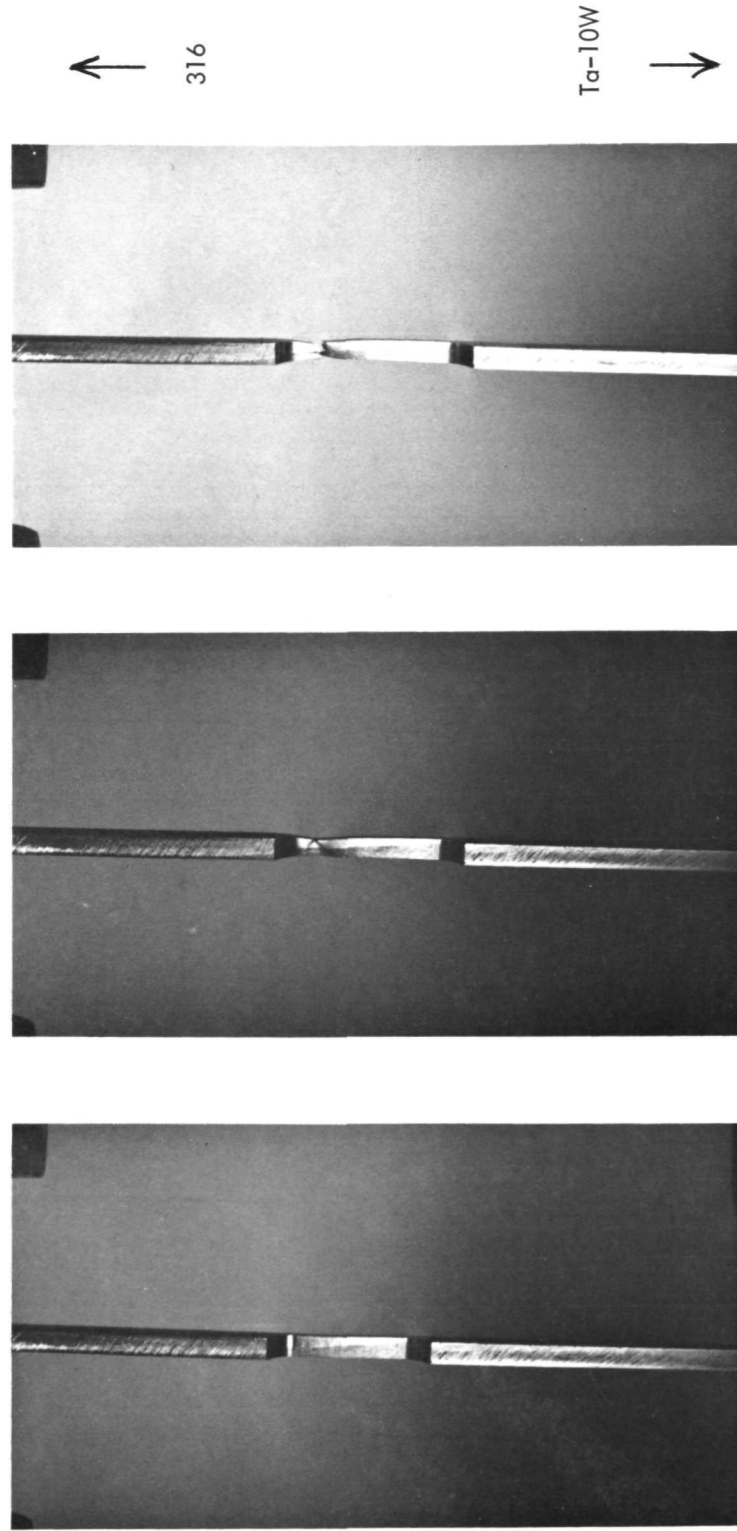
Figure VI-18. Results of Tensile Test on Thermally Cycled Specimen No. C23841-D

← 316

Ta-10W →

After Final Fracture on Ta-10W
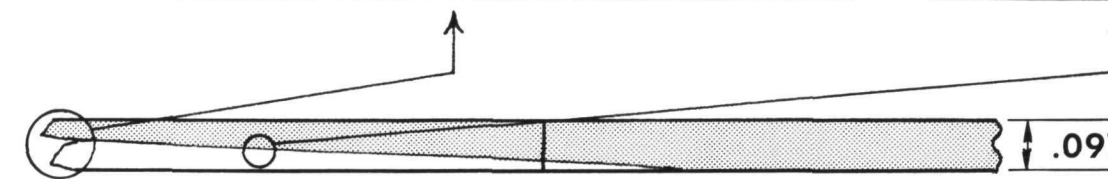Side of Intermetallic Bond.

Just Prior to Initial Fracture
Along Lower Maximum Shear
Plane on 316 Side of Intermetallic
Bond.

No Load.

Figure VI-19. Failure Sequence of Cut-Down Tensile Specimen No. C23841-D,
Tested at 0.002 In/Min Crosshead Speed

C23841-D
TESTED AT 0.002 IN/MIN
CROSSHEAD SPEED

316 S. ST.

.091

1.0

.125

Ta-10W

.250
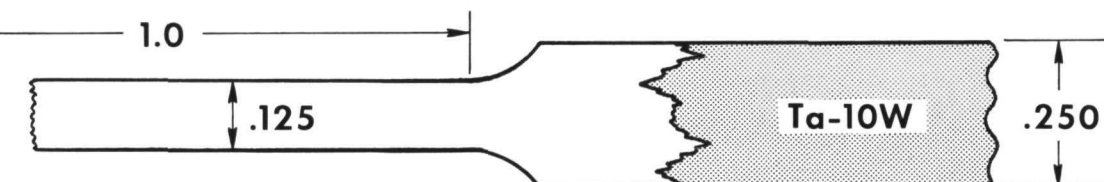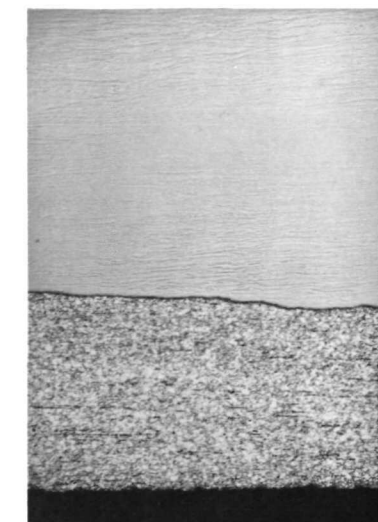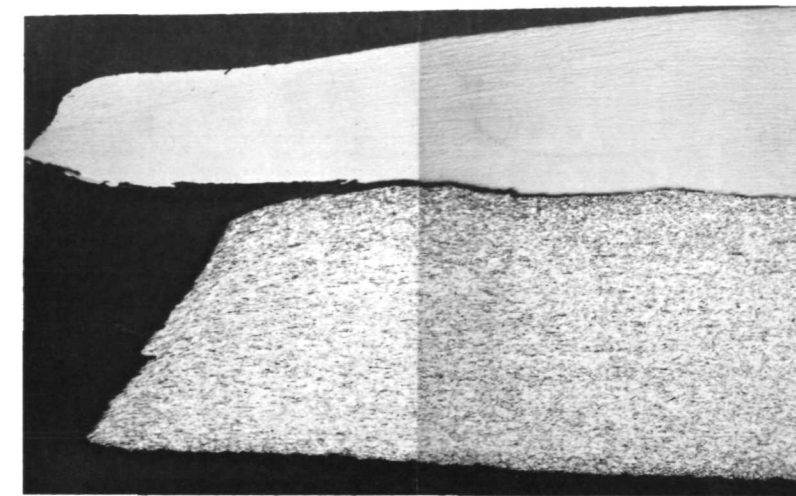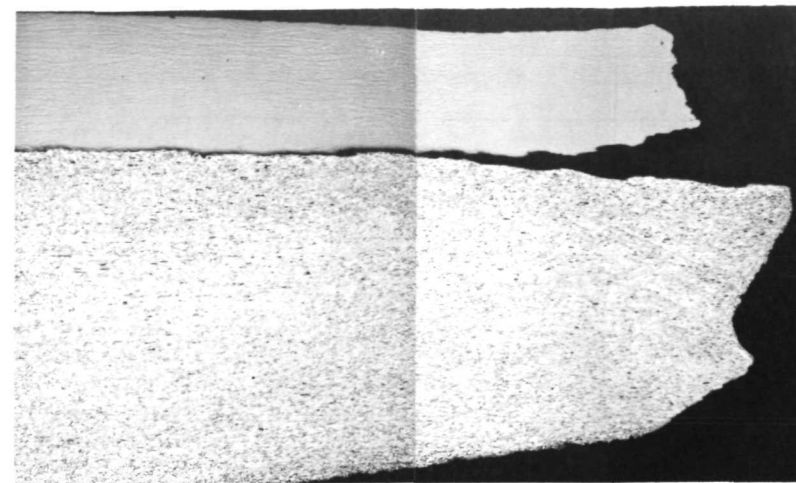
C23841-A
TESTED AT 0.01 IN/MIN
CROSSHEAD SPEED
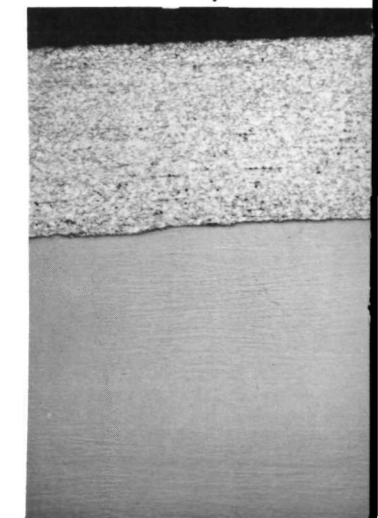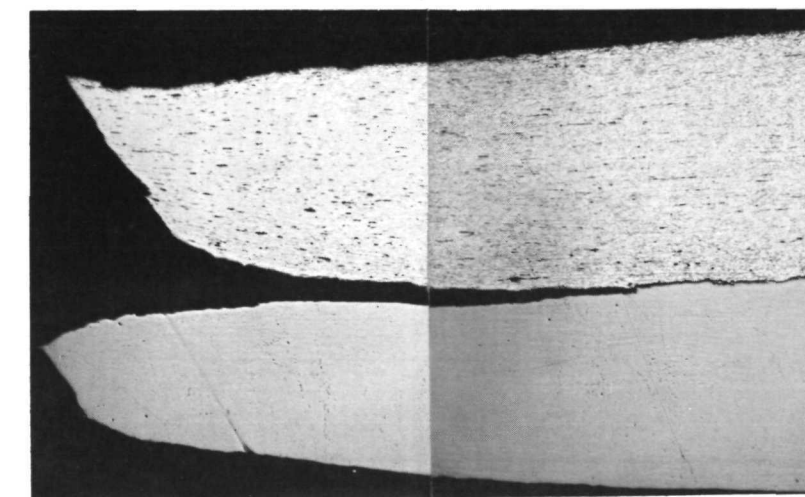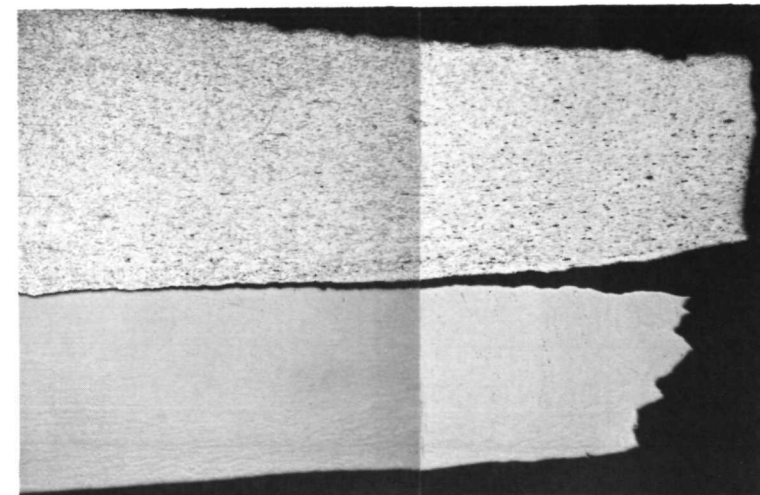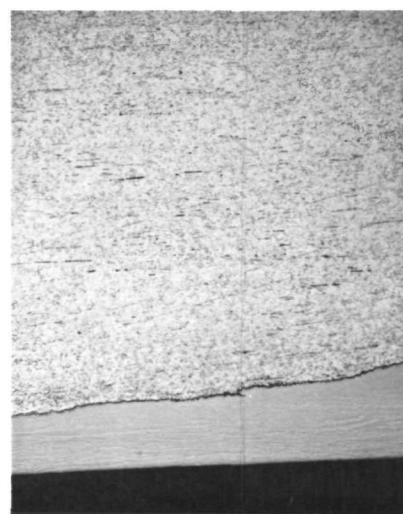
Figure VI-20. Microstructure at Fracture Location and Far from Fracture Location of Thermally Cycled Tensile Specimens Constrained to Fail in Intermetallic Bond Portion – Etched to Exhibit 316 Grain Structure 50 x (Reduced 60 Percent for Reproduction)

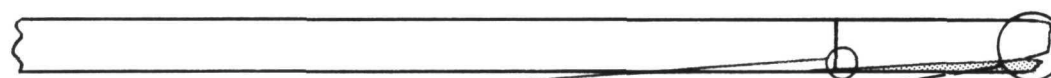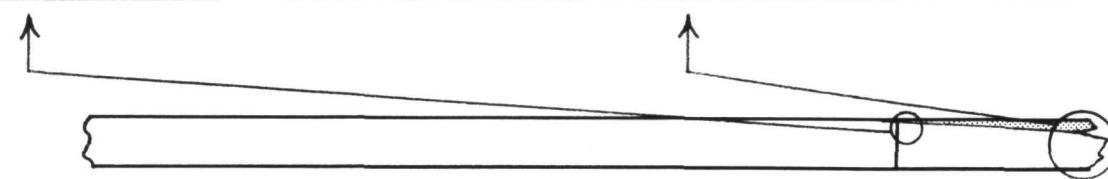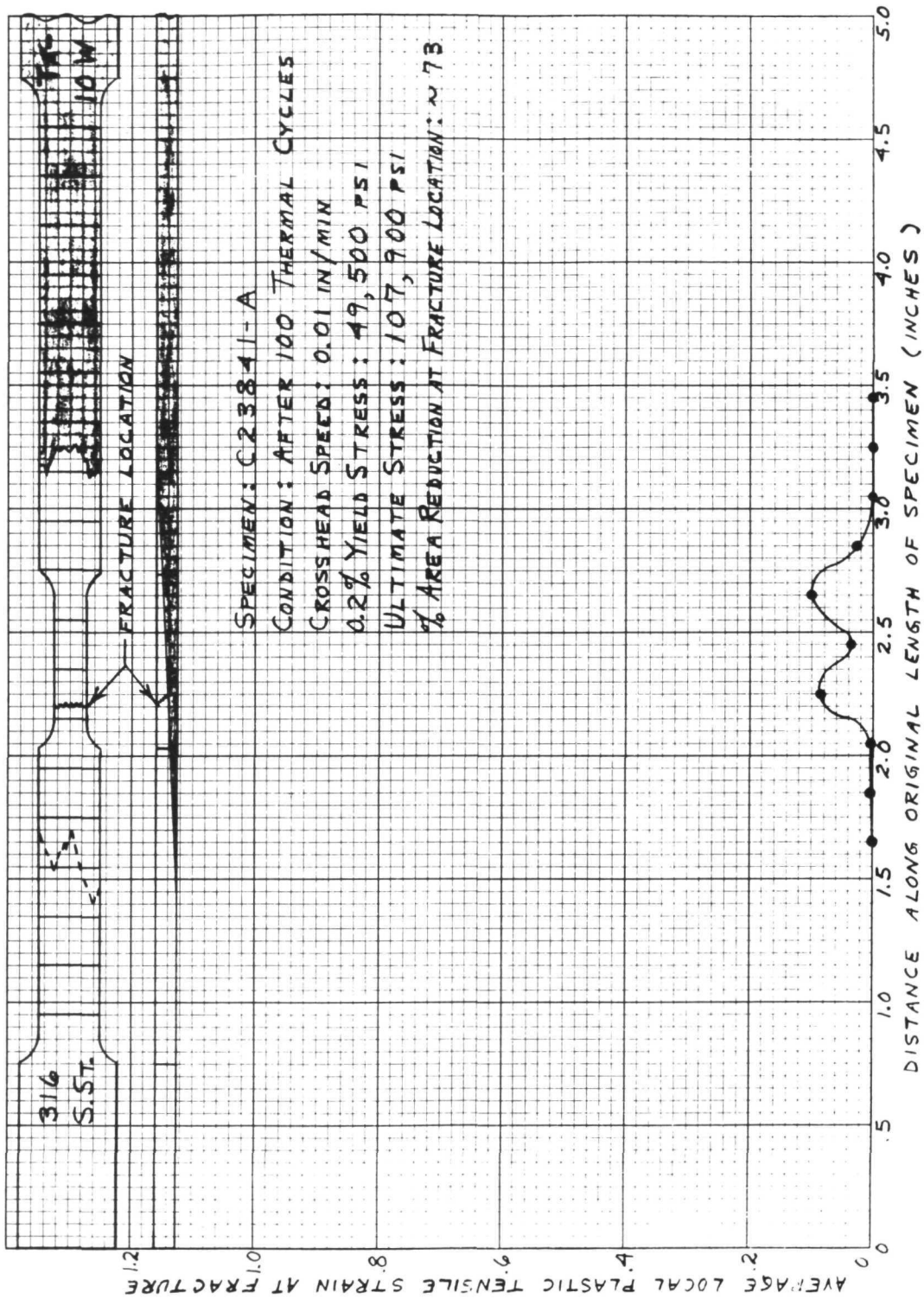Figure VI-21. Results of Tensile Test on Thermally Cycled Specimen No. C23841-A

Specimen: C23841-A
Condition: After 100 Thermal Cycles
Crosshead Speed: 0.01 in/min
0.2% Yield Stress: 49,500 psi
Ultimate Stress: 107,900 psi
% Area Reduction at Fracture Location: ~ 73

FRACTURE LOCATION

316 S.St.

DISTANCE ALONG ORIGINAL LENGTH OF SPECIMEN (INCHES)

AVERAGE LOCAL PLASTIC TENSILE STRAIN AT FRACTURE

316 ←

Ta–10W →

No Load

Just Prior to Initial Fracture

After Final Fracture

Figure VI-22. Failure Sequence of Cut-Down Tensile Specimen No. C23841-A,
Tested at 0.01 In/Min Crosshead Speed

Qualitatively, the various aspects of this specimen are similar to those of C23841-D.
The extent of heavy 316 deformation and secondary fracture propogation is about doubled
in this case, probably due to the increased strain rate. There is no ready explanation for
the curious double-peaked shape of the plastic strain distribution curve; it is probably
reasonable to suspect that an error was made in measuring the gage mark separation after
fracture.

The metallographically prepared sections of all five tensile specimens were
carefully examined at high magnification along the entire length of the intermetallic
bond layer. No evidence of bond separation or cracks in the base metals was seen (except,
of course, at the fracture locations in the cut-down specimens). Since these observations
were made on five planes equally-spaced around the circumference of the original specimen,
this casts further suspicion on the validity of the ultrasonic tests which indicated severe
unbonding conditions along the intermetallic region.

The principal conclusion drawn from the work in this section is that the
Ta-10W/316SS bimetal joint can survive 100 thermal cycles from 260 to 593°C at 16.7C°/
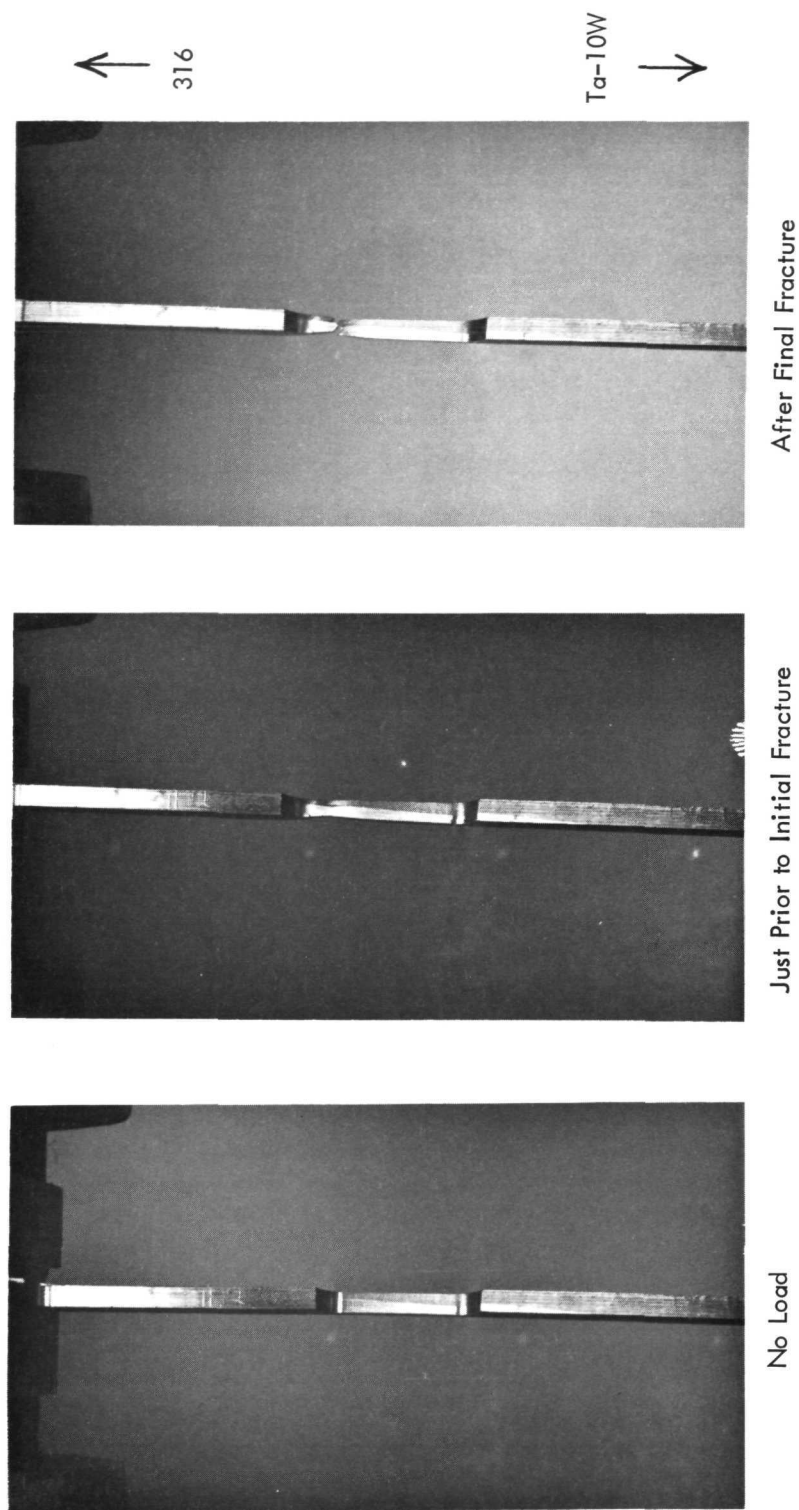min without suffering any significant dimensional, physical or mechanical changes or
damage. On this basis, then, the bimetal TEM-X inner clad is considered to be qualified
for cyclic operation under the given conditions.

4. Diffusional Growth of Intermetallic Bond Layer

It has been experimentally shown [1] that when metallurgical bonded refractory
metal/austenitic alloy combinations are exposed to elevated temperatures, the thickness
of the intermetallic bond layer increases due to solid state diffusion and reactions at the
bond layer/base metal interfaces. At a given temperature T, the growth process is conven-
iently described by the simple parabolic expression:

$$G(T,t) = K(T) \cdot t^{1/2}$$

[1] R. W. Buckman, Jr. and R. C. Goodspeed, "Evaluation of Refractory/Austenitic Bimetal
Combinations, "WANL-PR-(EE)-004, August, 1969, final report, Contract NAS-37634.

where　　　　$G(T, t)$ = increase in layer thickness (inches) due to exposure at temperature T for time t,

　　　　　　$K(T)$ = parabolic growth rate constant (in - hr$^{-1/2}$) at temperature T,

and　　　　　t = exposure time (hours).

The parabolic rate constant is generally assumed to obey the Arrhenius rate equation

$$K(T) = K_o \exp(-Q/RT)$$

where　　　　K_o = a constant (in - hr$^{-1/2}$),

　　　　　　Q = an "activiation energy" (calories/mole),

　　　　　　R = gas constant (1.987 cal/K^o - mole),

and　　　　　T = absolute temperature (^{o}K).

　　　　The reference work showed that when the bond layer thickness in these combinations reaches a value of order 12.7 μm (5×10^{-4} in), the bond becomes extremely brittle and the joint susceptible to failure under very small thermal stresses or applied loads. In view of this, it was of great importance to determine for the specific Ta-10W/316SS combination of the TEM-X inner clad the time required at the 650°C peak operating temperature for the bond layer thickness to reach the critical 12.7 μm value. (It should be understood that 12.7 μm is not a precisely defined value which holds with absolute validity for every conceivable refractory metal/austenitic alloy combination, but rather a rule-of-thumb type value obtained by consideration of results obtained on nine specific base metal pairs. In applying such a criterion to a high reliability thermoelectric system, a liberal margin of safety would of course be adopted. The best approach would obviously be to perform a series of diffusional growth/mechanical test experiments to define a unique critical value for the Ta-10W/316 SS combination of actual interest in the TEM-X program, but the amount of additional work involved to do this was beyond the support and schedular scope of this task.)

The particular combination studied in the reference work which was most similar to our Ta-10W/316 SS system was the system Ta/321 SS. The nominal compositions of the two stainless steels are:

316: 17 Cr-12 Ni - 2 Mn (max) - 1 Si (max) - .08C (max) - 2.5 Mo - bal. Fe

321: 18 Cr-10.5 Ni - 2 Mn (max) - 1 Si (max) - .08C (max) - (5 x C) Ti - bal. Fe

On the rather tenuous basis that at a given temperature diffusion coefficients tend to be smaller for higher melting point elements, it might be expected that interdiffusion would be somewhat slower in 316 systems (M.P. of Mo = 2610°C) than in 321 systems (M.P. of Ti = 1668°C), and similarly slower in Ta-10W systems (M.P. of W = 3410°C) than in pure Ta systems (M.P. of Ta = 2996°C). On this basis, intermetallic layer growth in our Ta-10W/ 316 SS system should be slower than in the Ta/321 SS reference system. However, diffusion in multicomponent systems is far too complicated a process to permit using reasoning of this type for drawing important conclusions without some specific experimental verification.

The parabolic growth rate constants measured for the Ta/321 SS reference system are plotted in Figure VI-23, from which it is seen that a serious problem existed in attempting to use this data for making estimates for this program. If the indicated slope change in the K(T) vs. 1/T curve is real, indicating a change in the rate controlling mechanism, and if a similar slope change occurred for our Ta-10W/316 SS system, as would be most reasonable to believe, then data from high temperature experiments (where large, easily-measured amounts of intermetallic layer growth could be obtained in relatively short times, greatly simplifying the experimental work) cannot be accurately extrapolated back to 650°C to give the sought-after K(650°C) vlaue. On the other hand, if one of the two end data points is in error and we arbitrarily choose one of the two branches to work with, then if we chose the incorrect branch we would be led far astray in making temperature choices and growth rate estimates. The approach which was taken is as follows:

      a.   Assumed that the Ta/321 SS reference data in Figure VI-23 is correct, that the slope change is real and that a similar slope change would occur in our Ta-10W/316 SS system.
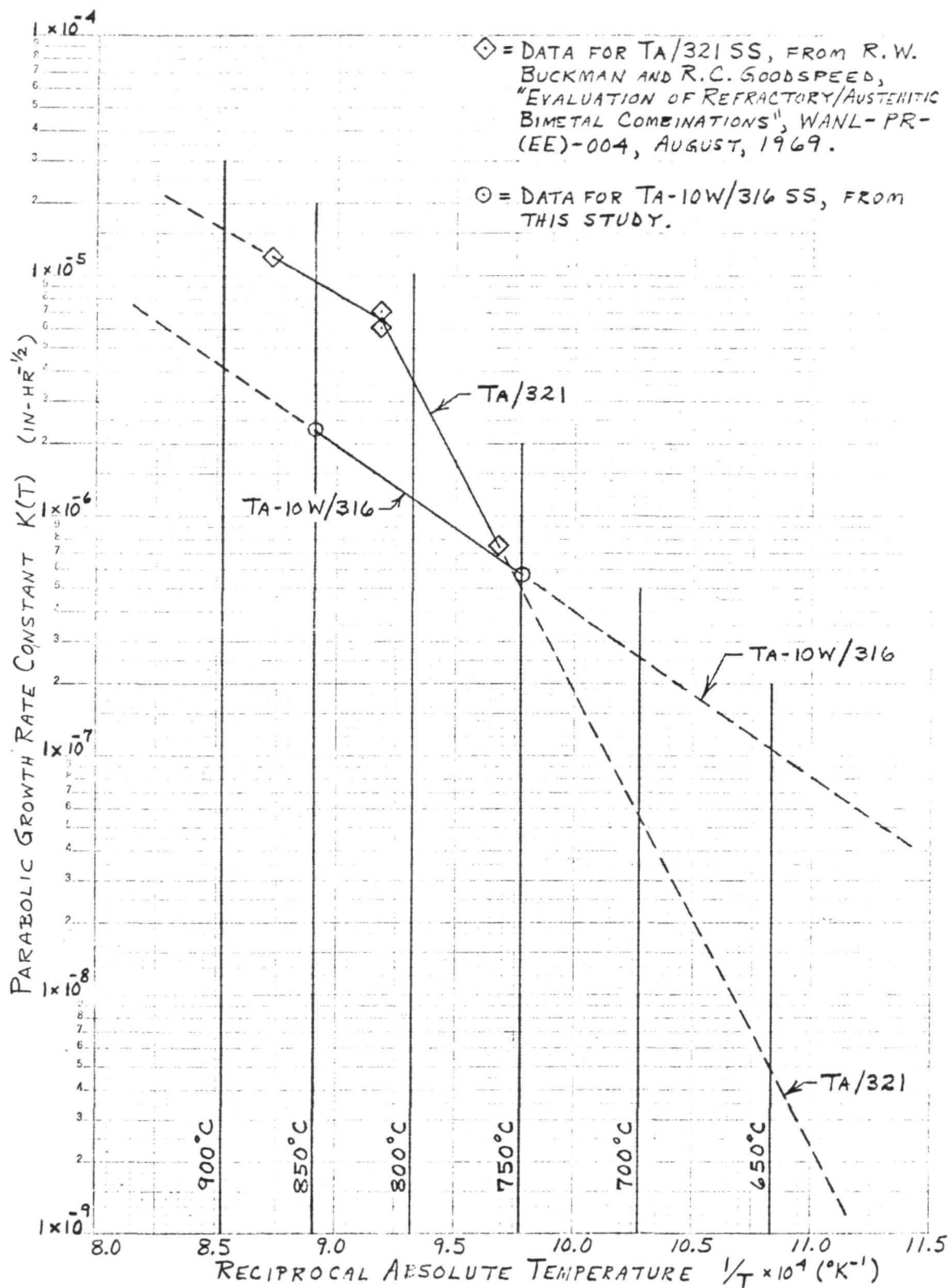
Figure VI-23. Parabolic Growth Rate Constant Versus Reciprocal Temperature for Intermetallic Bond Layer Growth in Ta/321 SS and Ta-10W/316 SS Bimetal Systems

b. Extrapolated the lower temperature branch of the Ta/321 SS reference curve back to 650°, yielding a K (650°C) value of 4.9×10^{-9} in $- hr^{-1/2}$. Calculated for this system that 44,000 hours of exposure at 650°C would produce 2.6×10^{-2} µm (1.03×10^{-6} in) of intermetallic layer growth. (This alone was a very encouraging result, as this is well over two orders of magnitude less than the 12.7 µm critical value, and we did not a priori expect the rate constants of the two systems to differ by as much as one order of magnitude.)

c. Calculated for the Ta/321 SS system that 100 hours of exposure at a temperature T* of 714°C would produce the same 2.6×10^{-2} µm of intermetallic layer growth that was predicted for 44,000 hours of exposure at 650°C.

d. Based on the above results, plus the fact that the slope change in the Ta/321 SS reference curve occurs at 816°C, selected the three temperatures 750, 800 and 850°C at which to experimentally measure the intermetallic layer growth rate in our Ta-10W/316 SS system. It was believed that this selection would (1) encompass the temperature of slope change in the Ta-10W/316 SS system, if any, and (2) permit an accurate extrapolation of the K(T) vs. 1/T curve back to 650°C to obtain the desired K(650°C) value for Ta-10W/316 SS.

Bimetal joint C23839 was then randomly selected from the remaining defect-free group and cut axially into twelve equal-width strips. Each strip was then cropped to the ends of the intermetallic bond region, mounted and metallographically polished. A series of electron beam microprobe experiments was initiated to determine the as-received intermetallic bond layer thickness by measuring concentration profiles of the major elements present as the beam spot traversed the bond layer. However, the results of an extensive program of running microprobe traces on both the bimetal specimens and precision calibration

standards led to the conclusion that the effective beam spot size of the WANL microprobe was too large (3 to 7 microns in diameter, depending on the accelerating voltage) to permit accurate measurement of the as-received bond layer width. Consequently, the specimens were repolished and etched, and 2000 X photomicrographs were made at selected parts of the bond layer for each specimen. Layer thickness measurements were then made on these photographs, and a suitable averaging technique was used to calculate a representative mean thickness for each specimen.

The results of layer thickness measurements on the as-received specimens are given in Table VI-2. The overall mean value for bimetal joint C23839 is 1.12 μm (4.41 × 10^{-5} in), an order of magnitude less than the cirtical 12.7 μm value representing an embrittled bond. It should be noted, however, that local variations in thickness along the bond layer are quite large. This is seen, for example, in the upper half of Figure VI-24 for strip specimen A. Extreme localized thickness-transition regions and anomalous areas were avoided in making thickness measurements from the photomicrographs. Such additional work tasks as determining the composition and crystal structure of the intermetallic layer(s), or investigating the spheroidal precipitate (or inclusion) aggregation in the Ta-10W adjacent to the intermetallic layer, were beyond the support scope of this program.

After completing photomicrography for the as-received condition, the specimens were demounted, cleaned and divided into four groups of three each. One group was designated for 2000-hour annealing runs at each of the temperatures 750, 800 and 850°C, with the fourth group being held aside for possible annealing at higher temperatures and/or longer times should this prove necessary. Each annealing group was wrapped in an envelope of clean, high-purity tantalum foil (which has been shown [1] to provide an effective barrier to interstitial contaminants in vacuum heat treating atmospheres), instrumented with two monitoring thermocouples whose hot junctions were wired tightly against the tantalum

---

[1] H. Inouye, "The Contamination of Refractory Metals in Vacua Below 10^{-6} Torr", in Refractory Metals and Alloys III: Applied Aspects (ed. R.I. Jaffee), Gordon and Breach, New York, 1966.

TABLE VI-2

RESULTS OF INTERMETALLIC BOND LAYER THICKNESS MEASUREMENTS

| Specimen	Diffusional Growth Annealing Temperature (°C)	As-Received (As-Extruded)	Mean Intermetallic Bond Layer Thickness (µm) — After 2000-Hour Growth Anneal			
			Near Originally Polished Face	.015 in. Below Originally Polished Face	Near Originally Unpolished Face	.015 in. Below Originally Unpolished Face
D	None	1.28	–	–	–	–
H	None	0.889	–	–	–	–
L	None	1.13	–	–	–	–
A	750	0.983	1.76	1.48	2.08	1.61
E	750	1.01	1.48	1.63	1.89	1.78
I	750	1.05	1.76	1.79	1.49	1.47
Overall Mean for 750°C Specimens		1.014	1.667	$\Delta = +0.653$	(Mean growth in 2010 hours at 750°C)	
B	800	1.11	–	–	–	–
F	800	1.06	–	–	–	–
J	800	0.952	–	–	–	–
C	850	1.14	3.33	3.97	3.35	3.19
G	850	1.02	3.93	4.30	3.67	3.46
K	850	1.84	4.54	4.02	3.22	3.68
Overall Mean for 850°C Specimens		1.333	3.933	$\Delta = +2.600$	(Mean growth in 2000 hours at 850°C)	
Overall Bimetal Joint Mean		1.12				
Range of Individual Thickness Readings		0.25 to 4.70	750°C: 0.51 to 5.84		850°C: 1.52 to 8.89	

316

|← 1 μm →|
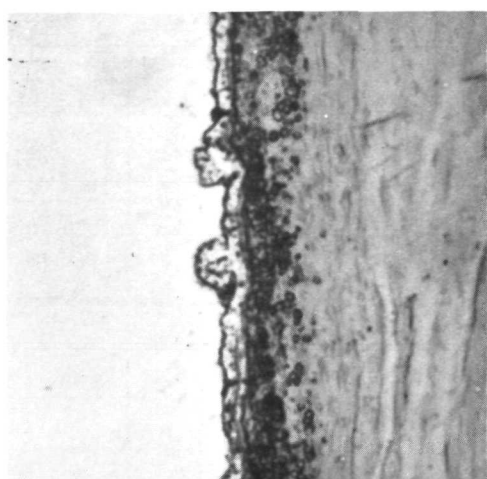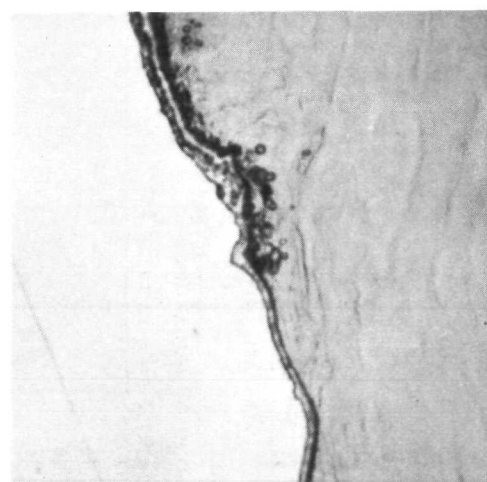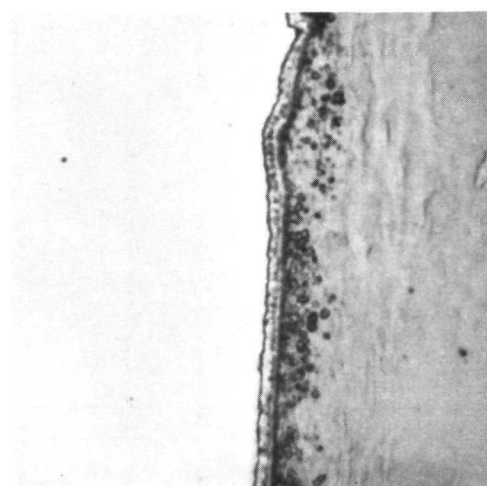
Ta-10W

As-Received (As-Extruded)

316

|← 1 μm →|
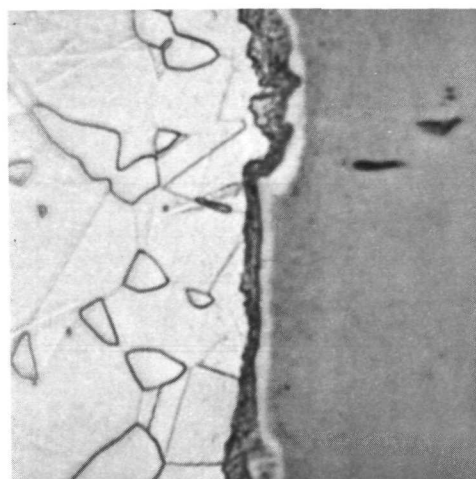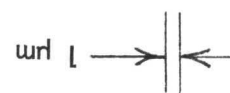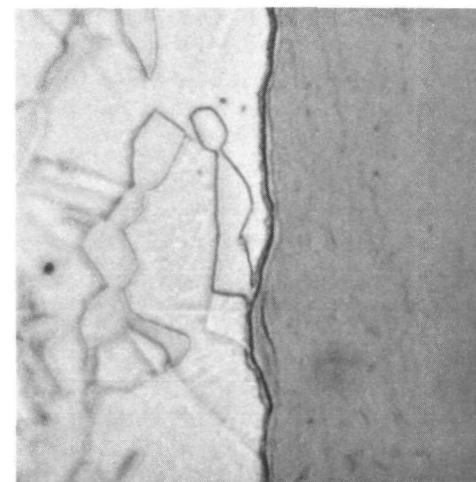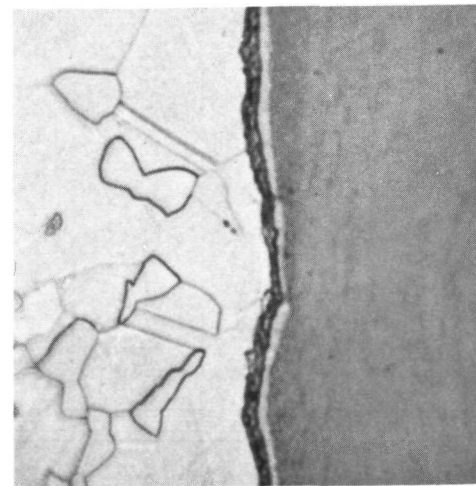
Ta-10W

After 2010 Hours at 750°C

Figure VI-24. Selected Regions of Intermetallic Bond Layer in Ta-10W/316 SS Diffusional

envelope, and installed in a Varian ion-pumped ultrahigh vacuum furnace. The groups
were then annealed for 2000 hours at their respective temperatures. Average furnace
pressures during the runs were 2.3×10^{-9} torr at $750^{\circ}C$, 7.2×10^{-9} torr at $800^{\circ}C$ and
1.2×10^{-8} torr at $850^{\circ}C$.

It was most unfortunately the case that, after about 250 hours of annealing at
$800^{\circ}C$, the combination of a power supply malfunction and a failure of the overtemperature
protection system for that particular furnace permitted the $800^{\circ}C$ specimen group to exper-
ience a 15 minute excursion to some unknown temperature greater than $975^{\circ}C$ (this being
the upper scale limit on the temperature recorder being used to monitor the system). At
the time, it was decided to continue the run on these specimens, for the following reasons:

a. It was believed that the 316 stainless steel had not melted (solidus
temperature = $1371^{\circ}C$), since it would then have attacked and penetrated
the tantalum envelope and this would have been visible through the
furnace sight port.

b. After consideration of the available data for the Ta/321 SS system, it
was believed that the amount of accelerated intermetallic layer growth
that occurred during the temperature excursion would be negligible
compared to the total growth to be obtained in 2000 hours at $800^{\circ}C$,
and thus the results would not be significantly affected.

While these reasons were proved to be valid ones, it turned out that another problem (dis-
cussed below) had occurred, evidently during the temperature excursion, which ruined the
$800^{\circ}C$ group of specimens with regard to obtaining layer thickness measurements.

At the end of the annealing runs, the specimen groups were cooled to room tempera-
ture and removed from the furnaces. The tantalum foil envelopes were removed, whereupon
it was found that a noticeable film had been deposited on the inside of the $850^{\circ}C$ foil, a
heavy film on the $800^{\circ}C$ foil and no visible film on the $750^{\circ}C$ foil. These films were undoubt-
edly composed of manganese and chromium which had evaporated from the surface of the
316 stainless steel and deposited on the adjacent tantalum surface. The fact that the $800^{\circ}C$

foil exhibited a much heavier film than the 850°C foil was an indication of the severity of the temperature excursion experienced by the former.

The specimens were then visually and microscopically examined, where it was found that the 800°C group exhibited almost complete fracture along the bond interface, and the 850°C group exhibited some fracture indications as well. The 750°C group appeared to be physically intact. Figure VI-25 shows the intersection of the bond interfaces with the specimen outer surfaces for all three groups; fracturing of both the 800 and 850°C specimens is plainly visible.

Figure VI-26 through VI-28 show selected areas of the as-annealed, unprepared specimen surfaces on the side originally polished and etched for layer thickness measurements in the as-received condition. The rather exotic thermally etched or decorated appearance of the 316 stainless steel is due to selective or biased evaporation of material from the grain boundary/surface intersections, austenitic matrix and various precipitated phase transformation products[1] developed in the stainless due to the 2000 hour elevated temperature exposures. The 750°C specimen bonds appear to be unperturbed, but the nearly totally fractured condition of the 800°C specimen bonds is markedly evident. The 850°C specimen bonds appeared to be largely intact except near the feather edges or tips at both ends of the bond region. Some bond layer cracks were seen toward the axial center of the bond region, and these are selectively displayed in the figure.

It was obvious that the bond layer cracking and fracturing in the 800 and 850°C specimens was due to the thermal stresses developed as a consequence of the difference in thermal expansion coefficients between the Ta-10W and the 316 stainless steel. However, it was impossible to determine whether the damage occurred immediately upon heating to the respective temperatures (i.e., the as-extruded bond was unable to withstand the thermal stresses developed at these temperatures) or whether failure had occurred only after the intermetallic bond layer had grown to some thickness representing an embrittled condition.

---

[1]See, for example, B. Weiss and R. Stickler: "Phase Instabilities During High Temperature Exposure of 316 Austenitic Stainless Steel", Met. Trans. 1972, Vol. 3, pp. 851 - 865. No attempt will be made here to identify precipitate phases by their micrographic appearance, but their presence is duly noted.
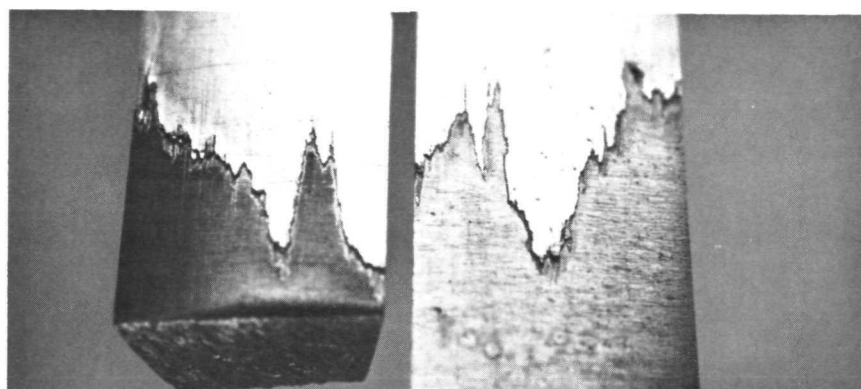
316

Ta-10W

850°C Specimens
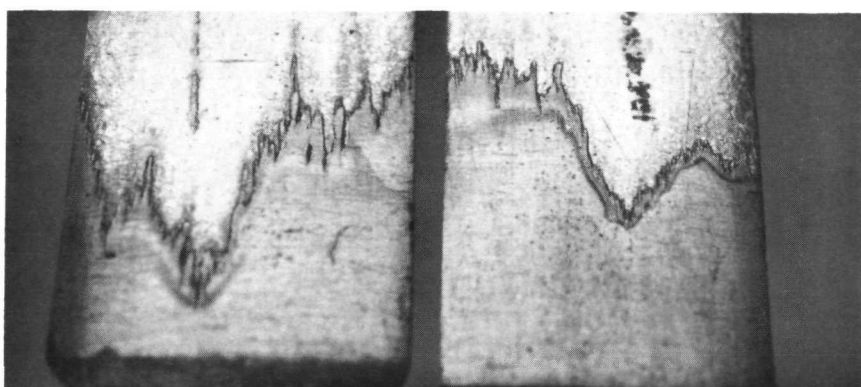
316

Ta-10W

800°C Specimens
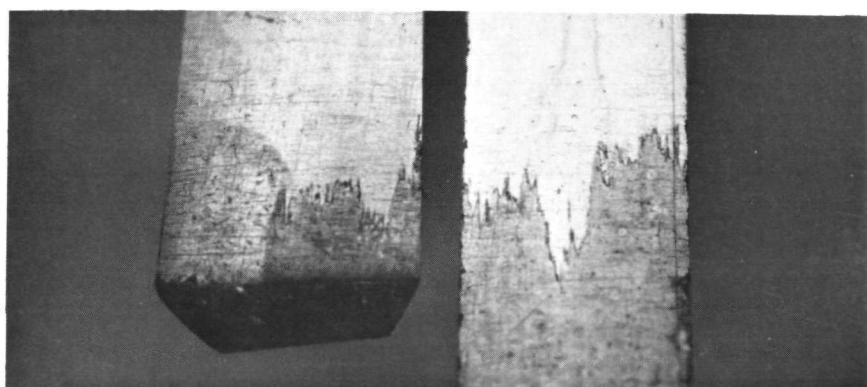
316

Ta-10W

750°C Specimens

Figure VI-25. Bond Layer Intersections with Outer Surfaces of
Diffusional Growth Specimens after 2000 Hour Annealing Runs - 9X
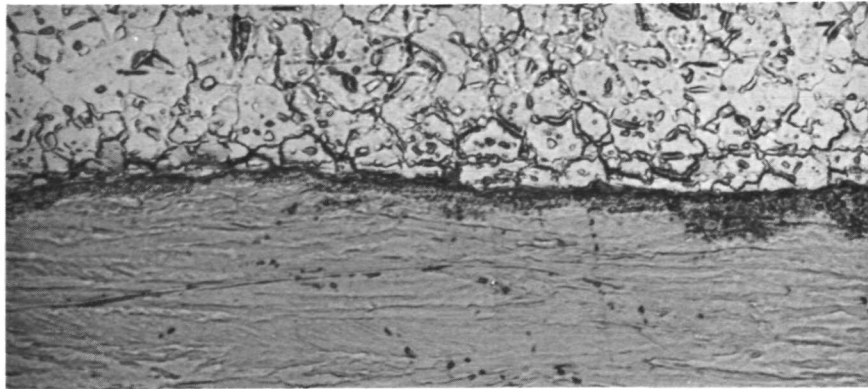
316

Ta-10W

Specimen A
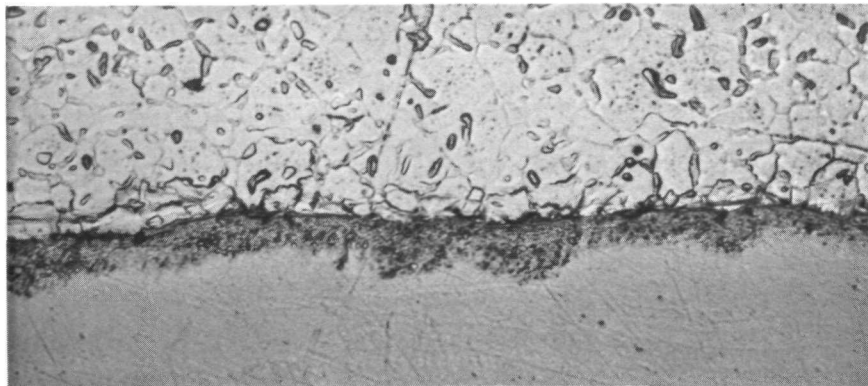
316

Ta-10W

Specimen E
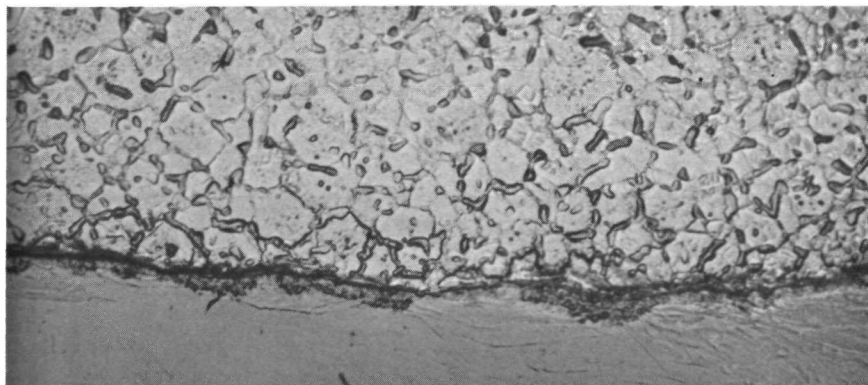
316

Ta-10W

Specimen I

Figure VI-26. As-Annealed (No Surface Preparation) Appearance of Ta-10W/316 SS Growth Specimens Exposed 2010 Hours at 750° C - 400X
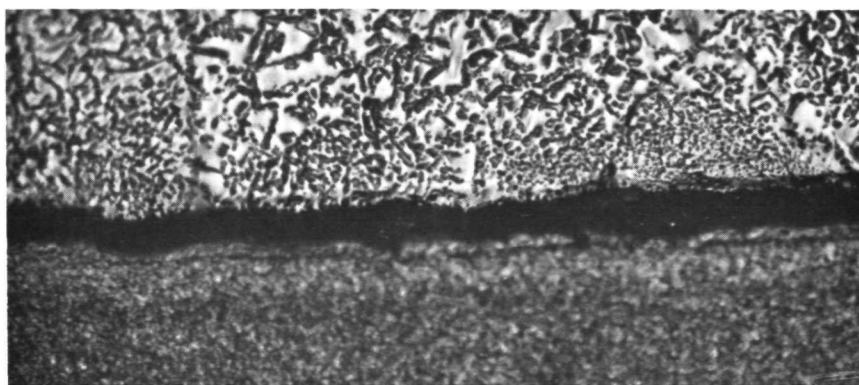
316

Ta-10W

Specimen B (Note complete bond fracture)
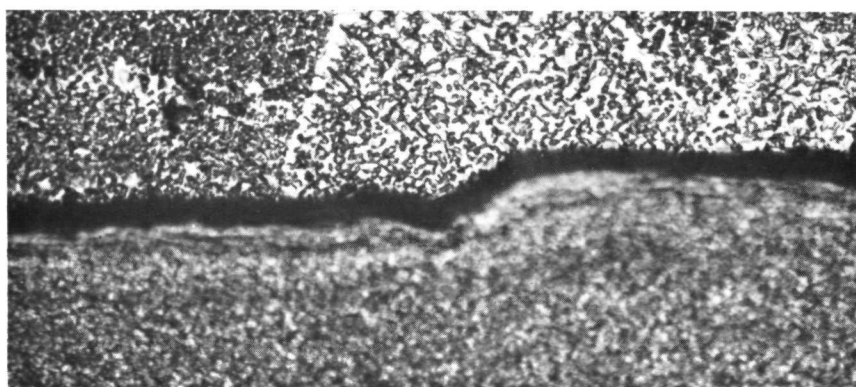
316

Ta-10W

Specimen F (Note complete bond fracture)
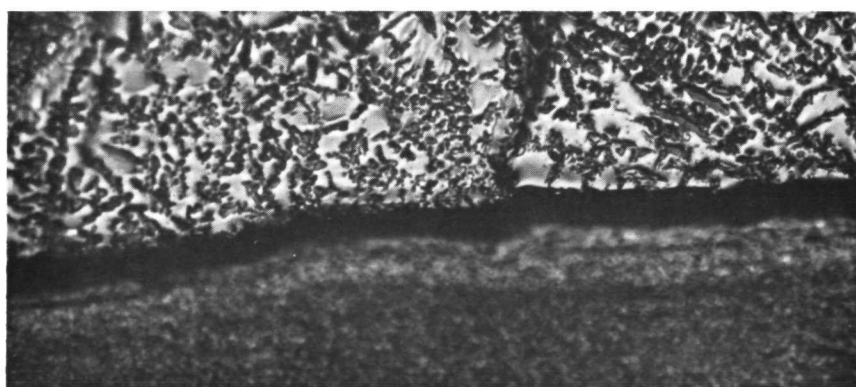
316

Ta-10W

Specimen J (Note complete bond fracture)

Figure VI-27. As-Annealed (No Surface Preparation) Appearance of Ta-10W/316 SS
Growth Specimens Exposed 2000 Hours at 800°C Plus 15 Minutes at Unknown
Temperature > 975°C - 400X
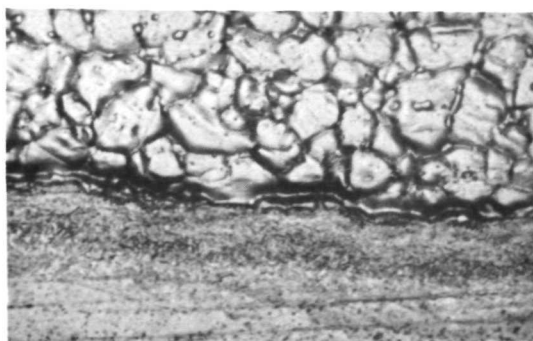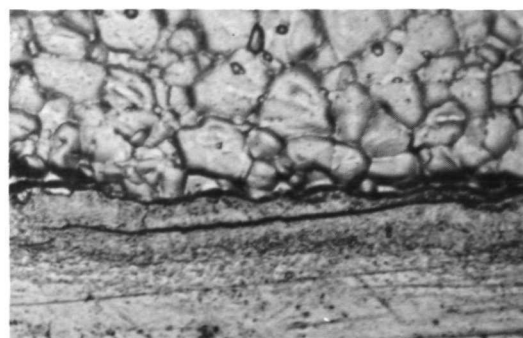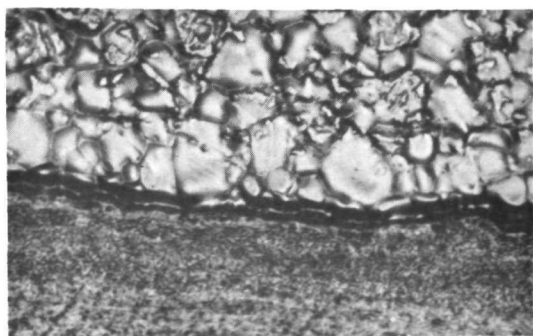
316

Ta-10W

Intact Bond Area   Cracked Bond Area

Specimen C

316

Ta-10W

Intact Bond Area   Cracked Bond Area

Specimen G

316
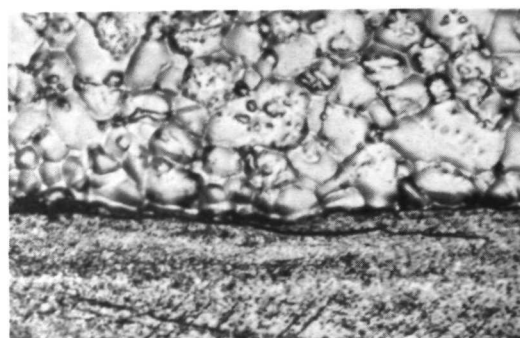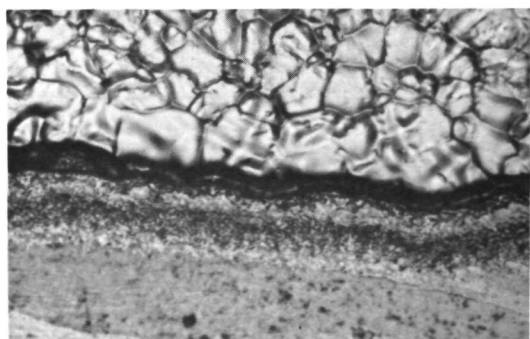
Ta-10W

Intact Bond Area   Cracked Bond Area
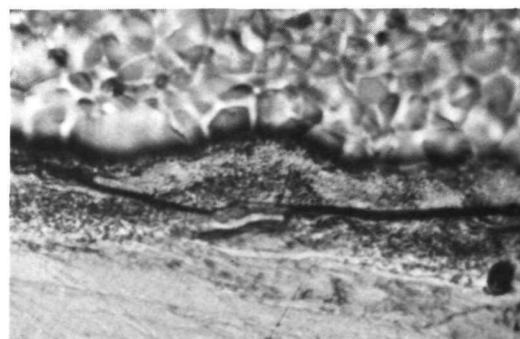
Specimen K

Figure VI-28. As-Annealed (No Surface Preparation) Appearance of Ta-10W/316 SS
Growth Specimens Exposed 2000 Hours at 850°C - 400X

To help formulate an answer to this question, specimens from the group which had been held aside were installed one each in the 800°C and 850°C annealing furnaces, heated to those temperatures at roughly the same rate ($\sim 10C^{o}$/min) used for the 2000 hour groups, held at temperature for 6 hours and then cooled to room temperature. These specimens were removed from the furnaces and examined visually and microscopically; no indications of bond layer fracture or cracking were seen in either case.

All of the specimens from the 2000 hour annealing groups were then mounted, and the sides which had been originally polished and etched for as-received measurements were re-prepared for metallographic examination with the minimum possible amount of material ($\sim$.001 inch) being removed. Figure VI-29 shows representative microstructures for each annealing group after etching to emphasize the 316 stainless steel grain structure, together with a comparative micrograph of an as-received specimen similarly prepared. It is seen that little or no grain growth occurred in the 2010 hour – 750°C specimens, while in the 2000 hour – 850°C specimens the average 316 grain size has at most doubled. The enormous size of the 316 grains in the 2000 hour – 800°C specimens indicates that their 15 minute temperature excursion must have been to a temperature fairly close to the melting point.

At this point, the following conclusions were drawn regarding bond layer fracture and cracking in the 2000 hour specimen groups:

a. The 800°C specimens fractured during their 15 minute temperature excursion, as the strength of the (essentially) as-extruded bond was inadequate to withstand the extremely high thermal stresses which were developed.

b. The bond layer cracks and feather-edge fractures in the 850°C specimens developed only after the intermetallic bond layer had grown in localized areas to a thickness representing an embrittled condition.

(It should be pointed out that all of the foregoing discussion of bond layer fracture and cracking has concerned the sliced and cropped diffusional growth specimens which are essentially bimetal strips with skewed interfaces. The state of stress developed in such

Specimen K

Specimen F

Specimen I

Specimen H

316
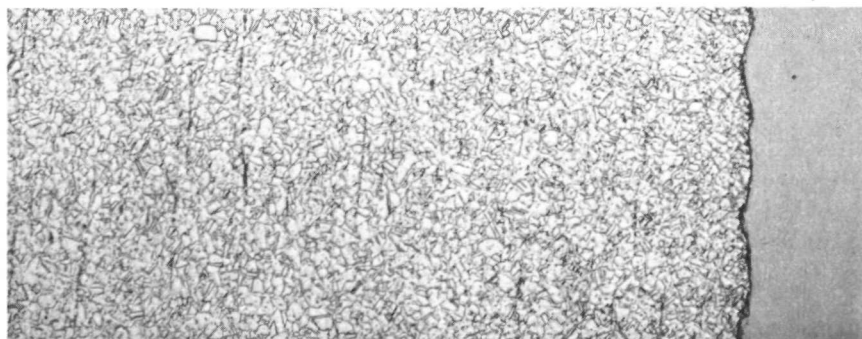
Ta-10W

After 2000 hours at 850°C

After 2000 hours at 800°C plus 15 minute excursion to unknown temperature >975°C

After 2010 hours at 750°C

As-received (as-extruded)
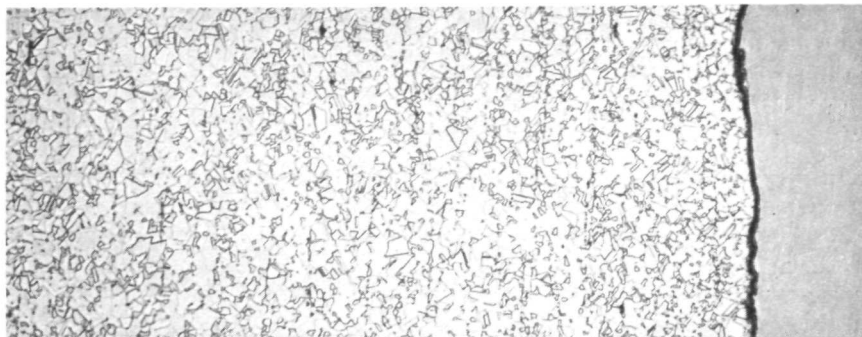
Figure VI-29. Effects of Diffusional Growth Anneals on the Microstructure of Specimens from Bimetal Joint No. C23839 - Etched to Display Stainless Steel Grain Boundaries - 100X

a strip upon heating to a given temperature is vastly different from that developed in a full tubular bimetal joint (i.e. in a TEM-X inner clad), so that the fact that fracture and cracking occurred in the strips implies little or nothing about the fate of a full joint similarly heated.)

The specimens were then lightly repolished and etched to bring out the boundaries of the intermetallic bond layers. 2000X photomicrographs were then made, and layer thicknesses measured and mean thicknesses calculated as in the as-received condition. To determine whether the effects of surface diffusion had produced an anomalously large amount of layer growth at this plane (which was .001 - .002 inches from the as-annealed surface), additional specimen preparation was performed and layer thickness determinations made at planes which were (1) 0.015 inches below the originally polished surface, (2) as close as possible to the originally unpolished surface and (3) 0.015 inches below the originally unpolished surface. All of the results are given in Table VI-2. In comparing average layer thicknesses near a given surface with the corresponding values 0.015 inches below that surface, it is found that the near-to-surface layer thickness is significantly larger in six cases, significantly smaller in four cases and about the same in two cases. This is sufficiently random to warrant concluding that the potential effects of surface diffusion are in fact not present.

In view of the above, only the layer thickness measurements made near the originally polished surfaces were used to calculate the 2000 hour layer growth values, since these should be most accurately related to the as-received thickness values. Mean layer thickness growth values of 0.653 μm in 2010 hours at 750°C and 2.600 μm in 2000 hours at 850°C were thus obtained. From these were calculated the parabolic growth rate constants

$$K (750°C) = 5.73 \times 10^{-7} \text{ in - hr}^{-1/2}$$

and $$K (850°C) = 2.29 \times 10^{-6} \text{ in - hr}^{-1/2},$$

which are plotted in Figure VI-23, and the general Arrhenius-type expression

$$K (T) = (3.284 \text{ in - hr}^{-1/2}) \exp (-31,600 \text{ cal/mole}/RT)$$

for our Ta-10W/316 SS system.

From the Arrhenius expression, or by a straight-line extrapolation through the two data points of Figure VI-23, a value of

$$K (650^{\circ}C) = 1.06 \times 10^{-7} \text{ in} - \text{hr}^{-1/2}$$

is obtained for Ta-10W/316 SS. If an initial intermetallic bond layer thickness of 1.12 μm is assumed, then 11.58 μm of layer growth is required to reach the 12.7 μm critical value which has been taken to represent an embrittled bond condition; at a temperature of 650°C, this growth will occur over a period of 1.67×10^{6} hours or 191 years. (It should be appreciated that this is an extremely conservative prediction; having failed to obtain layer thickness data at 800°C, it cannot be determined whether a slope change occurs in the K (T) versus 1/T curve in the 750 - 850°C range. If such a change does really occur, analogous to that shown for the Ta/321 SS system in Figure VI-23, then the true K (650°C) value for Ta-10W/316 SS is orders of magnitude less than the value found above, and the critical growth period correspondingly longer.) For 44,000 hours of operation at 650°C, the operational criterion specified for this qualification program, our results predict that the intermetallic bond layer will grow to a thickness of 1.68 μm, which is nearly an order of magnitude less than the critical 12.7 μm value. In 100 hours, this same 0.56 μm of layer growth should be obtained at a temperature T* of 848°C; however, experimental verification of this prediction was not performed due to termination of the program.

The micrographic appearance of the bond layer region after the 2000 hour growth runs is shown for a 750°C specimen in the lower half of Figure VI-24 and for two 850°C specimens in Figure VI-30. From these it is seen that two distinct intermetallic layers are present in the 750°C specimens and three layers are present in the 850°C specimens. This means that overall bond layer growth must be a very complex process involving diffusion in four (750°C) or five (850°C) phases, in each of which each diffusing element would have a different diffusion coefficient, plus reactions at three (750°C) or four (850°C) phase boundaries which could also be rate-controlling processes. Thus it appears that the single parabolic growth rate constant K(T) is not a parameter having fundamental significance with regard to the atomistic mechanism of layer growth, but rather a sort of

316   1 μm   Ta-10W
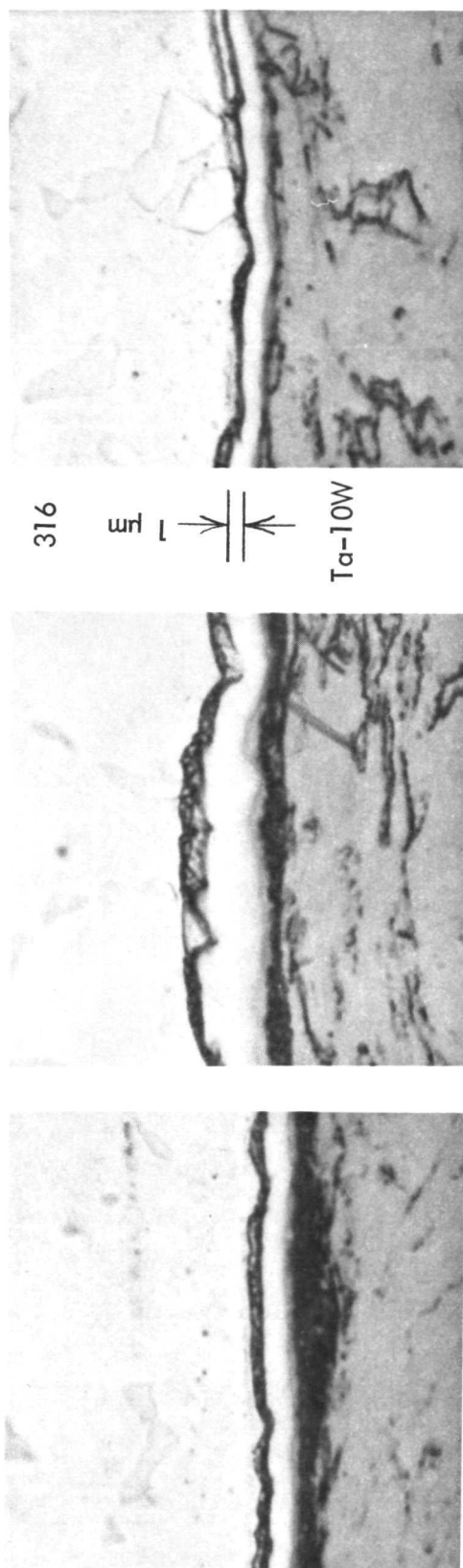
Specimen No. C23839-C, Near Originally Polished Surface

316   1 μm   Ta-10W
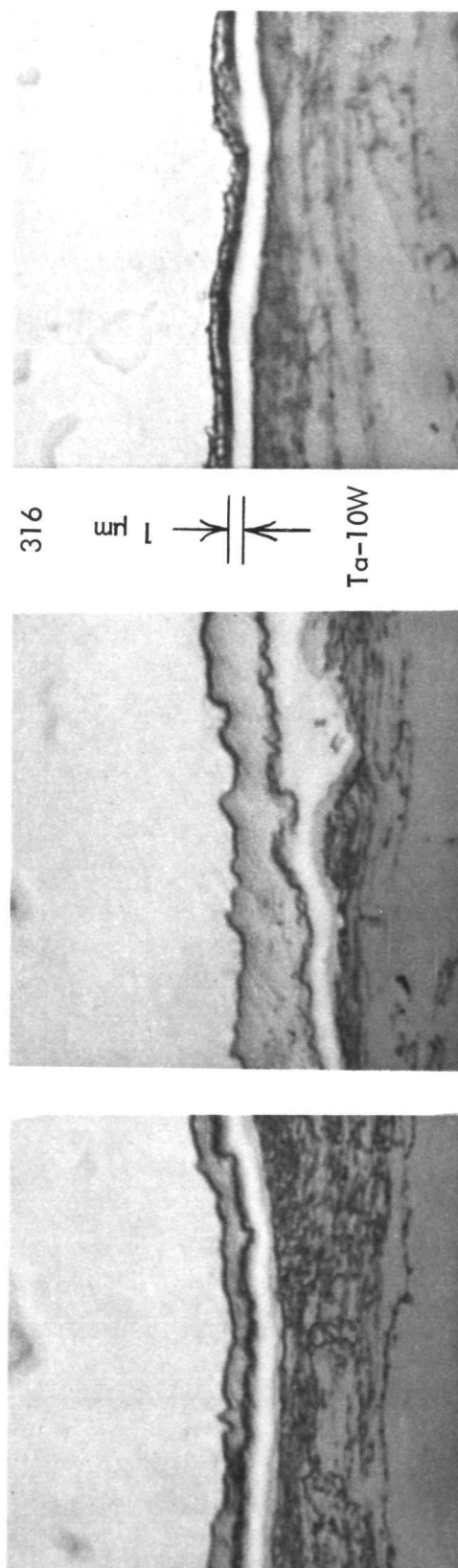
Specimen No. C23839-K, Near Originally Polished Surface

Figure VI-30. Selected Regions of Intermetallic Bond Layers in Ta-10W/316 SS
Diffusional Growth Specimens after 2000 Hours at 850°C – Etched, 2000X

averaging device which conveniently describes the process in a way that is adequate for engineering purposes.

In brief summary, it has been shown that the Ta-10W/316 SS bimetal joint can easily operate for 44,000 hours at 650°C without developing an embrittled bond due to excessive diffusional growth of the intermetallic bond layer. The bimetal TEM-X inner clad is thus considered to be qualified for use at these conditions.

5. Conclusions

The following conclusions, based on the work discussed in detail in the preceding subsections, are now presented:

a. The existing procedures and equipment used for dimensional inspection, borescope examination of inner surfaces, x-ray radiography, liquid penetrant testing and helium leak testing are all satisfactory for evaluating their respective intended aspects of the Ta-10W/316 SS bimetal inner clad.

b. The existing procedure/equipment combination used for ultrasonic inspection of the intermetallic bond region is satisfactory for detecting localized, three-dimensional defects but has not been proved reliable for detecting planar defects or "unbonding" at the bond interface. Should the program be resumed at some future date, either more work should be devoted to making the ultrasonic test reliable, or another method (e.g. eddy current testing) should be developed for detecting bond layer defects.

c. The Ta-10W/316 SS bimetal inner clad can withstand 100 thermal cycles from 260 to 593°C at 16.7 C°/min (in a noncontaminating environment) with no significant changes in or damage to its dimensional, physical and mechanical characteristics.

d. When subjected to axial loading, the bimetal inner clad does not fail by a delaminating-type fracture along the intermetallic bond interface. If the clad is stressed uniformly along its axis, then failure occurs by a

tensile-type fracture in the stainless steel. If it is stressed in such a way
that failure must occur within the intermetallic bond region, then the
failure mode is a primary tensile-type fracture in either the Ta-10W or
the stainless steel, followed by secondary fracture propogations which
are largely of academic interest.

e. The intermetallic bond layer in the as-extruded Ta-10W/316 SS bimetal
joint is not a uniform layer of reasonably constant thickness, but rather
a layer which exhibits numerous abrupt thickness transitions and a thickness
range of $\pm$ 400 percent of the nominal 1.1 µm value.

f. The diffusional growth of the intermetallic bond layer in the Ta-10W/316 SS
system is described by the expression

$$G(T,t) = t^{1/2}(3.284 \text{ in-hr}^{-1/2}) \exp \left({-31,600 \text{ cal/mole}}/{RT} \right)$$

where $G(T,t)$ = growth (inches) in time t at temperature T

$\qquad$ t = time (hours)

$\qquad$ T = absolute temperature ($^{\circ}$K)

$\qquad$ R = gas constant (1.987 cal/K$^{\circ}$ - mole)

g. In 44,000 hours at 650°C, the intermetallic bond layer thickness in the
Ta-10W/316 SS bimetal inner clad will grow from an initial value of 1.1
µm to a final value of 1.7 µm, far less than the critical 12.7 µm value which
reference work has shown to represent an embrittled condition in similar
refractory metal/austenitic alloy systems. There is some evidence that
the actual critical value for the specific Ta-10W/316 SS system may be
somewhat less than 12.7 µm, but it is in any case far greater than 1.7 µm.

h. The Ta-10W/316 SS bimetal inner clad is considered to be qualified for use
in TEM-X modules operating 44,000 hours or less in a noncontaminating
environment at peak inner clad temperatures not exceeding 650°C and
experiencing not more than 100 thermal cycles from average inner clad
temperatures of 260 to 593°C at a cycling rate not exceeding 16.7 C$^{\circ}$/min.

D.   GLASS SEAL DEVELOPMENT

As described above, failure of the duplex refractory clad was diagnosed to be caused by air leaking into the module at the ends where the power pins emerged through the BN insulators. A study of the problem resulted in a decision to develop a glass seal which would bond to the nickel conductor pin and the stainless steel end plate. Further, the glass was intended to remain in compression during operation and remain helium leak tight (HLT) after 50 thermal cycles (17 - 18C° per minute) and 44,000 hours of operation. In addition, the electrical resistance of the glass had to remain reasonable high, relative to the internal resistance of the module, to prevent current leakage.

1.   Test Specimen Geometry

The initial phase of the study was performed using flat plates with a central hole containing a BN sleeve and a nickel pin, all whose diameters were identical to the as fabricated dimensions of the corresponding parts used in actual modules. As experience was gained in forming glass seals on these single pin, flat plate mock-ups, four pin, and finally an eight pin, flat plate mock-up was fabricated. This latter mock-up duplicated a module end with the exception that all parts were a slip fit, whereas, in a processed module, the BN and nickel pin were tightly fitted and under compression as a result of the hot isostatic compression process. Eventually, mock-ups were fabricated to duplicate a module end and processed through hot isostatic compression. The use of the latter type mock-ups were more representative of the actual conditions under which the glass would have to operate. The usefulness of these mock-ups is further described below.

During the course of these experiments, it was found that two modifications in geometry materially affected the ability of the seals to remain HLT. First, the length of the BN sleeve was reduced so that a well was formed into which the glass, when it was melted, could flow, and subsequently would be placed under compression by the stainless plate as the assembly cooled. Second, the shoulders of the hole in the stainless steel were rounded, rather than squared. The latter configuration prevented objectionable sharp

corners from which cracks in the glass would originate if the glass overflowed the annulus between the nickel pin and the stainless steel.

2. Glass Application

Initially the glass was applied to the annulus in powder form, and then the pin/plate assembly was heated with a hydrogen torch until the glass melted and flowed. However, over the course of the project, experimental work gradually changed the procedure to one which proved more workable and consistently produced HLT seals. After assembly, the mock-up was sandblasted and the pins and plates pre-oxidized. Upon cooldown, the glass was applied in the form of a paste, using distilled water to make the mixture. The use of glass pre-forms seemed attractive, because it would allow the application of a pre-set amount of glass at each pin and prevent overspill which occurred when too much glass was applied. However, it was found that it was more difficult to obtain HLT seals with the preforms. The difficulty was attributed to retained binder which resulted in random, rather than uniform, wetting of the stainless steel and nickel. Accordingly, the paste mixture, described above, was used in all cases.

At first the glass was melted using a gas hand torch. Each pin was individually sealed in sequence. While this technique produced acceptable seals, the method depended to a large degree on the operators ability to judge the amount of heat necessary to form a seal. To circumvent this type of processing, an RF heating procedure was developed. Glass seals were then made on all eight pins simultaneously by proper coil design. In addition, the whole assembly was limited to a maximum predetermined temperature as determined by a thermocouple mounted on the stainless steel plate on the same bolt circle as the conductor pins.

3. Test Procedure

After the glass seals were formed they were leak checked on a Veeco helium leak detector. HLT was defined as no indications on the most sensitive scale, 3×10^{-10}

atm - cc/sec full scale. Cycling of the seals was performed under atmospheric conditions in an electrical furnace that was programmed to cycle the temperature between 530°C and 210°C at a rate of 17C° per minute with a one-half hour dwell time at the high and low points. Periodically, the seals would be removed and checked for leak tightness as described above. Life tests were also conducted under the same test conditions.

Seals were also placed on isothermal test, although in actual operation a radial temperature gradient would exist across the plate. At various time intervals, which increased as the integrity of the seals proved to be reliable, the seals would be removed and tested for their ability to remain HLT. Two in-situ tests were also conducted. One consisted of monitoring the pin to plate resistance as a function of time, and the other used an experimental set-up which allowed monitoring of HLT at the test temperature. However, the latter test which necessitated a more elaborate setup, including preheating of the helium to prevent thermal shock of the glass, was not within the scope of defined work, and so was a one of a kind experiment.

4. Results

The maximum temperature to which the seals would be exposed was calculated to be around 420°C. A temperature of 500°C was chosen for both the upper limit of thermal cycling and isothermal testing on the assumption it would provide a form of accelerated testing for the seals which might conceivably be exposed to an overtemperature. The problems inherent in the validity of such assumptions which try to accelerate time by increasing the temperature will become apparent as further details are described.

Once a proper glass[1] was identified, eight pin and gas pressure sintered (GPS) mock-ups were successfully cycled a minimum of 50 times while retaining their ability to remain HLT. One seal was cycled to failure, which required 77 cycles to destroy the HLT capacity. Life tests at 500°C were so successful, i.e., no leaks for the times at test, that further accelerated testing on eight pin flat plate mock-ups was done at 540, 570 and 600°C to allow a failure analysis at 420°C.

[1] The glass used in these experiments was developed on company funds at the Westinghouse Research and Development Center.

The failure mechanism proposed to explain the results was essentially one caused by devitrification of the glass. This process, where amorphous glass (V_1) transforms to crystalline solid (V_2), apparently causes a volume change ($V_2 < V_1$), pin holes and the resulting inability to provide a helium leak tight seal. A model of the process was made by assuming the crystallization followed first order kinetics. Letting n equal the fraction of glass crystallized

$$\frac{dn}{dt} = A\, e^{-Q/RT}$$

The time to failure, t_f, was assumed to occur when n equals unity, or some critical fraction n_c. In either case,

$$t_f = A'\, e^{Q/RT}$$

where $A' = 1/A$ or nc/A.

Hence, a plot of the log of failure time versus $1/T$ was made to allow an estimate of seal life at any specific operating conditions. Such a curve is shown in Figure VI-31 where the data for the four previously discussed temperatures is plotted. The data was obtained on six eight pin mockups tested at temperature $\geq 500^\circ$C, and one single pin mockup at 500°C. The time spread indicates the interval over which the seal failed, i.e., went from a helium leak tight condition to a state which permitted the passage of helium. The data allowed a reasonable straight line curve fit over the temperature range studied. The longer time data range at 500°C corresponds to the failure of three eight pin mockups and one single pin mockup over virtually an identical time interval. The lower temperature data corresponds to a possible helium leak indication of a single pin on an eight pin mockup after 2373 hours. However, it was not detected after the next check at 2642 hours.

Also shown on the plot is a point labeled goal. This point represented the five year desired life of a glass seal during air operation at the maximum operating temperature at the pin seal bolt circle (420°C) for a module operating at $\overline{T}_H = 585^\circ$C. However,

it should be noted that system temperatures were still not defined at the termination of the work. In fact higher temperatures were in vogue so it did not seem unreasonable to expect that one end (inlet side) of the module might have been exposed to a higher temperature. Further, it is pertinent to point out that the use of these modules in space, oxygenless environment, precluded the necessity for glass seals other than for a relatively short time ground checkout, 1000 - 2000 hours. Nonetheless, a 44,000 hour seal was the goal. It was apparent that extrapolation of the data to the lower operating temperature assured a more than adequate operating time, by a factor of ten, for these glass seals. In addition, measurements of temperature on a module whose $\overline{T}_H$ was 635°C showed a temperature of 387°C at the pin seal. Hence, regardless of how conservatively the data was handled, the prognosis for successful thermal capability of the glass seal appeared good.

However, testing at lower temperatures, 400°C disclosed seal failures occurring in the hundreds of hours for flat plate mock-ups. The GPS samples, on the other hand, did not fail even at the low temperatures. Obviously, the mechanism postulated above adequately explained seal pin failures at temperatures from 500°C upwards. Somewhere between 400° and 500°C the model breaks down for flat plate mock-ups. Table VI-3 shows the mockups that were on test when the program was terminated.

The ability of the gas pressure sintered end mock-ups (MEM) to maintain HLT capability for extended periods is evident. Obviously the glass seal is subjected to a more stringent test using a slip fit mock-up, i.e., assembly clearances to be filled by the glass, than a compacted end. That the latter statement appears to be true is pointed out in the successful performance of the TEM X S/N-3 modules that had glass seals applied prior to testing.

TABLE VI-3
GLASS SEAL LIFE TEST

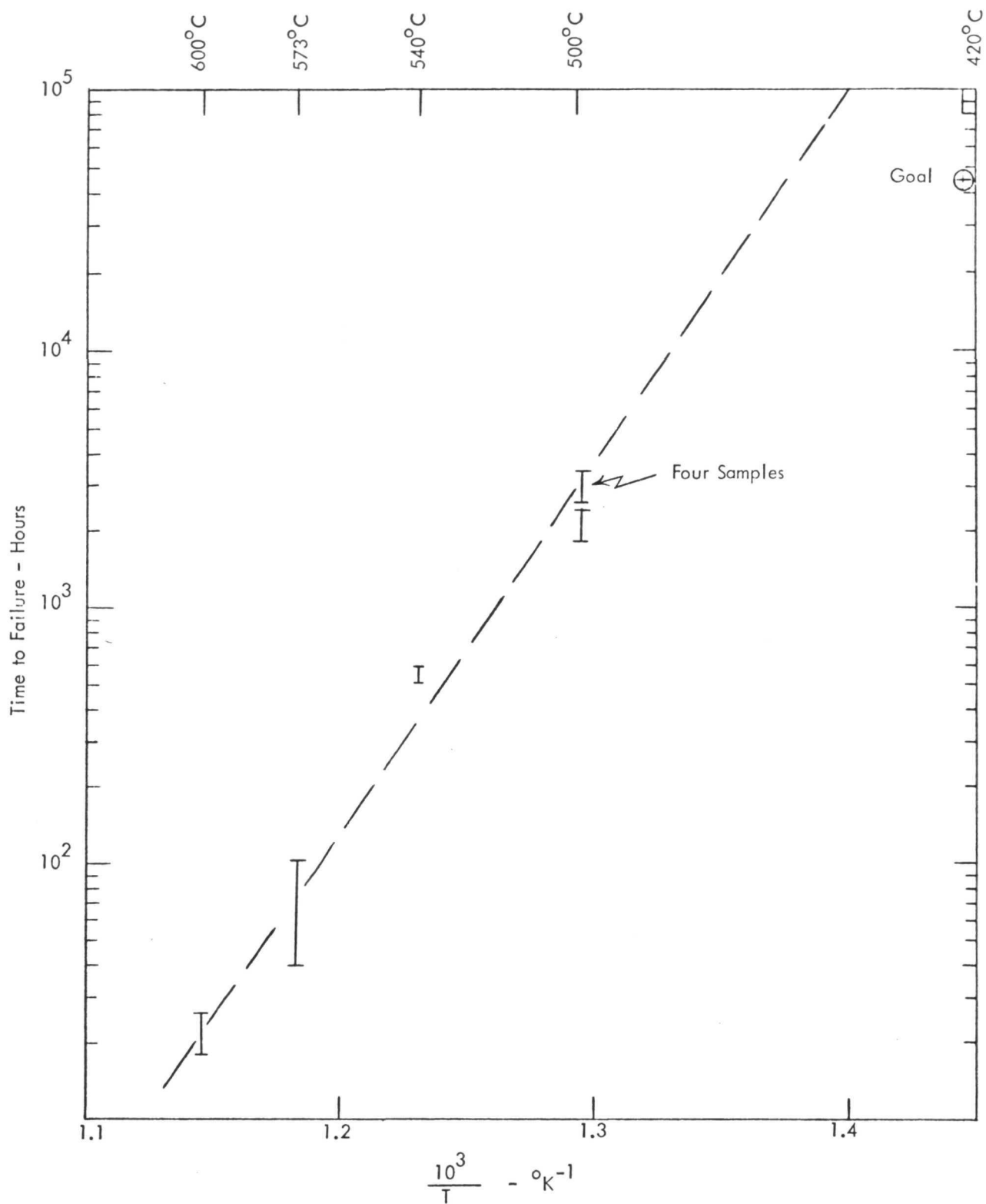| Seal and Glass	Temp. Tested	Hrs. Tested	Last Leak Check Hrs. HLT
8P-II LB (7571 No. 1)	500°C	4602	4602
8P-13LA (7571 No. 2)	500°C	4198	4198
MEM No. 3 (7571 No. 1) NOTE: Previously tested at 500°C for 3,634 hours	400°C	3110	3110
MEM No. 4 (7571 No. 1)	400°C	4207	4207
MEM No. 5A (7571 No. 2)	400°C	419	419

Figure VI-31. Failure Time of Glass Seals Versus Inverse Temperature

VII. WELDING DEVELOPMENT

Relatively little welding development has been performed or required in the continuation of tubular module fabrication since the end of Phase II-C of the Compact Thermoelectric Converter Program (June, 1969). New joints in TEM-13, TEM-X, TEM-15 and TEM-14 series modules have been handled for the most part by making straightforward engineering extrapolations from existing procedures and welding parameters, and making qualification specimens, welds and examinations in the few cases where the extrapolations exceeded the limits permitted by the controlling welding specification (WANL PS 597983). Such cases included welding of the Inconel 718 end stiffeners used on TEM-X S/N-1, discussed in Section I of this report, the electron beam welds in the 316/304 stainless steel outer clad joints in TEM-15A S/N-1, (see Section III), and the welding of the hermetic end caps to TEM-X S/N-3 series modules as discussed in Section VI: all of these proceeded success-fully and without incident.

Late in the program, a series of welding experiments was conducted in connection with the conductor pin/external collector ring joint for the three-module assembly of TEM-14B electromagnetic pump power modules (see Section II). In an attempt to minimize external I^2R losses in the high current circuit, experimental TIG and EB welds were performed on nickel conductor pin/copper collector ring specimens (as opposed to the nickel pin/nickel ring combination used in previous pump modules). In the TIG welding case, heat inputs far in excess of those normally used or allowed for thermoelectric module welds were required to obtain fusion in the self-chilling copper ring, and it was felt that damage to either the module or the collector ring/bus assembly braze joint could too easily occur under such conditions. The EB welding experiments indicated a severe problem in obtaining simultaneous fusion of both pin and ring when using the assembly clearances anticipated to be required for the three-module array. At this point it was decided that although a satisfactory nickel/copper joining procedure could eventually be developed, the amount of development required was beyond the existing work scope and the schedule could not tolerate the time required, so the nickel/copper approach was abandoned.

A series of EB welds was then performed on nickel pin/nickel ring specimens, anticipating that weld heat input to both module and braze joint would be minimal for the EB process. Although this indeed appeared to be the case, and adequate penetration was easily obtainable, two problems were encountered. First, burnoff of the thin web around the conductor pin hole at the collector ring I.D. invariably occurred, with the molten web material running down the inner surface of the ring (where it could drip onto the module end face and/or retaining ring stretch neck); second, the welding parameters could not be fixed for the total range of anticipated assembly clearances. It was thus decided in the interest of reliability and simplicity to work with a nickel pin/nickel ring TIG welded joint. A design and procedure were evolved in which a 0.1 inch wide x 0.1 inch deep x 240° "pocket", oriented opposite to the collector ring I.D., was milled around each conductor hole, as shown in Figure VII-1; the pin was then welded to the bottom of the pocket with a simple fusion pass, after which the pocket was filled in with a high-nickel-content alloy to develop an electrical contact area about 1.5 times the cross-sectional area of a conductor pin. Several demonstration joints of this type were welded with satisfactory results, and this approach (with slight modifications to ease the assembly fit-up problems of the three-module array) was committed for the TEM-14B application.

A weld specimen of precisely the final joint design was then fabricated and a series of qualification welds performed. During this work, it was determined that shrinkage cracks at the beginning and end of the initial fusion pass could be eliminated by adding a significant volume of ASTM B3 4 Class ERNi-3 filler metal[1] at these points, and this detail was incorporated into the final procedure. Completed qualification welds were sectioned, examined metallographically and found to be satisfactory; an example is shown in Figure VII-2. An electrical resistance of 0.07 milliohms was measured from the pin to the collector ring. Accordingly, the joint design and welding procedure were designated as qualified for the TEM-14B assembly.

---

[1]This alloy is also used to fill in the pocket above the end of the conductor pin.

Prior to initiating the actual welding of the three-module array, the program was terminated. In retrospect, if the work were to be later continued, two changes to the existing procedure would be made. First, the initial fusion pass of each joint would be converted to a complete filler pass instead of adding filler metal only at the beginning and end points; and second, the procedure would be requalified to develop operator technique for making all welds in an inert atmosphere welding chamber, to simplify the problems of avoiding oxidation of the unwelded pin/ring surfaces and of the copper bus straps brazed to the collector rings.
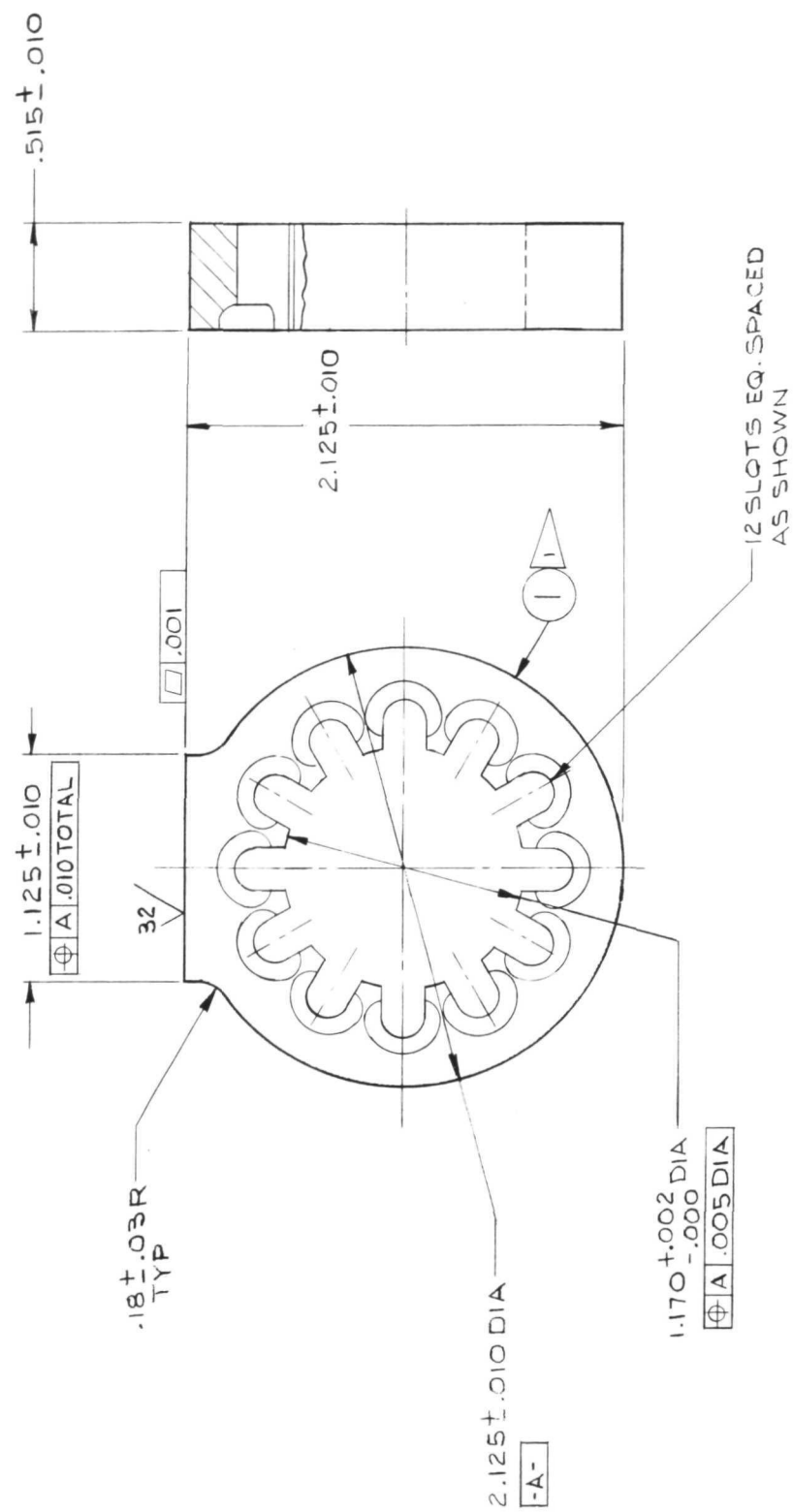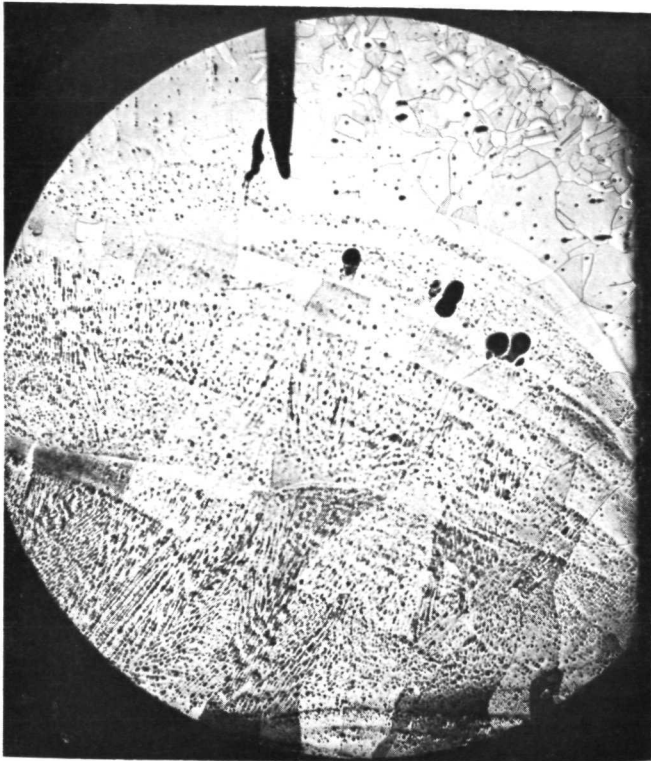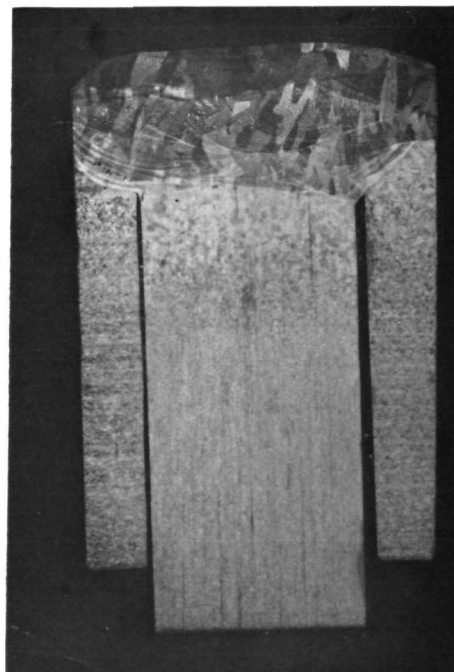
Figure VII-1. External Collector Ring, TEM-14B Pump Module

30 X

30 X

5 X

◀ Collector Ring

◀ Collector Pin

Figure VII-2. Photomicrographs of Etched Section of Typical TEM-14B
Conductor Pin/External Collector Ring Qualification Weld

VIII. 5 KWe SYSTEM MODULE ANALYSIS AND DESIGN

A.   GOALS AND ACHIEVEMENTS

In GFY 1973 work was initiated on the design of a 5 KWe reactor/thermoelectric demonstration system. The overall objective of the thermoelectric module portion of this program conducted by Westinghouse was to develop technology leading to the delivery of compact tubular thermoelectric converter modules capable of producing at least 5 KWe net power output at 30 volts at the end of a five year mission. To meet this objective a substantial effort was completed at Westinghouse to provide parametric module performance information as required in support of the 5 KWe system design conducted at Atomics International.

The initial portion of this effort involved the investigation of various design improvements on efficiency levels of reactor power modules. This effort was followed by the generation of reactor power module and E.M. pump module performance calculations over a range of operating temperatures and module dimensions leading toward the selection of reference designs for use in the 5 KWe system. Particular attention was given to effects of operating temperatures and design dimensions relative to module degradation rates allowing the reference designs to be optimized for end-of-life conditions.

Although the work had not been completed prior to the termination, a preliminary reference module design had been selected.

B.   MODULE IMPROVEMENT EFFECTS STUDY

        The objective of this effort was to quantify the performance improvement associated
with seven individual modifications considered feasible for incorporation into the state-of-
the-art TEM-X S/N-3 series modules.

        The design improvements considered in this analysis were:

        1.   Incorporation of ternary materials. For these calculations the ternary thermo-
electric material properties quoted by RCA[1] were substituted directly for the standard lead
telluride.

        2.   Reduced mica thickness and EBVD barrier. These two improvements were
paired since it appears that the incorporation of reduced axial thickness must be accompanied
by a thin electron beam vapor deposited diffusion barrier. The mica axial thickness con-
sidered here was .0015 inch.

        3.   Increased radial thickness thermoelectric washers. Washer radial thickness
increased to .200 inch from .145 inch was considered to improve efficiency.

        4.   Low heat loss end closure. By redesigning the existing TEM-X S/N-3 type
end closure, it is considred feasible to reduce the end closure conductances by 50 percent.

        5.   Thin inner clad. Using the swirl generator for internal radial support, it is
considered feasible to reduce the inner clad thickness by approximately 50 percent, thus
reducing the temperature drop across the clad.

        6.   Thin outer clad. Using the NaK shroud swirl generator for external radial
support, it is considered feasible to reduce the outer clad thickness by approximately 50
percent.

        7.   Segmented thermoelectric washers. By varying the dopant levels in the ternary
materials, it is possible to shift the peak in the figure-of-merit curve to lower temperatures.
Segmenting of the thermoelectric washers would allow the outer portion of the washer,

------

[1]RCA Quarterly Progress Report NYOO-3886-4.

which operates in a lower temperature range, to be doped such that it more efficiently uses the existing temperature gradient.

Since the effect associated with each modification was found to be dependent on the order in which the modifications were considered, two sets of calculations were generated. First, claculations were performed considering each individual design improvement, incorporated, one at a time, into the existing TEM-X S/N-3 design. The calculated overall efficiency for the existing TEM-X S/N-3 is 4.64 percent. The improvement effect, then, was defined by the expression

$$\Phi_i = 100\left(\frac{\eta_i}{\eta_b} - 1\right),$$

$$\eta_b = 4.64 \text{ percent},$$

where Φ_i is the percent improvement associated with each design modification; η_b (4.64 percent) and η_i are the calculated overall efficiencies before and after the incorporation of the improvement, respectively. Hence the improvement number represents the percent by which the TEM-X S/N-3 efficiency would be improved by the incorporation of each individual design improvement.

In the second phase of the work, each design improvement was investigated, one at a time, after the incorporation of all other improvements. The improvements effect in this case was defined by

$$\Phi_i = 100\left(\frac{\eta_b}{\eta_i} - 1\right),$$

$$\eta_b = 7.41 \text{ percent}.$$

Here Φ_i is the percent improvement associated with each design modification, η_b (7.41 percent) and η_i are the calculated overall efficiencies with all improvements and with all except the ith improvement, respectively.

Table VIII-1 summarizes the calculated module improvement effects associated with each design improvement. All numbers were generated using TEMOD, the tubular thermoelectric module performal calculational code.

TABLE VIII-1

CALCULATED MODULE IMPROVEMENT EFFECTS

	Improvement Effect (Pct.)	
Design Modification	Added to TEM-X S/N-3	Last Addition to Optimized Module
1. Ternary thermoelectric	19.3	23.1
2. Reduced mica and EBVD barrier	13.9	14.6
3. Increased T/E radial thickness	5.1	1.7
4. Low heat loss end closure	2.4	3.6
5. Thin inner clad	0.6	0.5
6. Thin outer clad	3.5	1.8
7. Segmented T/E washers	5.0	5.0
Accumulative	59.8	59.8

NOTE:

1. Improvement No. 7 cannot be added to TEM-X S/N-3 without incorporation of improvement No. 1.

2. The accumulative total is not the arithmetic sum of the individual effects since the effects compound one another.

The results indicated that the first two improvements resulted in substantial efficiency increases whereas the last five were much less effective. Primary emphasis, then, was placed on the development of ternary thermoelectric materials and electron beam vapor deposited barriers during GFY 1973.

C.   REACTOR MODULE PARAMETRIC ANALYSIS AND PRELIMINARY DESIGN

System calculations performed at Atomics International in conjunction with preliminary module performance parametric calculations resulted in the end-of-life (5 year) reactor power module performance requirements listed in Table VIII-2. To meet the specified requirements, the following "ground rules" were established to allow the determination of the circuit component dimensions of the "reference module" for the 5 KWe Demonstration System:

1.   The radial and overall axial dimensions of the reference module will be identical to those of the current TEM-X series modules. Preliminary system studies indicated the performance improvements associated with modifications in the overall module dimensions are relatively small.

2.   The reference module will incorporate thin film EBVD (electron beam vapor deposit) diffusion barriers allowing the use of 0.0015 inch intercouple mica insulators. This barrier configuration eliminates the need for the tungsten foil and .010 inch mica insulators used in the TEM-X S/N-3 series modules resulting in a substantial reduction in shunt heat losses.

3.   The reference module will incorporate ternary thermoelectric materials resulting in a substantial performance improvement over that obtainable using the current p- and n-type lead tellurides. The improvement results primarily because of a reduction in thermal conductivity exhibited by the ternary materials.

4.   The beginning-of-life efficiency will be 6.5 percent when the module is operated at $\overline{T}_H = 1085^\circ F / \overline{T}_C = 507^\circ F$ under matched load conditions. This represents a 30 percent (relative increase above the 5.0 percent efficiency level demonstrated by current TEM-X S/N-3 series modules at the same operating conditions). This improvement results from the use of thin film EBVD barriers and ternary thermoelectric materials. Calculations indicated, however, that with these two improvements, an efficiency level somewhat above 6.5 percent is theoretically obtainable. Accordingly the thermal conductivity

TABLE VIII-2

PRELIMINARY MATCHED LOAD END-OF-LIFE 5 KWe
REACTOR MODULE REQUIREMENTS

	Per Module	System
Average Module Inner Clad Temperature (^{o}F)	1140	--
Number of Modules	--	16
Power Output (watts)	320.6	5130
Load Voltage (volts)	3.86	30.9
Total Power Degradation (pct.)	7.0	7.0

of the ternary materials was <u>increased</u> by a factor of 1.028 to meet the 30 percent improvement goal which can be demonstrated without achieving the full theoretical improvement potential available in the ternary materials.

5. The reference module will incur a total power output degradation of 7.0 percent during the five years of operation of the system. Degradation, D, is defined by the expression

$$D = \frac{100 \, (P_{BOL} - P_{EOL})}{P_{BOL}},$$

where P_{BOL} and P_{EOL} are the beginning and end-of life matched load power outputs at a given set of operating temperatures.

Module degradation was accurately accounted for in the mathematical model by increasing the resistivity of the n-leg thermoelectric material by the factor necessary to cause a 7.0 percent reduction in power output at any given set of operating temperatures. Although voltage changes had been observed during operation of modules, these changes are much smaller in magnitude than the resistance changes. In addition, the experimental data indicated that the voltage initially increases, goes through a maximum, and then tends to decrease with time. These changes occur at a rate such that over a five-year period, the total voltage change should be negligible.

It was determined that, in the absence of voltage changes, a 7.0 percent reduction in power relates to 7.9 percent increase in resistance. A 7.9 percent increase in module resistance, in turn, relates to an 18 percent increase in n-leg resistivity. On this basis, a factor of 1.18 was applied to the resistivity of the n-type ternary material for the calculation of E.O.L. performance. By taking the effects of degradation into account, as described above, it was possible to perform parametric calculations to optimize end-of-life performance. That is, the n-leg to p-leg axial thickness ratio was maintained at that value which optimally compensates for the effects of degradation.

Maintaining the constraints ("ground rules") discussed above, there is one and only one module design which will satisfy the matched load voltage and power requirements

shown in Table VIII-2. The voltage requirement was met by varying the number of couples to be incorporated in the fifteen inch thermoelectric circuit. The power requirement was met by varying the average cold clad temperature of the module. Parametric calculations revealed that a 15 inch module incorporating 48 thermoelectric couples when operated at $\overline{T}_H = 1140^\circ F / \overline{T}_C = 542^\circ F$ satisfies all the requirements simultaneously. This module, then, was designated as the "reference module" for the 5 KWe Demonstration System.

Table VIII-3 presents a dimensional and performance description of the reference module. The radial dimensions, as specified, are identical to those of the current TEM-X series modules. The axial dimensions of the reference module differ somewhat from those of the TEM-X S/N-3 series modules which were designed for optimum B.O.L. (performance and n-leg axial thicknesses) and incorporate 38 couples and .009 inch mica/tungsten foil insulating barriers. The p-leg and n-leg washers of the TEM-X S/N-3 series modules have a post processing axial thickness of .189 inches.

Matched load performance calculations for the reference module are listed for $\overline{T}_H = 1085^\circ F / \overline{T}_C = 507^\circ F$ and $\overline{T}_H = 1140^\circ F / \overline{T}_C = 542^\circ F$. Both B.O.L. and E.O.L. performance is listed at the latter conditions. As can be seen, the module will produce an efficiency of 6.5 percent at $\overline{T}_H = 1085^\circ F / \overline{T}_C = 507^\circ F$, or 30 percent better than the TEM-X demonstrated efficiency at these temperatures. The end-of-life $\overline{T}_H = 1140^\circ F / \overline{T}_C = 542^\circ F$ performances very closely satisfies the system requirements specified in Table VIII-2 In addition, the total degradation of the module is 7.0 percent, as specified.

These results were transmitted to Atomics International for use in the 5 KWe Demonstration System calculations. Additional work was in progress to develop a series of accurate closed-form analytical expressions describing the performance (i.e., voltage, resistance, power, and efficiency) of the reference module as functions of average hot and cold clad temperatures, load resistance, and degradation. These relationships are necessary to allow a determination of the system performance as a function of time and to determine the starting operating temperatures that will allow the reactor outlet temperatures to be continually increased with time to offset degradation such that the final (five year) reactor outlet temperature is $1200^\circ F$. This corresponds to an average module temperature of $1140^\circ F$.

TABLE VIII-3

DIMENSIONS AND PERFORMANCE OF THE REFERENCE MODULE FOR THE 5 KWe DEMONSTRATION SYSTEM

I.   RADIAL DIMENSIONS AFTER PROCESSING

		Inner Radius (Inches)	Outer Radius (Inches)
1.	Ta/10W Inner Clad	.375	.463
2.	Inner Boron Nitride Insulating Sleeve	.463	.489
3.	Mo/W Inner Conductor Rings	.489	.520
4.	Ternary Lead Telluride Washers	.520	.662
5.	Molybdenum Outer Conductor Rings	.662	.682
6.	Outer Boron Nitride Insulating Sleeve	.682	.717
7.	Stainless Steel Outer Clad	.717	.822

II.   AXIAL DIMENSIONS

		Length (Inches)
1.	N-Type Ternary Thermoelectric Washer	.161
2.	P-Type Ternary Thermoelectric Washer	.149
3.	Mica Intercouple Insulator with EBVD Barrier	.0015
4.	Total Circuit (48 couples)	15.024

III.   MATCHED LOAD PERFORMANCE

		B.O.L. 1085/507	B.O.L. 1140/542	E.O.L. 1140/542
1.	Load Voltage (volts)	3.66	3.86	3.87
2.	Internal Resistance (milliohms)	39.1	43.3	46.7
3.	Power Output (watts)	342	345	321
4.	Module Heat Input (watts)	5250	5420	5300
5.	Overall Efficiency (pct.)	6.50	6.37	6.06

D.   PUMP MODULE PARAMETRIC CALCULATIONS

The 5 KWe reactor/thermoelectric system, like previous systems, was to incorporate tubular modules designed to operate the system electromagnetic pumps. Design of these pump power modules was complicated by the fact that the E.M. pump electrical requirements could not be explicitly defined.

Initial parametric calculations were performed to determine axial dimensions and numbers of couples for optimum TEM-14 pump modules having various voltage/current characteristics. For the first parametric study, the existing TEM-14 pump module radial dimensions were held fixed and $\overline{T}_H = 1168^\circ F/\overline{T}_C = 522^\circ F$ clad temperatures were selected on the basis of preliminary system analysis results received from Atomics International. The object of the study was to indicate the effects of pump module current and load voltage requirements on overall pump module efficiency and circuit length (hence module weight).

To complete the analysis, a computer code was developed to calculate the number of thermoelectric couples and washer axial thicknesses required to produce a given load voltage and current. The code was then used to calculate optimum TEM-14 parameters for voltages ranging from 0.1 volt to 0.3 volt, and load currents ranging from 500 amps to 900 amps.

Results of the study are presented in Figures VIII-1 and VIII-2. Figure VIII-1 shows the effect of operating requirements on overall module efficiency. For a fixed load voltage, efficiency varies inversely with current. This is because the module power output increases only linearly with current, whereas the Joule power losses (I^2R) in the electrical access pins (a significant parameter in pump module operation) increases with the square of the current. For a fixed current, efficiency varies directly with load voltage since the Joule power losses in the electrical access pins remain constant while the module power output is increased.

The relationship between circuit length and operating requirements is shown in Figure VIII-2. The characteristic shapes of the parametric curves shown in this figure result from the fact that circuit length varies directly with the electrical power requirement for a fixed set of operating temperatures.
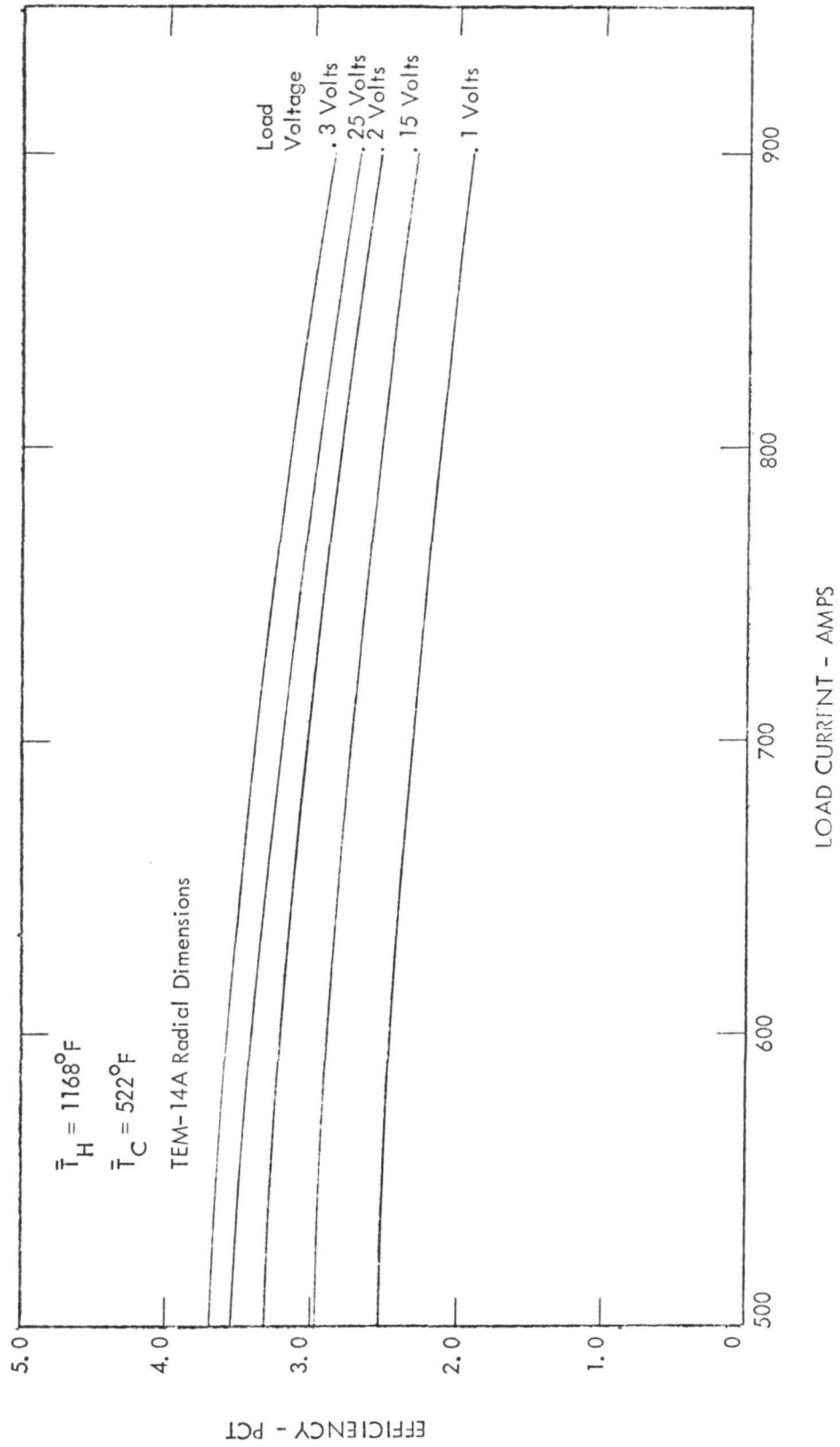
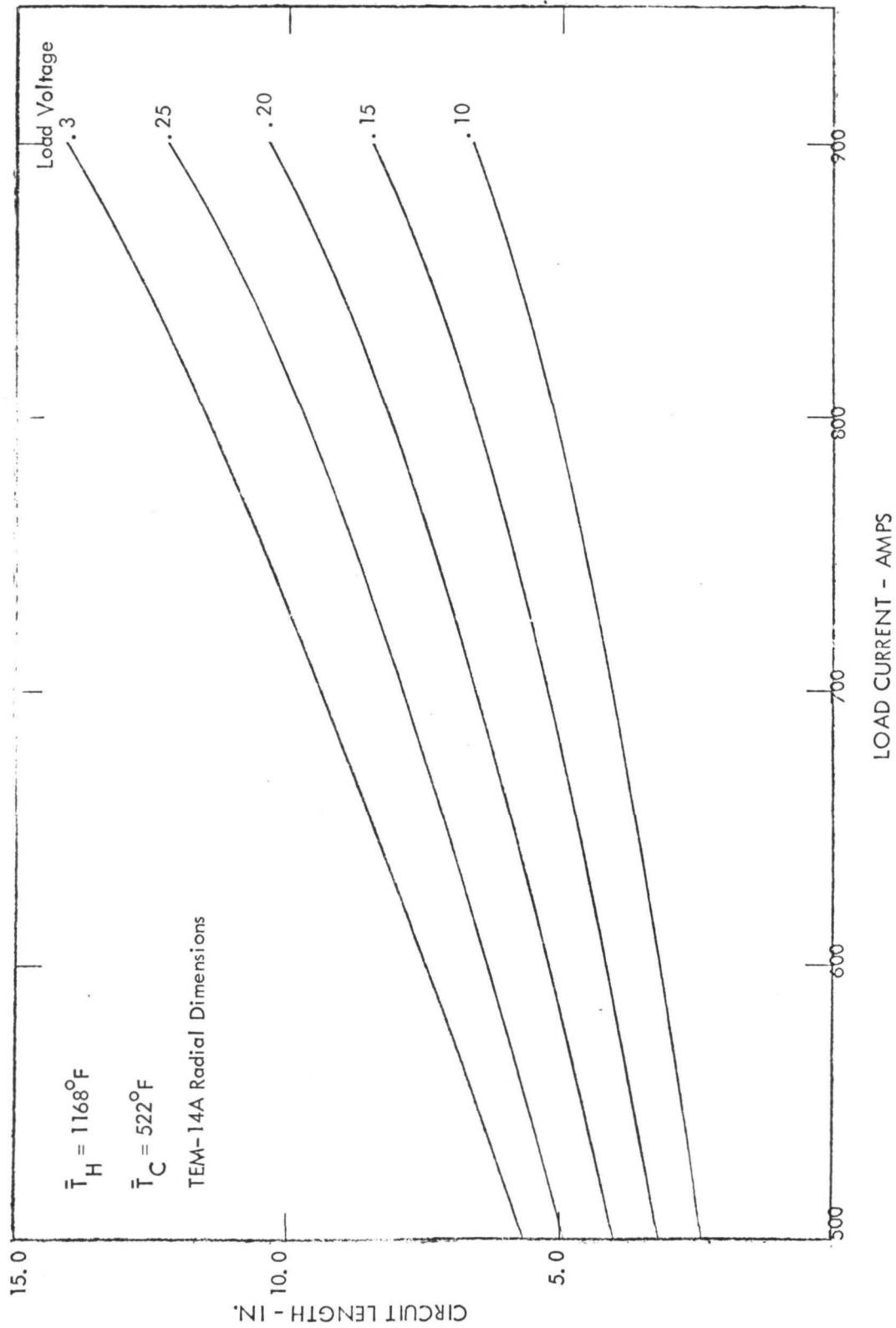Figure VIII-1. E. M. Pump Module 1168/522 Parametric: Efficiency Versus Current

Figure VIII-2. E. M. Pump Module 1168/522 Parametric: Circuit Length Versus Current

Additional sets of similar calculations were completed for various operating temperatures. These calculations indicated although the efficiency levels and circuit lengths varied as the temperatures were modified, the relationships between these parameters and operating characteristics of the module were relatively insensitive to temperatures.

Based on this information and system trade studies performed at Atomics International end-of-life performance requirements for the pump power module to be incorporated into the 5 KWe reactor/thermoelectric demonstration system were established. Electromagnetic pump of the primary and secondary liquid metal loops would be provided by an integrated E.M. pump/pump module assembly. The assembly would consist of three modules connected both in hydraulic and electrical parallel in an arrangement similar to that shown previously in Figure II-4. End-of-life pump module performance requirements for the 5 KWe demonstration system are listed in Table VIII-4.

An additional set of parametric calculations was then performed. In these calculations variations in inner and outer conductor ring radial thicknesses, lead telluride radial thickness and numbers of thermoelectric couples were considered for modules meeting end-of-life performance requirements specified in Table VIII-4. Module degradation was accounted for using the same techniques described in the reactor power module parametrics. In this case, however, a total 8.75 percent degradation rate was assumed based on experimental data from TEM-14A series pump power modules.

In the final set of parametric calculations, only one design improvement was considered for incorporation into the reference pump module for the system. The demonstration system pump module was assumed to incorporate nickel-clad copper electrical power pins having a cross section comprised of 15 percent nickel and 85 percent pure copper. The effective resistivity of a pin having this configuration would be approximately 17 percent of the presently used solid nickel pin. This reduction in pin circuit resistance results in a substantial improvement in performance (efficiency increases by about 20 percent). The module resistance and load voltage were taken to be measured from the outer ends of the pins at one end of the module to the outer ends of pins at the other end (i.e., external collector ring resistance and voltage drop were included in the load circuit).

TABLE VIII-4

PRELIMINARY END-OF-LIFE 5 KWe REACTOR
PUMP MODULE REQUIREMENTS

	Module	System*
Average Module Inner Clad Temperature ($^\circ$F)	1128	--
Average Module Outer Clad Temperature ($^\circ$F)	550	--
Pin-to-Pin Load Voltage (volts)	.201	.201
Current (amps)	564	1692
Total Power (watts)	113	340
Total Power Degradation (pct.)	8.75	8.75

*The system consists of three modules connected in hydraulic and electrical parallel.

The study showed that performance (i.e., efficiency) increased continuously as conductor ring radial thicknesses were increased. Thus, inner and outer conductor ring thickness were selected at 0.225 inch and 0.075 inch, respectively, on the basis of being able to insure full compaction during processing of the module. (The TEM-14A series modules employ 0.225 inch and 0.050 inch inner and outer conductors, respectively.)

Calculations were made for modules having both three and four thermoelectric couples. The results of the calculations are presented in Figures VIII-3 through VIII-5. Curves are presented for overall efficiency, module weight (including end closures), internal resistance, open circuit voltage, and module circuit length as functions of lead telluride radial thickness. In each case, the module component axial dimensions were selected to maintain the prescribed .201 load voltage and 564 amp system current requirement.

As can be seen in Figure VIII-3, the three-couple design becomes more efficient than the four-couple design for lead telluride radial thicknesses greater than 0.100 inch. The lead telluride radial thickness in the current TEM-14A and TEM-14B designs is 0.100 inch. It was anticipated that dimensions for the TEM-14C module, the reference pump module for the 5 KWe demonstration system, would be selected from these parametric results based on the trade-off between increasing module weight and decreasing radiator weight (due to increasing efficiency) as a function of increasing lead telluride thickness.
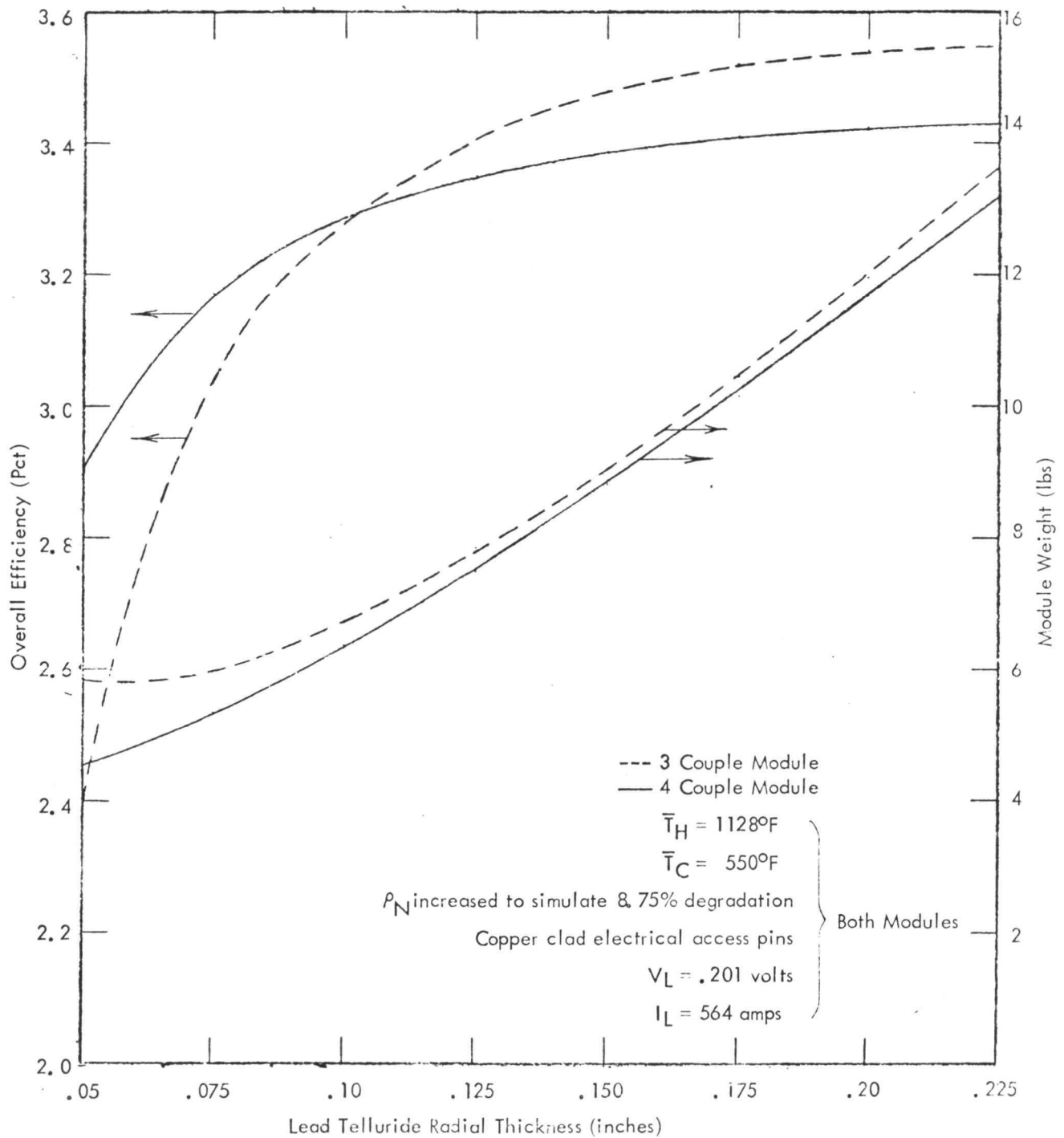
Figure VIII-3. Efficiency and Weight as Functions of PbTe Thickness for 3 and 4 Couple .201 Volt, 564 Amp Pump Modules Operated at $\overline{T}_H = 1128°F/\overline{T}_C = 550°F$
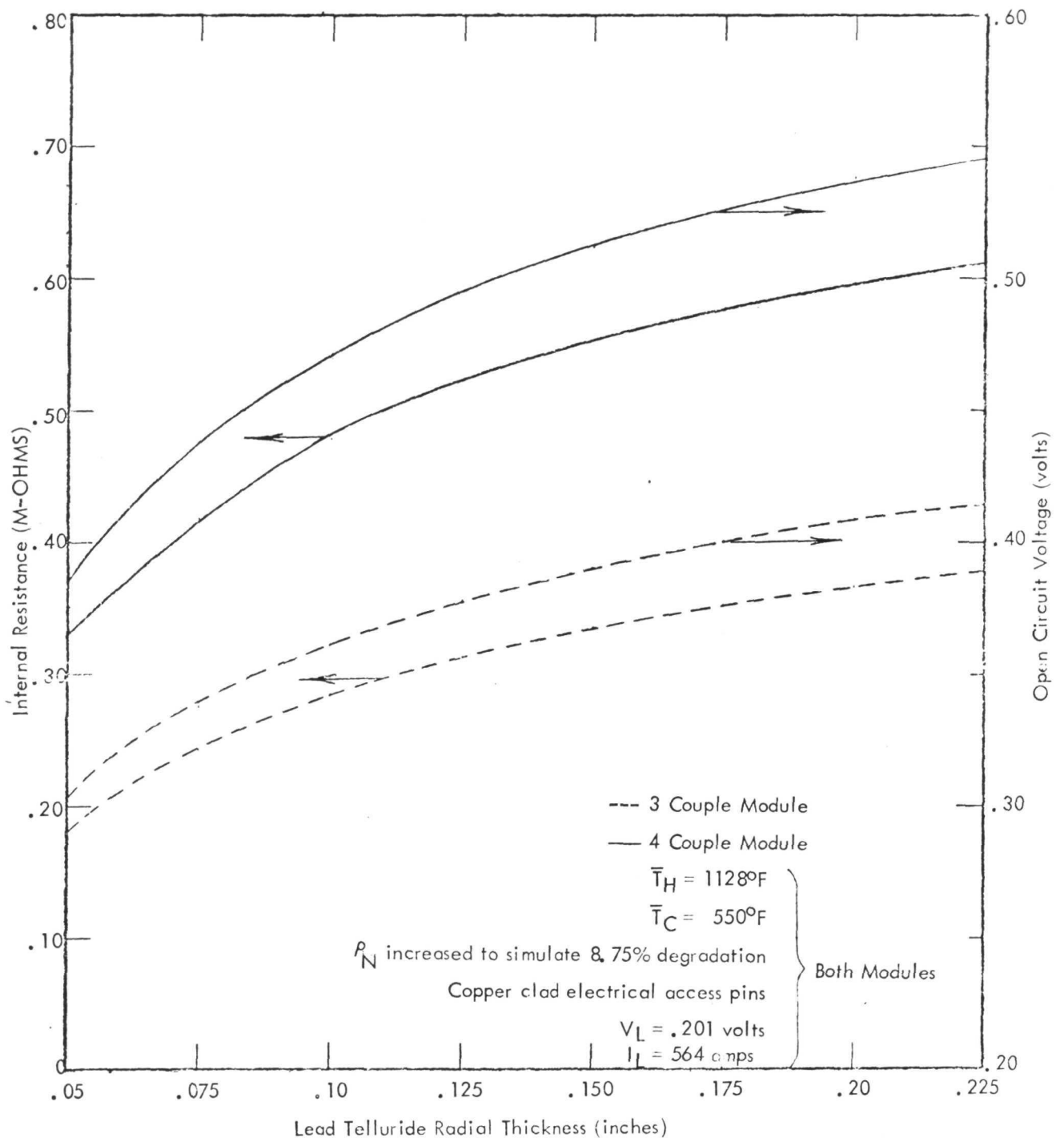
Figure VIII-4. Resistance and Open Circuit Voltage as Functions of PbTe Thickness for 3 and 4 Couple .201 Volt 564 Amp Pump Modules Operated at $\overline{T}_H = 1128°F/\overline{T}_C = 550°F$
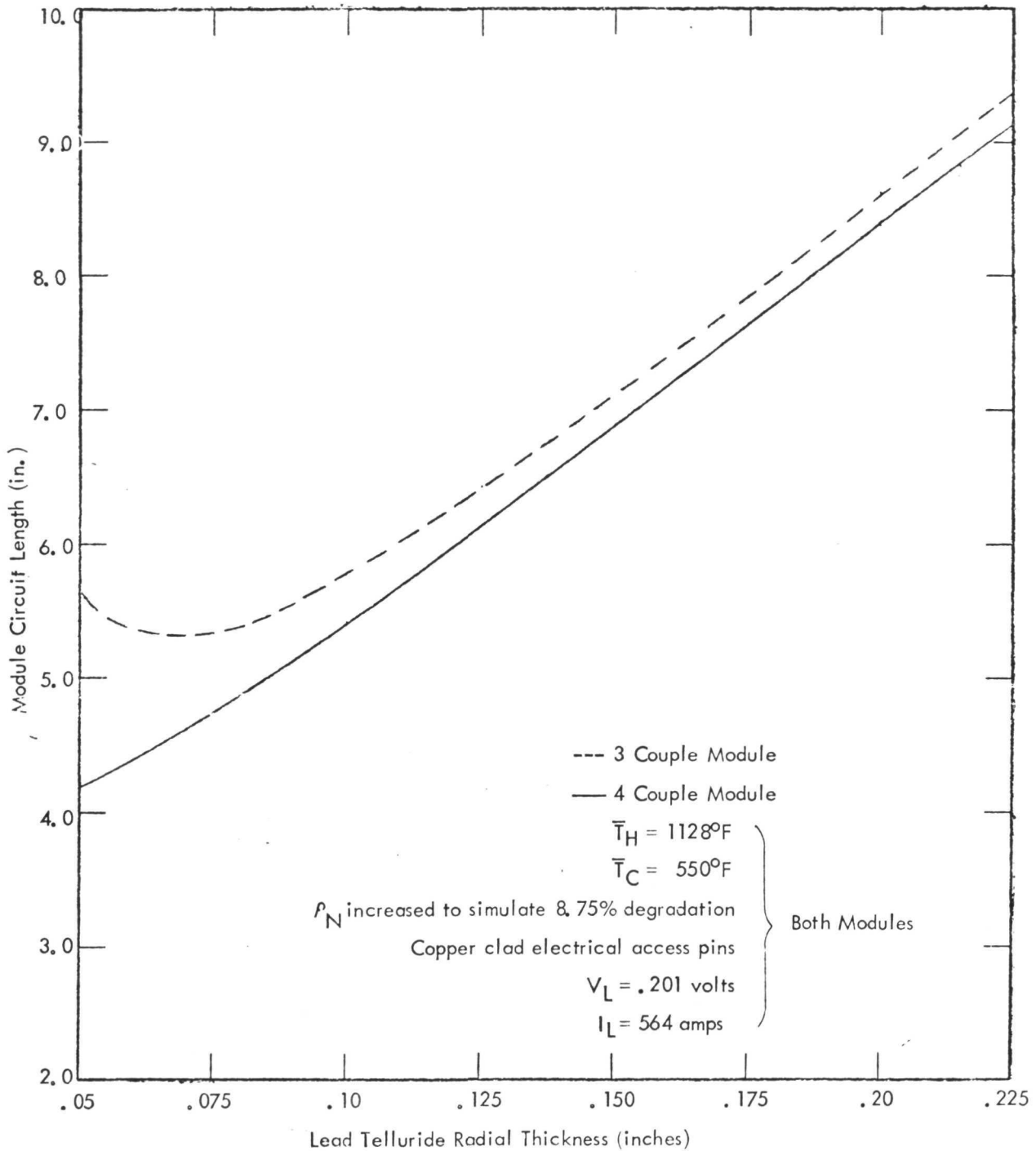
Figure VIII-5 Total Circuit Length as Functions of PbTe Thickness for 3 and 4 Couple
.201 Volt 546 Amp Pump Modules Operated at $\overline{T}_H = 1128°F/\overline{T}_C = 550°F$

APPENDIX A

LIST OF MODULE ASSEMBLY DRAWINGS

Initial Prototype Reactor Power Modules			Refractory Metal Clad Reactor Power Modules			Sublength Technology Modules		
Module			Module			Module		
TEM	S/N	Dwg. No.	TEM	S/N	Dwg. No.	TEM	S/N	Dwg. No.
13A	1	914E365	X	1	914E573	15	1	982D180
13A	2	914E365	X	2	914E734	15	2	982D180
13B	1	914E365	X	3	914E734	15A	1	914E590
13B	2	914E365	X	3A	914E734	15A	4	914E590
13C	1	914E365	X	3B	914E734	15A	4A	914E590
13C	2	914E365	X	3C	914E734	15A	4B	914E590
13D	1	914E365	X	3D	914E734	15A	4C	914E590
13D	2	914E365	X	3E	914E734	15A	4D	914E590
13F	1	914E489	X	3F	914E734	15A	4E	914E590
13F	2	914E489	X	3G	914E734	15A	4F	914E590
13F	3	914E489	X	3H	914E734	15A	4G	914E590
13G	1	914E573	X	3J	914E734	15A	4H	914E890
13G	2	914E573	X	3K	914E734	15A	4J	914E590
13G	3	914E573	X	3M	914E734	15A	5	914E590
13G	4	914E573				15A	8	914E590
13G	5	914E573				15B	4	914E590
13G	6	914E573				15B	4A	914E590
13G	7	914E573				15B	4B	914E590
13G	8	914E573				15B	4C	914E590
13G	9	914E573				15B	4D	914E890
13G	10	914E573				15C	4	914E590
13G	11	914E573				15C	4A	914E590
13G	12	914E573				15C	8	914E590
			Pump Power Modules			15D	4	914E737
			14A	1	914E383	15E	4	914E858
			14A	2	914E383	15F	4	914E858
			14A	3	914E383	15H	4	914E590
			14B	1	914E867	15P	1	914E877
			14B	2	914E867			
			14B	3	914E867			

APPENDIX B

NOMENCLATURE

a_o, b_o, c_o,	Crystal Lattice Parameters
$\overset{o}{A}$	Angstrom Unit
Alsimag 222	Aluminum/Silicon/Magnesium Insulating Material
ANX	Ternary N-Type PbTe-GeTe Composition Thermoelectric Material
APX	Ternary P-Type PbTe-PbSe Material
BOL	"Beginning-Of-Life" in Reference to the First Data Set Recorded at Design Operating Conditions
BN	Chemical Symbol for Boron Nitride Insulating Material
^{o}C	Degrees Centrigrade
CC	Cubic Centimeter
$\mathcal{C}_L$	Centerline
CVD	Chemical Vapor Deposition
DC	Direct Current
EB	Electron Beam (welding process)
EBVD	Electron Beam Vapor Deposition Process
EM	Electromagnetic
EOL	End-Of-Life
EXC	Experimental Capsule
^{o}F	Degrees Fahrenheit
GE-nl	A Stoichiometric N-Type Lead Iodide Doped Lead Telluride
I	Electrical Current
ID	Inner Diameter
I_L	Electrical Current Drawn through Load Resistor, R_L
^{o}K	Degrees Kelvin

k	Thermal Conductivity
KWe	Kilowatts (electrical power)
ML	Matched Load Module Operating Conditions ($R_L = R_G$)
NaK	Sodium-Potassium Liquid Metal Eutechtic Composition
n-type	Semi-Conductor Material Doped with an Excess of Negative Charge Carriers (electrons)
OC	Open Circuit Module Operating Conditions
OD	Outer Diameter
P_e	Electrical Power
p-type	Semi-Conductor Material Doped with an Excess of Positive Charge Carriers (holes)
Q_c	Thermal Power Delivered to Module Thermoelectric Circuit
Q_e	Thermal Power Loss through Module End Closures
Q_t	Total Thermal Power Delivered to Tubular Module
$^\circ R$	Degrees Rankin
R	Electrical Resistance
R_c	Electrical Resistance Measured from Module Circuit to Ground (clad)
RF	Radio Frequency
R_g	Internal Resistance of Module Measured from Positive to Negative External Collector Ring
R_L	Load Resistance into which Module Operates
SS	Stainless Steel
T	Temperature
$\overline{T}$	Average Module Temperature Defined $1/2 \, (\overline{T}_H + \overline{T}_C)$
$\overline{T}_C$	Mean Outer Clad Surface Temperature of a Module
T/E	Thermoelectric
TEGS-2P	3M Company Designation for Sodium Doped P-Type Lead Telluride

TEGS-3P	3M Company Designation for P-Type Lead-Tin-Telluride Containing Manganese and Sodium
TEM	Tubular Thermoelectric Module
$\bar{T}_H$	Mean Inner Clad Surface Temperature of a Module
TI	Thermal Impedance of a Module (defined: $\Delta\bar{T}/Q_T$)
TIG	Tungsten Inert Gas (welding procedure)
T_P	Peak Temperature Measured on Inner Clad of Module
V_L	Voltage Measured between Positive and Negative External Collector Rings with Load Resistor R_L Applied to Module
V_{oc}	Voltage Measured between Positive and Negative Terminals of Module with no Load Resistor Applied
WANL	Westinghouse Astronuclear Laboratory
Z	Figure-Of-Merit
a	Seebeck Coefficient
$\bar{a}$	Effective Seebeck Coefficient of a Module (defined: $\dfrac{V_{oc}}{\Delta T}$)
β	Crystal Lattice Parameter
$\Delta\bar{T}$	Mean Inner Clad to Outer Clad Temperature Drop across Module
ΔT_C	Axial Temperature Drop along Outer Clad of Module
ΔT_H	Axial Temperature Drop along Inner Clad of Module
ϵ	Emissivity
η	Efficiency
η_c	Carnot Efficiency
μm	Micro-meter
μV	Micro-volts
Ω	Ohms
$m\Omega$	Milliohms

NASA Lewis Research Center
21000 Brookpark Road
Cleveland, Ohio 44135
Attention: Martin J. Saari (15)
M. S. 60-6

NASA Lewis Research Center
21000 Brookpark Road
Cleveland, Ohio 44135
Attention: Leonard W. Schopen (1)
M. S. 500-206

NASA Lewis Research Center
21000 Brookpark Road
Cleveland, Ohio 44135
Attention: Norman T. Musial (1)
M. S. 500-113

NASA Lewis Research Center
21000 Brookpark Road
Cleveland, Ohio 44135
Attention: Librarian (2)
M. S. 60-3

NASA Lewis Research Center
21000 Brookpark Road
Cleveland, Ohio 44135
Attention: P. E. Foster (1)
M. S. 3-19

NASA Lewis Research Center
21000 Brookpark Road
Cleveland, Ohio 44135
Attention: G. Mervin Ault (1)
M. S. 3-5

NASA Lewis Research Center
21000 Brookpark Road
Cleveland, Ohio 44135
Attention: Robert E. English (1)
M. S. 500-201

NASA Lewis Research Center
21000 Brookpark Road
Cleveland, Ohio 44135
Attention: Henry O. Slone (1)
M. S. 501-6

NASA Lewis Research Center
21000 Brookpark Road
Cleveland, Ohio 44135
Attention: Donald Packe (4)
M. S. 500-201

NASA Lewis Research Center
21000 Brookpark Road
Cleveland, Ohio 44135
Attention: B. T. Lundin (1)

NASA Lewis Research Center
21000 Brookpark Road
Cleveland, Ohio 44135
Attention: B. Lubarsky (1)
M. S. 3-3

NASA Lewis Research Center
21000 Brookpark Road
Cleveland, Ohio 44135
Attention: Samuel J. Kaufman (3)
M. S. 49-2

NASA Lewis Research Center
21000 Brookpark Road
Cleveland, Ohio 44135
Attention: V. F. Hlavin (1)
M. S. 3-10

NASA Lewis Research Center
21000 Brookpark Road
Cleveland, Ohio 44135
Attention: Neal T. Saunders (3)
M. S. 105-1

NASA Lewis Research Center
21000 Brookpark Road
Attention: Report Control Office
Cleveland, Ohio 44135
Attention: A. P. Dill (1)
M. S. 5-5

NASA Scientific and Technical
Information Facility
Acquisitions Branch
Post Office Box 33
College Park, Maryland 20740 (10)

National Aeronautics and
Space Administration
Washington, D. C. 20546
Attention: P. R. Miller (3)
Code RNP

National Aeronautics and
Space Administration
Washington, D. C. 20546
Attention: D. S. Gabriel (2)
Code NS 2

Jet Propulsion Laboratory
4800 Oak Grove Drive
Pasadena, California 91103
Attention: Library (1)

National Aeronautics and
Space Administration
Geo. C. Marshall Space Flight Center
Marshall Space Flight Center,
Alabama 35812
Attention: Library (1)

NASA Flight Research Center
P. O. Box 273
Edwards, California 93523
Attention: Library (1)

NASA Ames Research Center
Moffett Field, California 94035
Attention: Library (1)

NASA Goddard Space Flight Center
Greenbelt, Maryland 20771
Attention: Library (1)

NASA Langley Research Center
Langley Station
Hampton, Virginia 23365
Attention: Library (1)

NASA Manned Spacecraft Center
Houston, Texas 77058
Attention: Library (1)